

VOLUME 80

OCTOBER 7, 1976

3mm
/ NUMBER 21

JPCHA x

THE JOURNAL OF
PHYSICAL
CHEMISTRY



PUBLISHED BIWEEKLY BY THE AMERICAN CHEMICAL SOCIETY

New and Recent Titles for the Physical Chemist...

THE HYDROLYSIS OF CATIONS

Charles F. Baes, Jr. & Robert E. Mesmer

A general reference which assists the reader in dealing with the array of hydroxy species that complicate the chemical behavior of metallic elements in aqueous solutions. It critically evaluates information on identities and stabilities of species in solution and the solid hydroxides and oxides produced therefrom:

489 pp. (0 471 03985-3) 1976 \$29.95

HANDBOOK OF CHEMICAL LASERS

Edited by R.W.F. Gross & J.F. Bott

Collects and critically reviews all available literature and the entire body of research work in the field of chemical lasers published and performed between 1967 and 1974. Provides a reference sourcebook for the engineers and systems analysts who are going to plan and perform the future development of the field.

864 pp. (0 471 32804-9) 1976 \$39.95

AN INTRODUCTION TO RADIATION CHEMISTRY, 2nd Ed.

J.W.T. Spinks & R.J. Woods

The Second Edition of the first comprehensive introduction to the subject of radiation chemistry. Fully updated to include such major topics as the techniques of pulse radiolysis and major revisions of the chapters on water, organic compounds, and industrial radiation chemistry.

504 pp. (0 471 81670-1) 1976 \$24.95

PROGRESS IN INORGANIC CHEMISTRY, Vol. 22

Edited by Stephen J. Lippard

CONTENTS: The Coordination and Bioinorganic Chemistry of Molybdenum. The Derivation and Application of Normalized Spherical Harmonic Hamiltonians. Chemical Applications of Magnetic Anisotropy Studies on Transition Metal Complexes. Oxidatively Induced Cleavage of Transition Metal-Carbon Bonds. Subject Index. Cumulative Index. *Progress in Inorganic Chemistry Series.*

432 pp. (0 471 54092-7) 1976 \$25.95

SURFACE AND COLLOID SCIENCE, Vol. 9

Edited by Egon Matijevic

CONTENTS: The Stability of Emulsions and Mechanisms of Emulsion Breakdown. Nuclear Magnetic Resonance of Surfactant Solutions. Micellar Aspects of Casein. The Adsorption of Gases on Porous Solids. Author Index. Subject Index. Cumulative Index. *Surface and Colloid Science Series.*

384 pp. (0 471 57638-7) 1976 \$34.95

HANDBOOK OF PROTON IONIZATION HEATS

And Related Thermodynamic Quantities

James J. Christensen, Lee D. Hansen, Reed M. Izatt

Brings together for the first time a complete listing of the heats of proton ionization, ΔH , together with the related thermodynamic quantities, pK_a , ΔS , and ΔC_p , where available. Includes all acids for which ΔH values are available (approximately 1200 entries) and three indexes.

CONTENTS: Preface. Use of Tables and Indexes. Table. Empirical Formula Index. Synonym Index. Reference Index.

320 pp. (0 471 01991-7) 1976 \$22.50

TOPICS IN PHOSPHORUS CHEMISTRY, Vol. 8

Edited by E.J. Griffith & Martin Grayson

CONTENTS: The Chemistry of Phosphorohydrazides and Azides. The Mass Spectra of Organophosphorus Compounds. NMR Parameters of the Proton Directly Bonded to Phosphorus. Phosphorus Sulfides. A Study of Isolated Complexes of Neutral Ligands. Chemical Analysis of Phosphate Rock. The Chemistry of P-C-N Systems. The Reaction of Disulfides with Trivalent Phosphorus Compounds. Subject Index. Cumulative Index. *Topics in Phosphorus Chemistry Series.*

approx. 720 pp. (0 471 32789-1) 1976 \$22.50 (tent.)

TOPICS IN PHOSPHORUS CHEMISTRY, Vol. 9

Edited by E.J. Griffith & Martin Grayson

Provides the generalist as well as the specialist with a series of critical evaluations and reviews of progress in the diverse areas of phosphorus chemistry.

CONTENTS: Transition Metal Complexes of Phosphorus Ligands. Phosphate Ceramics. ESR of Phosphorus Compounds. *Topics in Phosphorus Chemistry Series.*

544 pp. (0 471 32782-4) 1976 \$43.50

STATISTICAL MECHANICS, 2nd Ed.

Joseph Edward Mayer & the late Maria Goepfert Mayer

Updated introduction to the logic and fundamental structure of statistical mechanics including an introduction of historical perspective and 19th century perfect gas kinetic theory.

512 pp. (0 471 57985-8) 1976 \$23.50

THERMOCHEMICAL KINETICS, 2nd Ed.

Methods for the Estimation of
Thermochemical Data and Rate Parameters

Sidney W. Benson

A text with a molecular approach to the techniques for rapid and relatively quantitative estimation of thermochemical data and reaction-rate parameters for chemical reactions in the gas phase.

336 pp. (0 471 06781-4) 1976 \$22.50

THEORY AND APPLICATIONS OF MOLECULAR PARAMAGNETISM

E.A. Boudreaux & L.N. Mulay

A lucid treatment of the basic theory of paramagnetic phenomena from both classical and quantum mechanical viewpoints.

510 pp. (0 471 09106-5) 1976 \$35.50

TECHNIQUES INVOLVING EXTREME ENVIRONMENT, NONDESTRUCTIVE TECHNIQUES, COMPUTER METHODS IN METALS RESEARCH, AND DATA ANALYSIS, Vol. 7, Part 2

Edited by R.F. Bunshah

CONTENTS: Internal Friction Measurements. Nondestructive Testing. Techniques. Statistical Design of Experiments and Regression Analysis in Metallurgical Research. Measurement of Surfaces of Engineering Materials. Author Index. Subject Index.

448 pp. (0 471 12241-6) 1976 \$44.00

THE EXCITED STATE IN CHEMICAL PHYSICS

Edited by **J. Wm. McGowan**

Contributions by eight experts using interdisciplinary material to examine excited states in chemistry and physics.

CONTENTS: The Production of Excited Simple Chemical Reactions. Potential Energy Surface Considerations for Excited State Reactions. Vibrational and Rotational Excitation in Gaseous Collisions. Sensitized Fluorescence and Quenching. Theory of Nonadiabatic Collision Processes Including Excited Alkali Atoms. Excitation De-excitation Processes Relevant to the Upper Atmosphere. Applications to Lasers. *Advances in Chemical Physics Series, Vol. 28.*

492 pp. (0 471 58425-8) 1975 \$25.50

PHYSICAL CHEMISTRY OF SURFACES, 3rd Ed.

Arthur W. Adamson

Brings more emphasis to the molecular approach and the long list of phenomena including AES, APS, EIS, LEED, and SIMS. Notes the growing bridge between such studies and heterogeneous catalysis. For this new edition all chapters were updated with respect to the literature of the field, new problems were added, and the ordering of the problems section was brought into approximate parallel with that of the subjects covered in the chapters.

720 pp. (0 471 00794-3) 1976 \$24.95

from Wiley-Interscience

DYNAMIC LIGHT SCATTERING

With Applications to Chemistry, Biology and Physics

Bruce J. Berne & Robert Pecora

An introduction to the principles underlying laser light scattering, emphasizing the time dependence of fluctuations in fluid systems. The book is also useful as an introduction to the theory of time correlation functions and contains chapters on projection operator techniques in statistical mechanics.

376 pp. (0 471 07100-5) 1976 \$24.95

CRYOCHEMISTRY

Martin Moskovits & Geoffrey A. Ozin

Matrix and preparative cryochemistry cover much common ground in areas such as reaction intermediates and products, reaction pathways, thermodynamics and kinetics, reaction feasibility, and product yields. An intelligent combination of the two techniques can complement and supplement each other. This volume provides the student with a working knowledge of both topics in a coherent and logical scheme.

560 pp. (0 471 61870-5) 1976 \$32.50

EXCITED STATES OF BIOLOGICAL MOLECULES

Edited by **J.B. Birks**

The fourth book in the series to be devoted to the photophysics of organic molecules. The experimental and theoretical methods developed in the study of simple aromatic molecules are extended to more complex biological molecules such as DNA, the proteins, the porphyrins and the retinols. Its contents provide a broad topical survey of this branch of biochemical physics, and are based on an International Conference on the Excited States of Biological Molecules. *Chemical Physics Series.*

652 pp. (0 471 07415-6) 1976 \$45.00

ADVANCES IN CHEMICAL PHYSICS SERIES, Vols. 31-35

Edited by **I. Prigogine & Stuart A. Rice**

Vol. 31 NON-SIMPLE LIQUIDS A Topical Volume in Advances

CONTENTS: Theory and Molecular Models for Water. The Structure of Polar Fluids. The Kinetic Theory of Dense Polyatomic Fluids. Theory of Liquid Crystals. Theory of Electron States in Liquid Metals. Low Energy Electrons in Nonpolar Fluids. Solutions of Metals in Molten Salts.

496 pp. (0 471 69933-0) 1975 \$34.95

Vol. 32 PROCEEDINGS OF THE CONFERENCE ON INSTABILITY AND DISSIPATIVE STRUCTURES IN HYDRODYNAMICS

CONTENTS: On the Mechanism of Instabilities in Nonlinear Systems. On a Unified Thermodynamic Approach to a Large Class of Instabilities of Dissipative Continua. Concepts in Hydrodynamic Stability Theory. Some Remarks on Variational Methods, The Local Potential, and Finite Element Methods with Applications to Certain Continuum Mechanics Problems. Glandsdorff-Prigogine Criterion and Statistical Theory. Numerical Models for Convection. The Effect of Prandtl Number on Finite Amplitude Benard Convection. Light Scattering from Nonequilibrium Fluid Systems. Magnetic Fields and Convection. Stability of Supercritical Benard Convection and Taylor Vortex Flow. Laboratory Experiments on Double-Diffusive Instabilities. Cylindrical Couette Flow Instabilities in Nematic Liquid Crystals. Theoretical and Experimental Study of Stationary Profiles of a Water-Ice Mobile Solidification Interface. Stellar Evolutionary Stability in Relation to Spectral Theory. Stellar Atmospheres, Nonequilibrium Thermodynamics, and Irreversibility. The Benard Instability in Liquid Mixtures. On the Nature of Oscillatory Convection in Two-Component Fluids. Finite Amplitude Instability in the Two-Component Benard Problem.

333 pp. (0 471 69934-9) 1975 \$27.50

Vol. 33 ADVANCES IN CHEMICAL PHYSICS

CONTENTS: Mobilities of Charge Carriers in Superfluid Helium. Intermolecular Forces and Crystal Structures for D, N, O, F, and CO. Cooperative Conformational Kinetics of Synthetic and Biological Chain Molecules. The Electrodynamics of Atoms and Molecules. Spectral Line Shapes in Gases in the Binary-Collision Approximation. Time-Reversal Invariance, Representations for Scattering Wave Functions, Symmetry of the Scattering Matrix, and Differential Cross-Sections. Transition States Stabilization Energy as a Measure of Chemical Reactivity. The Thermodynamics of Evolving Chemical Systems and the Approach to Equilibrium.

462 pp. (0 471 69935-7) 1975 \$32.00

Vol. 34 ADVANCES IN CHEMICAL PHYSICS

CONTENTS: The Rotation of Molecules in Dense Phases. Roles of Repulsive and Attractive Forces in Liquids: The Equilibrium Theory of Classical Fluids. Recent Advances in the Study of Liquids by X-Ray Diffraction. Diffraction by Molecular Liquids. The Expansion of the Master Equation.

324 pp. (0 471 69936-5) 1976 \$28.95

Vol. 35 ADVANCES IN CHEMICAL PHYSICS

CONTENTS: Theories of Chemically Induced Electron Spin Polarization. Kinetic Theory and Rheology of Macromolecular Solutions. Kinetic Theory of Gravitational Systems. Magnetic Circular Dichroism. Time-Dependent Perturbation of a Two-State Quantum System by a Sinusoidal Field.

358 pp. (0 471 69937-3) 1976 \$29.75

Available at your bookstore or write to Nat Bodian, Dept. 2092.

Prices subject to change without notice.



WILEY-INTERSCIENCE

a division of John Wiley & Sons, Inc.

605 Third Avenue, New York, N.Y. 10016

In Canada: 22 Worcester Road, Rexdale, Ontario

THE JOURNAL OF PHYSICAL CHEMISTRY

BRYCE CRAWFORD, Jr., *Editor*
STEPHEN PRAGER, *Associate Editor*
ROBERT W. CARR, Jr., **C. ALDEN MEAD**, *Assistant Editors*

EDITORIAL BOARD: C. A. ANGELL (1973-1977), F. C. ANSON (1974-1978), V. A. BLOOMFIELD (1974-1978), J. R. BOLTON (1976-1980), L. M. DORFMAN (1974-1978), H. L. FRIEDMAN (1975-1979), H. L. FRISCH (1976-1980), W. A. GODDARD (1976-1980), E. J. HART (1975-1979), W. J. KAUZMANN (1974-1978), R. L. KAY (1972-1976), D. W. McCLURE (1974-1978), R. M. NOYES (1973-1977), W. B. PERSON (1976-1980), J. C. POLANYI (1976-1980), S. A. RICE (1976-1980), F. S. ROWLAND (1973-1977), R. L. SCOTT (1973-1977), W. A. STEELE (1976-1980), J. B. STOTHERS (1974-1978), W. A. ZISMAN (1972-1976)

Published by the
AMERICAN CHEMICAL SOCIETY
BOOKS AND JOURNALS DIVISION
D. H. Michael Bowen, Director

Editorial Department: Charles R. Bertsch,
Head; Marianne C. Brogan, Associate
Head; Celia B. McFarland, Joseph E.
Yurvati, Assistant Editors

Graphics and Production Department:
Bacil Guiley, Head

Research and Development Department:
Seldon W. Terrant, Head

Advertising Office: Centcom, Ltd., 50 W.
State St., Westport, Conn. 06880.

© Copyright, 1976, by the American
Chemical Society. No part of this publication
may be reproduced in any form without
permission in writing from the American
Chemical Society.

Published biweekly by the American
Chemical Society at 20th and Northampton
Sts., Easton, Pennsylvania 18042. Second
class postage paid at Washington, D.C. and
at additional mailing offices.

Editorial Information

Instructions for authors are printed in
the first issue of each volume. Please conform
to these instructions when submitting man-
uscripts.

Manuscripts for publication should be
submitted to *The Journal of Physical
Chemistry*, Department of Chemistry, Uni-
versity of Minnesota, Minneapolis, Minn.
55455. Correspondence regarding **accepted
papers and proofs** should be directed to the
Editorial Department at the ACS Easton
address.

Page charges of \$60.00 per page are as-
sessed for papers published in this journal.
Ability to pay does not affect acceptance or
scheduling of papers.

Bulk reprints or photocopies of indi-
vidual articles are available. For information
write to Business Operations, Books and
Journals Division at the ACS Washington
address.

Requests for **permission to reprint**
should be directed to Permissions, Books and
Journals Division at the ACS Washington
address. The American Chemical Society and
its Editors assume no responsibility for the
statements and opinions advanced by con-
tributors.

Subscription and Business Information

1976 Subscription rates—including surface
postage

	U.S.	PUAS	Canada, Foreign
Member	\$24.00	\$29.75	\$30.25
Nonmember	96.00	101.75	102.25
Supplementary material	15.00	19.00	20.00

Air mail and air freight rates are avail-
able from Membership & Subscription Ser-
vices, at the ACS Columbus address.

New and renewal subscriptions should
be sent with payment to the Office of the
Controller at the ACS Washington address.

Changes of address must include both old
and new addresses with ZIP code and a recent
mailing label. Send all address changes to the
ACS Columbus address. Please allow six
weeks for change to become effective. **Claims**
for missing numbers will not be allowed if loss
was due to failure of notice of change of ad-
dress to be received in the time specified; if

claim is dated (a) North America—more than
90 days beyond issue date, (b) all other for-
eign—more than 1 year beyond issue date; or
if the reason given is "missing from files".
Hard copy claims are handled at the ACS
Columbus address.

Microfiche subscriptions are available
at the same rates but are mailed first class to
U.S. subscribers, air mail to the rest of the
world. Direct all inquiries to Business Oper-
ations, Books and Journals Division, at the
ACS Washington address or call (202) 872-
4444. **Single issues** in hard copy and/or mi-
crofiche are available from Special Issues
Sales at the ACS Washington address. Cur-
rent year \$4.75. Back issue rates available
from Special Issues Sales. **Back volumes** are
available in hard copy and/or microform.
Write to Special Issues Sales at the ACS
Washington address for further information.
Microfilm editions of ACS periodical pub-
lications are available from volume 1 to the
present. For further information, contact
Special Issues Sales at the ACS Washington
address. **Supplementary material** must be
ordered directly from Business Operations,
Books and Journals Division, at the ACS
Washington address.

	U.S.	PUAS, Canada	Other Foreign
Microfiche			
Photocopy	\$2.50	\$3.00	\$3.50
1-7 pages	4.00	5.50	7.00
8-20 pages	5.00	6.50	8.00

Orders over 20 pages are available only on
microfiche, 4 × 6 in., 24X, negative, silver
halide. Orders must state photocopy or mi-
crofiche if both are available. Full biblio-
graphic citation including names of all au-
thors and prepayment are required. Prices
are subject to change.

American Chemical Society
1155 16th Street, N.W.
Washington, D.C. 20036
(202) 872-4600

Member & Subscription Services
American Chemical Society
P.O. Box 3337
Columbus, Ohio 43210
(614) 421-7230

Editorial Department
American Chemical Society
20th and Northampton Sts.
Easton, Pennsylvania 18042
(215) 258-9111

Volume 80, Number 21 October 7, 1976

JPCHAx 80(21) 2313-2436 (1976)

ISSN 0022-3654

Kinetics of the Reaction of Ozone with Tetrafluoroethene	Frina S. Toby and Sidney Toby*	2313 ■
Steady State and Pulse Radiolysis Studies of Molybdenum Octacyanate in Aqueous Solutions	M. Faraggi	2316
Direct and Indirect Effects in Pulse Irradiated Concentrated Aqueous Solutions of Chloride and Sulfate Ions	Kang-Jin Kim and William H. Hamill*	2320
Pulse Radiolysis of Concentrated Aqueous Solutions of Chloride, Iodide, and Persulfate Ions	Kang-Jin Kim and William H. Hamill*	2325
Spin Trapping of Cyanoalkyl Radicals in the Liquid Phase γ Radiolysis of Nitriles	S. W. Mao and Larry Kevan*	2330
Enthalpy-Entropy Compensation. 1. Some Fundamental Statistical Problems Associated with the Analysis of van't Hoff and Arrhenius Data	R. R. Krug,* W. G. Hunter, and R. A. Grieger	2335 ■
Enthalpy-Entropy Compensations. 2. Separation of the Chemical from the Statistical Effect	R. R. Krug,* W. G. Hunter, and R. A. Grieger	2341 ■
An Elementary Molecular Theory of Classical Fluids. Pure Fluids	Isaac C. Sanchez* and Robert H. Lacombe	2352
Statistical Mechanical Derivation of the Lippmann Equation. The Dielectric Constant	Jerry Goodisman	2363
Correlations of Cracking Properties of Mg-Y Zeolites with Their Acidic and Basic Sites	Claude Mirodatos, Antoine Abou Kais, Jacques C. Vedrine, Pierre Pichat, and Denise Barthomeuf*	2366
A Study of the Chemisorption of Nitric Oxide on PdY Zeolite. Evidence for a Room Temperature Oxidative Dissolution of Pd Crystallites	M. Che, J. F. Dutel, P. Gallezot, and M. Primet*	2371
Solute-Solvent Interactions in Water- <i>tert</i> -Butyl Alcohol Mixtures. 7. Enthalpies of Transfer for LiCl and HCl as Obtained through Dilution of an Aqueous Concentrated Electrolyte Solution in Hydroalcoholic Media	Yvon Pointud, Jean-Pierre Morel, and Jean Juillard*	2381 ■
Bonding in Silver Thionamides Studied by Infrared, Laser-Raman, and X-Ray Photoelectron Spectroscopy.	L. J. Gerenser, M. G. Mason,* and P. J. Trotter	2384
Luminescence of Yttrium(III), Lutetium(III), and Thorium(IV) Porphyrin Complexes	Louis A. Martarano, Ching-Ping Wong, William DeW. Horrocks, Jr., and Antonio M. Ponte Goncalves*	2389
Proton Magnetic Resonance Study of Aluminum(III) Complexes in the Aluminum Perchlorate-Acetonitrile-Water System	Yakir Ruben and Jacques Reuben*	2394

Electron Spin Resonance Studies on Hydrogen Atoms Formed in Pure and Acidic Ices under Electron Irradiation. Motional Narrowing and Electron Spin Polarization Effect Hirotsugu Shiraishi, Hajime Kadoi, Yosuke Katsumura, Yoneho Tabata,* and Keichi Oshima	2400
Kinetics of the Reaction of Atomic Oxygen with Phosphorus Trifluoride. Electron Spin Resonance Determination Ira B. Goldberg* and Harry R. Crowe	2407
Effect of Molecular Parameters on the Carbon-13 Spin-Lattice Relaxation Behavior in Alicyclic Compounds Richard A. Komoroski and George C. Levy*	2410
Axial and Equatorial Bond Orientation around Phosphorus in 1,3,2-Dithiaphosphorinanes. Use of $J(^{31}\text{P}^1\text{H})$ and $J(^{31}\text{P}^{13}\text{C})$ for Stereochemical Assignments J. Martin, J. B. Robert,* and C. Taieb	2417
Intramolecular Torsional Potential and Dielectric Properties of 2,3-Butanedione Giles L. Henderson* and Gevert H. Meyer	2422
Free Radical Oxidation of Organic Disulfides M. Bonifačić and K.-D. Asmus*	2426

COMMUNICATIONS TO THE EDITOR

Dependence of Molybdenum(V) Electron Paramagnetic Resonance Signals on Temperature Suheil Abdo, R. B. Clarkson, and W. Keith Hall*	2431
Comment on "Biological Ion Exchanger Resins. VI. Determination of the Donnan Potentials of Single Ion Exchange Beads with Microelectrodes", by M. Goldsmith, D. Hor, and R. Damadian F. F. Cantwell* and Rolf Saetre	2432
Reply to "Comment on Biological Ion Exchanger Resins. VI. Determination of the Donnan Potentials of Single Ion Exchange Beads with Microelectrodes", by F. Cantwell and R. Saetre Michael Goldsmith	2433
Ferrioxalate Actinometry. A Warning on Its Correct Use W. D. Bowman and J. N. Demas*	2434
Enthalpy-Entropy Compensation and Order in Alkane and Aqueous Systems D. Patterson* and M. Barbe	2435

■ Supplementary material for this paper is available separately (consult the masthead page for ordering information); it will also appear following the paper in the microfilm edition of this journal.

* In papers with more than one author, the asterisk indicates the name of the author to whom inquiries about the paper should be addressed.

AUTHOR INDEX

Abdo, S., 2431	Gerenser, L. J., 2384	Kim, K.-J., 2320, 2325	Pointud, Y., 2381
Asmus, K.-D., 2426	Goldberg, I. B., 2407	Komoroski, R. A., 2410	Primet, M., 2371
Barbe, M., 2435	Goldsmith, M., 2433	Krug, R. R., 2335, 2341	Reuben, J., 2394
Barthomeuf, D., 2366	Goncalves, A. M. P., 2389	Lacombe, R. H., 2352	Robert, J. B., 2417
Bonifačić, M., 2426	Goodisman, J., 2363	Levy, G. C., 2410	Ruben, Y., 2394
Bowman, W. D., 2434	Grieger, R. A., 2335, 2341	Mao, S. W., 2330	Saetre, R., 2432
Cantwell, F. F., 2432	Hall, W. K., 2431	Martarano, L. A., 2389	Sanchez, I. C., 2352
Che, M., 2371	Hamill, W. H., 2320, 2325	Martin, J., 2417	Shiraishi, H., 2400
Clarkson, R. B., 2431	Henderson, G. L., 2422	Mason, M. G., 2384	Tabata, Y., 2400
Crowe, H. R., 2407	Horrocks, W. D., Jr., 2389	Meyer, G. H., 2422	Taieb, C., 2417
Demas, J. N., 2434	Hunter, W. G., 2335, 2341	Mirodatos, C., 2366	Toby, F. S., 2313
Dutel, J. F., 2371	Juillard, J., 2381	Morel, J.-P., 2381	Toby, S., 2313
Faraggi, M., 2316	Kadoi, H., 2400	Oshima, K., 2400	Trotter, P. J., 2384
Gallezot, P., 2371	Kais, A. A., 2366	Patterson, D., 2435	Vedrine, J. C., 2366
	Katsumura, Y., 2400	Pichat, P., 2366	Wong, C.-P., 2389
	Kevan, L., 2330		

THE JOURNAL OF PHYSICAL CHEMISTRY

Registered in U. S. Patent Office © Copyright, 1976, by the American Chemical Society

VOLUME 80, NUMBER 21 OCTOBER 7, 1976

Kinetics of the Reaction of Ozone with Tetrafluoroethene

Frina S. Toby and Sidney Toby*

School of Chemistry, Rutgers, The State University, New Brunswick, New Jersey 08903 (Received February 17, 1976)

The reaction between ozone and tetrafluoroethene was measured in the gas phase in the temperature range 0–110 °C. The rate law found could be represented by $-d[O_3]/dt = k_1[O_3][C_2F_4] + k_2[O_3]^2[C_2F_4]$ where $\log(k_1/M^{-1} s^{-1}) = 8.2 \pm 0.5 - (9500 \pm 700)/2.3RT$, and $\log(k_2/M^{-2} s^{-1}) = 14.6 \pm 0.4 - (10100 \pm 600)/2.3RT$. O_2 was found to be a minor product, but experiments done in the presence of added O_2 showed an uptake of O_2 . Loss of C_2F_4 was measured so that the stoichiometry $\Delta C_2F_4/\Delta O_3$ was obtained. Other products were not determined here, but have been previously reported. A mechanism was postulated which accounts for the major findings with respect to product formation, the observed rate law, and the chemiluminescence associated with this system.

Introduction

Both the kinetics and the accompanying chemiluminescence of the gas-phase reactions of ozone with alkenes have been much studied¹ but there has been very little reported work on the corresponding reactions with fluoroalkenes. We have recently found that chemiluminescence accompanies the reactions of O_3 with tetrafluoroethene, 1,1-difluoroethene, *cis*-1,2-difluoroethene, *trans*-1,2-difluoroethene, and hexafluoropropene.² The emission from the $O_3 + C_2F_4$ system was particularly intense and was identified as due to CF_2 in its first electronically excited singlet state. The reactions of O_3 with some perfluoroalkenes were studied by Heicklen.³ Products were measured but very limited kinetic data were available for C_2F_4 . Gozzo and Camaggi⁴ studied the reaction between O_3 and C_2F_4 in gas and liquid phases and products were studied in some detail. In the present study the rate law, rate constants, and mechanism of the reaction were investigated and Arrhenius parameters are given for the first time.

Experimental Section

The apparatus and methods used have been described previously.⁵ The quartz cylindrical reaction vessel of length 10.0 cm and volume 450 cm³ was mounted in a thermostatted (± 0.5 °C) oven. The ozone concentration was monitored with a beam of 254-nm radiation and linear Beer plots were obtained over the ozone concentration range used. At the highest temperature employed the rate of disappearance of O_3 alone was 0.1% of the corresponding rate in the presence of substrate. Under most conditions the transmitted light would return to its value for an evacuated reaction vessel showing that all O_3 was destroyed and that products did not appreciably absorb 254-nm light.

Ozone was generated by passing oxygen (Matheson Ultra-pure grade) through a discharge from a Tesla coil. The ozone was condensed at -196 °C and the oxygen pumped away. Tetrafluoroethene (Columbia Organic Chemicals) was distilled and degassed before use and check runs were done with aliquots which had been distilled twice. No impurities in the C_2F_4 were found by gas chromatographic analysis. Some runs were done in the presence of sulfur hexafluoride (Matheson) which had been distilled.

The temperature range employed was 0–110 °C and the pressure range was 0.01–0.2 Torr for O_3 and 0.3–15 Torr for C_2F_4 . At the end of some experiments, excess C_2F_4 was measured by gas chromatography using a 10-ft molecular sieve (13X) column at 100 °C.

Results

Stoichiometry. Carbonyl fluoride, oxygen, tetrafluoroethylene oxide, and cyclohexafluoropropene have been identified as products in this system⁴ and only O_2 was measured here. The stoichiometry of (C_2F_4 used/ O_3 used) was measured at 30 °C and the results are shown in Figure 1.

O_2 has been reported as a minor product⁴ and we confirmed that when products were cooled to -196 °C there was some residual pressure. However, when runs were carried out in the presence of added O_2 the pressure of noncondensables at the end of the run was actually reduced. With the assumption that the noncondensable pressure consisted of O_2 (CO has not been reported as a product) the stoichiometry of O_2 production and consumption was measured for some runs and this is shown in Table I.

Kinetics. The overall order of the reaction appeared to be between 1 and 2. Single order plots did not normally give

TABLE I: Production and Consumption of O₂

Temp, °C	Initial pressure, Torr			Final p, Torr O ₂	(ΔO ₂)/ (O ₃) ₀
	O ₃	C ₂ F ₄	O ₂		
30	0.060	3.0	0	0.007	+0.1
	0.060	3.3	0	0.002	+0.03
	0.060	5.7	0	0.004	+0.07
	0.060	7.9	0	0.006	+0.1
	0.11	5.2	0.17	0.015	-1.4
	0.11	5.2	0.35	0.135	-1.9
110	0.11	5.2	0.41	0.275	-1.2
	0.058	5.2	0.11	0.006	-1.8
	0.058	5.2	0.22	0.015	-3.5
	0.058	5.2	0.55	0.030	-9.0
	0.058	5.2	1.62	1.53	-1.6

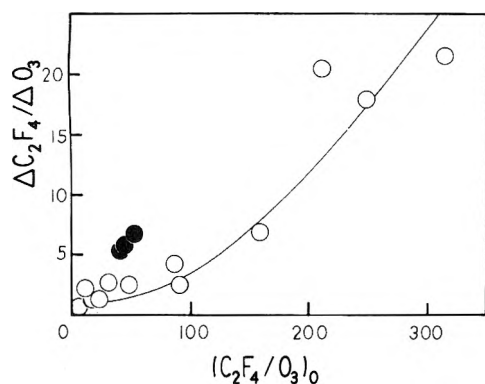


Figure 1. Stoichiometry plot of (C₂F₄ used)/(O₃ used) as a function of initial (C₂F₄)/(O₃) at 30 °C. Filled points refer to runs with 0.4 Torr added O₂.

straight lines although second-order plots were usually the least curved. We postulate that the rate law can be written

$$-d[\text{O}_3]/dt = k_1[\text{O}_3][\text{C}_2\text{F}_4]^m + k_2[\text{O}_3]^2[\text{C}_2\text{F}_4]^n \quad (1)$$

For runs done with a large excess of C₂F₄ we define the pseudoconstants $k_a = k_1[\text{C}_2\text{F}_4]^m$ and $k_b = k_2[\text{C}_2\text{F}_4]^n$. Equation 1 may be integrated to give

$$\ln \{[\text{O}_3]/(1 + K[\text{O}_3])\} = k_a t + \ln \{[\text{O}_3]_0/(1 + K[\text{O}_3]_0)\} \quad (2)$$

where $K = k_b/k_a$. A new method for obtaining the rate constants was used. Trial values of K were inserted in the left-hand side of eq 2 which was then plotted against time using an APL program.⁶ This typically resulted in a curved line but as the value of K was increased the line straightened and the correlation coefficient passed through a maximum which exceeded 0.99. The value of K for the maximum correlation coefficient together with the slope of that line gave k_a and k_b .⁶ In some cases no maximum correlation coefficient could be obtained but these were runs which obeyed simple order kinetics and only one rate constant could be measured.

The resulting values of k_a and k_b were measured over a range of initial O₃ concentrations at 0, 30, 70, and 110 °C with the C₂F₄ concentrations held constant at each temperature and typical results are shown in Figure 2. A series of experiments was then carried out with [O₃]₀ held constant at each temperature over a range of C₂F₄ concentrations. The resulting values of k_a and k_b were plotted against [C₂F₄] and typical results are shown in Figure 3. These plots show reasonably good linearity and we therefore write the rate law as

$$-d[\text{O}_3]/dt = k_1[\text{O}_3][\text{C}_2\text{F}_4] + k_2[\text{O}_3]^2[\text{C}_2\text{F}_4] \quad (3)$$

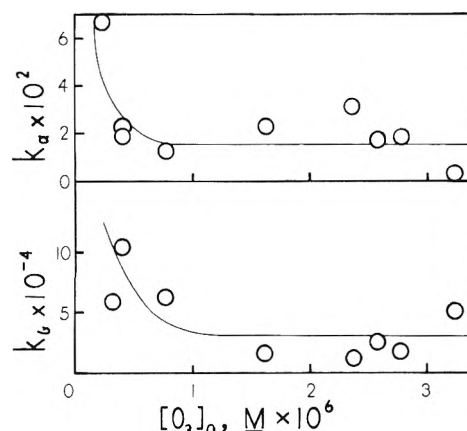


Figure 2. Plot of k_a and k_b as a function of [O₃]₀ at 70 °C with [C₂F₄]₀ = 1.4 × 10⁻⁴ M. Units of k_a are s⁻¹, and of k_b are M⁻¹ s⁻¹.

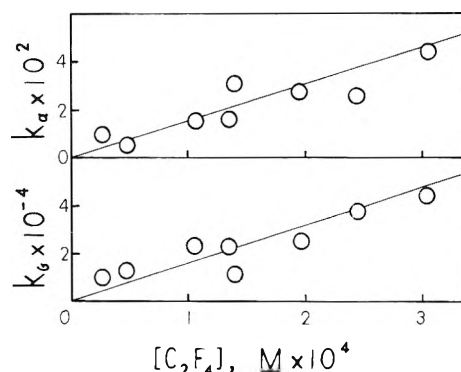


Figure 3. Plot of k_a and k_b as a function of [C₂F₄] at 70 °C with [O₃]₀ = 2.1 × 10⁻⁶ M.

An Arrhenius plot of k_1 and k_2 with estimated error limits is given in Figure 4 and yields $\log (k_1/\text{M}^{-1} \text{s}^{-1}) = 8.2 \pm 0.5 - (9500 \pm 700)/2.3RT$, and $\log (k_2/\text{M}^{-2} \text{s}^{-1}) = 14.6 \pm 0.4 - (10\,100 \pm 600)/2.3RT$.

The reaction of O₃ with C₂F₄ was slowed by the effect of added O₂ and an induction period was noted after the reactants were mixed before appreciable reaction occurred. The plots of transmitted light vs. time were not smooth curves and we were unable to make a kinetic analysis of these runs. Some experiments were done in the presence of added SF₆ and no significant change in k_a or k_b was found.⁶

Discussion

Heicklen³ studied the O₃ + C₂F₄ system at room temperature with excess O₃ present and found COF₂ as a product together with some O₂ which could have come from the background decomposition of O₃. Gozzo and Camaggi⁴ measured products from the reaction in inert solvent at 0 °C. When C₂F₄ was in large excess the products were COF₂ and the epoxide C₂F₄O together with small quantities of O₂ and c-C₃F₆. When O₃/C₂F₄ was closer to unity, O₂ became a major product and the ozonide C₂F₄O₃ was found. We found O₂ to be a minor product (about 7% of the O₃ used) as shown in Table I and also observed a rather surprising uptake of O₂ when it had been added to the system. The reaction of C₂F₄ with O₂ has been previously investigated by Gozzo and Camaggi^{7,8} and was found to be very slow in the gas phase but strongly accelerated by ozone. Molecular oxygen can thus be a reactant and a product in the C₂F₄ + O₃ system and we shall consider possible mechanisms for this effect shortly.

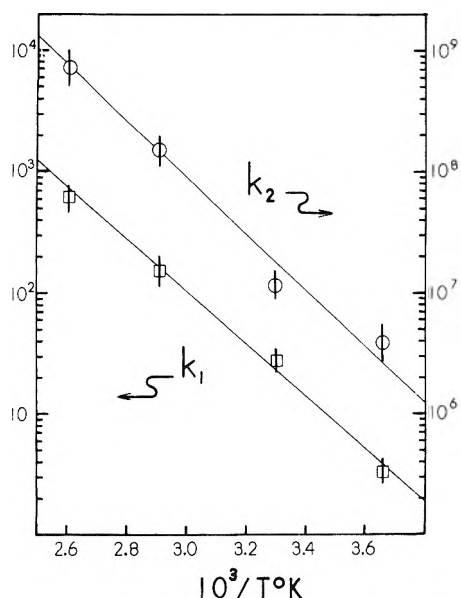
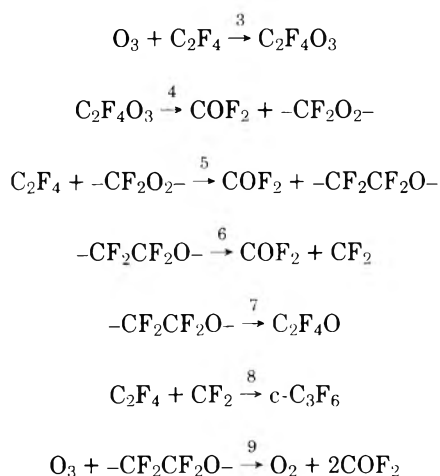


Figure 4. Arrhenius plot of k_1 (in $M^{-1} s^{-1}$) and k_2 (in $M^{-2} s^{-1}$). Vertical bars are estimated error limits.

Because of the uncertainties involved in extracting two rate constants from the observed rate, individual points in Figures 2 and 3 are subject to appreciable error. Nevertheless the trends shown are clear: the values of k_a and k_b are reasonably independent of $[O_3]_0$ over nearly all of the range studied. However, at the lowest pressures employed (~ 0.03 Torr) k_b showed an increase which has also been found for the rate constants corresponding to k_b in the O_3 + allene and O_3 + butadiene systems^{5,9} and for which we have no satisfactory explanation. Both k_a and k_b are proportional to $[C_2F_4]$ as shown by Figure 3, and in comparison plots of k_a and k_b against $[C_2F_4]^2$ showed distinct curvature.

We can explain the basic features of the reaction in terms of the following simplified mechanism:



The chemiluminescence from this system² is due to singlet excited CF_2 and is associated with energy of up to 117 kcal mol^{-1} . The sequence suggested by Gozzo and Camaggi⁴ for the formation of CF_2 is only 72 ± 8 kcal mol^{-1} exothermic: $C_2F_4 + O_3 \rightarrow COF_2 + CF_2O_2$, $CF_2O_2 \rightarrow CF_2 + O_2$. The sequence of reactions 3, 4, 5, 6, and 7 is exothermic overall by 220 ± 14 kcal mol^{-1} ¹⁰ and is analogous to the multistep activation or energy pooling which has been proposed in peroxide¹¹ and singlet molecular oxygen¹² chemiluminescence.

Taking steady states¹³ in $C_2F_4O_3$, $-CF_2O_2-$, $-CF_2CF_2O-$, and CF_2 , and assuming that $(k_6 + k_7) \gg k_9[O_3]$ yields

$$-d[O_3]/dt = k_3[C_2F_4][O_3] + k_3k_9[C_2F_4][O_3]^2/(k_6 + k_7) \quad (4)$$

which is of the same form as eq 3.

We know of no published values for the Arrhenius parameters of O_3 + haloalkenes with which the present work can be compared, but comparisons with alkenes are possible. Our value for the Arrhenius factor $A_3 = 10^{8.2} M^{-1} s^{-1}$ corresponds to $\Delta S_c^\ddagger = -25.0 \pm 2$ cal $mol^{-1} deg^{-1}$ at 25 °C. The A factor is slightly larger than the values of $10^{6.3}$ and $10^{6.9}$ reported for $O_3 + C_2H_4$ by DeMore¹⁴ and Becker, Schurath and Seitz,¹⁵ respectively. DeMore¹⁴ has estimated that a five-membered ozonide transition state would correspond to $A = 10^{7.1}$, whereas a linear complex would result in $A = 10^{10.6}$, thus our results favor a cyclic complex for $O_3 + C_2F_4$.

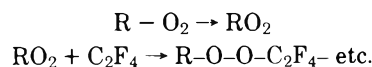
Our activation energy $E_3 = 9.5$ kcal mol^{-1} is much higher than the values of 4.9 and 4.7 reported for ethylene^{14,15} and comparable with the value $E = 10.8$ kcal mol^{-1} measured for acetylene.¹⁴

Gozzo and Camaggi⁴ measured products in various solvents at 0 °C using much higher O_3/C_2F_4 ratios than used here, nevertheless some comparisons may be made. Our mechanism predicts that the order of abundance of products is $c-C_3F_6 < C_2F_4O < O_2 < COF_2$. This is the correct order with the exception of O_2 which was always a minor product other than for two runs where O_3/C_2F_4 approached unity. Our data (Table I) also show O_2 is a minor product and that it is actually consumed in runs with added O_2 .

Our mechanism predicts that $d[C_2F_4O]/d[C_3F_6] = k_7/k_6$, and a plot of C_2F_4O/C_3F_6 formed vs. O_3 flow rate (omitting one point where O_3 was comparable to C_2F_4) shows no clear trend with an average value of $k_7/k_6 \sim 40$. The mechanism also leads to $d[COF_2]/d[C_2F_4O] \approx 2 + 2k_9[O_3]/k_7$ and if we approximate this relationship by plotting COF_2/C_2F_4O formed vs. O_3 flow rate (again minus the highest O_3 point⁴) there is a reasonably linear relationship with a correlation coefficient of 0.91 and an intercept of 1.95.

Missing Steps in the Mechanism. Although the postulated mechanism explains most of the observed kinetics and formation of products, it is incomplete with respect to the consumption of O_2 , and the overall uptake of O_3 and of C_2F_4 . We can only offer qualitative explanations for these aspects of the reaction.

The consumption of added oxygen shown in Table I is in accord with the findings of Gozzo and Camaggi.⁷ They found that C_2F_4 reacted with O_2 very slowly in the gas phase but that the reaction was very fast in the presence of O_3 . The uptake of O_2 led to the formation of an unstable poly(tetrafluoroethylene peroxide) $(C_2F_4O_2)_n$ via free radical intermediates:



A stable polymer $(C_2F_4O)_n$ was also formed. Such reactions would consume far more C_2F_4 than O_3 and account for the high $\Delta C_2F_4/\Delta O_3$ ratios which we found and which are plotted in Figure 1. In the absence of added O_2 , the O_2 normally obtained as a product in ozone reactions becomes a reactant. When O_2 is deliberately added, the $\Delta C_2F_4/\Delta O_3$ ratio increases even more: Figure 1 shows that the addition of 0.4 Torr of O_2 approximately doubled the resulting value of $\Delta C_2F_4/\Delta O_3$. The quenching effect of added O_2 on the CF_2 chemiluminescence in this system² can be similarly ascribed to the scavenging of precursor radicals by O_2 .

Equation 4 may be written $R = R_1 + R_2$, where R_1 and R_2 are the rates of the primary and secondary processes consuming O_3 . Under the conditions of our experiments R_2/R_1 reached a maximum value of 2.5 and this is only possible if short chains of ozone decomposition occur. Such chains occur in the $O_3 +$ alkene systems and have been shown to be thermochemically feasible for $O_3 + C_2H_4$.¹ Although the identity of the chain carriers for the $O_3 + C_2F_4$ system cannot be established from our work, such a chain leads to the catalytic destruction of O_3 . This would normally form O_2 as a major product but, as previously discussed, the resulting O_2 is consumed in this system to form oxygen-containing polymers.⁷

In summary, the reaction of O_3 with C_2F_4 is an extraordinarily complex system involving chains of both reactants and exhibiting both O_2 production and O_2 uptake. We have attempted to account quantitatively for the observed rate law and have given a qualitative description of the complex aspects of the kinetics.

Acknowledgment. We thank the Rutgers University Research Council for the support of this work.

Supplementary Material Available: Tables A–F of kinetic

data at 0, 30, 70, and 110 °C and effects of added SF_6 at 30 °C along with a computer program for obtaining rate constants (6 pages). Ordering information is available on any current masthead page.

References and Notes

- (1) F. S. Toby, S. Toby, and H. E. O'Neal, *Int. J. Chem. Kinet.*, **8**, 25 (1976), especially ref 1–11.
- (2) R. S. Sheinson, F. S. Toby, and S. Toby, *J. Am. Chem. Soc.*, **97**, 6593 (1975).
- (3) J. Hecklen, *J. Phys. Chem.*, **70**, 477 (1966).
- (4) F. Gozzo and G. Camaggi, *Chim. Ind. (Milan)*, **50**, 197 (1968).
- (5) F. S. Toby and S. Toby, *Int. J. Chem. Kinet.*, **6**, 417 (1974).
- (6) See paragraph at end of the text regarding supplementary material.
- (7) F. Gozzo and G. Camaggi, *Tetrahedron*, **22**, 1765 (1966).
- (8) F. Gozzo and G. Camaggi, *Tetrahedron*, **22**, 2181 (1966).
- (9) F. S. Toby and S. Toby, *Int. J. Chem. Kinet., Symp.*, **1**, 197 (1975).
- (10) S. W. Benson, "Thermochemical Kinetics", Wiley, New York, N.Y., 1968.
- (11) S. R. Abbott, S. Ness, and D. M. Hercules, *J. Am. Chem. Soc.*, **92**, 1128 (1970).
- (12) E. A. Ogryzlo and A. E. Pearson, *J. Phys. Chem.*, **72**, 2913 (1968).
- (13) Gozzi and Camaggi⁴ found small quantities of ozonide in the products of the liquid phase reaction at 0 °C at high O_3/C_2F_4 ratios, but not in the gas phase reaction.
- (14) W. B. DeMore, *Int. J. Chem. Kinet.*, **1**, 209 (1969).
- (15) K. H. Becker, U. Schurath, and H. Seitz, *Int. J. Chem. Kinet.*, **6**, 725 (1974).

Steady State and Pulse Radiolysis Studies of Molybdenum Octacyanate in Aqueous Solutions

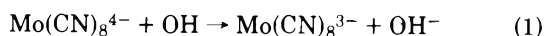
M. Faraggi

Nuclear Research Centre-Negev, P.O.B. 9001, Beer Sheva, Israel (Received January 8, 1976)

The oxidation of oxygen saturated solutions of $Mo(CN)_8^{4-}$ at different pH values was studied by steady state and pulse radiolysis techniques. It was shown that $Mo(CN)_8^{3-}$ is the oxidation product formed. G values of the Mo(V) octacyanate complex varied with the pH of the solution. It was of the order of 13 at pH 0 (1 M $HClO_4$) and approaching zero at pH >7. The high G values in acid solutions are explained by the oxidation of the Mo(IV) complex ion in the reactions with OH and HO_2 radicals and by H_2O_2 . The H_2O_2 reaction with Mo(IV) ion was found to be a very slow reaction and 75% effective only. In neutral and alkaline solutions the low G values are interpreted by the reduction of the Mo(V) ions formed by the O_2^- radicals. Confirmation of the above mechanism was established by using the pulse radiolysis technique. The formation of $Mo(CN)_8^{3-}$, the oxidation product of $Mo(CN)_8^{4-}$ in the reactions with OH and HO_2 radicals, was followed at 385 nm. The rate constants (in $M^{-1} s^{-1}$) are $(5.8 \pm 0.5) \times 10^9$ and $(5.7 \pm 0.6) \times 10^4$, respectively. These values were unaffected by the presence of H^+ or unreactive alkaline cations. O^- reacts with $Mo(CN)_8^{4-}$ much more slowly (estimated to be $\sim 1 \times 10^7 M^{-1} s^{-1}$). O_2^- reduces the $Mo(CN)_8^{3-}$ to $Mo(CN)_8^{4-}$, the rate constant found was $3.0 \pm 0.5 \times 10^5 M^{-1} s^{-1}$.

Introduction

In recent years, two studies have been published on the steady state (γ rays) and pulse radiolysis of aqueous molybdenum(IV) octacyanate solutions.^{1,2} Sharma¹ reported that $Mo(CN)_8^{4-}$ ions in 0.4 M H_2SO_4 solutions (oxygenated) react with OH radicals via a single electron transfer reaction to give $Mo(CN)_8^{3-}$



This study¹ also reports that $G(Mo(CN)_8^{3-}) = 2.7$ and concludes therefore that neither HO_2 nor H_2O_2 oxidize the $Mo(CN)_8^{4-}$ complex. However, a close examination of his results (ref 1, Figure 1) indicates that $G(Mo(CN)_8^{3-}) = 1.3$ rather than 2.7.

Waltz et al.² measured the rate constant of reaction 1 via the competition pulse radiolysis method³ and found a value of $(5.8 \pm 0.6) \times 10^9 M^{-1} s^{-1}$.

Cyanide complexes have been extensively studied in the

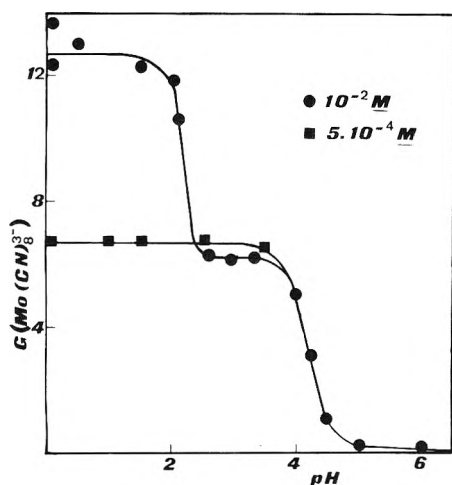


Figure 1. Mo(V) octacyanate ions yield (G value) as function of pH.

ferro-ferri system.⁴⁻²⁰ This system has been used for the determination of radical and molecular yields in the radiolysis of water and as a dosimeter in pulse radiolysis studies of aqueous solutions. It is generally known that OH radicals oxidize ferrocyanide and e_{aq}^- and H atoms reduce ferricyanide. Absolute rate constants for these reactions were measured by the pulse radiolysis technique. The peroxy radical in its acid form (HO_2) oxidizes the ferro complex while its alkaline form (O_2^-) reduces the ferri complex.

The aim of this work was to study the radiation chemistry of $Mo(CN)_8^{4-}$ and to compare its behavior to $Fe(CN)_6^{4-}$.

Experimental Section

Materials. Triply distilled water was used to prepare all solutions. $Mo(CN)_8^{4-}$ was prepared according to Furman and Miller²¹ and was recrystallized before use. $Mo(CN)_8^{3-}$ was prepared from $Mo(CN)_8^{4-}$ by electrolytic oxidation at +1.0 V. The purity of the complexes was confirmed analytically and spectrophotometrically.²² Solutions of these light sensitive complexes were prepared and studied in blackened vessels. All other materials used were of analytical grade.

γ Irradiations. Irradiations were performed with a 17 kCi cobalt 60 γ source providing a dose rate of about 1.2×10^6 rads/h as determined by ferrous sulfate dosimeter assuming $G(Fe^{3+}) = 15.6$. Saturation of the solutions was made by continuous bubbling of purified gases (Matheson Co. Inc.) for 30 min. The pH of the solutions was adjusted by addition of either $HClO_4$ or $NaOH$.

The yield of $Mo(CN)_8^{3-}$ was determined spectrophotometrically using a Cary 17 spectrophotometer at λ 386 nm. At this wavelength the absorption coefficient (ϵ) of $Mo(CN)_8^{4-}$ is $150 M^{-1} cm^{-1}$ and that of $Mo(CN)_8^{3-}$ is $1300 M^{-1} cm^{-1}$.²²

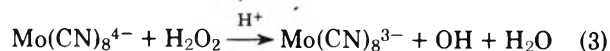
Pulse Radiolysis. The experiments were carried out using the Hebrew University linear accelerator. It was operated at 5 Mev, 200 mA and pulse length of 0.1–1.0 μs giving a dose range of 150–2000 rads per pulse. Other experimental procedures, the apparatus optical detection system, cell filling technique, and the evaluation of the kinetic curves have been previously described.²³

Results and Discussion

Steady State Radiolysis. Oxygen saturated solutions of different $Mo(CN)_8^{4-}$ ion concentrations and pH were irradiated. Linear plots of $Mo(CN)_8^{3-}$ concentration, as measured

at λ 386 nm, vs. dose were obtained. From the slope of these curves $G(Mo(CN)_8^{3-})$ values were determined. Figure 1 shows the results as function of pH at two different concentrations (5×10^{-4} and 10^{-2} M). It should be pointed out that due to the slow reaction between H_2O_2 and $Mo(CN)_8^{4-}$ (vide infra) measurements of the $Mo(CN)_8^{3-}$ ion concentration were made at different periods after irradiation. This was at least 15 h, during which the irradiated solutions were kept at dark, for the 10^{-2} M $Mo(CN)_8^{4-}$ solutions. In the 5×10^{-4} M $Mo(CN)_8^{4-}$ solutions the determination of the Mo(V) cyano complex concentration was made immediately after irradiation (~ 5 min).

Figure 1 clearly demonstrates that at high acid and $Mo(CN)_8^{4-}$ concentrations the $G(Mo(CN)_8^{3-})$ reaches a value of approximately 13 ± 0.5 (plateau value) reflecting the fact that under these conditions the oxidation reactions of $Mo(CN)_8^{4-}$ cannot be explained only by the reaction of the complex ion with OH radicals (reaction 1). Hence, the reactions of the HO_2 radicals, produced via the $H + O_2$ reaction, and the H_2O_2 with $Mo(CN)_8^{4-}$ are also suggested to participate in the oxidation process



Thus:

$$G(Mo(CN)_8^{3-}) = G_{OH} + 3G_{HO_2} + 2G_{H_2O_2} \\ = 2.95 + 3 \times 3.65 + 2 \times 0.8 = 15.5^{24}$$

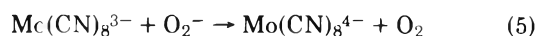
The difference between the calculated value and the experimental one is probably the result of the fact that reaction 3 compared to reactions 1 and 2 is slow and is only 75–80% effective. This behavior is similar to that observed in the $H_2O_2 + Fe(CN)_6^{4-}$ reaction.²⁵

Between pH 2.5 and 4 another plateau value is found and $G(Mo(CN)_8^{3-}) = 6.2 \pm 0.3$. This result shows that in this pH range only reactions 1 and 2 are taking place. Thus, $G(Mo(CN)_8^{3-}) = G_{OH} + G_{HO_2} = 6.0$ in good agreement with the experimental results. Similar results were found in the 5×10^{-4} M concentration indicating again that at this low solute concentration and after a short period after the irradiation, reaction 3 does not take place even at high acid concentration. When solutions of higher pH values were irradiated $G(Mo(CN)_8^{3-})$ decreased approaching to zero at $pH > 7$. At this pH value the perhydroxyl radical is transformed to its basic form O_2^-



with a pK of 4.88 ± 0.1 .²⁶

The G values at the neutral pH solutions found could be explained if it is assumed that the $Mo(CN)_8^{3-}$ produced via reaction 1 is reduced by O_2^- produced via $e_{aq}^- + O_2 \rightarrow O_2^-$ according to



and that H_2O_2 does not react with $Mo(CN)_8^{4-}$. Thus, as $G_{OH} < G_{e_{aq}^-} + G_H$ then

$$G(Mo(CN)_8^{3-}) = G_{OH} - G_{O_2^-} < 0$$

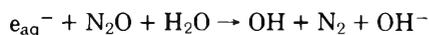
Reaction 4 is similar to that proposed for the reaction of ferrocyanide in the ferro-ferri irradiated system.

In separate experiments reaction 3 was followed in oxygen saturated aqueous solutions containing 10^{-2} M $Mo(CN)_8^{4-}$,

5×10^{-5} to 5×10^{-4} M H_2O_2 , and 1 M HClO_4 . It was found that the oxidation reaction is a slow process and approximately only 75% of the H_2O_2 reacted via reaction 3. Mo(V) equilibrium concentration was attained after at least 15 h. Both the Mo(V) yield and the time to attain equilibrium were found to depend on Mo(CN)_8^{4-} ion concentration. The results are again similar to those obtained in the Fe(CN)_6^{4-} - H_2O_2 acid solution system. The $\text{Mo(CN)}_8^{4-} + \text{H}_2\text{O}_2$ reaction is acid dependent. To attain the equilibrium concentration value of Mo(CN)_8^{3-} ions at a reasonable time scale solutions containing 1 M HClO_4 were necessary. This might indicate that prototropic equilibria involving the Mo(IV) complex exist in this acid range and reaction 3 might be observable only for protonated complexes. The slowness of the reaction could be a result of the high dissociation constant of the complex,²⁷ leaving a low concentration of the protonated form.

Pulse Radiolysis. The reaction of Mo(CN)_8^{4-} with OH radical was followed directly by the observation of the production of Mo(CN)_8^{3-} at 385 nm. The rate constant calculated was found to be $(5.8 \pm 0.5) \times 10^9 \text{ M}^{-1} \text{ s}^{-1}$ in neutral solutions (pH 6.5).

In order to check that reaction 1 produces exclusively Mo(CN)_8^{3-} , neutral and acid solutions were irradiated and the optical absorption in the 300–500-nm wavelength range was determined. It was found that this spectrum is similar to that of Mo(CN)_8^{3-} - Mo(CN)_8^{4-} difference spectrum.²² It is stable for at least 100 μs , independent of Mo(CN)_8^{4-} concentration (up to 5×10^{-2} M) and pH.¹⁻⁸ A similar spectrum was observed in N_2O saturated solutions. However, the optical densities values obtained in this solution doubled as compared to the oxygen saturated one. This is the result of e_{aq}^- conversion to OH radical in the N_2O saturated solutions via

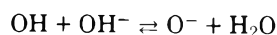


and that $G_{e_{\text{aq}}^-} \sim G_{\text{OH}}$. The results in oxygen and N_2O saturated solutions seem to indicate that Mo(CN)_8^{3-} is the species produced.

Table I shows the reaction rate constant k_1 measured in the presence of different additives and as a function of pH (acid and neutral). This table shows that except for the effect of 0.1 M of K^+ no other change in the rate constant could be observed. The behavior is different from that obtained for Fe(CN)_6^{4-} by Zahavi and Rabani²⁰ where association and ion pair formation between ferrocyanide and H^+ affected the reactivity of the OH radical. Our results may be due to the fact that Mo(CN)_8^{4-} does not associate with the added hydrogen ions to a greater extent or, that the associated ion pair(s) reacts with the OH radical with similar rates. However, Kolthoff and Tomsicek²⁷ studying cations effect on the standard electron potential of Mo(CN)_8^{4-} suggested that $\text{H}_4[\text{Mo(CN)}_8]$ unlike $\text{H}_4[\text{Fe(CN)}_6]$ is a strong tetrabasic acid. Thus, it seems that in our conditions most of the Mo(CN)_8^{4-} ions were not associated with H^+ .

Association of Mo(CN)_8^{4-} with positive ions to form ion pairs has no effect or a small one on k_1 in agreement with ref 20.

Rabani and Matheson¹¹ have shown that in alkaline solutions radicals dissociate to O^- radical ions according to



they reported a $\text{p}K_{\text{OH}}$ value of 11.9 ± 0.2 . Using revised rate constant values, Zehavi and Rabani reported a value of 11.85.²⁰ Rabani and Matheson¹¹ have also shown that O^- reacts slowly, compared to OH, with Fe(CN)_6^{4-} . They developed an equa-

TABLE I: Effect of Cations (Hydrogen and Alkaline Ions) on the Second-Order Rate Constant of the Reaction of OH + Mo(CN)_8^{4-}

[Mo(IV)]	Additives	$k_{\text{OH} + \text{Mo(IV)}}, 10^9 \text{ M}^{-1} \text{ s}^{-1}$
5×10^{-5} to 1.6×10^{-4}	$\text{HClO}_4, 10^{-5}$ to 1 M	5.8 ± 0.5
	$\text{LiClO}_4, 10^{-2}$ to 1 M	6.4 ± 0.7
	$\text{NaClO}_4, 10^{-2}$ to 1 M	6.6 ± 0.7
	$\text{CsClO}_4, 10^{-2}$ to 10^{-1} M	5.5 ± 0.7
	$\text{KClO}_4, 10^{-3}$ to 10^{-2} M	5.4 ± 0.4
	$\text{KClO}_4, 10^{-1}$ M	1.9 ± 0.2

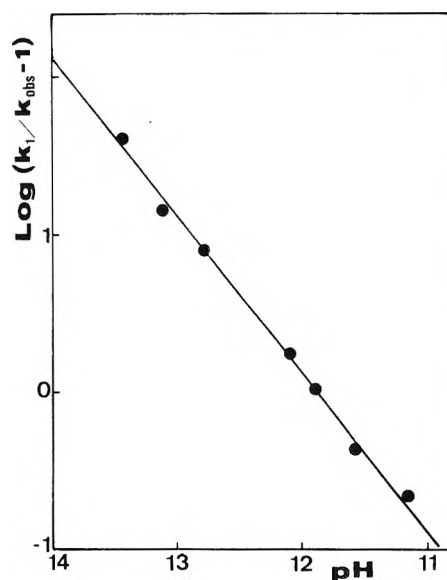


Figure 2. k_{obsd} , the observed rate constant of OH + Mo(CN)_8^{4-} , as a function of pH.

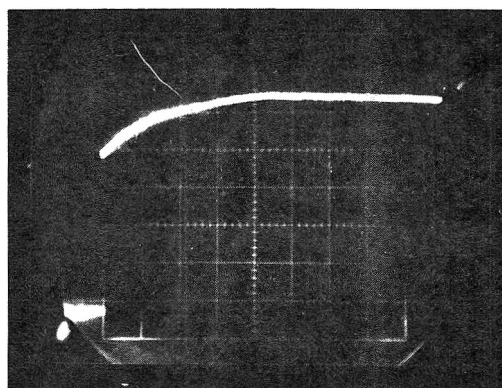


Figure 3. Oscilloscope trace at λ 385 nm of the pseudo-first-order reaction of HO_2 radicals with Mo(CN)_8^{4-} . Oxygen saturated solution of 2×10^{-3} M Mo(CN)_8^{4-} at pH 2.5 (HClO_4) irradiated with a 1.0- μs pulse. Vertical displacement corresponds to change in the optical transmission (1 large division = 3.8%) horizontal to time (1 large division = 5 ms).

tion relating the effective rate constant (k_{obsd}) for the OH (O^-) reaction with the pH value of the solution.

$$\log \left(\frac{k_1}{k_{\text{obsd}}} - 1 \right) = \text{pH} - \text{p}K$$

Figure 2 shows a plot of k_{obsd} in the pH range of 11.2–13.3 according to this equation. From this figure the $\text{p}K$ of OH is 11.8 ± 0.2 in good agreement with the published value.^{11,20}

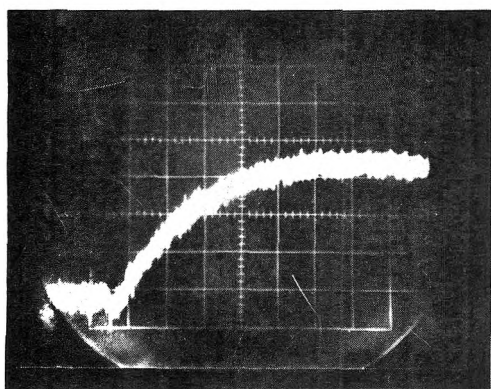


Figure 4. Oscilloscope trace at λ 385 nm of the pseudo-first-order reaction of HO_2 radicals with $\text{Mo}(\text{CN})_8^{4-}$. Oxygen saturated solution of 9.3×10^{-3} M $\text{Mo}(\text{CN})_8^{4-}$ and 0.3 M HCOO^- at pH 2.0 (HClO_4) irradiated with a 1.0- μs pulse. Vertical displacement corresponds to changes in the optical transmission (1 large division = 1.4%) horizontal to time (1 large division = 1 ms).

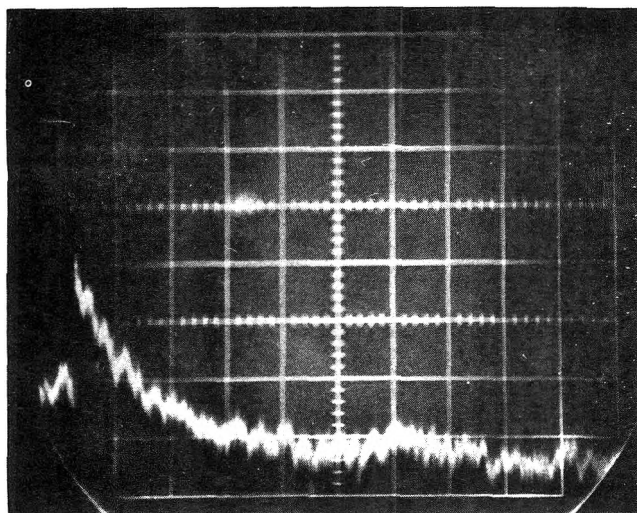


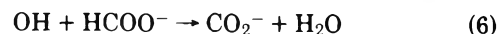
Figure 5. Oscilloscope trace at λ 385 nm of the pseudo-first-order reaction of O_2^- radicals with $\text{Mo}(\text{CN})_8^{3-}$. Oxygen saturated solution of 3.1×10^{-4} M $\text{Mo}(\text{CN})_8^{3-}$, 4.0×10^{-4} M $\text{Mo}(\text{CN})_8^{4-}$ + 5×10^{-3} M NaClO_4 at pH 10.0 (NaOH) irradiated with 1.0- μs pulse. Vertical displacement corresponds to changes in transmission (1 large division = 2.1%), horizontal to time (1 large division = 10 ms).

From Figure 4 the rate constant for the reaction of O_2^- with $\text{Mo}(\text{CN})_8^{4-}$ was estimated to be $\sim 1 \times 10^7 \text{ M}^{-1} \text{ s}^{-1}$.

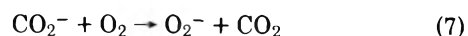
Reaction of HO_2 with $\text{Mo}(\text{CN})_8^{4-}$. O_2 saturated solutions containing 1×10^{-3} to 1×10^{-2} M $\text{Mo}(\text{CN})_8^{4-}$ in the pH range of 2.5–4.0 were investigated by pulse radiolysis. Figure 3 shows the oscilloscope trace observed. The first step is the rapid formation of $\text{Mo}(\text{CN})_8^{3-}$ due to the rapid reaction of OH radicals with $\text{Mo}(\text{CN})_8^{4-}$. The e_{aq}^- and H atoms are converted into peroxy radicals HO_2 and O_2^- . The relative concentrations of the peroxy radicals are determined by the pK of HO_2 which is 4.8.²⁴ As stated, the reaction of H_2O_2 with molybdenum(IV) octacyanate is a very slow reaction. The O_2^- radical ion is also unreactive toward $\text{Mo}(\text{CN})_8^{4-}$. This was confirmed by following pulse radiolysis experiments in oxygen saturated alkaline solution (pH 9) of 10^{-2} M $\text{Mo}(\text{CN})_8^{4-}$. After the formation of $\text{Mo}(\text{CN})_8^{3-}$ via reaction 1 was completed, its decay was observed in the 100-ms time range. This decay can be attributed to the reaction of $\text{Mo}(\text{CN})_8^{3-}$ with O_2^- . Thus, the

oxidation reaction of HO_2 with $\text{Mo}(\text{CN})_8^{4-}$ is separated in time from other reactions of the molybdenum(IV) and molybdenum(V) octacyanate.

In order to determine the oxidation rate constants of HO_2 with $\text{Mo}(\text{CN})_8^{4-}$ oxygenated solutions containing 5 to 10×10^{-3} M of the solute and 0.3 M formate ($2 \leq \text{pH} \leq 4$) were used. In these solutions the OH radical reacts mainly with the formate ions (>95%)



with $k_6 = 3.8 \times 10^9 \text{ M}^{-1} \text{ s}^{-1}$.³ The CO_2^- transfers its electron to O_2 via



with $k_7 = 2.4 \times 10^9 \text{ M}^{-1} \text{ s}^{-1}$.²⁸

Thus, all radicals (e_{aq}^- , H, and OH) are converted to the peroxy radical and its reaction with $\text{Mo}(\text{CN})_8^{4-}$ could be followed. Figure 4 shows the experimental result. In these experiments only reaction 2 is studied.

The value of k_2 was derived from the equation

$$k_2 = k_{\text{obsd}} \left(1 + \frac{K_4}{[\text{H}^+]} \right)$$

and was found to be $6 \pm 1 \times 10^4 \text{ M}^{-1} \text{ s}^{-1}$.

Reaction of the O_2^- Radical Ion with $\text{Mo}(\text{CN})_8^{3-}$. This reaction was followed in oxygenated solutions containing Mo(IV) and Mo(V) octacyanate at pH 8.3–10.4. Under these conditions $\text{Mo}(\text{CN})_8^{4-}$ reacted with the OH radicals according to reaction 1 to produce $\text{Mo}(\text{CN})_8^{3-}$ already present in the solution. Thus, after a short time, the system contains only Mo(IV) and Mo(V) octacyanate and O_2^- radical ions. At the pH studied the radical is relatively stable. Figure 5 shows the experimental result from which it can be seen the O_2^- reduced $\text{Mo}(\text{CN})_8^{3-}$ (reaction 5) with a rate constant of $3.0 \pm 0.3 \times 10^5 \text{ M}^{-1} \text{ s}^{-1}$.

The reactivity of Mo(IV) and Mo(V) octacyanate toward OH, HO_2 , and O_2^- radical and H_2O_2 is similar to that observed for ferro- and ferricyanide. It seems however that the molybdenum complexes reactivities are less affected by ion pair formation.

Acknowledgments. The author wishes to thank J. Ogdan for the operation of the linear accelerator and Mrs. A. Saraf for her aid in the experimental work.

References and Notes

- (1) B. K. Sharma, *Can. J. Chem.*, **46**, 2757 (1968).
- (2) W. L. Waltz, S. S. Akhtar, and R. L. Eager, *Can. J. Chem.*, **51**, 2525 (1973).
- (3) L. M. Dorfman and G. E. Adams, *Natl. Stand. Ref. Data Ser., Natl. Bur. Stand., No. 46*, (1973).
- (4) J. Rabani and G. Stein, *Trans. Faraday Soc.*, **58**, 2150 (1962).
- (5) (a) F. S. Dainton and W. S. Watt, *Nature (London)*, **195**, 1294 (1962); (b) *Proc. R. Soc., Ser. A*, **275**, 447 (1963).
- (6) (a) G. Hughes and C. Willis, *J. Chem. Soc.*, 2848 (1962); (b) *Discuss. Faraday Soc.*, **36**, 223 (1963).
- (7) (a) S. Gordon, E. J. Hart, M. S. Matheson, J. Rabani, and J. K. Thomas, *J. Am. Chem. Soc.*, **85**, 1375 (1963); (b) *Discuss. Faraday Soc.*, **36**, 193 (1963).
- (8) (a) E. Masri and M. Haissinsky, *J. Chim. Phys.*, **60**, 397 (1963); (b) M. Haissinsky, A. M. Koulkes, and E. Masri, *ibid.*, **63**, 1129 (1966).
- (9) (a) E. Hayon, *Trans. Faraday Soc.*, **61**, 723 (1965); (b) *ibid.*, **61**, 734 (1965).
- (10) G. E. Adams, J. W. Boag, and B. D. Michael, *Trans. Faraday Soc.*, **61**, 492 (1965).
- (11) (a) J. Rabani and M. S. Matheson, *J. Am. Chem. Soc.*, **86**, 3175 (1964); (b) *J. Phys. Chem.*, **70**, 761 (1966).
- (12) C. E. Burchill, F. S. Dainton, and D. Smithies, *Trans. Faraday Soc.*, **63**, 932 (1967).
- (13) S. Ohno and G. Tsuchihashi, *Radioisotopes*, **16**, 26 (1967).
- (14) J. Rabani and D. Meyerstein, *J. Phys. Chem.*, **72**, 1599 (1968).
- (15) G. Czapski and E. Peled, *Isr. J. Chem.*, **6**, 421 (1968).

- (16) J. Sobkowski, *Nukleonika*, **14**, 253 (1969).
 (17) G. E. Adams and R. L. Willson, *Trans. Faraday Soc.*, **65**, 2981 (1969).
 (18) G. C. Barker, P. Fowles, and B. Stringer, *Trans. Faraday Soc.*, **66**, 1509 (1970).
 (19) D. Zehavi and J. Rabani, *J. Phys. Chem.*, **75**, 1738 (1971).
 (20) D. Zehavi and J. Rabani, *J. Phys. Chem.*, **76**, 3703 (1972).
 (21) N. H. Furman and C. O. Miller in "Inorganic Synthesis", Vol. 3, L. F. Audrieth Ed., McGraw-Hill, New York, N.Y., 1950, p 160.
 (22) J. R. Perumareddi, A. D. Liehr, and A. W. Adamson, *J. Am. Chem. Soc.*, **85**, 249 (1963).
 (23) M. Faraggi and A. Feder, *Inorg. Chem.*, **12**, 236 (1973).
 (24) A. O. Allen, "The Radiation Chemistry of Water and Aqueous Solutions", Van Nostrand, Princeton, N.J., 1961, p 41.
 (25) J. Sobkowski, *Roczn. Chem.*, **43**, 1729 (1969).
 (26) D. Behar, G. Czapski, J. Rabani, L. M. Dorfman, and H. A. Schwarz, *J. Phys. Chem.*, **74**, 3209 (1970).
 (27) I. M. Kolthoff and J. W. Tomsicek, *J. Phys. Chem.*, **40**, 247 (1936).
 (28) G. E. Adams and R. L. Willson, *Trans. Faraday Soc.*, **65**, 2981 (1969).

Direct and Indirect Effects in Pulse Irradiated Concentrated Aqueous Solutions of Chloride and Sulfate Ions

Kang-Jin Kim and William H. Hamill*

Department of Chemistry and Radiation Laboratory,¹ University of Notre Dame, Notre Dame, Indiana 46556 (Received April 15, 1976)

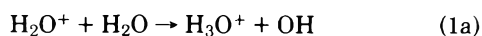
Publications costs assisted by the U.S. Energy Research and Development Administration

Yields of Cl_2^- have been measured in concentrated aqueous solutions of NaCl which contained ethanol to suppress ClOH^- and HCO_3^- to neutralize the acid spur. Yields of SO_4^- and Cl_2^- have been measured in solutions of $(\text{NH}_4)_2\text{SO}_4$, some containing 50 mM NaCl to convert SO_4^- to Cl_2^- . Yields of SO_4^- are considerably larger for solutions of $(\text{ND}_4)_2\text{SO}_4$ in D_2O . Optical spectra, extinction coefficients, and rate constants have been measured as needed for confirmation. Yields of oxidized species are attributed principally to electron transfer from the reagent R to ionized solvent S, with some contribution from direct effect. The effective electron fraction of R is $\phi = f_{\text{R}}[\text{R}]/(f_{\text{R}}[\text{R}] + f_{\text{S}}[\text{S}])$ in terms of oscillator strengths f , with $f_{\text{R}}/f_{\text{S}}$ adjustable. For direct and indirect primary yields G_{d}^0 and G_{i}^0 the yield is described by $G = G_{\text{d}}^0\phi + G_{\text{i}}^0(1 - \phi)\nu_1[\text{R}]/(\nu_1[\text{R}] + \nu_2[\text{S}])$ where $\nu_1[\text{R}]$ is the frequency of electron transfer and $\nu_2[\text{S}]$ is the frequency of dry hole localization, e.g., by formation of H_3O^+ . For $1 - \phi \sim 1$, the direct and indirect yields are algebraically indistinguishable. Large yields of SO_4^- in D_2O cannot be explained by ϕ . They are attributed to the vibration-limited frequency ν_2 which increases the lifetime of D_2O^+ .

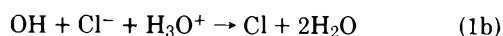
Introduction

The possibility of electron transfer from a solute to the primary positive hole in aqueous systems is of fundamental interest in radiation chemistry. Anions should be particularly suitable. For pulse radiolysis the oxidized species should provide an appropriate optical transient and OH, as precursor, capable of being excluded.

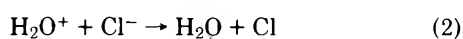
Electron transfer from an anion to H_2O^+ in aqueous solution was considered by Anbar and Thomas.² They observed first that chloride ion is rapidly oxidized by OH under pulse radiolysis in acidic aqueous solutions, the rate of formation of Cl_2^- being first order in the concentrations of OH, Cl^- , and H^+ .² The rate constant is $\sim 10^{10} \text{ M}^{-2} \text{ s}^{-1}$. In neutral or slightly alkaline solutions Cl_2^- was observed only at $>0.1 \text{ M Cl}^-$ and the reaction was considered to occur in spurs as a consequence of reactions



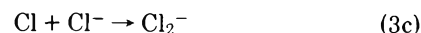
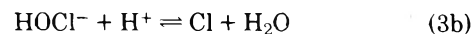
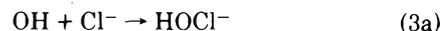
and



They also considered the following as a possible mechanism



but thought it to be unlikely. Another mechanism which was also considered is



The preceding results for large $[\text{Cl}^-]$ and neutral pH were subsequently attributed by Hamill to reaction 2.³ The possibility that Cl_2^- at neutral pH is produced principally by eq 1b or 3b in the acid spur was examined by Peled et al.⁴ who showed that in 2 M NaCl the yield of Cl_2^- was unchanged by 0.4 M Na_2HPO_4 or 0.5 M Na_2SO_4 as buffers. They concluded that either (i) H_2O^+ and e^- do not annihilate, or (ii) partial annihilation is much too fast for interference by scavengers. Concurrently, Fisher and Hamill⁵ had found that the yield of Cl_2^- was unaffected by 1 M Na_2SO_4 and concluded that reaction 2 occurred within $\sim 10^{-14} \text{ s}$.

Later work by Ogura and Hamill⁶ showed that at pH ~ 7 and large $[\text{Cl}^-]$, yields of Cl_2^- are $\sim 20\%$ larger in D_2O than in H_2O while the rate constant for reactions 3a-c is 17% greater in H_2O . Again, reaction 2 was invoked.

Pucheault et al.⁷ studied neutral solutions of LiCl up to 14 M. The 100-eV yield, $G(\text{Cl}_2^-)$, was a maximum at 3.4 in 9 M

LiCl. There appears to be no direct effect according to the authors. They concluded that the yield of primary species was ~ 4.7 .

There is a recent report by Hunt et al.⁸ that Cl_2^- and similar species have been observed at 30 ps in concentrated neutral solutions of Cl^- , Br^- , and SCN^- . Reaction 2 and its analogues were proposed.

The equilibrium reaction 3a has been confirmed by Jayson et al.⁹ with forward and reverse rate constants $k_f = 4.3 \times 10^9 \text{ M}^{-1} \text{ s}^{-1}$ and $k_r = 6.1 \times 10^9 \text{ s}^{-1}$. For reaction 3b, $k_f = 2.1 \times 10^{10} \text{ M}^{-1} \text{ s}^{-1}$ and $k_r = 1.3 \times 10^3 \text{ M}^{-1} \text{ s}^{-1}$. The spectrum of HOCl^- is very similar to that for Cl_2^- with $\lambda_{\text{max}} = 350 \text{ nm}$, $\epsilon = 3.7 \times 10^3 \text{ M}^{-1} \text{ cm}^{-1}$ and $\lambda_{\text{max}} = 340 \text{ nm}$, $\epsilon = 8.8 \times 10^3 \text{ M}^{-1} \text{ cm}^{-1}$, respectively. These authors found that reactions 3a-c sufficed to describe their results.

Recent work in this laboratory has disclosed another complication in earlier results since SO_4^{2-} at high concentrations gives appreciable yields of SO_4^- . Also, SO_4^- oxidizes Cl^- .^{10,11} Sulfate ion reacts very slowly with OH, even at low pH, and its efficient photoionization indicates its possible utility as an electron donor for H_2O^+ and OH^+ (the ionization potentials are 12.6 and 13.2 eV¹²) since it appears to be free of side effects which complicate the use of Cl^- . Also, SO_4^- provides an appropriate optical transient.

Radiolysis of concentrated solutions of sulfate ions may entail large contributions to $G(\text{SO}_4^-)$ from direct effect because of the large formular weight. To allow for this we define the effective electron fraction ϕ for R in S by

$$\phi = f_R[\text{R}]/(f_R[\text{R}] + f_S[\text{S}]) \quad (\text{I})$$

where the f 's are oscillator strengths. The ratio f_S/f_R is considered to be an adjustable parameter.

In earlier studies of this series^{5,6} eq II has been used for a simple, empirical description of the 100-eV yields of Cl_2^- in aqueous NaCl.

$$G(\text{Cl}_2^-) = G^0(1 + \nu_2[\text{H}_2\text{O}]/\nu_1[\text{Cl}^-])^{-1} \quad (\text{II})$$

It implies an indirect energy or charge transfer, $\nu_1[\text{Cl}^-]$, in competition with self-quenching or self-trapping, $\nu_2[\text{H}_2\text{O}]$, where the ν 's are appropriate frequencies when $[\text{Cl}^-]$ and $[\text{H}_2\text{O}]$ are expressed as mole fractions.

In eq II one may consider that $\nu_1[\text{Cl}^-]$ is the rate of electron transfer to the dry positive hole, $\text{S}^+ + \text{R}^z \rightarrow \text{S} + \text{R}^{z+1}$, while ν_2 is taken as the frequency of some self-trapping mechanism, such as formation of H_3O^+ in water. For very concentrated solutions of R in S it may be necessary to modify eq II to

$$G = (1 - \phi)G^0(1 + \nu_2[\text{S}]/\nu_1[\text{R}])^{-1} \quad (\text{III})$$

A still more general type of dependence which allows for both direct and indirect contributions from G_d^0 and G_i^0 is given by

$$G = \phi G_d^0 + (1 - \phi)G_i^0(1 + \nu_2[\text{S}]/\nu_1[\text{R}])^{-1} \quad (\text{IV})$$

For $G_d^0 = 0$, eq IV becomes eq III.

The objectives of this work include: (i) measuring $G(\text{Cl}_2^-)$ vs. $[\text{Cl}^-]$ relatively free of complications due to OH and acid; (ii) measuring $G(\text{SO}_4^-)$ vs. $[\text{SO}_4^{2-}]$ under conditions which eliminate measurable contributions from OH and acid; (iii) considering direct effects; (iv) examining the evidence for electron transfer from Cl^- and SO_4^{2-} to H_2O^+ and OH^+ , as well as D_2O^+ and CD^+ .

Experimental Section

Irradiations were performed with an ARCO LP-7 linear accelerator which provided 10-ns pulses of ~ 8 -MeV electrons,

approximating 5 krads. Dosimetry was based on the optical density (OD) of e_{aq}^- at 600 nm using $\epsilon = 1.17 \times 10^4 \text{ M}^{-1} \text{ cm}^{-1}$ and $G(e_{\text{aq}}^-) = 3.3$ at 10 ns. Ordinary corrections for density have been applied.

Water was triply distilled, chemicals were reagent grade, and all solutions were purged with argon or nitrogen.

Experimental procedures were those used previously except that dose monitoring of every pulse with a Faraday cup has been introduced. It samples part of the beam passing through the cell and a 5-mm hole in an aluminum plate. The cell holder is mounted on the plate and the assembly attached to the bolt ring of the LINAC window. The cell holder has three compartments, the middle being empty for testing, the top and bottom containing cells. One usually contains water for dosimetry. The cell holder moves vertically, being positioned reproducibly by a motor, gear train, and limit switches. In addition to improved pulse monitoring, the operating efficiency has been markedly improved.

Results

To minimize formation of Cl_2^- in the acidic spur requires an added base. Preliminary tests confirmed an earlier observation⁵ that NH_3 reacts rather rapidly with Cl_2^- . Nevertheless, by extrapolating optical densities to the end of the pulse for 1 M NaCl with 0.05 M $\text{C}_2\text{H}_5\text{OH}$ to remove OH, the addition of 0.1 and 1.0 M NH_3 decreased $G(\text{Cl}_2^-)$ by ~ 9 and $\sim 39\%$, respectively. Addition of 0.1 and 0.7 M NaHCO_3 to 1 M NaCl decreased $G(\text{Cl}_2^-)$ by 16 and 33%, respectively, and there was no appreciable reaction with Cl_2^- .

The 100-eV yields, $G(\text{Cl}_2^-)$, for solutions of NaCl also containing 0.1 M $\text{C}_2\text{H}_5\text{OH}$ to suppress OH and ClOH^- , are given by (O) in Figure 1. For a second series of measurements with solutions containing only NaCl (not shown), the optical density depends upon both $G(\text{Cl}_2^-)$ and $G(\text{ClOH}^-)$. Taking $K = 0.45 \text{ M}^{-1}$ for $\text{OH} + \text{Cl}^- = \text{ClOH}^-$,¹³ and $G(\text{oxid}) = 2.9$, calculated values of $G(\text{Cl}_2^-)$ and $G(\text{ClOH}^-)$ are obtained, shown by (+) and (---), respectively, in Figure 1. The $G(\text{OH})$ dependence is included (---). The observed and calculated values of $G(\text{Cl}_2^-)$ support the model, except for large $[\text{NaCl}]$ where the combined yields of Cl_2^- , OH, and ClOH^- may exceed 2.9. The decrease in $G(\text{ClOH}^-)$ at large $[\text{NaCl}]$ is a consequence of scavenging H_2O^+ and suppressing $G(\text{OH})$.

Another series of experiments was performed with solutions containing both 0.1 M $\text{C}_2\text{H}_5\text{OH}$ and also 0.24 M NaHCO_3 . The latter should neutralize acid in the spur at $t > 10^{-10}$ s to suppress reaction 1b. The combined reagents suppress OH at $t > 10^{-8}$ s and remove interfering optical absorption by ClOH^- .⁹ Higher concentrations of NaHCO_3 were precluded by its limited solubility in concentrated solutions of NaCl. These results are presented in Figure 2 according to eq II by data points (+) using the lower scale of abscissa. The yield of oxidizing precursors is $G^0 \sim 5.4$ and the scavenging efficiency is $\nu_1/\nu_2 = 7.5$. Using eq IV, $[\text{H}_2\text{O}] \sim 55.5 - 1.13[\text{Cl}^-]$ and setting $G_i^0 = 0$, the data points (O) and the upper scale of abscissa give $G_d^0 \sim 5.0$ and $f(\text{Cl}^-)/f(\text{H}_2\text{O}) = 7.0$. Note that diametrically opposed models produce approximately the same initial yields.

The primary yield of oxidizing species agrees approximately with recent results from dry-electron scavenging by Cd^{2+} for which $G^0 = 5.2$.¹⁴

Nitrate ion was tested as a possible electron donor for H_2O^+ . Since NO_3^- absorbs very weakly but has a very large electron affinity, a second electron donor, not oxidized by OH, is required to produce an absorbing transient. In 2 M NaNO_3 and 0.05 M NaCl at neutral pH there was a transient absorption

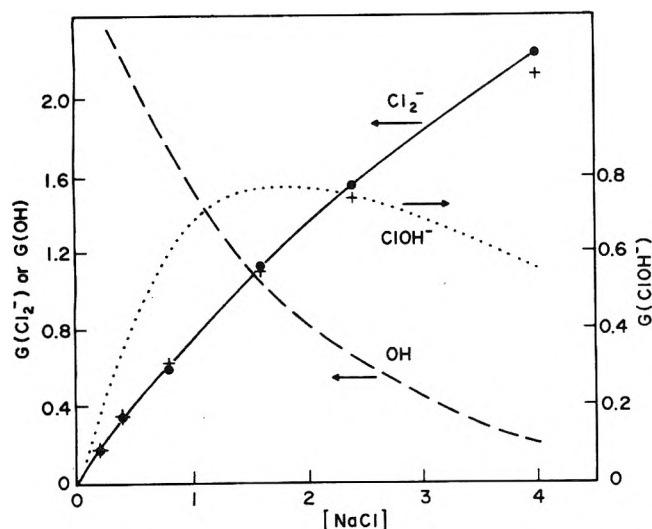


Figure 1. The 100-eV yields of Cl_2^- in solutions of NaCl with 0.1 M $\text{C}_2\text{H}_5\text{OH}$ to remove OH (O). Corrected yields of Cl_2^- for NaCl alone, based on $K = 0.45 \text{ M}^{-1}$ for eq 3a are included (+), together with calculated values of $G(\text{ClOH}^-)$ and $G(\text{OH})$.

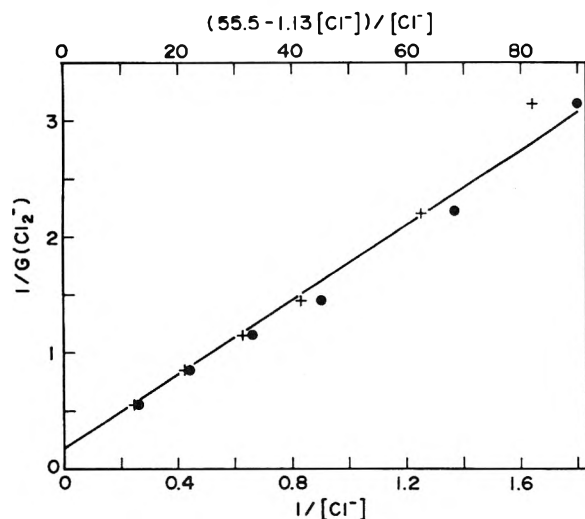


Figure 2. Yields of Cl_2^- in solutions of NaCl with 0.1 M $\text{C}_2\text{H}_5\text{OH}$ and 0.24 M NaHCO_3 in terms of eq II for $G_d^0 = 0$ lower scale (+), and eq IV $G_i^0 = 0$, upper scale (O). The line is drawn arbitrarily to fit (+).

with $\lambda_{\text{max}} = 345 \text{ nm}$. The spectrum was indistinguishable from that of Cl_2^- in 0.05 M NaCl at pH 2 and $G(\text{Cl}_2^-) = 0.58$. For comparison, the results of Figure 2 give $G(\text{Cl}_2^-) = 1.0$ in 2 M NaCl. The rate constant for converting NO_3^- to Cl_2^- was $1.0 \times 10^8 \text{ M}^{-1} \text{ s}^{-1}$, based on the slow increase in OD_{345} , obtained from Figure 5. Because of its relatively low efficiency, NO_3^- was not considered further.

The simplest reagent found for H_2O^+ (by hypothesis) was SO_4^{2-} . It is not oxidized in dilute solutions, viz. by OH, but is oxidized at high concentrations to yield an observable transient, SO_4^- . There appears to be no prior report of this effect. Although the extinction coefficient of SO_4^- is only $\epsilon = 1100 \text{ M}^{-1} \text{ cm}^{-1}$,¹⁵ the very slow oxidation of SO_4^{2-} by OH, even at low pH, recommended the use of this system.

In 2 M $(\text{NH}_4)_2\text{SO}_4$ with 0.01 M NaNO_3 to scavenge e_{aq}^- , a transient absorption spectrum with $\lambda_{\text{max}} = 450 \text{ nm}$ was observed to be the same as that for 0.1 M $(\text{NH}_4)_2\text{S}_2\text{O}_8$ which produces SO_4^- by dissociative attachment. These spectra, which appear in Figure 3, agree with published spectra for

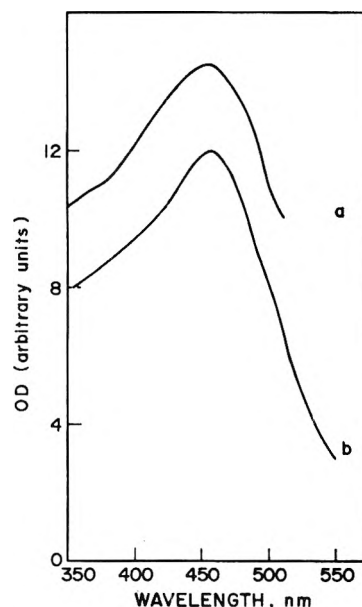


Figure 3. The spectra of SO_4^- from the pulse radiolysis of 2 M $(\text{NH}_4)_2\text{SO}_4$ (a), and 0.1 M $(\text{NH}_4)_2\text{S}_2\text{O}_8$ (b). The OD's have been normalized at λ_{max} and the upper spectrum has been shifted vertically.

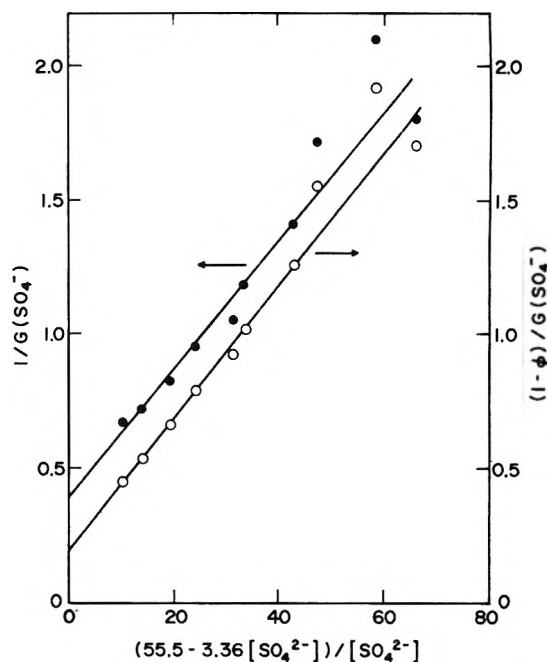


Figure 4. Yields of SO_4^- in solutions of $(\text{NH}_4)_2\text{SO}_4$ in terms of eq IV for $G_d^0 = 0$ and $f(\text{SO}_4^{2-})/f(\text{H}_2\text{O}) = 4.0$, arbitrarily, by points (O) and $G_i^0 = 0$ (●).

SO_4^- .¹⁵ The dependence of $G(\text{SO}_4^-)$ on $[\text{SO}_4^{2-}]$ by eq IV in terms of $[\text{H}_2\text{O}] \sim 55.5 - 3.5[\text{SO}_4^{2-}]$ for the case $G_d^0 = 0$ is given by points (●) in Figure 5, with $G_d^0 = 2.6$ and $f(\text{SO}_4^{2-})/f(\text{H}_2\text{O}) = 17$. For eq IV, letting $G_d^0 = 0$ and $f(\text{SO}_4^{2-})/f(\text{H}_2\text{O}) = 4$, arbitrarily, $G_i^0 = 5.0$ and $\nu_2/\nu_1 = 0.125$ given by points (O) in Figure 4.

The utility of SO_4^{2-} as an electron donor can be enhanced by converting SO_4^- to Cl_2^- to improve the signal intensity. The transient spectrum coincided with that of Cl_2^- . Additional support for the oxidation of Cl^- by SO_4^- is provided in Figure 5. For 2 M Na_2SO_4 , $k = 4.1 \times 10^8$ and for 2 mM $(\text{NH}_4)_2\text{S}_2\text{O}_8$, $k = 1.3 \times 10^8 \text{ M}^{-1} \text{ s}^{-1}$. For both solutions, 50 mM

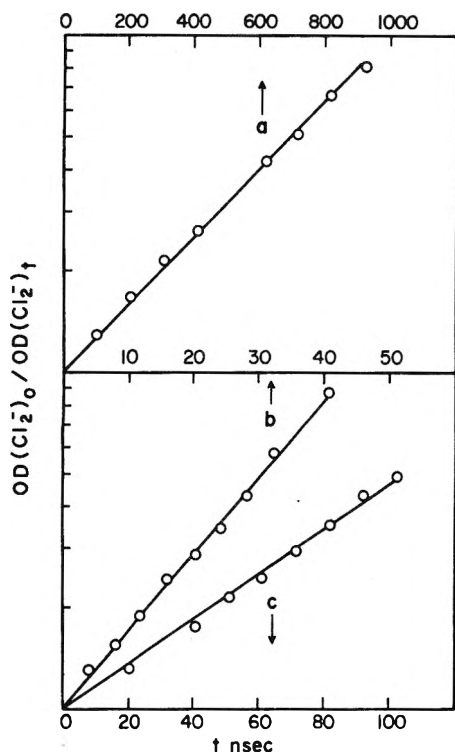


Figure 5. The rates of oxidation of Cl^- in 0.05 M NaCl by NO_3^- from 2 M NaNO_3 (a), by SO_4^{2-} from 2 M Na_2SO_4 (b), and by SO_4^{2-} from 2 mM $(\text{NH}_4)_2\text{S}_2\text{O}_8$ (c).

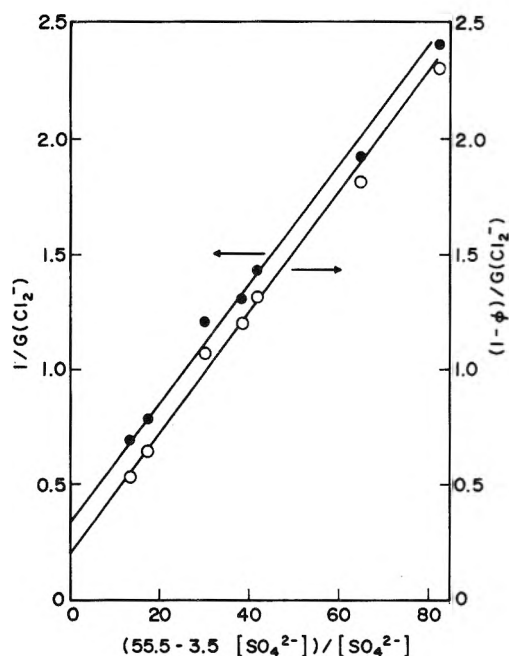


Figure 6. Yields of Cl_2^- in solutions of $(\text{NH}_4)_2\text{SO}_4$ with 0.05 M NaCl in terms of eq IV for $G_d^0 = 0$, (O), and $G_i^0 = 0$ (●).

NaCl was used. The higher rate constant in 2 M Na_2SO_4 is consistent with ionic strength effects.

Yields of Cl_2^- in solutions of SO_4^{2-} containing 50 mM NaCl appear in Figure 6. In terms of eq IV, when $G_i^0 = 0$, one obtains $f(\text{SO}_4^{2-})/f(\text{H}_2\text{O}) = 14$ and $G_d^0 = 2.9$ from points (●). For $G_d^0 = 0$, the best fit occurs for $f(\text{SO}_4^{2-})/f(\text{H}_2\text{O}) = 3$ giving $G_i^0 = 4.8$ and $\nu_2/\nu_1 = 0.122$ from the points (O).

The dependence of $G(\text{SO}_4^-)$ on $[(\text{NH}_4)_2\text{SO}_4]$ in H_2O for G_d^0

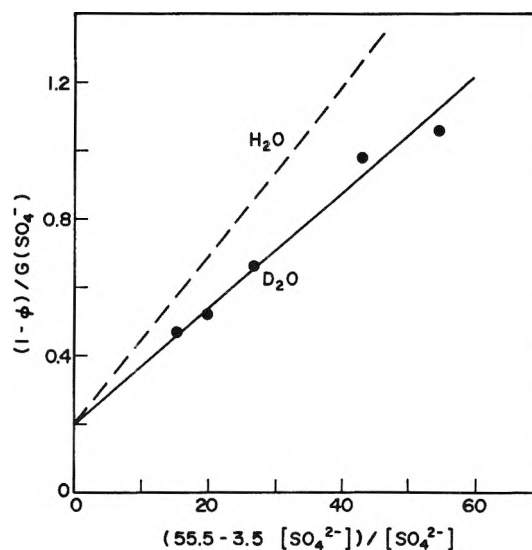


Figure 7. Yields of SO_4^- in solutions of $(\text{ND}_4)_2\text{SO}_4$ in D_2O in terms of eq IV for $G_d^0 = 0$ taking $f(\text{SO}_4^{2-})/f(\text{D}_2\text{O}) = 4$.

TABLE I: Values of the Parameters for Eq IV

Reagent	Transient	f_R/f_S	ν_2/ν_1	G_d^0	G_i^0
Cl^-	Cl_2^-	7.0		5.0	0
SO_4^{2-}	SO_4^-	17		2.6	0
		4^a	0.13	0	5.0
		$4^{a,b}$	0.085	0	5.0
SO_4^{2-}	Cl_2^-	14		2.9	0
		3^a	0.12	0	4.8

^a Arbitrary values. ^b Solvent D_2O , all others H_2O .

= 0 is compared in Figure 7 with the corresponding results with $(\text{ND}_4)_2\text{SCl}_4$ in D_2O . Choosing $f(\text{SO}_4^{2-})/f(\text{D}_2\text{O}) = 4$, $G_d^0 = 5.0$, and $\nu_2/\nu_1 = 0.085$. The isotope effect is $(\nu_1/\nu_2)_{\text{H}_2\text{O}} = 1.45(\nu_1/\nu_2)_{\text{D}_2\text{O}}$.

All parameters for Figures 2, 4, and 6 are summarized in Table I.

Discussion

It will be assumed that indirect action in solutions of NaCl is described by eq 2 and analogously for other anions. There is a minor contribution to $G(\text{Cl}_2^-)$ from spur reactions of Cl^- , but there is no comparable reaction for SO_4^{2-} . Both oxidized species (i.e., the trapped holes) decay rather slowly and e_{aq}^- is not kinetically significant. The yield and fate of OH^+ cannot be resolved by these experiments. It may annihilate by electron transfer from anions or H_2O and therefore resembles H_2O^+ .

The three constructed curves of Figure 1 depend upon the equilibrium $G(\text{ClOH}^-)/G(\text{OH}) = 0.45[\text{Cl}^-]$ and one assumption, $G(\text{OH}) + G(\text{ClOH}^-) + G(\text{Cl}_2^-) = 2.9$. Consequently, using the data of Figure 2 for $G(\text{Cl}_2^-)$, both $G(\text{OH})$ and $G(\text{ClOH}^-)$ can be evaluated. The combined decrease in $G(\text{ClOH}^-)$ and $G(\text{OH})$ is a consequence of eq 1a and 2.

In Figure 2 the trial assumption that $G(\text{Cl}_2^-) = \phi G_d^0$ led to the requirement that $f(\text{Cl}^-) = 7f(\text{H}_2\text{O})$, which is clearly unacceptable. Consequently, some other mechanism for producing Cl_2^- is required, either in whole or in part.

It should be noted that for $G_i^0 = 0$ and $[\text{H}_2\text{O}] \sim 55$, a constant, eq IV is experimentally indistinguishable from eq II. Also, provided ϕ is small and $[\text{H}_2\text{O}]$ nearly constant for the other limiting case that $G_d^0 = 0$, eq IV again approximates eq II. It is clearly very difficult to distinguish between the two

extreme cases on the basis of algebraic form. The choice of any linear combination must rest on other considerations. The problem has been examined in detail by Mozumder.¹⁶

Although eq II provides a convenient approximation of eq IV for both extremes to describe high [NaCl], it is a much poorer approximation for high [(NH₄)₂SO₄] because of its large formular weight. The choice $G_i^0 = 0$ can be eliminated, because of the unacceptably high values for $f(\text{SO}_4^{2-})/f(\text{H}_2\text{O})$, but the choice $G_d^0 = 0$ cannot, from the parameters of Table I. To test this case by letting $\phi = 0$, since the f 's are only very roughly known, is not an acceptable approximation and it is much better to assign $f(\text{SO}_4^{2-})/f(\text{H}_2\text{O})$ some arbitrary but plausible value. Since the data can be fitted by this approach without requiring unacceptable values of the parameters, no linear combination of direct and indirect terms (by fitting ϕ and G_d^0) can cause a significant improvement. The ratio of the direct and indirect effects of eq IV tends to be roughly constant below 1 or 2 M scavenger and this compounds the difficulty of resolving them. Curves in Figures 2, 4, and 6 for the nominal case $G_d^0 = 0$ unavoidably contain some admixture from both mechanisms, due to their algebraic resemblance.

The ratio of solute to solvent oscillator strengths for Cl⁻ from Figure 2 and Table I is independent of any assumption about contributions from Na⁺. It was found, however, that for 3 M LiCl, 3 M NaCl, and 1.5 M BaCl₂, $G(\text{Cl}_2^-)$ was 1.98, 1.89, and 1.94. Since the first excited states of these cations are relatively high, e.g., 33 eV for crystalline sodium halides,^{18,19} energy deposited in such cations in the crystal is transferred to Cl⁻ and contributes to the yield of secondary electrons. In aqueous solutions the energy will be transferred principally to H₂O from which part will be transferred to Cl⁻. Energy deposited in the higher states of Cl⁻ can also transfer to H₂O and then back to a lower state of Cl⁻. The oscillator strengths of the cations have not been considered further. It is doubtful that "direct effects" can be defined operationally for electron energy losses at ≥ 25 eV, or even lower.

Poucheault et al.⁷ concluded that there is no direct effect in $G(\text{Cl}_2^-)$ for ≤ 14 M LiCl. The maximum which they observed at 9 M LiCl is not inconsistent with partial direct effect according to eq IV. The charge transfer term is changing weakly at 9 M. Since ϕG_d^0 increases monotonically vs. [Cl⁻] with decreasing curvature while $(1 - \phi)G_i^0$ decreases more rapidly the higher the concentration, there may be a maximum according to eq IV.

Matthews et al.²⁰ have presented kinetic evidence for direct action of ⁶⁰Co irradiation on H₂SO₄ to form SO₄⁻ (or HSO₄). Lesigne et al.²¹ also reported evidence for the direct effect in 0.4, 2, and 4 M H₂SO₄ based on the linearity of $G(\text{SO}_4^-)$ vs. the electron fraction ϕ of H₂SO₄ at ~ 12 ns. Their prompt $G(\text{SO}_4^-)$ was 1.4 for 4 M H₂SO₄, about the same as that for Figures 4 and 6. They found $G(\text{OH})$ approximately proportional to $\phi(\text{H}_2\text{O})$ and attribute this to direct effect. However, since $G(\text{OH}) + G(\text{SO}_4^-) \sim 2.9$ from their data, they are not inconsistent with $G_d^0 = 0$, decreased $G(\text{OH})$ resulting from $\text{H}_2\text{O}^+ + \text{HSO}_4^- \rightarrow \text{H}_2\text{O} + \text{HSO}_4$. Once more, the evidence can be interpreted by either extreme.

The conversion of SO₄⁻ to Cl₂⁻ is supported by earlier observations,¹¹ by the spectra of SO₄⁻ and Cl₂⁻, and by the rates in Figure 5. Since $\epsilon(\text{SO}_4^-) = 1.1 \times 10^3 \text{ M}^{-1} \text{ cm}^{-1}$ at 460 nm and $\epsilon(\text{Cl}_2^-) = 8.6 \times 10^3 \text{ M}^{-1} \text{ cm}^{-1}$ at 345 nm, both redetermined in this work, improved accuracy is to be expected. The approximate agreement of the results in Figure 6 with those in Figure 4 show that there is no detectable oxidation of 0.05 M Cl⁻ except that from SO₄⁻, and no transient absorption at 345 nm except that of Cl₂⁻ after $\sim 10^{-7}$ s.

The extreme cases in Figure 6, $G_i^0 = 0$ (●, upper curve) and $G_d^0 = 0$ (○, lower curve) are logically unacceptable but experimentally difficult to distinguish. They are in adequate agreement with the results of Figure 4.

It is now clear that the apparent failure of 0.5 or 1 M Na₂SO₄ to decrease $G(\text{Cl}_2^-)$ in concentrated NaCl solutions by buffering the spur⁵ was due to two opposing effects. The buffering reaction does decrease $G(\text{Cl}_2^-)$ arising from mechanism 3a-c. However, the combined yield of scavenging H₂O⁺ by Cl⁻ and SO₄²⁻ is increased by the greater concentration of reactive anions and both scavengers produce one measurable product, Cl₂⁻.

Substantially no isotope effect is expected for $G_d^0\phi$, either in G_d^0 or in ϕ . Consequently, for Figure 7 at given [SO₄²⁻], the difference between $G_{\text{D}_2\text{O}}$ and $G_{\text{H}_2\text{O}}$ depends only on the indirect term in eq IV. The primary ionization yields are 5.2 in H₂O and 4.9 in D₂O¹⁴ and the coefficient $1 - \phi$ has a common value for given [SO₄²⁻]. The more efficient oxidation of SO₄²⁻ in D₂O arises almost entirely from ν_2/ν_1 . The electron transfer frequency ν_1 is not expected to contribute to the isotope effect but ν_2 , the frequency to form H₃O⁺ or D₃O⁺, cannot be faster than the stretching vibrational frequencies. There is no detectable activation energy and it has been proposed that H-atom transfer from H₂O to H₂O⁺ occurs at the vibrational frequency since the reaction partners are already aligned by H bonding.⁶ If direct and indirect actions could be separated, the isotope effect would be described by the ratio of $(\nu_1/\nu_2)_{\text{D}_2\text{O}}/(\nu_1/\nu_2)_{\text{H}_2\text{O}}$. By interpolation at 1 M SO₄²⁻, however, $G(\text{SO}_4^-)_{\text{D}_2\text{O}}/G(\text{SO}_4^-)_{\text{H}_2\text{O}} = 1.47$ provides qualitative evidence for a relatively large indirect effect.

There is an alternative (and possibly preferable) mechanism for localizing the dry positive hole, H₂O⁺, which is probably indistinguishable from the preceding. The molecular configuration of H₂O⁺ produced by a vertical transition is that of H₂O, bent, while the ground state of H₂O⁺ is approximately linear.²² Configurational relaxation is an efficient mechanism for self-trapping with substantially the same vibrational frequencies as H₂O (or D₂O) and therefore the same isotope effects and frequencies as for protonation.

It is of interest that ν_1/ν_2 is, by eq IV, the number of electron transfers from molecule to hole prior to self-trapping, e.g., 12 in D₂O. This chain is terminated by an impurity donor or by self-trapping. If $\nu_2 \sim 10^{14} \text{ s}^{-1}$, then $\nu_1 \sim 10^{15} \text{ s}^{-1}$ and the velocity of hole migration is $\sim 2 \times 10^7 \text{ cm s}^{-1}$, which is not implausible.

Acknowledgment. The authors are indebted to Dr. A. Mozumder for helpful discussions concerning direct effects.

References and Notes

- (1) The Radiation Laboratory of the University of Notre Dame is operated under contract with the U.S. Energy Research and Development Administration. This is ERDA Document No. COO-38-1041.
- (2) M. Anbar and J. K. Thomas, *J. Phys. Chem.*, **68**, 3828 (1964).
- (3) W. H. Hamill, *J. Phys. Chem.*, **73**, 1341 (1969).
- (4) E. Peled, D. Meisel, and G. Czapski, *J. Phys. Chem.*, **76**, 3677 (1972).
- (5) M. M. Fisher and W. H. Hamill, *J. Phys. Chem.*, **77**, 171 (1973).
- (6) H. Ogura and W. H. Hamill, *J. Phys. Chem.*, **77**, 2952 (1973).
- (7) R. J. Woods, B. Lesigne, L. Gilles, C. Ferradini, and J. Poucheault, *J. Phys. Chem.*, **79**, 2700 (1975).
- (8) J. W. Hunt, R. K. Wolff, and S. G. Chenery, "Fast Processes in Radiation Chemistry and Biology", G. E. Adams, E. M. Fielden, and B. D. Michael, Ed., The Institute of Physics, London; Wiley, London, 1975, p 109.
- (9) G. G. Jayson, B. J. Parsons, and A. J. Swallow, *J. Chem. Soc., Faraday Trans. 1*, **69**, 1597 (1973).
- (10) Results of K.-J. Kim.
- (11) O. P. Chawla and R. W. Fessenden, *J. Phys. Chem.*, **79**, 2693 (1975).
- (12) J. L. Franklin, J. G. Dillard, H. M. Rosenstock, J. T. Herron, K. Draxl, and F. H. Field, *Natl. Stand. Ref. Data Ser., Natl. Bur. Stand.*, **No. 26** (1969).

- (13) R. W. Fessenden, private communication.
 (14) Cz. Stradowski and W. H. Hamill, *J. Phys. Chem.*, **80**, 1431 (1976).
 (15) E. Heckel, A. Henglein, and G. Beck, *Ber. Bunsenges. Phys. Chem.*, **70**, 149 (1966).
 (16) A. Mozumder, to be submitted for publication.
 (17) L. Dogliotti and E. Hayon, *J. Phys. Chem.*, **71**, 2511 (1967).
 (18) K. Hiraoka and W. H. Hamill, *J. Chem. Phys.*, **57**, 3881 (1972).
 (19) M. Kreuzberg, *Z. Phys.*, **196**, 433 (1966).
 (20) R. W. Matthews, H. A. Mahlman, and T. J. Sworski, *J. Phys. Chem.*, **76**, 1265 (1972).
 (21) B. Lesigne, C. Ferradini, and J. Pucheault, *J. Phys. Chem.*, **77**, 2156 (1973).
 (22) G. Herzberg, "Electronic Spectra of Polyatomic Molecules", Van Nostrand, New York, N.Y., 1966, p 489.

Pulse Radiolysis of Concentrated Aqueous Solutions of Chloride, Iodide, and Persulfate Ions

Kang-Jin Kim and William H. Hamill*

Department of Chemistry and the Radiation Laboratory,¹ University of Notre Dame, Notre Dame, Indiana 46556 (Received May 14, 1976)

Publication costs assisted by the U.S. Energy Research and Development Administration

Yields of Cl_2^- per 100 eV at pH 1 in solutions of NaCl are the same as those for HCl, up to 4 M Cl^- , being nearly constant at $G(\text{Cl}_2^-) = 3.2$. In solutions of KI at pH ~ 8 , $G(\text{I}_2^-)$ increased almost linearly from 3.25 at 10^{-2} M to 3.60 at 1.8 M while $2G(\text{I}_3^-)$ increased from ~ 0 to 1.45. At pH 2, $G(\text{I}_2^-) + 2G(\text{I}_3^-)$ was greater by ~ 0.4 over the range, with $2\Delta G(\text{I}_3^-) \approx 3\Delta G(\text{I}_2^-)$. In 10^{-2} M KI, $G(\text{I}_2^-)$ increased from 3.25 to 3.70 as pH decreased from ~ 3 to 0.5. Two geminate one-electron oxidations of I^- at low pH are indicated and suggest transient $\text{O}(\text{1D})$ or $\text{O}(\text{3P})$, but not H_2O^* . The reaction $\text{OH}^+ + \text{H}_2\text{O} \rightarrow \text{H}_3\text{O}^+ + \text{O}(\text{3P})$ is indicated. In solutions of $(\text{NH}_4)_2\text{S}_2\text{O}_8$, $G(\text{SO}_4^-)$ increased to 6.0 at 1.2 M. With addition of 5×10^{-2} M NaCl, SO_4^- is converted to Cl_2^- , but $G(\text{Cl}_2^-) - G(\text{SO}_4^-) \approx 1.2$ over most of the range. The increase is attributed to $\text{H}_2\text{O}(\text{3B}_1) + \text{Cl}^-(\text{1S}_0) \rightarrow \text{H}_2\text{O}(\text{1A}_1) + \text{Cl}^-(\text{3P}_1)$ followed by electron transfer to $\text{S}_2\text{O}_8^{2-}$. At 0.05 M $\text{S}_2\text{O}_8^{2-}$ the additional yield of Cl_2^- was time resolved for ≥ 0.025 M Cl^- . The evidence suggests that 3B_1 is produced by recombination of the dry charge pair, H_2O^+ and e^- .

Introduction

In concentrated aqueous solutions of NaCl with added $\text{C}_2\text{H}_5\text{OH}$ to suppress ClOH^- and with HCO_3^- to suppress reaction with OH in the acid spur, Cl_2^- can be formed both by direct ionization of Cl^- and by prompt electron transfer from Cl^- to H_2O^+ .² The results can be described in principle by

$$G(\text{Cl}_2^-) = G_d^\circ \phi + G_i^\circ (1 - \phi) \times \{ \nu_1 [\text{Cl}^-] / \nu_1 [\text{Cl}^-] + \nu_2 [\text{H}_2\text{O}] \} \quad (\text{I})$$

where the effective electron fraction of NaCl in terms of oscillator strengths f is given by

$$\phi = f(\text{NaCl}) / [f(\text{NaCl}) + f(\text{H}_2\text{O})] \quad (\text{II})$$

G_d° and G_i° are the direct and indirect primary yields, ν_1 is the frequency of electron transfer between H_2O^+ and H_2O or the impurity Cl^- , and ν_2 is the frequency of H transfer to H_2O^+ from H_2O . It has been shown by Hunt et al.³ that the spectrum of Cl_2^- in 5 M NaCl is present at 30 ps and $G(\text{Cl}_2^-)$ is ~ 5 .

In ≤ 4 M NaCl solutions, setting $G_i^\circ = 0$ leads to unacceptable values of $f(\text{NaCl})/f(\text{H}_2\text{O})$ and G_d° . The approximation $G_d^\circ = 0$ is much more nearly acceptable.²

A serious limitation in working with chloride ion is that the expected spur products Cl_2 and Cl_3^- are difficult to measure. The former absorbs weakly and the latter strongly (at 220 nm) and $[\text{Cl}_3^-] = 0.2[\text{Cl}_2][\text{Cl}^-]$.⁴ Iodide ion, on the other hand, is an efficient reagent for OH, is expected to be efficient for

H_2O^+ , and both I_2^- and I_3^- are readily measurable. Triiodide ion is a significant radiolytic product.⁵ It has not been shown to form in the spur, although that is expected. Iodide ion offers the possibility of measuring the total yield of oxidation for comparison with the primary yield of dry electrons, e^- , which was found (by extrapolation) to be $G(e^-) = G(\text{Cd}^+) = 5.2/100$ eV.⁶ Since Cd^{2+} is not reduced by H atoms and Cd^+ is unaffected by acid in the spur, the comparison of these yields may provide the basis for an estimate of the extent of dissociation of excited water.

Persulfate ion is a possibly useful detector for excited water since SO_4^- can be measured. The lowest excited state of water is $\text{H}_2\text{O}(\text{3B}_1)$ at 6.65 eV⁷ and this lies well above the dissociation energy of $\text{S}_2\text{O}_8^{2-}$. The accuracy of the method is somewhat limited by the large background of SO_4^- from reaction of electrons and hydrogen atoms with $\text{S}_2\text{O}_8^{2-}$, but this is partially offset since each excited state produces two SO_4^- . Alternatively, or additionally, $\text{S}_2\text{O}_8^{2-}$ may serve as a detector for the excited state $\text{Cl}^-(\text{3P}_1)$ since evidence has been presented that this species is readily oxidized.⁸

In the context of the preceding considerations, it should be noted that Allen⁹ has called attention to an apparent deficiency of oxidizing products in some ^{60}Co -irradiated aqueous solutions at high pH.

The objectives of the present work include: (i) scavenging OH and H_2O^+ by concentrated Cl^- at low pH; (ii) scavenging OH and H_2O^+ by concentrated I^- with measurement of both I_2^- and I_3^- ; (iii) scavenging e^- , e_{aq}^- , and H by $\text{S}_2\text{O}_8^{2-}$; (iv)

measuring the yield of excited water; (v) considering the balance of $G(\text{oxid})$ and $G(\text{red})$.

Experimental Section

Ten-ns pulses of ~ 8 -MeV electrons were used for all experiments. Doses were 3–4 krad except for acidulated solutions of iodide ion when doses approximated 1 krad. To protect these solutions from photolysis, which caused inconveniently high and unpredictable base lines, a filter of 5 M KI with 10^{-3} M $\text{Na}_2\text{S}_2\text{O}_3$ was interposed. For all solutions of KI which produced both I_2^- and I_3^- the light beam was split and measurements made simultaneously at 290 and 345 nm. Other procedures have been described.²

Results

Chloride Ion. Chloride ion at low pH is an efficient scavenger for OH. The 100-eV yields, $G(\text{Cl}_2^-)$, increase very gradually from 2.9 in 0.1 M HCl to 3.2 in 4 M NaCl with 0.1 M HCl, as shown in Figure 1. In solutions of HCl alone the results are indistinguishable from those for NaCl. The dependence of $G(\text{Cl}_2^-)$ on $[\text{NaCl}]$ at neutral pH with 0.1 M $\text{C}_2\text{H}_5\text{OH}$ to remove OH was reported previously² and is included for comparison. The yields of Cl_2^- are based on $\epsilon(\text{Cl}_2^-) = 8.6 \times 10^3 \text{ M}^{-1} \text{ cm}^{-1}$ at 345 nm for $G(\text{OH}) = 2.9$ at 10^{-7} s for 0.1 M NaCl and 0.01 M HCl.

In solutions containing 4 M Cl^- at low pH all oxidizing species are scavenged as H_2O^+ or OH (possibly some OH^+) and $G(\text{oxid}) \geq 5.2$ is expected in order to match $G(e^-)$ as well as the unknown contribution from homolytic dissociation of H_2O . Since $G(\text{Cl}_2^-) = 3.2$ was observed, the missing oxidation products are expected to be Cl_2 and Cl_3^- . The former absorbs weakly at 220 nm where Cl_3^- absorbs strongly with $\epsilon(\text{Cl}_3^-) = 1 \times 10^4 \text{ M}^{-1} \text{ cm}^{-1}$. The best available light source was rather weak at 220 nm and the equilibrium constant for $[\text{Cl}_3^-]/[\text{Cl}_2][\text{Cl}^-] = K$ is only 0.2 and evaluated at low ionic strength.⁴ In 2, 3, and 4 M HCl, the combined yields $G(\text{Cl}_2) + G(\text{Cl}_3^-)$ were ~ 0.6 , or approximately 1.2 Cl atoms per 100 eV.

Iodide Ion. Iodide ion has some advantages as an OH scavenger. These include a high rate constant ($\sim 10^{10} \text{ M}^{-1} \text{ s}^{-1}$), $\epsilon(\text{I}_3^-) = 3.9 \times 10^4 \text{ M}^{-1} \text{ cm}^{-1}$ at 290 nm (where there is no overlap from I_2^-), and $\epsilon(\text{I}_2^-) = 8.2 \times 10^3 \text{ M}^{-1} \text{ cm}^{-1}$ at 380 nm. The latter overlaps the 352-nm band of I_3^- , but measured optical densities (OD) at 290 and 380 nm provide reliable yields of both products. The value of $\epsilon(\text{I}_2^-)$ is based on $G(\text{OH}) = 2.8$ for 10^{-3} M NaI.

The yields of products $G(\text{I}_3^-)$, $G(\text{I}_2^-)$, and their sum for 5×10^{-3} to 2 M NaI are summarized in Figure 2, expressed as I atoms. All yields are higher at pH 2 (\square and \circ) than at pH ~ 8 (\blacksquare and \bullet). The gradual rise in $G(\text{I}_2^-)$ resembles that for $G(\text{Cl}_2^-)$ in Figure 1, but $G(\text{I}_2^-)$ is 3.65 for 1.8 M I^- at pH 2 while $G(\text{Cl}_2^-)$ is 3.05 for 2 M Cl^- at pH ≤ 1 . The top curve is the combined yield with 10^{-2} M HClO_4 added, both I_2^- and I_3^- contributing to the increase. The average combined increase from pH 8 to 2 was $\Delta G = 0.35$ of which $\sim 75\%$ derived from I_3^- , all expressed as atomic iodine.

The doubly oxidized species I_3^- is probably formed in the spur by $\text{I} + \text{I}$, or $\text{I}_2^- + \text{I}_2^-$, and is analogous to H_2O_2 .¹⁰ Comparison of $G(\text{I}_3^-)$ with the decrease $\Delta G(\text{H}_2\text{O}_2)$ caused by addition of KI, from Hayon's results, appears in Figure 3¹¹ and supports the comparison.

In 10^{-2} M NaI with 10^{-2} M NaNO_3 to scavenge e_{aq}^- , $G(\text{I}_2^-)$ was 3.28 and there was no measurable yield of I_3^- . Addition of $[\text{HClO}_4]$ from 10^{-3} to 0.3 M in 10^{-2} M KI increased $G(\text{I}_2^-)$ to 3.70, as shown in Figure 4. Referring again to Figure 2 for

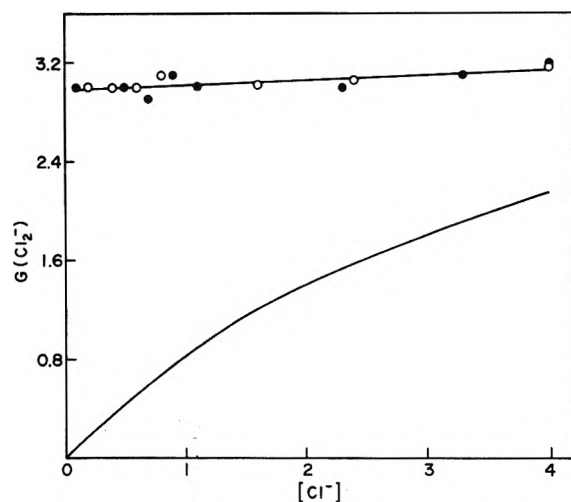


Figure 1. The dependence of $G(\text{Cl}_2^-)$ on $[\text{NaCl}]$ with 0.1 M HCl (\bullet) and on $[\text{HCl}]$ (\circ). The lower curve describes $G(\text{Cl}_2^-)$ vs. $[\text{NaCl}]$ at neutral pH, from ref 2.

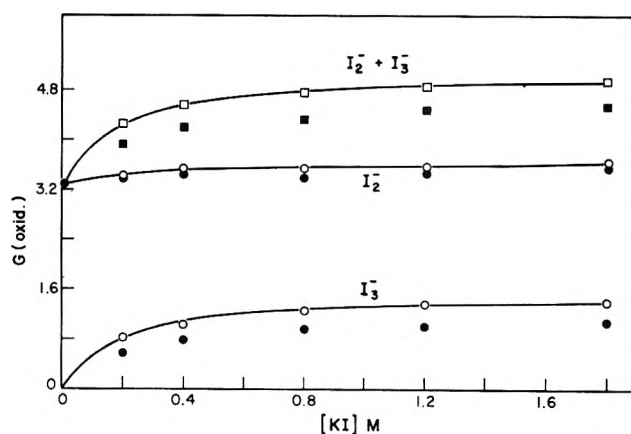


Figure 2. $G(\text{I}_3^-)$ and $G(\text{I}_2^-)$ vs. $[\text{KI}]$ at neutral pH (\bullet) and at pH 2 (\circ); the combined yields at pH ~ 8 (\blacksquare) and pH 2 (\square), all in terms of iodine atoms.

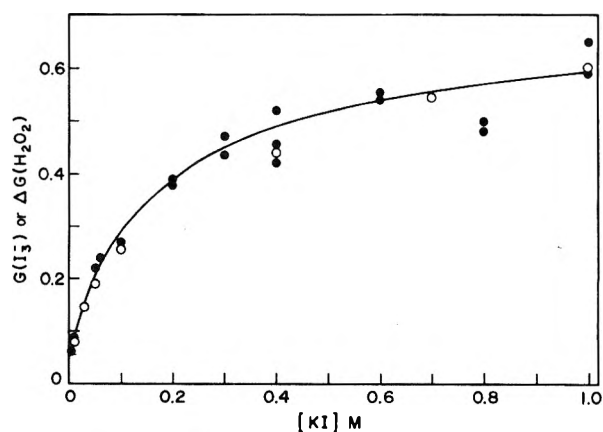


Figure 3. The yield of I_3^- and the decrease in the yield of H_2O_2 vs. $[\text{KI}]$, both at neutral pH. Yields of H_2O_2 (\circ) from Hayon.¹¹

the combined yield at pH 2, the increase due to acid appears only for appreciable concentrations of I^- , which demonstrates a concerted reaction or sequence involving both H^+ and I^- .

Persulfate Ion. Persulfate ion is expected to react according to eq 1–2; eq 3 is hypothetical; eq 4 requires prior energy transfer from H_2O^* to Cl^- .

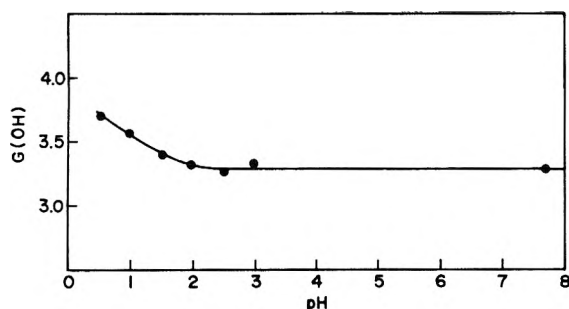


Figure 4. The yield of OH, measured as I_2^- , for 10^{-2} M KI with addition of HClO_4 .

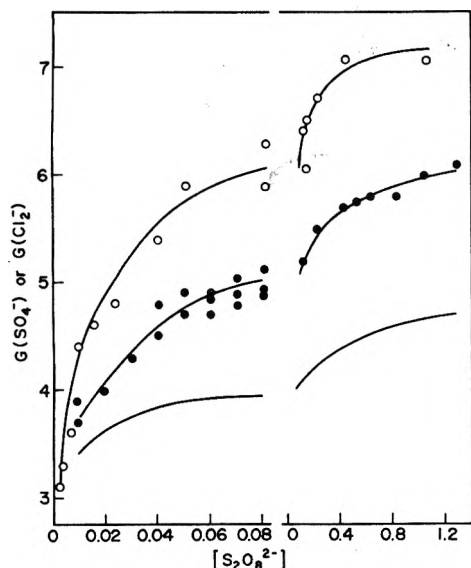
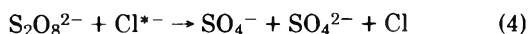
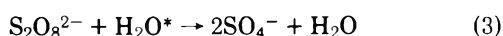
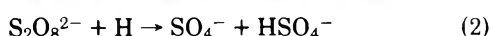
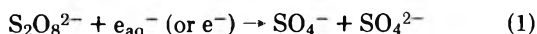
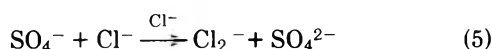


Figure 5. The yields of Cl_2^- (O) and SO_4^- (●) from $(\text{NH}_4)_2\text{S}_2\text{O}_8$ and the calculated yields of SO_4^- for reaction 1 (lowest curve). For measurements of $G(\text{Cl}_2^-)$ solutions contained 0.05 M NaCl.



In Figure 5 the lowest curve presents the calculated yields of SO_4^- for reactions of e_{aq}^- and e^- with $k = 1.06 \times 10^{10} \text{ M}^{-1} \text{ s}^{-1}$ for dilute solutions and $k = 1.8 \times 10^{10} \text{ M}^{-1} \text{ s}^{-1}$ for concentrated solutions from the work of Lam and Hunt.¹² The next curve (●) presents the measured $G(\text{SO}_4^-)$ for solutions of $(\text{NH}_4)_2\text{S}_2\text{O}_8$. The top curve (O) gives $G(\text{Cl}_2^-)$ for solutions of persulfate which also contained 0.05 M NaCl. The spectra for both transients were measured for comparison with the literature and they have been reported, together with the rate constant for reaction 5, for which $k_5 = 1.3 \times 10^8 \text{ M}^{-1} \text{ s}^{-1}$ at low concentrations.²



The nearly constant difference between $G(\text{Cl}_2^-)$ and $G(\text{SO}_4^-)$ in Figure 3 correlates with a slow reaction which appears to be first order in $[\text{S}_2\text{O}_8^{2-}]$ and is tentatively attributed to step 4. However, since $[\text{NaCl}]$ was only 0.05 M it was not adequately time resolved from eq 5.

To examine this effect further, the slow increase of $G(\text{Cl}_2^-)$ was measured at various $[\text{NaCl}]$ for 0.1 M $(\text{NH}_4)_2\text{S}_2\text{O}_8$ and the results are presented in Table I. For solutions containing only NaCl, the optical density in column 3, nominally attributed to Cl_2^- , contains an appreciable contribution from ClOH^- .² Both of these components contribute to the OD's of columns 4 and 6. They are removed by subtraction to give the data in columns 5 and 7.

There are three components in $G(\text{Cl}_2^-)$. One is due to prompt electron transfer from Cl^- to H_2O^+ , the second to reactions 1, 2, and 5 which are fast at $\geq 1 \text{ M NaCl}$,² and the third is due to the relatively slow sequence eq 4 + 5. The second of these components, $\Delta G(\text{Cl}_2^-)_{t=0}$ in column 5, is constant for 1–5 M NaCl and the average value has been adopted. The values for $\text{OD}(\text{Cl}_2^-)_{t=\infty}$ in column 6 include all three components and were corrected for slow decay by linear extrapolation to $t = 0$. Yields $\Delta G(\text{Cl}_2^-)_{t=\infty}$ in column 7 have been corrected for contributions from column 3. The yields in columns 8 and 9 measure the slow component. For 1–5 M NaCl these yields were fully time resolved and can also be obtained from the difference of columns 4 and 6.

At $\geq 1 \text{ M NaCl}$ the slow growth is due almost entirely to reaction 4 and $k \approx 2 \times 10^8 \text{ M}^{-1} \text{ s}^{-1}$.

An attempt to develop $\text{S}_2\text{O}_8^{2-}$ as a scavenger for H by scavenging electrons with Cd^{2+} was unsuccessful. In 0.1 M $\text{S}_2\text{O}_8^{2-}$, $G(\text{SO}_4^-)$ was unchanged by 0.5, 1, and 2 M $\text{Cd}(\text{ClO}_4)_2$. Simultaneous measurements at 310 and 460 nm showed that Cd^+ decayed and SO_4^- increased. Consequently, Cd^+ is oxidized and the final $G(\text{SO}_4^-)$ is unchanged.

Discussion

Chloride Ion. The very weak dependence of $G(\text{Cl}_2^-)$ on $[\text{Cl}^-]$ above 0.1 M in Figure 1 indicates that mostly homogeneously distributed OH is contributing to the measured yield, except for some direct ionization of Cl^- . A yield of 3.0 for Cl_2^- from Figure 1 is approximately the expected value of the primary yield of OH at 10 ns. It is well known that the yield of H_2O_2 is strongly suppressed by Cl^- at low pH by efficient scavenging of precursor OH in the spurs.¹³ Consequently, Cl and Cl_2^- in the spurs must also dimerize with about the same efficiency as CH. The combined yields of Cl_2 and Cl_3^- , $\sim 1.2 \text{ Cl}/100 \text{ eV}$, though only approximate, supports this interpretation. If the primary yield of H_2O_2 is taken to be 0.80, then only a total $G(\text{OH}) = 4.6$ can be accounted for. Since $G^0(e^-) = 5.2$,⁶ there may be an undetected oxidized radiolytic product, but not at high pH as Allen has proposed.⁹

At large $[\text{Cl}^-]$ a considerable fraction of the yield of Cl_2^- in Figure 1 is produced directly by H_2O^+ , given by the lower curve. There is no evidence of this in the upper curve. The lifetime of H_2O^+ is $\sim 10^{-14} \text{ s}^2$ and that of OH, for these experiments, $\sim 10^{-10} \text{ s}$. Consequently, the spatial distribution of Cl and its daughter species should be substantially independent of the relative contributions of the two mechanisms. The rather small change in $G(\text{Cl}_2^-)$ from $[\text{H}^+][\text{Cl}^-] = 10^{-2}$ to 16 implies that $-\Delta G(\text{H}_2\text{O}_2) \approx G(\text{Cl}_2^-) + G(\text{Cl}_3^-)$.

The similarity of results for NaCl and HCl shows the unimportance of direct action on cations, already noted for LiCl and BaCl_2 .² It also shows the independence of the primary yield G_{OH} on $[\text{H}^+]$ in the range observed. The data of Anbar and Thomas,¹⁴ for more dilute solutions, show that for a constant $[\text{H}^+][\text{Cl}^-]$, $G(\text{Cl}_2^-)$ is independent of pH. Stradowski has recently found that the yield of Cd^+ is independent of pH in the range 7 to 0.¹⁵

Iodide Ion. Figure 3 shows that $G(\text{I}_3^-) = -\Delta G(\text{H}_2\text{O}_2)$, that I_3^- forms in the spur, and that the rate constants for reactions

TABLE I: Slow Increase of $G(\text{Cl}_2^-)$ in Solution of NaCl with 0.1 M $(\text{NH}_4)_2\text{S}_2\text{O}_8$

$[\text{Cl}^-]$, M	$[\text{S}_2\text{O}_8^{2-}]$, M	OD- $(\text{Cl}_2^-)_{t=0^a}$	OD- $(\text{Cl}_2^-)_{t=0^b}$	ΔG - $(\text{Cl}_2^-)_{t=0^c}$	OD- $(\text{Cl}_2^-)_{t=\infty}$	ΔOD - $(\text{Cl}_2^-)^f$	ΔOD - $(\text{Cl}_2^-)^{e,g}$	ΔG - $(\text{Cl}_2^-)^{e,h}$	$\Delta G(\text{Cl}_2^-)$ calcd
0.1	0	0.05							
0.1	0.1		~1.4	(4.30) ^d	2.44	2.39	0.87	2.5	2.4
0.5	0	0.23							
0.5	0.1		~1.6	(4.30) ^d	2.38	2.15	0.63	1.8	2.1
1.0	0	0.41							
1.0	0.1		0.96	4.38	2.54	2.13	0.61	1.7	1.7
1.5	0	0.54							
1.5	0.1		2.09	4.38	2.53	1.99	0.47	1.3	1.4
2.0	0	0.62							
2.0	0.1		2.12	4.23	2.40	1.78	0.26	0.7	1.1
3.0	0	0.79							
3.0	0.1		2.27	4.17	2.42	1.63	0.11	0.3	0.6
5.0	0	0.98							
5.0	0.1		2.52	4.34	2.46	1.48	~0	~0	0
				Av 4.30 ± 0.08	2.45 ± 0.05				

^a The prompt yields of Cl_2^- from H_2O^+ and of ClOH^- , from Cl^- only, observed previously. ^b These yields include a second component from reaction 5, not well resolved from the slow component in 0.1 and 0.5 M NaCl. ^c From the difference of columns 3 and 4. ^d The average value for ≥ 1 M NaCl. ^e These yields are due to the slow component time resolved. ^f Column 6 minus column 3. ^g Column 7 minus column 5. ^h From column 8.

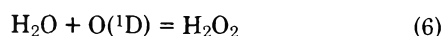
between $\text{OH} + \text{OH}$, $\text{OH} + \text{I}_2^-$, $\text{I}_2^- + \text{I}_2^-$, and so on, are rather similar. This is to be expected if all reactions are substantially diffusion controlled. It suggests that there may be appreciable losses of I_2^- and I_3^- by spur reactions with e_{aq}^- and H by analogy with reactions of OH. Analogously, the limiting yield, $G(\text{Cd}^+) = 5.2$,⁶ is a minimal value.

The higher yields of I_2^- relative to Cl_2^- are due in part to a weak linear dependence which suggests greater direct ionization, but mostly from an effect of acid in the spur.

The dependence of $G(\text{I}_2^-)$ on pH in Figure 4 is not due to an effect on $G(\text{OH})$. The change in yield is due to the limited lifetime of a reactive precursor since the maximum optical density was achieved at ~ 50 ns in all solutions. For acidic solutions in Figure 2 the maximum OD was reached within 10 ns of the end of the pulse for both I_2^- and I_3^- , indicating that the lifetime depends upon $[\text{H}^+][\text{I}^-]$.

The selection of a pH-sensitive transient precursor of I_2^- and I_3^- depends on three critical considerations. One is that it must be able to convert spontaneously into a much less reactive species (and thereby escape detection at low scavenger concentrations), or convert to OH or H_2O_2 , or react similarly. Another is that the total yield increases with $[\text{I}^-]$ as well as with $[\text{H}^+]$, even at concentrations far greater than are required for efficient scavenging of OH. Concurrent or fast consecutive action is required. The third is that if only one precursor species is involved, it must produce two one-electron oxidations of I^- since both $G(\text{I}_3^-)$ and $G(\text{I}_2^-)$ were increased by acid. The additional I_3^- cannot be attributed to a conventional spur reaction because $\Delta G(\text{I}_3^-)$ was about three times greater than $\Delta G(\text{I}_2^-)$, indicating a geminate pair of I atoms, and the spur is already quite acidic.

Excited molecular species do not satisfy the second and third critical requirements. This can be seen at once for H_2O^* , OH^* , and $\text{OH}^{*\cdot}$. There remain $\text{O}(^3\text{P})$ and $\text{O}(^1\text{D})$ as the least implausible candidates. The latter was shown by Taube to generate H_2O_2 quantitatively¹⁶ by reaction 6 (which satisfies the lifetime condition)

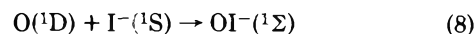


whereas in the low pressure vapor the process is



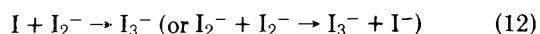
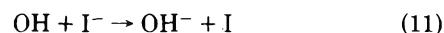
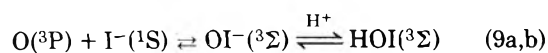
with $k_7 = 1.8 \times 10^{10} \text{ M}^{-1} \text{ s}^{-1}$ and somewhat slower than collision controlled.¹⁷ Since $\Delta H_7 = -2.8$ eV in the vapor, the product in reaction 6 is collision stabilized in water.

If $\text{O}(^1\text{D})$ is responsible for the effects under consideration, the first step is expected to be



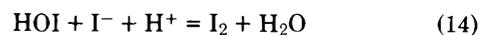
for which $\Delta H_8 = -3.4$ eV. Consequently, the efficiency of scavenging $\text{O}(^1\text{D})$ depends strongly on $[\text{I}^-]$ and weakly on $[\text{H}^+]$, contrary to observation. At neutral pH, OI^- does not yield I_3^- , but in the acidic spur the reaction is fast. This may contribute to $G(\text{oxid})$ at neutral bulk pH, however, and is not inconsistent with Figure 3. It may account for the difference between $G(\text{I}_2^-)$ and $G(\text{Cl}_2^-)$, amounting to ~ 0.6 .

In terms of $\text{O}(^3\text{P})$, deferring the problem of its spontaneous disappearance, the mechanistic steps 9 through 13 are proposed:



From the electron affinity of I_2 , 2.58 eV,¹⁸ $\Delta H_f(\text{I}_{2\text{aq}}^-) \simeq -3.9$ eV. Reaction of $\text{HOI}(^1\Sigma)$ with I_{aq}^- is then nearly thermo-neutral and step 10 must be exothermic. Since OI_{aq}^- is yellow, the $^3\Sigma$ state lies below ~ 3.0 eV. Formation of $\text{HOI}(^1\Sigma)$ from $\text{O}(^3\text{P})$ is exothermic by ~ 3.4 eV and for $\text{HOI}(^3\Sigma)$ it is still exothermic. There is no evident thermochemical implausibility in the proposed mechanism and no need for a termolecular mechanism which would produce $\text{I}_2(^3\Sigma)$.

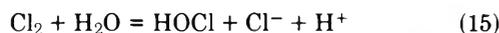
The rate constant for a reaction attributed to



has been reported¹⁹ to be $1.3 \times 10^{10} \text{ M}^{-1} \text{ s}^{-1}$, but a "considerably" smaller value was also proposed.²⁰ This is not inconsistent with two one-electron oxidations and the fast

overall reaction observed, about tenfold slower than a diffusion controlled bimolecular process.

The analogous reaction with HOCl is slow since $K_{15} \approx 10^{-4}$ and this is



consistent with the insensitivity of $G(\text{Cl}_2^-)$ on $[\text{H}^+]$ in Figure 1.

Mechanism 9–13 can also account qualitatively for decay of the precursor unless $[\text{H}^+][\text{I}^-] \geq 10^{-3}$, indicating that $\text{HOI}({}^3\Sigma)$ is a much stronger acid than $\text{HOI}({}^1\Sigma)$. Rate constants for reactions 9a and 10 must be $\geq 10^9 \text{ M}^{-1} \text{ s}^{-1}$.

Reaction 11 is very fast and reaction 12 describes the reaction of geminate species from consecutive reactions.

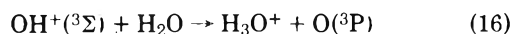
There must be an efficient mechanism to reduce the lifetime of $\text{O}({}^3\text{P})$. Conversion to OH is rather endothermic and it may be necessary to postulate formation of $\text{H}_2\text{O}_2({}^3\text{B})$. The corresponding formation of $\text{H}_2\text{O}_2({}^1\text{A})$ is 1.4 eV exothermic and the mechanism requires $\Delta H \leq 1.4 \text{ eV}$ for ${}^1\text{A} \rightarrow {}^3\text{B}$. Since $D(\text{HO}-\text{OH}) = 2.12 \text{ eV}$, the proposed reaction is not excluded.

There is also a quite simple way to account approximately for the disappearance of $\text{O}({}^3\text{P})$ within $\sim 10^{-7} \text{ s}$, viz., by spur reactions. The doublets e_{aq}^- , H, and OH can probably react very rapidly with $\text{O}({}^3\text{P})$ in the spur to form O^- , OH, and HO_2 and reduce the $\Delta G(\text{oxid})$ from 0.35 to considerably less than half as much since the combined $G^\circ(\text{doublets})$ is ~ 10 . This small residual yield would be rather difficult to detect at $> 10^2 \text{ ns}$ because slow growth of I_3^- , e.g., cannot be resolved from slow decay.

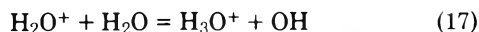
The greater part of the $\Delta G(\text{oxid})$ from I^- , indicated by $G(\text{I}_2^-) - G(\text{Cl}_2^-) \approx 0.6$, arises from the acidity of the spur at neutral bulk pH by eq 9 and 10. Consequently, the primary yield of $\text{O}({}^3\text{P})$ may be ~ 1.0 equiv (or 0.5 atoms/100 eV).

The highest yield in Figure 2 is $G(\text{oxid}) = 4.9$ and for 1 M Cd^{2+} , $G(\text{Cd}^+) = 4.9$, but the yields are not directly comparable since $G(\text{cations}) = G(\text{oxid}) - G(\text{OH}^+)$, by hypothesis. Also, Cd^+ was produced principally by dry electrons, but under the present conditions there is no evidence for H_2O^+e^- recombination not followed formation of OH. The value $G(e_{\text{aq}}^-) \approx 4.0$ at 30 ps⁶ is probably the appropriate yield for the present purpose. If $G(\text{OH}^+) \approx 0.5$, as proposed, then $G(\text{cations}) \approx 4.9 - 0.5$, about the same as $G(e_{\text{aq}}^-)$.

Formation of $\text{O}({}^3\text{P})$ is almost a logical necessity, although its chemistry is not very well known. About 18% of the ionizations of water vapor produce OH^+ which then reacts by



This reaction was observed by Thynne and Harrison²¹ to have the same rate constant as



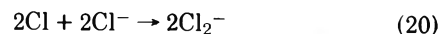
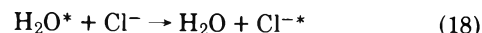
Consequently, simple electron transfer cannot be a dominant process in the low-pressure vapor. Since $\Delta H_{16} = -1.52 \text{ eV}$, these authors concluded that $\text{O}({}^3\text{P})$ was formed.

Ryan²² found that reaction 17 is very fast at low kinetic energy, $< 0.8 \text{ eV}$, while charge transfer only occurs at $> 0.8 \text{ eV}$. Consequently, there is a possibility that $G \approx 1$ for $\text{O}({}^3\text{P})$ in water, or $\sim 18\%$ of $G^2(e^-) = 5.2$.

Persulfate Ion. It is uncertain whether $G(\text{SO}_4^-)$ at large $[\text{S}_2\text{O}_8^{2-}]$ in Figure 5 contains a contribution from excited states. The difficulty rests on the uncertainty in primary G_{H} under these conditions, since $\text{S}_2\text{O}_8^{2-}$ is an efficient scavenger for both dry and hydrated electrons¹² as well as for H atoms. Stradowski¹⁵ used the H-atom adduct of acetophenone as a measure of the primary yield of G_{H} at 10^{-8} s . The yield de-

creased smoothly from 0.92 to 0.55 as $[\text{Cd}^{2+}]$ increased to $\geq 0.5 \text{ M}$. If this result is due only to suppression of H by electron scavenging, then the predicted yield of $G(\text{SO}_4^-)$ is 5.2 for electrons⁶ and 0.55 for H. The observed yield was 5.7 at $\sim 0.5 \text{ M S}_2\text{O}_8^{2-}$ and there is no clear evidence for a contribution from excitation.

The difference $\Delta G(\text{oxid}) = G(\text{Cl}_2^-) - G(\text{SO}_4^-)$ in Figure 5, about 1.2, is attributed to excited states, represented arbitrarily by H_2O^* , according to the reactions



The data of Table I provide indirect qualitative support for those of Figure 5 as regards $\Delta G(\text{oxid})$. Excepting the solution containing 0.1 M NaCl from Table I, even approximate comparisons are not possible. Observed values of $\Delta G(\text{Cl}_2^-)_{t=0}$ in column 5 are less than expected. However, it is $\Delta G(\text{Cl}_2^-)_{t=\infty}$ in column 9 with which we are particularly concerned and these differences are relatively less subject to errors of measurement and interpretation.

Formation of Cl^{*-} cannot arise from direct excitation of Cl^- because the yield is greatest in 0.1 M NaCl. The decrease of $G(\text{Cl}_2^-)$ with increasing $[\text{NaCl}]$ is not due to self-quenching because the growth half-time decreases only about 50% from 0.5 to 5 M NaCl, approximately that expected for kinetic salt effect. Efficient energy transfer from Cl^{*-} to 10^{-4} M TI^+ requires a long-lived state, $\text{Cl}^-({}^3\text{P}_1)$,⁸ which then implies $\text{H}_2\text{O}({}^3\text{B}_1)$ at 6.65 eV.⁷ The latter excludes direct excitation by electrons with energy much above resonance. A plausible mechanism is dry electron recombination with H_2O^+ , with partial randomization of spins in the spur. The primary yield of these recombinations is $\geq 1.2/100 \text{ eV}$ since $G^c(\text{Cd}^+)$ is 5.2 for dry electron scavenging while $G^\circ(e_{\text{aq}}^-)$ is ~ 4.0 .³ The latter value is expected to apply for material balance.

To assess the possibility that $\text{H}_2\text{O}({}^3\text{B}_1)$ is produced principally by recombination, the yields of column 9 were compared with earlier yields of Cl_2^- from electron transfer. They are approximately linearly related according to

$$\Delta G(\text{Cl}_2^-)_{t=\infty} = 2.5 - 1.2G(\text{Cl}_2^-)_{t=0} \quad (21)$$

The factor 1.2 arises from the fitted 50% efficiency to yield $\text{H}_2\text{O}({}^3\text{B}_1)$ and formation of 2SO_4^- for each $\text{Cl}^-({}^3\text{P}_1)$. The calculated values appear in column 10 of Table I. The model provides too weak a dependence on $[\text{NaCl}]$ at high concentrations and there may be additional fast quenching mechanisms in the spur. There are, for example, three triplet states of Cl_2 in the range 2.2 to 8.4 eV and probably related states of Cl_3^- . In addition ClOH^- may be effective.

References and Notes

- (1) The Radiation Laboratory of the University of Notre Dame is operated under contract with the U.S. Energy Research and Development Administration. This is ERDA Document No. COO-38-1043.
- (2) K.-J. Kim and W. H. Hamill, *J. Phys. Chem.*, preceding paper in this issue.
- (3) J. W. Hunt, R. K. Wolff, and S. G. Chenery, "Fast Processes in Radiation Chemistry and Biology", G. E. Adams, E. M. Fielden, and B. D. Michael, Ed., The Institute of Physics and Wiley, London, 1975, p. 109.
- (4) G. Zimmerman and F. C. Strong, *J. Am. Chem. Soc.*, **79**, 2063 (1957).
- (5) M. M. Fisher and W. H. Hamill, *J. Phys. Chem.*, **77**, 171 (1973).
- (6) Cz. Stradowski and W. H. Hamill, *J. Phys. Chem.*, **80**, 431 (1976).
- (7) C. Naleway, Ph.D. Dissertation, University of Notre Dame, 1973.
- (8) T. Huang and W. H. Hamill, *J. Phys. Chem.*, **79**, 2465 (1975).
- (9) A. O. Allen, *Radiat. Res.*, **51**, 269 (1972).
- (10) Formation of I^+ would also yield I_3^- , but the cross section is expected to be small.

- (11) E. Hayon, *Trans. Faraday Soc.*, **61**, 723 (1965).
 (12) K. Y. Lam and J. W. Hunt, *Int. J. Radiat. Phys. Chem.*, **7**, 317 (1975).
 (13) A. O. Allen, "The Radiation Chemistry of Water and Aqueous Solutions", Van Nostrand, Princeton, N.J., 1961.
 (14) M. Anbar and J. K. Thomas, *J. Phys. Chem.*, **68**, 3829 (1964).
 (15) Cz. Stradowski, unpublished results.
 (16) H. Taube, *Trans. Faraday Soc.*, **53**, 656 (1957).
 (17) D. Biedenkapp, L. G. Hartshorn, and E. J. Blair, *Chem. Phys. Lett.*, **5**, 379 (1970).
 (18) W. A. Chupka, J. Berkowitz, and D. Gutman, *J. Chem. Phys.*, **55**, 2724 (1971).
 (19) E. Abel, *Z. Phys. Chem.*, **136**, 161 (1928).
 (20) H. A. Liebafsky, *J. Am. Chem. Soc.*, **54**, 3499 (1932).
 (21) J. C. D. Thynne and A. G. Harrison, *Trans. Faraday Soc.*, **62**, 2468 (1966).
 (22) K. R. Ryan, *J. Chem. Phys.*, **52**, 6009 (1970).

Spin Trapping of Cyanoalkyl Radicals in the Liquid Phase γ Radiolysis of Nitriles

S. W. Mao[†] and Larry Kevan*

Department of Chemistry, Wayne State University, Detroit, Michigan 48202 (Received April 23, 1976)

The following radicals have been identified in the liquid phase γ radiolysis of several nitriles by spin trapping with phenyl *tert*-butyl nitron: CH_2CN in acetonitrile, H and $\text{CH}_3\text{CHCN}(\text{?})$ in propionitrile, $\text{CH}(\text{CN})_2$ in malononitrile, and H, CN, and $\text{CH}_2\text{CH}_2\text{CN}$ in succinonitrile. γ proton splittings are observed for the CH_2CN and $\text{CH}(\text{CN})_2$ spin adducts. The results are discussed in comparison with solid phase radiolysis data and with alkyl radical spin adduct splittings.

Introduction

The radicals produced in the γ radiolysis of alkyl cyanides (nitriles) have been studied to some extent in the solid phase by electron paramagnetic resonance (EPR), but definite radical identification has proved difficult due to lack of spectral resolution.¹ Here we report liquid phase studies on acetonitrile, propionitrile, malononitrile, and succinonitrile in which the radicals produced by γ radiolysis are "spin trapped" by addition to phenyl *tert*-butyl nitron (PBN) to form a radical stable in solution.² PBN is advantageous as a spin trap because it forms a very stable radical adduct, but its main disadvantage is that the spin adduct does not generally show hyperfine couplings from magnetic nuclei in the trapped radical itself. The EPR spectrum of the spin adduct with PBN is generally a triplet of doublets due to splitting by the nitrogen and the β proton. The identification of the trapped radicals is based on small changes in the magnitudes of the nitrogen and β -proton coupling constants of PBN which vary with the size and electronegativity of the trapped radical. Positive identification of the trapped radical is dependent upon synthesis of a series of spin adducts and correlations from the trends deduced. However, for several of the cyanoalkyl radicals reported here, the hyperfine structure of the trapped radical in the PBN spin adduct is resolved. This seems to be related to the electronegativity of the cyano group.

Experimental Section

The nitriles were obtained from Aldrich Chemical Co. and Fisher Chemical Co. Acetonitrile (CH_3CN) and propionitrile ($\text{CH}_3\text{CH}_2\text{CN}$) were further purified by repeated distillation.

[†] Current address: Department of Chemistry, Tunghai University, Taichung, Taiwan.

Malononitrile (NCCH_2CN) and succinonitrile ($\text{NCCH}_2\text{CH}_2\text{CN}$) were purified by vacuum sublimation. Purified PBN was obtained from Dr. N. A. LeBel of this Department. Samples were prepared by dissolving some PBN into the above compounds. The solution was then degassed under vacuum and sealed in a 2-mm i.d. Spectrosil quartz tube. The γ irradiation was usually carried out at room temperature to a typical dose of 0.02 Mrad in a ^{60}Co source with a dose rate of ~ 0.23 Mrad/h. The EPR spectra were obtained with a Varian E-4 spectrometer.

After a spin adduct was formed, the solvent could be changed, if desired, by pumping out the original solvent under vacuum and distilling another solvent (typically benzene) into the sample tube.

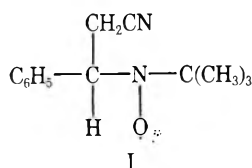
Most spin adducts were found to be very stable; they typically lasted for several days. Nevertheless, fresh samples were prepared for each run, and EPR spectra were taken immediately after γ irradiation to avoid complications from slow secondary reactions.

Results

Acetonitrile (CH_3CN). For a typical dose of 0.02 Mrad an EPR spectrum similar to that shown in Figure 1 is obtained for 0.1 M PBN in acetonitrile. The EPR spectrum can be observed after only 0.002 Mrad dose, increases with dose to 0.01 Mrad, and then remains constant at higher doses. Identical spectral were also obtained for PBN concentrations down to 0.01 M. Although a large concentration of the radical cannot be produced by high irradiation dose, the adduct radical is stable for as long as several days at room temperature. The six-line triplet of doublets typical of PBN spin adducts is further split into approximately 1:2:1 triplets which are attributed to the hyperfine splitting of two equivalent γ protons. The radical trapped by PBN is thus identified as $\cdot\text{CH}_2\text{CN}$. The spin adduct has the following structure:

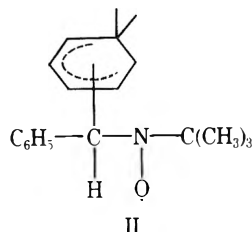


Figure 1. EPR spectrum of the spin adduct in γ irradiated 0.1 M phenyl *tert*-butyl nitron in acetonitrile (CH_3CN) at room temperature at 0.2 Mrad dose in benzene solvent. The spectrum is assigned to the $\cdot\text{CH}_2\text{CN}$ adduct.



where radical I has the following splitting constants: $A^{\text{N}} = 14.9$ G, $A_{\beta}^{\text{H}} = 3.9$ G, and $A_{\gamma}^{\text{H}} = 0.65$ G when CH_3CN is used as solvent.

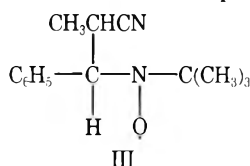
A good comparison of splitting constants for various spin adducts can be made only if they are in same solvent. We have used benzene as a common solvent throughout the work since many previous data compiled for PBN spin adducts were obtained in benzene. First, we attempted to use a mixture of CH_3CN and benzene as a solvent. However, upon γ irradiation of benzene the cyclohexadienyl radical is also produced.³ Therefore, in addition to radical I, we observed a second spin adduct presumably due to the trapping of cyclohexadienyl radical by PBN, i.e.



The splitting constants measured for this radical in pure benzene are: $A^{\text{N}} = 14.5$ G and $A_{\beta}^{\text{H}} = 2.25$ G. Both the nitrogen and β proton splittings are distinctly larger than for the phenyl radical trapped by PBN.⁴ We believe the assignment of radical II seems quite reasonable.

Since the spectrum was complicated by the occurrence of two spin adduct species, an alternate method was used to produce radical I in pure benzene. Radical I was first produced in acetonitrile, the solvent was then pumped off, and benzene was added to the spin adduct on a vacuum line. Figure 1 shows the EPR spectrum of radical I in benzene, where $A^{\text{N}} = 14.7$ G, $A_{\beta}^{\text{H}} = 3.7$ G, and $A_{\gamma}^{\text{H}} = 0.6$ G. The solvent effect is found to be very small for radical I. Splitting constants of radical II, however, were found to be quite sensitive to solvent. This will be discussed in the succinonitrile section.

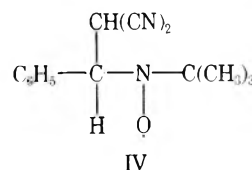
Propionitrile ($\text{CH}_3\text{CH}_2\text{CN}$). Upon irradiating 0.1 M PBN in propionitrile to a dose of 0.02 Mrad, only one spin adduct is observed. The splitting constants are $A^{\text{N}} = 14.8$ G and $A_{\beta}^{\text{H}} = 3.65$ G; no γ proton splittings are observed. In benzene these splitting constants are $A^{\text{N}} = 14.6$ G and $A_{\beta}^{\text{H}} = 3.6$ G so there is little change with solvent. Assuming an α proton is most easily lost, a possible structure of this spin adduct is



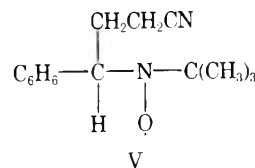
although the $\cdot\text{CH}_2\text{CH}_2\text{CN}$ adduct is also quite possible.

At lower dose, <0.008 Mrad, a second species is observed with $A^{\text{N}} = 13.9$ G and $A_{\beta}^{\text{H}} = 2.4$ G, but it disappears upon further irradiation. These splittings, in particular the small β proton splitting, appear similar to the splittings for phenyl and substituted phenyl spin adducts⁴ and may suggest a radical derived from an impurity species. The $\cdot\text{CH}_2\text{CH}_2\text{CN}$ adduct is expected to have splitting similar to those for radical III so it is not assigned to the new low dose spectrum. The H atom spin adduct is also observed with $A^{\text{N}} = 15.5$ G and $A_{\beta}^{\text{H}} = 8.2$ G at low dose when the PBN concentration is increased to 0.2 M. The large A_{β}^{H} splitting is quite distinctive for H atom adducts. Figure 2 shows the EPR spectrum of 0.2 M PBN in $\text{CH}_3\text{CH}_2\text{CN}$ after a γ dose of 0.008 Mrad with benzene as solvent. The H atom adduct, the CH_3CHCN adduct (III), and the possible impurity adduct are all observed. Figure 3 shows the EPR spectrum of only radical III in benzene.

Malonitrile (NCCH_2CN). Figure 4a shows the EPR spectrum taken at 310 K of PBN in $\text{CH}_2(\text{CN})_2$ with a mole ratio of approximately 1:100 after γ irradiation to a dose of 0.02 Mrad at 310 K. Identical spectra are obtained at room temperature except that the high field lines are broader. When benzene is added, the splitting constants change significantly as shown in Figure 4b. The solubility of $\text{CH}_2(\text{CN})_2$ in benzene is low; the most concentrated solution that can be obtained is about 0.4 M. However, at lower concentrations of $\text{CH}_2(\text{CN})_2$ the values of A^{N} and A_{β}^{H} are almost constant. Therefore the values for the splitting constants are considered to be valid values for benzene solvent. The γ proton splitting is also resolved. The doublet γ hyperfine splitting indicates that the structure of the trapped radical is $\cdot\text{CHX}_2$; the spin adduct can be immediately identified as



Succinonitrile ($\text{NCCH}_2\text{CH}_2\text{CN}$). When PBN is dissolved in succinonitrile in a mole ratio of 1:50 (PBN:succinonitrile), only one spin adduct is found after the sample has been γ irradiated. The splitting constants are $A^{\text{N}} = 14.7$ G and $A_{\beta}^{\text{H}} = 3.75$ G. In benzene the spin adduct has essentially the same splitting constants. These values are extremely close to the values obtained for radical III; the line width is also similar in both cases, 1.05 G for radical III compared to 1.0 G for the radical observed here. The spin adduct observed may well be the same as radical III. However it is also possible that the spin adduct may be



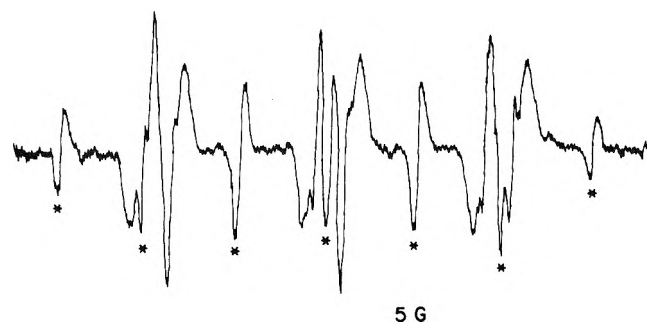


Figure 2. EPR spectrum of the spin adducts in γ irradiated 0.2 M phenyl *tert*-butyl nitron in propionitrile ($\text{CH}_3\text{CH}_2\text{CN}$) at room temperature after 0.008 Mrad dose in benzene solvent. Lines due to the H atom adduct are marked by asterisks. There appear to be two other spin adducts with characteristic six-line spectra which are assigned to the $\text{CH}_3\dot{\text{C}}\text{HCN}$ adduct and to a possible impurity adduct. At higher dose only the $\text{CH}_3\dot{\text{C}}\text{HCN}$ adduct spectrum is observed.

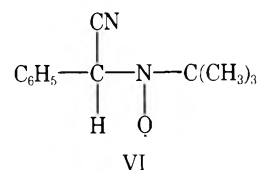
which is expected to have similar splitting constants to III. Radical V seems to be the best assignment since the $\cdot\text{CN}$ radical is also observed which will be discussed later. We could distinguish III from V if a γ proton splitting were observed, but none is.

If we dissolve succinonitrile in benzene and then add PBN, the results are quite interesting. At low concentrations of succinonitrile (≤ 0.3 M), we only observe the spin adduct of γ irradiated benzene, radical II. However, the splitting constants are increased slightly over the values in pure benzene and appear to increase with succinonitrile concentration. This

may suggest specific molecular interactions between the spin adduct and succinonitrile but we have not investigated this further.

Upon increasing the concentration of succinonitrile, an unresolved shoulder on each peak is observed, probably due to radical V, but we have never resolved this radical well in benzene solution under any conditions. Figure 5 shows the EPR spectrum of benzene containing 0.1 M PBN and 0.8 M succinonitrile after γ irradiation to a dose of 0.02 Mrad and Figure 6 shows the EPR spectrum of benzene containing 0.2 M PBN and 1.2 M succinonitrile at the same dose. The differences between Figures 5 and 6 are that the H atom spin adduct is clearly observed at the higher concentration of PBN and a broad shoulder background, attributed to radical V, is clearly shown in Figure 6. The H adduct has splitting constants of $A^{\text{N}} = 15.4$ G and $A_{\beta}^{\text{H}} = 8.1$ G.

There is a third spin adduct in Figures 5 and 6, most clearly shown in Figure 5, with a large splitting. After careful analysis, we concluded that these peaks are due to nitrogen triplets as shown by the stick diagram in Figure 5. The radical is assigned as



where $A^{\text{N}(1)} = 14.4$ G, $A_{\beta}^{\text{H}} = 5.5$ G, and $A^{\text{N}(2)} = 1.2$ G. This assignment seems very reasonable when the magnitudes of A_{β}^{H} for different cyanoalkyl spin adducts are compared. Table

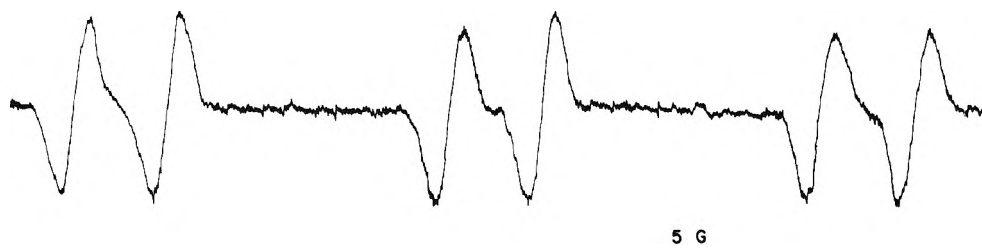


Figure 3. EPR spectrum of the spin adduct in γ irradiated 0.1 M phenyl *tert*-butyl nitron in propionitrile ($\text{CH}_3\text{CH}_2\text{CN}$) at room temperature at 0.02 Mrad dose in benzene solvent.

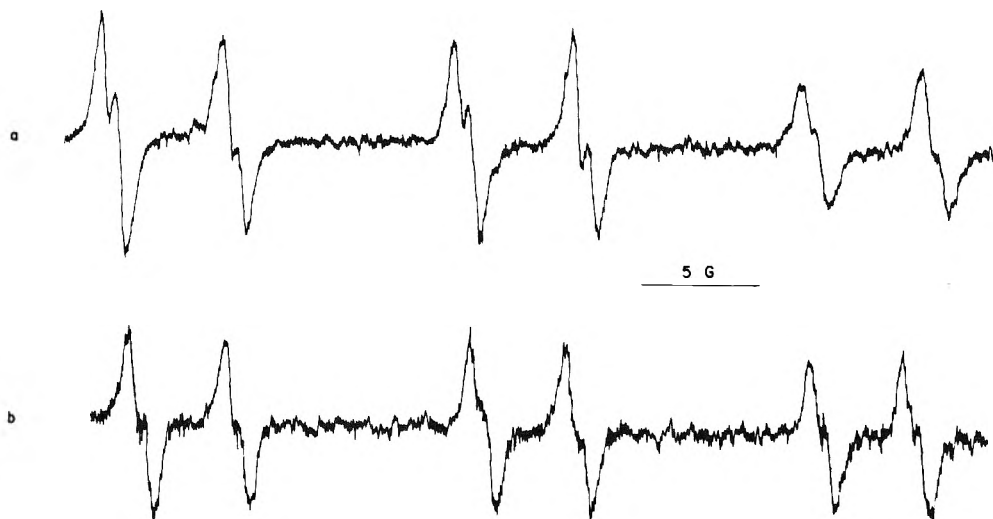


Figure 4. (a) EPR spectrum of phenyl *tert*-butyl nitron in malonitrile (NCCH_2CN) with mole ratio of 1:100 (PBN:NCCH₂CN) at 310 K after 0.02 Mrad ^{60}Co γ irradiation. The spectrum is assigned to the $\cdot\text{CH}(\text{CN})_2$ adduct. (b) EPR spectrum of the same radical as in (a) in benzene at room temperature.

TABLE I: Hyperfine Coupling Constants of *tert*-Butyl α -Substituted Benzyl nitroxides [$C_6H_5CHRNOC(CH_3)_3$] at Room Temperature

R	Solvent	$A^N,^a$ G	$A_{\beta}^H,^a$ G	$A_{\gamma}^H,^b$ G	$A_{\gamma}^N,^a$ G
CH ₂ CN	CH ₃ CN	14.9	3.9	0.65	
	C ₆ H ₆	14.7	3.7	0.6	
CH ₃ CHCN or CH ₂ CH ₂ CN	CH ₃ CH ₂ CN	14.8	3.6		
	C ₆ H ₆	14.6	3.6		
CH ₂ CH ₂ CN	NCCH ₂ CH ₂ CN	14.7	3.75		
	C ₆ H ₆	14.6	3.7		
CH(CN) ₂	CH ₂ (CN) ₂	14.8	5.0	0.68	
	C ₆ H ₆	14.5	3.9	0.65	
CN	C ₆ H ₆ ^c	14.4	5.5		1.2
H	CH ₃ CH ₂ CN	15.5	8.2		
H	C ₆ H ₆ ^c	15.4	8.1		
C ₆ H ₇	C ₆ H ₆	14.5	2.25		

^a ± 0.1 G. ^b ± 0.05 G. ^c 1.2 M succinonitrile, NCCH₂CH₂CN.

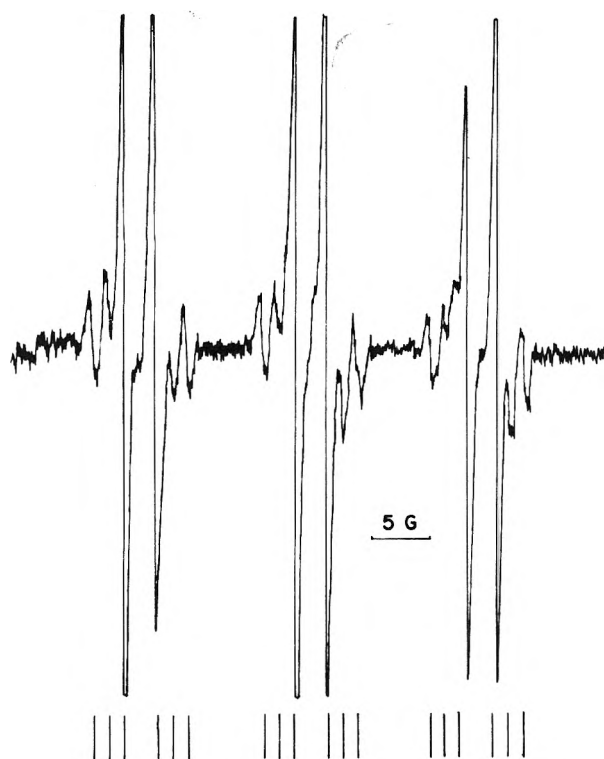


Figure 5. EPR spectrum of 0.1 M phenyl *tert*-butyl nitroxide and 0.8 M succinonitrile (NCCH₂CH₂CN) in benzene at room temperature after 0.02 Mrad ⁶⁰Co γ irradiation. The stick diagram shows the lines for the *tert*-butyl- α -cyanobenzyl nitroxide radical.

I summarize the splitting constants for the various cyanoalkyl and other spin adducts detected.

Discussion

Relation to Radiolysis Studies. In liquid acetonitrile radiolysis we observe a γ proton splitting in the PBN spin adduct and can definitely identify \cdot CH₂CN. Previous radiolysis studies of acetonitrile have been in the solid phase at 77 K where the radicals are trapped directly.⁵⁻⁹ A broad triplet is observed in the solid and is assigned to \cdot CH₂CN. In addition methyl radicals⁶ have been reported and hydrogen atoms⁹ have been implied in irradiated solid acetonitrile. We did not observe the CH₃ spin adducts under the same conditions that we observed the CH₂CN adduct and feel that this argues for its absence in liquid phase radiolysis. We are less confident

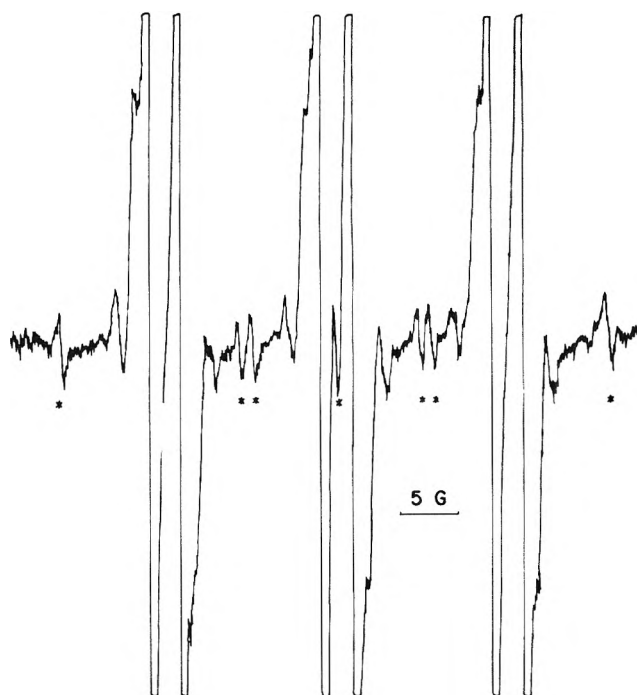


Figure 6. EPR spectrum of 0.2 M phenyl *tert*-butyl nitroxide and 1.2 M succinonitrile (NCCH₂CH₂CN) in benzene at room temperature after 0.02 Mrad ⁶⁰Co irradiation. The peaks with asterisks are due to the H atom spin adduct with PBN; two additional lines are buried under the two sets of outer doublets.

about the implications of not observing the H spin adduct. Although H adducts are observed in propionitrile and succinonitrile they are always weak and require high PBN concentrations. Thus we feel that H atoms are likely produced in liquid acetonitrile radiolysis but react too fast for significant spin trapping by PBN.

In liquid propionitrile radiolysis we definitely identify H and tentatively identify either CH₃CHCN or CH₂CH₂CN as present. The absence of a resolvable γ proton splitting might favor CH₂CH₂CN, but we also expect that an α proton would be more easily lost from the molecule. The EPR spectrum of irradiated solid propionitrile at 77 K has been interpreted as CH₃CHCN but the intensity ratio of the EPR lines cannot be described by this radical alone.⁸ C₂H₅ and CH₃CHCN have been reported in another study,⁶ but we feel we would have spin trapped C₂H₅ if it were formed in the liquid phase radiolysis.

In liquid malonitrile radiolysis we can observe a γ proton splitting and can definitely identify $\text{CH}(\text{CN})_2$. We do not see the H adduct. However we postulate that H atoms are formed but react too readily for significant spin trapping by PBN. Irradiated malonitrile has been studied at 77 K⁶ but the spectra are complex and cannot readily be identified.

Our results in liquid succinonitrile radiolysis are of particular interest since we observe three radicals by spin trapping: H, CN, and $\text{CH}_2\text{CH}_2\text{CN}$. The identification of $\text{CH}_2\text{CH}_2\text{CN}$ is somewhat tentative, but it is strongly supported by the definite observation of CN. The observation of H adducts suggests that perhaps a radical such as CNCHCH_2CN is formed, but we do not believe much of this is formed or we would probably be able to identify it from its expected γ proton splittings. In solid succinonitrile at 77 K, EPR studies¹⁰ indicate that a dimeric molecule anion is formed which can be thermally bleached to give $\text{CH}_2\text{CH}_2\text{CN} + \text{CN}^-$. Our studies indicate that in the liquid some CN is formed by C-C bond scission.

Splitting Constant Trends. Table I shows that all four cyanoalkyl radical spin adducts have about the same splittings ($A^N \sim 14.6$ G and $A_{\beta}^H \sim 3.7$ G) when observed in the same solvent (benzene). These splittings are only slightly larger than those for alkyl radicals (methyl, ethyl, butyl) in benzene for which $A^N \sim 14.1$ G and $A_{\beta}^H \sim 3.2$ G.⁴ The small difference can perhaps best be attributed to a small shift in spin density from the nitroxide oxygen due to the more electronegative cyanoalkyl substituents. This electronegativity effect could account for the resolved γ proton splittings in the CH_2CN and $\text{CH}(\text{CN})_2$ spin adducts although it is somewhat surprising that the γ proton splitting in the $\text{CH}(\text{CN})_2$ adduct is not somewhat larger than the splitting in the CH_2CN adduct. The only other reported γ proton splitting in a PBN spin adduct of which we are aware is that for the gas phase trapping of CHO ($A^N = 14.02$ G, $A_{\beta}^H = 3.17$ G, $A_{\gamma}^H = 1.36$ G). This large γ proton splitting has not been explained, but electronegativity effects do not seem to be important.

The CN spin adduct shows only a slight decrease in A^N but a significant increase in A_{β}^H in benzene compared to the cyanoalkyl adducts. This may be consistent with a spin density shift due to the electronegativity of CN, but it could also be due to a small conformational change. The β proton splitting is related to the dihedral angle θ between the β hydrogen-carbon-nitrogen plane and the carbon-nitrogen-p orbital plane. From the approximate relationships¹² $A_{\beta}^H(\text{G}) \sim 50 \cos^2 \theta \rho_N$ and $A^N(\text{G}) \sim 35.6 \rho_N$, an A_{β}^H change from 3.7 to 5.5 G only corresponds to a change in θ from 65 to 59°. It is interesting to compare the CN adduct splittings with those for the Cl adduct in benzene ($A^N = 12.1$ G and $A_{\beta}^H = 0.75$ G).¹² The small A_{β}^H splitting for the Cl adduct has been attributed to a conformation with $\theta = 18^\circ$.

Acknowledgment. We are grateful for support of this work by the Energy Research and Development Administration under Contract No. E(11-1)-2086. We thank Dr. N. LeBel for providing the nitron.

References and Notes

- (1) L. Kevan, *Actions Chim. Biol. Radiat.*, **15**, 81-143 (1971).
- (2) E. G. Janzen, *Acc. Chem. Res.*, **4**, 31 (1971); M. J. Perkins, *Chem. Soc., Spec. Publ.*, No. 24, 97 (1970); C. Lagercrantz, *J. Phys. Chem.*, **75**, 3466 (1971).
- (3) S. Ohnishi, T. Tanei, and I. Nitta, *J. Chem. Phys.*, **37**, 2402 (1962).
- (4) E. G. Janzen and B. J. Blackburn, *J. Am. Chem. Soc.*, **91**, 4481 (1969).
- (5) P. B. Ayscough, H. Drawe, and P. Kohler, *Radiat. Res.*, **33**, 263 (1968).
- (6) P. B. Ayscough, R. G. Collins, and T. J. Kemp, *J. Phys. Chem.*, **70**, 2220 (1966).
- (7) K. Takeda and F. Williams, *Mol. Phys.*, **17**, 677 (1969).
- (8) N. V. Eliseeva, B. V. Kotov, V. A. Sharpatyi, and A. N. Pravednikov, *Opt. Spektrosk.* **18**, 842 (1965) (*Opt. Spectrosc.*, **18**, 470 (1965)).
- (9) D. Dubar, D. Hale, L. Harrah, R. Rondeau, and S. Zakanycz, *Develop. Appl. Spectrosc.*, **3**, 361 (1963).
- (10) A. Campion and F. Williams, *J. Chem. Phys.*, **54**, 4510 (1971).
- (11) E. G. Janzen, I. G. Lopp, and T. V. Morgan, *J. Phys. Chem.*, **77**, 139 (1973).
- (12) E. G. Janzen, B. R. Knauer, L. T. Williams, and W. B. Harrison, *J. Phys. Chem.*, **74**, 3025 (1970).

Enthalpy-Entropy Compensation. 1. Some Fundamental Statistical Problems Associated with the Analysis of van't Hoff and Arrhenius Data

R. R. Krug,^{*1a} W. G. Hunter,^{1b} and R. A. Grieger^{1a}

Chemical Engineering Department, and Statistics Department and Engineering Experiment Station, University of Wisconsin, Madison, Wisconsin 53706 (Received March 8, 1976)

A statistical analysis of the enthalpy-entropy compensation effect is presented. The correlation coefficient and functionality of the statistical compensation line are derived. A hypothesis test is proposed for application to enthalpy-entropy data to determine if any extrathermodynamic factors are distinguishable from the statistical compensation effect. A review of reported compensations in the literature reveals that detectable extrathermodynamic enthalpy-entropy effects are rare.

Introduction

Plots of enthalpies vs. entropies often form straight lines. Several standard chemistry texts^{2,3} treat these linear plots as authentic representations of an extrathermodynamic relationship, which is sometimes called the isokinetic effect, enthalpy-entropy compensation effect, or simply the compensation effect. Some authors⁴⁻⁶ believe the compensation is linear because of the functionality of the temperature dependence of the Hammett parameter. This functionality has not been verified experimentally, however.^{7,8}

Tables summarizing enthalpy-entropy data from the literature have been published^{2a,5} for which the correlation coefficient exceeds 0.95. Such high values of the correlation coefficient are taken to imply chemical causation for the linear correlations. Perhaps for this reason investigators still plot enthalpies vs. entropies and publish the resulting linear plots when the estimated correlation coefficients are near unity or, equivalently, when regression analysis gives a straight line that fits the data well.

In this paper reasons are given for believing that, when data are plotted in the usual way, the true functional dependence, if any, is usually masked by a dominant statistical compensation pattern that arises solely from experimental errors. That is, the observed distribution of data points along straight lines in the enthalpy-entropy plane is more often due to the propagation of measurement errors than to chemical variations. Presented here is a detailed analysis of the propagation of experimental errors pattern that is confounded with chemical variations. This pattern has previously been suspected⁹⁻¹⁷ but has not been adequately accounted for statistically.

In this article we review the statistics of the estimation situation for data plotted in the enthalpy-entropy plane. We derive the correlation coefficient and the slope of the regression line for the case in which the chemical variation is small compared to the experimental error. We also develop a hypothesis test for determining whether the observed compensation effect has a strong chemical contribution or whether the observed distribution of data in the enthalpy-entropy plane is indistinguishable from a statistical pattern generated by random errors.

This analysis only treats the case for which enthalpies, entropies, and free energies are estimated from the variation of rate or equilibrium constants with temperature. We do not treat the case for which enthalpies are determined by inde-

pendent calorimetric measurements or free energies are determined independently.

Theory

Both kinetic and equilibrium enthalpy and entropy determinations can be made using plots of experimental observations vs. inverse temperatures. The results of the analyses presented below will be identical for both cases because of the formal similarity of the rate and equilibrium constants with their respective thermodynamic parameters. Enthalpies are determined from the slopes of data on Arrhenius or van't Hoff plots and entropies are determined from the respective intercepts. Errors associated with the measurements, $\ln k_i$ and $\ln K_i$, are assumed to be normally and independently distributed with zero mean and constant variance. To avoid redundancy we present the details only for the case of kinetic observations.

A more complete analysis would take into account possible systematic deviations from van't Hoff and Arrhenius plots that are caused by large differences in standard heat capacities and heat capacities of activation. Since the data reviewed by us did not generally show such structured lack of fit to Arrhenius or van't Hoff plots, we did not treat this case in the following analysis.

I. *The Correlation Coefficient.* For estimation of activation enthalpy ΔH^\ddagger and activation entropy ΔS^\ddagger the Arrhenius equation is usually linearized so that the slope and intercept may be determined by ordinary linear regression. Thus the i th observation of data taken at n temperatures has the following temperature dependence

$$\ln k_i = \ln A - E/R \cdot 1/T_i$$

The complete data set may be summarized in matrix notation by

$$\mathbf{y} = \mathbf{X}\boldsymbol{\theta}$$

where the observation vector is $\mathbf{y}' = (\ln k_1, \ln k_2, \dots, \ln k_n)$, the parameter vector is $\boldsymbol{\theta}' = (\ln A, -E/R)$, and the design matrix is

$$\mathbf{X}' = \begin{bmatrix} 1 & 1 & \dots & 1 \\ 1/T_1 & 1/T_2 & \dots & 1/T_n \end{bmatrix}$$

Furthermore, enthalpies and entropies are determined from the estimates of $\boldsymbol{\theta}$.

$$\Delta S^\ddagger = R \ln A - R \ln (kT_e/h) = R\theta_1 + C_1$$

$$\Delta H^\ddagger = E - RT = -R\theta_2 + C_2$$

These relationships may be formulated as

$$\psi = \mathbf{Z}\theta + \mathbf{C}$$

where the thermodynamic parameter vector is $\psi = (\Delta S^\ddagger, \Delta H^\ddagger)$, the additive constant vector is $\mathbf{C} = (-R \ln (kT_e/h), -RT)$, and the matrix \mathbf{Z} is

$$\mathbf{Z} = \begin{bmatrix} R & 0 \\ 0 & -R \end{bmatrix}$$

Let a caret ($\hat{}$) denote an estimated value, for example, $\Delta \hat{H}^\ddagger$ is an estimate of ΔH^\ddagger . The correlation coefficient between $\Delta \hat{H}^\ddagger$ and $\Delta \hat{S}^\ddagger$ is determined from the elements of the variance-covariance matrix

$$\mathbf{V}(\hat{\psi}) = \mathbf{V} \begin{bmatrix} \Delta \hat{H}^\ddagger \\ \Delta \hat{S}^\ddagger \end{bmatrix} = \mathbf{Z}(\mathbf{X}'\mathbf{X})^{-1} \mathbf{Z}\sigma^2$$

$$= \begin{bmatrix} \sum (1/T)^2 & \sum 1/T \\ \sum 1/T & n \end{bmatrix} \frac{R^2\sigma^2}{\Delta}$$

where σ^2 is the variance of the observations y and Δ is the determinant of $\mathbf{X}'\mathbf{X}$. The correlation coefficient observed between $\Delta \hat{H}^\ddagger$ and $\Delta \hat{S}^\ddagger$ in the absence of any extrathermodynamic effect is^{18,19}

$$\rho = \frac{\text{Cov}(\Delta \hat{H}^\ddagger, \Delta \hat{S}^\ddagger)}{\sqrt{V(\Delta \hat{H}^\ddagger)}\sqrt{V(\Delta \hat{S}^\ddagger)}} = \frac{\sum 1/T}{\sqrt{n \sum (1/T)^2}}$$

Notice that this correlation coefficient depends only on the choice of experimental temperatures. The result is identical for equilibrium data because \mathbf{Z} and \mathbf{X} are the same for both the kinetic and equilibrium expressions. For equilibrium data, however, $\mathbf{y}' = (\ln K_1, \ln K_2, \dots, \ln K_n)$ and $\mathbf{C}' = (0, 0)$. It can be shown that, as the experimental temperature range becomes small, the correlation coefficient approaches unity. Note, for instance, in the limiting case if all the T 's are equal, $\rho = 1$. If the chemical variations in ΔH and ΔS are small compared to the uncertainty of the estimates of these parameters, the experiments are essentially replications and the estimated correlation coefficient r

$$r = \frac{\sum (\Delta H - \langle \Delta H \rangle)(\Delta S - \langle \Delta S \rangle)}{\sqrt{\sum (\Delta H - \langle \Delta H \rangle)^2} \sqrt{\sum (\Delta S - \langle \Delta S \rangle)^2}}$$

is an estimate of the population parameter ρ

$$\lim_{n \rightarrow \infty} r = \rho$$

The brackets ($\langle \rangle$) indicate an averaged quantity.

Thus data taken over narrow temperature ranges will have relatively uncertain enthalpy estimates and $\Delta H - \Delta S$ correlation coefficients approaching unity. In fact, whenever experimental errors are large compared to thermodynamic variations, the estimated correlation coefficient will tend toward ρ , which is usually much larger than 0.95. Wold¹⁶ has demonstrated that the converse is also true: as the thermodynamic effect becomes dominant, the estimated correlation coefficient from $\Delta H - \Delta S$ estimates will usually decrease. Thus a large value of the estimated correlation coefficient r from $\Delta H - \Delta S$ estimates is a poor reason for inferring chemical causation, but a good reason to expect either the absence

of a thermodynamic effect or that the data lack the precision to display such an effect. In any case nothing conclusive can be inferred from a large value of r determined from $\Delta H - \Delta S$ estimates.

Correlated parameter estimates are obtained in other chemical investigations as well. In enzyme studies, for example, the Michaelis-Menten parameter estimates \hat{v}_{\max} and \hat{K}_m are highly correlated when estimated from a Lineweaver-Burk plot when the range of inverse substrate concentration is small. The magnitude of this correlation can be found by an analysis parallel to the one given above.

II. *The Statistical Compensation Equation.* To determine the distribution of enthalpy and entropy estimates in the $\Delta H - \Delta S$ plane due to experimental or measurement errors we first consider the shape of the relevant confidence regions.^{20,21}

Since the form of the model to which the data are fitted is linear, the confidence region at any level of significance α is elliptical. That is, upon repeated sampling, the probability is $1 - \alpha$ that the true value of any ($\Delta H, \Delta S$) pair will be located in a region bounded by the ellipse

$$(\psi - \hat{\psi})' \mathbf{Z}^{-1} \mathbf{X}' \mathbf{X} \mathbf{Z}^{-1} (\psi - \hat{\psi}) = 2s^2 F(2, n - 2, 1 - \alpha)$$

where $F(2, n - 2, 1 - \alpha)$ is the upper α point of the F statistic with $2, n - 2$ degrees of freedom and s^2 is, under suitable assumptions, an estimate of σ^2 .

$$s^2 = \frac{\sum (y_i - \hat{\theta}_1 - \hat{\theta}_2/T_i)^2}{n - 2}$$

Since $T_i \gg 1$ in either the Rankin or Kelvin temperature scales for most kinetic and equilibrium experiments, the ratio of the major to minor axis of the ellipse is always much greater than unity and may be approximated by

$$a/b \cong \sqrt{n / \sum (1/T - \langle 1/T \rangle)^2} \gg 1$$

Typically the value a/b will exceed 10 000!

The extreme elongation of the ellipse gives it the appearance of a line. Just as the true value of a parameter has a probability $1 - \alpha$ of being within such an ellipse, if the chemical variations are small compared to experimental errors, $(1 - \alpha)100$ percent of these "approximate replications" will fall within a similar ellipse centered about the true value.

Canonical analysis of the elliptic equation shows that the major axis has a slope of $T_{\text{hm}} = \langle 1/T \rangle^{-1}$, the harmonic mean of the experimental temperatures. Thus enthalpy and entropy estimates will fall along a line with slope T_{hm} when the experimental errors are large compared to thermodynamic variations.

That the experimental or measurement errors would propagate into a consistent pattern on $\Delta H^\ddagger - \Delta S^\ddagger$ plots has been previously recognized. The slope of the line in which these errors are distributed has been called the "error slope".^{9,11,12} For the special case of two temperatures, derivations have been published which claim to show that this slope is equal to the harmonic mean,^{11,12} the arithmetic mean,²² the quantity¹⁰ $2T_1T_2/(3T_1 - T_2)$, or is approximated by the geometric mean¹¹ of the experimental temperatures. We have shown above for the general case of any $n \geq 2$ experimental temperatures that the error slope is equal to T_{hm} when enthalpies and entropies are estimated by ordinary linear regression (i.e., least squares).

The statistical compensation pattern may also be derived by considering the transformation that makes the slope and

intercept estimates independent of one another and discovering what compensation between variables will keep the slope and intercept values independent. To accomplish this the independent variable, inverse experimental temperatures, is centered about its mean. Thus the linearized form of the Arrhenius equation may be rewritten such that

$$\ln k = \{\ln A - E\langle 1/T \rangle / R\} - E/R\{1/T - \langle 1/T \rangle\}$$

the slope $-E/R$ and intercept $\{\ln A - E\langle 1/T \rangle / R\}$ estimates are independent with correlation coefficient $\rho = 0$.¹⁸ The intercept is a measure of the free energy at T_{hm} .

$$\Delta G^\ddagger (\text{at } T = T_{\text{hm}}) = \Delta G^\ddagger_{T_{\text{hm}}} = -RT_{\text{hm}}\{\ln A - E/RT_{\text{hm}}\} + RT_{\text{hm}} \ln (kT_{\text{hm}}e/h) - RT_{\text{hm}}$$

Thus any error in the value of E/R must be fully compensated for by a corresponding error in the value of $\ln A$ to keep the value of $\{\ln A - E/RT_{\text{hm}}\}$ independent of deviations in E/R . Rewriting this compensation equation

$$\{\ln A - E/RT_{\text{hm}}\} = \ln A - E/RT_{\text{hm}}$$

in terms of the definitions of ΔH^\ddagger , ΔS^\ddagger , and ΔG^\ddagger yields the statistical compensation pattern.

$$-\Delta G^\ddagger_{T_{\text{hm}}} = T_{\text{hm}}\Delta S^\ddagger - \Delta H^\ddagger$$

alternately

$$\Delta H^\ddagger = T_{\text{hm}}\Delta S^\ddagger + \Delta G^\ddagger_{T_{\text{hm}}}$$

Shimulis²³ has derived the corresponding statistical compensation line in $E - \ln A$ coordinates. Thus data plotted in $\Delta H - \Delta S$ coordinates with a high correlation coefficient and slope near T_{hm} must be suspect of having experimental errors masking any chemical or physical effect that may be present.

III. *A Hypothesis Test.* A useful hypothesis test should discriminate between the statistical compensation pattern and any linear chemical compensation pattern^{5,24}

$$\Delta H = \beta \Delta S - \Delta G (\text{at } T = \beta) = \beta \Delta S + \Delta G_\beta$$

Since the two linear compensation patterns are identical except for one parameter, it is sufficient to merely test the value of that parameter. The null hypothesis is then

$$H_0: \beta = T_{\text{hm}}$$

Unless this hypothesis can be rejected there is no reason to suspect the existence of chemical causation and hence no reason to create theories to explain it (apart from purely statistical ones).

Since the vast majority of compensation temperatures that have been reported in the literature have been determined using least squares, it would be useful to formulate a hypothesis test using this method in order to screen literature values of compensation temperatures. Many authors^{5,9-11,13,22,24-26} have warned that plots with slopes approximately equal to the experimental temperatures may be simply manifestations of the propagation of experimental errors. Other authors^{12,15-17} have criticized regression of $\Delta \hat{H}$ on $\Delta \hat{S}$ because of the large covariance between these two estimates. We maintain, however, that such regressions are useful to test the null hypothesis that the observed linear

pattern arises only because of the propagation of experimental errors. An ordinary least-squares analysis will reflect the statistical compensation effect that is always present. If an important chemical effect is also present, the data will tend to fall away from the statistical compensation line. If the data are sufficiently far from the statistical compensation line, the estimate $\hat{\beta}$ will be significantly different from T_{hm} . H_0 may then be rejected, which would suggest the possible presence of a detectable chemical compensation.

The argument for accepting linear regression results to test H_0 is based on the following analysis. The line that describes the major axis of the ellipse for any single data pair can be derived from a canonical analysis to be given by the equation

$$(\Delta H - \Delta \hat{H}) = T_{\text{hm}}(\Delta S - \Delta \hat{S})$$

alternately

$$\Delta H = T_{\text{hm}}\Delta S + \Delta \hat{G}_{T_{\text{hm}}}$$

This expression may be written in terms of the true value of the free energy $\Delta G_{T_{\text{hm}}}$ and its measurement error $\epsilon(\Delta G_{T_{\text{hm}}})$

$$\Delta H = T_{\text{hm}}\Delta S + \Delta G_{T_{\text{hm}}} + \epsilon(\Delta G_{T_{\text{hm}}})$$

Thus under the assumption that a series of data pairs $(\Delta \hat{H}, \Delta \hat{S})$ vary only as a consequence of measurement errors from a single fixed value of thermodynamic parameters $(\Delta H, \Delta S)$ and that the resulting probability ellipse is very elongated (i.e., $b/a \rightarrow 0$, which is a good approximation for usual experimental temperature ranges) the data $(\Delta \hat{H}, \Delta \hat{S})$ will be distributed essentially along a line characterized by a known slope, T_{hm} , and unknown intercept $\Delta G_{T_{\text{hm}}}$ and deviations from that line in the direction of the ΔH axis have the magnitude of the error of the free energy estimate as might be estimated from repeated application of the Gibbs equation to the $(\Delta \hat{H}, \Delta \hat{S})$ data and averaging. Since these errors have zero mean $E(\epsilon(\Delta G_{T_{\text{hm}}})) = 0$ and constant variance $V(\epsilon(\Delta G_{T_{\text{hm}}})) = \mathbf{I}\sigma^2(\Delta G_{T_{\text{hm}}})$, the application of linear regression is fairly well justified. In particular, it is readily shown that the spread of data along the statistical compensation line is generally much greater than that away from the statistical compensation line

$$\frac{s_{\Delta H}^2}{s_{\Delta \hat{G}}^2} = \frac{(\sum 1/T)^2}{n \sum (1/T - \langle 1/T \rangle)^2} \gg 1$$

for the usual experimental temperature ranges so that the true orientation of residuals will not significantly affect the values of the slope and intercept estimates.²⁷

To test the null hypothesis, then, the slope $\hat{\beta}$ should be compared with T_{hm} . An approximate $(1 - \alpha)100$ percent confidence interval for $\hat{\beta}$ may be calculated from

$$(1 - \alpha)100\% \text{ CI } \hat{\beta} \approx \hat{\beta} \pm t_{m-2, \alpha/2} \sqrt{V(\hat{\beta})}$$

where

$$\hat{\beta} = \frac{\sum (\Delta H - \langle \Delta H \rangle)(\Delta S - \langle \Delta S \rangle)}{\sum (\Delta S - \langle \Delta S \rangle)^2}$$

$$V(\hat{\beta}) = \frac{\sum (\Delta H - \Delta \hat{G}_\beta - \hat{\beta} \Delta S)^2}{(m - 2) \sum (\Delta S - \langle \Delta S \rangle)^2}$$

and m is the number of $(\Delta H, \Delta S)$ data pairs.

If T_{hm} falls within this interval, the hypothesis may not be

TABLE I: A Comparison of Observed with Statistical Compensation Temperatures

Reaction	$(\Delta\hat{H}, \Delta\hat{S})$ pairs	T_{hm}	95% CI of $\hat{\beta}$	Ref		Comments
				Data	Reviews	
1. Isomerization of substituted 5-aminotriazoles	4	414.5	(742.6, 323.8)	30	2a	
2. Decomposition in toluene of p -XC ₆ H ₄ N=NC(C ₆ H ₄) ₃	5	335.9	(509.3, 165.7)	31	2a	
3. Decomposition in various solvents of C ₆ H ₅ N=NC(C ₆ H ₅) ₃	7	321.9	(327.9, 296.7)	32	2a	
4. Alcoholysis of substituted benzhydryl chlorides	5	287.7	(409.5, 298.7)	33	2a	Systematic error in kinetic data
5. Same as 4	5	295.6	(400.6, 276.6)	33	2a	Just data at 20 and 25 °C
6. Solvolysis of para-substituted benzoyl chlorides in acetone-water	4	285.1	(429.7, 264.5)	34	2a	R = Br, H, Me, MeO
7. Alkaline hydrolysis of primary alkyl acetates	7	298.1	(332.2, 259.4)	35	2a	Without 2,2-diethyl-1-butyl and 2-ethyl-3,3-dimethyl-1-butyl compounds
8. Same as 7	9	298.1	(327.2, 22.2)	35	2a	All data
9. Hydrolysis of substituted benzoic anhydrides	6	341.8	(783.4, 264.8)	36	2a	
10. Decomposition of para-substituted triphenylmethyl azides	8	452.8	(484.0, 447.6)	37	2a	All solvents
11. Same as 10	6	452.8	(517.7, 451.7)	37	29	Only dibutyl carbitol solvent
12. Hydrolysis of meta-substituted phenyl potassium sulfates	7	336.2	(460.9, 373.5)	38	2a	
13. Esterification of substituted benzoic acids	14	342.8	(403.8, 282.0)	39	2a	
14. Complex formation between iodine and amines	7	298.1	(850.1, 147.1)	40	2a	
15. Oximation of carvacryl ketones	6	308.1	(330.0, 36.0)	28	2a,5,12,26	All data
16. Same as 15	5	308.1	(342.8, 230.5)	28	2a,5,12,26	Deleting methylated compound
17. Oximation of thymyl ketones	7	308.1	(401.3, 226.1)	28	2a,5,12,26	All data
18. Same as 17	6	308.1	(328.3, 285.7)	28	2a,5,12,26	Deleting methylated compound
19. Hydrolysis of ethyl benzoate in various solvents	12	292.6	(431.3, 401.3)	41	5	
20. Esterification of substituted benzoic acids in cyclohexanol	6	338.0	(371.5, 278.5)	42	11	
21. Hydrolysis of aliphatic ethyl esters in aqueous acetone	4	307.7	(468.6, 190.0)	43	11	
22. Racemization of 2,2-dimethoxy-6,6-dicarboxybiphenyl	10	362.6	(398.6, 322.2)	44	11	"Lowest family"
23. Dimethyl esters of 22	12	362.6	(388.9, 298.5)	44	11	Did not find cyanobenzene data
24. Diamides of 22	4	362.6	(422.9, 330.1)	44	11	"Higher family"
25. Racemization of a biphenyl	4	362.6	(454.8, 166.7)	45	11	"Intermediate group"
26. Same as 25	7	362.6	(362.0, 277.2)	45	11	"Lowest group" all data
27. Same as 25	6	362.6	(426.9, 221.3)	45	11	"Lowest group" deleting glycol
28. Cleavage of carbon-metal bonds	5	298.4	(304.3, 285.3)	46	12	R = H, 4-F, 3-Me, 2,4-dimethyl-, dihexylmercury
29. Saponification of substituted ethyl phenoxyacetates	13	287.4	(332.7, 231.1)	24	12	
30. Decomposition of a propionitrile in various solvents	4	342.7	(401.0, 326.2)	10	12	
31. Lossen rearrangement of dihydroxamic acid salts	17	308.1	(353.8, 205.8)	47	12,15	
32. Reaction of 1,1-dinitro compounds with formaldehyde	9	301.1	(564.4, 419.4)	48	15	"Best" line
33. Same as 32	14	301.1	(755.1, 121.9)	48	15	"Next best" line
34. Formation of amino triphenyl carbinols	9	338.0	(341.4, 328.0)	49	15	"Best fit" of meta para data
35. Same as 34	13	338.0	(396.9, 331.7)	49	15	All meta para data
36. Same as 34	6	338.0	(490.2, 274.0)	50	15	All ortho data deleting SO ₃ H
37. Same as 34	5	338.0	(553.0, 214.4)	50	15	Ortho data without NO ₂ and SO ₃ H compounds
38. Ionization of azomethanes	5	303.9	(277.3, -44.7)	51	15	
39. Binding of SCN ⁻ to human hemoglobin C	7	293.1	(391.1, 267.3)	52	29	All data
40. Same as 39	4	293.1	(299.3, 256.3)	52	29	For pH ≤ 7.5

TABLE I (Continued)

Reaction	$(\Delta\hat{H}, \Delta\hat{S})$ pairs	T_{hm}	95% CI of $\hat{\beta}$	Ref		Comments
				Data	Reviews	
41. Binding of SCN^- to human hemoglobin A	6	293.0	(553.2, 195.4)	52	29	All data
42. Same as 41	4	293.0	(672.2, 112.9)	52	29	For $pH \geq 7$
43. Reaction of sperm whale metmyoglobin with azide	11	290.7	(345.7, 180.1)	53	29	
44. Ionization of vertebrate methaemoglobins ($I = 0.05$)	6	285.7	(309.1, 285.7)	54	29	Low temperature group
45. Same as 44	5	292.7	(323.9, 288.1)	54	29	High temperature group
46. Same as 44 ($I = 1.0$)	11	285.7	(297.8, 262.0)	54	29	
47. Same as 44 ($I = 0.05$)	11	285.7	(323.0, 282.6)	55	29	

rejected at the α level of significance. Recall the hypothesis is that the observed distribution of data in the $\Delta H - \Delta S$ plane is a reflection solely of the propagation of experimental errors, not chemical factors.

Application to Chemical Examples

Data for the oximation of alkyl thymyl ketones²⁸ have been discussed as perhaps displaying an isokinetic relationship.^{2a,5,12,26} For these data taken at 30, 35, and 40 °C the correlation coefficient between estimates of an individual enthalpy-entropy pair is almost unity (see Figure 1).

$$\rho = \frac{\sum 1/T}{\sqrt{n \sum (1/T)^2}} = 0.999\ 91$$

If the variation of $(\Delta\hat{H}^\ddagger, \Delta\hat{S}^\ddagger)$ pairs in the $\Delta H^\ddagger - \Delta S^\ddagger$ plane is merely a reflection of the propagation of experimental errors the estimated correlation coefficient r is an estimate of ρ . Since $r = 0.9988$ for the data deleting the methylated compound and $r = 0.9724$ for the entire data set, it appears that the distribution of data may be the consequence of experimental errors for all but the methylated compound. Figure 2b confirms that the free energy estimate of the methylated compound is measurably different than the rest. The clustering of the free energy estimates for all but the methylated compound indicates that they may fall along the same statistical compensation line because the enthalpy variations are small compared to the statistical uncertainty of the enthalpy estimates.

A plot of the joint confidence regions in Figure 2a further suggests the propagation of errors as the reason for a linear distribution of data in $\Delta H^\ddagger - \Delta S^\ddagger$ coordinates. The ellipses are so elongated that they appear as lines. The ratio of major to minor axes is very large, $a/b = 232\ 52$, and the variance of $\Delta\hat{G}^\ddagger$ is very small compared to that of $\Delta\hat{H}^\ddagger$.

$$\frac{s_{\Delta H^\ddagger}^2}{s_{\Delta G^\ddagger}^2} = \frac{(\sum 1/T)^2}{n \sum (1/T - (1/T))^2} = 5696$$

Because these ratios are large, it is reasonable to use linear regression to test the null hypothesis $H_0: \beta = T_{hm}$.

The 95% confidence interval for $\hat{\beta}$ for the oximation of thymyl ketones is (401.3, 226.1) and includes the harmonic mean of the experimental temperatures, 308.1 K. The corresponding confidence interval for the data set deleting the methylated compound is (328.3, 285.7). Thus the hypothesis

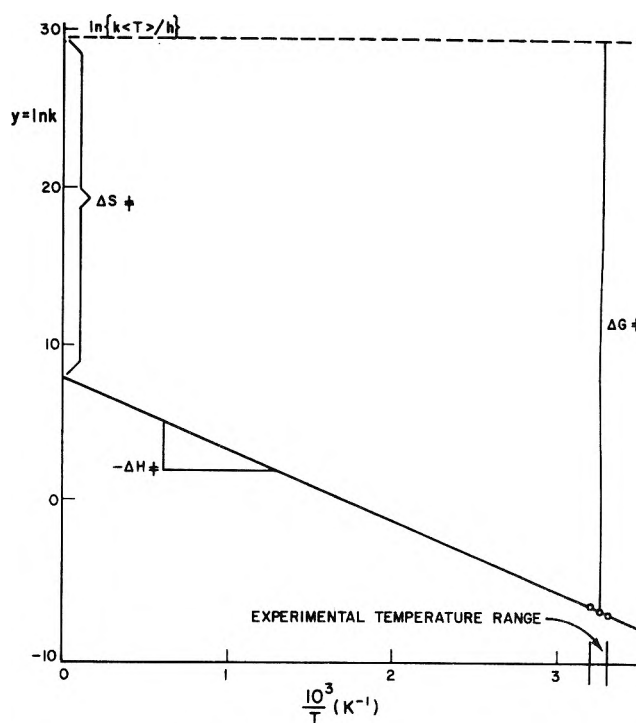


Figure 1. Geometric interpretation of the parameter estimates. The indicated lengths are proportional to ΔG^\ddagger and ΔS^\ddagger and the indicated slope is proportional to $-\Delta H^\ddagger$. These data for the oximation of methyl thymyl ketone²⁸ indicate a strong dependence of the intercept estimate on the slope estimate because the data were taken over a very small temperature range far from the origin. The three data points are designated by dots. Reprinted with copywrite permission from *Nature*.¹⁸

that the observed compensation between regression parameter estimates is just a consequence of the propagation of experimental errors cannot be rejected at the 5% level of significance for this data set.

Many other data sets were similarly tested. These examples of linear compensations were taken from major reviews in the literature.^{2a,5,12,15,26,29} Only data that were thermally consistent were considered so T_{hm} would be exactly defined. The Leffler reviews,^{2a,5} however, were so extensive that only data he included in figures were reviewed. Furthermore, since the t statistic becomes very large at one degree of freedom, only data sets with four or more $(\Delta H, \Delta S)$ pairs were considered. Both kinetic and equilibrium data were reviewed. The results are listed in Table I.

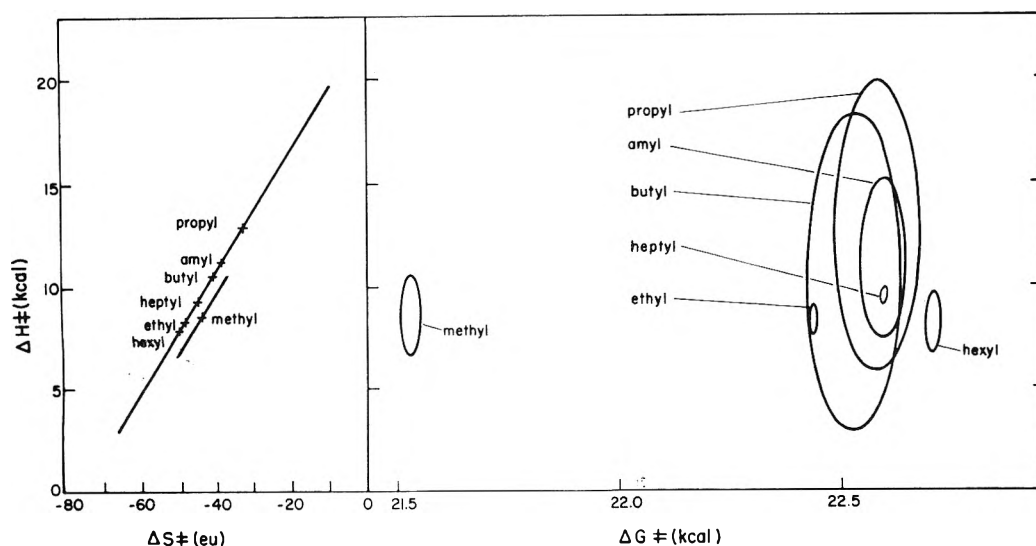


Figure 2. The 50% joint confidence regions for the oximation of alkyl thymyl ketones.²⁸ The $\Delta H^\ddagger - \Delta S^\ddagger$ ellipses are so narrow that they appear as lines. Departure of the methylated compound from a common ΔG^\ddagger value causes it to fall off the statistical compensation "line" between ΔH^\ddagger and ΔS^\ddagger estimates. Notice that ΔG^\ddagger is estimated more precisely than ΔH^\ddagger . All values were calculated for $T = T_{\text{hm}} = 308.1$ K. Reprinted with copyright permission from *Nature*.¹⁸

Most of the compensation relationships in Table I have the harmonic mean of the experimental temperatures well within the 95% confidence intervals for the regression estimates of the compensation temperatures. Thus in most cases reviewed, the hypothesis that the observed compensation behavior is fully explained as a statistical compensation of regression parameter estimates cannot be rejected at the 5% level of significance.

Notable exceptions are entries 12, 19, and 38. Other exceptions may have plausible explanations. For example, systematic error in the residuals of entry 4 when fitting Arrhenius parameters indicates that one of the three reported temperatures may be misquoted. Rejecting the data at 0 °C gave good agreement.

Examples 32 and 34 represent "best lines" by rejecting portions of a data set and retaining only those data that appear to conform to linear compensation as determined by Exner's novel technique.¹⁵ The lack of robustness of the alleged compensations was demonstrated by examples 33 and 35.

A drawback of the technique described above is if a chemical compensation effect exists but is such that β differs only slightly from T_{hm} , the hypothesis test will indicate that the observed pattern is indistinguishable from the statistical compensation pattern. This hypothesis test, however, is the best that can be formulated if the researcher restricts analysis to enthalpy and entropy estimates alone. A more sensitive procedure, which involves reparameterization, is described in part 2 of this work.⁵⁶

Summary and Conclusions

The statistical compensation pattern for enthalpy-entropy data pairs is the usual compensation between regression parameter estimates that occurs because the range of variation of the independent variable (the inverse experimental temperatures) is small. Consequently the estimated slopes of the regression lines have values near the harmonic mean of the experimental temperatures and the estimated correlation coefficients have values near unity. Standard deviations of free energies estimated from the standard deviations of enthalpies and entropies must take into account this correlation.¹⁹

Because the statistical compensation pattern is linear, with

a high correlation coefficient, linear plots of enthalpy-entropy data do not necessarily imply that a chemical phenomenon is responsible for the observed correlation. For regression in the enthalpy-entropy plane, large experimental errors tend to raise the estimated value of the correlation coefficient, rather than lower it.

The hypothesis that the observed line in the enthalpy-entropy plane is a manifestation of only the statistical compensation pattern may be rejected if the slope estimate is sufficiently different from T_{hm} as determined by a t test.

Most of the enthalpy-entropy compensation effects presented in the literature reviews on this subject appear to be indistinguishable from the statistical compensation effect described here.

Supplementary Material Available: Details of the mathematical arguments used in this article (9 pages). Ordering information is available on any current masthead page.

References and Notes

- (1) (a) Chemical Engineering Department. (b) Statistics Department and Engineering Experiment Station.
- (2) (a) J. E. Leffler and E. Grunwald, "Rates and Equilibria of Organic Reactions", Wiley, New York, N.Y., 1963, pp 315-402; (b) L. P. Hammett, "Physical Organic Chemistry", 2d ed, McGraw-Hill, New York, N.Y., 1970, pp 391-408.
- (3) K. J. Laidler, "Chemical Kinetics", 2d ed, McGraw-Hill, New York, N.Y., 1965, pp 251-253.
- (4) H. H. Jaffe, *Chem. Rev.*, **53**, 191 (1953).
- (5) J. E. Leffler, *J. Org. Chem.*, **20**, 1202 (1955).
- (6) C. D. Ritchie and W. Sager, *Prog. Phys. Org. Chem.*, **2**, 323 (1964).
- (7) M. Charton, *J. Org. Chem.*, **29**, 1222 (1964).
- (8) T. E. Bitterwolf, R. E. Linder, and A. C. Ling, *J. Chem. Soc. B*, 1673 (1970).
- (9) D. A. Blackadder and C. Hinshelwood, *J. Chem. Soc.*, 2720 (1958).
- (10) R. C. Petersen, J. H. Markgraf, and S. D. Ross, *J. Am. Chem. Soc.*, **83**, 3819 (1951).
- (11) R. F. Brown, *J. Org. Chem.*, **27**, 3015 (1962).
- (12) O. Exner, *Coll. Czech. Chem. Commun.*, **29**, 1094 (1964); *Nature (London)*, **201**, 488 (1964).
- (13) R. C. Petersen, *J. Org. Chem.*, **29**, 3133 (1964).
- (14) J. E. Leffler, *J. Org. Chem.*, **31**, 533 (1966).
- (15) O. Exner, *Coll. Czech. Chem. Commun.*, **37**, 1425 (1972).
- (16) S. Wold, *Chem. Script.*, **2**, 145 (1972).
- (17) S. Wold and O. Exner, *Chem. Script.*, **3**, 5 (1973).
- (18) R. R. Krug, W. G. Hunter and R. A. Grieger, *Nature (London)*, **261**, 566 (1976).
- (19) Thus when estimating the standard deviation of a free energy estimate from

- ($\Delta\bar{H}$, $\Delta\bar{S}$) values using $\Delta\bar{G} = \Delta\bar{H} - T\Delta\bar{S}$, the estimated variance $s_{\Delta\bar{G}}^2$ (square of standard deviation) is $s_{\Delta\bar{G}}^2 = s_{\Delta\bar{H}}^2 + T^2s_{\Delta\bar{S}}^2 - 2T\rho s_{\Delta\bar{H}}s_{\Delta\bar{S}}$, where ρ is given above. Unfortunately, the covariance term has usually been ignored in the literature.
- (20) N. Draper and H. Smith, "Applied Regression Analysis", Wiley, New York, N.Y., 1966.
 - (21) J. Mandel and F. J. Linning, *Anal. Chem.*, **29**, 743 (1957).
 - (22) J. E. Leffler, *J. Org. Chem.*, **31**, 533 (1968).
 - (23) V. I. Shimulis, *Kinet. Katal.*, **10**, 1026 (1968); *Kinet. Catal.*, **10**, 837 (1968).
 - (24) R. F. Brown and H. C. Newsom, *J. Org. Chem.*, **27**, 3010 (1962).
 - (25) D. A. Blackadder and C. Hinshelwood, *J. Chem. Soc.*, 2728 (1958).
 - (26) J. E. Leffler, *Nature (London)*, **205**, 1101 (1965).
 - (27) For data distributed in an ellipse which is approximated by a line, other more complicated procedures are possible, for example, the method of maximum likelihood or the minimization of the weighted residuals perpendicular to the line. Since these latter residuals are small ($a/b \gg 1$), the numerical values of the slope and intercept will not be significantly different from those obtained by least squares. Such elaborate methods could be formulated but are not warranted for the present case.
 - (28) M. J. Craft and C. T. Lester, *J. Am. Chem. Soc.*, **73**, 1127 (1951).
 - (29) R. Lumry and S. Rajender, *Biopolymers*, **9**, 1125 (1970).
 - (30) E. Lieber, C. N. R. Rao, and T. S. Chao, *J. Am. Chem. Soc.*, **79**, 5962 (1957).
 - (31) G. L. Davies, D. H. Hey, and G. H. Williams, *J. Chem. Soc.*, 4397 (1956).
 - (32) M. G. Alder and J. E. Leffler, *J. Am. Chem. Soc.*, **76**, 1425 (1954).
 - (33) G. Baddeley, S. Varma, and M. Gordon, *J. Chem. Soc.*, 3171 (1958).
 - (34) G. E. K. Branch and A. C. Nixon, *J. Am. Chem. Soc.*, **58**, 2499 (1936).
 - (35) S. Sarel, L. Tsai, and M. S. Newman, *J. Am. Chem. Soc.*, **78**, 5420 (1956).
 - (36) E. Berliner and L. H. Altschul, *J. Am. Chem. Soc.*, **74**, 4110 (1952).
 - (37) W. H. Saunders, Jr., and J. C. Ware, *J. Am. Chem. Soc.*, **80**, 3328 (1958).
 - (38) G. N. Burkhardt, C. Horrex, and D. I. Jenkins, *J. Chem. Soc.*, 1649 (1936).
 - (39) R. J. Hartman, H. M. Hoogsteen, and J. A. Moede, *J. Am. Chem. Soc.*, **66**, 1714 (1944).
 - (40) H. Yada, J. Tanaka, and S. Nagakura, *Bull. Chem. Soc. Jpn.*, **33**, 1660 (1960).
 - (41) R. A. Fairclough and C. N. Hinshelwood, *J. Chem. Soc.*, 538 (1937).
 - (42) R. J. Hartman, L. B. Storms, and A. G. Gassman, *J. Am. Chem. Soc.*, **61**, 2167 (1939).
 - (43) H. A. Smith and R. R. Myers, *J. Am. Chem. Soc.*, **64**, 2362 (1942).
 - (44) B. M. Graybill and J. E. Leffler, *J. Phys. Chem.*, **63**, 1461 (1959).
 - (45) J. E. Leffler and W. H. Graham, *J. Phys. Chem.*, **63**, 687 (1959).
 - (46) R. E. Dessey and J. Y. Kim, *J. Am. Chem. Soc.*, **83**, 1167 (1961).
 - (47) R. D. Bright and C. R. Hauser, *J. Am. Chem. Soc.*, **61**, 618 (1939).
 - (48) V. K. Krylov and I. V. Tselinskii, *Reakts. Sposoln. Org. Soedin.*, **7**, 78 (1970); *Org. React.*, **7**, 33 (1970).
 - (49) G. S. Idlis and O. F. Ginsburg, *Reakts. Sposoln. Org. Soedin.*, **2**, 47 (1965).
 - (50) G. S. Idlis and O. F. Ginsburg, *Reakts. Sposoln. Org. Soedin.*, **2**, 54 (1965).
 - (51) V. A. Bren, E. N. Malysheva and V. I. Minkin, *Reakts. Sposoln. Org. Soedin.*, **5**, 763 (1968); *Org. React.*, **5**, 314 (1968).
 - (52) A. C. Anusiem, J. G. Beetlestone, and D. H. Irvine, *J. Chem. Soc. A*, 960 (1968).
 - (53) J. E. Bailey, J. G. Beetlestone, and D. H. Irvine, *J. Chem. Soc. A*, 241 (1969).
 - (54) J. G. Beetlestone and D. H. Irvine, *J. Chem. Soc. A*, 3271 (1965).
 - (55) J. G. Beetlestone and D. H. Irvine, *J. Chem. Soc. A*, 5090 (1964).
 - (56) R. R. Krug, W. G. Hunter, and R. A. Grieger, *J. Phys. Chem.*, following article in this issue.

Enthalpy-Entropy Compensation. 2. Separation of the Chemical from the Statistical Effect

R. R. Krug,^{*1a} W. G. Hunter,^{1b} and R. A. Grieger^{1a}

Chemical Engineering Department, and Statistics Department and Engineering Experiment Station, University of Wisconsin, Madison, Wisconsin 53706 (Received March 8, 1976)

For problems concerning enthalpy-entropy compensations, an appropriate regression procedure is presented for the estimation of functional dependencies between thermodynamic parameters. Unbiased parameter estimates and their confidence intervals are derived for the case of a linear dependence between thermodynamic parameters. It is demonstrated that nonlinear as well as linear functional dependencies are readily detectable when enthalpy estimates are plotted vs. free energy estimates. Some linear and nonlinear examples of functional dependencies between thermodynamic parameters are analyzed and discussed.

Introduction

In the first part of this article² we demonstrated that the propagation of experimental errors will tend to distribute enthalpy and entropy estimates along a line characterized by a slope equal to the harmonic mean of the experimental temperatures. The associated correlation coefficient will likewise tend to be near unity.

The method of ordinary linear regression, which is valid for data that have no error in the independent variable, will also give unbiased parameter estimates for linear models when such errors are present if they are *uncorrelated* with those of the dependent variable and if the independent variable is sampled at predetermined values.^{3,4} For the linear enthalpy-entropy effect, unfortunately, the errors in the enthalpy estimates are highly *correlated* with errors in the entropy estimates and the values of entropy at which enthalpies are measured are not controlled. Thus ordinary linear re-

gression will give biased estimates. Furthermore ordinary linear regression is an insensitive procedure for determining the existence of an enthalpy-entropy compensation effect because the results will be confounded with the statistical compensation pattern.

Here we use (1) a transformation that gives rise to uncorrelated errors between dependent and independent variables and (2) a regression procedure that properly accounts for the relative magnitude of error in the independent variable to that in the dependent variable. Hence true chemical compensations will not be confounded with any statistical compensation between parameter estimates when this procedure is used. The transformation indicates that *regression should be of enthalpy estimates on free energy estimates evaluated at the harmonic mean of the experimental temperatures instead of enthalpy on entropy*,⁵ as is customarily done. An analysis of the results obtained using this regression procedure indicates that weighted least squares is generally sufficient be-

TABLE I: Chronology of Correct Statistical Regression Procedures for Detecting a Linear Extrathermodynamic Compensation

Author (year)	Method	Limitations
1. Exner ⁶ (1964)	Correlation analysis of $\ln k_1$ vs. $\ln k_2$	(1) Assumes a linear compensation (2) Limited to 2 experimental temperatures (3) Exaggerates errors ^{9,10}
2. Exner ⁷ (1970, 1972)	Regression of $\ln k_i$ on $-e_0/R\beta - b_i(1/T_i - 1/\beta)$	(1) Assumes a linear compensation (2) Assumes prior knowledge of the uncertainty of rate constant measurements (3) Reliability interval of $\hat{\beta}$ is not exactly defined (4) Data must be evaluated at consistent temperatures
3. Wold and Exner ⁸ (1973)	Nonlinear regression of $\ln k_i$ on extended Arrhenius equation	(1) Assumes a linear compensation (2) Limited to 3 experimental temperatures (3) Reliability interval of $\hat{\beta}$ not exactly defined

cause the free energy estimates are determined with much greater precision than the enthalpy estimates.

Several statistical procedures for estimating the isokinetic temperature have already been presented in the literature⁶⁻⁸ and are summarized in Table I. These procedures are correct in the sense that the application of each procedure does not violate the assumptions upon which it is formulated, as is the case with ordinary linear regression of enthalpy estimates on entropy estimates. Each of these procedures is more limited than the one presented in this article, however, and they have their utility more in determining whether a linear extrathermodynamic effect is detectable, rather than in determining the actual parameter values associated with such an effect. The most severe limitation of these procedures is that they all assume that the extrathermodynamic effect is linear and they have no provision for determining if a nonlinear or symmetric effect exists. Another possibility is the use of a dispersion analysis to determine if a linear extrathermodynamic effect may be present.¹¹

The first procedure in Table I is limited to data sampled at only two temperatures and consequently has been criticized for its inability to detect nonlinear effects⁹ and exaggeration of errors.¹⁰ The second procedure assumes a prior knowledge of the magnitude of errors in the rate constants and the third procedure uses estimates of these errors from the fit to the extended Arrhenius equation but is limited to data taken at three temperatures.

The procedure presented here is not limited to data taken at any number of temperatures, and moreover a prior knowledge of the magnitude of uncertainty of rate or equilibrium constants is unnecessary. Estimates of the uncertainty of the data are obtained from the lack of fit to the Arrhenius or van't Hoff equations and the data are plotted in an unbiased manner. Hence visual inspection of plotted data may be used to determine if a quadratic, exponential, or other nonlinear functionality is appropriate. The maximum likelihood estimate and confidence interval for the linear compensation temperature are also presented in this article.

Analysis of the estimation situations for correlated and uncorrelated cases reveals that, by ignoring the assumptions implicit in the formulation of ordinary linear regression, investigators were estimating from the data the "worst" instead of the "best" value of the compensation temperature as defined by the likelihood function. Various data sets have been reviewed using these transformation and regression techniques and several cases that appear to display either linear or nonlinear chemical compensations are discussed.

Theory

The only assumptions necessary for the derivation of the procedure given here are: (1) that the experimental temperatures are determined with much greater accuracy and precision than experimentally measured rate and equilibrium constants, (2) that the Arrhenius and van't Hoff equations are adequate mathematical models to represent kinetic and equilibrium data over the respective experimental temperature ranges, (3) that the data were taken at the same temperatures for all of the systems being investigated, and (4) errors associated with the measurements, $\ln k_i$ and $\ln K_i$, are assumed to be normally and independently distributed with zero mean and constant variance.

Assumptions 1, 2, and 4 are almost universally accepted and assumption 3 is also required by all of the previous statistical treatments listed in Table I. Although the data reviewed by us did comply with this last requirement, if data are taken at different but close temperatures, extrapolations may be made using assumption 2 to obtain the best estimates possible from the available data. Again for brevity we choose to limit detailed discussions to the case of kinetic data although all the results are equally applicable to equilibrium data as well.

I. Functional Dependencies between Thermodynamic Parameters. As a consequence of the first and second laws of thermodynamics, the potentials H , G , E , and A are related to each other and S , T , P , and V by the Maxwell equations. That a linear enthalpy-entropy effect should also appear to be linear in other coordinates as a consequence of these interrelationships was first noted by Ritchie and Sager.¹² In particular, the linear enthalpy-entropy relationship^{13,14}

$$\Delta H = \beta \Delta S + \Delta G(\text{at } T = \beta) = \beta \Delta S + \Delta G_\beta$$

must be consistent with the Gibbs equation

$$\Delta G = \Delta H - T \Delta S$$

such that a linear relationship also exists between ΔH and ΔG

$$\Delta H = \gamma \Delta G + (1 - \gamma) \Delta G_\beta$$

where

$$\gamma = 1/(1 - T/\beta)$$

Thus to observe an extrathermodynamic relationship between ΔH and ΔS , the researcher has three possible planes ($\Delta H - \Delta S$, $\Delta H - \Delta G$, $\Delta G - \Delta S$) in which to plot the experimental data. More planes are possible if constraints other than

the Gibbs equation are invoked. Furthermore, these parameters must be evaluated at some arbitrary temperature. Typically the data have been plotted in the $\Delta H - \Delta S$ plane at some reference temperature, usually 25 °C.

II. *Uncorrelated Errors.* Given a regression situation where the slope and intercept are the desired parameters, their estimates may be made uncorrelated by translating the intercept to the arithmetic mean of the range of the independent variable. The following equivalent formulation of the Arrhenius equation accomplishes this⁵

$$\ln k_i = \ln A - E/R \cdot 1/T_i \\ = \{\ln A - E\langle 1/T \rangle/R\} - E/R\{1/T_i - \langle 1/T \rangle\}$$

where the estimates of $\{\ln A - E/RT_{\text{hm}}\}$ and $-E/R$ are uncorrelated. Since these parameters are measures of $\Delta G^\ddagger_{T_{\text{hm}}}$ the free energy at the harmonic mean of the experimental temperatures and ΔH^\ddagger the activation enthalpy, the correlation coefficient between ΔH^\ddagger and $\Delta G^\ddagger_{T_{\text{hm}}}$ is zero, as was previously shown.^{2,5}

$$\rho_{\Delta H^\ddagger, \Delta G^\ddagger_{T_{\text{hm}}}} = \frac{\Sigma(1/T - \langle 1/T \rangle)}{\sqrt{n\Sigma(1/T - \langle 1/T \rangle)^2}} = 0$$

For consistency we also evaluate the enthalpy estimate at $T = T_{\text{hm}}$.

Although estimates may be evaluated at any arbitrary temperature and may be plotted in any of three different possible planes, the only estimates that are statistically independent are those that are evaluated at T_{hm} and plotted in the $\Delta H - \Delta G$ plane. Variations in this plane due to the propagation of experimental errors have a completely random distribution. Thus any observed structured pattern must be the result of chemical factors alone.⁵ Ritchie and Sager¹² have suggested that a linear $\Delta H - \Delta S$ effect should be determined in $\Delta H - \Delta G$ coordinates but they failed to specify at what temperature the parameters should be evaluated.

III. *Regression with Error in Both Variables.* Several articles have been published that present solutions of various special cases in which there is error in the independent variable.^{4,15-17} For the regression of $\Delta H_{T_{\text{hm}}}$ onto $\Delta G_{T_{\text{hm}}}$, the likelihood function is maximized by minimizing the weighted sum of squares

$$\min_{a, \gamma} \sum_{j=1}^m \frac{(\Delta \hat{H}_j - a - \gamma \Delta \hat{G}_j)^2}{\sigma_j^2}$$

assuming a linear functionality where

$$\sigma_j^2 = V[\Delta \hat{H}_j - a - \gamma \Delta \hat{G}_j] \\ = V[(\Delta H_j + \epsilon_{\Delta H_j}) - a - \gamma(\Delta G_j + \epsilon_{\Delta G_j})] \\ = \sigma_{\Delta H_j}^2 + \gamma^2 \sigma_{\Delta G_j}^2 \\ = \sigma_{\Delta G_j}^2(\lambda + \gamma^2) \\ \cong s_{\Delta G_j}^2(\lambda + \gamma^2)$$

where σ^2 refers to the errors ϵ in the estimates of ΔH and ΔG , and λ has been derived previously²

$$\lambda = \frac{\sigma_{\Delta H_j}^2}{\sigma_{\Delta G_j}^2} = \frac{(\Sigma 1/T)^2}{n\Sigma(1/T - \langle 1/T \rangle)^2}$$

Notice the ratio λ depends only on the choice of experimental temperatures. Also the variance estimate $s_{\Delta G_j}^2 \cong V(\Delta \hat{G}_j)$ is proportional to the sum of squares of residuals after regressing either $\ln k_{i,j}$ or $\ln K_{i,j}$ onto $\{1/T_i - \langle 1/T \rangle\}$.

$$s_{\Delta G_j}^2 = \left[\frac{(RT_{\text{hm}})^2 \sum_{i=1}^n (1/T_i - \langle 1/T \rangle)^2}{|\mathbf{W}'\mathbf{W}|} \right] s_j^2$$

where

$$\mathbf{W}' = \begin{bmatrix} 1 & 1 & \dots & 1 \\ 1/T_1 - \langle 1/T \rangle & 1/T_2 - \langle 1/T \rangle & \dots & 1/T_n - \langle 1/T \rangle \end{bmatrix} \\ s_j^2 = \frac{\sum_{i=1}^n (y_{i,j} - \hat{\delta}_{1,j} - \hat{\delta}_{2,j}\{1/T_i - \langle 1/T \rangle\})^2}{(n-2)}$$

and $y_{i,j} = \ln k_{i,j}$ or $\ln K_{i,j}$ for $i = 1, n$ temperatures and $j = 1, m$ data sets. Thus the function to be minimized to obtain unbiased estimates of a and γ is

$$\min_{a, \gamma} \sum_{j=1}^m \frac{(\Delta H_j - a - \gamma \Delta G_j)^2}{s_j^2(\lambda + \gamma^2)}$$

The solution of this problem for $\hat{\gamma}$ is¹⁵⁻¹⁷

$$\hat{\gamma} = \theta \pm \sqrt{\theta^2 + \lambda} \quad \text{sgn}(\sqrt{\theta^2 + \lambda}) = \text{sgn}(s_{HG})$$

where s_{HH} , s_{GG} , and s_{HG} are the estimated variances of the enthalpies, free energies, and the estimated covariance of these two, respectively, and

$$\theta = (s_{HH} - \lambda s_{GG})/2s_{HG}$$

The minimum likelihood estimate (the "worst" value of the parameter given the data) is given by

$$\hat{\gamma}^* = \theta \pm \sqrt{\theta^2 - \lambda} \quad \text{sgn}(\sqrt{\theta^2 - \lambda}) = -\text{sgn}(s_{HG})$$

A t test has been derived by Creasy¹⁶ for the angle ϕ that the regression line makes through the plane for which there is error in both variables

$$t_{\alpha/2, m-2} = \sqrt{\frac{(m-2)\{(s_{HH} - s_{GG})^2/4 + s_{HG}^2\}}{s_{HH}s_{GG} - s_{HG}^2}} \sin 2(\phi - \hat{\phi})$$

where ϕ is related to γ by

$$\gamma = \sqrt{\lambda} \tan \phi$$

Geometrically, the regression procedure minimizes the weighted residuals between the data points and the regression line through the plane. Instead of the residuals being the vertical distances between the data and the regression line as is the case when there is no error in the ordinate variable, the residuals are the distances between the data and the regression line at some angle that depends on the relative magnitude λ of the variances of the two variables.

IV. *Regression Algorithm.* Given kinetic or equilibrium data, (\mathbf{k}, \mathbf{T}) or (\mathbf{K}, \mathbf{T}) , the following algorithm may be used to obtain unbiased estimates of ϕ , γ , a , ΔG_β , and β (the compensation temperature) for $j = 1, m$ systems evaluated at $i = 1, n$ temperatures.

(1) Regress $y_j = \ln k_j$ or $\ln K_j$ onto $\{1/T - \langle 1/T \rangle\}$ to obtain parameter estimates $\hat{\zeta}_j$ and residual sums of squares s_j^2 . Let

$$y_j = \mathbf{W} \zeta_j = \eta_j + \epsilon_j$$

$$\mathbf{W}' = \begin{bmatrix} 1 & 1 & \dots & 1 \\ 1/T_1 - \langle 1/T \rangle & 1/T_2 - \langle 1/T \rangle & \dots & 1/T_n - \langle 1/T \rangle \end{bmatrix}$$

$$\zeta_j' = \{\ln A - E/RT_{\text{hm}}\}_j, \{-E/R\}_j$$

for kinetic data, $y_{i,j} = \ln k_{i,j}$

$$= (-\Delta G_j^0/RT_{\text{hm}}, -\Delta H_j^0/R)$$

for equilibrium data, $y_{i,j} = \ln K_{i,j}$

Calculate

$$T_{\text{hm}} = n/\Sigma 1/T_i = \langle 1/T \rangle^{-1}$$

$$\hat{\zeta}_j = (\mathbf{W}'\mathbf{W})^{-1}\mathbf{W}'y_j$$

or more explicitly

$$\zeta_j' = \left[\frac{\sum_{i=1}^n y_{i,j}}{n}, \frac{\sum_{i=1}^n y_{i,j}(1/T_i - \langle 1/T \rangle)}{\sum_{i=1}^n (1/T_i - \langle 1/T \rangle)^2} \right]$$

and

$$s_j^2 = \frac{\sum_{i=1}^n (y_{i,j} - \zeta_{1,j} - \zeta_{2,j}(1/T_i - \langle 1/T \rangle))^2}{(n-2)}$$

(2) Then calculate enthalpy and free energy estimates from the slope and intercept estimates. For kinetic data

$$\Delta \hat{G}_j^\ddagger = -RT_{\text{hm}} \zeta_{1,j} + \{RT_{\text{hm}} \ln(kT_{\text{hm}}e/h) - RT_{\text{hm}}\}$$

$$\Delta \hat{H}_j^\ddagger = -R\zeta_{2,j} - RT_{\text{hm}}$$

and for equilibrium data

$$\Delta \hat{G}^\circ = -RT_{\text{hm}} \zeta_{1,j}$$

$$\Delta \hat{H}^\circ = -R\zeta_{2,j}$$

In matrix notation this may be written as

$$\Psi_j = \mathbf{A} \zeta_j + \mathbf{B}$$

where

$$\mathbf{A} = \mathbf{A}' = \begin{bmatrix} -RT_{\text{hm}} & 0 \\ 0 & -R \end{bmatrix}$$

$$\Psi_j' = (\Delta \hat{G}_j^\ddagger, \Delta \hat{H}_j^\ddagger) \quad \text{for kinetic data}$$

$$= (\Delta \hat{G}_j^\circ, \Delta \hat{H}_j^\circ) \quad \text{for equilibrium data}$$

$\mathbf{B}' = (\{RT_{\text{hm}} \ln(kT_{\text{hm}}e/h) - RT_{\text{hm}}\}, -RT_{\text{hm}})$ for kinetic data
 $= (0, 0)$ for equilibrium data

(3) The data may be plotted with joint confidence regions determined by the elliptic equation

$$(\Psi_j - \hat{\Psi}_j)' \mathbf{A}^{-1} \mathbf{W}' \mathbf{W} \mathbf{A}^{-1} (\Psi_j - \hat{\Psi}_j) = 2s_j^2 F(2, n-2, 1-\alpha)$$

or the data may be plotted along with one standard deviation increments from the maximum likelihood estimates from 2.

$$V(\hat{\Psi}_j) = \mathbf{A}(\mathbf{W}'\mathbf{W})^{-1} \mathbf{A} s_j^2$$

$$SD_{\Delta \hat{G}_j} = \sqrt{V(\Delta \hat{G}_j)} = (T_{\text{hm}} R) \sqrt{s_j^2/n}$$

$$SD_{\Delta \hat{H}_j} = \sqrt{V(\Delta \hat{H}_j)} = R \sqrt{s_j^2/\Sigma(1/T - \langle 1/T \rangle)^2}$$

If a linear regression appears to be justified from this plot then proceed with 4 and 5. If a nonlinear functionality is to be fitted, use an appropriate weighted nonlinear technique. The weighting factors are the estimated values of the residual sum of squares s_j^2 from step 1 or $s^2_{\Delta \hat{H}_j} = V(\Delta \hat{H}_j)$ from above.

(4) Calculate the following

$$\lambda = (\Sigma 1/T)^2 / (n \Sigma (1/T - \langle 1/T \rangle)^2)$$

$$s_{GG} = \Sigma \Delta G_j^2 / s_j^2 - (\Sigma \Delta G_j / s_j^2)^2 / \Sigma 1/s_j^2$$

$$s_{HH} = \Sigma \Delta H_j^2 / s_j^2 - (\Sigma \Delta H_j / s_j^2)^2 / \Sigma 1/s_j^2$$

$$s_{HG} = \Sigma \Delta H_j \Delta G_j / s_j^2 - \Sigma \Delta H_j / s_j^2 \Sigma \Delta G_j / s_j^2 / \Sigma 1/s_j^2$$

$$\theta = (s_{HH} - \lambda s_{HG}) / 2s_{HG}$$

$$\hat{\gamma} = \theta \pm \sqrt{\theta^2 + \lambda} \quad \text{sgn}(\sqrt{\theta^2 + \lambda}) = \text{sgn}(s_{HG})$$

$$\hat{\phi} = \tan^{-1}(\hat{\gamma}/\sqrt{\lambda})$$

$$\hat{a} = (\Sigma \Delta H_j / s_j^2 - \hat{\gamma} \Sigma \Delta G_j / s_j^2) / \Sigma 1/s_j^2$$

$$\Delta \hat{G}_\beta = \hat{a} / (1 - \hat{\gamma})$$

$$\hat{\beta} = T_{\text{hm}} / (1 - 1/\hat{\gamma})$$

(5) Finally $(1 - \alpha)100$ percent confidence intervals may be calculated from the following upper and lower bound estimates.

$$\hat{\phi}_\nu = \hat{\phi}$$

$$\pm \frac{1}{2} \sin^{-1} \left[2t_{\alpha/2, m-2} \sqrt{\frac{\lambda(s_{HH}s_{GG} - s_{HG}^2)}{(m-2)(\lambda s_{GG} - s_{HH})^2 + \lambda s_{HG}^2}} \right]$$

$$\hat{\gamma}_\nu = \sqrt{\lambda} \tan \hat{\phi}_\nu$$

$$\hat{a}_\nu = (\Sigma \Delta H_j / s_j^2 - \hat{\gamma}_\nu \Sigma \Delta G_j / s_j^2) / \Sigma 1/s_j^2$$

$$\Delta \hat{G}_{\beta\nu} = \hat{a}_\nu / (1 - \hat{\gamma}_\nu)$$

$$\hat{\beta}_\nu = T_{\text{hm}} / (1 - 1/\hat{\gamma}_\nu)$$

We have presented here the regression algorithm and its derivation for the determination of unbiased parameter estimates and their confidence intervals for a linear functional dependence between ΔH and ΔG for both kinetic and equilibrium data. For convenience we will refer to this *modification* of ordinary linear regression as M-linear regression. M-linear regression takes into account the ratio of variances of the two independent variables. Note that ordinary linear regression is a special case of M-linear regression for the case of no uncertainty in one of the independent variables. We have also presented the transformations that relate these parameter estimates and their confidence intervals to those that characterize a linear dependence between ΔH and ΔS . We have also alluded to how parameter estimations may be obtained between other thermodynamic parameters by transformations of the results in the $\Delta H - \Delta G$ plane and also for parameter estimation for nonlinear functionalities.

Because this parameter estimation situation is different from most, being twice removed from the original data, some rather unusual results occur from the straightforward application of this algorithm. In these next few sections several unusual results are discussed: the interpretation of the *minimum* likelihood values $\hat{\gamma}^*$ and $\hat{\beta}^*$, confidence intervals for γ that are not symmetric about $\hat{\gamma}$, and confidence intervals for β that appear at first glance to exclude $\hat{\beta}$. Interpretation of the results of the regression algorithm to accept or reject the hypothesis that a linear enthalpy-entropy effect has been detected is also discussed. Finally experimental design considerations are reviewed so that an experimenter who, on the basis of an initial set of experiments, suspects the existence of a linear effect may plan additional experiments to enhance his chances of detecting it if, in fact, it does exist.

V. *The Minimum Likelihood Estimate.* We have shown that an unbiased estimate of chemical compensation is displayed only in $\Delta H - \Delta G_{T_{\text{hm}}}$ coordinates. A linear relationship in these coordinates with slope γ is a reflection of a linear relationship in $\Delta H - \Delta S$ coordinates with slope

$$\beta = T_{\text{hm}} f(\gamma) = T_{\text{hm}} / (1 - 1/\gamma)$$

Because experimental temperatures are less than infinity the ratio of variances of enthalpy to free energy will always be greater than unity ($\lambda > 1$). In fact, for all the cases reviewed by us, $\lambda > 250$, indicating that the residuals to be minimized will be very nearly the vertical distances between any fitted line and the data points. At $\lambda = 1$ the residual is the perpendicular distance between each data point and the regression line. These residuals become the vertical displacements as λ increases to infinity. Thus the least likely line to be fitted for any $\lambda \gg 1$ is the vertical line $\gamma^* = \infty$ which by substitution into the above relationship yields $\beta^* = T_{\text{hm}}$.

Another way to arrive at this result is to consider the geo-

metrical representation of the compensation effect presented by Petersen,^{18a} Exner,⁷ and Wold.^{18b} They argue that Arrhenius plots must show an intersection of the regression lines at a true compensation temperature. The same geometrical requirement is also necessary for van't Hoff plots. Thus the maximum likelihood estimate $\hat{\beta}$ is located where the lines comes closest together. This is where all y_j are projected to have the same value. The minimum likelihood estimate $\hat{\beta}^*$ occurs where all y_j are least likely to have the same value. This location corresponds to the point at which the confidence bands about the regression lines are farthest apart, as is illustrated in Figure 1. Since the confidence band about any given line is the narrowest at $T = T_{hm}$, the estimate $\hat{\beta}^*$ will always be near T_{hm} . In fact $\hat{\beta}^*$ equals T_{hm} for either of the following cases: (1) all lines are exactly parallel or (2) the sum of positive deviations from some arbitrary line equals the sum of negative deviations. This second case is essentially the case of no detectable linear compensation. It is precisely for this case, however, that the application of ordinary least squares to data in the $\Delta H - \Delta S$ plane gives $\hat{\beta} \cong T_{hm}$ whereas the proper regression procedure gives $\hat{\beta}^* \cong T_{hm}$. Thus the researcher will generally estimate the worst possible instead of the best possible value of the compensation temperature by applying linear regression to regress enthalpy estimates on entropy estimates.

VI. *Hypothesis Testing.* The various confidence intervals, $(\hat{\gamma}_L, \hat{\gamma}_U)$ and $(\hat{\beta}_L, \hat{\beta}_U)$, give a measure of the precision of the estimates of the diagnostic parameter γ and the chemical compensation temperature β . The simplest hypothesis test for detection of a linear extrathermodynamic effect is $H_0: \gamma = 1$. Rejection of this hypothesis would indicate that the extra thermodynamic equation

$$\Delta H = \gamma \Delta G + (1 - \gamma) \Delta G_\beta$$

where

$$\Delta G_\beta = \Delta H - \beta \Delta S = \Delta H + \gamma T_{hm} \Delta S / (1 - \gamma)$$

is not identical with the thermodynamic expression at $T = T_{hm}$

$$\Delta H = \Delta G - T_{hm} \Delta S$$

Hence rejection of H_0 by the $(1 - \alpha)100$ percent confidence interval $(\hat{\gamma}_L, \hat{\gamma}_U)$ not including unity means rejection of the hypothesis at the α level of significance that only the thermodynamic effect is being observed. Notice that $\hat{\gamma}$ is not necessarily centered in $(\hat{\gamma}_L, \hat{\gamma}_U)$, but depends on the magnitude and uncertainty of the angle ϕ that the regression line makes through the plane.

Similarly the confidence interval $(\hat{\beta}_L, \hat{\beta}_U)$ for β is a measure of the precision with which the compensation temperature is estimated. The expression for β in terms of γ has a pole at $\gamma = 1$, however. Thus when only the thermodynamic effect is dominant, γ approaches unity and the confidence interval for β tends to include all possible values, both positive and negative, except those near T_{hm} . If a linear compensation functionality is forced to fit these data, the result is that the intersection of regression lines may be somewhere far removed from the experimental range both at higher or lower values. When this result is obtained, it is safe to conclude that only the thermodynamic effect was observed from the data and no extrathermodynamic effect was detected.

VII. *Experimental Design Considerations.* Selection of experimental temperatures prior to experimentation is the

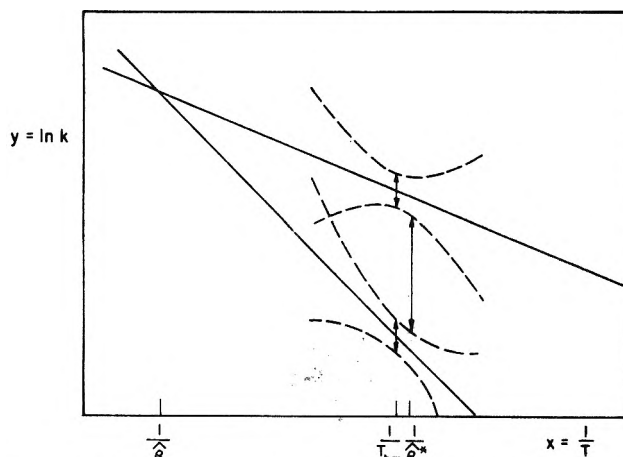


Figure 1. Plot of $y_{i,j} = \ln k_j$ or $\ln K_j$ vs. $1/T_i$ for two hypothetical data sets. The temperature at which the y values are predicted to coincide is the maximum likelihood estimate of the compensation temperature $\hat{\beta}$ and is located at the intersection of the regression lines.^{7,18} The minimum likelihood estimate of the compensation temperature $\hat{\beta}^*$ is where the values of y are least likely to coincide and that corresponds to the value for which the confidence bands are farthest apart.

selection of the experimental design. Typically the experimenter will wish to select a design that will maximize the precision of the parameters that he is estimating. Recalling that

$$\beta = T_{hm} / (1 - 1/\gamma)$$

the precision of the β estimate may be approximately obtained from the precision of the γ estimate by considering a truncated Taylor series expansion

$$V(\hat{\beta}) = \left[\frac{T_{hm}}{\gamma^2(1 - 1/\gamma)^2} \right]^2 V(\hat{\gamma})$$

The value of β is estimated with greatest precision when the value of γ becomes very large. In the limit, as γ is increased, the variance of $\hat{\beta}$ becomes vanishingly small.

$$\lim_{\gamma \rightarrow \pm\infty} V(\hat{\beta}) = 0$$

This may be accomplished two ways.

(1) Set all experimental temperatures exactly equal to β . This can be seen from the earlier definitions

$$\lambda = \frac{(\sum 1/T)^2}{n \sum (1/T - \langle 1/T \rangle)^2}$$

$$\hat{\gamma} = \Theta \pm \sqrt{\Theta^2 + \lambda}$$

then

$$\lim_{T_i=T_j \neq i} \lambda = \infty = \pm \lim_{T_i=T_j \neq i} \hat{\gamma}$$

In this case the experimenter would obtain an estimate $\hat{\beta}$ from previous experimentation and would merely compare the value of the various rate constants after repeated sampling with the experimental temperature set equal to $\hat{\beta}$.

(2) The experimental temperatures may be varied but centered about $\hat{\beta}$ such that the harmonic mean of these temperatures is as close as possible to the value of β estimated from previous experiments. This result may be seen from the definition

$$\gamma = 1/(1 - T_{\text{hm}}/\beta)$$

then

$$\lim_{\beta \rightarrow T_{\text{hm}}} \hat{\gamma} = \infty$$

$$\lim_{\gamma \rightarrow \infty} V(\hat{\beta}) = 0$$

Leffler⁹ has previously argued that data should be taken at temperatures near the compensation temperature in order to observe linear compensations. He explained that nonlinear effects may otherwise be observed due to competing compensations of similar intensity. Ritchie and Sager,¹² however, have shown that compensation temperatures may themselves be temperature dependent and should be reported along with the experimental temperature at which they were observed. Thus an experimenter may not be able to run his experiments at temperatures as close to a compensation temperature as he would like.

Application to Chemical Examples

We used the M-linear regression algorithm to screen data from the literature in a search for linear compensation effects. We now demonstrate the usefulness of this regression procedure, discuss the inferences that can be made about many data sets in light of the results obtained using this powerful analytical method, and compare findings obtained from the usual application of least squares.

I. *Correlation Analysis.* The need to analyze enthalpy-entropy compensation data using proper regression procedures is best exemplified by comparing a data set that clearly has a chemical compensation effect with one that does not. To make this comparison the logarithms of rate constants were regressed on both $1/T_j$ and $\{1/T_j - \langle 1/T \rangle\}$ to obtain the estimates $\Delta\hat{H}^\ddagger$, $\Delta\hat{S}^\ddagger$, and $\Delta\hat{G}^\ddagger_{T_{\text{hm}}}$ for two chemical examples. $\Delta\hat{H}^\ddagger$ and $\Delta\hat{S}^\ddagger$ were then evaluated at T_{hm} and all these parameter estimates are plotted in Figures 2 and 3.

The random distribution of data in Figure 2b indicates that all the apparent linear structure in Figure 2a can be explained solely on the basis of the propagation of experimental errors. The data in Figure 3b, however, clearly show a chemical effect. The correlation coefficients are summarized in Table II.

In the oximation example no significant correlation is detected²¹ after removal of the statistical compensation pattern. This is in contrast to the hydrolysis example in which a strong correlation is evident even after the statistical effect is removed.

II. *Parameter Estimation.* The parameter estimates were obtained for these two data sets assuming a linear extrathermodynamic functionality. Three regression procedures were used: (a) the procedure presented here that accounts for the relative magnitude of errors, (b) weighted linear least squares of $\Delta\hat{H}_{T_{\text{hm}}}$ on $\Delta\hat{G}_{T_{\text{hm}}}$ using the variance estimates $s^2_{\Delta\hat{H}_j}$ (see Regression Algorithm Step 3) as the weighting factors, and (c) ordinary least squares of $\Delta\hat{H}_{T_{\text{hm}}}$ on $\Delta\hat{S}_{T_{\text{hm}}}$. The maximum likelihood estimates of γ and β are given in Table III along with their 95% confidence intervals. The minimum likelihood estimate of the compensation temperature β^* and the values of λ and T_{hm} are also listed.

For all cases note that $\hat{\beta}^* \cong T_{\text{hm}}$ and that weighted least squares gives nearly identical results with the M-linear regression procedure presented here. Because $\lambda \gg 1$, the alignment of the residuals that were minimized was not far from vertical, the alignment that is appropriate for the case of or-

dinary linear regression. Hence the close agreement between the estimates by methods a and b.

The hydrolysis data showed a slight bias of $\hat{\beta}$ toward T_{hm} when regression was performed of $\Delta\hat{H}^\ddagger$ on $\Delta\hat{S}^\ddagger$ using method c, as was expected. The close agreement with the proper regression results, however, indicates that the assumptions made in developing the hypothesis test proposed in the first article² were reasonable. The hydrolysis data are plotted in Figure 4 along with the regression lines and the maximum likelihood point of intersection is also marked along with its 95% confidence interval.

The oximation data are plotted in Figure 5 and do not appear to have a common point of intersection. At the 95% level of confidence, the location of a common point of intersection for this data set, for example, could not be below 417 K nor above 212 K. The maximum likelihood point of intersection is at -1328 K. Thus at this level of probability the intersection or compensation temperature could be almost anywhere, except near where the data were sampled. Given the data, then, there is no detectable chemical compensation effect.

Why the confidence interval includes all numbers above and below certain bounds, instead of just the numbers inbetween, is shown in Figure 6. For the hydrolysis example the probability density function for γ_1 given the data $p(\gamma_1 | \mathbf{k}_1, \mathbf{T}_1)$ is reflected into the well-behaved probability density function for β_1 given the data $p(\beta_1 | \mathbf{k}_1, \mathbf{T}_1)$ through the transformation $\beta = T_{\text{hm}} f(\gamma) = T_{\text{hm}}/(1 - 1/\gamma)$. The oximation example, however, has a density function $p(\gamma_2 | \mathbf{k}_2, \mathbf{T}_2)$ that straddles the pole at $\gamma = 1$. The density function $p(\beta_2 | \mathbf{k}_2, \mathbf{T}_2)$ is then thinly dispersed over a wide range of numbers. Thus the probability is vanishingly small that a compensation temperature exists in any finite temperature interval. We conclude that no chemical compensation is detected for cases where $p(\gamma | \mathbf{k}, \mathbf{T})$ overlaps unity.

III. *The Case of Other Independent Variables.* Since $\lambda \gg 1$ and $\rho_{\Delta H, \Delta S} \cong 1$, the most precisely determined measure of a thermodynamic variable readily obtainable from kinetic or equilibrium data is $\Delta\hat{G}_{T_{\text{hm}}}$. Thus this parameter should get greater attention when considering the effect of some independent variable on the thermodynamics of a chemical series. For the oximation example, the number of carbon atoms n_c in a side chain is such an independent variable. Plots of the enthalpies and free energies vs. n_c in Figure 7 reveal a true chemical effect, with some asymptotic dependence on n_c , even though no chemical compensation is detectable. Since the enthalpy is not causing the variation in free energy, the effect must be the result of entropy as was deduced by the experimenters.

The free energy remains relatively constant for the last six chemicals of the series and appear to form an asymptote for $n_c \geq 2$. By application of M-linear regression presented above we conclude that $\Delta\hat{H}^\ddagger$ and $\Delta\hat{S}^\ddagger$ are probably also relatively invariant for $n_c \geq 2$ for this data set.

IV. *Other Examples.* Although the simple hypothesis test using regression in the $\Delta H - \Delta S$ plane as was suggested in the first article² gave correct results when applied to the oximation and hydrolysis data, in general it may not discriminate well when β numerically approaches T_{hm} . The proper regression procedure given here does provide good discrimination between β and T_{hm} since the variance and standard deviation of β becomes vanishingly small near T_{hm} . Thus if the value of β is near T_{hm} , it will be determined with the greatest precision possible (see Experimental Design Considerations).

Our review of the literature revealed that the data listed in Table IV have at least a linear compensation distinguishable

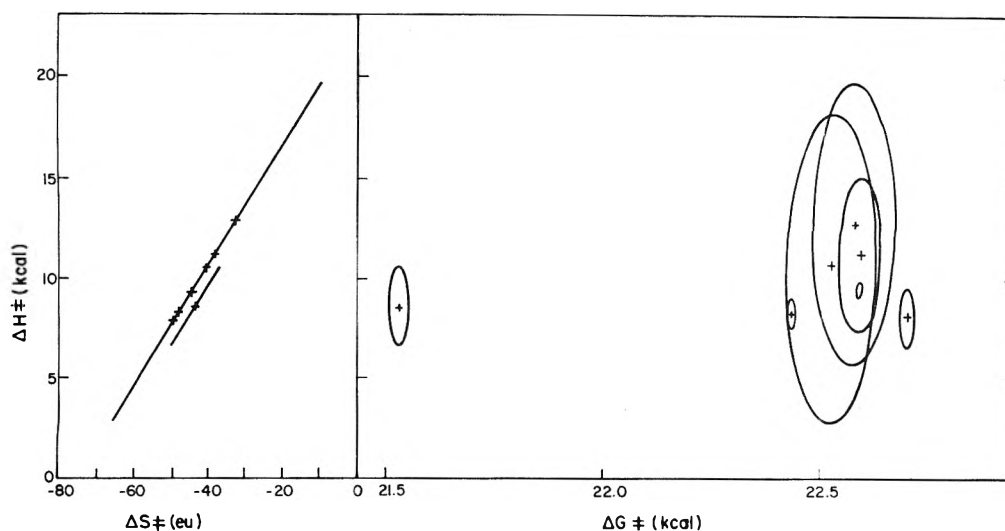


Figure 2. Plots of thermodynamic parameter estimates and their respective 50% confidence regions for the oximation of thymyl ketones.¹⁹ The lack of structure in the $\Delta H^\ddagger - \Delta G^\ddagger$ plot indicates that the apparent linear distribution of estimates in the $\Delta H^\ddagger - \Delta S^\ddagger$ plot is just a realization of the propagation of experimental errors. No chemical effect is detected. The data are evaluated at $T_{\text{hm}} = 308.1$ K.

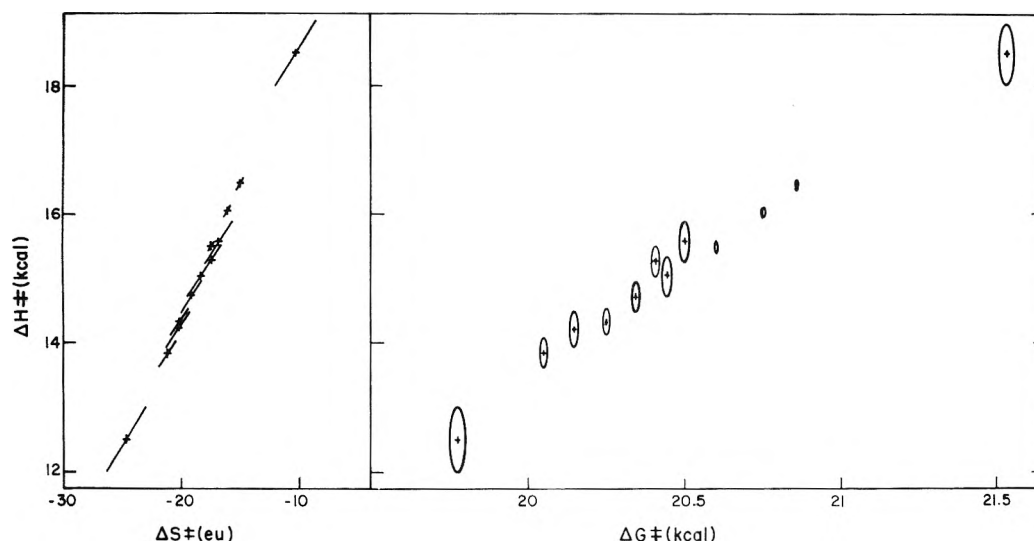


Figure 3. Plots of thermodynamic parameter estimates and their respective 50% confidence regions for the hydrolysis of ethyl benzoate.²⁰ The linear structure in the $\Delta H^\ddagger - \Delta G^\ddagger$ plot indicates that a linear chemical compensation is detected. The data are evaluated at $T_{\text{hm}} = 292.6$ K.

TABLE II: Correlation Coefficients

Reaction	$\Delta \hat{H}^\ddagger - \Delta \hat{S}^\ddagger$		$\Delta \hat{H}^\ddagger - \Delta \hat{G}^\ddagger$		<i>m</i>
	ρ	<i>r</i>	ρ	<i>r</i>	
1. Oximation of alkyl thymyl ketones ¹⁹	0.9999	0.9724	0	-0.2273	7
2. Same as (1) but deleting the methylated compound	0.9999	0.9988	0	0.0770	6
3. Hydrolysis of ethyl benzoate ²⁰	0.9988	0.9987	0	0.9929	12

from the thermodynamic restraint imposed by the Gibbs equation. That is, for these data sets the hypothesis $H_0: \gamma = 1$ is rejected at the 5% level of significance that the observed distribution of points is more than just randomly distributed about the line

$$\Delta H = \Delta G + T\Delta S$$

because unity is not contained in the 95% confidence intervals

of these estimates of γ . The data sets that were reviewed in the first part of this article² but that do not appear here did not have an extrathermodynamic effect detectable at the 5% level of significance. The only solvent effects listed in Table IV are entries 7, 9, 13, 14, and 17. The rest are substituent effects. There are about twice as many cases of the compensation temperatures being higher than the experimental temperatures as lower than the experimental temperatures. There

TABLE III: Parameter Estimates

Reaction		$\hat{\gamma}$	$(\hat{\gamma}_L, \hat{\gamma}_U)$	$\hat{\beta}$	$(\hat{\beta}_L, \hat{\beta}_U)$	Other
1. Oximation of alkyl thymyl ketones ¹⁹	a	0.812	(-2.220, 3.846)	-1328.01	(212.41, 416.35)	$T_{hm} = 308.10$
	b	0.811	(-2.214, 3.835)	-1319.46	(212.23, 416.77)	$\hat{\beta}^* = 308.05$
	c			313.7	(226.1, 401.3)	$\lambda = 5695.88$
2. Same as (1) but deleting the methylated compound	a	3.485	(-6.251, 13.338)	432.07	(265.60, 333.07)	$T_{hm} = 308.10$
	b	3.456	(-6.096, 13.009)	433.53	(265.68, 333.75)	$\hat{\beta}^* = 307.91$
	c			307.0	(285.7, 328.3)	$\lambda = 5695.88$
3. Hydrolysis of ethyl benzoate ²⁰	a	3.257	(2.979, 3.535)	422.29	(408.03, 440.47)	$T_{hm} = 292.62$
	b	3.255	(2.977, 3.533)	422.36	(408.12, 440.59)	$\hat{\beta}^* = 290.31$
	c			416.3	(401.3, 431.3)	$\lambda = 410.26$

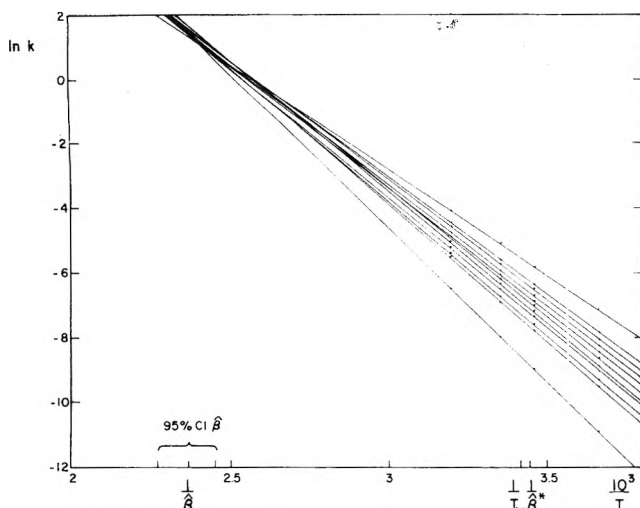


Figure 4. Plot of $\ln k_{i,j}$ vs. $1/T_i$ for the hydrolysis of ethyl benzoate.²⁰ Notice that the data suggest that a common point of intersection is plausible within the extrapolation error of the regression lines. The 95% confidence interval for such a compensation temperature is indicated as well as the location of the least likely temperature at which a common intersection may occur given the data.

is only one example (5) of an estimated negative compensation temperature (for this example the 95% confidence interval does extend into the region of positive values). Exner calls data with negative β values examples of "anti-compensation".⁶ Three other examples (2, 6, 18) have compensation temperatures so low that their 95% confidence intervals extend below zero.

Examples 9 and 12 have compensation temperatures sufficiently close to the experimental temperatures that the compensation temperature estimate is determined rather precisely. Example 15 has such good fit to the linear extra-thermodynamic relationship that the compensation temperature is also estimated very precisely.

Examples 7, 8, 10, 13, and 15 have slight curvatures that may be the realizations of the type of compensation that results from a consideration of the vibrational energies as discussed by Laidler.³⁴ Other examples of curvature of the $\Delta H - \Delta G$ function are the racemization of a biphenyl in butanol-water²⁷ and the racemization of a dicarboxydiphenyl in methanol-water and methanol-benzene.³⁵ In fact these two data sets display $\Delta H - \Delta G$ functions that appear to pass through minima.

Examples 4, 10, 12, 16, and 20 are subsets of the complete data sets in examples 3, 1, 9, 11, and 19, respectively. All but examples 16 and 11 demonstrate that essentially the same compensation is operative throughout the data set as is evidenced by the overlapping confidence intervals of the pa-

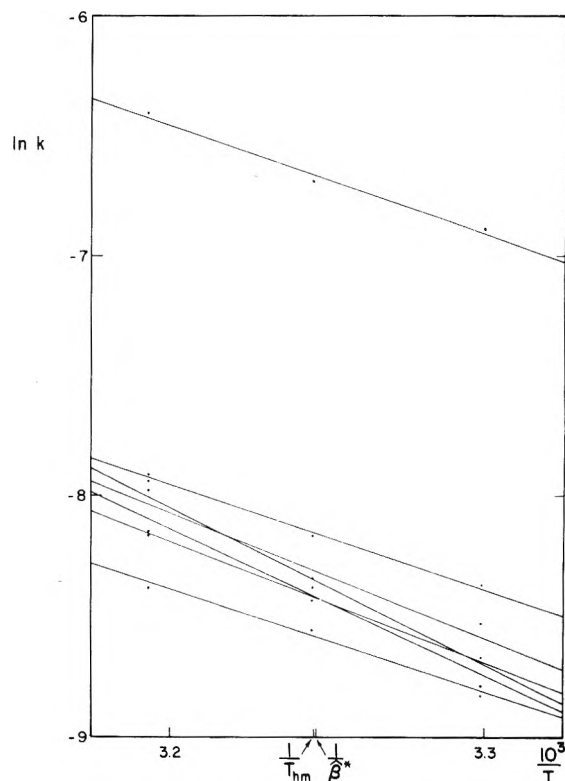


Figure 5. Plot of $\ln k_{i,j}$ vs. $1/T_i$ for the oximation of thymyl ketones.¹⁹ Notice no common point of intersection is suggested by the data. The minimum likelihood estimate for the temperature for such an intersection point is near T_{hm} .

parameter estimates. Figure 8 contains a plot of the data set in example 16. Lack of fit to a line is indicated. It is informative to note that the range of variation of $\Delta \bar{H}$ and especially $\Delta \bar{G}$ is substantially wider for this case and hence gives a more complete view of the overall functionality. A comparison of example 16 with example 11 shows how a sampling over a sufficiently restricted range of one variable might lead the investigator to believe that he is sampling from a linear function whereas he might actually be sampling from a local linearity of an otherwise nonlinear function.

Again the 50% joint confidence regions are plotted for the data in Figure 8. The precision of the parameter estimates is so great, however, that these ellipses appear as small line segments. The extrema of the ellipses are delineated by horizontal bars. The same short line segments represent the one standard deviation increments from the maximum likelihood values of the enthalpies. The one standard deviation increments for the free energy estimates are too small to be discernible on this plot.

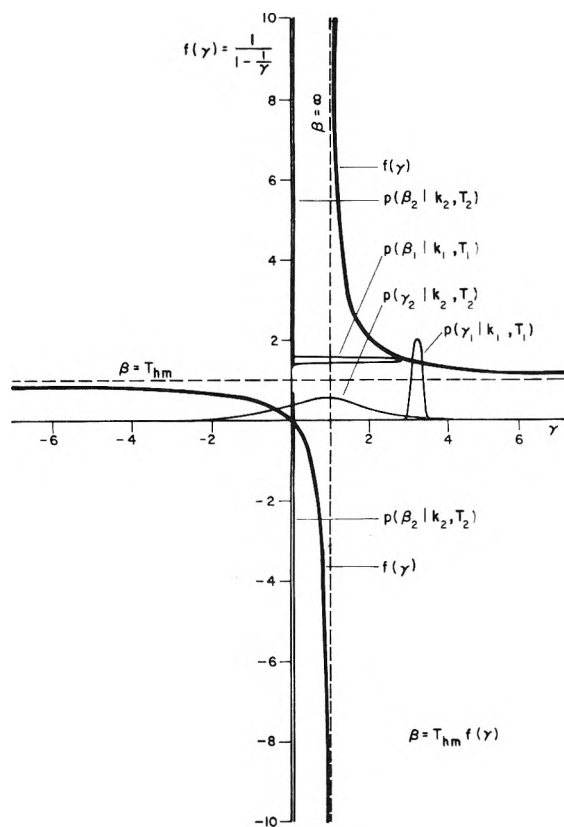


Figure 6. Probability density functions for γ and β . The bold line is the function $f(\gamma)$ through which the well-behaved probability density functions $p(\gamma|k, T)$ are mapped into either well behaved or skewed density functions $p(\beta|k, T)$. The footnote "1" represents parameters obtained from the hydrolysis of ethyl benzoate²⁰ and "2" represents parameters obtained from the oximation of thymyl ketones.¹⁹

Leffler⁹ has warned that the regression and plotting methods of Exner⁶ are inadequate because multiple interaction mechanisms will produce nonlinear compensations. The regression techniques of Exner and Wold assume a linear functionality of the extrathermodynamic relationship.⁶⁻⁸ This carbinol formation example, (16), however, appears to be nonlinear. The thermodynamic and statistical mechanical arguments of Laidler,³⁴ Hammett,³⁶ Ritchie and Sager,¹² and Leffler^{9,30} all suggest a general nonlinear functionality that degenerates to the linear case when certain order of magnitude criteria are met. In a similar vein, Wold³⁷ and Daudel³⁸ merely make a Taylor series expansion and assume higher order terms are negligible for the linear extrathermodynamic relationships. We will now test the hypothesis that only the first-order expansion is detectable.

Given a general nonlinear functional dependence of ΔH on ΔG , the function may be expanded in a Taylor series to give an N th order polynomial that essentially converges in some finite number of terms N .

$$\Delta H = C_0 + \sum_{i=1}^N C_i \Delta G^i$$

where the coefficients C_i are the derivatives of ΔH with respect to ΔG

$$C_i = \left(\frac{\partial^i \Delta H}{\partial \Delta G^i} \right)_{\Delta G = \Delta G_{T_{hm}}}$$

To test whether additional terms in the expansion give sig-

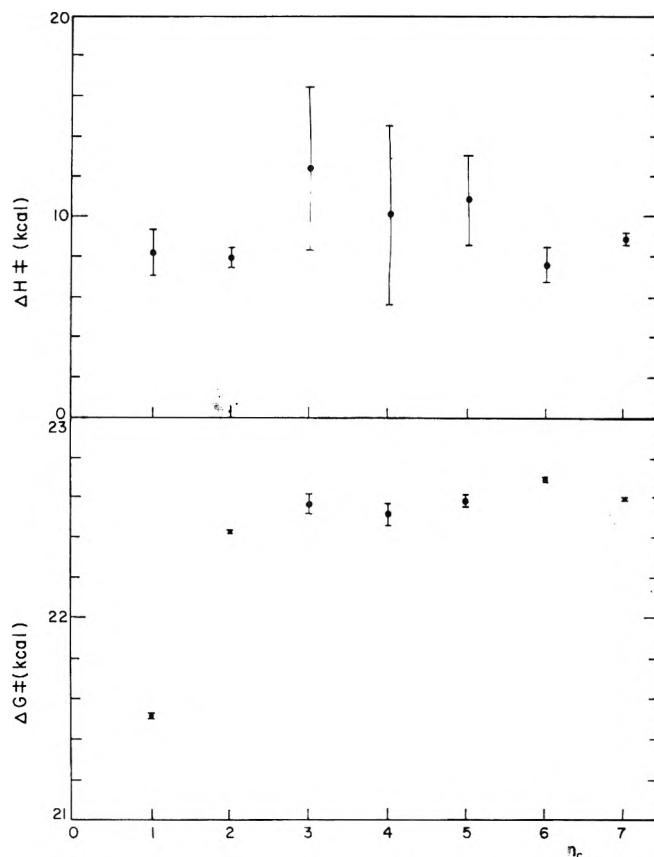


Figure 7. Plots of thermodynamic parameters vs. an independent variable for the oximation of thymyl ketones.¹⁹ The number of carbon atoms, n_c , may be considered to be free of error and the $\Delta G^\ddagger_{T_{hm}}$ estimates are determined with much greater precision than the ΔH^\ddagger estimates. One standard deviation increments are plotted. The greater precision of the $\Delta G^\ddagger_{T_{hm}}$ estimates is the reason for its utility when subtle chemical variations are to be detected.

nificant reductions in the sum of squares of residuals to the fit of the polynomial the principle of extra sum of squares is used.³⁹ Since $\lambda = 709 \gg 1$ for this example the uncertainty of the free energy estimates is much smaller than the uncertainty of the enthalpy estimates. Thus the use of weighted least squares is justified. For the comparison of a p variable vs. a q variable model that is linear in the parameters where $p > q$ the significance of the reduction in sums of squares of weighted residuals from S_q to S_p is given by the F test.

$$\frac{(S_q - S_p)/(p - q)}{s_v^2} = F(p - q, v, 1 - \alpha)$$

The expected sum of squares s_v^2 is estimated from the variances of the enthalpy estimates determined by regression on the linearized Arrhenius or van't Hoff equations. Since these variances are also used as the weights for the determination of S_p and S_q , then s_v^2 is given by

$$s_v^2 = \frac{\sum_{j=1}^m s^2_{\Delta H_j} / s^2_{\Delta H_j}}{m - 1} = \frac{m}{m - 1}$$

A significant reduction in the sums of squares did not occur until an expansion of $N = 4$. Surprisingly the linear term in ΔG was negligible but the $l = 2, 3$, and 4 coefficients were significant. The $l = 5$ coefficient was also insignificant in the sense that its 95% confidence interval included zero. An ex-

TABLE IV: Linear Extrathermodynamic Compensations

Reaction	$\hat{\gamma}$	$(\hat{\gamma}_L, \hat{\gamma}_U)$	$\hat{\beta}$	$(\hat{\beta}_L, \hat{\beta}_U)$	T_{hm}	m
1. Hydrolysis of aryl sulfuric acids ²²	2.67	(2.22, 3.13)	537.1	(494.0, 611.8)	336.2	23
2. Esterification of benzoic acids ²³	-0.379	(-0.989, 0.231)	94.1	(-103.2, 170.4)	342.8	22
3. Carbinol formation from malachite dyes ²⁴	5.37	(4.13, 6.63)	366.0	(350.7, 393.1)	297.8	13
4. Same as (3) but deleting the <i>p</i> -N(CH ₃) ₂ compound	5.72	(4.56, 6.89)	360.9	(348.3, 331.5)	297.8	12
5. Esterification of aromatic acids ²⁵	0.102	(-0.414, 0.619)	-36.1	(-514.0, 92.7)	316.4	12
6. Esterification of aromatic acids ²⁶	-0.354	(-0.872, 0.164)	81.3	(-61.2, 144.9)	311.1	11
7. Racemization of a biphenyl in MeOH-H ₂ O ²⁷	4.40	(3.34, 5.46)	469.3	(443.8, 517.5)	362.6	8
8. Hydrolysis of amides ²⁸	3.25	(1.19, 5.39)	500.6	(425.7, 2200.4)	346.7	8
9. Rearrangement of triarylmethyl azides ²⁹	20.4	(14.8, 26.4)	476.2	(470.7, 435.6)	452.8	8
10. Same as (1) but just those data that form a 7 point line in Figure 9-30 of Lefler's text ³⁰	4.43	(2.62, 6.30)	434.1	(399.6, 543.6)	336.2	7
11. Carbinol formation of σ -substituted malachite dyes ³¹	2.49	(1.32, 3.67)	497.8	(409.4, 1228.0)	297.7	7
12. Same as (9) but only in dibutyl carbitol	20.4	(12.8, 28.8)	476.1	(469.1, 491.2)	452.8	6
13. Racemization of a biphenyl in acetic acid-benzene ²⁷	2.60	(1.15, 4.04)	589.8	(481.6, 2706.3)	362.6	6
14. Racemization of a biphenyl in acetic acid-water ²⁷	5.11	(3.56, 6.68)	450.8	(426.4, 504.1)	362.6	6
15. Hydrolysis of phenyl acetates ³²	-2.42	(-2.77, -2.08)	228.8	(218.3, 237.4)	323.1	6
16. Same as (11) but deleting H and SO ₃ H substituted compounds	8.59	(4.87, 12.63)	337.0	(323.3, 374.7)	297.7	5
17. Racemization of a biphenyl in Me ₂ SO-H ₂ O ²⁷	2.45	(1.48, 3.43)	612.8	(512.0, 1125.4)	362.6	5
18. Hydrolysis of benzyl acetates ³²	-1.82	(-4.40, 0.66)	208.7	(-633.8, 263.3)	323.1	5
19. Isomerization of aminotriazoles, k_2 ³³	2.18	(1.93, 2.43)	607.7	(558.3, 683.8)	328.8	5
20. Same as (19) but deleting the C ₆ H ₅ CH ₂ substituted compound	2.21	(1.94, 2.48)	600.4	(550.5, 678.9)	328.8	4

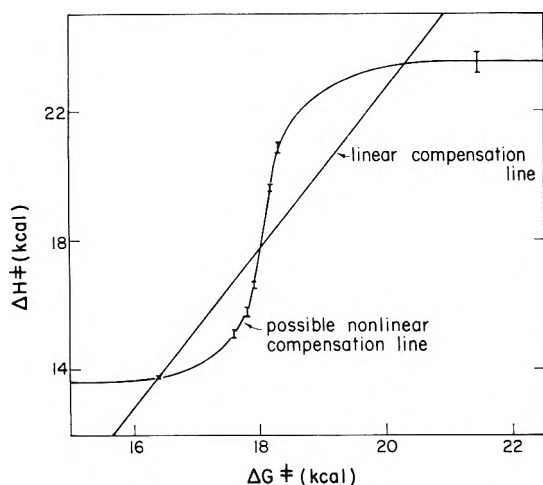


Figure 8. Carbinol formation from malachite dyes.³¹ The data are plotted along with 50% confidence ellipses or one standard deviation increments. The variances of the $\Delta G^\ddagger_{T_{hm}}$ estimates are too small to be noticed on this plot. A nonlinear functionality appears to be suggested by the data. The data are evaluated at $T = T_{hm} = 297.7$ K.

pansion that adequately describes the extrathermodynamic functionality for this carbinol formation is

$$\Delta H = 2026 - 2.6\Delta G - 35.8\Delta G^2 + 2.6\Delta G^3 - 0.052\Delta G^4$$

where ΔH and ΔG are expressed in kilocalories per mole. The 95% confidence intervals for these parameters are (1253, 2800), (-23.5, 18.3), (-48.4, -23.2), (1.7, 3.5), and (-0.071, -0.034), respectively. Note that the confidence interval for C_1 includes zero, so if a more parsimonious form were desired, the regression may be repeated deleting that term. The $C_{l \neq 1}$ coefficients appear to be essentially unchanged after deleting the $C_{l=1}$ term giving

$$\Delta H = 2061 - 36.9\Delta G^2 + 2.7\Delta G^3 - 0.054\Delta G^4$$

The reduction in sums of squares of either of these two ex-

pressions compared with the fit to the simple linear model (containing only terms up to $l = 1$) was very significant by the F test, which indicates the inadequacy of truncating the expansion after the linear term for this data set. Since the range of variation of ΔG was substantially greater for this example than for examples where only a linear effect was detected, one might infer that the previous linear examples are merely examples of local linearity as might be expected by sampling from just a small range of an otherwise nonlinear function. Although we have not found the exact functionality of this nonlinear compensation, knowledge of the magnitude of the first five partial derivatives may imply the existence of one or more of the theoretical nonlinear functionalities discussed earlier. We recommend that regressions of functionalities between thermodynamic variables be performed in the $\Delta H_{T_{hm}} - \Delta G_{T_{hm}}$ plane because, provided certain reasonable assumptions discussed above are satisfied, unbiased estimates of the parameters will be obtained and nonlinear effects are both readily seen and evaluated.

Summary and Conclusions

Chemical enthalpy-entropy compensation effects are detectable by a regression procedure that gives unbiased parameter estimates and confidence intervals for linear dependencies between thermodynamic parameters. Most reported examples of linear $\Delta H - \Delta S$ compensations in the literature, however, appear to be merely the statistical compensation pattern that is independent of the chemistry of the observed reactions and equilibria. A review of chemical theory and plots of $\Delta H_{T_{hm}}$ vs. $\Delta G_{T_{hm}}$ estimates suggested that linear chemical compensation between ΔH and ΔS may be considered a local linearity of an otherwise nonlinear function. Both variations in solvents and substituents appeared to generate linear compensations for chemical reactions. No linear compensations were detected for equilibria, but perhaps a more thorough review would uncover some.

The regression procedure presented here involves the regression of enthalpy estimates on free energy estimates evaluated at the harmonic mean of the experimental tempera-

tures. These are the only two thermodynamic potentials that define a plane into which the experimental errors propagate in a statistically uncorrelated manner. Unbiased estimates of slope and intercept are obtained in this plane using a procedure that accounts for the relative magnitude of uncertainty of the ΔH and ΔG estimates. Unbiased estimates of slopes and intercepts in other planes, for example $\Delta H - \Delta S$, can then be obtained from these estimates and their respective confidence intervals.

A review of the parameter estimation situation revealed that the determination of the compensation temperature by the application of ordinary least squares (regressing ΔH estimates on ΔS estimates) usually gives a number close to the "worst" rather than the "best" value of the compensation temperature. The modified linear regression procedure presented here gives an unbiased estimate of the compensation temperature and confidence interval estimates at any level of probability. The experimental design problem of obtaining precise measures of the compensation temperature was also discussed along with the application of weighted least squares to obtain parameter estimates for nonlinear dependencies between thermodynamic parameters.

Supplementary Material Available: Details of the mathematical arguments that have not already been presented in the first article² (5 pages). Ordering information is available on any current masthead page.

References and Notes

- (1) (a) Chemical Engineering Department. (b) Statistics Department and Engineering Experiment Station.
- (2) R. R. Krug, W. G. Hunter, and R. A. Grieger, *J. Phys. Chem.*, preceding article in this issue.
- (3) (a) J. Berkson, *J. Am. Stat. Assoc.*, **45**, 164 (1950); (b) G. E. P. Box, *Bull. Int. Stat. Inst.*, **38**, 339 (1961).
- (4) W. G. Cochran, *Technometrics*, **10**, 637 (1968).
- (5) R. R. Krug, W. G. Hunter, and R. A. Grieger, *Nature (London)*, **261**, 566 (1976).
- (6) O. Exner, *Coll. Czech. Chem. Commun.*, **29**, 1094 (1964); *Nature (London)*, **201**, 488 (1964).
- (7) O. Exner, *Nature (London)*, **227**, 366 (1970); *Coll. Czech. Chem. Commun.*, **37**, 1425 (1972).
- (8) S. Wold and O. Exner, *Chem. Script.*, **3**, 5 (1973).
- (9) J. E. Leffler, *Nature (London)*, **205**, 1101 (1965).
- (10) R. Lumry and S. Rajender, *Biopolymers*, **9**, 1125 (1970).
- (11) V. I. Shimulis, *Kinet. Katal.*, **10**, 1026 (1969); *Kinet. Catal.*, **10**, 837 (1969); B. Dzhuntini and V. I. Shimulis, *Kinet. Katal.*, **15**, 210 (1974); *Kinet. Catal.*, **15**, 180 (1974).
- (12) C. D. Ritchie and W. Sager, *Prog. Phys. Org. Chem.*, **2**, 323 (1964).
- (13) R. F. Brown and H. C. Newsom, *J. Org. Chem.*, **27**, 3010 (1962).
- (14) J. E. Leffler, *J. Org. Chem.*, **20**, 1202 (1955).
- (15) A. Madansky, *J. Am. Stat. Assoc.*, **54**, 173 (1959).
- (16) M. A. Creasy, *J. R. Stat. Soc. B*, **18**, 65 (1956).
- (17) D. V. Lindley, *J. R. Stat. Soc. Suppl.*, **9**, 218 (1947).
- (18) (a) R. C. Petersen, *J. Org. Chem.*, **29**, 3133 (1964); (b) S. Wold, *Chem. Script.*, **2**, 145 (1972).
- (19) M. J. Craft and C. T. Lester, *J. Am. Chem. Soc.*, **73**, 1127 (1951).
- (20) F. N. David, "Tables of the Correlation Coefficient", Cambridge University Press, Cambridge, England, 1954.
- (21) G. N. Burkhardt, C. Horrex, and D. i. Jenkins, *J. Chem. Soc.*, 1649 (1936).
- (22) R. J. Hartman, H. M. Hoogsteen, and J. A. Moede, *J. Am. Chem. Soc.*, **66**, 1714 (1944).
- (23) G. S. Idlis and O. F. Ginzburg, *Reakts. Sposoln. Org. Soedin.*, **2**, 46 (1965).
- (24) R. J. Hartman and A. G. Gassmann, *J. Am. Chem. Soc.*, **62**, 1559 (1940).
- (25) R. J. Hartman and A. M. Borders, *J. Am. Chem. Soc.*, **59**, 2107 (1937).
- (26) J. E. Leffler and W. H. Graham, *J. Phys. Chem.*, **63**, 687 (1959).
- (27) I. Meloche and K. J. Laidler, *J. Am. Chem. Soc.*, **73**, 1712 (1951).
- (28) W. H. Saunders and J. C. Ware, *J. Am. Chem. Soc.*, **80**, 3328 (1958).
- (29) J. E. Leffler and E. Grunwald, "Rates and Equilibria of Organic Reactions", Wiley, New York, N.Y., 1963, pp 315-402.
- (30) G. S. Idlis and O. F. Ginzburg, *Reakts. Sposoln. Org. Soedin.*, **2**, 54 (1965).
- (31) E. Tommila and C. N. Hinshelwood, *J. Chem. Soc.*, 1801 (1938).
- (32) E. Lieber, C. N. Rao, and T. S. Chao, *J. Am. Chem. Soc.*, **79**, 5962 (1957).
- (33) K. J. Laidler, *Trans. Faraday Soc.*, **55**, 1725 (1959).
- (34) B. M. Graybill and J. E. Leffler, *J. Phys. Chem.*, **63**, 1461 (1959).
- (35) L. P. Hammett, "Physical Organic Chemistry", 2d ed., McGraw-Hill, New York, N.Y., 1970, pp 391-408.
- (36) S. Wold, *Chem. Script.*, **5**, 97 (1974).
- (37) R. Daudel, "Quantum Theory of Chemical Reactivity", Reidel, Boston, Mass., 1973, pp 10-12.
- (38) N. R. Draper and H. Smith, "Applied Regression Analysis", Wiley, New York, N.Y., 1966, pp 67-69.

An Elementary Molecular Theory of Classical Fluids. Pure Fluids

Isaac C. Sanchez* and Robert H. Lacombe

Materials Research Laboratory and Polymer Science and Engineering, University of Massachusetts, Amherst, Massachusetts 01002
(Received April 22, 1976)

A molecular theory of classical fluids based on a well-defined statistical mechanical model is presented. Since the model fluid reduces to the classical lattice gas in one special case, it can be best characterized as an Ising or lattice fluid. The model fluid undergoes a liquid-vapor transition. Only three molecular parameters are required to describe a fluid; these parameters have been determined and tabulated for several fluids. The molecular weight dependence of the critical point and boiling point of a homologous series of fluids such as the normal alkanes is correctly predicted. The equation of state does not satisfy a simple corresponding states principle, although polymeric liquids of sufficiently high molecular weight do satisfy a corresponding states principle. The Ising fluid better correlates experimental saturated vapor pressures and liquid-vapor densities than the van der Waals or related theories. When applied to polymeric liquids it correlates experimental density data as well as less tractable equations derived from cell theories. The basic simplicity and structure of the theory readily suggests a generalization to mixtures.

I. Introduction

In a previous communication,¹ a new molecular theory of fluids was briefly outlined. Assumptions and details of the statistical mechanical model not discussed previously are fully explored in the present paper. Also, the theory will be compared with experiment and the van der Waals, lattice gas, hard sphere, and cell model theories.

The basic motivation of this work is to establish a foundation for a general theory of mixed molecular fluids of arbitrary geometry and size. The basic simplicity and structure of the pure fluid formalism readily suggests a suitable generalization to mixtures. Further, the pure fluid theory is sufficiently accurate so that the resulting mixture theory enjoys a high level of predictive capability. Details of the mixture theory will be presented in a second paper.

In statistical mechanics the Gibbs free energy G is related to the configurational partition function Z in the pressure ensemble by

$$G = -kT \ln Z(T,P) \quad (1)$$

$$Z(T,P) = \sum_V \sum_E \Omega(E,V,N) \exp[-\beta(E + PV)] \quad (2)$$

where $\Omega(E,V,N)$ is the number of configurations available to a system of N molecules whose configurational (potential) energy and volume are E and V , respectively. The summations extend over all values of E and V . In the ensemble of systems under consideration, the temperature T ($\beta \equiv 1/kT$) and pressure are fixed. The Gibbs potential and the associated pressure ensemble are the most convenient of the potential ensembles to utilize in the study of fluid phase equilibria. The properties derived from the pressure ensemble in the thermodynamic limit are identical with those of the more commonly used canonical and grand canonical ensembles.²

II. Description of the Model

The fundamental problem is to determine Ω . Solution of this problem is very difficult even when a lattice is used to enumerate configurations. In the lattice formulation, the problem is to determine the number of configurations available to a system of N molecules each of which occupies r sites (a r -mer) and N_0 vacant lattice sites (holes). This problem has

yet to be solved completely for the simple case of dimers and holes on a rectangular lattice,³ although the case of the completely filled lattice (no holes) has yielded to solution.⁴⁻⁶ When it is realized that the exact mathematical solution of the latter problem is isomorphic with the solution of the two-dimensional Ising model, the difficulty of the problem is appreciated.

Some time ago, Guggenheim⁷⁻⁹ obtained an *approximate* value of Ω for a multicomponent mixture of r -mers on a lattice. The Guggenheim solution for a binary mixture of r -mers and monomers (holes) will be used to evaluate the partition function, eq 2, in a *mean field approximation*. Before displaying Guggenheim's solution the following notation is introduced:

(1) The total number of lattice sites for a binary mixture of N r -mers and N_0 empty sites is

$$N_r = N_0 + rN \quad (3)$$

(2) The coordination number of the lattice is z . Each interior mer of a linear chain is surrounded by $z - 2$ nearest nonbonded neighbors and two bonded neighbors; mers at the chain ends have $z - 1$ nearest nonbonded neighbors and one bonded neighbor. Thus, each r -mer is surrounded by qz nearest nonbonded neighbors where

$$qz = (r - 2)(z - 2) + 2(z - 1) = r(z - 2) + 2 \quad (4)$$

(3) The total number of nearest neighbor pairs in the system is $(z/2)N_r$. Only $(z/2)N_q$ are nonbonded pairs where

$$N_q = N_0 + qN \quad (5)$$

The numbers N_r , N_q , N_0 , and N are related by

$$(z/2)N_q = (z/2 - 1)N_r + N + N_0 \quad (6)$$

(4) A r -mer is characterized by a symmetry number σ . For example, for a linear r -mer it is equal to two if the chain ends are indistinguishable and to unity if the chain ends are distinguishable. As will be seen, the exact value of σ is of inconsequential importance.

(5) A r -mer is also characterized by a "flexibility parameter", δ . It is equal to the number of ways in which the r -mer can be arranged on the lattice after one of its mers has been fixed on a lattice site. It is a measure of the r -mer's *internal*

degrees of freedom.¹⁰ For molecules occupying a single site, $\delta = 1$; for molecules occupying two sites, $\delta = z$. For $r = 3$ there are three distinct cases: if the trimer is *linear* and *rigid* $\delta = z$. If the trimer is *nonlinear* and *rigid* $\delta = zz'$ where z' is the number of allowable sites for the third mer after the first two mers have been placed ($z' \leq z - 1$). If the trimer is *flexible* then $\delta = z(z - 1)$. In general, for a r -mer the maximum value for δ is

$$\delta_{\max} = z(z - 1)^{r-2} \quad (7)$$

This is the maximum value because a long, flexible r -mer has certain configurations, especially the more compact ones, that are forbidden. These configurations involve multiple occupancy of one or more sites (the intramolecular excluded volume effect).

The number of configurations available to a system of N r -mers and N_0 empty sites is⁷⁻⁹

$$\Omega = \left(\frac{\delta}{\sigma}\right)^N \frac{N_r!}{N_0!N!} \left(\frac{N_0!}{N_r!}\right)^{z/2} \quad (8a)$$

Using Sterling's approximation $[n! \approx (n/e)^n]$ and eq 6 it can be shown that eq 8a has the following limiting form for large z :

$$\lim_{z \rightarrow \infty} \Omega = \left(\frac{1}{f_0}\right)^{N_0} \left(\frac{\omega}{f}\right)^N \quad (8b)$$

$$\omega = \delta r / \sigma e^{r-1} \quad (9)$$

and where the empty site fraction f_0 and the fraction of occupied sites f are given by

$$f_0 = N_0/N_r \quad f = rN/N_r \quad (10)$$

The large z limit, eq 8b, is known as the "Flory approximation" because a similar formula was first obtained by Flory.¹¹ Although eq 8a was first obtained by Huggins¹² and Miller,¹³ Guggenheim's derivation of (8a) is unique because he makes use of an elegant grand canonical partition function formalism. This approach has the virtue of clearly defining the approximate nature of the derivation. Exact calculation of Ω requires the correct determination of pair and higher order probabilities. Guggenheim's evaluation of Ω assumes⁹ "that when two sites are not occupied by the same molecule, the probabilities of being occupied or vacant are *independent* for the two sites". This mean field approximation decouples the probabilities and makes the evaluation of Ω possible. Guggenheim⁹ has analyzed the error on various types of lattices for binary mixtures of dimers and monomers. Surprisingly, eq 8a is only slightly better than the large z approximation, eq 8b, and neither is in serious error. Error estimates for the general case of r -mers and monomers are not yet available.

Equation 8a is strictly applicable only to linear or branched chain r -mers. Cyclic r -mers have slightly different formulae.⁹ However, all formulae for Ω reduce to eq 8b for large z ; calculations in this paper will be based on eq 8b and it will be applied to all types of molecular geometries. In addition, the following two assumptions will be made:

(1) It will be assumed that the flexibility parameter δ is independent of temperature and pressure. Any thermodynamic property, such as heat capacity, that depends in part on internal degrees of freedom is a property that this model will not correlate well. A generalization which considers the case of determining δ when some of the internal molecular configurations are not energetically equivalent has been given.¹⁴⁻¹⁶ The generalization leads to a temperature dependent δ , but

it does not contribute to the PVT equation of state; this refinement is ignored in this paper.

(2) It will be assumed that the *close packed* volume rv^* of a molecule is independent of temperature and pressure. The close packed volume of a mer is v^* ; it is also the volume of a lattice site. The close packed volume of the N r -mers (no holes) is

$$V^* = N(rv^*) \quad (11)$$

If ρ^* is the close packed *mass* density, then the close packed molecular volume is given by

$$rv^* = M/\rho^* \quad (12)$$

where M is the molecular weight. As a first approximation ρ^* is equal to the crystal density. Equation 12 provides a useful means of estimating the close packed molecular volume, rv^* .

The volume associated with an empty lattice site (a hole) is also equal to v^* ; the volume of the system is therefore:

$$\begin{aligned} \text{volume} &= (\text{number of sites}) \times (\text{site volume}) \\ V &= (N_0 + rN)v^* = N_r v^* = V^*/f \end{aligned} \quad (13)$$

The energy of the lattice depends only on nearest neighbor interactions. In general, the lattice energy (attractive) can be written as

$$E = -(z/2)N_r \sum_i \sum_j p(i,j)\epsilon_{ij} \quad (14)$$

where ϵ_{ij} is the pair interaction energy between components i and j and $p(i,j)$ is the pair (joint) probability of an (i,j) pair in the system. In the present case, there are only two components: "holes" and "mers". The only nonzero pair interaction energy is the one associated with nonbonded, mer-mer interactions; hole-hole, hole-mer, and bonded mer-mer pairs are assigned a zero energy. If we assume random mixing of holes and molecules, i.e., the same approximation invoked in the evaluation of Ω , then the pair probability of a nonbonded, mer-mer interaction is⁷⁻⁹

$$p(\text{mer,mer}) = (qN)^2/N_q N_r \quad (15a)$$

or in the large z limit becomes

$$\lim_{z \rightarrow \infty} p(\text{mer,mer}) = (rN/N_r)^2 \equiv f^2 \quad (15b)$$

Thus, from eq 14 and 15, the lattice (potential) energy is

$$E = -N_r(z\epsilon/2)f^2 \quad (16a)$$

or by using eq 11 and 13

$$E/rN = -\epsilon^*(V^*/V) = -\epsilon^*f \quad (16b)$$

where ϵ is the nonbonded, mer-mer interaction energy and

$$\epsilon^* \equiv z\epsilon/2 \quad (17)$$

is the total interaction energy per mer. The quantity $r\epsilon^*$ is the characteristic interaction energy per molecule in the absence of holes; ϵ^* is also the energy required to create a lattice vacancy (hole).

Since E and Ω are functions of a single parameter, the number of holes in the lattice, the double sum over E and V required in the evaluation of the partition function can be replaced by a single sum over N_0 :

$$Z(T,P) = \sum_{N_0=0}^{\infty} \Omega \exp[-\beta(E + PV)] \quad (18)$$

In statistical mechanics the standard procedure is to approximate the above sum by its maximum term; the maximum term is overwhelmingly larger than any other for a macroscopic system. Mathematically, this is equivalent to equating the free energy to the logarithm of the generic term in the partition function and then finding the minimum value of the free energy [see eq 1 and 2]; thus

$$G = E + PV - kT \ln \Omega \quad (19a)$$

Using eq 8b, 13, and 16, eq 19a can be expressed in dimensionless variables as

$$G/(Nr\epsilon^*) \equiv \bar{G} = -\bar{\rho} + \bar{P}\bar{v} + \bar{T} \left[(\bar{v} - 1) \ln(1 - \bar{\rho}) + \frac{1}{r} \ln(\bar{\rho}/\omega) \right] \quad (19b)$$

where \bar{T} , \bar{P} , \bar{v} , and $\bar{\rho}$ are the reduced temperature, pressure, volume, and density:

$$\bar{T} \equiv T/T^* \quad T^* \equiv \epsilon^*/k \quad (20)$$

$$\bar{P} \equiv P/P^* \quad P^* \equiv \epsilon^*/v^* \quad (21)$$

$$\bar{v} \equiv 1/\bar{\rho} \equiv V/V^* \quad V^* \equiv N(rv^*) \quad (22)$$

The fraction of occupied sites f and the empty site fraction f_0 [see eq 10] are related to the mass density ρ and the close packed mass density ρ^* by

$$f = \rho/\rho^* \equiv \bar{\rho} \equiv 1/\bar{v} \quad (23a)$$

$$f_0 = 1 - \bar{\rho} \quad (23b)$$

The minimum value of the free energy is found in the usual way:

$$\partial \bar{G} / \partial \bar{v} |_{\bar{T}, \bar{P}} = 0 \quad (24a)$$

which yields

$$\bar{\rho}^2 + \bar{P} + \bar{T} \left[\ln(1 - \bar{\rho}) + \left(1 - \frac{1}{r}\right) \bar{\rho} \right] = 0 \quad (24b)$$

Equation 24b is the *equation of state* for the system. It must always be kept in mind that in the pressure ensemble $\bar{\rho}$ is the dependent variable and \bar{P} and \bar{T} are the independent variables. Therefore, eq 24b defines the value of $\bar{\rho}$ at given (\bar{T}, \bar{P}) that minimizes the free energy. Equation 24b can also be obtained directly from the standard thermodynamic equation of state relation, $V = \partial G / \partial P |_T$.

Equations 19 and 24b contain the complete thermodynamic description of the model fluid; all other thermodynamic properties follow from the standard thermodynamic formulae. For example, the thermal expansion coefficient α and isothermal compressibility β are given by

$$\alpha \equiv \frac{1}{V} \left. \frac{\partial V}{\partial T} \right|_P = - \left. \frac{\partial \ln \bar{\rho}}{\partial T} \right|_P \quad (25a)$$

$$\beta \equiv - \frac{1}{V} \left. \frac{\partial V}{\partial P} \right|_T = \left. \frac{\partial \ln \bar{\rho}}{\partial P} \right|_T \quad (26a)$$

$$T\alpha = \frac{1 + \bar{P}\bar{v}^2}{\bar{T}\bar{v}[1/(\bar{v} - 1) + 1/r] - 2} \quad (25b)$$

$$P\beta = \frac{\bar{P}\bar{v}^2}{\bar{T}\bar{v}[1/(\bar{v} - 1) + 1/r] - 2} \quad (26b)$$

III. Liquid-Vapor Transition

The solution of eq 24b must be obtained by numerical

techniques. The character of the solution can be seen by rewriting the equation as follows:

$$\bar{\rho} = 1 - \exp[-\bar{\rho}^2/\bar{T} - (1 - 1/r)\bar{\rho} - \bar{P}/\bar{T}] \equiv h(\bar{\rho}) \quad (24c)$$

In general there are three solutions to eq 24 as illustrated in Figure 1.

The solutions at the lowest and highest values of $\bar{\rho}$ correspond to minima in the Gibbs function, eq 19b; the intermediate solution corresponds to a maximum in G . Figure 2 illustrates the situation schematically. The high density minima corresponds to a liquid while the lower density corresponds to a gas. At a given pressure there will be a unique temperature at which the two minima are equal. This temperature and pressure are defined as the *saturation* temperature and pressure. The locus of all such saturation points defines the *saturation* or *coexistence* line and is defined by

$$\bar{G}[\bar{T}, \bar{P}, \bar{\rho}_1(\bar{T}, \bar{P})] = \bar{G}[\bar{T}, \bar{P}, \bar{\rho}_g(\bar{T}, \bar{P})] \quad (27)$$

Equation 27 shall also be referred to as the *binodal* condition and the binodal curve is illustrated by the solid line in Figure 3.

If the pressure is increased isothermally, the vaporlike minimum will disappear; if the pressure is decreased isothermally, the liquidlike minimum will eventually disappear. Similar comments also apply if the temperature is increased or decreased isobarically. In other words, the model fluid undergoes a liquid-vapor phase transition.

If at a given pressure and temperature two minima appear, the higher free energy minimum corresponds to a metastable state. The locus of the pressures and temperatures (\bar{P}_s, \bar{T}_s) that define the metastability limit of a phase is called the *spinodal* and is illustrated by the dashed curves in Figure 3. The spinodal condition may be envisioned in Figure 1 as that situation where the function $h(\bar{\rho})$ is exactly tangent to the 45° line.

The notion of metastable states is controversial. It has been shown that in the thermodynamic limit the free energy function calculated from a partition function is a convex function of ρ ,¹⁷⁻¹⁹ and thus, it cannot exhibit the behavior (the relative maximum) shown in Figure 2. More precisely, the argument is that the spinodal should coincide with the binodal; the fact that they do not in the present theory (they only coincide at the critical point) can be attributed to the approximate evaluation of the partition function.

It is assumed that when the model fluid is in that part of the \bar{P} - \bar{T} plane, where metastable states are possible, the "equilibrium state" of the fluid is that of lower Gibbs free energy. Thus, the equilibrium value of the free energy \bar{G}_{eq} in Figure 2 is

$$\bar{G}_{eq}(\bar{T}, \bar{P}) = \bar{G}[\bar{T}, \bar{P}, \bar{\rho}_g(\bar{T}, \bar{P})] \quad (28)$$

since the gaslike solution of the equation of state corresponds to the lower free energy. This rule is equivalent to the Maxwell construction required in van der Waals theory. It yields a free energy which is a convex function of ρ and thus avoids the problem of metastable states.

In practice the spinodal is very useful in the numerical analysis of eq 27 because it sets useful bounds on the solution of that equation. As mentioned previously the spinodal condition can be obtained from eq 24c and the tangency condition

$$\partial h(\bar{\rho}) / \partial \bar{\rho} = 1 \quad (29)$$

Thus, if $\bar{\rho}_s$ is the spinodal density, the reduced spinodal temperature is

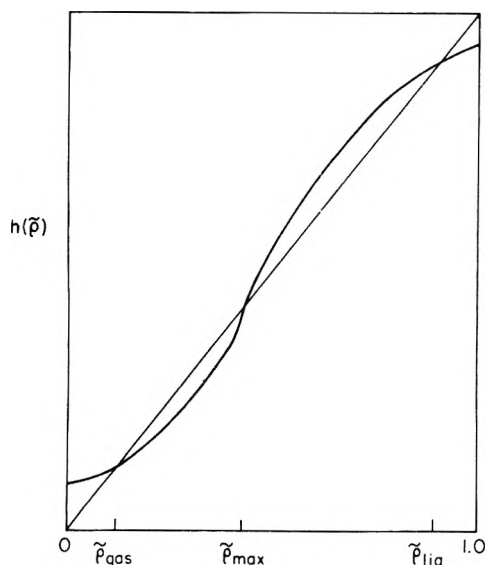


Figure 1. Schematic representation of the solutions of the equation of state (eq 24c). Solutions at the lowest and highest values of \tilde{p} correspond to minima in the Gibbs free energy; the intermediate solution corresponds to a maximum in G . See Figure 2.

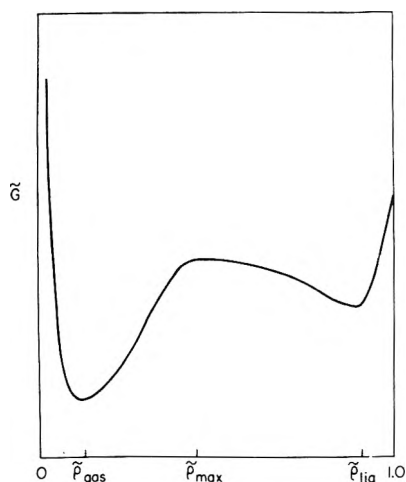


Figure 2. Schematic of the variation of the reduced Gibbs free energy, eq 19b, with reduced density at a pressure and temperature where a liquid phase is metastable with respect to the vapor phase.

$$\tilde{T}_s = \frac{2\tilde{\rho}_s(1 - \tilde{\rho}_s)}{\tilde{\rho}_s + (1 - \tilde{\rho}_s)(1/r)} \quad (30)$$

and the spinodal pressure is

$$\tilde{p}_s = - \frac{2\tilde{\rho}_s(1 - \tilde{\rho}_s) \ln(1 - \tilde{\rho}_s) + (1 - 1/r)\tilde{\rho}_s^2(1 - \tilde{\rho}_s) + \tilde{\rho}_s^2}{\tilde{\rho}_s + (1 - \tilde{\rho}_s)(1/r)} \quad (31)$$

for all values of $\tilde{\rho}_s$ for which $\tilde{P}_s > 0$.

The critical point is obtained when the density of the two phases become equal so that the critical point not only satisfies eq 29 but also the condition

$$\partial^2 h(\tilde{p}) / \partial \tilde{p}^2 = 0 \quad (32)$$

These conditions on $h(\tilde{p})$, eq 29 and 32, can be shown to be completely equivalent to the usual conditions for the critical point, that is

$$\left. \frac{\partial P}{\partial V} \right|_T = 0 \quad \left. \frac{\partial^2 P}{\partial V^2} \right|_T = 0 \quad (33)$$

Equations 24, 29, and 32 then yield

$$\tilde{\rho}_c = 1/(1 + \sqrt{r}) \quad (34)$$

$$\tilde{T}_c = 2r/(1 + \sqrt{r})^2 \quad (35)$$

$$\tilde{P}_c = [2/(1 + \sqrt{r})^2] \left[r \ln \left(1 + \frac{1}{\sqrt{r}} \right) + \frac{1}{2} - \sqrt{r} \right] \quad (36)$$

Another quantity of interest is the critical compressibility factor Z_c :

$$Z_c = \frac{P_c V_c}{R T_c} = r \frac{\tilde{P}_c \tilde{\rho}_c}{\tilde{T}_c} = (1 + \sqrt{r}) \left[r \ln \left(1 + \frac{1}{\sqrt{r}} \right) + \frac{1}{2} - \sqrt{r} \right] \quad (37)$$

$$Z_c(r = 1) = 2 \ln 2 - 1 = 0.386 \quad (38a)$$

and

$$\lim_{r \rightarrow \infty} Z_c = \frac{1}{3} \quad (38b)$$

Since Z_c of most simple molecules is less than 0.3, the present theory is clearly unsatisfactory near the critical point.

Figure 3 illustrates several other important facets of the liquid-vapor behavior:

(1) Since this is a P - T diagram in reduced variables, it emphasizes that the present theory does not obey a simple corresponding states principle.

(2) The limits of metastability of liquid and vapor states determined from eq 30 and 31 are clearly defined. Any \tilde{P}, \tilde{T} point in the metastable region yields a free energy diagram similar to Figure 2. Any point outside of the metastable region yields a free energy with a single minimum.

(3) Notice that the reduced critical temperature increases with r and the reduced critical pressure decreases with r . Below the critical point and along an isobar, a saturation temperature also increases with r . The implication, at least qualitatively, is that the critical temperature should increase, the critical pressure should decrease, and the normal boiling point should increase for a homologous series of fluids of increasing molecular weight. This predicted dependence of the critical point and normal boiling point on molecular weight is exemplified by the normal alkanes.

(4) Since $P_c \rightarrow 0$ as $r \rightarrow \infty$, it should become increasingly difficult if not impossible to vaporize a high molecular weight liquid. High molecular weight polymers have negligible vapor pressures at ordinary temperatures and none can be vaporized.

IV. Determination of the Molecular Parameters

A pure fluid is completely characterized by three molecular parameters: v^* , v^* , and r , or equivalently, the scale factors T^* , P^* , and ρ^* . The number of sites r occupied by the molecule and its molecular weight M are related to the scale factors by

$$RT^* \rho^* / P^* = v^* \rho^* = M/r \quad (39)$$

and

$$P^* v^* / RT^* = 1 \quad (40)$$

In principle any thermodynamic property can be utilized to determine these parameters, but saturated vapor pressure data are particularly useful because they are readily found in

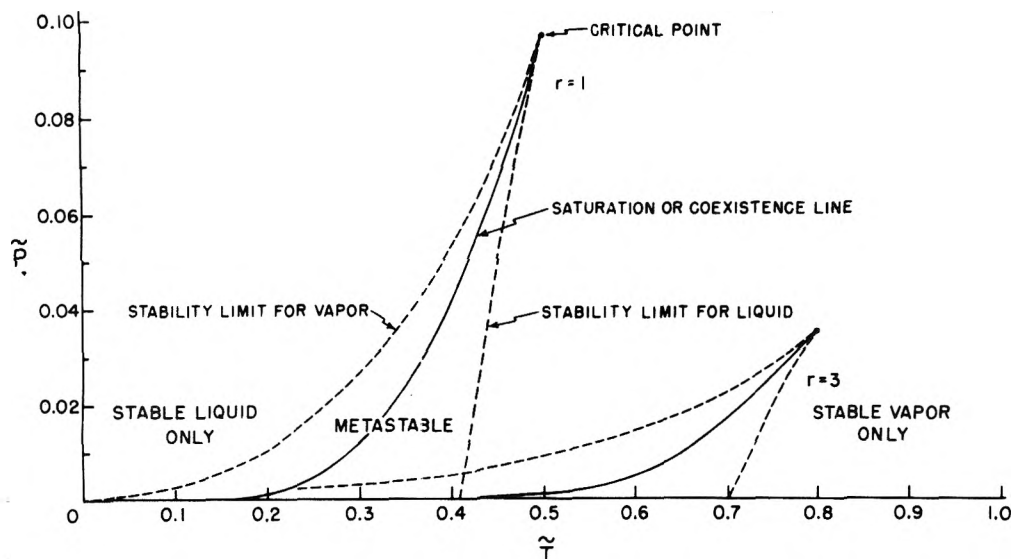


Figure 3. Reduced pressure-temperature diagrams for $r = 1$ and 3. Any \tilde{P}, \tilde{T} point in a metastable region yields a free energy diagram similar to Figure 2. Any point outside of a metastable region yields a free energy with a single minimum.

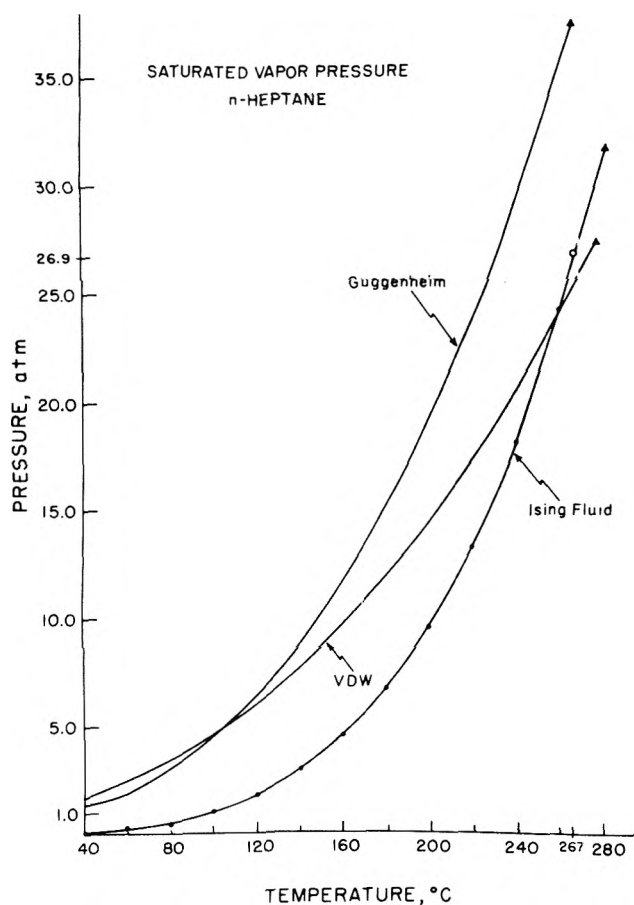


Figure 4. A comparison of experimental saturated vapor pressure data of *n*-heptane with the present theory (Ising fluid), van der Waal's theory, and Guggenheim's theory. The corresponding comparison of experimental orthobaric densities with the various theories is shown in Figure 5. Solid circles are experimental points.²⁰ Solid triangles are theoretical critical points. The open circle is the experimental critical point. Equation of state parameters for *n*-heptane can be found in Table I.

the literature for a wide variety of fluids. A useful compendium of such data is available for organic liquids.²⁰

Saturated vapor pressure data for many liquids can be fitted to within experimental error to as near as 25 °C of the critical point. Near the critical point the theoretical P - T curve never possesses the proper curvature. Figure 4 illustrates a typical nonlinear least-squares fit of saturated vapor pressure data for *n*-heptane.

A number of comments are in order concerning the procedure used to fit the data shown in Figure 4. Experimental points closer than 15–20 °C of the critical point are deliberately omitted since the theory is not expected to hold near the critical point. As previously discussed, the close packed mass density ρ^* can be estimated from known crystalline densities. However, ρ^* is treated as a free parameter and is chosen so that the density of the liquid at the normal boiling point is correctly predicted. This value of ρ^* is usually within 10% of the crystal density. The scaling temperature T^* is simultaneously adjusted to correctly fit the central data point (the midpoint) of the vapor pressure curve. This procedure scales the theoretical fit and defines T^* and P^* as a function of r . With r being the only independent parameter left, it is chosen to give a best fit of eq 27 to the rest of the vapor pressure data in the usual least-squares sense.

Although this fitting procedure is not unique, its main justification is that the resulting computer algorithm is fast, stable, and yields excellent fits. Table I lists a number of fluids to which the above procedure was used to determine the characteristic parameters.

Three exceptions to the above fitting procedure are noted:

(1) In those cases where the density of the liquid at the normal boiling point was unavailable, ρ^* was chosen to give the proper liquid density at one atmosphere and 20 °C.

(2) In the case of the two fatty acids listed in Table I, vapor pressure data were unavailable; instead, liquid orthobaric densities (liquid densities at saturation pressure and temperature) were used and the determination of the parameters was accomplished as follows: ρ^* was chosen so that the largest liquid density is correctly fit (lowest temperature); this again

TABLE I: Molecular and Scale Parameters^a

	ϵ^* , kcal/mol	v^* , cm ³ /mol	r	T^* , K	P^* , atm	ρ^* , g/cm ³
Methane	0.446	7.52	4.26	224	2450	0.50
Ethane	0.627	8.00	5.87	315	3230	0.64
Propane	0.737	9.84	6.50	371	3090	0.69
<i>n</i> -Butane	0.802	10.40	7.59	403	3180	0.736
Isobutane	0.791	11.49	7.03	398	2840	0.72
<i>n</i> -Pentane	0.876	11.82	8.09	441	3060	0.755
Isopentane	0.843	11.45	8.24	424	3040	0.765
Neopentane	0.824	12.97	7.47	415	2620	0.744
Cyclopentane	0.957	10.53	7.68	491	3750	0.867
<i>n</i> -Hexane	0.947	13.28	8.37	476	2940	0.775
2,2-Dimethylbutane	0.904	13.77	8.10	455	2710	0.773
2,3-Dimethylbutane	0.920	13.31	8.29	463	2850	0.781
Cyclohexane	0.987	10.79	8.65	497	3780	0.902
<i>n</i> -Heptane	0.967	13.09	9.57	487	3050	0.80
<i>n</i> -Octane	0.998	13.55	10.34	502	3040	0.815
<i>n</i> -Nonane	1.027	14.00	11.06	517	3030	0.828
<i>n</i> -Decane	1.053	14.47	11.75	530	3000	0.837
<i>n</i> -C ₁₁ H ₂₄	1.077	14.89	12.40	542	2990	0.846
<i>n</i> -C ₁₂ H ₂₆	1.098	15.28	13.06	552	2970	0.854
<i>n</i> -C ₁₃ H ₂₈	1.113	15.58	13.79	560	2950	0.858
<i>n</i> -C ₁₄ H ₃₀	1.132	15.99	14.36	570	2920	0.864
<i>n</i> -C ₁₇ H ₃₆	1.184	17.26	15.83	596	2830	0.88
Benzene	1.039	9.80	8.02	523	4380	0.994
Chlorobenzene	1.162	11.14	8.58	585	4310	1.206
Toluene	1.080	11.22	8.50	543	3970	0.966
<i>p</i> -Xylene	1.115	12.24	9.14	561	3760	0.949
<i>m</i> -Xylene	1.114	12.11	9.21	560	3800	0.952
<i>o</i> -Xylene	1.135	12.03	9.14	571	3890	0.965
<i>trans</i> -Decalin	1.234	16.37	9.03	621	3110	0.935
<i>cis</i> -Decalin	1.255	15.74	9.15	631	3290	0.960
Tetralin	1.278	16.37	9.03	621	3110	0.935
Phenanthrene	1.591	17.67	9.95	801	3720	1.013
H ₂ S	0.759	5.19	6.00	382	6049	1.095
CS ₂	1.126	9.15	5.95	567	5090	1.398
CCl ₄	1.064	11.69	7.36	535	8020	1.788
Chloroform	1.017	9.33	7.58	512	4500	1.688
Methylene chloride	0.967	7.23	7.64	487	5520	1.538
1,1-Dichloroethylene	0.970	7.93	7.10	488	5050	1.722
1,1,1-Trichloroethane	1.025	11.35	7.74	516	3730	1.518
Nitromethane	1.232	5.57	7.36	620	9130	1.490
H ₂ O	1.238	1.93	8.46	623	26520	1.105
Methanol	0.931	3.24	10.72	468	11860	0.922
Ethanol	0.821	3.21	14.89	413	10550	0.963
Propanol	0.834	3.93	15.72	420	8750	0.972
2-Propanol	0.793	3.89	15.83	399	8420	0.975
2-Methyl-2-propanol	0.891	5.38	14.47	448	6840	0.952
Phenol	1.052	5.55	14.23	530	7830	1.192
Ethyl formate	0.926	7.80	8.82	466	4900	1.076
Ethyl acetate	0.930	8.49	9.87	468	4520	1.052
<i>n</i> -Butyl acetate	0.990	10.50	11.03	498	3890	1.003
Diethyl ether	0.857	9.88	8.52	431	3580	0.870
Acetone	0.961	7.54	8.40	484	5260	0.917
Methyl ethyl ketone	1.019	9.54	8.28	513	4410	0.913
Aniline	1.220	8.11	10.30	614	6210	1.115
Pyridine	1.125	8.57	8.55	566	5420	1.079
2,6-Lutidine	1.098	10.60	9.92	552	4280	1.019
β -Picoline	1.168	9.97	8.97	588	4846	1.041
γ -Picoline	1.168	9.92	9.03	588	4860	1.039
Triethylamine	0.951	12.78	9.39	479	3070	0.843
Acetic acid	1.116	5.43	9.51	562	8500	1.164
<i>n</i> -Stearic acid	1.373	20.92	14.91	691	2710	0.912
<i>n</i> -Palmitic acid	1.356	18.89	14.77	682	2960	0.919

^a Three parameters, either ϵ^* , v^* , r or T^* , P^* , ρ^* , completely characterize a fluid. The parameters are related to one another by eq 39 and 40.

scales the theoretical fit. The size parameter r is then chosen so that one saturation point (one saturation pressure and temperature was given²⁰) is fitted correctly. This determines r as a function of T^* which is chosen so that the remaining density data are given a best fit in the least-squares sense.

(3) Since vapor pressure data are unavailable for polymer liquids, the molecular parameters are determined by a conventional nonlinear least-squares analysis of liquid density data. That is, experimental density data above the glass transition temperature are fitted to the theoretical equation of state, eq 24b.

Once the molecular parameters are known for a fluid, all other thermodynamic properties can be calculated. In the next section this theory will be compared with other theories and experiment.

V. Comparison with Other Theories and Experiment

A. van der Waals (VDW) Fluid. The present theory in some respects is similar to that of VDW. The similarity is more apparent if eq 24b is expanded in virial form:

$$PV/NkT = r\bar{v}/\bar{T} = 1 + r(1/2 - 1/\bar{T})\bar{\rho} + (r/3)\bar{\rho}^2 + (r/4)\bar{\rho}^3 + \dots \quad (24d)$$

The VDW equation may be written as [cf. eq 24b]

$$\bar{\rho}^2 + \bar{P} - \bar{T}\bar{\rho}(1 - \bar{\rho})^{-1} = 0 \quad (41a)$$

and has the following virial expansion:

$$PV/NkT = \bar{P}\bar{v}/\bar{T} = 1 + (1 - 1/\bar{T})\bar{\rho} + \bar{\rho}^2 + \bar{\rho}^3 + \dots \quad (41b)$$

where the reduced variables are defined as

$$\begin{aligned} \bar{v} &= 1/\bar{\rho} = V/Nb \\ \bar{T} &= T/(a/bR) \\ \bar{P} &= P/(a/b^2) \end{aligned} \quad (42)$$

The parameters a and b are the usual ones defined in the VDW theory.

Second virial coefficients in both theories are identical in functional form (linear functions of $1/T$). This is a consequence of the mean field approximation invoked in both theories that yields a potential energy that is proportional to density. An energy dependence on volume of this type is commonly referred to in the literature as a VDW energy.

Kac, Uhlenbeck, and Hemmer^{21,22} have renewed interest in the VDW form of the potential energy because they have shown that it is obtained *exactly* in systems that have weak, long-range potentials. Longuet-Higgins and Widom²³ and Guggenheim^{24,25} have also argued that the VDW energy is the appropriate form at *high densities* for a system of hard, attractive spheres.

The difference between the present theory and VDW theory is in the entropy. The VDW entropy is given by

$$S_{VDW} = R \ln(\bar{v} - 1) + \text{constant} \quad (43)$$

and in the present theory by

$$S = R[\ln \bar{v} - r(\bar{v} - 1) \ln(1 - \bar{\rho})] + \text{constant} \quad (44)$$

The VDW entropy is exact for a one-dimensional hard rod fluid, i.e., a Tonk's gas.^{19,26} Both theories yield the same correct limiting value of $R \ln \bar{v}$ for very large values of \bar{v} (gaslike densities), but the VDW entropy diverges as \bar{v} approaches unity (dense fluid) whereas the entropy of the present theory is well-behaved in the same limit. More importantly, the entropy of the present theory depends explicitly on molecular

size through r , whereas the VDW entropy is independent of molecular size.

The VDW theory yields a value of 0.375 for the critical compressibility, $P_c V_c / RT_c$; the present theory [see eq 37] yields the same value of 0.375 for a dimer ($r = 2$).

The Boyle temperature T_B is defined as that temperature for which the second virial coefficient is zero. Inspection of eq 41b shows that this occurs at $\bar{T}_B = 1$ for a VDW fluid; it is easily shown that the ratio of T_B to the critical temperature T_c is

$$T_B/T_c = 27/8 = 3.375 \quad \text{VDW fluid} \quad (45)$$

and for the present theory $\bar{T}_B = 2$ and

$$T_B/T_c = (1 + \sqrt{r})^2/r \quad (46)$$

For a dimer, $T_B/T_c = 2.91$. Experimentally the average value for Ar, Kr, Xe, and CH₄ is 2.70.

At the critical point, $\partial P/\partial V|_T$ and $\partial^2 P/\partial V^2|_T$ are zero and $\partial^3 P/\partial V^3|_T$ is negative in both theories. Theories that satisfy these conditions at the critical point are classified as VDW theories by Rowlinson.²⁷

Experimentally, it is strongly suspected that the critical point is nonanalytic; theoretically, Fisher²⁸ has shown that the critical point may be an essential singularity. The singularity at the critical point of VDW like theories is not an essential singularity since $\partial^3 P/\partial V^3|_T$ exists, but more closely resembles a simple pole.²⁹

Figure 5 compares the predictions of the present theory and the VDW theory with experimental orthobaric densities of *n*-heptane. Except near the critical point, the present theory adequately describes both vapor and liquid densities. By comparison, VDW theory only predicts vapor densities well. The VDW parameters used to determine the curve in Figure 5 were taken from a CRC handbook (1972–1973) and were ostensibly adjusted to give a good fit to the critical point. The predicted vapor pressure curve is shown in Figure 4 and, as can be seen, the VDW theory is in considerable error. However, the VDW parameters can be adjusted to fit the vapor pressure data, but then the critical point and liquid densities are in serious error (not shown). It is clear, therefore, that the present theory offers a substantial improvement over the VDW theory.

Further evidence of the adequacy of the present theory is given in Tables II and III where calculated and experimental values of *first-* and *second-* order thermodynamic properties of *n*-heptane are compared. A first-order property is related to a first derivative on the Gibbs free energy and a second-order property is related to a second derivative.

B. Lattice Gas. A special case of the present model fluid is the classical lattice gas. For a lattice gas, a lattice site is either vacant or occupied by a single atom ($r = 1$). If the partition function for the lattice gas is evaluated in a mean field (Bragg-Williams) approximation then eq 24b is obtained with $r = 1$.³⁰ Lee and Yang³¹ have shown that the lattice gas is mathematically equivalent to an Ising spin model. Spin up corresponds to an occupied site and spin down to a vacant site. Thus, for the more general case of $r > 1$, the model can be characterized as an *Ising* or *lattice fluid*.

C. Hard Sphere Fluids. 1. Repulsive Forces Only. A model fluid that has been extensively studied is that of rigid, hard spheres. Equations of state for hard sphere fluids have been recently reviewed.^{32,33}

The Percus-Yevick compressibility equation has been solved for a hard sphere fluid with the result

$$PV/NkT = (1 + y + y^2)/(1 - y)^3 \quad (47)$$

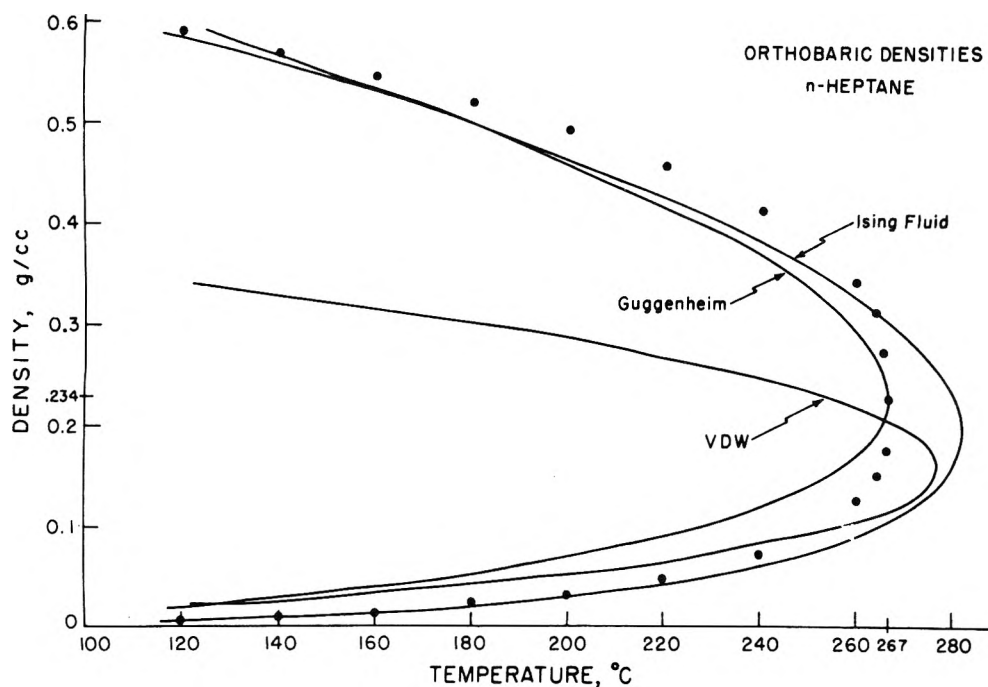


Figure 5. Comparison of experimental orthobaric densities of *n*-heptane with various theories. The corresponding comparison of experimental saturated vapor pressures with the various theories are shown in Figure 4. Solid circles are experimental points.²⁰

TABLE II: Comparison of Experimental and Calculated Values for Some First-Order Thermodynamic Properties of *n*-Heptane^a

Property	Temp, °C	Expt	Theor	% error
Heat of vaporization, kcal/mol	98.7	7.576	7.610	+0.4
Liquid density, g/cm ³	25	0.6795	0.6909	+1.6
Vapor density, g/cm ³	100	0.0036	0.0034	-5.0
Cohesive energy density, cal/cm ³	25	55.3	55.1	-0.4

^a The normal boiling point of *n*-heptane is 98.7 °C.

TABLE III: Comparison of Experimental and Calculated Values at Atmospheric Pressure for Some Second-Order Thermodynamic Properties of *n*-Heptane

Property	Temp, °C	Expt	Theor	% error
Thermal expansion coefficient, K ⁻¹	25	1.2×10^{-3}	1.3×10^{-3}	+8
Isothermal compressibility, atm ⁻¹	25	1.4×10^{-4}	1.7×10^{-4}	+21
Internal pressure, atm	20	2530	2310	-9

where

$$y = b/4V \quad b = N(2\pi\sigma^3/3) \quad (48)$$

σ is the hard sphere diameter and b is the usual VDW excluded volume parameter; y attains its maximum value of $\pi\sqrt{2}/6 = 0.740$ for closest packing of spheres (face centered cubic or hexagonal close packed). The same equation of state, eq 47, has also been obtained from scaled particle theory.³⁴ It is considered to be the most accurate theoretical equation of state for nonattractive hard spheres.^{32,33}

Many other approximate equations of state have been derived or empirically suggested; a particularly simple and accurate one is due to Guggenheim:^{9,24}

$$PV/NkT = 1/(1 - y)^4 \quad (49)$$

The VDW equation yields in the absence of attractive interactions ($a = 0$):

$$PV/NkT = 1/(1 - 4y) \quad (50)$$

The equation of state for the Ising fluid can be written as

$$PV/NkT = 1 - r[1 + \ln(1 - \bar{\rho})/\bar{\rho}] \quad (51)$$

in the limit of zero attractive interactions ($\epsilon^* = 0$).

To compare this latter equation with other hard sphere equations, a relation between $\bar{\rho}$ and y must be established. By its definition $\bar{\rho} = 1$ for closest molecular packing; $y = 0.74$ for hexagonal close packing and $y = 0.63$ for random close packing of spheres.³⁵ Molecular dynamic studies³⁶ of hard sphere fluids have shown that a liquid–solid (disorder–order) transition occurs at about $y = 0.5$, but none of the above theories predict such a transition. Since eq 51 is intended to describe the fluid (disordered state), the following identification is made for hard spheres:

$$\bar{\rho} = y/0.63 \quad (52)$$

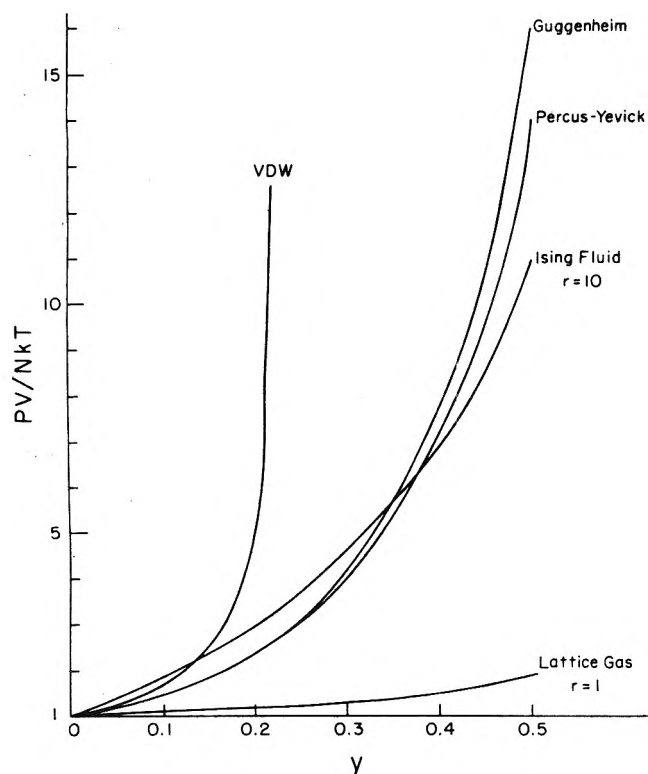


Figure 6. Equations of state for hard sphere fluids in the absence of attractive interactions. The Percus-Yevick equation is the most accurate.

In Figure 6 a comparison is made of the above equations of state and the Ising fluid for $r = 1$ and $r = 10$. The Percus-Yevick equation (eq 47) is the most accurate^{32,33} in that it reproduces the molecular dynamic results very well up to the transition at about $y = 0.5$. Although the Ising fluid equation is not as good as the PY or Guggenheim equations, it is certainly superior to the VDW equation.

For the Ising fluid, the repulsive core of the molecule is considered only approximately through the parameter r . The potential energy is $+\infty$ if two mers are at the same site, $-\epsilon$ if they are nearest neighbors, and zero otherwise. Thus a r -mer has a repulsive core proportional to r .

2. *Repulsive Plus Attractive Forces.* As mentioned previously in section VA, Longuet-Higgins and Widom²³ and Guggenheim^{9,24,25} have argued that a system of hard, attractive spheres should have an attractive potential energy that is proportional to the fluid density (VDW interaction energy). The equation of state of this model would then take the form

$$P = P_0 - a/V^2 \quad (53)$$

where P_0 is the pressure of a hard sphere fluid in the absence of an attractive potential. The effect of the potential lowers the pressure by the amount $\partial E/\partial V|_T = a/V^2$. This is the form of the equation of state for the present model; P_0 is given by eq 51 and the VDW type interaction energy, eq 16b, follows in a natural way from the mean field approximation.

A problem arises immediately with the extension of eq 53 to a *nonspherical* molecular fluid since P_0 is not in general calculable from theory. Herein lies the strength of the Ising fluid model: the theory has been developed approximately for molecules of arbitrary size and shape and P_0 is given by eq 51. To illustrate the importance of obtaining an accurate estimate

of P_0 , a comparison is made in Figure 5 of the Ising fluid model, the VDW and the Guggenheim theories against the orthobaric densities of a fluid that does not obey a simple corresponding states principle (*n*-heptane). The parameters of the Guggenheim theory were chosen to correctly predict the critical point as shown. The impression is given in Figure 5 that the Guggenheim theory is comparable with the present theory. However, this is not true. As can be seen in Figure 4 the predicted vapor pressure curve from the Guggenheim theory is in error. On the other hand, if the Guggenheim equation of state parameters are chosen to fit the vapor pressure data, then the critical point and the orthobaric liquid densities are in considerable error (not shown). This was the same result that obtained with VDW theory, i.e., if the equation of state parameters are chosen to fit vapor pressure data, then the predicted critical point and liquid orthobaric densities are in serious error.

Since the present theory is able to simultaneously correlate vapor pressure and orthobaric vapor and liquid densities of fluids that substantially deviate from a simple corresponding states principle, the conclusion is that the present theory is superior to the VDW or Guggenheim theories. Recall that the three theories have the same VDW attractive energy term and only differ in P_0 , or more correctly, in the entropy associated with a system of hard core molecules.

D. *Cell Models and "c" Parameter Theories.* Several theoretical studies have been made to determine the equation of state of a chain or polymer liquid.³⁷⁻⁴³ Curro⁴⁴ has reviewed developments in this field up to 1973. These theories appeal to Prigogine's³⁷ fundamental idea that the *external* degrees of freedom attributable to a mer in a polymer chain are less than those for a similar small molecule. External degrees of freedom are assumed to depend only on intermolecular forces, whereas *internal* degrees of freedom are associated with the chemical bond forces.

Prigogine³⁷ introduced a new parameter, c , to characterize the decrease in the external degrees of freedom. This parameter is in addition to those ordinarily used in the *cell model* of Lennard-Jones and Devonshire.⁴⁵ The assumption is made that the configurational partition function can be factored into a product. One factor depends on internal degrees of freedom and the other factor on external degrees of freedom:

$$Z(T, V) = Z_{\text{int}}(T) [z_{\text{ext}}(T, V)]^{3cN} \exp(-E_0/kT) \quad (54)$$

where E_0 is the potential energy when all the mers are at cell centers. The internal degrees of freedom are assumed to be independent of density, and thus, only z_{ext} contributes to the *PVT* equation of state.

A similar factorization of the partition function occurs naturally in the present theory, but without explicitly introducing the c parameter. Equation 8 can be expressed as

$$\Omega = \Omega_{\text{int}} \Omega_{\text{ext}} \quad (55)$$

where

$$\Omega_{\text{int}} = \delta^N \quad (56)$$

Recall that δ is the number of configurations available to a r -mer after one of its mers has been *localized* on a lattice site. It is a direct measure of the r -mer's internal degrees of freedom.

However, the r -mer has additional degrees of freedom, Ω_{ext} , because the first mer of a r -mer can be placed at any of the available empty lattice sites. The additional (external) degrees of freedom will depend on the number of empty sites N_0 , or equivalently the density. Thus

TABLE IV: Comparison of Experimental^a and Calculated Thermal Expansion Coefficients, α , Isothermal Compressibilities, β , and Internal Pressures, $\partial E/\partial V|_T$, for Poly(vinyl acetate)^b

Poly(vinyl acetate)		$T\alpha$		$P\beta$		$\partial E/\partial V _T$	
			% error		% error	atm	% error
32 °C, 1 atm	expt	0.217	-4	5.0×10^{-5}	-4	4350	0
	calcd	0.209		4.8×10^{-5}		4350	
80 °C, 1 atm	expt	0.254	+13	5.9×10^{-5}	+20	4310	-6
	calcd	0.287		7.1×10^{-5}		4040	
70 °C, 800 atm	expt	0.203	-13	0.0324	-17	4210	+5
	calcd	0.177		0.0270		4430	

^a Reference 46. ^b The equation of state parameters used in the calculations were $T^* = 591$ K, $P^* = 5090$ atm, and $\rho^* = 1.284$ g/cm³. The glass transition temperature is 32 °C.

$$\Omega_{\text{ext}} = \frac{N_r!}{\sigma^N N_0! N!} \left(\frac{N_q!}{N_r!} \right)^{z/2} \quad (57a)$$

As the volume of the system becomes large, the low density limit, Ω_{ext} , becomes

$$\lim_{\substack{z \rightarrow \infty \\ N_0 \rightarrow \infty}} \Omega_{\text{ext}} = \frac{(N_0 + rN)^N}{\sigma^N N!} \sim \frac{V^N}{N!} \gg 1 \quad (57b)$$

This result, eq 57b, is the partition function for an ideal gas. It is exactly the result expected for a system of noninteracting or widely separated particles. For molecules that occupy space (repulsive cores) at even moderate densities, eq 57b will grossly overestimate Ω_{ext} .

In the limit of high density, Ω_{ext} becomes

$$\lim_{\substack{z \rightarrow \infty \\ N_0 \rightarrow 0}} \Omega_{\text{ext}} = (r/\sigma e^{r-1})^N \quad (57c)$$

Replacing δ by δ_{max} there obtains in the high density limit

$$\lim_{\substack{z \text{ and } r \rightarrow \infty \\ N_0 \rightarrow 0}} \Omega_{\text{int}} \Omega_{\text{ext}} = \left(\frac{z-1}{e} \right)^{rN} \quad (58)$$

This is an interesting result. A mer belonging to an isolated chain that is localized on the lattice has approximately $(z-1)$ degrees of freedom. This is the situation at low densities, but as the density increases, intermolecular interference reduces the degrees of freedom per mer. For a long r -mer, the degrees of freedom per mer becomes $(z-1)/e$ at the highest density. The physical implications of this result for a temperature dependent δ are discussed elsewhere.¹⁴⁻¹⁶

As in the Prigogine theory it is assumed that Ω_{int} is density independent and only Ω_{ext} contributes to the PVT equation of state.

For a polymer liquid in which $r \rightarrow \infty$, the equation of state (eq 24b) becomes

$$\bar{\rho}^2 + \bar{P} + \bar{T}[\ln(1 - \bar{\rho}) + \bar{\rho}] = 0 \quad (59)$$

Thus, all polymer liquids of sufficiently high molecular weight satisfy a corresponding states principle.

This equation is able to reproduce experimental liquid densities of poly(vinyl acetate) with a mean error of less than 0.1% in the temperature range 35–100 °C and in the pressure range 0–800 bars. Experimental errors were estimated to be about 0.01%.⁴⁶ In Table IV calculated and experimental thermal expansion and compressibility coefficients and internal pressures are compared.

The same data have been analyzed using an equation of state obtained from a modified (c parameter) cell theory.⁴⁷ The correlation of the density data is comparable to the present theory, but the cell model equation of state is mathematically cumbersome by comparison.

In summary, the assumptions required for the Ising fluid model are very similar to those invoked by Prigogine³⁷ in his generalization of cell model theories but the former does not require the introduction of the c parameter. Preliminary indications are that the Ising fluid yields an equation of state for polymer liquids which works as well as other more complicated equations based on cell models. Furthermore, cell models yield a very strong density dependent potential energy which is more characteristic of solids than fluids.⁴⁴ This deficiency in the cell model can be remedied by the ad hoc adoption of a VDW potential energy.³⁸

VI. Conclusions

The main conclusions of this paper are summarized as follows:

(1) The theory is based on a well-defined statistical mechanical model and is amenable, in principle, to systematic improvement. Since the model reduces to the classical lattice gas for $r = 1$, it can be properly characterized as an Ising or lattice fluid.

(2) A liquid–vapor transition is predicted.

(3) The effect of chain length on the critical point and boiling points of the normal alkanes has been correctly predicted. Also, the theory correctly predicts that it should be very difficult to vaporize a high molecular weight (polymeric) liquid.

(4) Only three molecular parameters (ϵ^* , v^* , r) are required to describe any molecular fluid. These parameters have been tabulated (Table I) for many common fluids and the procedures for their determination have been outlined.

(5) The attractive part of the potential energy of the Ising fluid is a van der Waals type energy; i.e., it is proportional to the fluid density. This particular form of the energy is a consequence of the mean field approximation used to evaluate the partition function.

(6) Unlike the VDW theory, the Ising fluid equation of state does not satisfy a simple corresponding states principle. The deviation is directly related to the magnitude of the repulsive part of the potential as measured by the parameter r .

(7) For real fluids that do not satisfy a corresponding states principle, the Ising fluid better correlates experimental saturated vapor pressures and liquid and vapor densities than either the VDW or Guggenheim theories.

(8) For nonattractive hard spheres, the Ising fluid equation

of state is not as accurate as the Percus–Yevick or Guggenheim equations, but it is much better than the VDW equation at liquid densities.

(9) When applied to polymeric liquids, the Ising fluid equation of state correlates density data as well as more mathematically complicated equations of state based on modified cell models. Polymeric liquids of high molecular weight satisfy a corresponding states principle.

(10) It has been demonstrated that the Ising fluid model is capable of semiquantitatively describing the thermodynamic properties of a wide variety of molecular fluids of arbitrary size and geometry. The theory is nevertheless simple. Generalization of the theory to fluid mixtures is relatively straightforward. Details of the mixture theory will follow soon in a separate publication.

References and Notes

- (1) I. C. Sanchez and R. H. Lacombe, *Nature (London)*, **252**, 381 (1974).
- (2) M. B. Lewis and J. F. Siegert, *Phys. Rev.*, **101**, 1227 (1956).
- (3) O. J. Heilmann and E. H. Lieb, *J. Math. Phys.*, **24**, 1412 (1970).
- (4) H. N. Y. Temperley and M. E. Fisher, *Phil. Mag.*, **6**, 1061 (1961).
- (5) P. W. Kasteleyn, *Physica*, **27**, 1209 (1961).
- (6) M. E. Fisher, *Phys. Rev.*, **124**, 1664 (1961).
- (7) E. A. Guggenheim, *Proc. R. Soc. London, Ser. A*, **183**, 203 (1944).
- (8) E. A. Guggenheim, "Mixtures", Oxford University Press, London, 1952, Chapters X and XI.
- (9) E. A. Guggenheim, "Application of Statistical Mechanics", Oxford University Press, London, 1966, Chapters 4 and 7.
- (10) Guggenheim uses the symbol ρ for the flexibility parameter instead of δ ; ρ is used in this paper to represent density. The notation adopted in this paper differs from that of ref 1, but more closely conforms to that used by others.
- (11) P. J. Flory, *J. Chem. Phys.*, **10**, 51 (1942).
- (12) M. L. Huggins, *Ann. N.Y. Acad. Sci.*, **43**, 9 (1942).
- (13) A. R. Miller, *Proc. Comb. Phil. Soc. Math. Phys., Sci.*, **39**, 54 (1943).
- (14) P. J. Flory, *Proc. R. Soc. London, Ser. A*, **234**, 60 (1956).
- (15) J. H. Gibbs and E. A. DiMarzio, *J. Chem. Phys.*, **28**, 373 (1958); E. A. DiMarzio and J. H. Gibbs, *ibid.*, **28**, 807 (1958).
- (16) J. F. Nagle, *Proc. R. Soc. London, Ser. A*, **337**, 569 (1974).
- (17) D. Ruelle, "Statistical Mechanics", W. A. Benjamin, New York, N.Y., 1969.
- (18) J. L. Lebowitz, *Annu. Rev. Phys. Chem.*, **19**, 389 (1968).
- (19) C. J. Thompson, "Mathematical Statistical Mechanics", Macmillan, New York, N.Y., 1972.
- (20) J. Timmermans, "Physico-Chemical Constants of Pure Organic Compounds", American Elsevier, New York, N.Y.: Vol. I, 1950 and Vol. II, 1965.
- (21) M. Kac, G. E. Uhlenbeck, and P. C. Hemmer, *J. Math. Phys.*, **4**, 216 (1963).
- (22) G. E. Uhlenbeck, P. C. Hemmer, and M. Kac, *J. Math. Phys.*, **4**, 219 (1963); P. C. Hemmer, M. Kac, and G. E. Uhlenbeck, *ibid.*, **5**, 60 (1964).
- (23) H. C. Longuet-Higgins and B. Widom, *Mol. Phys.*, **8**, 549 (1964).
- (24) E. A. Guggenheim, *Mol. Phys.*, **9**, 43 (1965).
- (25) E. A. Guggenheim, *Mol. Phys.*, **9**, 199 (1965).
- (26) L. Tonks, *Phys. Rev.*, **50**, 955 (1936).
- (27) J. S. Rowlinson, "Liquids and Liquid Mixtures", Plenum Press, New York, N.Y., 1969, Chapter 3.
- (28) M. E. Fisher, *J. Math. Phys.*, **5**, 944 (1964).
- (29) M. E. Fisher, *Physics*, **3**, 255 (1967).
- (30) T. L. Hill, "Introduction to Statistical Thermodynamics", Addison-Wesley, Reading, Mass., 1960, Chapter 14.
- (31) T. D. Lee and C. N. Yang, *Phys. Rev.*, **87**, 410 (1952).
- (32) F. Kohler, "The Liquid State", Verlag Chemie, Weinheim/Bergstr., Germany, 1972, Chapter 7.
- (33) T. M. Reed and K. E. Gubbins, "Applied Statistical Mechanics", McGraw-Hill, New York, N.Y., 1973, Chapter 9.
- (34) N. R. Reiss, H. L. Frisch, and J. L. Lebowitz, *J. Chem. Phys.*, **31**, 369 (1959).
- (35) J. D. Bernal, "Liquids Structure, Properties, Solid Interactions", T. J. Hughel, Ed., Elsevier, Amsterdam, 1965.
- (36) B. J. Alder and T. E. Wainwright, *J. Chem. Phys.*, **31**, 459 (1959); **33**, 1439 (1960).
- (37) I. Prigogine, "The Molecular Theory of Solutions", North-Holland Publishing Co., Amsterdam, 1957, Chapter XVI.
- (38) P. J. Flory, R. A. Orwoll, and A. Vrij, *J. Am. Chem. Soc.*, **86**, 197 (1964); P. J. Flory, *ibid.*, **87**, 1833 (1965).
- (39) R. Simha and T. Somcynsky, *Macromolecules*, **2**, 342 (1969).
- (40) T. Somcynsky and R. Simha, *J. Appl. Phys.*, **42**, 4545 (1971).
- (41) T. Nose, *Polym. J.*, **2**, 124 (1971).
- (42) T. Nose, *Polym. J.*, **2**, 427 (1971).
- (43) S. Beret and J. M. Prausnitz, *Macromolecules*, **8**, 878 (1975).
- (44) J. G. Curro, *J. Macromol. Sci.-Rev. Macromol. Chem.*, **C11**, 321 (1974).
- (45) J. E. Lennard-Jones and A. F. Devonshire, *Proc. R. Soc. London, Ser. A*, **163**, 63 (1937).
- (46) J. E. McKinney and M. Goldstein, *J. Res. Natl. Bur. Stands., Sect. A*, **78**, 331 (1974).
- (47) J. E. McKinney and R. Simha, *Macromolecules*, **7**, 894 (1974).

Statistical Mechanical Derivation of the Lippmann Equation. The Dielectric Constant

Jerry Goodisman

Department of Chemistry, Syracuse University, Syracuse, New York 13210 (Received April 30, 1976)

Publication costs assisted by Syracuse University

We consider the polarizable electrochemical interface with spherical symmetry, and show that the common assumption of an invariant dielectric constant violates the mechanical equilibrium condition, unless its value is that of vacuum. The polarizable particles must be taken into account explicitly, which we do by deriving distribution functions for interacting charged and polarizable particles, neglecting short-range forces and short-range correlations. Calculating the change in surface tension when the distributions change so as to keep constant the temperature and the pressure inside and outside the interface, we obtain the Lippmann equation.

Introduction

The Lippmann equation, which relates the surface tension and surface charge density of the ideally polarizable interface to the potential drop across the interface, is of fundamental importance to our understanding¹ of the electrochemical double layer. The proof by thermodynamics was given 100 years ago² but a general statistical mechanical proof, in terms of the molecular species which make up the interface, is not available. Since only such a proof can give the interpretation on the molecular level of such quantities as surface charge density, we have attempted, in several recent publications,^{3,4} to construct such a proof. Starting from the balance of forces for interacting ions, the Lippmann equation was obtained³ when only the changes in long-range (electrostatic) forces were considered. To take into consideration polarizable molecules, we assumed a Boltzmann distribution for their density. As shown in the next paragraph, the common assumption that these molecules may be taken into account by insertion of a dielectric constant into the force laws is in contradiction to the mechanical equilibrium condition. It is the purpose of the present paper to show how the Lippmann equation follows from the general statistical mechanical equilibrium conditions for interacting charged and polarizable species.

The explicit consideration of the polarizable (solvent) species is necessary for a consistent proof of the Lippmann equation. Their behavior cannot be subsumed under a dielectric constant ϵ of fixed value. If the solvent molecules are not allowed to readjust to changes in electrical conditions, mechanical equilibrium is violated, as we now show.⁵ The mechanical equilibrium condition in the presence of an electric field is⁶

$$\frac{dp}{dx} = \frac{d}{dx} [(\epsilon - \frac{1}{2}\epsilon_0)E^2] \quad (1)$$

where the system is supposed to be homogeneous in the y and z directions, so that the electric field E is necessarily in the x direction. If the derivative of the pressure p involves only the derivative of the densities n_i of charged species (ions) and these obey a Boltzmann distribution, (1) becomes

$$kT \frac{d}{dx} \sum_i n_{i0} e^{-e_i\psi(x)/kT} = (\epsilon - \frac{1}{2}\epsilon_0) \frac{d}{dx} E^2 \quad (2)$$

Here, n_{i0} is the density of ionic species i for $x = \infty$, where the electrical potential ψ is zero. These assumptions are the con-

ventional ones, used in the Gouy–Chapman, Debye–Hückel, and other theories, and can be used to generate a proof of the Lippmann equation.^{5,7} However, the left side of eq 2 may be written:

$$kT \sum_i n_i \frac{d}{dx} (-e_i\psi/kT) = - \sum_i n_i e_i \frac{d\psi}{dx} = E\rho = E \frac{d(\epsilon E)}{dx}$$

using the Poisson equation appropriate to a region of dielectric constant ϵ . Equation 2 now becomes

$$\epsilon E dE/dx = (2\epsilon - \epsilon_0)E dE/dx$$

This can hold only for $\epsilon = \epsilon_0$ (no dielectric present).

For $\epsilon \neq \epsilon_0$ there is a contradiction between the assumptions and the mechanical equilibrium condition (1), although both should follow from thermal equilibrium. A proof of the Lippmann equation^{5,7} from the density distributions of the Gouy–Chapman theory, which require $\epsilon = \text{constant}$, is unsatisfactory for this reason. A more consistent proof can be given⁵ using the assumptions of the theory, which are not themselves inconsistent for low enough ion densities.

Basic Equations

We turn now to a proof from general statistical mechanical relations. For simplicity, we consider only the solution side of the metal–solution interface, so that the metal side serves only as a source of fields which act on the particles of the solution. The potential drop across the metal surface is supposed to be unchanged when the surface charge density changes. (It is possible⁴ to treat the entire interface, including both metal and solution sides, but the present treatment conforms to the usual models discussed for the metal–solution interface.) For a spherical interface with surface tension ρ and surface of tension at radius r_σ , we showed³

$$\Delta\rho r_\sigma^2 = - \int_{r_i}^{r_e} r^2 dr (\Delta p_T + \frac{1}{2}\epsilon_0 \Delta E^2) \quad (3)$$

where “ Δ ” means “change in” and p_T is the pressure in the tangential direction, except for the contribution of long-range forces, which have been separated out in the last term. The electric field E is in the radial direction, and vanishes at $r = r_e$ (far outside the interfacial region). The metal surface is at $r = r_i$. Included in p_T are forces due to short-range interactions and correlations as well as the “kinetic” contribution. Only the latter will be considered here, so that

$$p_T = \sum_{i=0}^n n_i kT \quad (4)$$

assuming thermal equilibrium where n_i is the number density of species i . There are n chemical species, with n_0 referring to the solvent, whose molecules are uncharged and polarizable; the other species have charged but nonpolarizable molecules.

The balance of forces between the molecules is treated, as previously,³ using a formalism given by Mazur.⁸ Under conditions of equilibrium and constant temperature

$$\nabla(\rho_k kT) = \langle m_k \ddot{\mathbf{R}}_k \delta(\mathbf{R}_k - \mathbf{R}) f \rangle \quad (5)$$

where f is the distribution function in phase space, ρ_k is the number density of particle k at point \mathbf{R} , and fences indicate integration over phase space. \mathbf{R}_k gives the position of the center of mass of k . The charged particles which make up particle k are labeled ki and have charges e_{ki} , while those making up particle l have charges e_{lj} , so that

$$m_k \ddot{\mathbf{R}}_k = -(4\pi\epsilon_0)^{-1} \sum_i \nabla_{ki} \sum_{j \neq k} \sum_l e_{ki} e_{lj} |\mathbf{R}_{ki} - \mathbf{R}_{lj}|^{-3} \quad (6)$$

The position of particle ki is given by

$$\mathbf{R}_{ki} = \mathbf{R}_k + \mathbf{r}_{ki} \quad (7)$$

with \mathbf{r}_{ki} supposed to be small. This allows us to write, after carrying out the differentiation in (6) and expanding $|\mathbf{R}_{ki} - \mathbf{R}_{lj}|^{-3}$ in a power series

$$\begin{aligned} -4\pi\epsilon_0 m_k \ddot{\mathbf{R}}_k = & \sum_i e_{ki} \sum_{j \neq k} \sum_l e_{lj} [\mathbf{R}_l + \mathbf{r}_{lj} \\ & - (\mathbf{R}_k + \mathbf{r}_{ki})] |\mathbf{R}_k - \mathbf{R}_l|^{-3} + \mathbf{r}_{ki} \cdot \nabla_{R_k} |\mathbf{R}_k - \mathbf{R}_l|^{-3} \\ & + \mathbf{r}_{lj} \cdot \nabla_{R_l} |\mathbf{R}_k - \mathbf{R}_l|^{-3} + \mathbf{r}_{ki} \mathbf{r}_{lj} \cdot \nabla_{R_k} \nabla_{R_l} |\mathbf{R}_k - \mathbf{R}_l|^{-3} \end{aligned} \quad (8)$$

Terms like $\mathbf{r}_{ki} \mathbf{r}_{kj}$ have been dropped; they correspond to moments higher than first order.

After multiplying out the terms we introduce the total charges of the molecules

$$e_k = \sum_i e_{ki}, \quad e_l = \sum_j e_{lj}$$

and the molecular dipole moments

$$\boldsymbol{\mu}_k = \sum_i e_{ki} \mathbf{r}_{ki}, \quad \boldsymbol{\mu}_l = \sum_j e_{lj} \mathbf{r}_{lj}$$

Then we multiply (8) by $\delta(\mathbf{R}_k - \mathbf{R}) f$ and integrate over phase space. The leading term on the right side is

$$\begin{aligned} & \sum_{j \neq k} \int d\mathbf{R}' \langle e_{ki} e_{lj} \delta(\mathbf{R}_k - \mathbf{R}) \delta(\mathbf{R}_l - \mathbf{R}') f(\mathbf{R}_k - \mathbf{R}_l) |\mathbf{R}_k - \mathbf{R}_l|^{-3} \rangle \\ & = \sum_{j \neq k} \int d\mathbf{R}' \rho_{kl}(\mathbf{R}, \mathbf{R}') e_{ki} e_{lj} |\mathbf{R}' - \mathbf{R}| |\mathbf{R} - \mathbf{R}'|^{-3} \end{aligned} \quad (9)$$

where ρ_{kl} is a two-particle distribution function. Ignoring short-range correlations, $\rho_{kl}(\mathbf{R}, \mathbf{R}')$ becomes $\rho_k(\mathbf{R}) \rho_l(\mathbf{R}')$. Correlation terms are also being dropped from p_T , but we have so far been unable to demonstrate explicit cancellation of all the correlation terms in the Lippmann equation. We ignore the short-range correlations for all terms when averaging (8) over phase space. Now grouping together the particles by species, we find for species h (note $n_h = \sum_k^{(h)} \rho_k$)

$$\begin{aligned} & -4\pi\epsilon_0 \sum_k^{(h)} m_h \langle \ddot{\mathbf{R}}_k \delta(\mathbf{R}_k - \mathbf{R}) \rangle \\ & = \int d\mathbf{R}' [e_h n_h(\mathbf{R}) \rho_h(\mathbf{R}') |\mathbf{R} - \mathbf{R}'|^{-3} \\ & + (e_h n_h(\mathbf{R}) P(\mathbf{R}') - \bar{\boldsymbol{\mu}}_h(\mathbf{R}) n_h(\mathbf{R}) \rho_h(\mathbf{R}')) |\mathbf{R} - \mathbf{R}'|^{-3} \\ & + (\mathbf{R}' - \mathbf{R}) (\bar{\boldsymbol{\mu}}_h(\mathbf{R}) n_h(\mathbf{R}) \rho_h(\mathbf{R}') - e_h n_h(\mathbf{R}) P(\mathbf{R}')) \\ & \cdot \nabla_{R'} |\mathbf{R} - \mathbf{R}'|^{-3} + (P(\mathbf{R}') n_h(\mathbf{R}) \bar{\boldsymbol{\mu}}_h(\mathbf{R}) \\ & + n_h(\mathbf{R}) \bar{\boldsymbol{\mu}}_h(\mathbf{R}) P(\mathbf{R}')) \cdot \nabla_{R'} |\mathbf{R} - \mathbf{R}'|^{-3} \\ & + (\mathbf{R} - \mathbf{R}') n_h(\mathbf{R}) \bar{\boldsymbol{\mu}}_h(\mathbf{R}) P(\mathbf{R}') \cdot \nabla_{R'} \nabla_{R'} |\mathbf{R} - \mathbf{R}'|^{-3} \end{aligned} \quad (10)$$

Here $\rho(\mathbf{R})$ is the electric charge density at \mathbf{R}

$$\rho(\mathbf{R}) = \sum_k e_k n_k(\mathbf{R}) \quad (11)$$

and $P(\mathbf{R})$ the polarization at \mathbf{R}

$$P(\mathbf{R}) = \sum_k \bar{\boldsymbol{\mu}}_k(\mathbf{R}) n_k(\mathbf{R}) \quad (12)$$

In (10) and (12), $\bar{\boldsymbol{\mu}}_h$ is the average electric dipole moment of a molecule of species h at point \mathbf{R} . Unlike the molecular charge e_h , it depends on position in space. We will assume below, consistent with our neglect of short-range forces, that $\bar{\boldsymbol{\mu}}_h(\mathbf{R})$ depends only on the electric field at \mathbf{R} .

Equation 10 may be simplified using the definition of the electric field,

$$\begin{aligned} \mathbf{E} = & -(4\pi\epsilon_0)^{-1} \int d\mathbf{R}' \rho(\mathbf{R}') (\mathbf{R}' - \mathbf{R}) |\mathbf{R}' - \mathbf{R}|^{-3} \\ & - (4\pi\epsilon_0)^{-1} \int d\mathbf{R}' P(\mathbf{R}') \cdot \nabla_{R'} \nabla_{R'} |\mathbf{R} - \mathbf{R}'|^{-1} \end{aligned} \quad (13)$$

Then, combining with eq 5, we find, for the case of spherical symmetry

$$kT dn_k/dr = e_k n_k(r) E(r) + \bar{\boldsymbol{\mu}}_k(r) n_k(r) dE/dr$$

For a charged particle ($\bar{\boldsymbol{\mu}}_k = 0$) this leads to

$$d(\ln n_k)/dr = (e_k/kT) (-d\psi/dr)$$

or

$$n_k(r) = n_k(r_e) e^{-e_k(\psi - \psi_e)}$$

where $\psi_e = \psi(r_e)$. In our previous treatment³ we introduced an additional term in the exponential, corresponding to short-range ("chemical") forces due to the metal, so that

$$n_k(r) = n_k(r_e) e^{-e_k(\psi - \psi_e + W_k(r))/kT} \quad (14)$$

For the uncharged but polarizable solvent molecules

$$d(\ln n_0)/dr = (kT)^{-1} \bar{\boldsymbol{\mu}}_0(r) dE/dr$$

or

$$n_0(r) = n_0(r_e) \exp \left[(kT)^{-1} \int_{r_e}^r dr \bar{\boldsymbol{\mu}}_0(r) (dE/dr) \right]$$

Introducing an additional force due to the metal and assuming that $\bar{\boldsymbol{\mu}}_0$ depends only on E , we have

$$n_0(r) = n_0(r_e) \exp \left[\left(\int_0^E \bar{\boldsymbol{\mu}}_0(E) dE - W_0(r) \right) / kT \right] \quad (15)$$

The distributions (14) and (15), except for the W_i short-range terms, have now been shown to follow directly from the condition of mechanical equilibrium (5) and the electrostatic force law.

The electric field (13) leads to the Maxwell equation $\nabla \cdot \mathbf{D} = \rho$. (Mazur⁸ has derived this fact from the definition of \mathbf{E} in terms of the component charges e_{ki} and e_{lj} .) To see this, we calculate $\nabla \cdot \mathbf{E}$ as follows:

$$\begin{aligned} \nabla_R \cdot \mathbf{E} &= -(4\pi\epsilon_0)^{-1} \int d\mathbf{R}' \rho(\mathbf{R}') \nabla_R \cdot \nabla_R |\mathbf{R} - \mathbf{R}'|^{-1} \\ &+ (4\pi\epsilon_0)^{-1} \int d\mathbf{R}' P(\mathbf{R}') \cdot \nabla_R \nabla_R \cdot \nabla_R |\mathbf{R} - \mathbf{R}'|^{-1} \\ &= \epsilon_0^{-1} \int d\mathbf{R}' \rho(\mathbf{R}') \delta(\mathbf{R} - \mathbf{R}') - \epsilon_0^{-1} \int d\mathbf{R}' P(\mathbf{R}') \\ &\quad \cdot \nabla_R \delta(\mathbf{R} - \mathbf{R}') \end{aligned}$$

Carrying out the second integral by parts and rearranging, we find

$$\nabla \cdot (\epsilon_0 \mathbf{E}) + \nabla \cdot P = \rho \quad (16)$$

Defining \mathbf{D} as $\epsilon_0 \mathbf{E} + P$ or as $\epsilon \mathbf{E}$, we have the desired equation. In our model for the ionic solution, the polarization $P(R)$ is just $n_0(\mathbf{R})\bar{\mu}_0(\mathbf{R})$.

Lippmann Equation

We now use (14), (15), and (16) to derive the Lippmann equation. Using (14) and (15) in (4), the change in the tangential pressure is

$$\begin{aligned} \Delta p_T &= \sum_{i=0}^n \Delta n_i kT = n_0 \Delta \left[\int_0^E \bar{\mu}_0(E) dE - W_0(r) \right] \\ &\quad + \sum_{i=1}^n n_i \Delta [-e_i \psi(r) + e_i \psi_e - W_i(r)] \end{aligned}$$

Assuming W_0 and W_i are invariant to the change in electrical conditions, we have

$$\Delta p_T = n_0 \bar{\mu}_0(E) \Delta E - \rho (\Delta \psi - \Delta \psi_e)$$

to be substituted into (3). This gives

$$\Delta \sigma r_\sigma^2 = - \int_{r_i}^{r_e} r^2 dr (P \Delta E - \rho \Delta \psi + \rho \Delta \psi_e + \epsilon_0 E \Delta E) \quad (17)$$

Using (16) and integrating by parts

$$\begin{aligned} \int_{r_i}^{r_e} r^2 dr \rho \Delta \psi &= \int_{r_i}^{r_e} r^2 dr \left[\frac{1}{r^2} \frac{d}{dr} r^2 (\epsilon_0 E + P) \right] \Delta \psi \\ &= [r^2 (\epsilon_0 E + P) \Delta \psi]_{r_i}^{r_e} - \int_{r_i}^{r_e} r^2 dr (\epsilon_0 E + P) \frac{d \Delta \psi}{dr} \end{aligned}$$

Now E and P vanish for $r = r_e$, while $\epsilon_0 E + P$ at $r = r_i$ is equal to the electric displacement D within the metal, which vanishes, plus Q , the charge per unit area on the metal. Thus we have (note that $d \Delta \psi / dr = -\Delta E$)

$$\int_{r_i}^{r_e} r^2 dr \rho \Delta \psi = -r_i^2 Q \Delta \psi_i + \int_{r_i}^{r_e} r^2 dr (\epsilon_0 E + P) \Delta E$$

On substituting this into (17), we find, after cancellation of terms

$$\Delta \sigma r_\sigma^2 = -(\Delta \psi_e) \int_{r_i}^{r_e} r^2 dr \rho - r_i^2 Q \Delta \psi_i \quad (18)$$

The overall electroneutrality of the interface means that the total charge on the solution side must equal $-Q r_i^2$. Furthermore, the change in U , the potential drop across the interface, is equal to $\Delta(\psi_i - \psi_e)$. Therefore (18) gives us the Lippmann equation

$$\Delta \sigma r_\sigma^2 = -Q r_i^2 \Delta U$$

Since the thickness of the interface is small compared to the radius of the metal drop, r_σ is essentially equal to r_i .

References and Notes

- (1) P. Delahay, "Double Layer and Electrode Kinetics", Wiley-Interscience, New York, N.Y., 1955.
- (2) G. Lippmann, *Wied. Ann.*, **11**, 316 (1880); J. W. Gibbs, "Collected Works", Vol. I, Dover Publications, New York, N.Y., 1961, p. 336.
- (3) J.-P. Badiali and J. Goodisman, *J. Phys. Chem.*, **79**, 223 (1975).
- (4) J.-P. Badiali and J. Goodisman, *J. Electroanal. Chem.*, **65**, 523 (1975).
- (5) J. Goodisman, *J. Chim. Phys.*, **72**, 143 (1975).
- (6) A. Sanfeld, "Introduction to the Theory of Charged and Polarized Layers", Wiley-Interscience, London, 1968, Section 17-VI.
- (7) K. Herzfeld, *Phys. Z.*, **21**, 28 (1920).
- (8) P. Mazur, *Adv. Chem. Phys.*, **1**, 309 (1958).

Correlations of Cracking Properties of Mg-Y Zeolites with Their Acidic and Basic Sites

Claude Mirodatos, Antoine Abou Kais,[†] Jacques C. Vedrine, Pierre Pichat, and Denise Barthomeuf*

Institut de Recherches sur la Catalyse—CNRS, 79, boulevard du 11 novembre 1918, 69626 Villeurbanne, Cedex, France
(Received May 19, 1976)

Publication costs assisted by the Centre National de la Recherche Scientifique

The catalytic activity for isooctane cracking, the surface acidity (using colored indicators and ir spectra of chemisorbed pyridine), and the concentrations in various OH groups (by means of ir and ESR spectroscopies) have been measured for Mg-Y zeolites having various H⁺ and Mg²⁺ contents and the same Na⁺ content. The influence of Mg²⁺ cations on these properties are discussed in terms of cation location and polarizing field. On the basis of the influence of CO₂ at 400 °C, it is suggested that a part of the protons giving rise to the ir band at 3640 cm⁻¹ and the ESR line of 4.1-Oe width may be inhibited for the catalytic cracking by the basic Mg(OH)⁺ species associated with the 3685-cm⁻¹ ir band. The role played by CO₂ in the increase of catalytic properties has been cleared up.

Introduction

Y-zeolites exchanged with Mg²⁺ cations exhibit a great catalytic activity for reactions involving carbonium ions.¹⁻³ Moreover their hydroxyl groups and acid sites show a high thermal stability.⁴ Their catalytic activity for *o*-xylene isomerization has been correlated with the concentration in OH groups vibrating at 3640 cm⁻¹ and in pyridinium ions remaining after evacuation at 250 °C.⁵ The magnesium ion location was also studied.⁶ On the other hand, it has been recently reported⁷ that after certain heat treatments, Mg-Y zeolites with a constant sodium level may contain Mg(OH)⁺ species whose concentration depends on the magnesium content. The catalytic activity for isooctane cracking of these samples is enhanced by introduction of CO₂ in the reactants. It has been shown that CO₂ reacts with the Mg(OH)⁺ species giving rise to new acidic OH groups.⁷ In the present work, the activity for isooctane cracking was measured for a series of samples with various Mg content in order to find out if the presence of these Mg(OH)⁺ species, which have a basic character, changes the catalytic properties of the acid sites by modifying their environment. Particularly, the role of the protonic sites was investigated. For this purpose, the acidity was measured using various methods: colored indicators, ir spectra of chemisorbed pyridine, and ESR spectra of hydrogen atoms formed in zeolites after γ irradiation at 77 K. The same measurements were also carried out after reaction of the samples with CO₂ at 400 °C in order to facilitate the interpretations.

Experimental Section

Materials. The starting zeolite was Union Carbide Na-Y material. An exchange of Na⁺ by NH₄⁺ ions using chloride solutions was first performed. The residual sodium content was close to 1.2%, i.e., ~ 7 Na⁺ per unit cell. NH₄⁺ ions were then progressively exchanged for Mg²⁺ ions in chloride solutions. Two or three successive treatments with the chloride

* Address correspondence to this author at Laboratoire de Catalyse Organique, L. A. CNRS no. 231, Ecole Supérieure de Chimie Industrielle de Lyon, 43, bd. du 11/11/1918, 69621 Villeurbanne, France.

[†] Permanent address: Faculté des Sciences, Université Libanaise Hadath, Liban et C.N.R.S. libanais.

solution were required to obtain high magnesium levels. The sample with the highest Mg content was exchanged at 100 °C for 48 h. After drying at 110 °C, the materials were heated at 380 °C in a dry air flow for 15 h in order to evolve NH₃ and then at 550 °C for the same time. This heating procedure tends to avoid ultrastabilizing effects. X-ray diffraction measurements showed the samples to be highly crystalline. Chemical compositions of the catalysts referred to by the total number of equivalents of cation (Na⁺ + 2Mg²⁺) per unit cell are given in Table I.

Ir Studies. Wafers of 30–40 mg of zeolite pretreated as described above were inserted in a quartz sample holder which was introduced in the infrared cell.⁸ They were heated (5 deg/min) to 465 °C in a dry oxygen flow in order to evolve carbonaceous deposits. After 15 h at this temperature, the samples were cooled to room temperature and the oxygen was pumped off. The materials were then heated under vacuum at 400 °C for 15 h and the spectra recorded at room temperature. Reaction with CO₂ was studied by introducing this gas under a 100 Torr pressure in the ir cell at room temperature and heating at 400 °C for 15 h. The zeolites were then outgassed at room temperature for 30 min and the spectra recorded. CO₂ purity was better than 99.998%. Pyridine adsorption was performed as usual at room temperature and spectra were recorded after evacuation at 250 and 350 °C.

Some experiments were carried out after pretreatment of the ir wafers in a hydrogen stream at 465 °C instead of in vacuo at 400 °C in order to compare ir and catalytic studies.

Spectra were scanned on a Perkin-Elmer Model 125 grating spectrophotometer. The reference beam was attenuated.

ESR Studies. The samples underwent the same pretreatment as for ir experiments. Zeolite powder (about 30 mg) was inserted in conventional ESR tubes, with a breakseal when necessary, and γ irradiated at 77 K for doses of about 0.3 Mrad. ESR spectra were recorded with a Varian E9 spectrometer using a dual cavity. Quantitative data were obtained by integrating the derivative lines.

Butylamine Titration. The 380–550 °C heated zeolites were titrated with *n*-butylamine and colored indicators as previously described.⁹ Because of the deep coloration of Mg zeolites in benzenic solution, only the total acidity (strength $\geq 3 \times 10^{-4}\%$ H₂SO₄) was measured.

TABLE I: Analysis of the Zeolites

Catalysts	Na ⁺ ions/uc	Mg ²⁺ ions/uc	Total cation equiv/uc ^a
Na-HY	7.5	0	7.5
Mg-17.7	7.1	5.3	17.7
Mg-23.4	8.2	7.6	23.4
Mg-26.2	8.0	9.1	26.2
Mg-32.1	7.1	12.5	32.1
Mg-37.5	8.1	14.7	37.5
Mg-46.1	7.5	19.3	46.1

^a The difference with 56 (number of charges to be neutralized) represents the theoretical number of H⁺ per unit cell after the NH₄⁺ decomposition.

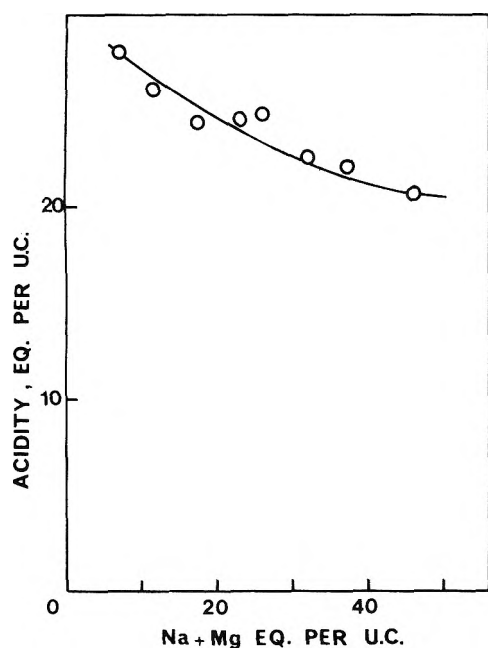


Figure 1. Acidity (strength $\geq 3 \times 10^{-4}$ % H₂SO₄) of zeolites from *n*-butylamine titration.

Catalytic Activity Measurements. The isooctane cracking was studied at 465 °C in a microcatalytic reactor under flowing hydrogen as previously described.⁹ Before the test, the 380–550 °C treated samples were heated in situ at 465 °C for 15 h in a hydrogen stream. The isooctane partial pressure was 100 Torr. The activity was measured after steady state conditions were reached (i.e., 1 or 2 h). Reaction products were analyzed by gas chromatography. The activity is expressed by the percentage of isooctane transformed (precision >0.1%). Some experiments were done under CO₂ atmosphere by continuously introducing this gas in flowing hydrogen during the catalytic test (partial pressure 40 Torr).

Results

Butylamine Titration. A decrease in total acidity with increasing Mg content is observed (Figure 1). It should be stressed that the experimental conditions used (pretreatment, liquid phase) for these titrations are quite different from those corresponding to the ir and ESR studies described below. Consequently, no attempt has been made to relate the total acidity thus measured to the number of OH groups (or H atoms) and pyridinium ions chemisorbed at various temperatures.

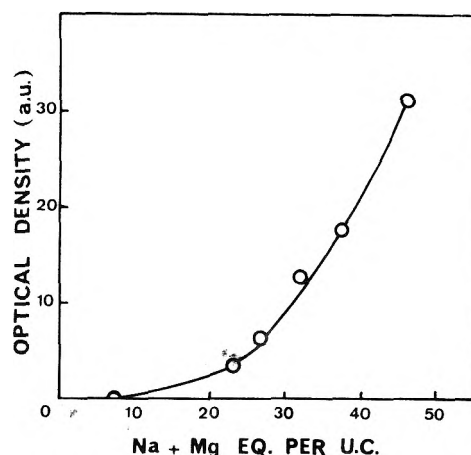


Figure 2. Intensity of the 1449-cm⁻¹ band referring to pyridine bonded to Mg²⁺ cations after evacuation at 350 °C for zeolites pretreated in a H₂ stream at 465 °C.

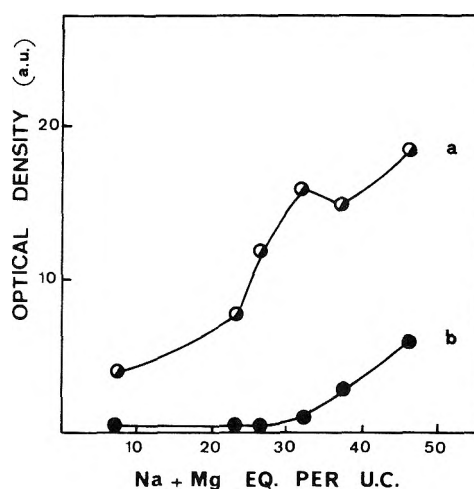


Figure 3. Intensity of the 1545-cm⁻¹ band referring to pyridinium ions (Brønsted acidity) after evacuation at: (a) 250 °C, (b) 350 °C, for zeolites pretreated in a H₂ stream at 465 °C.

Pyridine Titration. The 19 b vibrational mode of pyridine bonded to various zeolitic sites gives rise to bands at 1449 cm⁻¹ (Mg²⁺ cations), 1451 cm⁻¹ (Lewis acid sites), and 1545 cm⁻¹ (Brønsted acid sites). The optical densities of the 1449- and 1545-cm⁻¹ bands are reported in Figures 2 and 3, respectively, as a function of cation exchange level for evacuation at various temperatures. These results refer to 465 °C H₂-pretreated materials.

As shown in Figure 2, the 1449-cm⁻¹ band appears as soon as divalent cations are introduced in the zeolite and increases as a function of cation exchange level. The number of 250 °C bonded pyridinium ions rises with increasing Mg contents (Figure 3a), whereas the strongest protonic acidity begins to appear only at about 30 cation equivalents per unit cell (Figure 3b). Lewis acidity is difficult to determine, because the 1451-cm⁻¹ band appears only as a shoulder on the 1449-cm⁻¹ band. However, it is possible to note a small linear increase in the strongest acidity (350 °C coordinated pyridine) with increasing Mg content.

Figure 4 reports the changes in Brønsted acid sites (1545-cm⁻¹ band) on 400 °C evacuated samples before and after exposure to CO₂ at 400 °C. The comparison with Figure 3 shows that the severe 400 °C evacuation does not modify the shape of curve b, but that the curve referring to 250 °C bonded

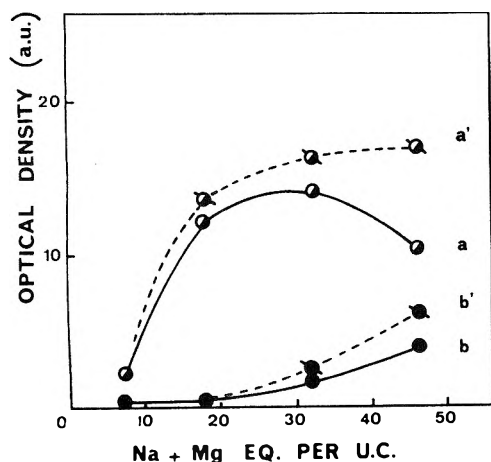


Figure 4. Intensity of the 1545-cm^{-1} band referring to pyridinium ions (Bronsted acidity) after evacuation at: (a, a') 250°C , (b, b') 350°C , for zeolites pretreated at 400°C , first under vacuum (a, b), and subsequently in CO_2 (a', b').

pyridinium ions presents a maximum in the intermediate range of cation content, which emphasizes the importance of the pretreatment. Concerning CO_2 -pretreatment influence, an increase in the intensity of Brønsted acidities is observed at the two evacuation temperatures especially for the most cationated samples. By contrast, a large decrease of the intensity of the cation pyridine interaction band (1449 cm^{-1}) is observed after the 400°C CO_2 exposure.

Ir Hydroxyl Bands. Besides the 3740-cm^{-1} band not related to catalysis, three other bands are observed at 3550 , 3640 , and 3685 cm^{-1} . The first two bands are generally present in Mg zeolites⁴ and correspond to acidic OH groups. The 3685-cm^{-1} band has been attributed to $\text{Mg}(\text{OH})^+$ groups exhibiting a basic character.⁷ The optical densities of all these OH bands, which were used as a measure of the concentrations in OH groups, are reported in Figures 5 and 6 before and after the 400°C CO_2 exposure. As may be seen from Figure 5b the 3550-cm^{-1} band intensity is very weak, which is in agreement with its known low stability upon 400°C evacuation.⁴ The 3640 - and 3685-cm^{-1} bands increase with increasing cation content (Figures 5a and 6a). Results obtained for hydrogen-pretreated materials were similar and would not be considered further. Reaction with CO_2 causes an increase in the intensity of the two acidic bands for samples with the highest magnesium levels (Figure 5a' and 5b'), whereas the intensity of the 3685-cm^{-1} band varies in an opposite way (Figure 6a').

It may be noted that the increase in the number of OH groups vibrating at 3640 cm^{-1} (Figure 5a) is not reflected in the curve referring to the pyridinium ions stable at 250°C for 400°C evacuated samples (Figure 4a). Differences in acid strength may account for this phenomenon.

ESR Results. The ESR spectrum of H atoms trapped in Y type zeolite (doublet of about 500 Oe hyperfine splitting) has widely been studied previously.¹⁰ Each H atom ESR line is the superposition of a narrow (1.4 Oe) and a broad (4.1 Oe) line with hyperfine splittings equal to 501.8 and 499.8 Oe, respectively. The difference in line width indicates that H atoms are trapped in two different sites. The experimental results for both lines are given in Figure 7 as a function of Mg content, before and after 400°C CO_2 exposure.

Catalytic Activity. The percentage of isooctane transformed is presented in Figure 8 as a function of cation content. All the Mg exchanged samples are more active for isooctane

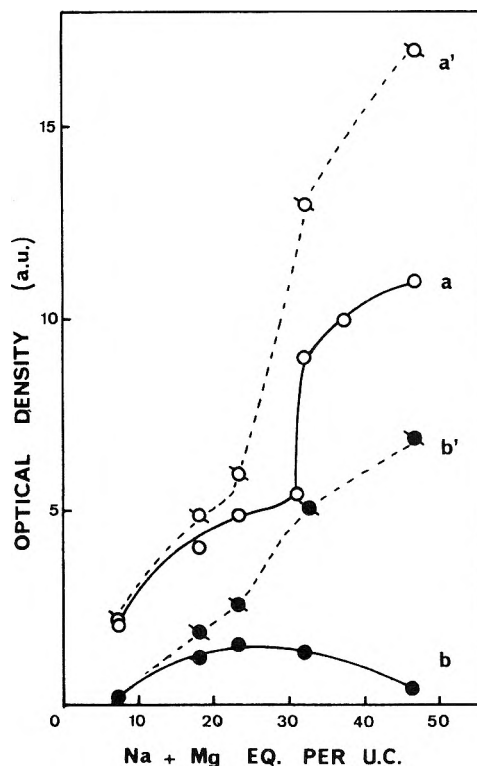


Figure 5. Intensity of the 3640-cm^{-1} band (a and a') and 3550-cm^{-1} OH band (b and b') for zeolites pretreated at 400°C first under vacuum (a and b) and subsequently in CO_2 (a' and b').

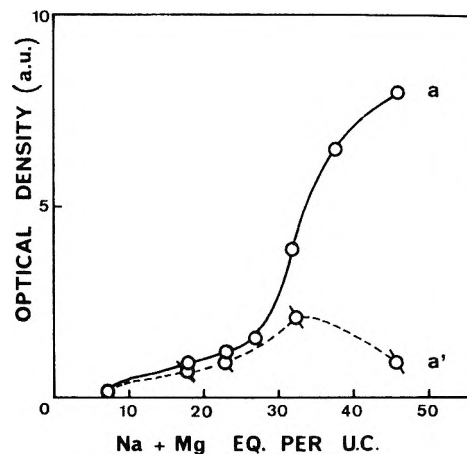


Figure 6. Intensity of the 3685-cm^{-1} OH band for zeolites treated at 400°C first under vacuum (a), subsequently in CO_2 (a').

cracking than a Na-HY zeolite with the same sodium content. The favorable influence of CO_2 on catalytic activity is more marked for zeolites containing large amounts of Mg^{2+} ions than for less cation exchanged samples and nonexistent for the protonic faujasite. No significant change in selectivity was detected on adding CO_2 to the reactants.

Discussion

In this part the influence of Mg^{2+} cations on the catalytic activity and acidity is first presented in terms of cation location and polarizing field. Then, on the basis of the data obtained by allowing Mg-Y zeolites to react with CO_2 , we discuss the participation in catalytic cracking of the different types of protons, measured by ir and ESR spectroscopies.

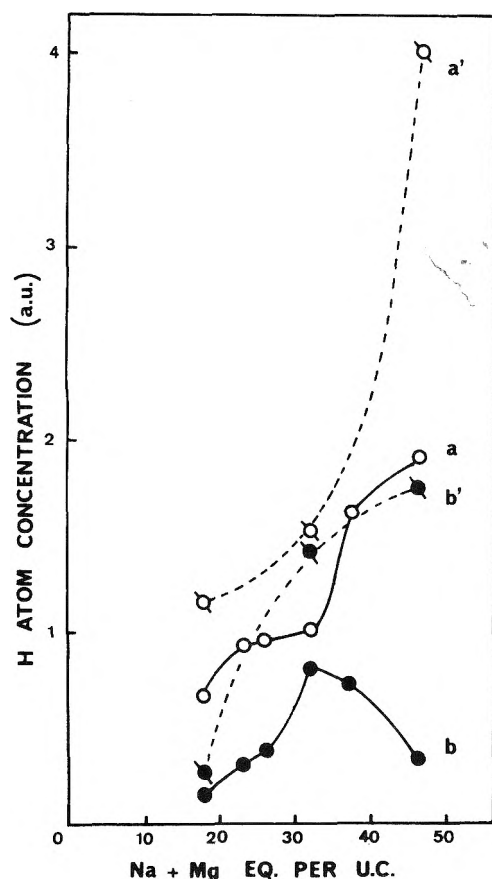


Figure 7. Intensity of the 4.1-Oe signal (a and a') and the 1.4-Oe signal (b and b') for zeolites pretreated at 400 °C, first under vacuum (a and b) and subsequently in CO₂ (a' and b').

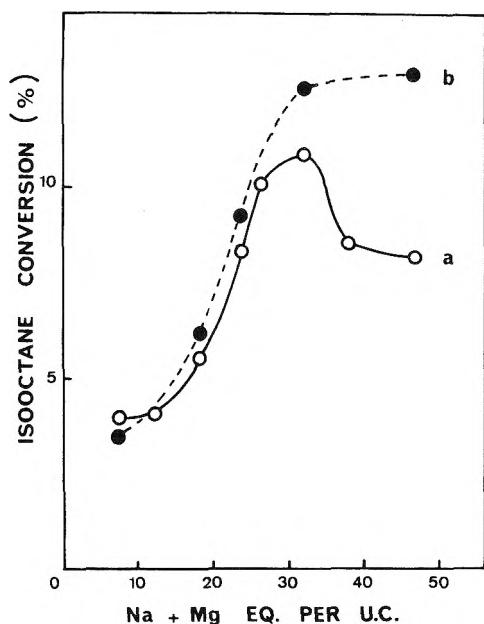


Figure 8. Percent conversion in isooctane cracking with (b) or without (a) CO₂ in the reactants.

I. Location and Polarizing Effect of Mg²⁺ Cations. From the occurrence of the 1449-cm⁻¹ band assigned to the 19 b vibrational mode of pyridine molecules bonded to Mg²⁺ cations in the zeolite, the presence of Mg²⁺ cations in the supercages may be inferred, since the pyridine cannot enter the

sodalite cages. However, this conclusion is true only if it is supposed that the pyridine does not displace these cations from inaccessible sites.

Figure 2 shows that the 1449-cm⁻¹ band is observed even for the lowest Mg content. This datum differs from the one reported by Ward,⁶ using also pyridine as probe. This author found that Mg²⁺ cations are not in the supercages for low ions contents. This discrepancy may be due to the different composition and heat treatment of the zeolites. Nevertheless, considering the increase in slope of the curve for the highest Mg contents, it is inferred that the fraction of Mg cations located in the supercages increases more for levels greater than 30 cation equivalents per unit cell.

For all the samples considered here and whatever their Mg content, a magnesium influence on the catalytic properties is likely to occur, because of the location of some of these cations in the supercages, although effects of the cations sited in the other cages may come into play as previously proposed.²

In the following paragraphs, we consider the changes in acidity and catalytic activity which are expected on replacing NH₄⁺ ions by Mg²⁺ ions in Y zeolites.

First, this replacement corresponds to the loss of two protons for each Mg²⁺ cation introduced. Therefore a complete exchange should reduce the protonic acidity to zero, which is not the case as may be seen from Figure 1.

To explain this observation, it is suggested that, because of the polarizing effect of Mg²⁺ cations on adsorbed water molecules, the following reaction¹¹ occurs:



Consequently, the number of protonic acid sites would not tend to zero for a completely exchanged Na-Mg-Y zeolite.

Secondly, it has been shown that Mg²⁺ cations increase the thermal stability of the zeolitic OH groups.¹ This last effect should cause a rise in catalytic activity with increasing Mg content, whereas, on the contrary, the decrease in the number of acid sites (Figure 1) should correspond to a progressive decline of the catalytic activity. Therefore, these effects, as a whole, may account for the maximum found in the catalytic activity (Figure 8) as a function of Mg content. Such a maximum was also obtained for *o*-xylene isomerization.⁵

This interpretation is not entirely satisfactory, since, on the basis of the same arguments, the catalytic activity of other polyvalent cation exchanged zeolites for reactions involving carbonium ions should also pass through a maximum, which has not been observed. Therefore, effects due specifically to the Mg²⁺ cations should be considered in addition to the preceding phenomena. The high polarizing power of Mg²⁺ cations has been previously invoked to explain the great catalytic activity of a magnesium hydrogen zeolite for *o*-xylene isomerization.² The formation of very strong Brønsted acid sites for the highest Mg levels (Figure 3c), in agreement with the ideas of Hirschler¹² and Richardson,¹³ as well as an increase in the electron acceptor power of the framework Al atoms (Lewis acidity) with increasing Mg content have been found in the present work. These results may be attributed to the polarizing effect of the Mg²⁺ cations. Furthermore, it is tentatively suggested that the Mg²⁺ cation field could polarize hydrocarbon molecules, so that the activation of C-C bonds by acid sites is favored. Hence, the electrostatic field of these cations^{2,14,15} would play a part in one step of the cracking mechanism. This view would account for the great catalytic activity of the Mg-Y zeolites even for low divalent cation contents.

II. Correlations between Catalytic Activity and OH Groups. The question arises as to whether these changes in catalytic activity may be related to changes in the intensity of the OH ir bands and ESR signals due to atomic hydrogen.

In regard to the ESR signals, it has been shown that when trapping strength and trapping sites as determined via hyperfine splitting constant and the ESR line width, respectively, are identical, the H atom yield characterizes a given range of acidity strength.¹⁶ Moreover, a close relationship between this yield and the catalytic activity for isooctane cracking has been observed for H-Y zeolites aluminum-deficient or not.¹⁷

The two H atom ESR lines (1.4 and 4.1 Oe) have been correlated with the 3550- and 3640-cm⁻¹ ir bands, respectively.¹⁸ These correlations are supported by curves of Figures 5 and 7 which have roughly the same patterns. This is interesting, since, in the case of samples exhibiting only weak OH ir bands, ESR spectroscopy may be used successfully with an improved accuracy because of its greater sensitivity.

For short, in what follows, the 3550-cm⁻¹ band and the 1.4-Oe line on the one side, and the 3640-cm⁻¹ band and the 4.1-Oe line on the other side, will be considered by pairs and designated LF-N bands (low frequency-narrow) and HF-B bands (high frequency-broad), respectively.

The curves showing the LF-N bands as a function of Mg content (Figures 5b and 7b) have a maximum as expected from the effects considered at the beginning of this discussion part, i.e., increase in the thermal stability of the protons and decrease in their number with increasing Mg content. Moreover, the maximum corresponds to approximately 30 equiv per unit cell as in the case of catalytic activity. However, it would be questionable to conclude that only the LF-N bands refer to active sites, since samples which do not exhibit these bands are active. Nevertheless, their participation cannot be excluded, although the HF-B band is usually considered as more important in catalysis by acid sites.^{5,19}

In a previous study,⁵ the catalytic activity of Mg-Y zeolites for *o*-xylene isomerization has been correlated to protons giving rise to the band at 3640 cm⁻¹ and capable of retaining pyridine at 250 °C. In the present case such a correlation is not clear. The HF-B bands, as well as the number of strongest acid sites, increase markedly for high Mg content, which is not consistent with the expected decrease in the number of protons.

These increases may be understood if one considers the change in the 3685-cm⁻¹ band upon ion exchange. In an earlier study,⁷ the 3685-cm⁻¹ band was attributed to Mg(OH)⁺ species having a basic character, whereas the 3640-cm⁻¹ band is usually related to acidic hydroxyl groups O₁H. For samples containing more than 30 equivalents of cations per unit cell, both the HF-B bands and the 3685-cm⁻¹ band rise sharply (Figures 5a, 6a, 7a), which may be explained by equilibrium 1, provided the protons formed give rise to O₁H groups specifically. Reaction 1 would be favored or the OH formed would be more stable when a large number of Mg²⁺ cations is in the supercages.

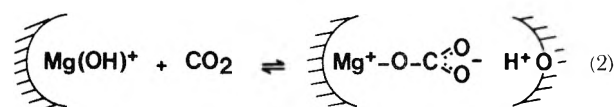
For the Mg-Y zeolites studied by Hansford and Ward,^{5,6} no nonacidic band was found around 3685 cm⁻¹ and there was no increase in the 3640-cm⁻¹ band for the highest Mg contents. These discrepancies may be due to a different pretreatment which precludes reaction 1. It must be emphasized that in our case no ultrastable material was detected according to ir and x-ray measurements.⁷ Consequently, the 3685-cm⁻¹ band cannot be due to OH groups at Al deficient sites.

TABLE II: Influence of CO₂ on ESR Signals of H Atoms, OH Ir Bands, and Catalytic Activity (Ratios of the Values with and without CO₂)

Catalysts	LF-N bands		HF-B bands		Catalytic activity
	1.4 Oe	3550 cm ⁻¹	4.1 Oe	3640 cm ⁻¹	
Mg-17.7	1.6	~1	1.6	1.3	1.1
Mg-32.1	1.8	~3	1.6	1.4	1.2
Mg-46.1	4.8	>6	2.1	1.5	1.5
Ca-51.1	<1	~1	5.8	7.5	4.0

In order to help to determine why the increase in the HF-B bands, whose associated protons are usually involved in the catalysis, and the appearance of very strong Brønsted acid sites, as determined from pyridine adsorption, correspond to a fall in the catalytic activity, the effect of CO₂ on the OH groups was investigated, since this molecule modifies the catalytic activity.⁷

Such a reaction involves the formation of new OH groups vibrating at 3550 and 3640 cm⁻¹ and of two types of unidentate carbonate species.⁷ One of these carbonate species has been assigned to the reaction of CO₂ with the basic Mg(OH)⁺ species (vibrating at 3685 cm⁻¹) which generates new structural acidic hydroxyl groups as follows:



The H⁺ formed would give a structural hydroxyl vibrating at 3550 cm⁻¹ and, to a lesser extent, at 3640 cm⁻¹ according to which type of framework oxygen it would be attached.⁷ Thus, the effects of heat treatment in the presence of CO₂ on OH group and H atom intensities as shown in Figures 5, 6, and 7 are quite consistent with reaction 2, whereas no effect was detected on Na-H-Y zeolites. Also, the decline of the 1449-cm⁻¹ band due to pyridine bonded to Mg²⁺ cations for CO₂ pretreated zeolites corroborates the fact that CO₂ reacts with some of the divalent cations.

A quantitative evaluation of the influence of CO₂ is tentatively given in Table II. This table depicts the ratios of the HF-B and LF-N band intensities and of the catalytic activities measured with and without CO₂ treatment. For generalization, a Ca-Y sample, containing 3.5Na⁺ and 23.8Ca²⁺ (i.e., 51.1 cation equivalents) per unit cell, has also been included.

Examination of Table II clearly shows that, as a function of Mg content, the effects of CO₂ are similar for the HF-B bands and catalytic activity, whereas the behavior of LF-N bands does not parallel that of the catalytic activity. This correlation is reinforced by the Ca zeolite results. Hence, the conclusion is similar, whatever the cation nature or content. This strongly supports the importance of the hydroxyl groups referring to the HF-B bands in catalysis.

Since CO₂ reacting with the Mg(OH)⁺ species increases both the HF-B band intensities and the catalytic activity, it is suggested that part of the OH groups formed in reaction 1 are inhibited in regard to catalysis by these basic species. After CO₂ treatment, the inhibited OH groups are released. Simultaneously, new acidic OH groups are also generated (reaction 2) and it is likely that at least part of them will play a role in the formation of carbonium ions. Moreover, it is conceivable that pyridine, which is a strong base, is capable of reacting with part of the OH groups responsible for the HF-B

bands even in the presence of basic $\text{Mg}(\text{OH})^+$ species, whereas hydrocarbons are not activated. This may account for the increase in the number of 350 °C bonded pyridinium ions in the case of samples with Mg contents greater than 30 cation equivalents per unit cell.

Conclusion

Although the participation of the protons responsible for the ir band at 3550-cm^{-1} and producing, under γ irradiation at 77 K, atomic H with an ESR line of 1.4 Oe cannot be excluded, it is proposed that the catalytic activity for isooctane cracking is related to the protons corresponding to the ir band at 3640-cm^{-1} and to the ESR line of 4.1-Oe width, since it appears that they are equally affected by reaction with CO_2 at 400 °C. However, part of these protons may be inhibited toward the catalytic cracking of hydrocarbons by basic $\text{Mg}(\text{OH})^+$ species. As a result of reaction with CO_2 , these basic sites are eliminated, so that the initially inhibited protons are released. Moreover, new acidic OH groups are also created. Consequently, the catalytic activity is increased. This phenomenon is also observed for a Ca-Y zeolite and might perhaps be extended to other polyvalent ion-exchanged zeolites interacting with acidic gases.

Acknowledgment. The authors thank the Laboratory of

Chemical Analysis. This work was assisted by the D.G.R.S.T. (Contract No. 74.7.1157).

References and Notes

- (1) J. W. Ward, *J. Catal.*, **26**, 451 (1972).
- (2) J. W. Ward, *J. Catal.*, **26**, 470 (1972).
- (3) L. N. Burenkova, V. I. Trunova, I. S. Thuong, and K. V. Topchieva, *Vestn. Mosk. Univ.*, **3**, 291 (1973).
- (4) J. W. Ward, *J. Catal.*, **11**, 251 (1968).
- (5) R. C. Hansford and J. W. Ward, *Adv. Chem. Ser.*, No. **102**, 356 (1971).
- (6) J. W. Ward, *J. Phys. Chem.*, **74**, 3021 (1970).
- (7) C. Mirodatos, P. Pichat, and D. Barthomeuf, *J. Phys. Chem.*, **80**, 1335 (1976).
- (8) M. V. Mathieu and P. Pichat in "La Catalyse au Laboratoire et dans l'Industrie", B. Claudel, E.J. Masson et Cie, Paris, 1967, p 319.
- (9) R. Beaumont and D. Barthomeuf, *J. Catal.*, **26**, 218 (1972).
- (10) A. Abou Kais, J. C. Vedin, J. Massardier, G. Dalmay-Imelik, and B. Imelik, *C.R. Acad. Sci. Paris, Ser. C*, **273**, 883 (1971); *J. Chim. Phys.*, **69**, 561 (1972).
- (11) J. W. Ward, *Adv. Chem. Ser.*, No. **101**, 380 (1971).
- (12) A. E. Hirschler, *J. Catal.*, **2**, 428 (1963).
- (13) J. T. Richardson, *J. Catal.*, **9**, 182 (1967).
- (14) V. J. Frette, P. B. Weisz, and R. L. Golden, *J. Catal.*, **1**, 301 (1962).
- (15) J. A. Rabo, P. E. Pickert, D. N. Stammers, and J. E. Boyle, *Proc. Int. Congr. Catal.* **2nd**, 2055 (1965).
- (16) A. Abou Kais, J. C. Vedin, J. Massardier, and G. Dalmay-Imelik, *J. Chem. Soc., Faraday Trans. 1*, **70**, 1039 (1974).
- (17) A. Abou Kais, J. C. Vedin, J. Massardier, and G. Dalmay-Imelik, *J. Catal.*, **34**, 317 (1974).
- (18) A. Abou Kais, J. Massardier, G. Dalmay-Imelik, and B. Imelik, *J. Chim. Phys.*, **69**, 570 (1972).
- (19) J. W. Ward and R. C. Hansford, *J. Catal.*, **13**, 364 (1969); J. W. Ward, *ibid.*, **11**, 259 (1968).

A Study of the Chemisorption of Nitric Oxide on PdY Zeolite. Evidence for a Room Temperature Oxidative Dissolution of Pd Crystallites

M. Che, J. F. Dutel, P. Gallezot, and M. Primet*

Institut de Recherches sur la Catalyse, C.N.R.S. 39, boulevard du 11 Novembre 1918, 69526, Villeurbanne, France (Received April 19, 1976)

Publication costs assisted by the Centre National de la Recherche Scientifique

Nitric oxide adsorption on a PdY zeolite in oxidized or reduced forms has been investigated by ir and EPR spectroscopies. Cations and metal atoms have been located in the zeolite framework by x-ray diffraction. Adsorption of NO on oxidized samples at 25 °C produced the migration of one-half of Pd^{2+} ions from the SI' sites in sodalite cages to the supercages. Two infrared bands near 1775 and 1875-cm^{-1} were attributed to NO molecules bonded to Pd^{2+} ions in sodalite cages and supercages, respectively. The band at 1775-cm^{-1} has a lower frequency probably because of a Pd-NO bent configuration. This attribution accounts for the different reactivities of the two species with respect to CO and H_2 . Encaged Pd(0) atoms produced by hydrogen reduction at room temperature are reoxidized in Pd^{2+} ions upon NO adsorption. This was proved by three techniques which together with mass spectrometry suggest that the reoxidation could be $2(\text{Z-OH}) + \text{Pd}(0) + 2\text{NO} \rightarrow \text{N}_2\text{O} + \text{H}_2\text{O} + 2(\text{Z-O})^-\text{Pd}^{2+}$. The 20-Å Pd crystallites formed in the bulk of the zeolite by reduction at higher temperature can also be reoxidized upon NO adsorption at room temperature. The reoxidative dissolution was clearly proved by the disappearance of the x-ray reflections due to Pd crystallites and by the reoccupancy of SI' sites by Pd^{2+} ions. The reversibility was also proved by ir and EPR results.

Introduction

From the standpoint of environmental science, the reduction of NO in automobile exhaust represents a difficult task because of the overall oxidizing conditions. This problem has been given much attention¹ and several reviews have recently

appeared on this subject.² From a more fundamental point of view, NO is a fascinating molecule because of the following properties: (i) it possesses an unpaired electron in the π antibonding orbital, whose degeneracy can be lifted by a crystal field and this can lead to characteristic EPR spectra; (ii) it can form nitrosyl complexes whose frequencies in ir spectra de-

pend largely on the availability of vacant orbitals or free electrons in the d shells of the coordination metal ion or atom;⁴ (iii) lastly, it can decompose in three different ways either according to a disproportionation reaction giving NO₂ and N₂O,⁵ or into N₂O and oxygen,⁶ or into its elements N₂ and O₂.⁷

In the present study, we have selected the PdY zeolite system because of its most unusual property to stabilize palladium in various oxidation states depending on the activation treatment of the sample. Thus, it is possible to obtain Pd³⁺ (4d⁷) or Pd²⁺ (4d⁸) ions after an oxidizing treatment and Pd⁺ (4d⁹) or Pd(0) atoms (4d¹⁰ after reduction by H₂ at room temperature.⁸⁻¹⁰ By reduction at higher temperature, Pd crystallites of various diameters can be produced.¹⁰ This gives the unique possibility of testing the influence of vacant d orbitals on the nature of nitrosyl complexes.

Apart from a brief account¹¹ there is at present no systematic work in the literature on the adsorption of NO on atomically dispersed metal nor on small crystallites and this represents the first attempt.

In this study, we have used the EPR technique, by which the participation of the odd electron in the bond is probed, the ir technique for measuring the change in the bond strength between the nitrogen and oxygen atoms, as manifested by the change in the vibration frequency of this bond, the x-ray technique in order to follow any possible migration of the ions which is known to occur for instance in NiY zeolite upon NO adsorption,^{12,13} and lastly the mass spectrometry for the analysis of the gas phase products.

Finally, it was interesting to compare the properties of PdY zeolite with similar systems (CaY,¹⁴ NiY,¹⁵ CuY¹⁶ in particular) known to catalyze the disproportionation reaction of NO with different rates.

Experimental Section

Materials. The sodium form of the Y-type zeolite with a ratio SiO₂/Al₂O₃ = 4.8 was supplied by the Linde Co. The palladium form was obtained by exchanging the NaY with cations from a tetramminepalladium(II) solution prepared by dissolving PdCl₂ in an ammonia solution. The exchanged zeolite was then washed until free from chloride ions and dried at 80 °C in air. Flame photometry and colorimetry methods were used for determining the sodium and palladium contents respectively and gave the following results: Pd_{12.5}Na_{19.5}(NH₄)_{11.5}Al₅₆Si₁₃₆O₃₈₄.

NO, NO₂, and N₂O received from a commercial source were purified by repeated distillations before use and special attention was given to avoid any trace amount of NO₂ and N₂O to be present in NO.

Sample Treatments. Infrared wafers (18 mm in diameter) of about 30 mg of zeolite were compressed at a pressure of 1000 kg cm⁻². The quartz sample holder and cell have been previously described¹⁷ except that in this study no joint nor stopcock was used. In the x-ray experiments, the zeolite samples were treated in a quartz cell possessing x-ray capillaries which were sealed off after the activated solid had been transferred into them. For the EPR study, the activation was carried out directly in silica EPR tubes. In all cases, the cells were supplied with break seals for many step activation process or further introduction of gases.

The activation procedure was adapted to each case so as to obtain a reproducible state of the Pd ions hereafter referred to as the oxidized PdY zeolite. The color and the EPR signals were found to be good probes for monitoring, after the thermal treatment, the oxidation states of palladium ions. A bright

beige pink color was always associated to palladium ions mostly in the Pd²⁺ state and a few percent in the Pd³⁺ state as proven by their characteristic EPR signal at $g_{iso} = 2.223$.⁸

The oxidized samples could only be obtained after NH₃ which issued from the decomposition of the tetramminepalladium complex had been carefully removed. Thus, the changes in the activation procedure for each technique depended on the geometry of the cells (diameter) and the state of the sample (compressed disks, thickness of the powder) as observed earlier.⁸

In the x-ray experiments, the zeolite was activated in a flow of dried oxygen up to 350 °C for several hours and then evacuated overnight at 600 °C under a pressure of 10⁻⁵ Torr. For the ir experiments, the samples were slowly heated in a flow of dried O₂ up to 500 °C, kept at this temperature for 10 h, sealed off under oxygen, and finally evacuated at 500 °C for 8 h under a pressure of 10⁻⁵ Torr. For the EPR measurements, the samples were heated in oxygen, in presence of a liquid nitrogen trap, up to 300 °C in 6 h, kept at this temperature for 8 h, and finally evacuated under vacuum (10⁻⁵ Torr) at 500 °C for 15 h. This last procedure was found far more reproducible than that described earlier.^{8,9}

Techniques. The ir spectra were recorded on a grating Perkin-Elmer spectrophotometer (Model PE 125). The resolution was better than 2 cm⁻¹ in the spectral range studied (4000–1200 cm⁻¹). The reference beam was attenuated and the instrument was flushed with air freed of H₂O and CO₂. The x-ray analysis has been performed following the method used earlier.¹⁰ In both cases, the recordings were made at room temperature.

The paramagnetic absorption of Pd ions and NO radicals was investigated both at room temperature and 77 K using Varian spectrometers (Models V 4502 and E-9) at X (9.5 GHz) and Q (35 GHz) bands. The g values were measured using a dual cavity and DDPH as a reference ($g = 2.0036$).

Results

I. X-Ray Study. The crystal structure of the oxidized PdY zeolite activated at 600 °C (sample A of ref 10) was refined again assuming that the SI sites were occupied by Na⁺ ions instead of Pd²⁺ as previously reported.¹⁰ As a matter of fact, it must be recalled that structure analysis gives only the electron density so that an absolute distinction between extraframework atoms with low occupancy factor can never be achieved exactly. SI' sites can readily be attributed to Pd²⁺ ions because of the high population of these sites and of the very short SI'-O(3) distances, whereas the assignment of Pd²⁺ to SI sites is groundless. The refinement yielded 6 Na⁺ instead of 1.3 Pd²⁺, i.e., exactly the 4.5 ratio of their atomic scattering factor. For the same reason as mentioned above, it is also quite possible that one or two Pd²⁺ ions might share the SII sites with Na⁺ ions.

Sample I was obtained by allowing the oxidized zeolite to equilibrate during 4 h with a 200 Torr gas pressure of NO at 25 °C.

Sample II was prepared as follows: the oxidized zeolite was reduced at 25 °C by H₂ under a 100 Torr pressure; the excess of hydrogen was then pumped off at 25 °C to 10⁻⁵ Torr; the sample was then equilibrated with a 200 Torr pressure of NO for 24 h at 25 °C.

Sample III was prepared as sample II and then evacuated from 25 to 200 °C at a rate of 1 °C/min.

The coordinates and population of extraframework species located in samples I, II, and III are given in Table I. The

TABLE I: Population and Coordinates of Extraframework Atoms

	SI	SI' (0.044)	SI' (0.068)	SI' (0.11)	U^a (0.125)	SII	Unit cell constant ($\pm 0.01 \text{ \AA}$), Final R index ^b
Sample A ^c	6 (1) Na ⁺ 0.0	10.6 (3) Pd ²⁺ 0.044 (1)				19 (1) Na ⁺ (or 14 Na ⁺ + 1 Pd ²⁺) 0.236 (1)	$a = 24.66$ $R = 0.097$
Sample I First refinement	14 (1) Na ⁺ 0.0		6.0 (2) Pd ²⁺ 0.068 (1)	10 (2) N or O 0.11 (1)		23 (1) Na ⁺ (or 14 Na ⁺ + 2Pd ²⁺) 0.238 (1)	$a = 24.72$ $R = 0.088$
Sample I Second refinement	14 (1) Na ⁺ 0.0		6.0 (2) Pd ²⁺ 0.068 (1)		13 (3) N or O 0.125	23 (1) Na ⁺ (or 14 Na ⁺ + 2Pd ²⁺) 0.238 (1)	$a = 24.72$ $R = 0.091$
Sample II	9 (1) Na ⁺ 0.0		3.8 (2) Pd ²⁺ 0.070 (1)		7 (3) N or O 0.125	27 (1) Na ⁺ (or 14 Na ⁺ + 3Pd ²⁺) 0.240 (1)	$a = 24.71$ $R = 0.092$
Sample III	6 (1) Na ⁺ 0.0	9.2 (3) Pd ²⁺ 0.043 (1)	2.9 (3) Pd ²⁺ 0.067		5 (3) N or O 0.125	17 (1) Na ⁺ 0.238 (1)	$a = 24.68$ $R = 0.097$

^a Atoms dispersed within a 1 Å radius sphere at $x = y = z = 0.125$. ^b $R = \Sigma ||F_o - |F_c|| / \Sigma |F_o|$, F_o and F_c are observed and calculated structure factors. ^c Reference 10.

complete list of crystallographic parameters and the listing of observed and calculated structure factors will be supplied upon request to the authors.

Refinement of sample I showed that only 6 out of the 10.6 Pd²⁺ ions are left on SI' sites, moreover they are shifted from $x = y = z = 0.044$ to 0.068 toward the center of the sodalite cage. In addition, scattering matter was found at $x = y = z = 0.11$ near the center of the sodalite cage ($x = y = z = 0.125$) and attributed to N or O atoms (N and O atoms cannot be distinguished from each other because of their nearly equal scattering factors) belonging to a NO molecule. The other atom of the molecule should be near $x = y = z = 0.135$ (about 1.2 Å apart corresponding to the NO bond length) but the refinement did not converge to acceptable occupancy factor and atomic coordinates. However, as there is much uncertainty in locating these light atoms in presence of heavy Pd²⁺ ions, an alternative refinement (sample I, refinement 2) has been performed using liquid scattering functions¹⁰ corresponding to a model where the NO molecules are randomly distributed within a sphere of 1 Å radius centered at $x = y = z = 0.125$. This yielded 13 ± 3 N or O atoms or about 6 NO molecules, however, the error is probably underestimated. The 6 unlocated Pd²⁺ ions have probably migrated toward the supercages. Part of them probably share SII sites with Na⁺ ions and this would account for the anomalous high Na⁺ population at these sites.

The distribution of Pd²⁺ ions in sample II is similar to that found in sample I except that a larger number of cations occupy the supercages.

In sample III, most of the Pd²⁺ ions (9.2 out of the initial 10.6 Pd²⁺) occupy SI' (0.044) sites again. However, 2.9 Pd²⁺ ions are still in interaction at SI' (0.068) sites with residual NO molecules.

The action of NO on PdY zeolites reduced at higher temperature was also investigated. In a previous paper¹⁰ it was shown that after a 300 °C reduction (sample AH 300) palladium atoms are completely removed from the sodalite cages and form 20-Å diameter crystallites. Examination by electron microscopy of ultramicrotome sections of this sample has shown that the palladium crystallites have grown inside the volume of the zeolite crystals (a limited breakdown of the framework around each Pd crystallites must occur). In the present investigation the PdY zeolite activated in O₂ at 500

°C was reduced for 6 h at 500 °C with a 300 Torr hydrogen pressure and then evacuated at the same temperature. The x-ray diffraction pattern is similar to that of AH 300,¹⁰ the zeolite diffraction lines have the same relative intensities and broad lines correspond to 20-Å diameter crystallites. The size of Pd crystallites does not increase between 300 and 500 °C because they are occluded in the bulk of the zeolite as reported above. The reduced zeolite was then contacted at 25 °C with a 300 Torr pressure of NO. The dark brown color of the powder turned to the beige pink color of oxidized palladium within about 20 min. This reoxidation of palladium was evidenced by x-ray analysis. After 2 days of contact with NO the diffraction lines of palladium crystallites completely vanished. Moreover after heating the zeolite at 200 °C under vacuum, the diffraction pattern of the zeolite was similar to those of samples A and III. From these results, one is led to conclude that the NO molecules have oxidized and subsequently complexed all the Pd atoms forming the crystallites which completely disappear. These complexes are then redistributed among the zeolite cages and on heating under vacuum at 200 °C the NO molecules are removed and the Pd²⁺ ions can move back to the SI' sites.

II. *Infrared Study.* (1) *NO Adsorption on Oxidized Samples.* The sample oxidized at 500 °C exhibited ν_{OH} bands like a NaY zeolite. Upon evacuation at 500 °C, these bands completely vanished. All the spectra presented a broad band near 1800 cm⁻¹ which was assigned to overtones or combinations of Si-O framework vibrations.

Upon contact with NO at 25 °C the PdY sample oxidized at 500 °C showed bands at 2025, 2175, 1780, and 1865 cm⁻¹ (Figure 1). Increasing the time of contact with NO only had little influence on the two first bands in contrast with the last two bands which increased in intensity, that at 1780 cm⁻¹ faster than that at 1865 cm⁻¹. After NO was pumped off at room temperature, the intensity of the bands at 2025 and 2175 cm⁻¹ strongly decreased while the two others were little changed (Figure 1). Evacuation at higher temperature eliminated the bands at 1780 and 1865 cm⁻¹, the latter between 150 and 200 °C (Figure 1) and the former between 300 and 350 °C. After the bands had reached their maxima, the ratio of the optical densities (OD) $r = [OD(1780 \text{ cm}^{-1})/OD(1865 \text{ cm}^{-1})]$ was dependent upon the heat treatment: $r = 1.2$ and 2.10 after 350 and 500 °C O₂ and vacuum treatment, respectively.

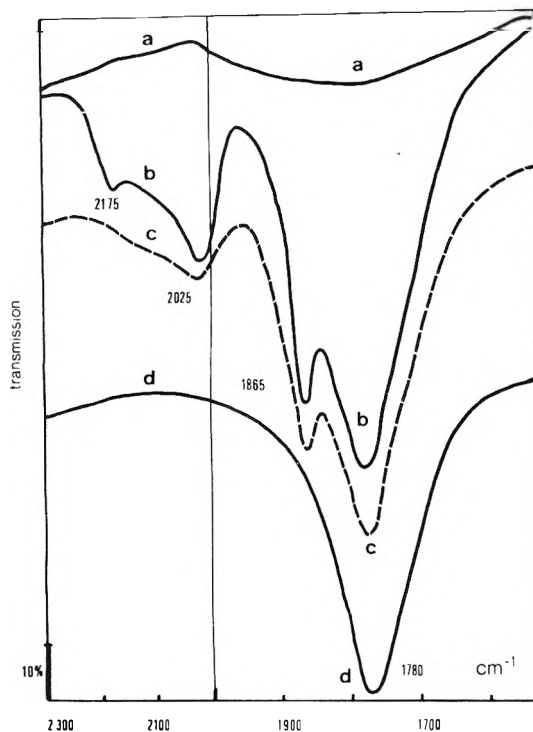


Figure 1. Infrared spectra of NO adsorbed on oxidized samples: (a) Pd^{2+}Y sample treated under O_2 and in vacuo at 500°C ; (b) sample a contacted with NO (pressure = 45 Torr) for 12 h at 25°C ; (c) evacuation of NO at 25°C ; (d) NO pumped off at 200°C for 12 h.

Subsequent addition of NO restored the bands in their initial intensities suggesting that no chemical change had occurred in the nature of the adsorption sites upon NO treatment and subsequent evacuation at 350°C .

The bands at 1780 and 1865 cm^{-1} were not altered upon treatment with oxygen at 25°C , in contrast to hydrogen which eliminated the bands at 1865 , 2025 , and 2175 cm^{-1} at 25°C and that at 1780 cm^{-1} at about 250°C ; simultaneously the hydrogen reduction process led to the appearance of bands at 1445 , 1640 , 3640 , and 3540 cm^{-1} . CO introduced onto irreversibly adsorbed NO led to the disappearance of the 1865 cm^{-1} band while the other band at about 1780 cm^{-1} increased in intensity and was broadened. Simultaneously, a sharp and intense band developed at 2140 cm^{-1} characteristic of CO adsorbed on Pd^{2+} ions⁹ (Figure 2). Upon evacuation of CO at 25°C , the 2140 cm^{-1} band was eliminated and the ν_{NO} bands at 1780 – 1865 cm^{-1} were observed with intensities slightly smaller than originally (Figure 2). On the other hand, CO directly introduced onto oxidized samples produced only very weak IR bands at 2135 and 2110 cm^{-1} (Figure 5a).

(2) *NO Adsorption on Reduced Samples.* (a) *Reduction at 25°C .* The reduced samples containing atomically dispersed palladium were obtained by contacting the oxidized samples with 100 Torr of H_2 at 25°C ;^{9,10} this produced an increase of the ν_{OH} bands which were then well resolved (3540 – 3640 cm^{-1}) and, at the same time, the water formation was detected by its $\delta_{\text{H}_2\text{O}}$ band at 1640 cm^{-1} (Figure 3). After H_2 had been pumped off, NO was admitted at room temperature under a pressure of 30 Torr which produced bands at 1795 and 1865 cm^{-1} (Figure 3). These bands showed the same behavior as that observed for the oxidized samples upon adsorption and desorption of NO and further contact with H_2 , O_2 , or CO. In addition, a small doublet near 2200 cm^{-1} due to gas phase N_2O was also observed. For the reduced samples, at equilibrium,

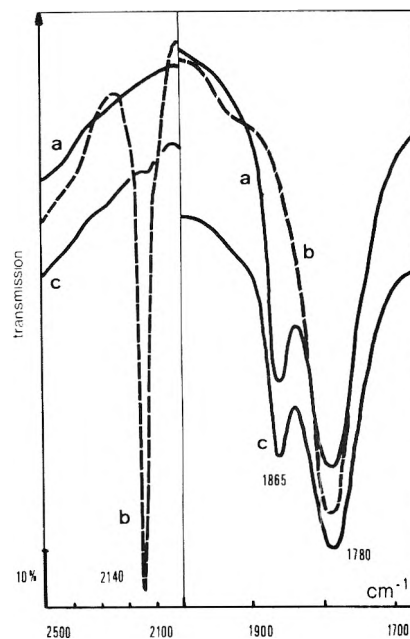


Figure 2. Infrared spectra of CO adsorbed on oxidized samples containing nitrosyl complexes: (a) Pd^{2+}Y treated under O_2 and in vacuo at 350°C , then contacted with NO at 25°C , for 4 h; NO is pumped off at room temperature; (b) sample a contacted with CO (pressure = 20 Torr) at 25°C ; (c) CO evacuated at 25°C .

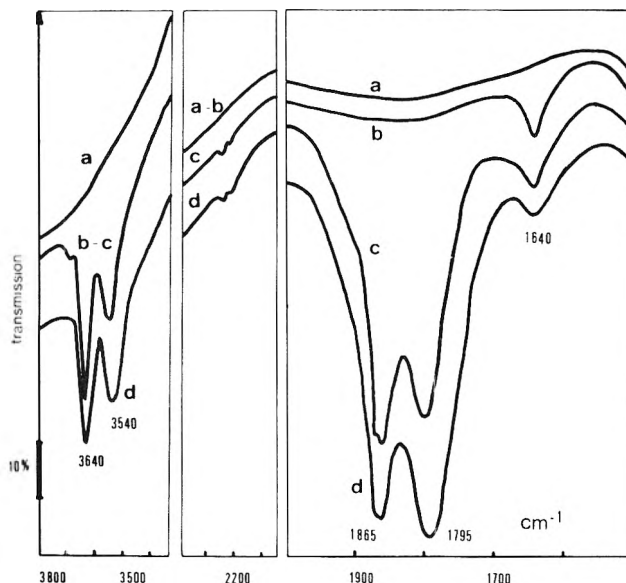


Figure 3. Infrared spectra of NO adsorbed on sample reduced by hydrogen at room temperature: (a) Pd^{2+}Y calcined under O_2 at 500°C , then evacuated at 500°C ; (b) sample a reduced by H_2 (pressure = 300 Torr) for 8 h at 25°C and evacuated at 25°C ; (c) introduction of NO (pressure = 50 Torr) for 5 min at 25°C ; (d) same as c but contact time was 12 h at 25°C .

the optical density ratio of the two bands was $r = 1.15$ (Figure 3d).

In order to check the oxidation state of palladium accessible to CO, NO was completely eliminated by desorption at 350°C and CO introduced onto the sample. No band characteristic of CO adsorbed on metallic palladium⁹ could be detected. After CO had been pumped off at 25°C , only two weak bands at 2135 and 2110 cm^{-1} were observed which corresponded to CO adsorbed on Pd^{2+} ions.⁹

(b) *Reduction at Higher Temperatures.* A treatment by H_2

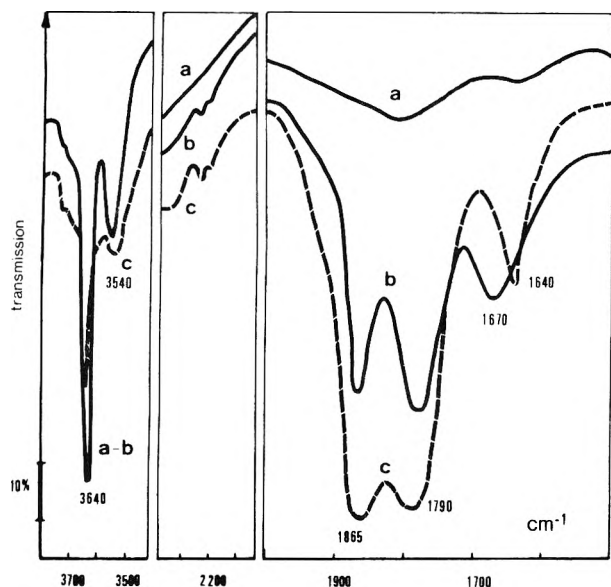


Figure 4. Infrared spectra of NO adsorbed on sample reduced by hydrogen at 500 °C: (a) Pd²⁺Y sample reduced by H₂ at 500 °C, then evacuated at 500 °C; (b) NO introduced on the previous sample (pressure = 20 Torr) at 25 °C for 5 min; (c) same as b but contact time was 5 h.

at 150 °C reduces Pd²⁺ ions to the Pd(0) state. After reduction by H₂ at 150 °C, the sample was evacuated at 25 °C and NO allowed to contact it. The ν_{OH} bands at 3640–3540 cm⁻¹ produced by the reducing treatment were slightly altered, while a doublet at 2235, 2210 cm⁻¹ and three more intense bands at 1675, 1790, and 1865 cm⁻¹ were observed. When the time of contact was increased, the last two bands grew in intensity while that at 1675 cm⁻¹ finally disappeared. After evacuation at 25 °C the optical density ratio of the remaining bands was $r = 0.96$, while at 400 °C the bands were no longer observed. Subsequent CO adsorption did not yield bands encountered with metal but weak peaks at 2135 and 2110 cm⁻¹.

Reduction of H₂ at 500 °C yields 20-Å Pd crystallites.¹⁰ After H₂ had been pumped off at 500 °C, the sample exhibited two intense and well-resolved ν_{OH} bands at 3540 and 3640 cm⁻¹ (Figure 4). Addition of NO at 25 °C had the same effect as that observed with the sample reduced at 150 °C: bands at 2235–2210 and 1865–1790 cm⁻¹ developed progressively while that at 1670 cm⁻¹ slowly disappeared at the same time, ν_{OH} bands decreased and the formation of water was detected by a band at 1640 cm⁻¹. After 12 h of contact and subsequent evacuation of excess NO, the intensity ratio of the bands at 1790 and 1865 cm⁻¹ was $r = 0.84$ while the doublet at 2235, 2210 cm⁻¹ was no longer observed. It was necessary to evacuate the sample at 400 °C to remove NO from the sample. Subsequent CO adsorption at 25 °C onto the resulting solid produced very weak bands characteristic of the presence of Pd²⁺ ions only, but not of metal (Figure 5).⁹

III. EPR Study. (1) *NO Adsorption on Oxidized Samples.* Oxidized samples exhibit a bright beige pink color and at 77 K an EPR signal at $g_{iso} = 2.223$ assigned to Pd³⁺ ions.⁸ After exposure of the samples at 25 °C to 5–100 Torr of NO for 1–4 days, the color did not change and no EPR signal could be detected at room temperature. However, when cooled to 77 K, the samples became intensely purple while a signal at $g \approx 1.95$ developed and the Pd³⁺ EPR signal progressively decreased to a low intensity (Figure 6). When 150–200 Torr NO pressures were used the Pd³⁺ EPR signal completely disappeared while the $g \approx 1.95$ EPR signal developed with a poorer

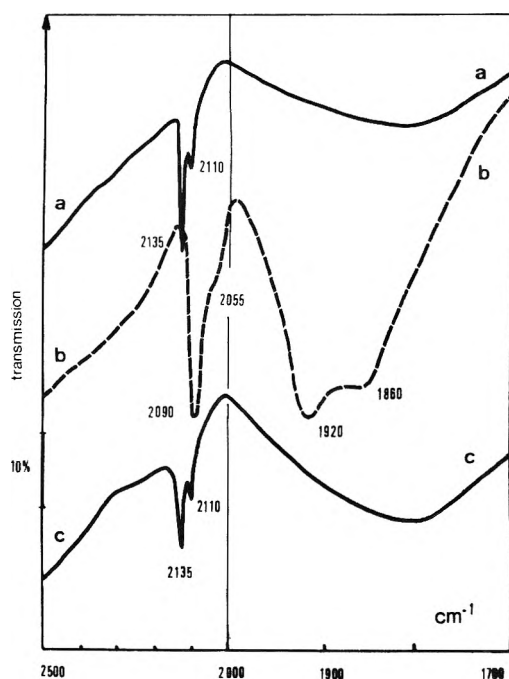


Figure 5. Infrared spectra of CO adsorbed at 25 °C on palladium supported zeolites: (a) oxidized samples treated at 500 °C under O₂, evacuated at 500 °C, CO irreversibly adsorbed; (b) reduced samples, treated by H₂ at 300 °C, spectrum taken under 10 Torr of CO pressure; (c) reduced samples, treated by H₂ at 500 °C, contact with NO at 25 °C for 18 h, desorption at 450 °C for 4 h, CO irreversibly adsorbed.

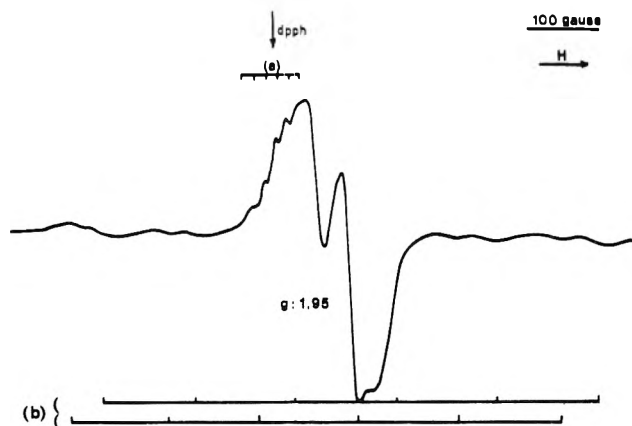


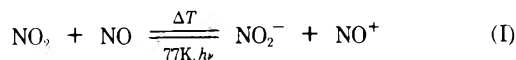
Figure 6. EPR signal at $g = 1.95$ observed at 77 K for an oxidized sample contacted with NO (pressure = 50 Torr) at 25 °C for 48 h, then evacuated at room temperature for 5 min: (a) hyperfine lines due to Al nuclei; (b) hyperfine lines due to ¹⁰⁵Pd nuclei.

resolution. Evacuation of the gas phase led to the resolution obtained with low pressures.

Evacuation of NO at room temperature for several hours restored the Pd³⁺ EPR signal to its original intensity and eliminated both the signal at $g \approx 1.95$ and the purple coloration when the sample was cooled to 77 K. The bright beige pink color of the sample was not altered by successive adsorption and desorption of NO. It was further learned that the results obtained upon NO adsorption and subsequent evacuation could be repeated several times, showing the complete reversibility. Both EPR signals of Pd³⁺ ions and that at $g \approx 1.95$ were not observable at 25 °C because of line broadening while they were much narrower and easily observed at 77 K. The signal at $g \approx 1.95$ could be eliminated by contacting the samples with H₂ at 25 °C. In presence of excess oxygen, it was

broadened beyond detection but could be regenerated upon evacuation of excess oxygen.

It has been shown by Kasai and Bishop¹⁵ that NO₂ produced by NO disproportionation in NiY zeolites reacts with NO following the equilibrium:



Thus, uv irradiation at 77 K should produce NO₂ and NO radicals if disproportionation occurs, which has been observed with Y-type zeolites exchanged with various cations.¹⁵ In the PdY zeolite case, after NO had been pumped off, uv irradiation at 77 K produced only a minute signal due to NO₂ radicals. Moreover, the resolution of the EPR signal at $g \approx 1.95$ did not depend on the contact time but on the pressure, in contrast to the results obtained for NaY, BaY, and ZnY zeolites which catalyze disproportionation.¹⁵

(2) *NO Adsorption on Reduced Samples.* (a) *Reduction at 25 °C.* At 25 °C, hydrogen converted irreversibly Pd³⁺ ions into Pd²⁺ ions characterized by an anisotropic EPR signal at $g_{\perp} = 2.10$ and $g_{\parallel} = 2.33$,⁸ observable at 77 K or 25 °C with no appreciable increase in the line width. This conversion was accompanied at 25 °C by a color change from bright beige pink to ash-grey. After evacuation of hydrogen and upon contact with NO at 25 °C, the samples changed in color from ash-grey to bright beige pink, the characteristic color of the oxidized samples. Cooling the sample to 77 K caused the color to change again to intense purple and examination at 77 K by EPR showed that the Pd²⁺ signal had disappeared and that at $g \approx 1.95$ had developed with the same characteristics as for oxidized samples. Increasing the NO pressure accelerated the rate of disappearance of the Pd²⁺ EPR signal and decreased the resolution of the signal at $g \approx 1.95$, which could be improved upon evacuation of the gas phase. Evacuation of NO at 25 °C for several hours strongly decreased the intensity of the EPR signal at $g \approx 1.95$, while no restoration of the Pd²⁺ EPR signal could be obtained. Readmission of NO, as previously, increased the EPR signal at $g \approx 1.95$ to its original intensity.

In order to investigate the nature of the adsorption site of NO leading to the EPR signal at $g \approx 1.95$, the following procedure was used: the oxidized PdY zeolite was reduced at 25 °C with H₂ which was then pumped off. The Pd²⁺ ions thus produced were reoxidized into Pd³⁺ ions with O₂ at 150 °C. This last reoxidation step was monitored by the decrease in intensity of the Pd²⁺ EPR signal until its complete disappearance. NO was then allowed to react with the Pd³⁺ Y zeolite. This produced only the EPR signal at $g \approx 1.95$ with no simultaneous appearance of Pd³⁺ or Pd²⁺ EPR signal showing that Pd²⁺ ions were the adsorption sites. The EPR signal at $g \approx 1.95$ had the same behavior toward H₂ and O₂ as for the oxidized samples. Pd²⁺ ions did not react with N₂O at 25 °C but gradually converted between 200 and 300 °C in a N₂O atmosphere into Pd³⁺ ions ($g_{\text{iso}} = 2.223$). In contrast Pd²⁺ ions reacted at 25 °C with NO₂ as their EPR signal irreversibly disappeared. Simultaneously, a signal due to NO₂ radicals developed. By evacuation at 25 °C, this signal was not altered but no EPR signal due either to Pd²⁺ or Pd³⁺ ions was observed.

(b) *Reduction at Higher Temperatures.* If the sample reduced by H₂ at 25 °C was further heated in H₂ to 150 °C, the Pd²⁺ EPR signal converted into an "inverted" anisotropic signal (Figure 7) at $g_{\perp} = 2.30$ and $g_{\parallel} = 2.05$ with $g_{\perp} > g_{\parallel}$ in contrast with the g tensor of the "normal" Pd²⁺ ion with $g_{\parallel} > g_{\perp}$. Q band measurements showed that the line shape of this

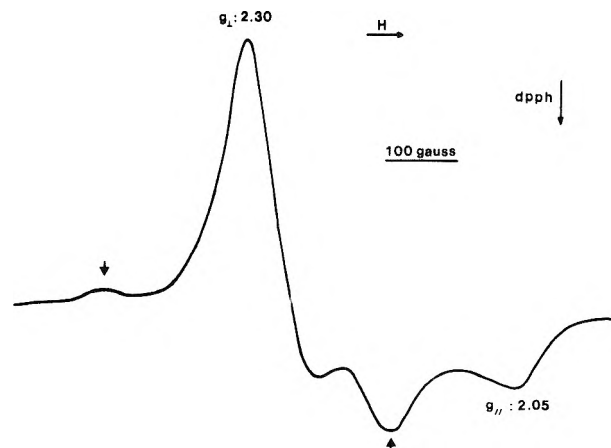


Figure 7. EPR inverted anisotropic signal observed at 77 K for an oxidized sample further reduced by hydrogen at 150 °C for 2 h. The weak signal marked by arrows is due to normal Pd²⁺ ions which remain after reduction by hydrogen at 150 °C.

new signal was due to the g tensor alone and confirmed the g values. This new signal is due to Pd²⁺ ions in a different environment. After, evacuation of H₂ at 25 °C and upon contact with 100 Torr of NO, the "inverted" signal first converted into the normal Pd²⁺ signal whose intensity in turn decreased while the signal at $g \approx 1.95$ developed. Evacuation of NO at room temperature did not produce any new signal and strongly decreased the signal at $g \approx 1.95$. Admission of NO₂ at 25 °C converted the inverted signal into the normal one which in turn further reacted with NO₂ as described previously in the preceding paragraph.

When the PdY zeolite was reduced at 500 °C by H₂ which was then pumped off at 500 °C, a broad EPR signal (line width 180 G) was detected. Admission of 100 Torr of NO at 25 °C produced the signal at $g \approx 1.95$ that could be eliminated by evacuation at room temperature and reproduced by subsequent NO admission. NO₂ admitted on the sample reduced at 500 °C produced a signal due to NO₂ radicals but no other signal.

IV. Mass Spectrometry Study. In the case of samples reduced at high temperatures by hydrogen, the ir results have shown that NO undergoes a decomposition reaction yielding N₂O. For lower reduction temperatures, it was interesting to use mass spectrometry to confirm the decomposition of NO yielding N₂O.

The samples were prepared as follows: one was a conventional EPR cell (sample A) with about 40 mg of solid, the other (sample B) was a larger cell with about 400 mg. They both were treated simultaneously on the same gas handling line. After the oxidizing heat treatment (presence of the EPR signal of Pd³⁺ ions), the samples were reduced at 25 °C for 15 h by hydrogen which was then pumped off at the same temperature (presence of the EPR signal of Pd²⁺ ions). NO was then admitted under a pressure of 300 Torr at 25 °C on both samples (disappearance of the EPR signal due to Pd²⁺ ions and appearance of the EPR signal at $g \approx 1.95$) and in a reference cell to test the purity of the NO gas.

For the larger cell, the analysis of the gas phase products was performed after increasing time intervals. In the case of the EPR cell, the analysis was carried out after 72 h of contact with NO. The mass spectrometry results are presented in Table II. It is conspicuous that the sole product of NO decomposition is N₂O in agreement with ir results.

TABLE II: Mass Spectrometry Results

Samples	Time contact with NO, h	N ₂ O, %	H ₂ , %	N ₂ , %
A	72	2		
B	1	0.3	Traces	Traces
	3	0.75	Traces	Traces
	20	2.4	Not detected	Traces
	27	2.9	Not detected	0.1
	49	3.4	Not detected	0.1
	68	3.8	Not detected	0.1
Reference NO gas		No impurity detected		

Discussion

Table III summarizes most of the experimental results.

I. *Oxidized Samples.* (a) *Origin of the Ir Bands near 1780 and 1865 cm⁻¹.* The oxidized samples contain mainly Pd²⁺ ions and a small fraction of Pd³⁺ ions.⁹ Thus owing to their large intensities, the two bands at 1780 and 1865 cm⁻¹ are assigned to nitrosyl complexes¹⁸ involving Pd²⁺ ions. On HY and NaY zeolites¹⁴ and on NH₄Y¹⁹ it is known that NO adsorption does not produce any intense ir bands at 25 °C in this spectral region confirming that the palladium ions are the adsorption sites.

In a number of ir investigations on NO adsorption, the presence of two bands in this spectral region has been reported and assigned to different species: N₂O₂^{20,21} or nitrosyl complexes formed from transition metal ions in oxidized and reduced states.⁶ The N₂O₂ dimer is stable only at low temperatures even on surfaces^{20,21} and from the different behavior of the two bands in presence of H₂, this assumption can be ruled out.

The x-ray technique demonstrates that in oxidized samples before NO adsorption palladium occupy cation sites (sample A, Table I) while no Pd⁺ ions and only a small concentration of Pd³⁺ ions can be detected by EPR. The color of the sample after NO adsorption similar to that of the oxidized sample also indicates that NO does not reduce the oxidized sample. Thus, the simultaneous presence of reduced and oxidized states of Pd as the adsorption sites of NO can be ruled out. This discussion confirms that NO molecules adsorb mainly at Pd²⁺ sites.

There are two possibilities to account for the presence of bands at 1780 and 1865 cm⁻¹, namely, (a) two molecules of NO adsorbed on one Pd²⁺ ion, (b) NO molecules adsorbed on Pd²⁺ ions in different environments. Assumption (a) cannot explain the experimental results, e.g., the different rate of formation of the two bands, their different thermal stability, their intensity variation as function of the heat treatment conditions, and their different reactivity toward H₂ and CO. Moreover, it has been shown by Zecchina et al.²² that Cr^{II}(NO)₂ complexes on Cr₂O₃/SiO₂ catalysts were able to add one CO ligand, which caused a shift and a variation in intensity of the two NO bands besides the formation of a third band produced by the CO ligand. The ir data disagree with Zecchina's results. Thus assumption (a) can be discarded.

The x-ray results indicate that in oxidized samples (sample A, Table I) about 11 Pd²⁺ ions occupy the SI' sites. As these ions tend to be the most dispersed among the eight sodalite cages, statistically three cages are occupied by two Pd²⁺ ions and the others by one Pd²⁺ ion. After NO adsorption, six Pd²⁺

ions remain at SI' sites slightly displaced toward the center of the cage because they interact with NO molecules; the others have migrated toward the supercages. It is tempting to assume that only the Pd²⁺ ions initially alone in their cage can migrate whereas those which are two per cage remain. Therefore the possibility for a NO molecule entering the sodalite cage to interact with two Pd²⁺ ions cannot be discarded (although six Pd²⁺ ions and six NO molecules were detected, the 1:1 stoichiometry cannot be taken for granted in view of the large and probably underestimated error on the population of NO molecules statistically distributed in a 1-Å radius sphere). Whatever the situation, it turns out that the NO molecules are bonded with Pd²⁺ in different environments (six Pd²⁺ ions in sodalite and supercage units, respectively) and this strongly supports assumption (b). This hypothesis is further supported by the higher sensitivity of the ir band at 1865 cm⁻¹ compared to that at 1780 cm⁻¹ when the sample is evacuated or contacted with H₂ or CO. These results are well explained if it is assumed that the ir bands at 1865 and 1780 cm⁻¹ are due to nitrosyl complexes in the supercage and sodalite units, respectively. In fact the CO molecules do not enter the sodalite cages at room temperature (adsorption of CO on oxidized samples where most Pd²⁺ ions are at SI' sites lead only to very weak ν_{CO} bands while intense bands were observed after NO had induced the migration of half the Pd²⁺ ions to the supercages). It is also probable that H₂ molecules do not enter the sodalite cages at room temperature since the kinetic diameter of the H₂ molecule (2.89 Å)³⁴ is larger than the cage aperture (2.2 Å).

We suggest the ir bands at 1780 and 1865 cm⁻¹ be used as probes for the following: (i) Monitoring by their intensities the amount of Pd²⁺ ions in the supercage and sodalite units, respectively; this can prove a general property since the presence of two ν_{NO} bands has also been observed in CrY zeolite in the same spectral region.²³ (ii) Studying the accessibility of simple molecules in the supercage and sodalite units, respectively. As for CO, the ir results seem to point to the inaccessibility of H₂ into the sodalite unit at room temperature.

(b) *Structure of the Nitrosyl Complexes.* It is necessary now to discuss in more detail the frequencies of the two ν_{NO} bands. There are three possibilities to account for the lower frequency of the band attributed to NO bonded with Pd²⁺ in sodalite cages (1780 cm⁻¹) with respect to that corresponding to Pd²⁺ in supercages (1865 cm⁻¹):

(i) The difference may be due to different bonding strength between the framework oxygen atoms and the Pd²⁺ in sodalite and supercage units, respectively. It is highly probable that the Pd²⁺ ions are less strongly bonded to the framework oxygens in supercages than in SI' sites. This in turn would mean that the Pd²⁺ (SI') ions are more electron deficient than the Pd²⁺ in the supercages and consequently the back-donation for nitrosyl complex formation less efficient for Pd²⁺ (SI'). From this, one would then anticipate a higher ν_{NO} frequency for nitrosyl complexes in the sodalite cages than that for the complexes in the supercages, which contradicts our conclusion on ir bands assignments. Therefore, the difference in the frequencies of the two bands must be due to a different bonding scheme for the two types of nitrosyl complexes.

(ii) One may assume that a NO molecule interacts with two Pd²⁺ ions in the sodalite cages, since the ν_{NO} frequency of a bridged NO is lower than that of a linear NO. Thus in Ru₃(CO)₁₀(NO)₂,²⁴ the ν_{NO} frequency of NO bridging two Ru atoms is 1500 cm⁻¹, whereas linear NO groups absorb above 1800 cm⁻¹ in ruthenium nitrosyls.²⁵ However, the distance

TABLE III: Summary of Experimental Results

Sample	After activation	Contact with NO at room temp	Evacuation of NO
Oxidized samples	Color beige pink ν_{OH} bands (vw) Signal at $g_{\text{iso}} = 2.223$ (Pd^{3+}) 10.6 Pd^{2+} SI' (0.044)	Color beige pink ν_{OH} bands unchanged ν_{NO} 2025, 2175 cm^{-1} (w) ν_{NO} 1780–1865 cm^{-1} (vs) Signal at 2.223 disappears Signal at $g \approx 1.95$ ($\text{NO}\cdot$) 6.0 Pd^{2+} SI' (0.068) 13 N or O (in sodalite cages) 6 Pd^{2+} ions unlocated (probably in supercages)	Color beige pink At room temp ν_{OH} bands unchanged ν_{NO} 2025, 2175 cm^{-1} disappear slowly Signal at $g_{\text{iso}} = 2.223$ (Pd^{3+}) reappears Signal at $g \sim 1.95$ ($\text{NO}\cdot$) disappears At 200 °C ν_{NO} 1865 cm^{-1} disappears At 300 °C ν_{NO} 1780 cm^{-1} disappears Color beige pink
Samples reduced with hydrogen at room temp and then evacuated at room temp	Color ash-grey $\nu_{\text{OH}} = 3540\text{--}3640$ cm^{-1} (m) $\delta_{\text{H}_2\text{O}} = 1640$ cm^{-1} (m) Signal at $g_{\perp} = 2.10$ \uparrow Pd^+ $g_{\parallel} = 2.33$ \downarrow Pd^+ 4 Pd^{2+} SI' (0.078) (sample AH25 ref 10) 1.5 Pd^{2+} SI' (0.052) Others as Pd(0) atoms in sodalite cages at random positions	Color beige pink ν_{OH} and $\delta_{\text{H}_2\text{O}}$ unchanged ν_{NO} 1795–1865 cm^{-1} (vs) Pd ⁺ signal disappears Signal at $g \approx 1.95$ ($\text{NO}\cdot$) 3.8 Pd^{2+} SI' (0.070) 7 N or O (in sodalite cages) 8 Pd^{2+} ions unlocated (probably in supercages)	At room temp = signal at $g \approx 1.95$ ($\text{NO}\cdot$) disappears At 200 °C $\delta_{\text{H}_2\text{O}}$ (1640 cm^{-1}), ν_{NO} (1865 cm^{-1}) disappear 9.2 Pd^{2+} SI' (0.043) 2.9 Pd^{2+} SI' (0.067) 5 N or O (in sodalite cages) At 350 °C ν_{NO} (1795 cm^{-1}) disappears Color beige pink
Samples reduced with hydrogen at 500 °C then evacuated at 500 °C	Color dark brown ν_{OH} 3540–3640 cm^{-1} (v.s.) 20-Å diameter Pd(0) crystallites occluded in the zeolite crystals	Color beige pink ν_{OH} 3540–3640 cm^{-1} decrease 2235–2210 cm^{-1} (w) (N_2O) ν_{NO} (1790–1865) cm^{-1} growing with time $\delta_{\text{H}_2\text{O}} = 1640$ cm^{-1} (m) ν_{NO} (1670 cm^{-1} decreasing with time) Signal at $g \approx 1.95$ ($\text{NO}\cdot$) Disappearance of Pd crystallites	Color beige pink At room temp signal at $g \approx 1.95$ ($\text{NO}\cdot$) disappears 2235–2210 cm^{-1} (N_2O) disappear At 200 °C ν_{NO} (1865 cm^{-1}) and $\delta(\text{H}_2\text{O})$ disappear At 350 °C ν_{NO} (1790 cm^{-1}) disappears Diffraction patterns similar to oxidized samples after activation (most of Pd^{2+} ions in SI')

between two Pd^{2+} (SI') ions in the sodalite cage is too large (5.64 Å) to expect a bridged nitrosyl group.

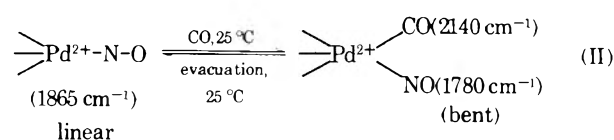
(iii) Earlier work on nitrosyl complexes has shown that in general the ν_{NO} frequency for a bent terminal group was lower than that of a linear terminal group.²⁶ In particular, in the complex $(\text{RuCl}(\text{NO})_2(\text{PPh}_3)_2)^+$, a ν_{NO} frequency of 1687 cm^{-1} was found for the bent terminal group and 1845 cm^{-1} for the linear terminal group.²⁶ This would suggest that the nitrosyl complexes within the supercage have a linear structure (1865 cm^{-1}) and those in the sodalite cages a bent structure (1780 cm^{-1}). The bent structure can also explain the fact that crystal structure analysis of sample I (refinement 1) detected scattering matter at $x = y = z = 0.11$ which would correspond to the N atom of a NO molecule but fails to detect electron density at $x = y = z = 0.135$ which would correspond to the oxygen atom of the molecule. In fact, with a bent geometry the oxygen atom would be outside the ternary axis and therefore could not be detected.

From the above discussion, it is likely that the lower frequency of NO bonded to Pd^{2+} ions in sodalite cage (1780 cm^{-1}) is due a Pd–NO bent structure, whereas the higher frequency of NO bonded to Pd^{2+} ions in supercages is due to a linear Pd–NO group.

(c) *Reactivity of the Nitrosyl Complexes.* In view of the previous conclusions, one can then discuss the reactivity of the nitrosyl complexes toward carbon monoxide. When CO

is contacted with nitrosyl complexes, it can react within the supercage units only following two possible ways: either replacing NO or adding as another ligand. Since the ν_{NO} bands are restored upon evacuation of CO at 25 °C, the former possibility can be ruled out. The most likely complex would then have two extraframework ligands CO and NO leading to bands at 2140 (ν_{CO}) and 1780 cm^{-1} (ν_{NO}), respectively.

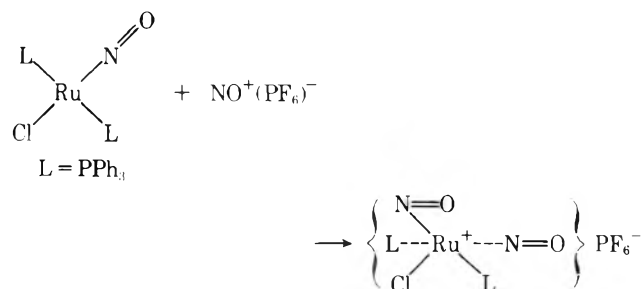
The addition of the CO ligand alters the original nitrosyl complex from a linear to a bent structure for the NO ligand, and this explains the broadening and the increase in intensity of the original ν_{NO} band at 1780 cm^{-1} along with the disappearance of the ν_{NO} band at 1865 cm^{-1} . Evacuation of excess CO restores the original bands so that the following scheme can be proposed:



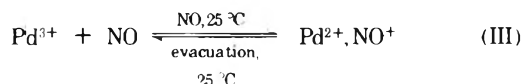
It is interesting to note that a similar complex has been observed but with two extraframework CO ligands in the same PdY zeolite.⁹

In coordination chemistry, an interconversion²⁷ bent–linear has been invoked to explain the number of ir bands; this

phenomenon was attributed to a modification of the coordination sphere according to the scheme:



(d) *Origin of the Ir Bands at 2025 and 2175 cm⁻¹.* In contrast to the bands at 1780 and 1865 cm⁻¹, the bands at 2025 and 2175 cm⁻¹ are of low intensity and are thus related to NO adsorption on Pd³⁺ ions present in small concentration in the oxidized sample.⁹ As, upon evacuation of excess NO, the Pd³⁺ EPR signal is restored and the 2025 and 2175 cm⁻¹ bands eliminated, the reversibility can be explained by the reaction



Thus, the ir bands at 2025 and 2175 cm⁻¹ can be attributed to NO⁺ ions. The vibration frequency ν_{NO} in the free molecule is 1876 cm⁻¹ and the N–O bond is strengthened by the loss of an electron to form a positive ion leading to frequencies in the 2100-cm⁻¹ range. An alternative explanation would be the formation of a Pd³⁺ NO complex which would be largely broadened because of electron–electron dipolar interaction. This can be ruled out because of the constant line width of the Pd³⁺ EPR signal throughout the cycle described by reaction III. Similar reversible reductions have been observed in Cu²⁺Y¹⁶ and Ni²⁺Y¹⁵ zeolites.

(e) *Paramagnetic Species.* Both the EPR signal at $g \approx 1.95$ and the purple color observed at 77 K are due to adsorbed NO radicals whose π orbital degeneracy has been removed by the zeolite crystal field. The EPR signal is a composite spectrum and the presence of hyperfine lines due to Al nuclei ($I = 5/2$, 100% natural abundance) and ¹⁰⁵Pd nuclei ($I = 5/2$, 22.6% natural abundance) shows that NO radicals can be adsorbed at both sites. The adsorption at Al³⁺ sites here is similar to that described earlier for NH₄Y zeolites.²⁸

The thermal behavior of the EPR signal at $g \approx 1.95$ is different from that of any of the ir bands and it is probable that the type of bonding involved is also different. In particular, because of the hyperfine interaction, the π^* electron of the NO radical is partly delocalized on Al nuclei and Pd nuclei and this type of bonding is weak since degassing the sample at 25 °C destroys the EPR signal. The EPR signal at $g \approx 1.95$ can be generated from samples exhibiting no Pd⁺ or Pd³⁺ EPR signals and one can thus conclude that the palladium ions which adsorb NO to give the $g \approx 1.95$ EPR signal are in a divalent state. The reversible broadening of the signal at $g \approx 1.95$ by gas phase oxygen further indicates that the corresponding radicals are located in the supercage unit.

Kasai and Bishop have shown that the zeolite crystal field could be modified by the formation of NO⁺ and NO₂⁻ ions produced by the disproportionation reaction of NO.¹⁵ This caused the EPR spectra of NO radicals, on standing at room temperature for several days, to become sharp and well defined. The fact, that, for PdY zeolite, the resolution is not time dependent shows that such reaction does not occur. This is

further substantiated by the ir and EPR results which show that it was not possible to detect, if disproportionation occurs, (i) any EPR signal due to NO₂ radicals even after uv irradiation at 77 K, and (ii) any ir band directly or indirectly connected with reaction products NO₂ and N₂O, in particular the two bands at 1400 cm⁻¹ observed by Kasai and Bishop for BaY zeolite.¹⁵

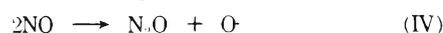
The present results are similar to those obtained with CuNaY zeolites with different copper exchange levels.¹⁶ The extent of NO disproportionation was shown to decrease when the copper content increased. It is probable that the palladium exchange level is too high for the reaction to occur in the present case.

II. *Samples Reduced by Hydrogen at Room Temperature.* Previous work¹⁰ has shown that when the PdY zeolite is reduced at room temperature the Pd(0) atoms produced remain in the sodalite cages. For reduction at higher temperature, these atoms migrate and form 20-Å Pd crystallites. The present investigation shows that if the reduced zeolite is contacted with NO and subsequently evacuated at 200 °C nearly all the palladium ions are found at SI' cations sites (sample III, Table I), i.e., those occupied in the oxidized samples (sample A). This clearly indicates that the Pd(0) atoms have been reoxidized into Pd²⁺ ions by NO. Simultaneously a color change of the reduced sample from ash-grey to beige pink, the characteristic color of the oxidized samples, is observed.

The oxidation process is also proved by the other techniques. When NO is adsorbed onto reduced samples, the EPR signal at $g \approx 1.95$ develops as in the oxidized samples. Moreover the same ir results as those observed for oxidized samples were obtained except that bands at 2025 and 2125 cm⁻¹ were no longer observed while, instead a small doublet near 2200 cm⁻¹ was detected in gas phase.

It is noteworthy that the reoxidation process produces only Pd²⁺ ions but not Pd³⁺ ions as the EPR signal of the latter is not observed nor are the associated ir bands at 2025 and 2175 cm⁻¹. The doublet near 2200 cm⁻¹ was assigned to gaseous or weakly adsorbed N₂O since such frequencies have been reported for N₂O adsorbed on NaA zeolite²⁹ (2260 cm⁻¹) and on CaY and HY zeolite¹⁴ (2250 and 2200 cm⁻¹). Mass spectrometry data (Table II) also prove the formation of N₂O.

The whole set of results points to a reoxidation process of Pd atoms into Pd²⁺ ions. The mechanism is certainly complex because of the different palladium oxidation states involved, however, the detection of N₂O both by ir (small doublet near 2200 cm⁻¹) and mass spectrometry shows that NO decomposes according to the following reaction:



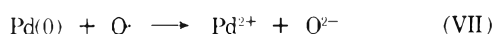
There is strong evidence that the O· species is the oxidizing agent for the EPR results show that N₂O along does not react at 25 °C with reduced samples since it has no effect on the Pd⁺ EPR signal nor does it alter their ash-grey color. Moreover, the possibility of a disproportionation reaction on reduced samples can be ruled out in view of the EPR results: NO₂ adsorbed on reduced samples leads to an EPR signal due to NO₂ radicals while upon NO adsorption no such signal is observed even after uv irradiation at 77 K. The failure to detect O₂ in the gas phase products and NO₂ by EPR demonstrates that the processes



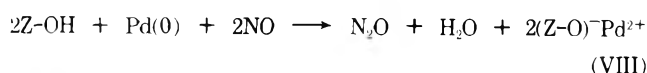
and



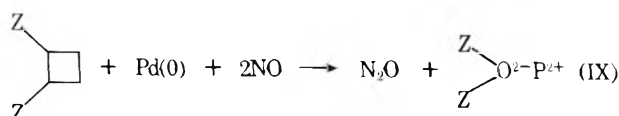
do not take place and that the O· species react instead with Pd⁺ ions and Pd(0) atoms following the reaction:



The O²⁻ ions produced in reaction VII do not remain bonded to the Pd²⁺ ions as an extraframework anion because the NO molecules subsequently bonded to these ions would have different frequencies than those observed on oxidized samples. They either react with the H⁺ formed during reduction to yield an H₂O molecule or fill an oxygen framework vacancy so that the overall reoxidation process would be



or



where Z represents the zeolite framework and the square an oxygen vacancy.

III. Samples Reduced by Hydrogen at Higher Temperatures. Once the reoxidation process of Pd atoms by NO was established, it was interesting to know what would happen to samples reduced at higher temperatures and containing no longer atomically dispersed palladium but 20-Å crystallites. Surprisingly enough, the x-ray, ir, and EPR results point to a reoxidative dissolution of the crystallites back into Pd²⁺ ions at room temperature. This astonishing reversibility is directly observed by x-ray diffraction: after 2 days of contact with NO, it is no longer possible to detect any crystallite; moreover the SI' sites are reoccupied by Pd²⁺ ions after NO has been pumped off at 200 °C.

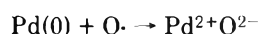
The reoxidation process, as earlier, is also shown by the following: (i) the color change from dark brown to bright beige pink, the characteristic color of oxidized samples; (ii) the presence of bands at 1785–1865 cm⁻¹ due to Pd²⁺ nitrosyl complexes and of the doublet near 2200 cm⁻¹ attributed to N₂O; the formation of N₂O shows that the oxidative process of Pd crystallites is the same whatever the reduction temperature; (iii) the transformation of the inverted signal into the normal EPR signal due to a change in the coordination of Pd²⁺ ions for reduction temperatures of about 150 °C; (iv) the disappearance of the normal EPR signal due to Pd⁺ ions when present (i.e., for reduction temperatures lower than 150 °C) and then the formation in any case of the EPR signal at *g* ≈ 1.95 due to Pd²⁺ NO radicals. The EPR results suggest that for reduction temperatures higher than 150 °C, the oxidation of Pd crystallites back into Pd²⁺ ions does not involve the production of Pd⁺ ions as an intermediate step or if so, they escape observation by EPR, probably because of their short lifetime.

At this point, the various steps of the reoxidative process must be discussed. When NO is adsorbed on Pd crystallites, the first step is the formation of Pd-NO species. Although organic nitrite compounds of the type R-O-NO present bands near 1700 cm⁻¹,³⁰ the band at 1680 cm⁻¹ could be attributed to NO bonded to palladium metal; in fact, the ν_{NO} frequency of nitric oxide decreases with the atom oxidation state. For instance, NO adsorbed on Pt²⁺ ions in platinum loaded zeolites³¹ gives bands at 1905 cm⁻¹ whereas NO chemisorbed on platinum metal exhibits band near 1800 cm⁻¹.³² The rapid decrease of the band near 1680 cm⁻¹ is correlated to the increase of the 1785- and 1865-cm⁻¹ bands. This indicates that

the Pd²⁺ nitrosyl complexes are formed at the expense of the Pd crystallite atoms. As in the case of the samples reduced at room temperature, several successive reactions can be postulated to explain the oxidation of palladium: decomposition of NO

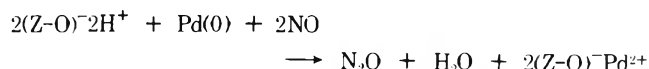


oxidation of Pd(0)



formation of Pd²⁺ nitrosyl complexes and migration of these species to neighboring zeolite cages; reaction of oxygen anion, formed during the oxidation of Pd(0) with zeolite protons. This reaction is proved by the decrease of bands due to hydroxyl groups and by the formation of water.

Therefore, the overall reoxidation process of Pd crystallites is



Conclusion

Besides the interest of showing various structural aspects of the chemistry of Pd²⁺ ions in zeolite, this work demonstrates that very unusual oxidation–reduction processes may occur with metal supported on zeolites. There are two important implications in the results of NO action on Pd atoms or crystallites: (a) NO can be reduced in N₂O, it acts as oxidant and gives harmless products, (b) palladium can be reoxidized to such an extent that all the metal atoms are redispersed as cations on the support.

While implication (a) has obvious practical interest for the elimination of NO in automobile exhaust, implication (b) may prove to be very important as far as aging of catalysts is concerned.

The behavior of palladium in zeolite seems very different from that described by Dunken and Hobert³³ in the study of the interaction of NO with silica supported palladium where no oxidation nor dissolution of metal was observed. Several properties of zeolites could account for this unique behavior: (i) palladium metal is more reactive toward NO because of its high state of dispersion, particularly in the case of reduction by H₂ at 25 °C; (ii) acid–base reactions can easily occur in zeolites; thus, oxygen anions produced during the reaction can react with the acid protons or vacancies of the zeolite; (iii) complex cations can readily migrate in the porous lattice and be fixed on the framework.

References and Notes

- (1) (a) M. L. Unland, *J. Phys. Chem.*, **77**, 1952 (1973); (b) T. P. Kobylinski and B. W. Taylor, *J. Catal.*, **33**, 376 (1974).
- (2) (a) M. Shelef and J. T. Kummer, *Chem. Eng. Prog., Symp. Ser.*, **67**, No. 155, 74 (1971); M. Shelef, *Catal. Rev. Sci. Eng.*, **11**, 1 (1975); (b) J. Blanco and J. Soria, *Quim. Ind.*, **19**, 23 (1973); (c) F. G. Dwyer, *Catal. Rev.*, **6**, 261 (1972).
- (3) J. H. Lunsford, *Adv. Catal.*, **22**, 265 (1972).
- (4) L. M. Roev and A. N. Terenin, *Opt. Spektrosk.*, **7**, 756 (1959).
- (5) W. E. Addison and R. M. Barrer, *J. Chem. Soc.*, 757 (1955).
- (6) G. W. Poling and R. P. Eischens, *J. Electrochem. Soc.*, **113**, 218 (1966).
- (7) K. J. Laidler, "Catalysis", Vol. 1, P. H. Emmet, Ed., Reinhold, New York, N.Y., 1954, p 149.
- (8) C. Naccache, J. F. Dutel, and M. Che, *J. Catal.*, **29**, 179 (1973).
- (9) C. Naccache, M. Primet, and M. V. Mathieu, *Adv. Chem. Ser.*, **No. 121**, 266 (1973).
- (10) P. Gallezot and B. Imelik, *Adv. Chem. Ser.*, **No. 121**, 66 (1973).
- (11) M. Che, J. F. Dutel, and M. Primet, "Molecular Sieves", J. B. Uytterhoven, Ed., Leuven University Press, 1973, p 394.
- (12) P. Gallezot, Y. Ben Taarit, and B. Imelik, *J. Catal.*, **26**, 481 (1972).

- (13) P. Gallezot, Y. Ben Taarit, and B. Imelik, *J. Phys. Chem.*, **77**, 2556 (1973).
- (14) C. C. Chao and J. H. Lunsford, *J. Am. Chem. Soc.*, **93**, 71 (1971).
- (15) P. H. Kasai and R. J. Bishop, Jr., *J. Am. Chem. Soc.*, **94**, 5560 (1972).
- (16) C. Naccache, M. Che, and Y. Ben Taarit, *Chem. Phys. Lett.*, **13**, 109 (1972).
- (17) M. V. Mathieu and P. Pichat, "La Catalyse au Laboratoire et dans l'Industrie", Masson, Paris, 1967, p 319.
- (18) L. H. Little, "Infrared Spectra of Adsorbed Species", Academic Press, London, 1966, p 84; N. G. Connelly, *Inorg. Chim. Acta Rev.*, **1**, 47 (1972).
- (19) Y. Ben Taarit, C. Naccache, and B. Imelik, *J. Chim. Phys.*, **70**, 728 (1973).
- (20) A. Lubezky and M. Folman, *Trans. Faraday Soc.*, **67**, 3110 (1971).
- (21) C. C. Chao and J. H. Lunsford, *J. Am. Chem. Soc.*, **93**, 6794 (1971).
- (22) (a) A. Zecchina, E. Garrone, C. Morterra, and S. Coluccia, *J. Phys. Chem.*, **79**, 978 (1975); (b) E. Garrone, G. Ghiotti, S. Coluccia, and A. Zecchina, *ibid.*, **79**, 984 (1975).
- (23) C. Naccache and Y. Ben Taarit, *J. Chem. Soc., Faraday Trans. 1*, **69**, 1475 (1973).
- (24) J. R. Norton, J. P. Collman, G. Dolcetti, and W. T. Robinson, *Inorg. Chem.*, **11**, 382 (1972).
- (25) D. M. Adams, "Metal Ligand and Related Vibrations", Edward Arnold, London, 1967, p 292.
- (26) F. A. Cotton and G. Wilkinson, "Advanced Inorganic Chemistry", Interscience, New York, N.Y., 1972, p 716.
- (27) J. P. Collman, P. Farnham, and G. Dolcetti, *J. Am. Chem. Soc.*, **93**, 1788 (1971).
- (28) J. H. Lunsford, *J. Phys. Chem.*, **72**, 4163 (1968).
- (29) E. Cohen de Lara and J. Vincent Geisse, *J. Phys. Chem.*, **76**, 945 (1972).
- (30) P. Tarte, *J. Chem. Phys.*, **20**, 1570 (1952).
- (31) M. Primet, unpublished results.
- (32) M. Primet, J. M. Basset, E. Garbowski, and M. V. Mathieu, *J. Am. Chem. Soc.*, **97**, 3655 (1975).
- (33) H. Dunken and H. Hobert, *Z. Chem.*, **3**, 398 (1963).
- (34) D. W. Breck, "Zeolite Molecular Sieves", Wiley, New York, N.Y., 1974, p 636.

Solute-Solvent Interactions in Water-*tert*-Butyl Alcohol Mixtures. 7. Enthalpies of Transfer for LiCl and HCl as Obtained through Dilution of an Aqueous Concentrated Electrolyte Solution in Hydroalcoholic Media

Yvon Pointud, Jean-Pierre Morel, and Jean Juillard*

Laboratoire d'Etude des Interactions Solutés-Solvants, Université de Clermont,
B.P. 45, 63170-Aubière, France (Received March 16, 1976)

Publication costs assisted by the Université de Clermont

Enthalpies for the process of transferring Li^+ , Cl^- and H^+ , Cl^- from water to mixtures containing up to 40% of *tert*-butyl alcohol are reported. They are derived from experimental heats of dilution of an aqueous concentrated solution of the electrolyte, both in pure water and in hydroalcoholic mixtures. Corresponding equations are obtained from classical thermodynamics of solution. It is shown that the enthalpies of transfer are related to experimental enthalpies, relative molal enthalpies of water, and dilution enthalpies in the two media. Data thus obtained are discussed in terms of structure of the water-*tert*-butyl alcohol mixtures.

Introduction

Enthalpies of transfer of electrolytes from one solvent to another are generally obtained by comparing enthalpies of solution in the two solvents. Such a method can only be employed in the case of dry solid electrolytes sufficiently soluble in the two solvents to obtain noticeable thermic effects. Recently, the reverse method in which enthalpies of transfer are derived from enthalpies of precipitation of insoluble compounds has been proposed and developed by Bright and Jezorek.¹

As far as gaseous solutes are concerned direct calorimetric measurements of enthalpies of solution although possible² are rather difficult and transfer enthalpies are generally obtained from Gibbs free energy changes with temperature.

In the course of a continuing study³ on thermodynamic quantities related to the transfer process of electrolytes from water to water-*tert*-butyl alcohol (TBA) mixtures, it appeared useful to record enthalpies of transfer of both a gaseous electrolyte (HCl) and an hygroscopic solid electrolyte (LiCl). Therefore the dilution of a concentrated aqueous electrolyte solution into both water and water-alcoholic solvents has been considered. Using a formal thermodynamic treatment it can

be shown that enthalpies of transfer can be derived from the experimental enthalpies thus obtained, changes in partial molal enthalpies of water, and dilution enthalpies in the two media. Such a treatment is here presented in the first part of this paper. This method is thus applied to the determination of the transfer of HCl and LiCl from water to water-TBA media (with a TBA content varying from 10 to 40 wt %).

Data concerning the other alkali metal have been reported earlier.⁴ All these results concerning thermodynamic functions of transfer (G , H , S) can then be considered.

Experimental Section

Heat measurements were performed using an LKB solution calorimeter (Type 8 700). The general experimental procedure has been described elsewhere.⁵ Ampoules containing weighed amounts (500 mg) of a stock aqueous solution of HCl or LiCl were crushed into 100 ml of either the mixed solvent or pure water. Final concentrations thus obtained are of the order of 2×10^{-2} mol kg^{-1} .

KCl and LiCl concentrations in stock solutions are determined through conductometric titration of a chloride ion by silver nitrate. HCl stock solutions have been prepared from

a Merck "titrisol" and their concentrations checked through precise indicator titration.

Purification of both solvents (water and TBA) has been done as previously reported.⁴ Solvents properties used in the calculations have been tabulated in a former paper.⁴

Theoretical

Small amounts of a concentrated aqueous solution of the electrolyte were poured into both water (process A) and the hydroorganic mixtures (process B). Process A is classical and well defined; it is a dilution. Process B is, on the contrary, more complicated since a change in the composition of the solvent media also occurs. In order to establish rigorously the relationship between the experimental heats and the standard enthalpy of transfer, we use the mathematical formalism relative to the functions of three variables, since a ternary mixture is here involved. At constant temperature and pressure the state of the system is defined by the number of moles of the three components: water, cosolvent, and electrolytes, n_w , n_s , n_e , respectively. The intensive nature of the partial molar quantities, which are homogeneous functions of the zero degrees, allows the use of the reduced variables

$$\frac{n_w}{n_w} = 1, \quad \frac{n_s}{n_w} = r, \quad \text{and} \quad \frac{n_e}{n_w} = \rho$$

that is to say, the molar ratio relative to water. The enthalpy of the system is then

$$H(n_w, n_s, n_e) = n_w \bar{H}_w(1, r, \rho) + n_s \bar{H}_s(1, r, \rho) + n_e \bar{H}_e(1, r, \rho) \quad (1)$$

The infinitely diluted state of the solute is noted as by the superscript θ . So, the expected standard enthalpy of transfer is

$$\Delta \bar{H}_t^\theta = \bar{H}_e^\theta(1, r, 0) - \bar{H}_e^\theta(1, 0, 0)$$

Process B

The aqueous concentrated solution of composition $(1, 0, \rho_i)$ which contains n_w moles of water and n_e moles of solute is poured into an initial mixture of composition $(1, r_i, 0)$ which contains N_w moles of water and N_s moles of cosolvent. A ternary mixture $(1, r_f, \rho_f)$ which contains $(N_w + n_w)$ moles of water, N_s moles of cosolvent, and n_e moles of solute is then obtained.

Under these conditions, the experimental enthalpy per mole of solute is

$$\begin{aligned} \Delta \bar{H}_B = & \left(\frac{n_w + N_w}{n_e} \right) \bar{H}_w(1, r_f, \rho_f) + \frac{N_s}{n_e} \bar{H}_s(1, r_f, \rho_f) \\ & + \bar{H}_e(1, r_f, \rho_f) - \frac{n_w}{n_e} \bar{H}_w(1, 0, \rho_i) - \bar{H}_e(1, 0, \rho_i) \\ & - \frac{N_w}{n_e} \bar{H}_w(1, r_i, 0) - \frac{N_s}{n_e} \bar{H}_s(1, r_i, 0) \quad (2) \end{aligned}$$

For the infinite dilution of the solute in the final mixture ($\rho \rightarrow 0$), the enthalpy per mole of solute becomes

$$\begin{aligned} \Delta \bar{H}_B^\theta = & \frac{1}{\rho_i} [\bar{H}_w(1, r_f, 0) - \bar{H}_w(1, 0, \rho_i)] \\ & + [\bar{H}_e^\theta(1, r_f, 0) - \bar{H}_e(1, 0, \rho_i)] \\ & + \frac{N_w}{n_e} [\bar{H}_w(1, r_f, 0) - \bar{H}_w(1, r_i, 0)] \\ & + \frac{N_s}{n_e} [\bar{H}_s(1, r_f, 0) - \bar{H}_s(1, r_i, 0)] \quad (3) \end{aligned}$$

The difference between these two enthalpies can be identified as the integral heat of dilution for the solute in the mixture of composition $(1, r_f, 0)$:

$$\begin{aligned} \Delta \bar{H}_B - \Delta \bar{H}_B^\theta = & \frac{n_w + N_w}{n_e} [\bar{H}_w(1, r_f, \rho_f) - \bar{H}_w(1, r_f, 0)] \\ & + \frac{N_s}{n_e} [\bar{H}_s(1, r_f, \rho_f) - \bar{H}_s(1, r_f, 0)] \\ & + [\bar{H}_e(1, r_f, \rho_f) - \bar{H}_e^\theta(1, r_f, 0)] \\ = & -\Delta \bar{H}_{\text{dil}}[(1, r_f, \rho_f) \rightarrow (1, r_f, 0)] \quad (4) \end{aligned}$$

Process A

The aqueous concentrated solution of composition $(1, 0, \rho_i)$ which contains n_w^* moles of water and n_e^* moles of solute is here poured into N_w^* moles of water.

The experimental molar enthalpy is thus

$$\Delta \bar{H}_A = \Delta \bar{H}_A^\theta - \Delta \bar{H}_{\text{dil}}[(1, 0, \rho_i^*) \rightarrow (1, 0, 0)] \quad (5)$$

and the molar enthalpy of the process at infinite dilution:

$$\begin{aligned} \Delta \bar{H}_A^\theta = & (1/\rho_i) [\bar{H}_w(1, 0, 0) - \bar{H}_w(1, 0, \rho_i)] \\ & + [\bar{H}_e^\theta(1, 0, 0) - \bar{H}_e(1, 0, \rho_i)] \quad (6) \end{aligned}$$

Enthalpy of Transfer. The combination of the previous equations yields

$$\begin{aligned} \Delta \bar{H}_B + \Delta \bar{H}_{\text{dil}}[(1, r_f, \rho_f) \rightarrow (1, r_f, 0)] - \Delta \bar{H}_A \\ - \Delta \bar{H}_{\text{dil}}[(1, 0, \rho_i^*) \rightarrow (1, 0, 0)] = & \bar{H}_e^\theta(1, r_f, 0) \\ - \bar{H}_e^\theta(1, 0, 0) + (1/\rho_i) [\bar{H}_w(1, r_f, 0) - \bar{H}_w(1, 0, 0)] \\ & + \frac{N_w}{n_e} [\bar{H}_w(1, r_f, 0) - \bar{H}_w(1, r_i, 0)] \\ & + \frac{N_s}{n_e} [\bar{H}_s(1, r_f, 0) - \bar{H}_s(1, r_i, 0)] \quad (7) \end{aligned}$$

The first two terms of the right-hand side correspond to the standard enthalpy of transfer for the electrolyte from water to the final mixture. This enthalpy of transfer is therefore

$$\begin{aligned} \Delta \bar{H}_t^\theta = & \Delta \bar{H}_B - \Delta \bar{H}_A - \Delta \bar{H}_c + \Delta \bar{H}_{\text{dil}}(\text{mixture}) \\ & - \Delta \bar{H}_{\text{dil}}(\text{water}) \quad (8) \end{aligned}$$

where $\Delta \bar{H}_c$, the heat of dilution of n_w moles of water in $(N_w + N_s)$ moles of the mixture divided by the number of moles of solute n_e , represents the three last terms in eq 7. $\Delta \bar{H}_c$ can be obtained breaking ampoules of water in the mixture in such a way that the number of moles n_w , N_w , and N_s be identical (or as near as possible) with the number of moles used in process B.

If the electrolytes final concentrations are low enough, the molar enthalpies of dilution can both be calculated using the Debye-Hückel relationship. The corresponding complete equation has recently been established within the scope of the Bjerrum theory for 1-1 electrolytes fully dissociated.^{4,6}

Equation 8 is, as far as the physical meaning of its various terms is concerned, identical with an equation previously derived from the MacMillan-Meyer formalism during the study of the experimental process of mixing dilute solutions of electrolytes and nonelectrolytes (eq 11 in the paper by Desnoyers et al.⁷).

It is worth noting that if n_w is negligible as compared to N_w , the last two terms in eq 7 are then equivalent to

$$(1/n_e)[N_w d\bar{H}_w(1, r_i, 0) + N_s d\bar{H}_s(1, r_i, 0)]$$

TABLE I: Relative Molal Enthalpy of Water [$\bar{H}_w(\text{mixture}) - \bar{H}_w(\text{water})$] in J mol^{-1}

X^a	$-\bar{L}_w^b$	$-\bar{L}_w^c$	X^a	$-\bar{L}_w^b$	$-\bar{L}_w^c$
5	11	8	25	647	636
10	67	96	30	711	703
15	242	243	35	750	736
20	502	506	40	777	761

^a Weight percent of TBA. ^b Our data. ^c Interpolated from ref 8 by H. Gillet, L. Avedikian, and J. P. Morel, *Can. J. Chem.*, **53**, 455 (1975).

TABLE II: Comparison of Transfer Enthalpies for K^+ , Cl^- from Water to TBA-Water Mixtures as Obtained through Different Methods (ΔH_t^θ , kJ mol^{-1})

X^a	b	c	X^a	b	c
10	2.82	2.77	30	8.72	8.31
20	7.72	7.60	40	7.64	7.27

^a X is the weight percent of TBA. ^b Previous data from heats solution of the solid electrolyte. ^c These measurements.

TABLE III: Enthalpies of Transfer for H^+ , Cl^- and Li^+ , Cl^- from Water to Water-TBA Mixtures

X^a	$\text{H}^+, \text{Cl}^-^b$	$\text{Li}^+, \text{Cl}^-^b$	X^a	$\text{H}^+, \text{Cl}^-^b$	$\text{Li}^+, \text{Cl}^-^b$
5	1.31	0.91	25	1.99	5.96
10	2.58	1.81	30	0.72	5.87
15	3.62	3.36	35	-0.72	5.53
20	3.38	4.79	40	-1.99	5.01

^a Weight percent of TBA. ^b ΔH_t^θ in kJ mol^{-1} .

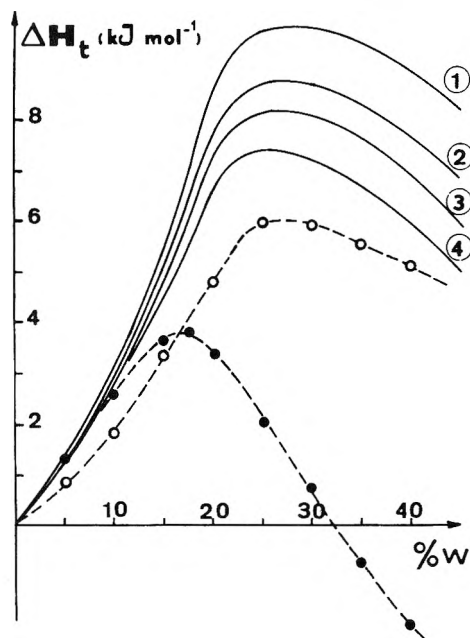


Figure 1. Enthalpy of transfer from water to water-TBA mixtures: NaCl, 1; KCl, 2; RbCl, 3; CsCl, 4, from ref 4; LiCl (O), and HCl (●) this work.

which is null in accordance to the Gibbs-Duhem relationship. It yields

$$\Delta \bar{H}_c \approx \frac{1}{\rho_i} [\bar{H}_w(\text{water}) - \bar{H}_w(\text{mixture})] = -\frac{\bar{L}_w}{\rho_i}$$

TABLE IV: Enthalpies of Transfer for H^+ , Cl^- following Various Authors ΔH_t^θ (kJ mol^{-1})

X^a	Das ^b	Roy ^c	Our data
10	6.96	3.18	2.6
20	7.32	5.49	3.4
40	4.18	0.99	-2.0

^a Weight percent of TBA. ^b Calculated from ΔG_1 and ΔS_1 given in ref 12. ^c From ref 11.

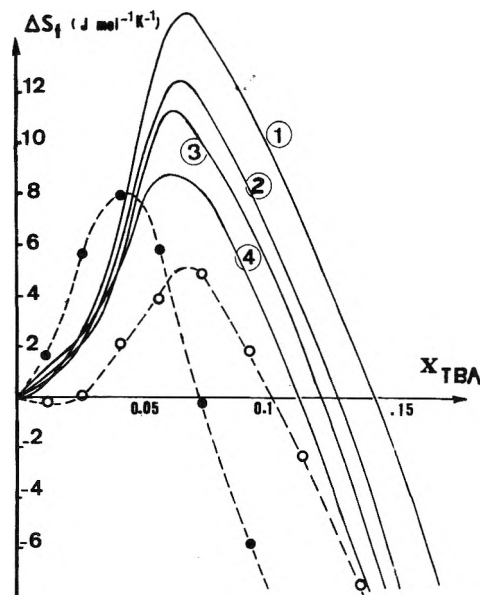


Figure 2. Entropies of transfer in the molal scale (same notations as in Figure 1).

Then, if the relative molal enthalpy \bar{L}_w is known (generally using the same approach) $\Delta \bar{H}_c$ can be calculated using this approximation, which is justified for the experimental process involved here.

Results and Discussion

In Table I are summarized data concerning changes of partial molal enthalpies of water when going from water to water-TBA. These results have been obtained from dilution of water in the mixtures. They agree fairly well with previous values calculated by Kentamaa⁸ from heat of mixing of water and TBA. Since, the method used here is expected to be more precise and has the advantage to be coherent with the following experiments, these new data will be preferred in the forthcoming calculations.

Enthalpies of transfer of KCl from water to some TBA mixtures have been previously derived from enthalpies of solution in these media.⁴ As a test of the method proposed here, new values were recorded. As can be seen in Table II, they compare favorably to the previous ones, discrepancies being at worst 0.4 kJ.

Experimental heat measurements for dilution of LiCl and HCl concentrated aqueous solutions in water and water-TBA mixtures are available as supplementary material to this paper. (See paragraph at end of text regarding supplementary material.) Only standard enthalpies of transfer estimated as described in the theoretical part are given in Table III. Their variations vs. the TBA content are shown in Figure 1 in addition to former results concerning Na, K, Rb, and CsCl in the same media.

Using Gibbs free energies of transfer of LiCl^9 and HCl^{10} in the same media, obtained from galvanic cell measurements, entropies of transfer have been calculated and are shown in Figure 2. Such entropies have been estimated for HCl, by two groups of authors,^{11,12} from the temperature coefficient of the standard potential of the $\text{Ag}|\text{AgCl}$ electrode in water-TBA mixtures. The reported ΔH are compared to our values in Table IV. Great discrepancies are observed. As a matter of fact, ΔS values obtained from ΔG at various temperatures are very sensitive to small variations of ΔG . In support of this opinion it must be noted that both Roy¹¹ and Bose¹² using the same standard potential data recorded by Roy obtain quite different values for the enthalpies of transfer. Therefore, it is our feeling that both of these results are in error. In this perspective, a systematic comparison of data obtained by our method for HCl to previous ΔH derived from galvanic cell in various hydroorganic mixtures is underway.

From Figures 1 and 2 it appears that the behavior of LiCl in water-TBA of both enthalpies and entropies of transfer are situated at 0.08 mole fraction of TBA (27 wt %). With the exception of the media richer in water ($x < 0.04$), the importance of the effect of transferring an alkali metal ion from water to water-TBA increases following the sequence $\text{Li}^+ < \text{Cs}^+ < \text{K}^+ < \text{Na}^+$. This order, observed here for enthalpies and entropies, has already been noted for Gibbs free energies,⁹ molar volumes, and heat capacities.¹³ We are working on qualitative and quantitative models able to explain all the thermodynamic property changes of these solutes in these media. More extensive discussion is thus delayed and will appear in a future paper.

As far as the transfer of HCl is concerned, it is worthwhile to note that the nature of the effects is quite different from those observed for alkali metal chlorides. Transfer entropies

as well as enthalpies are at maximum for a mole fraction of *t*-BuOH of 0.05 which is supposed to correspond to a maximum structuration of the TBA mixtures, a model which is supported by some thermodynamic and spectroscopic arguments.¹⁴⁻¹⁶

Supplementary Material Available: Additional experimental heat data for dilution of LiCl and HCl concentrated aqueous solutions in water and water-TBA mixtures (2 pages). Ordering information is available on any current masthead page.

References and Notes

- (1) L. L. Bright and J. R. Jezorek, *J. Phys. Chem.*, **79**, 800 (1975).
- (2) C. E. Vanderzee and J. D. Nutter, *J. Phys. Chem.*, **67**, 2521 (1963).
- (3) Part VI, N. Dollet and J. Juillard, *J. Solution Chem.*, **5**, 77 (1976).
- (4) Y. Pointud, J. Juillard, L. Avedikian, J. P. Morel, and M. Ducros, *Thermochim. Acta*, **8**, 423 (1974).
- (5) L. Avedikian, J. Juillard, J. P. Morel, and M. Ducros, *Thermochim. Acta*, **6**, 283 (1973).
- (6) J. Juillard, J. P. Morel, *C.R. Acad. Sci., Ser. C*, **277**, 825 (1973).
- (7) J. E. Desnoyers, G. Perron, L. Avedikian, and J. P. Morel, *J. Solution Chem.*, in press.
- (8) J. Kentamaa, E. Tommila, and M. Marti, *Ann. Acad. Sci. Fenn. AII*, **93**, 3 (1959).
- (9) Y. Pointud, J. Juillard, J. P. Morel, and L. Avedikian, *Electrochim. Acta*, **19**, 229 (1974).
- (10) J. P. Morel and J. Morin, *J. Chim. Phys.*, **67**, 2018 (1970).
- (11) R. N. Roy, W. Vernon, and A. L. M. Bothwell, *J. Chem. Soc. A*, 1242 (1971).
- (12) K. Bose, A. K. Das, and K. K. Kundu, *J. Chem. Soc., Faraday Trans. 1*, 1838 (1975).
- (13) L. Avedikian, G. Perron, and J. E. Desnoyers, *J. Solution Chem.*, **4**, 331 (1975).
- (14) M. C. R. Symons and M. J. Blandamer, "Hydrogen-Bonded Solvent Systems", A. K. Covington and P. Jones, Ed., Taylor and Francis, London, 1968, p 211.
- (15) E. K. Baumgartner and G. Atkinson, *J. Phys. Chem.*, **75**, 2236 (1971).
- (16) F. Franks and D. S. Reid, *Water: Compr. Treatise*, **2**, 356 (1975), and following.

Bonding in Silver Thionamides Studied by Infrared, Laser-Raman, and X-Ray Photoelectron Spectroscopy

L. J. Gerenser, M. G. Mason,* and P. J. Trotter

Research Laboratories, Eastman Kodak Company, Rochester, New York 14650 (Received January 19, 1976; Revised Manuscript Received July 8, 1976)

Publication costs assisted by the Eastman Kodak Company

Silver thionamide compounds have been structurally characterized. Laser-Raman, infrared, and x-ray photoelectron (ESCA) spectroscopies were employed in a complementary manner for analysis of tautomeric forms and bonding characteristics in these compounds. ESCA binding energies have been interpreted with the aid of CNDO and extended-Hückel molecular orbital calculations. Silver thionamides were shown to form mercaptide structures of the type $-\text{N}=\text{C}-\text{S}-$ -Ag. Thionamide silver nitrate complexes exhibited thione-silver ion coordination, $>\text{C}=\text{S}-$ -Ag⁺.

Introduction

Several spectroscopic studies of silver complexes utilizing the infrared method have been reported.¹⁻⁸ Thionamide silver complexes were found to be particularly difficult to characterize by means of ir alone.^{3,6} This difficulty is due primarily

to large uncertainties in assigning thione C=S vibrations⁹ in H-N-C=S containing ligands.¹⁰ In silver complexes of thionamides, the question arises whether an Ag- $-\text{N}-\text{C}=\text{S}$ complex is formed leaving the thione group intact,^{3,6} or whether silver may form a mercaptide complex of the structure $-\text{N}=\text{C}-\text{S}-$ -Ag. Since the precise structure and position

of these silver bonds are in doubt, we have attempted to characterize these molecular structures with the aid of the relatively new methods of laser-Raman and x-ray photoelectron spectroscopy (XPS) or ESCA. Results of this study show that laser-Raman spectroscopy is superior in determining thionamide tautomeric forms while ESCA provides direct evidence for silver-sulfur complexing.

The ESCA technique uses x-ray photoionization to measure binding energies of electrons in the individual atoms of the molecular system.¹¹ These binding energies may vary as the molecular environment is altered and such chemical shifts can be calculated with quite good accuracy from intermediate molecular orbital theories such as CNDO.¹² Binding energies, within a series of similar compounds, can be correlated with atomic charges by use of the "potential model" equation¹²

$$E_B^i = kq_i + V_i + l \quad (1)$$

E_B^i is the binding energy of a core level on atom i , relative to a chosen reference energy, q is the calculated charge on atom i , and k and l are empirical parameters determined by a least-squares fit of the experimental data to eq 1. The term V_i is referred to as the molecular potential and accounts for the electrostatic potential produced by the other charged atoms in the molecule. This potential has most commonly been calculated by a simple point-charge model in which

$$V_i = \sum_{j \neq i} q_j / R_{ij} \quad (2)$$

where R_{ij} is the interatomic distance between atoms i and j .¹² The atomic charges, q_j , were obtained from CNDO calculations¹³ and the R_{ij} values from crystallographic data or characteristic bond angles and distances.¹⁴

Calculations at this level are not possible for the silver complexes themselves. CNDO is, at best, restricted to atoms of the first and second rows of the periodic table.¹⁴ Therefore, we have used extended-Hückel (EH) calculations as a guide to the charge distribution and bonding in the silver complexes.

Experimental Section

The photoelectron spectra were recorded on a Hewlett-Packard 5950A ESCA spectrometer at about 100 K. When appropriate, the 1s lines from the ligand carbon atoms were used as references and assigned a binding energy of 284.6 eV. Alternatively, calibration was accomplished either by evaporation of a small amount of gold on the sample or physically mixing with graphite. The gold 4f_{7/2} line served as a standard with a binding energy of 84.1 eV. All spectra were stable with time and showed no indications of photolytic decomposition due to x-ray exposure. The Du Pont 310 curve resolver was used to determine binding energies of overlapping lines.

Raman spectra were excited at 6471 Å (270 mW) with a Spectra-Physics Model 165 krypton laser and were recorded on the Cary Model 82 Raman spectrometer. Spinning of the solid silver compounds combined with use of low-energy 6471-Å red excitation appeared to eliminate photolytic effects on most of these compounds. As an alternative method some silver compounds were run at low temperature using a liquid nitrogen cooled sample chamber. A Beckman IR-12 infrared spectrophotometer was used to obtain ir scans from 200 to 4000 cm⁻¹.

Silver compounds were formed by precipitation from stoichiometric solutions of AgNO₃ plus ligand in H₂O or in 50% aqueous ethanol. All compounds were verified as to correct stoichiometry by elemental analyses of Ag, C, H, N, and S.

TABLE I: The C=N Region for Compounds and Ions Investigated

	Structure	C=N region (1520–1580 cm ⁻¹)	
		Raman	Infrared
(1)		Blank	Blank
(1a)		1561 (w), 1522 (s) ^a	—
(1b)		1557 (s), 1526 (s)	1548 (shoulder)
(2)		Blank	Blank
(2a)		1540 (m) ^a	—
(2b)		1541 (m)	1540 (m)
(3)		Blank	Blank
(3a)		1564 (m) ^a	—
(3b)		1564 (m)	1562 (w)
(4)		1530 (m)	1540 (m)
(4a)		Blank	Blank
(5)		1558 (m)	(vw) ^b
(6)		1560 (m)	1560 (m-w)
(6a)		1557 (m)	(vw) ^b
(6b)		Blank	Blank

^a Ions run in aqueous NaOH at pH 12. ^b Very weak (vw) and difficult to locate.

Most of our studies were carried out on 1:1 silver:ligand compounds; other stoichiometries used are designated in the text and tables.

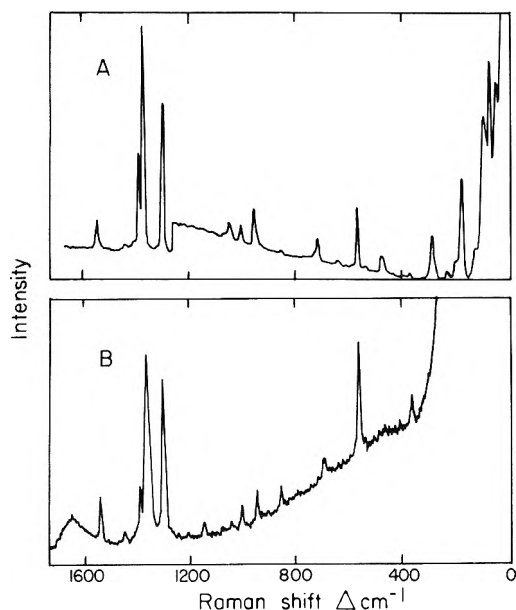
Results and Discussion

A. Silver Thionamide Complexes. In order to compare compounds of varying degrees of ring conjugation, we have examined 1:1 silver complexes formed from benzothiazole-

TABLE II: Raman Bands of Silver Salts Compared to Mercaptide Anions and Parent Ligands

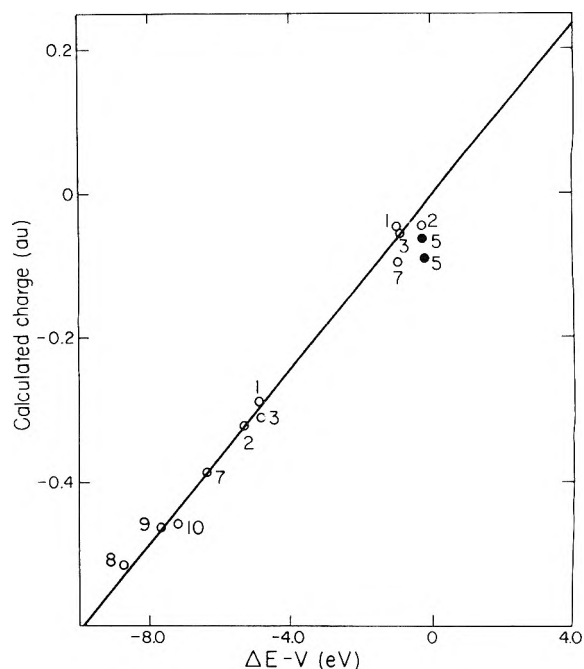
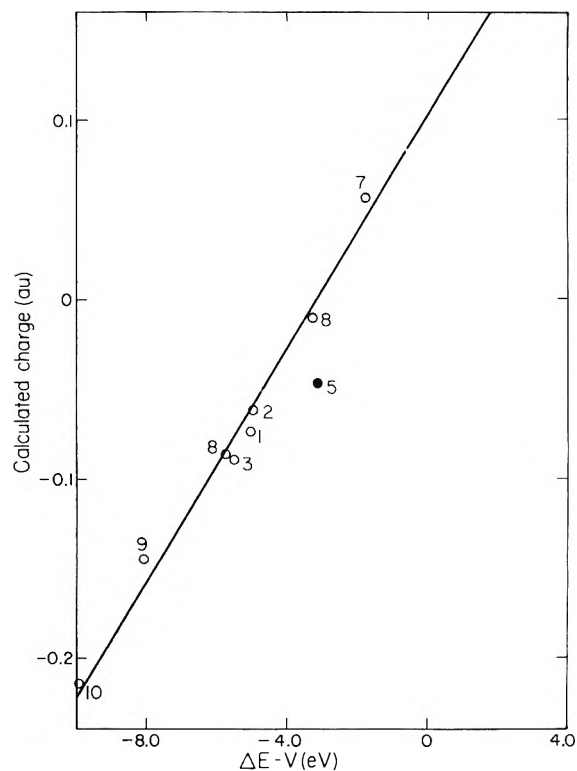
Compd	Main molecular Raman bands, cm^{-1}
1	(blank, C=N), ^a 1512w, 1468s, 1438m, 1375m, 1295s, 1258s, 1042s, 1000w, 935s, 707s, 653s, 591s, 435s
1a	1561(w-C=N), 1522s, 1458m, 1442m, 1313m, 927w, 713m, 575s, 433m
1b	1557(s-C=N), 1526s, 1455m, 1435m, 1306m, 940w, 713m, 580s, 443m
2	1602(s-C=C), (blank, C=N), ^a 1470s, 1385m, 1322m, 1265s, 1147m, 1059s, 679s, 555s, 463s
2a	1540(m-C=N), 1390m, 1361s, 1298s, 1000w, 943m, 850w, 688w, 558s
2b	1541(m-C=N), 1389m, 1371s, 1299s, 1000w, 948m, 855vw, 711w, 562s
3	1594m, (blank, C=N), ^a 1460m, 1320m, 1272m, 1255s, 1132m, 1077m, 1032m, 1014w, 708m, 608m, 502m, 397s
3a	1592m, 1564(m-C=N), 1457m, 1395vs, 1280s, 1247s, 1133s, (1022m, 1002m), 711s, 507s, 383m
3b	1593m, 1564(m-C=N), 1460m, 1408vs, 1281s, 1249s, 1136s, (1011s), 716s, 511s, 399m

^a The C=N region is 1520–1580 cm^{-1} for these ring structures.


Figure 1. Raman spectra of (A) the silver salt of 4-methyl-4-thiazoline-2-thione and (B) the ligand anion in basic solution.

2-thione, 4-methyl-4-thiazoline-2-thione, and thiazolidine-2-thione. Several N- and S-substituted model compounds were used in comparing known organic structures to those of the silver complex. Structures of the ligands and related model compounds are shown in Table I. These thionamides react with silver to eliminate the N-H proton and form sparingly water-soluble silver complexes.³⁻⁷

Infrared correlations of the main C=S vibration in structures related to thiazolidine-2-thione assign C=S to a strong band ranging from 1000 to 1200 cm^{-1} .^{9,10} Previous infrared studies of silver thiazolidine-2-thione have cited the presence of a strong band near the expected C=S position (1050 cm^{-1})⁹ as evidence for the thione^{3,6} form of the silver compound. However, utilizing the presence or absence of such thione

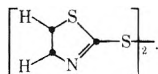

Figure 2. Correlation between calculated charge and measured S 2p binding energies. Numbers refer to those given in Tables I and IV. Least-squares fit gives $k = 16.8$, $l = -0.18$, and $\sigma = 0.31$. The structurally unique molecule 5 was not included in the least-squares analysis.

Figure 3. Correlation between calculated charge and measured N 1s binding energies. Numbers refer to those given in Tables I and IV. Least-squares fit gives $k = 31.2$, $l = -3.14$, and $\sigma = 0.36$. The structurally unique molecule 5 was not included in the least-squares analysis.

bands as an indication of silver complex structure is quite uncertain since many interfering absorptions^{9,10} may appear in this broad region. For example, model compounds 4, 5, and 6a (Table I) which have no C=S groups all have at least one

TABLE III: ESCA Binding Energies and Charges for Thionamides and Their Silver Complexes

Compd		Binding energy, eV						Calculated charge, au		
		N		S		=S		N	S	=S
		Calcd	Obsd	Calcd	Obsd	Calcd	Obsd			
1	HL	399.5	400.0	164.2	163.8	162.3	162.2	-0.07	-0.04	-0.29
	AgL		398.5		163.6		162.5			
	δ		-1.5		-0.2		+0.3			
2	HL	399.9	400.0	163.6	164.1	161.8	161.7	-0.06	-0.05	-0.32
	AgL		398.4		163.9		162.4			
	δ		-1.6		-0.2		+0.7			
3	HL	399.9	400.0	164.2	164.2	162.0	162.1	-0.09	-0.05	-0.31
	AgL		398.6		163.9		162.5			
	δ		-1.4		-0.3		+0.4			
5			398.3		164.0		164.0	-0.05 ^a	-0.06 ^a	-0.09 ^a

^a Actual molecule used in calculation was



strong band between 1000 and 1100 cm^{-1} which could be assigned to S-C-S stretching.¹⁵ Ring vibrations also occur in the same region.⁹ Another difficulty in assigning definite thione bands for thionamides arises from the presence of mixed vibrational modes involving C=S coupling to the N-C bond.^{16,17}

Raman spectra showing the presence or absence of C=N appear to indicate more reliably the tautomeric form present, as illustrated in Table I, and infrared spectra can often provide confirmation of C=N. Raman spectra of the anions (1a, 2a, and 3a, Table I) in aqueous solution at pH 12 also show C=N, indicating the mercaptide tautomeric form as shown. This confirms earlier evidence from ultraviolet spectra¹⁸ that anions from compounds such as 2 and 3 exist as mercaptides 2a and 3a (see Table I). Aqueous mercaptide spectra are compared with Raman bands of the silver complexes in Table II, and it is seen that the silver complexes match the mercaptide pattern. Bands from parent ligands are also listed in Table II for comparison. Figure 1 illustrates this analysis with spectra of the silver complex of 4-methyl-4-thiazoline-2-thione compared with that of its aqueous anion. Thus, this method of comparing silver complex spectra with C=N vibrations and Raman measurements of aqueous mercaptide ions has demonstrated that these silver complexes possess the mercaptide structure (-N=C-S⁻). This conclusion is contrary to that reached in earlier infrared work on silver plus thiazolidine-2-thione, wherein the hydrogen from the NH group was thought to be replaced by Ag, forming N-Ag with C=S intact.^{3,6}

The ESCA results are shown in Table III. The chemical shifts calculated from CNDO charges using 1 and 2 are shown graphically in Figures 2 and 3 for all silver complexing ligands considered in this work. The correlation between calculated and observed sulfur shifts is excellent. The poorest correlation is found for the structurally unique disulfide compound 5. The S 2p parameter $k = 16.8$ compares with the values of 14.1 determined from ab initio calculations of gross atomic charge¹⁹ and 14.0 from atomic calculations.²⁰ Similar correlation is found for the N 1s binding energies. The k value of 31.2 can be compared to the values of 31 determined by Stucky et al.²¹ for a series of gas phase compounds and 26 from the theoretical atomic calculations.²⁰

These calculations, while restricted to the ligands, are very useful in understanding the chemical shifts which occur in the silver complexes. In particular the large N 1s shift observed in the silver complexes might be interpreted as evidence of direct N-Ag coordination. However, a close examination of

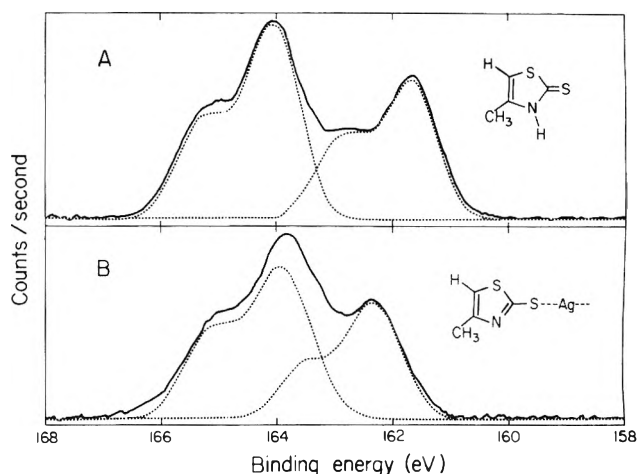


Figure 4. S 2p photoelectron spectra of (A) 4-methyl-4-thiazoline-2-thione and (B) its silver complex.

the chemical shifts, as predicted by CNDO calculations, shows that coordination most likely occurs at the thione sulfur. In analyzing the contributions of the various terms in eq 1 to the total binding energy, one sees that the N 1s values are determined primarily by the molecular potential V_i . The amide hydrogen is the dominant factor among the terms in the potential summation in eq 2, contributing about 4 eV to the total energy. It is easy, then, to understand why removal of this hydrogen can grossly affect the binding energy, even without direct N-Ag coordination. This effect is observed experimentally in the spectrum of the disulfide compound 5 listed in Table III. The N 1s binding energy for compound 5 is shifted relative to the monomer ligands to the same degree as in the silver complexes. In a contrary fashion, analysis of the calculated thione binding energy shows only a slight dependence on the amide hydrogen. Therefore, we conclude that the thione sulfur shifts shown in Table III and Figure 4 indicate direct Ag-S coordination. This agrees with extended-Hückel calculations which predict the mercaptide structure to be the most stable by 0.6 eV.

In summation the combined evidence from Raman spectra, ESCA, and molecular orbital calculations shows that the basic structural unit in the solid thionamide complexes is

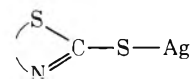
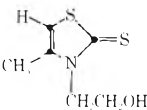
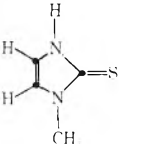
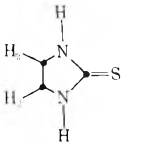
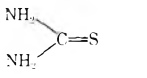
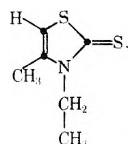


TABLE IV: ESCA Binding Energies and Charges for Thionamides and Their Silver Complexes

Structure		Binding energy, eV						Calculated charge, au		
		N		S		=S		N	S	=S
		Calcd	Obsd	Calcd	Obsd	Calcd	Obsd			
	L	400.8 ^a	400.5	163.5 ^a	164.1	161.7 ^a	161.7	+0.06 ^a	-0.10 ^a	-0.39 ^a
	AgLNO ₃ δ		400.7 +0.2		164.1 0		162.6 +0.9			
	L	398.9, 399.8	399.0, 399.8			161.3	161.1	-0.01, -0.09		-0.53
	Ag ₂ L ₃ (NO ₃) ₂ δ		399.2, 400.0 +0.2,+0.2				161.9 +0.8			
	L	398.9, 399.8	399.0, 399.8			161.2	161.1	-0.01, -0.09		-0.53
	AgL ₄ NO ₃ δ		399.2, 400.0 +0.2,+0.2				161.9 +0.8			
	L	399.7	399.2			162.0	161.9	-0.14		-0.46
	AgLNO ₃ δ		399.7 +0.5				162.6 +0.7			
	L	399.9	399.7			161.9	162.2	-0.21		-0.46
	AgL ₃ Cl δ		399.7 0				162.5 +0.3			

^a Calculated for the similar molecule



In view of the coordination tendencies of Ag, it seems reasonable to suggest a polymeric chain structure involving multiple S coordination. Silver thiocyanate has such a chain structure formed by S–Ag–N covalent bonds,²² and bis(thiourea)silver(I) chloride also exhibits a long polymeric chain of bridging S–Ag–S bonds.²³ This type of S–Mⁿ⁺–S bonding is also found in thiourea complexes with Mn²⁺, Co²⁺, Ni²⁺, Cd²⁺,²⁴ Pb²⁺,²⁵ and Cu⁺.²⁶ Such polymeric structures would account for the low solubility of the thionamide complexes, satisfy the coordination requirements of Ag, and not be inconsistent with any present experimental data. However, spectra presented here offer no direct evidence for or against any specific polymeric structure. Final determination of the exact crystal structure must await x-ray diffraction results.²⁷

B. Thionamide Silver Nitrate Complexes. In addition to the sparingly water-soluble silver complexes discussed in the previous section, we have also examined neutral thionamides which form soluble Ag⁺ complexes of the type Ag⁺_xL_y(NO₃)_z, without the elimination of H⁺. These complexes were examined in order to determine the effect of a blocking group on nitrogen. The ESCA and CNDO results for four such compounds are shown in Table IV and in Figures 2 and 3.

The ESCA spectra of the four ligands are all similar to those discussed in section A. The CNDO charge calculations show that both the thione sulfur and ring nitrogens have higher electron densities than in the ligands in section A. This redistribution of charge is caused by increased π bonding in the thione group and increased σ bonding between the nitrogens and the central carbon atom.

Upon complex formation, the thione sulfurs show binding energy shifts of the same degree as are observed for the ligands in section A. On the other hand, changes in N 1s binding energy are much smaller. This is to be expected since the immediate environment of the nitrogen atom has not been altered.

The coordination of Ag is easily satisfied in the 3:1 and 4:1 complexes. The 1:1 complexes would most likely form chains of the type suggested for the compounds in section A. Again, this would be consistent with the Ag–S–Ag bridging bonds formed in the thiourea complexes.²³

Conclusions

The combination of vibrational and photoelectron spectroscopies discussed here provides elucidation of structure and bonding in silver–organic complexes. CNDO calculations were used to determine charge distributions in the complexing ligands and show excellent correlation with measured S 2p and N 1s binding energies. For the class of thionamide–silver complexes discussed in section A, Raman spectra clearly show the –N=C–S tautomeric form by correlation with aqueous mercaptide –N=C–S[–] structures. Electron binding energies measured by ESCA corroborate this structure by comparison with several model compounds. Silver thione complexing (C=S–Ag⁺) was clearly indicated by ESCA binding energy shifts in thionamide–silver nitrate complexes.

Acknowledgments. We wish to thank R. C. Baetzold for his help with the molecular orbital calculations. Infrared spectra were run by T. F. Hall and R. Riley, and many of the silver

compounds were prepared by J. I. Cohen, R. A. LaRossa, and R. A. DeMauriac. We wish to thank J. W. Boettcher, D. L. Smith, A. H. Herz, D. D. Shiao, and Ms. T. J. Davis for many helpful discussions.

References and Notes

- (1) K. Nakamoto, "Infrared Spectra of Inorganic and Coordination Compounds", Wiley, New York, N.Y., 1963.
- (2) A. L. Geddes and G. L. Bottger, *Inorg. Chem.*, **8**, 802 (1969).
- (3) L. H. Little and R. H. Ottewill, *Can. J. Chem.*, **40**, 2110 (1962).
- (4) M. Tamura, H. Hada, J. Noguchi, and S. Hayashi, *J. Phys. Chem.*, **66**, 559 (1962).
- (5) W. I. Stephen and A. Townshend, *J. Chem. Soc. A*, 166 (1966).
- (6) L. H. Little, "Infrared Spectra of Adsorbed Species", Academic Press, New York, N.Y., 1966, Chapter 12.
- (7) A. Parentich, L. H. Little, and R. H. Ottewill, *Kolloid-Z. Z. Polym.*, **251**, 494 (1973).
- (8) A. Parentich, L. H. Little, and R. H. Ottewill, *J. Inorg. Nucl. Chem.*, **35**, 2271 (1973).
- (9) R. Mecke et al., *Chem. Ber.*, **90**, 957 (1957).
- (10) C. N. R. Rao and R. Venkataraghavan, *Spectrochim. Acta*, **18**, 541 (1962).
- (11) K. Siegbahn, C. Nordling, A. Fahlman, R. Nordling, K. Hamrin, J. Hedman, G. Johansson, T. Bergmark, S. E. Karlson, I. Lindgren, and L. Lindberg, "ESCA Atomic Molecular and Solid State Structure Studied by Means of Electron Spectroscopy", Almquist and Wiksells, Uppsala, 1967.
- (12) K. Siegbahn, C. Nordling, G. Johansson, J. Hedman, P. F. Heden, K. Hamrin, U. Gelius, T. Bergmark, L. O. Werme, R. Manne, and Y. Baer, "ESCA Applied to Free Molecules", Elsevier, New York, N.Y., 1969.
- (13) CNINDO, QCPE No. 141.1, Quantum Chemistry Program Exchange, University of Indiana, Bloomington, Ind.
- (14) J. A. Pople and D. L. Beveridge, "Approximate Molecular Orbital Theory", McGraw-Hill, New York, N.Y., 1970.
- (15) N. B. Colthup, L. H. Daly, and S. E. Wiberley, "Infrared and Raman Spectroscopy", Academic Press, New York, N.Y., 1964, p 409.
- (16) I. Suzuki, *Bull. Chem. Soc. Jpn.*, **35**, 1286, 1449, 1456 (1962).
- (17) C. N. R. Rao and C. C. Chaturvedi, *Spectrochim. Acta, Part A*, **27**, 520 (1971).
- (18) E. S. Stern and C. J. Timmons, "Electronic Absorption Spectroscopy in Organic Chemistry", St. Martin's Press, New York, N.Y., 1970, pp 229-231.
- (19) U. Gelius, B. Roos, and K. Siegbahn, *Chem. Phys. Lett.*, **4**, 471 (1970).
- (20) Reference 11, p 85.
- (21) G. D. Stucky, D. A. Matthews, J. Hedman, M. Klasson, and C. Nordling, *J. Am. Chem. Soc.*, **94**, 8009 (1972).
- (22) I. Lindqvist, *Acta Crystallogr.*, **10**, 29 (1957).
- (23) E. A. Vizzini, I. F. Taylor, and E. L. Amma, *Inorg. Chem.*, **7**, 1351 (1968).
- (24) M. Nardelli, L. Cavalca, and A. Braibanti, *Gazzetta*, **87**, 917 (1957); M. Nardelli, A. Braibanti, and G. Fava, *ibid.*, **87**, 1209 (1957).
- (25) M. Nardelli and G. Fava, *Acta Crystallogr.*, **12**, 727 (1959).
- (26) C. B. Knobler, Y. Okaya, and R. Pepinsky, *Z. Kristallogr.*, **111**, 385 (1959).
- (27) D. L. Smith and H. R. Luss have recently communicated to us the crystal structure of the 3:1 silver complex of 4-methyl-4-thiazoline-2-thione. Their results show covalent silver-thione sulfur bonding.

Luminescence of Yttrium(III), Lutetium(III), and Thorium(IV) Porphyrin Complexes

Louis A. Martarano, Ching-Ping Wong, William DeW. Horrocks, Jr., and Antonio M. Ponte Goncalves*

Department of Chemistry, The Pennsylvania State University, University Park, Pennsylvania 16802 (Received April 8, 1976)

Publication costs assisted by the Petroleum Research Fund

The luminescence of recently synthesized Y(III), Lu(III), and Th(IV) complexes of *meso*-tetraphenylporphyrin is reported. An unusual characteristic common to all three complexes is that they fluoresce from the second excited singlet state: $S_2 \rightarrow S_0$ (maximum ~ 425 nm). The quantum yield of this fluorescence is essentially the same for all three complexes (ϕ_f : 0.001, 0.001, 0.0004), even though the atomic number increases greatly from Y($Z = 39$) to Th($Z = 90$). This absence of heavy-atom effect indicates that the radiationless decay of S_2 proceeds primarily through internal conversion, presumably to S_1 . In contrast to the $S_2 \rightarrow S_0$ fluorescence, the quantum yield of the normal fluorescence, $S_1 \rightarrow S_0$ (maxima ~ 600 and ~ 650 nm), exhibits a clear heavy-atom effect (ϕ_f : 0.006, 0.001, ~ 0.0001). This trend is in agreement with previous evidence that the $S_1 \rightarrow S_0$ fluorescence in metalloporphyrins is internally quenched almost exclusively by intersystem crossing to the lowest triplet state. All three complexes phosphoresce strongly (ϕ_p : ~ 0.01 , ~ 0.02 , ~ 0.03), with lifetimes which decrease markedly with increasing atomic number of the metal ion (τ_p : 29, 2.8, ≤ 0.3 ms). The rate constants for spin-forbidden processes are estimated and the results are discussed. In particular, it is suggested that the apparent lack of heavy-atom effect in the comparison between the phosphorescences of the Zn(II) and Y(III) complexes may be due to a much larger deviation of Y(III) from the porphyrin plane, which results in a decreased metal-porphyrin interaction.

Introduction

The luminescence properties of porphyrin complexes with most metallic elements in the periodic table have been reported^{1,2} since the pioneering work of Allison and Becker³ more than a decade ago. Some of the very few remaining gaps are in group 3B, from which only the luminescence of Sc(III) porphyrins has been previously reported.⁴ The recent synthesis of lanthanide,⁵ yttrium, and thorium⁶ porphyrins has permitted us to explore further the luminescence of group 3B

porphyrin complexes. The interest of this type of porphyrin complex is twofold. First, lanthanide porphyrins are potentially valuable probes of heme proteins. The recent incorporation of Yb(III) mesoporphyrin IX into apomyoglobin indicates the feasibility and usefulness of such studies.⁷ Secondly, it will be shown that all three porphyrin complexes discussed in this paper fluoresce from the second excited singlet state, $S_2 \rightarrow S_0$. Although there are quite a few examples of strong $S_2 \rightarrow S_0$ emission,⁸⁻¹³ they are relatively rare considering the vast number of molecules known to fluoresce from the first excited

TABLE I: Absorption Spectrum Maxima (nm)^a

Porphyrin	B(0,0) ^b	Q(2,0)	Q(1,0)	Q(0,0)
YTPP(acac)	420	515	554	589
LuTPP(acac)	418	512	551	587
ThTPP(acac) ₂	419	510	551	591

^a In methanol at room temperature. ^b Soret band.

singlet state, $S_1 \rightarrow S_0$. The luminescence from S_2 becomes especially interesting in the light of recent reports of different photochemical behavior of S_1 and S_2 .^{14,15}

This paper is concerned with the fluorescence and phosphorescence of complexes of Y(III), Lu(III), and Th(IV) with *meso*-tetraphenylporphyrin (TPP): YTPP(acac), LuTPP(acac), and ThTPP(acac)₂, where (acac) designates the bidentate ligand, acetylacetonate. All three metal ions in these porphyrins are diamagnetic.¹⁶ The results are discussed in terms of the increased spin-orbit coupling (heavy-atom effect) in Y (atomic number 39) through Th (atomic number 90), and of its possible reduction because of deviations of the metal ions from the porphyrin plane. In the latter respect, a comparison is made between the Y(III) complex to the lighter (atomic number 30) and more closely planar Zn(II) complex.

Experimental Section

The preparation, purification, and characterization of YTPP(acac), LuTPP(acac), and ThTPP(acac)₂ were carried out as described elsewhere.^{5,6} Spectrophotometric grade methanol (Aldrich) was used as solvent in all room temperature measurements, and EPA (a 5:5:2 ether-isopentane-ethanol mixture) from Matheson Coleman and Bell was the solvent employed in the low temperature experiments. Successive dilutions were used in all experiments to ensure that the spectra were undistorted by reabsorption.¹⁷

Absorption spectra were obtained on a Cary 17 recording spectrophotometer. Fluorescence measurements were made on an Aminco-Bowman spectrophotofluorometer equipped with a Hamamatsu R446S photomultiplier tube (S-20 response). The wavelength calibration of this instrument was made with light from a mercury Pen-Ray lamp placed in the sample compartment. The wavelength readings are accurate to ± 1 nm. Phosphorescence measurements were performed either on the above instrument or on a home-made spectrometer in which the detection is made through a 0.25-m Jarrell-Ash monochromator and an RCA 7102 photomultiplier tube (S-1 response). This instrument permits detection at wavelengths as long as 960 nm. The wavelength settings of the Jarrell-Ash monochromator were calibrated with light from an argon ion light source, and are accurate to ± 0.3 nm. The RCA photomultiplier was cooled to -60 °C by boil-off from a liquid nitrogen dewar. The spectral response of the detection was measured in both systems using light from a standard tungsten lamp (GE Model 30A/T24/1). For the room temperature measurements no attempt was made to remove oxygen from the solutions. Several freeze-pump-thaw cycles were used to remove oxygen from the samples used in the low temperature experiments. All phosphorescence data were obtained at 77 K. Phosphorescence lifetimes were measured by interrupting the exciting light with a programable electronic shutter (Vincent Associates). The phosphorescence signal-to-noise ratio was improved with repeated accumulations on a signal averager (Tracor-Northern). The time resolution of this system is 0.3 ms.

Relative quantum yields were obtained by comparing the

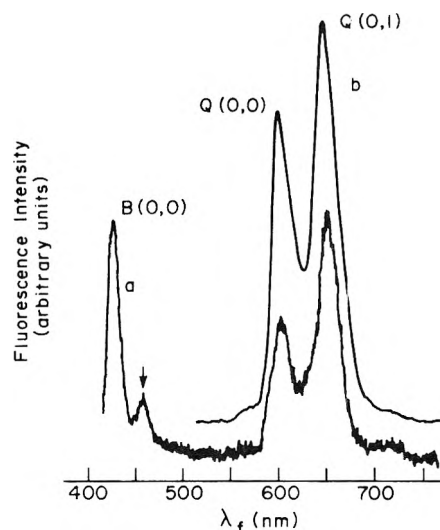


Figure 1. Uncorrected fluorescence spectra of YTPP(acac) in methanol at room temperature, with excitation at 400 (a) and at 425 nm (b). The peak labeled B(0,0) is the Soret fluorescence. The arrow indicates a solvent Raman peak. The apparent intensity ratio of the Q(0,0) and Q(0,1) maxima is different in (a) and (b) because of free base TPP contamination (see text).

areas under the corrected spectra. Absolute fluorescence quantum yields were determined from dilute solutions by comparison with zinc etioporphyrin in benzene ($\phi_f = 0.04$),¹⁸ after correcting for the difference in solvent index of refraction.¹⁷ Because of experimental difficulties to be discussed later, the fluorescence quantum yields reported here are believed to be accurate only to $\pm 30\%$.

Results

Absorption. The absorption spectra of all three complexes are very similar in both the positions and the extinction coefficients of the band maxima.^{5,6} The positions of the absorption band maxima are collected in Table I.

Fluorescence. Figure 1 shows uncorrected fluorescence spectra of YTPP(acac) obtained by excitation at 400 (a) and at 425 nm (b). We see that, in addition to the normal $S_1 \rightarrow S_0$ fluorescence bands, labeled Q(0,0) and Q(0,1), excitation at 400 nm produces the B(0,0) fluorescence in the Soret region. The small shoulder appearing on the short wavelength side of Q(0,0) in Figure 1b is not present at 77 K. An analogous band was observed by Quimby and Longo¹⁹ for ZnTPP, and was attributed to fluorescence from vibrationally excited S_1 states. The B(0,0), or Soret, fluorescence is attributed to emission from the second excited singlet state, $S_2 \rightarrow S_0$, and will be discussed in detail later on. Detection of the Soret fluorescence is somewhat difficult because of scattered incident light, and because of reabsorption by the intense Soret absorption band (which peaks at 420 nm). These problems can be minimized by excitation at wavelengths considerably shorter than the Soret absorption maximum, and by the use of very dilute solutions. Unfortunately, both measures considerably reduce the Soret fluorescence intensity. The position of the apparent Soret fluorescence maximum is strongly dependent on concentration because of reabsorption of the short wavelength edge of the fluorescence. In order to determine the position of the true maximum, successive dilutions were used until the B(0,0)/Q(0,0) fluorescence intensity ratio ceased to increase. The spectrum shown in Figure 1a was obtained in this limit and represents therefore our best estimate of the Soret fluorescence line shape.

Comparison of the two spectra in Figure 1 reveals a difference in the $Q(0,0)/Q(0,1)$ intensity ratios. This is due to the contamination of the sample by an impurity with emissions near 650 and 720 nm. The excitation spectrum of the 720-nm fluorescence is identical with that of free base TPP, showing in particular a band near 650 nm which is not found in the YTPP(acac) absorption spectrum. The prominence of the TPP contribution to the fluorescence in Figure 1a is a consequence of the much lower fluorescence quantum yield of YTPP(acac). The difference in the observed $Q(0,0)/Q(0,1)$ intensity ratios arises from the fact that, although the Soret band maxima of TPP and YTPP(acac) are very close, the TPP Soret band is much broader toward shorter wavelengths. Because of this, excitation at 400-nm magnifies the effect of the free base contamination (Figure 1a). The $Q(0,0)/Q(0,1)$ intensity ratio in free base TPP solutions, together with the intensity of the 720-nm band in Figure 1b, indicates that the contamination of the YTPP(acac) $Q(0,1)$ band by free base TPP fluorescence is less than 15%. Part of the free base TPP seems to be present in the initial YTPP(acac) sample, but it is also gradually produced by decomposition of the metalloporphyrin once in solution. In order to minimize this problem all solutions were freshly prepared shortly before the spectra were taken.

The mirror image relationship between the Soret fluorescence of Figure 1a and the Soret absorption is evident after consideration of the fluorescence excitation spectra of Figure 2. (This is also seen by comparing the first columns of Tables I and II.) Spectrum a of Figure 2 was detected at 618 nm and is identical with the YTPP(acac) absorption spectrum. Detection at 618 (a) and at 450 nm (b) lead to identical Soret bands and thus indicate that the observed Soret fluorescence originates in YTPP(acac). (Although the Soret absorption maxima of free base TPP and YTPP(acac) are fairly close, excitation of the free base would have been readily recognized since it is much broader toward the short wavelength end of the spectrum.)¹ Also, free base TPP solutions have been carefully explored for Soret fluorescence but none was found.²⁰ Thus we conclude that the observed Soret fluorescence is solely due to YTPP(acac).

Studies similar to those outlined above were conducted for LuTPP(acac) and ThTPP(acac)₂. The results are summarized in Table II. Since the level of free base TPP contamination is approximately the same for all three complexes, the difficulties it creates are increasingly severe because of the progressively smaller $S_1 \rightarrow S_0$ quantum yields. In the case of ThTPP(acac)₂ only the $S_2 \rightarrow S_0$ fluorescence could be detected by excitation at 400 nm. Excitation at the B(0,0) maximum in fairly concentrated solutions does produce a fluorescence at ~ 605 nm which has the appropriate excitation spectrum and is thus tentatively attributed to ThTPP(acac)₂. However, its $Q(0,1)$ band is totally hidden under free base TPP fluorescence. Thus our estimate of the quantum yield for the $S_1 \rightarrow S_0$ fluorescence in ThTPP(acac)₂ is only of a rough qualitative significance. Figure 3 shows the corrected fluorescence spectra of YTPP(acac) and LuTPP(acac), and indicates clearly the dramatic increase in the B(0,0)/ $Q(0,0)$ intensity ratio. Because of the free base TPP interference the corrected fluorescence spectra had to be obtained in two steps: (1) The line shape of the $S_1 \rightarrow S_0$ fluorescence was obtained with a minimum of free base TPP contamination by excitation at 425 nm. (2) The $S_2 \rightarrow S_0$ fluorescence line shape and the B(0,0)/ $Q(0,0)$ intensity ratio were determined by excitation at 400 nm.

Phosphorescence. The phosphorescence data are collected

TABLE II: Fluorescence Data^a

Porphyrin	B(0,0) ^{b,c}	Q(0,0) ^{b,c}	Q(0,1) ^b	$\phi_f(B)$ ^d	$\phi_f(Q)$ ^e
YTPP(acac)	425 (421)	589 (421) (~ 516) (584) (~ 589)	650	0.001	0.006
LuTPP(acac)	426 (419)	599 (419)	647	0.001	0.001
ThTPP(acac) ₂	429 (420)	~ 605 (~ 421)		0.0004	~ 0.0001

^a In methanol at room temperature. ^b Wavelength in nm. ^c The numbers in parentheses are maxima of the excitation spectrum. ^d Quantum yield of $S_2 \rightarrow S_0$. ^e Quantum yield of $S_1 \rightarrow S_0$.

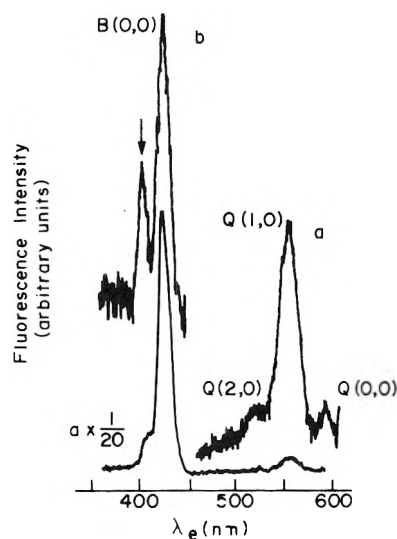


Figure 2. Uncorrected fluorescence excitation spectra of YTPP(acac) in methanol at room temperature, with detection at 618 (a) and at 450 nm (b). The arrow indicates a solvent Raman peak.

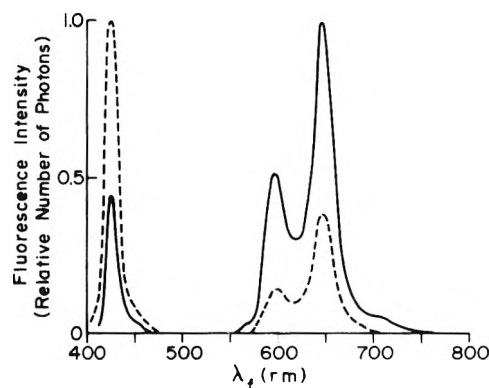


Figure 3. Corrected fluorescence spectra of YTPP(acac) (solid lines) and LuTPP(acac) (dashed lines) in methanol at room temperature. The fluorescence intensity is in arbitrary units so that no comparison is to be made between the intensity of the YTPP(acac) and LuTPP(acac) spectra. However, the intensities of the Soret and Q bands for each complex are to the same scale.

in Table III. Since free base porphyrin phosphorescence is always extremely weak,²¹ it posed no problem in the phosphorescence measurements. The phosphorescence lifetime of ThTPP(acac)₂ could not be measured because of the lim-

TABLE III: Phosphorescence Data^a

Porphyrin	T(0,0) ^b	I _p /I _f ^c	τ _p ^d	φ _p ^e
YTPP(acac)	779	3.6	29	0.01
LuTPP(acac)	769	120	2.8	0.02
ThTPP(acac) ₂	764	~700	≤0.3	~0.03

^a In EPA at 77 K. ^b Wavelength in nm. ^c Ratio of the intensities of the T(0,0) phosphorescence and Q(0,0) fluorescence maxima. ^d Phosphorescence lifetime in ms. ^e Phosphorescence quantum yield.

ited time resolution of our instrument (0.3 ms). Also, the relative intensities of the S₁ → S₀ fluorescence and phosphorescence for this complex could only be determined approximately because of the low S₁ → S₀ fluorescence quantum yield. The phosphorescence quantum yields in Table III were obtained with the assumption that the fluorescence quantum yield is the same at room temperature and at 77 K.

Discussion

Soret Fluorescence. Until a few years ago azulene was the only known case of strong S₂ → S₀ fluorescence.²² More recently, however, a number of other molecules have been shown to fluoresce from higher excited states^{8-13,22} but such cases are relatively rare. Two porphyrins, in particular, have been reported to fluoresce with moderate intensity from the second excited singlet state: zinc tetrabenzoporphyrin (TBP)^{9,10} and CdTBP.¹⁰ In each case the Soret fluorescence is about two orders of magnitude weaker than the S₁ → S₀ emission. In this work we found that all three metalloporphyrins studied exhibit a Soret fluorescence whose quantum yield is comparable to (or even larger than) that of the S₁ → S₀ fluorescence. We also found that the Soret fluorescence, in marked contrast with the S₁ → S₀ fluorescence, is unaffected by the increasing spin-orbit coupling in the sequence Y, Lu, Th. This shows, not unexpectedly, that the decay of S₂ is governed almost entirely by internal conversion, presumably to S₁.²² From the S₂ ← S₀ extinction coefficients⁶ and the S₂ → S₀ quantum yields we estimate that the internal conversion rate constants are of the order of 2–5 × 10¹¹ s⁻¹. Because of the relatively large S₂–S₁ energy gap the Soret fluorescences are not due to thermal repopulation of S₂ from S₁.²² We found, as expected, that the Soret fluorescences can only be excited through the Soret absorption band.⁹

At this point a question suggests itself: Is this Soret fluorescence a property of some porphyrins only, or is it a general characteristic? In the first instance, a good understanding of the correlation between porphyrin structure and the ability to fluoresce from S₂ would be extremely valuable in further clarifying the nature of photophysical processes in this class of molecules. A preliminary investigation of free base TPP has already shown²⁰ that the presence of the metal ions is necessary to the Soret fluorescence. On the other hand, it is entirely possible that most porphyrins have Soret fluorescences which have been overlooked in previous investigations. This is not unlikely because of the experimental difficulties in the detection of even moderately strong Soret fluorescence. Clearly, a systematic reexamination of other free bases and metalloporphyrins for Soret fluorescence is necessary before this question can be resolved.

Heavy Atom Effects. It has been shown for a variety of metalloporphyrins that the radiationless decay of S₁ occurs almost exclusively by intersystem crossing (rate constant, *k*_{isc}) to the lowest triplet state.²³ We shall assume that this is also

TABLE IV: Rate Constants for Spin-Forbidden Transitions

Porphyrin	Z	<i>k</i> _{isc} / <i>k</i> _f	<i>k</i> _p , s ⁻¹	<i>k</i> _{qp} , s ⁻¹
ZnTPP ^a	30	29	0.59	39
YTPP(acac)	39	170	0.35	35
LuTPP(acac)	71	10 ³	7.2	360
ThTPP(acac) ₂	90	~10 ⁴	≥10 ²	≥3 × 10 ³

^a Reference 23.

true of the three complexes investigated here. In that case we may write

$$k_{isc}/k_f = \phi_f^{-1} - 1$$

where *k*_f is the radiative decay rate constant for S₁ and φ_f is the quantum yield for S₁ → S₀. For a qualitative discussion of the heavy-atom effects encountered here we may also assume that *k*_f is roughly constant since the extinction coefficients of the Q bands of all complexes discussed below are very similar. For example, the extinction coefficients of the Q(1,0) bands for ZnTPP,¹⁹ YTPP(acac), LuTPP(acac), and ThTPP(acac)₂^{6,24} are respectively 2.3 × 10⁴, 1.9 × 10⁴, 1.9 × 10⁴, and 1.6 × 10⁴ M⁻¹ cm⁻¹. The calculated values of *k*_{isc}/*k*_f are collected in Table IV, together with the values of the phosphorescence rate constant, *k*_p, and of the radiationless decay rate constant, *k*_{qp}, of the triplet state. The rate constants *k*_p and *k*_{qp} have been obtained from the following relations:

$$\tau_p^{-1} = k_p + k_{qp}$$

$$\phi_p = (1 - \phi_f)k_p\tau_p$$

The comparison between ZnTPP (which also has a closed shell electronic configuration) and YTPP(acac) is quite striking. First, because of the increase in atomic number, the expected spin-orbit coupling enhancement should increase *k*_p and *k*_{qp}. However, this is not the case and these rate constants are very similar for the two complexes. The triplet states of ZnTPP and YTPP(acac) are quite similar in two other respects: (1) The positions of T(0,0) band maxima are 781 nm for ZnTPP¹⁹ and 779 nm for YTPP(acac). (2) The triplet state fine structure parameters of YTPP(acac), obtained²⁵ by electron paramagnetic resonance at 4.2 K, are *D* = 0.029 cm⁻¹ and *E* ≈ 0.010 cm⁻¹, which are very close to the values²⁶ for ZnTPP. The similarity between fine structure parameters indicates that there are no significant differences in triplet state configuration.^{26,27} The apparent lack of heavy-atom effect between ZnTPP and YTPP(acac) might be due to larger deviation from planarity in the latter complex, although this is not certain since other factors may be important (e.g., axial ligands, ring distortions). It has been suggested⁴ that the displacement of the metal ion from the porphyrin plane leads to smaller interaction between the empty e_g(π*) porphyrin orbitals and the metal d_π orbitals, and therefore to a decreased spin-orbit coupling.²⁸ The extent to which the metal ion deviates from the porphyrin plane depends very critically on its ionic radius. Horrocks and Wong²⁴ estimated the out-of-plane distance of the metal ion using the paramagnetic NMR shifts of the aryl protons in the complexes of tetraarylporphyrin with Eu(III) and Yb(III). The estimated out-of-plane distances are 1.8 Å for Eu(III) (ionic radius 0.95 Å) and 1.6 Å for Yb(III) (ionic radius 0.86 Å). Since Y(III), Lu(III), and Th(IV) have ionic radii of respectively 0.98, 0.85, and 0.96 Å, we expect a similar trend to exist in their out-of-plane distances in the corresponding porphyrin complexes.

On the other hand, Zn(II) (ionic radius 0.70 Å) is considerably closer to the porphyrin plane (~ 0.33 Å).²⁹ In contrast to the similarity between the ZnTPP and YTPP(acac) triplet state properties, k_{isc} is noticeably different. This is perhaps not surprising considering that k_{isc} and k_{qp} are governed by different vibronic coupling mechanisms.²⁷ Once the gap between ZnTPP and YTPP(acac) is bridged, the trend from YTPP(acac) through ThTPP(acac)₂ may be easily understood simply in terms of increasing spin-orbit coupling. It should be noticed that this heavy-atom effect perturbs k_{isc} , k_p , and k_{qp} in a substantially similar manner, in contrast to the change occurring between ZnTPP and YTPP(acac).

NOTE ADDED IN PROOF: After the present paper was submitted for publication, Professor M. Gouterman kindly informed us of work, subsequently published, which deals with the $S_1 \rightarrow S_0$ fluorescence and the phosphorescence of octaethylporphyrin complexes of yttrium and lanthanides. [M. Gouterman, C. D. Schumaker, T. S. Srivastava, and T. Yonetani, *Chem. Phys. Lett.*, **40**, 456 (1976).]

Acknowledgments. Acknowledgment is made to the donors of the Petroleum Research Fund, administered by the American Chemical Society, for support of this research through a grant to one of us (A.M.P.G.). The synthesis of the porphyrins investigated in this work was supported by the National Science Foundation through Grant No. MPS73-08550 to W. DeW. H. We thank E. G. Hove for recording the absorption spectra. A gift of zinc etioporphyrin by Professor D. G. Whitten of the University of North Carolina is gratefully acknowledged.

References and Notes

- (1) M. Gouterman in "Excited States of Matter", Vol. 2, C. W. Shoppee, Ed., Texas Tech University, Lubbock, Tex., 1973, p 63.

- (2) F. R. Hopf and D. G. Whitten in "Porphyrins and Metalloporphyrins", K. M. Smith, Ed., Elsevier, Amsterdam, 1975, p 667.
- (3) J. B. Allison and R. S. Becker, *J. Chem. Phys.*, **32**, 1410 (1960); R. S. Becker and J. B. Allison, *J. Phys. Chem.*, **67**, 2662, 2669 (1963).
- (4) M. Gouterman, L. K. Hanson, G.-E. Khalil, J. W. Buchler, K. Rohbock, and D. Dolphin, *J. Am. Chem. Soc.*, **97**, 3142 (1975).
- (5) C.-P. Wong, R. F. Venteicher, and W. DeW. Horrocks, Jr., *J. Am. Chem. Soc.*, **96**, 7149 (1974).
- (6) C.-P. Wong and W. DeW. Horrocks, Jr., *Tetrahedron Lett.*, **31**, 2637 (1975).
- (7) W. DeW. Horrocks, Jr., R. F. Venteicher, C. A. Spilburg, and B. L. Vallee, *Biochem. Biophys. Res. Commun.*, **64**, 317 (1975).
- (8) M. H. Hui, P. DeMayo, R. Suau, and W. R. Ware, *Chem. Phys. Lett.*, **31**, 257 (1975), and references therein.
- (9) L. Bajema, M. Gouterman, and C. B. Rose, *J. Mol. Spectrosc.*, **39**, 421 (1971).
- (10) I. E. Zaleskii, V. N. Kotlo, A. N. Sevchenko, K. N. Solov'ev, and S. F. Shirkman, *Dokl. Akad. Nauk SSSR*, **210**, 312 (1973), [*Sov. Phys. Dokl.*, **18**, 320 (1973)].
- (11) G. Eber, F. Grüneis, S. Schneider, and F. Dörr, *Chem. Phys. Lett.*, **29**, 397 (1974).
- (12) J. R. Huber and M. Mahaney, *Chem. Phys. Lett.*, **30**, 410 (1975).
- (13) L. Margulies and A. Yogev, *Chem. Phys. Lett.*, **37**, 291 (1976).
- (14) P. deMayo and H. Shizuka, *J. Am. Chem. Soc.*, **95**, 3492 (1973).
- (15) H. Shizuka, Y. Ishii, M. Hoshino, and T. Morita, *J. Phys. Chem.*, **80**, 30 (1976).
- (16) The complex with La(III) is also diamagnetic but was not studied because of difficulties arising from its instability.
- (17) J. B. Birks, "Photophysics of Aromatic Molecules", Wiley-Interscience, London, 1970, p 97, and references therein.
- (18) P. G. Seybold and M. Gouterman, *J. Mol. Spectrosc.*, **31**, 1 (1969).
- (19) D. J. Quimby and F. R. Longo, *J. Am. Chem. Soc.*, **97**, 5111 (1975).
- (20) A. M. Ponte Goncalves and L. A. Martarano, unpublished results.
- (21) M. Gouterman and G.-E. Khalil, *J. Mol. Spectrosc.*, **53**, 88 (1974).
- (22) J. B. Birks in "Organic Molecular Photophysics", Vol. 2, J. B. Birks, Ed., Wiley-Interscience, London, 1975, p 447.
- (23) A. T. Gradyushko and M. P. Tsvirko, *Opt. Spektrosk.*, **31**, 548 (1971) [*Opt. Spectrosc.*, **31**, 291 (1971)].
- (24) W. DeW. Horrocks, Jr., and C.-P. Wong, to be submitted for publication.
- (25) W. U. Spindel and A. M. Ponte Goncalves, unpublished results.
- (26) S. R. Langhoff, E. R. Davidson, M. Gouterman, W. R. Leenstra, and A. L. Kwiram, *J. Chem. Phys.*, **62**, 169 (1976).
- (27) W. G. van Dorp, W. H. Schoemaker, M. Soma, and J. H. van der Waals, *Mol. Phys.*, **30**, 1701 (1976).
- (28) M. Gouterman, F. P. Schwarz, P. D. Smith, and D. Dolphin, *J. Chem. Phys.*, **59**, 676 (1973).
- (29) J. L. Hoard in "Porphyrins and Metalloporphyrins", K. M. Smith, Ed., Elsevier, Amsterdam, 1975, p 317.

Proton Magnetic Resonance Study of Aluminum(III) Complexes in the Aluminum Perchlorate–Acetonitrile–Water System¹

Yakir Ruben

Department of Chemistry, Ben Gurion University, Beer Sheva, Israel

and Jacques Reuben*²

Isotope Department, The Weizmann Institute of Science, Rehovot, Israel (Received April 19, 1976)

The region of coordinated water in the proton magnetic resonance spectra of acetonitrile solutions of $\text{Al}(\text{ClO}_4)_3$ containing low concentrations of water reveal 24 distinct absorptions, which were assigned to the different aluminum(III) complexes in this system. For the spectral assignment the changes in line intensities effected by changing the water concentration and the temperature were analyzed. Distinct absorptions due to coordinated acetonitrile molecules were also observed. From the integrated intensities as well as from the multitude of lines it was concluded that at certain water contents the total solvation number of Al^{3+} is smaller than 6 and that the perchlorate anion participates in the first coordination sphere of the Al^{3+} ion. The coordination behavior of Al^{3+} with respect to water and perchlorate is in accord with the positive deviation from Raoult's law observed in acetonitrile–water mixtures. An estimate for the overall equilibrium quotient of water substitution in the first coordination sphere of Al^{3+} was obtained and thermodynamic parameters calculated from its temperature dependence. Analogies with other related systems are pointed out.

Introduction

The properties of electrolyte solutions depend largely upon the solvation states of the ions. The observation and monitoring of the coordination spheres of cations is conveniently achieved by nuclear magnetic resonance methods. Under conditions of slow (on the NMR time scale) ligand exchange separate resonances are usually observed for the molecules comprising the first coordination sphere of the cation. Therefore the aluminum(III) ion with a solvation sphere of a relatively long residence time³ has been one of the first⁴ and most thoroughly studied cations.^{5–21} The addition of water miscible organic solvents often permits the slowing down of ligand exchange processes by lowering the temperature.^{19–21} In the latter case, however, mixed solvation spheres have been observed^{18,19,21–25} and ion pair formation demonstrated.^{18,22,26} Results on the coordination behavior of cations in mixed aqueous solvents may have implications in widely different areas, e.g., desalination processes and the state of metal ions bound to biological macromolecules

In this communication we report the results of a proton NMR study of the aluminum(III) complexes in acetonitrile solutions of $\text{Al}(\text{ClO}_4)_3$ containing small amounts of water. In 1967 Supran and Sheppard demonstrated in a preliminary report that several distinct resonances belonging to water molecules in different mixed aquo complexes can be observed in this system.¹⁸ We have extended our studies over a wider range of water concentrations and temperatures and observed 24 resonances in the spectral region of coordinated water in addition to a number of absorptions in the region of the coordinated acetonitrile molecules. From the integration and assignment of the spectra a detailed picture emerges regarding the solvation and coordination state of Al^{3+} in this system.

Experimental Section

Solutions. Attempts to prepare acetonitrile solutions of $\text{Al}(\text{ClO}_4)_3$ using a salt that was dried in vacuo at 180 °C failed, probably because the drying process yields an insoluble crystal form. Therefore the solutions used in this work were prepared

by allowing the appropriate stoichiometric amounts of AlCl_3 to react with AgClO_4 , both dissolved in acetonitrile, and removing the AgCl precipitate. The solvent, a product of BDH, was distilled over P_2O_5 before use. The proton NMR spectra showed that the acetonitrile contained an impurity of benzene. Dry AlCl_3 was obtained from BDH sealed in an ampoule. The AgClO_4 was dried at 80 °C under reduced pressure and in the presence of P_2O_5 in the drying chamber. Thus a stock solution containing 0.123 ± 0.001 M $\text{Al}(\text{ClO}_4)_3$ was prepared. It was found that despite the precautions this solution contained 0.11 M water as determined by integrating the water absorptions in its NMR spectrum. Solutions of different water content were made up from the stock solution by pipeting predetermined amounts of doubly distilled water. Sixteen samples were prepared in this manner with water content (determined by NMR) ranging between 0.11 and 0.96 M. In the process of water addition an additional (albeit minor) precipitation of insoluble material occurred. At the lower water content, up to 0.56 M, the precipitate was identified as AgCl . At the higher water content minute amounts of a colloidal precipitate were found and identified as $\text{Al}(\text{OH})_3$. The concentration of Al^{3+} in each sample was determined by volumetric titrations (in duplicate) with standardized EDTA using Eriochrome Black T as the end-point indicator. The concentrations (± 0.001 M) were 0.123 M for the first nine samples (water content from 0.11 to 0.56 M) and from 0.120 to 0.114 M for the remaining seven samples (water content from 0.62 to 0.96 M). For convenience we will refer to the samples and to their water content by the relative water concentration expressed as²²

$$Z = [\text{H}_2\text{O}]/[\text{Al}^{3+}] \quad (1)$$

where the square brackets denote total concentrations.

NMR Measurements. Proton spectra were recorded at 100 MHz on a Varian XL-100 NMR spectrometer equipped with variable temperature accessories. Chemical shifts were referred to tetramethylsilane (TMS) in a reference solution of TMS in acetonitrile. Since the solvent acetonitrile contained an impurity of benzene, the chemical shift of the latter was determined in the reference solution and the benzene reso-

nance was used in fact as an internal reference. Spectra of all of the samples were taken at five temperatures: -34 , -15 , 0 , $+15$, and $+39$ °C. The temperature was determined before and after each run from the peak separation of a methanol sample using the calibration chart provided by the instrument manufacturer. During each run the temperature remained constant to within ± 1.5 °C. Several spectra were recorded for each sample and temperature so as to encompass the entire spectrum with sufficient resolution. Thus, e.g., the spectral region of coordinated water (7.0–9.0 ppm) was recorded at a sweep width corresponding to 0.2 Hz/cm. Line intensities were determined by integration. The integral of the low field ¹³C satellite of uncoordinated acetonitrile corresponding to the 0.105 M ¹³CH₃CN molecules was used for calibration.

Results

General Description of the Spectrum. The proton spectra of acetonitrile solutions of Al(ClO₄)₃ containing small amounts of water reveal the following general features.

(1) An intense sharp peak at 1.95 ppm due to the uncoordinated acetonitrile solvent.

(2) A band centered at ca. 2.5 ppm of overlapping low intensity lines belonging to the coordinated acetonitrile ligands.

(3) A sharp peak of low intensity at 2.6 ppm due to the uncoordinated ¹³CH₃CN molecules. A similar peak appears also on the upfield side of the solvent peak.

(4) At higher water concentrations a peak at 4.0 ppm appears due to the uncoordinated water molecules.

(5) A sharp peak of low intensity at 7.25 ppm is due to a small impurity of benzene.

(6) A wide band of many peaks is found in the region 7.0–9.0 ppm. These are the water resonances of the different water containing complexes of aluminum(III).

In general both the line positions and the line widths showed little or no temperature dependence.

Coordination Numbers. The average coordination numbers with respect to the acetonitrile (N_{AN}) or to the water (N_W) ligands were determined by integrating the corresponding absorptions in the proton spectra and normalizing by the Al³⁺ concentration. The results at -15 °C along with the total solvation number ($N_T = N_{AN} + N_W$) are plotted in Figure 1 as a function of Z . Some of the water absorptions could be assigned to complexes containing perchlorate in the first coordination sphere and from their relative intensities the average number of coordinated perchlorates (N_P) was estimated. The values of N_P are also given in Figure 1. It is seen from these results that the addition of water to the system leads to an increase in N_W and to a concomitant decrease in N_{AN} until at $Z > 6$ one has $N_T = N_W = 6.0 \pm 0.3$. At the lowest water concentration studied we find $N_{AN} = 4.9 \pm 0.3$, a value much larger than the values of 2.8 and 2.9 reported for anhydrous solutions.^{12,18} In our experiments such values for N_{AN} are found at $Z \approx 1.8$. The only explanation we can offer for this discrepancy is the possible presence of water traces in what was assumed to be an anhydrous system in previous work. In fact the spectrum of coordinated acetonitrile reported by O'Brien and Alei for an apparently anhydrous system¹² is almost identical with the spectrum we observe at $Z = 1.7$. The total solvation number displays a minimum of $N_T = 4.3 \pm 0.3$ at $Z \approx 2.7$. At the lowest Z as well as at $Z > 6$, $N_T = 6.0 \pm 0.3$. On the other hand N_P shows a maximum of 0.9 ± 0.3 at $Z \approx 2.3$ suggesting preferential coordination of perchlorate at certain water contents. It approaches zero at the lowest Z as

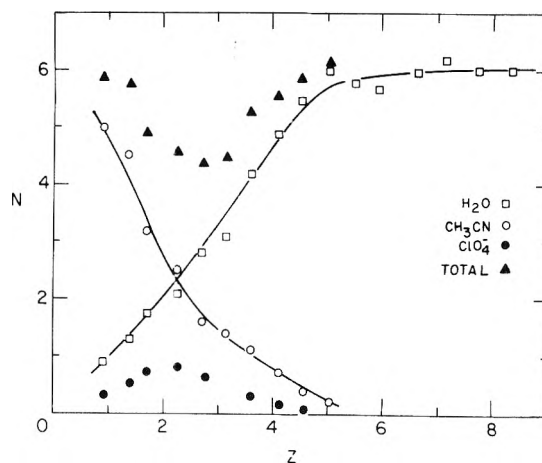


Figure 1. Solvation numbers of Al³⁺ in acetonitrile–water mixtures at -15 °C as a function of Z , the water/aluminum ratio. Total refers to $N_W + N_{AN}$. Lines are drawn to guide the eye.

well as at $Z > 4.5$. Qualitatively similar results were obtained at the other temperatures.

Assignment of the Water Resonances. The proton resonances of the water ligands of Al³⁺ appear in the spectral region 7.0–9.0 ppm. Inspection of the 16 samples (Z increasing from 0.9 to 8.4) revealed 24 distinct peaks of intensities varying with Z in a consistent manner. This dependence on water concentration is different at different temperatures. Representative spectra obtained at -15 °C are shown in Figure 2. Also given in Figure 2 is a stick diagram which will be used for peak identification. The 24 resonances can be divided into eight groups according to their positions and Z dependence of their relative intensities. These groups are listed in the legend of Figure 2 (see also Appendix). The following features were observed in the relative intensities (some of them can be seen in Figure 2). At low values of Z the first two groups (I and II) appear with high intensity, the other groups being of progressively lower intensity. With increasing Z the first groups lose in intensity until their disappearance: group I disappears first, then II, etc. Concomitantly groups III–V gain in intensity and then lose until at $Z > 7.5$ only the broad absorption 19 remains. From these observations it is clear that the first groups belong to complexes with a small number of water molecules (one, two), whereas groups V and VI correspond to complexes of higher hydration (five and six water molecules). Similar behavior has previously been observed for this system¹⁸ as well as for the Mg²⁺–acetone–water system.^{22,24,25} The breadth of the spectral range for each group increases with raising the temperature and its center shifts upfield. The following shifts (± 0.01 ppm) were measured between the centers of adjacent groups at the lowest four temperatures: $\delta_{I,II} = 0.22$ ppm, $\delta_{II,III} = 0.25$ ppm, $\delta_{III-IV} = 0.25$ ppm, $\delta_{IV-V} = 0.24$ ppm, $\delta_{V-VI} = 0.20$ ppm. If one assumes that each of these groups belongs to a complex containing from one to six water molecules, respectively, then the addition of one water molecule to the solvation shell results in an almost constant upfield increment in the shift of 0.23 ± 0.03 ppm.

The presence of several peaks within some of the groups suggests that different geometrical isomers of complexes of the type Al(H₂O)_{6-*i*}(CH₃CN)_{*i*},³⁺ with $i = 2, 3$, or 4, may give rise to slightly shifted absorptions. When $i = 0, 1$, or 5 there is only one possible arrangement of ligands. There are two isomers for each of $i = 2, 3$, or 4. Thus for $i = 4$ the following two arrangements are possible:

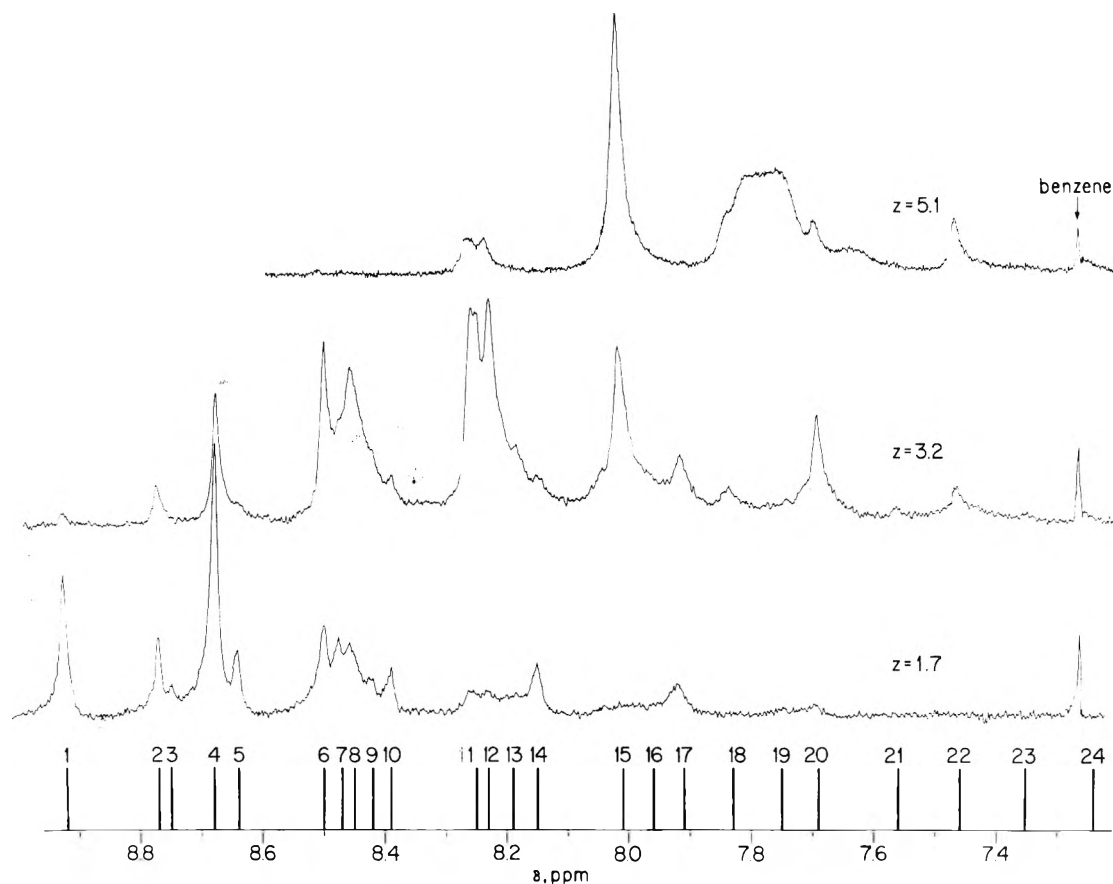
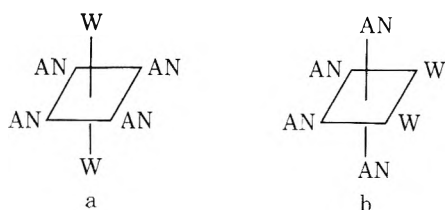


Figure 2. Spectra of coordinated water in the Al^{3+} -acetonitrile-water system at -15°C for different values of Z , the water/aluminum ratio. The stick diagram is for peak identification purposes. Group division: I, 1; II, 2-5; III, 6-10; IV, 11-14; V, 15-17; VI, 18-20; VII, 21,22; VIII, 23, 24.



where $W = \text{H}_2\text{O}$ and $\text{AN} = \text{acetonitrile}$. We will refer to the water ligands in a as apical or trans and to those in b as cis. Considering the neighboring ligands in each isomer it becomes clear that the water molecules reside in different magnetic environments in the different isomers. With the number of isomers taken into account and assuming chemical shift equivalence of the ligands within each isomer a total of nine absorptions is expected. If the latter assumption does not hold separate peaks should be present due to different positions within the same isomer. The intensity of such peaks should change in a parallel manner with changing temperature or Z . Parallel changes of this type were not observed except in the following cases. Peak 8 is relatively broad and may contain overlapping absorptions. Peak 18, which is in group VI, seems to belong to a complex containing a total of five water molecules and is tentatively assigned to the apical water molecule in $\text{Al}(\text{H}_2\text{O})_5(\text{CH}_3\text{CN})^{3+}$.

Measurements of the total solvation number of Al^{3+} in this system (vide supra) have shown that at the lower water concentrations $N_T < 6$ with a minimum of 4.3 at $Z = 2.7$. This finding together with the observation of a multitude of peaks in the spectral region of coordinated water suggests that

complexes containing at least one perchlorate in the first coordination sphere are present at low water concentrations. Consider complexes of the type $\text{Al}(\text{H}_2\text{O})_{5-i}(\text{CH}_3\text{CN})_i(\text{ClO}_4)^{2+}$. For $i = 0$ there will be one such complex. For $i = 1$ there will be two isomers with the perchlorate either cis or trans to the acetonitrile ligand. Similarly for $i = 4$ there will be two isomers with the perchlorate now cis or trans to the water ligand. For each of $i = 2$ and $i = 3$ there will be three geometrical forms. Thus there is a total of 11 possible species containing one coordinated perchlorate. These together with the nine $\text{Al}(\text{H}_2\text{O})_{6-i}(\text{CH}_3\text{CN})_i^{3+}$ complexes give a total of 20 species in accord with the number of peaks observed in the first six groups. We can now proceed with a detailed assignment of the individual peaks. The results are summarized in Table I. The arguments and details of the reasoning are given in an Appendix.

Peak 19, which is the broadest among the resonances of coordinated water, corresponds to the $\text{Al}(\text{H}_2\text{O})_6^{3+}$ complex and the broadening is due to unresolved spin-spin coupling with the spin $\frac{5}{2}$ aluminum-27 nucleus. Although the multiplet is unresolved, a lower limit for the coupling constant can be obtained from the overall line width, Δ , and taking the average line width of the other absorptions as representative of the proton relaxation rate, $1/T_2$, in these complexes. Thus $J \geq (\Delta - 1/\pi T_2)/5$ and we obtain $J \geq 1.7$ Hz.

Resonances of Coordinated Acetonitrile. The spectral region due to the coordinated acetonitrile ligands is shown in Figure 3 along with the low field ^{13}C satellite of the uncoordinated acetonitrile solvent. The intensity of this band decreases with increasing Z until it disappears at $Z > 5.0$ (cf.

TABLE I: Peak Assignment in the Spectral Region of Water Coordinated to Aluminum(III) at -15 °C

Peak ^a	Shift, ppm	Complex ^b			Structure ^c
		x	i	p	
1	8.92	1	5		
2	8.77	2	4		W,W-trans
3	8.75	1	4	1	W,P-trans
4	8.68	2	4		W,W-cis
5	8.64	1	4	1	W,P-cis
6	8.50	3	3		W,W,W-cis, trans
7	8.47	2	3		W,W-trans
8	8.45	3	3		W,W,W-cis, cis
9	8.42	2	3	1	W,W-cis, P-cis, cis
10	8.39	2	3	1	W,W-cis, P-cis, trans
11	8.25	4	2		AN,AN-cis
		3	2	1	AN,AN-trans
12	8.23	4	2		AN,AN-trans
13	8.19	3	2	1	AN,AN-cis, P-cis, trans
14	8.15	3	2	1	AN,AN-cis, P-cis, cis ^d
15	8.01	5	1		in-plane waters
16	7.96	4	1	1	AN,P-trans
17	7.91	4	1	1	AN,P-cis
18	7.83	5	1		apical water
19	7.75	6			
20	7.69	5		1	
21	7.56	Monohydroxo complexes			
22	7.46	Monohydroxo complexes			
23	7.35	Dihydroxo complexes			
24	7.25	Dihydroxo complexes			

^a Cf. stick diagram in Figure 2. ^b Al(H₂O)_x(CH₃CN)_i(ClO₄)_p^{3-p+}, x = 6 - i - p. ^c W = H₂O, AN = acetonitrile, P = perchlorate. ^d This peak may also contain contribution from an Al(H₂O)₂(CH₃CN)₂(ClO₄)₂²⁺ complex with a bidentate perchlorate.

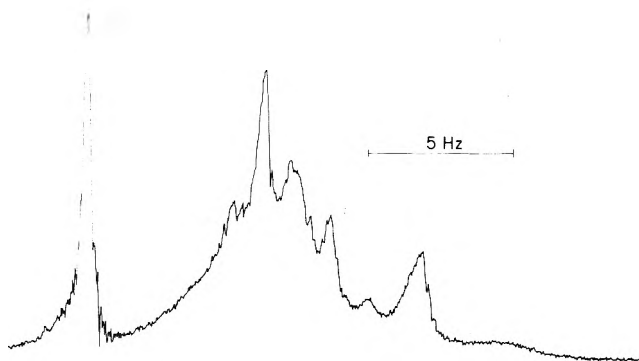


Figure 3. Spectrum of coordinated acetonitrile at -15 °C for Z = 1.4. The sharp peak at the left is centered at 2.6 ppm and is the low field component of the ¹³C satellites of uncoordinated acetonitrile.

Figure 1). In principle one would expect in this region as many peaks as those in the water region. Unfortunately the chemical shift differences here are too small and the overlap of lines is rather extensive. Therefore no assignment to individual complexes was attempted. In some instances however at least six distinct maxima were discernible (cf. Figure 3), which probably correspond to the six complexes containing from one to six coordinated acetonitrile ligands.

Resonances of Uncoordinated Water. For samples with high water content, Z > 6, an absorption due to uncoordinated water appears at 4.0 ppm and its intensity increases with increasing Z. This spectral region at -34 °C is shown in Figure

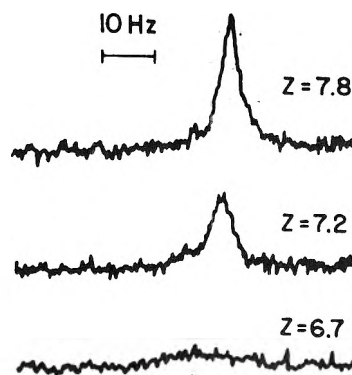
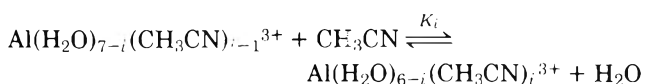


Figure 4. Spectra of uncoordinated water in the Al³⁺-acetonitrile-water system at -34 °C for different values of Z. The intense absorptions are centered at ca. 4.0 ppm.

4. For this lowest temperature it can be seen that the absorption is composed in fact of two lines: one sharp and intense and another, smaller and broader, shifted downward by 0.06 ppm. A similar feature has been observed in the Mg²⁺-acetone-water system.²² A possible origin for it is from a second solvation sphere.

Equilibrium Quotients. A treatment of the equilibria in the Al³⁺-acetonitrile-water system may be impractical because of the great complexity of the system. From the spectral analysis it was found that the Al³⁺ ion participates in at least 25 different complexes, i.e., there are at least 25 coupled equilibria in the system. The lire overlap within each group in the spectral region of coordinated water precludes accurate determinations of individual line intensities. Nevertheless, using some approximations (or oversimplifications) one may obtain order of magnitude estimates of the equilibrium quotients. Toward this end we have adopted the approach of Covington and Covington used for the Mg²⁺-acetone-water system and the reader is referred to their article for details not given here.²⁵

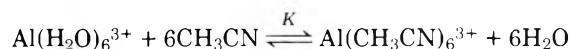
The system is assumed to be composed only of complexes of the type Al(H₂O)_{6-i}(CH₃CN)_i³⁺, where i = 0, 1, . . . , 6, which participate in equilibria of the type



with the equilibrium quotient given by

$$K_i = \frac{[\text{Al(H}_2\text{O)}_{6-i}\text{(CH}_3\text{CN)}_i\text{ }^{3+}][\text{H}_2\text{O}]}{[\text{Al(H}_2\text{O)}_{7-i}\text{(CH}_3\text{CN)}_{i-1}\text{ }^{3+}][\text{CH}_3\text{CN}]}$$

where the square brackets denote equilibrium concentrations of species. The sum of all equilibria can be represented by



Assuming a statistical distribution of species the equilibrium quotient of each step will be given by

$$K_i = K^{1/6}(7 - i)/i$$

It is convenient to express the abundance of each species by its fraction of the total aluminum(III) present:

$$\phi_i = [\text{Al(H}_2\text{O)}_{6-i}\text{(CH}_3\text{CN)}_i\text{ }^{3+}]/[\text{Al}^{3+}]_t$$

Using the known total concentrations and assuming a value for K^{1/6} these fractions are calculated according to the procedure of Covington and Covington.²⁵ The value of K^{1/6} is varied until a best fit with the experimental φ_i values is ob-

tained. We have taken as experimental values of ϕ_i the relative intensities of each of the groups I–VI as representing a definite Al^{3+} complex with a respective number of water molecules. Thus coordinated perchlorate is counted as being a water molecule and the species contributing to groups VII and VIII are neglected. The results thus obtained for -15°C are shown in Figure 5. It is seen that a good agreement between calculated and experimental values is obtained for the higher aquo complexes (ϕ_0, ϕ_1 , and ϕ_2). The agreement for the lower aquo complexes contributing mainly at the lower Z values is rather poor. This, of course, could be anticipated since here the contribution of the perchlorato complexes is significant and their equilibrium quotients are probably quite different. Similar results were obtained for the other temperatures. The temperature dependence of $K^{1/6}$ is depicted in Figure 6. From the straight line in Figure 6 the following thermodynamic parameters were calculated: $\Delta H = 5 \pm 1$ kcal/mol, $\Delta S = -2 \pm 3$ eu. They merely reflect the exothermic nature of the hydration process.

Discussion

We have presented a detailed, albeit tentative, assignment of the water proton resonances of the aquo–aluminum(III) complexes in the aluminum perchlorate–acetonitrile–water system. A general phenomenon is observed of upfield shifts with water or anion coordination. A similar phenomenon has also been observed for the Mg^{2+} –acetone–water system.^{22,24} In fact the spectra reported for that system (cf., e.g., Figure 8 in ref 24) resemble in certain aspects those obtained in the present work. However, due to smaller shifts and faster ligand exchange the line overlap in the Mg^{2+} system is extensive. There is also a similarity between the spectrum of the acetonitrile ligands (Figure 3) and that of acetone coordinated to Mg^{2+} (cf. Figure 2 in ref 24). Even the somewhat peculiar features of the free water resonances (Figure 4) are similar in the two systems (cf. Figure 7 in ref 22). These similarities suggest that the spectral assignments presented here might be helpful in the spectral analysis of other related systems.

The relatively low value of the total solvation number obtained at certain water contents and the multitude of peaks in the spectral region of coordinated water firmly establish the existence of perchlorato complexes of Al^{3+} in this system. Recent chlorine-35 NMR measurements on the $\text{Mg}(\text{ClO}_4)_2$ –acetonitrile–water system have shown that the ^{35}Cl resonance of perchlorate is broadened at low water concentrations demonstrating the participation of perchlorate in the coordination sphere of magnesium(II).²⁶ Perchlorate coordination to Al^{3+} has also been indicated in the infrared spectra and the possible action of perchlorate both as a monodentate and as a bidentate ligand has been pointed out.¹⁸ It thus seems that water coordination enhances the affinity of the cation for perchlorate and the coordination of perchlorate is preferred over that of acetonitrile at low water contents ($Z < 4$). We would expect the behavior of the conductivity in our system to be qualitatively similar to that reported for $\text{Mg}(\text{ClO}_4)_2$ in the same solvent system,²⁶ i.e., the conductance at low values of Z should change little (or might even decrease) with increasing Z and only at $Z > 4$ should it increase.

The solvation number of Al^{3+} in water^{5–7} as well as in a number of polar organic solvents^{9,14,19} has been firmly established to be 6.0. Our results show that in the Al^{3+} –acetonitrile–water system at water concentrations exceeding six times the Al^{3+} concentration, i.e., $Z > 6$, $\text{Al}(\text{H}_2\text{O})_6^{3+}$ is the only aluminum(III) species present. Only after the hydration of Al^{3+} is completed does the resonance of uncoordinated water

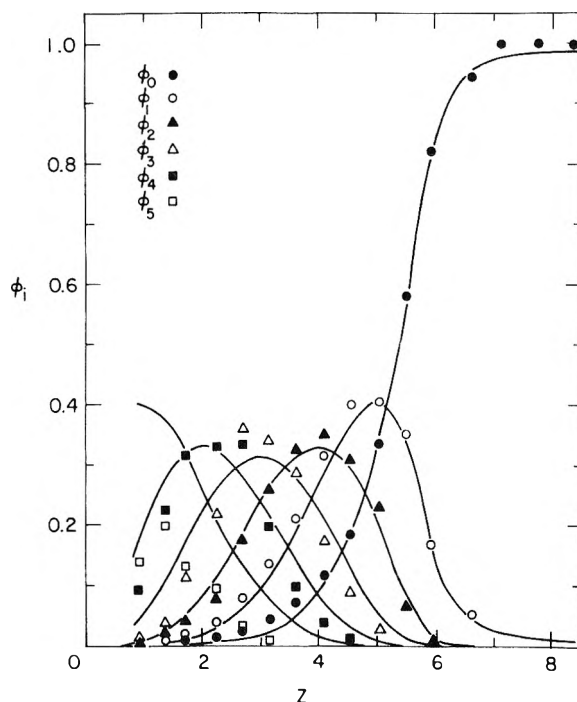


Figure 5. Relative populations of $\text{Al}(\text{H}_2\text{O})_6-(\text{CH}_3\text{CN})_i$ complexes at -15°C as a function of Z . Curves are calculated (see text).

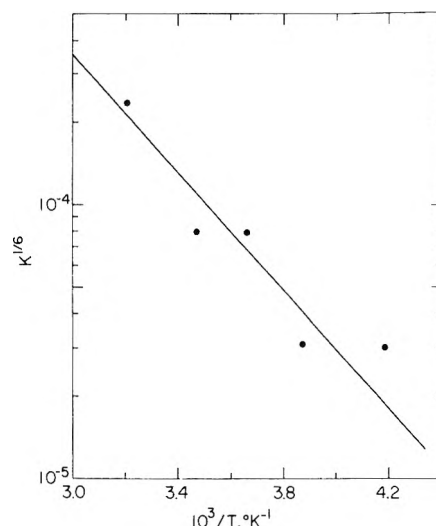


Figure 6. Temperature dependence of the overall equilibrium quotient for mixed aquo–acetonitrile complexes of aluminum(III).

appear in the spectrum. The preference for water coordination in this system is rather strong. The metal ion–water bond has in fact a partial covalent character as evidenced by the finite ^1H – ^{27}Al spin–spin coupling constant in the $\text{Al}(\text{H}_2\text{O})_6^{3+}$ complex.

A more quantitative comparison between the Al^{3+} –acetonitrile–water system and other related systems is afforded by the values of the equilibrium quotient for water substitution. The estimate obtained here is $K^{1/6} = 2 \times 10^{-5}$ at -15°C , which should be compared with $K^{1/6} = 1.1 \times 10^{-3}$ at -88°C reported for the Mg^{2+} –acetone–water system.²⁵ The much higher preference for water coordination to Al^{3+} relative to Mg^{2+} is thus clearly revealed. The origin for the different affinity is not only in the different cationic charges but also in the state of water in the two solvents. This difference is conspicuously expressed in the positive deviations of the systems

from Raoult's law.^{27,28} A positive deviation from Raoult's law is an indication of the tendency of water to escape from the solvent. It is likely that, in the presence of an electrolyte, water will tend to enter into the cation solvation sphere with a similar tendency. It might be expected that the mean residence time of the water molecule in the solvation sphere will be longer in such a mixed solvent system than in pure water. It is difficult to test this assertion in our system since the mean residence time of a water molecule in $\text{Al}(\text{H}_2\text{O})_6^{3+}$ is too long on the NMR time scale, ca. 6 s.⁸ For $\text{Ga}(\text{H}_2\text{O})_6^{3+}$, however, it is sufficiently short, ca. 5.5×10^{-4} s at 25 °C.⁸ Indeed inspection of published proton NMR spectra of the $\text{Ga}(\text{ClO}_4)_3$ -acetone-water system reveals marked line narrowing with increasing the acetone to water ratio (cf. Figures 1, 2, and 3 in ref 20). We ascribe this phenomenon as arising from the slowing of the water exchange process. The ability of an organic solvent to slow down the water exchange from the solvation spheres of cations is probably related to the deviation of the mixed solvent system from Raoult's law. Referring to these deviations for acetonitrile²⁷ and for acetone²⁸ one might expect water exchange processes to be slower in acetonitrile. Situations resembling those of mixed aqueous solvents may be found in biological systems, e.g., the interior of proteins. It may therefore be expected that water molecules will tend to bind stronger and reside longer in the coordination spheres of metal ions bound in the interior of protein molecules. Thus, e.g., while ligand substitution in the first coordination sphere of Mn^{2+} normally leads to enhanced water exchange rates,²⁹⁻³¹ the water exchange from Mn^{2+} bound in the interior of the protein concanavalin A is slower even than that for the aquo ion in water.³²

Appendix. Details of the Spectral Assignment

Group I. There is only peak 1 in this group. It appears already at $Z = 0.9$, is relatively intense at low values of Z , and disappears at $Z > 3.5$. This is the first peak to disappear from the spectrum with increasing Z . It is likely that it belongs to the complex of the lowest water content and is therefore assigned to the $\text{Al}(\text{H}_2\text{O})(\text{CH}_3\text{CN})_5^{3+}$ complex.

Group II. This group consists of the four peaks 2, 3, 4, and 5. It is also present at low Z values but disappears at $Z > 4.2$, i.e., it is still present after the disappearance of peak 1. This group contains the absorptions due to the two isomers of $\text{Al}(\text{H}_2\text{O})_2(\text{CH}_3\text{CN})_4^{3+}$. Assuming that coordination of perchlorate in the first sphere induces a shift similar to that of an additional water molecule, one would expect that this group will also include the two isomers of $\text{Al}(\text{H}_2\text{O})(\text{CH}_3\text{CN})_4(\text{ClO}_4)^{2+}$. The intensity of peaks 2 and 3 was found to be always smaller than that of peaks 4 and 5 by factors of 3-4. The relative statistical weights of isomers a and b are 1 and 4, respectively. Therefore peaks 2 and 3 may be assigned to isomers having the two water molecules or the water and the perchlorate in a trans configuration. It was also found (and can be seen in Figure 2) that the intensity of peaks 2 and 4 increases with increasing Z (at low Z values) more than that of peaks 3 and 5. Since the participation of perchlorate as a ligand has a relatively low probability, as evidenced by the fact that the minimum solvation number observed is $N_T = 4.3$, we conclude that the smaller peaks 3 and 5 belong to the complexes containing one perchlorate and one water. These assignments also suggest that when two water molecules (or a water and a perchlorate) are in a trans configuration their resonances are at slightly lower fields than when they are in a cis configuration. This observation will guide us in further assignments.

Group III. This group contains the five peaks 6, 7, 8, 9, and 10. While it appears already in the spectrum for $Z = 0.9$, its intensity is much lower than that of groups I and II. It disappears at $Z > 5.1$ and at the higher temperatures already at $Z > 4.5$. This behavior is found for other groups as well and arises from the temperature dependence of the equilibrium quotient for formation of aquo-aluminum(III) complexes in this system. From considerations similar to those given in the previous assignments we assign this group to the isomers of the complexes $\text{Al}(\text{H}_2\text{O})_3(\text{CH}_3\text{CN})_3^{3+}$ and $\text{Al}(\text{H}_2\text{O})_2(\text{CH}_3\text{CN})_3(\text{ClO}_4)^{2+}$. It was found that the intensities of peaks 6 and 8 increase predominantly with increasing Z (at low Z values). Therefore we assign these peaks to the $\text{Al}(\text{H}_2\text{O})_3(\text{CH}_3\text{CN})_3^{3+}$ species, with peak 6 corresponding to a cis, trans arrangement of the water molecules and peak 8 to a cis, cis arrangement. This assignment is made in analogy to that in group II. With one perchlorate in the complex there are three geometrical isomers. We assign peak 7 to the trans configuration of water molecules, peak 9 to a cis configuration with the perchlorate cis, cis and peak 10 to a cis configuration of waters with a cis, trans perchlorate.

Group IV. This group contains the four peaks 11, 12, 13, and 14. At the lower temperatures it appears at $Z = 1.7$, at the higher already at $Z = 1.3$ and disappears at $Z > 5.4$. This group contains the absorptions due to the two isomers of $\text{Al}(\text{H}_2\text{O})_4(\text{CH}_3\text{CN})_2^{3+}$ and the three isomers of $\text{Al}(\text{H}_2\text{O})_3(\text{CH}_3\text{CN})_2(\text{ClO}_4)^{2+}$. Thus five peaks are expected for these complexes. In fact peak 11 is broader than other peaks in this group and at -15 °C a small splitting in it is discernible (cf. Figure 2, $Z = 3.2$). The assignment of the peaks along the lines of the previous assignments is now straightforward. The assignment of peak 14, however, deserves further attention. It was found that this peak appears already at the lowest Z and that its intensity is less sensitive to changes in Z . Also, as may be seen in Figure 2, it is more intense than other members of this group at lower Z values. It thus seems that this peak contains absorptions belonging to two species differing in one water molecule. A plausible origin of an additional species is a complex in which perchlorate acts as a bidentate ligand. Such complexes have in fact been observed by Supran and Sheppard in the infrared spectra of this system.¹⁸

Group V. This group contains the peaks 15, 16, and 17. At the lower temperatures it appears at $Z = 1.3$, while at the higher at $Z = 2.0$. It disappears at $Z > 7.0$. The peaks are assigned to complexes containing one acetonitrile molecule.

Group VI. This group contains the peaks 18, 19, and 20. Peak 19 is the broadest among the proton resonances of coordinated water. The double resonance experiments of Supran and Sheppard have shown that this broadening arises from spin-spin coupling to the ²⁷Al nucleus.¹⁸ Aluminum-27 is a nucleus of spin 5/2 possessing a quadrupole moment. The interaction of the latter with intramolecular electric field gradients leads to rapid nuclear relaxation and as a result to effective decoupling of the protons. However, in the symmetrical environment of six water molecules in the $\text{Al}(\text{H}_2\text{O})_6^{3+}$ complex these gradients almost vanish and the effect of the ¹H-²⁷Al spin-spin coupling is apparent.

Groups VII and VIII. These groups contain the peaks 21, 22, 23, and 24. Peaks 21 and 22 appear at $Z = 2.6$ and disappear at $Z > 6.0$. Peaks 23 and 24 appear at $Z = 4.0$ and disappear at $Z > 6.8$. As was already mentioned in the Experimental Section, small amounts of $\text{Al}(\text{OH})_3$ precipitate with increasing water content. It could be assumed therefore that the lower hydroxo species $\text{Al}(\text{OH})_2^+$ and $\text{Al}(\text{OH})^{2+}$ might be present in solution. The appearance of groups VII and VIII

in the spectra of the samples for which a decrease in the Al^{3+} concentration has been observed suggests that these resonances belong to hydroxo complexes. In analogy to the previous assignments we assign group VII to monohydroxo and group VIII to dihydroxo complexes. Hydroxo complexes have also been observed in the Mg^{2+} -acetone-water system.²²

References and Notes

- (1) Taken in part from the M.Sc. Thesis of Y.R. Feinberg Graduate School, The Weizmann Institute of Science, Rehovot, 1976.
- (2) Present address: Department of Biochemistry and Biophysics, University of Pennsylvania School of Medicine, Philadelphia, Pa. 19174.
- (3) H. W. Baldwin and H. Taube, *J. Chem. Phys.*, **33**, 206 (1960).
- (4) J. A. Jackson, J. F. Lemons, and H. Taube, *J. Chem. Phys.*, **32**, 553 (1960).
- (5) R. E. Connick and D. N. Fiat, *J. Chem. Phys.*, **39**, 1349 (1963).
- (6) M. Alei, Jr., and J. A. Jackson, *J. Chem. Phys.*, **41**, 3402 (1964).
- (7) R. E. Schuster and A. Fratiello, *J. Chem. Phys.*, **47**, 1554 (1967).
- (8) D. Fiat and R. E. Connick, *J. Am. Chem. Soc.*, **90**, 608 (1968).
- (9) S. Thomas and W. L. Reynolds, *J. Chem. Phys.*, **44**, 3148 (1966).
- (10) H. H. Glaeser, H. W. Dodgen, and J. P. Hunt, *J. Am. Chem. Soc.*, **89**, 3065 (1967).
- (11) J. F. Hon, *Mol. Phys.*, **15**, 57 (1968).
- (12) J. F. O'Brien and M. Alei, Jr., *J. Phys. Chem.*, **74**, 743 (1970).
- (13) I. Y. Ahmed and C. D. Schmulbach, *Inorg. Chem.*, **11**, 228 (1972).
- (14) D. Richardson and T. D. Alger, *J. Phys. Chem.*, **79**, 1733 (1975).
- (15) J. F. Hinton, L. S. McDowell, and E. S. Amis, *Chem. Commun.*, 776 (1966).
- (16) J. F. Hinton and E. S. Amis, *Chem. Commun.*, 100 (1967).
- (17) J. F. Hinton, E. S. Amis, and W. Mettetal, *Spectrochim. Acta, Part A*, **25**, 119 (1969).
- (18) L. D. Supran and N. Sheppard, *Chem. Commun.*, 832 (1967).
- (19) A. Fratiello, R. E. Lee, V. M. Nishida, and R. E. Schuster, *J. Chem. Phys.*, **47**, 4951 (1967).
- (20) A. Fratiello, R. E. Lee, V. M. Nishida, and R. E. Schuster, *J. Chem. Phys.*, **48**, 3705 (1968).
- (21) A. Fratiello, R. E. Lee, V. M. Nishida, and R. E. Schuster, *Inorg. Chem.*, **8**, 69 (1969).
- (22) R. D. Green and N. Sheppard, *J. Chem. Soc., Faraday Trans. 2*, **68**, 821 (1972).
- (23) Y. Haas and G. Navon, *J. Phys. Chem.*, **76**, 1449 (1972).
- (24) F. Toma, M. Villemin, and J. M. Thiery, *J. Phys. Chem.*, **77**, 1294 (1973).
- (25) A. D. Covington and A. K. Covington, *J. Chem. Soc., Faraday Trans. 1*, **71**, 831 (1975).
- (26) H. A. Berman, H. J. C. Yeh, and T. R. Stengle, *J. Phys. Chem.*, **79**, 2551 (1975).
- (27) V. de Landsberg, *Bull. Soc. Chim. Belg.*, **49**, 59 (1940).
- (28) "International Critical Tables", Vol. 3, McGraw-Hill, New York, N.Y., 1928, p 290.
- (29) M. Grant, H. W. Dodgen, and J. P. Hunt, *Inorg. Chem.*, **10**, 71 (1971).
- (30) M. S. Zetter, M. W. Grant, E. J. Wood, H. W. Dodgen, and J. P. Hunt, *Inorg. Chem.*, **11**, 2701 (1972).
- (31) M. S. Zetter, H. W. Dodgen, and J. P. Hunt, *Biochemistry*, **12**, 778 (1973).
- (32) E. Meirovitch and A. J. Kaib, *Biochim. Biophys. Acta*, **303**, 258 (1973).

Electron Spin Resonance Studies on Hydrogen Atoms Formed in Pure and Acidic Ices under Electron Irradiation. Motional Narrowing and Electron Spin Polarization Effect

Hirotsugu Shiraishi, Hajime Kadoi, Yosuke Katsumura, Yoneho Tabata,* and Keichi Oshima

Department of Nuclear Engineering, Faculty of Engineering, University of Tokyo, Tokyo, Japan (Received June 4, 1975; Revised Manuscript Received June 21, 1976)

Hydrogen atoms formed in pure ice and in frozen solutions of sulfuric and hydrochloric acid were observed by ESR spectroscopy during continuous electron irradiation. In the sulfuric acid ice a large decrease in the hydrogen atom line width occurred around $-130^{\circ}C$. Above $-110^{\circ}C$ an anomaly which is characteristic of the spin polarization effect was concurrently observed with further gradual narrowing of the line width. While no hydrogen atom was detected in pure ice below $-130^{\circ}C$, a narrowed signal emerged above $-110^{\circ}C$. This also showed the polarization effect. The narrowing was attributed to diffusional motion of hydrogen atoms, and was analyzed with a simple classical method assuming an exponential correlation function for the fluctuating field. The narrowing around $-130^{\circ}C$ in sulfuric acid ice is related to an escape process from the solute trap, while above $-110^{\circ}C$ both acidic and pure ices seem to involve a similar diffusional process with a low activation energy. The polarization of hydrogen atoms observed was distinct from the reported result in the liquid phase in that the low-field line can sometimes be more strongly polarized than the high-field line. This point was discussed in terms of the radical pair theory, taking account of the relatively slow diffusion of hydrogen atoms in solid ice.

Introduction

The irradiated aqueous system is one of the important cases in which hydrogen atoms are directly observed by ESR spectroscopy. Much work has been done on trapped hydrogen atoms formed in acidic ices upon γ irradiation at 77 K ¹ since

they were first found by Livingston, Zeldes, and Taylor.² These hydrogen atoms are known to become unstable at slightly elevated temperatures. It was also reported that hydrogen atoms are stably trapped in pure ice at 4.2 K ,³ and that they disappear quickly below 50 K .⁴ The thermal decay of hydrogen atoms has been measured and analyzed in both pure⁴ and acidic ices, such as, sulfuric acid glass⁵ and perchloric acid glass.⁶ These decay curve studies are, however, mainly concerned with the deviation of decay kinetics from

* Correspondence should be addressed to the Nuclear Research Laboratory, Faculty of Engineering, University of Tokyo, 7-3-1 Hongo, Bunkyo-ku Tokyo, Japan.

a simple rule, and not much has been known about the diffusional process of hydrogen atoms in ice.

On the other hand, it has been reported by Fessenden and his co-workers^{7,8} and also by Smaller and his co-workers⁹ that an anomalous ESR signal of hydrogen atoms, comprising an emissive low-field line and an absorptive high-field line, was observed in aqueous solution irradiated with an electron beam at room temperature. This kind of anomaly, which was first noted by Fessenden and Schuler in 1963¹⁰ and is now called the chemically induced dynamic electron polarization, has recently been an interesting subject for an increasing number of researchers.¹¹ It is becoming clear that this phenomenon is not a special characteristic of a certain example but that it is rather commonly observed when radicals have a very short lifetime in the liquid phase. Particularly, it has been argued theoretically¹² and has been substantiated experimentally¹³ that a simple recombination reaction of radicals is responsible for at least some type of polarization. However, because of an inherent difficulty in the detection of polarization there is only a limited amount of data concerning this phenomenon, and further accumulation of experimental results under different conditions is required for its more complete elucidation.

In this study the authors have tried to observe ESR spectra of hydrogen atoms in both acidic and pure ices during irradiation at relatively high temperatures. The primary intention was to observe narrowing of the line width which is reasonably expected from large difference in the line width between hydrogen atoms in a liquid phase and those trapped at low temperatures. The narrowing was in fact found to take place around -130°C . In addition, hydrogen atom signals showed a clear indication of a polarization effect above -110°C . A preliminary account of the experiment on acidic ice was given previously,¹⁴ and here an analysis of the narrowing and some discussions on the polarization effect are presented together with the experimental results recently obtained.

The measurements were carried out during continuous irradiation from an electron accelerator coupled with a conventional ESR spectrometer. Sulfuric and hydrochloric acids were used as acidic solutes. The former is known for its relatively high efficiency of hydrogen atom trapping, while the latter possesses much less ability in that trapping.¹⁵ A relatively dilute solution, as compared to so-called acidic glass, was used in order to facilitate a comparison with the results obtained in pure ice. The presence of acidic solutes enabled a continuous observation of hydrogen atoms from -170°C , the lowest temperature available, to the vicinity of the melting point, while in pure ice hydrogen atoms were detectable only above -110°C .

To make the point clear, an argument is made here in advance about the origin of hydrogen atoms in acidic ices. Hydrated electrons in acidic solutions are known to react readily with protons to give hydrogen atoms, while there exist several pieces of evidence against the occurrence of the corresponding reaction in frozen acidic solutions at 77 K.¹⁶ The formation of trapped hydrogen atoms has been explained by the reaction of electrons with undissociated forms of acid or by the dissociation of excited water molecules.¹ The results at 77 K do not necessarily rule out the possibility of that reaction at higher temperatures. However, no such evidence has been obtained in the pulse radiolysis experiments^{17,18} on solid ice at higher temperatures except that a very small fraction of ejected electrons reacts similarly to the hydrated electrons. The result of the present experiment is also consistent with the view that this reaction makes a negligible contribution to the production of hydrogen atoms above -110°C in solid ice.

The physical backgrounds of the two phenomena, narrowing of the line width and polarization effect, are, of course, quite different. However, the narrowing observed here is due to the diffusional motion of hydrogen atoms, as described later. Since the development of electron spin polarization rests on time evolution of the relevant wave function, the motional state of hydrogen atoms is an important factor in the polarization process. It is not only for this reason but also because of their actual concurrence that the two phenomena are described together in this paper.

The narrowing of the line width is treated with a simple classical method assuming an exponential correlation function for the fluctuation of the local magnetic field. The polarization effect is discussed in terms of the radical pair theory which was first proposed by Kaptein and Oosterhoff¹⁹ and by Closs and Closs.²⁰ A quite different mechanism of the polarization of hydrogen atoms was proposed by Wan and his co-workers,²¹ who postulated nuclear and electron spin dependent relaxation from excited states of an isolated hydrogen atom. However, the experiment in the liquid phase by Verma and Fessenden⁸ shows that the polarization of hydrogen atoms is most likely the result of continuous pumping by radical pair interaction.

Most of the results on the polarization effect remain only descriptive here, and much has to be left for future exploration. This is mainly because of the lack of information about the rates of chemical reactions in solid ice or about temperature dependence of spin lattice relaxation. Secondary reactions, which inevitably took place in the present batch-sample method, make the situation more complicated. Attention is drawn to the fact that the emissive low-field line can sometimes be more intense than the corresponding high-field line in solid ice, and detailed discussion is made on how this fact is reconciled with the radical pair theory.

Experimental Section

The experimental setup is essentially the same as reported elsewhere.²² It consists of a conventional X-band ESR spectrometer with 100-kHz field modulation, which is coupled with a Dynamitron accelerator (Research Center for Nuclear Science and Technology, University of Tokyo). The accelerator was operated at 1.2 MeV. The output was monitored by current collected within the ESR cavity, and the dose rate was calibrated by the rate of production of peroxy radicals in polytetrafluoroethylene.²³ An improvement in the homogeneity of the magnetic field was made by putting a Helmholtz coil around the end of the hole through the pole piece. This resulted in a decrease of inhomogeneity to about 1.5×10^{-5} within an ordinary sample volume of 4 mm diameter and 7 mm length. Hyperfine splittings were measured by use of a proton NMR detector and a high frequency counter.

In order to avoid the trouble with spurious signals from hydrogen atoms trapped in sample tubes a bare sample of ice was used throughout this experiment. The procedure is as follows. After degassing with a vacuum line, the sample solution in a glass ampoule was frozen on the tip of a thin platinum tube. The ampoule was then sealed off and was reopened under an atmosphere of nitrogen. The sample was taken out bare and was stored in liquid nitrogen. A copper-constantan thermocouple was enclosed in the platinum tube as a sensor for the sample temperature.

Triply distilled water was used, and for a pure ice sample nitrogen was bubbled through to purge carbon dioxide. Commercial grade reagents were used to make the solutions without further purification.

Results and Discussions

A. Motional Narrowing. First a few points noted in the observation below $-140\text{ }^{\circ}\text{C}$ in 0.5 M sulfuric acid solution are briefly described. In this temperature range spectral features of hydrogen atoms concerning hyperfine splitting and line width are about the same as observed at 77 K. It was noted that the steady state concentration of hydrogen atoms, measured by the integrated signal intensity, decreased markedly as the irradiation proceeded. This dose effect is probably due to an increase of reaction of hydrogen atoms with accumulating radicals such as OH and SO_4^- .

When the temperature of this solution is raised, hydrogen atom signals become less intense due to an increase in the decay rate which corresponds to the detrapping process studied by Sprague and Schulte-Frohlinde.⁵ These authors have studied the decay kinetics of hydrogen atoms in sulfuric acid glass, and the existence of at least two types of traps, 5.79 and 4.1 kcal/mol deep, was deduced from the analysis of the complex decay curves. Hydrogen atom signal intensity during irradiation with a dose rate of 1.8 Mrads/min decreases from $-170\text{ }^{\circ}\text{C}$ with an apparent activation energy of about 4 kcal/mol. The situation here is complicated because of the coexistence of the first- and second-order decay processes, and actually the apparent activation energy tends to increase during the course of prolonged irradiation. No conclusive argument about the depth of traps can be made from these measurements, but the fact is that around $-130\text{ }^{\circ}\text{C}$ the signals become hardly discernible.

The narrowing begins at about $-140\text{ }^{\circ}\text{C}$. Narrower and clearer signals reappear above $-110\text{ }^{\circ}\text{C}$, and they are now oppositely polarized; the low-field line is in emission while the high-field line is in absorption. As the temperature is raised further, the derivative ESR signal increases in height and the line continues to narrow. Considering a large variation in the line width, derivative signals were doubly integrated, and these integrated intensities are plotted against temperature in Figure 1.²⁴ It is seen that the increase in the peak height above $-110\text{ }^{\circ}\text{C}$, as described in the previous paragraph, is just compensated by the decrease in the line width and that both narrowing and polarization are essential to the reappearance of the hydrogen atom signal, which in turn means that if neither narrowing nor polarization effect had existed, hydrogen atom signals could not be observed above $-130\text{ }^{\circ}\text{C}$. The small difference of the intensity of the two lines around $-150\text{ }^{\circ}\text{C}$ is indicative of the fact that a weak polarization effect, which is balanced by a relaxation effect, is already operative here. A slight decrease in the cavity Q value was noted above $-120\text{ }^{\circ}\text{C}$ in this 0.5 M sulfuric acid solution²⁵ when the sample was set in the cavity before irradiation, and above $-50\text{ }^{\circ}\text{C}$ the Q value decreased seriously, although the sample remained in the solid state.

In Figure 2 is shown the change of the line width measured at maximum slope. Because of a poor S/N ratio, which forced us to use undesirably large field modulation, those values contain considerable errors as indicated in the figure. The effect of inhomogeneity of the magnetic field was taken into account, but no correction was made with regard to the small sideband effect of 100-kHz field modulation. The widths of the two hyperfine lines were found to coincide within experimental errors. The hyperfine coupling constant was measured at two different temperatures in this solution. The result was $1415.9 \pm 1.0\text{ MHz}$ at $-167\text{ }^{\circ}\text{C}$ and $1418.7 \pm 1.0\text{ MHz}$ at $-70\text{ }^{\circ}\text{C}$. The latter value is closer to the free hydrogen atom value, 1420.4 MHz, than the former at $-167\text{ }^{\circ}\text{C}$. The fact that trapped hydrogen atoms in acidic ice have a smaller hyperfine

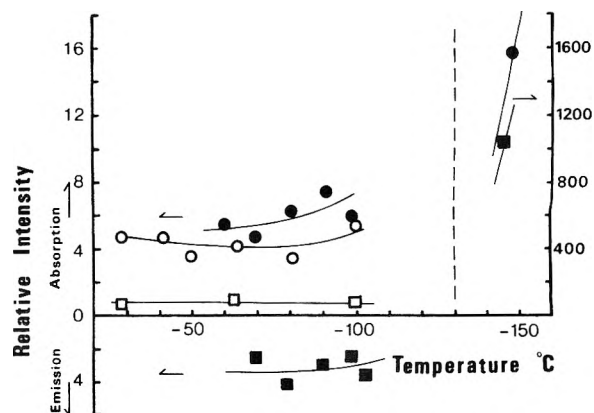


Figure 1. Temperature variation of the integrated signal intensity of hydrogen atoms in 0.5 M sulfuric acid solution (●, high-field line; ■, low-field line), and in pure ice (○, high-field line; □, low-field line); dose rate, 8 Mrad/min. See footnote 24 concerning the ordinate.

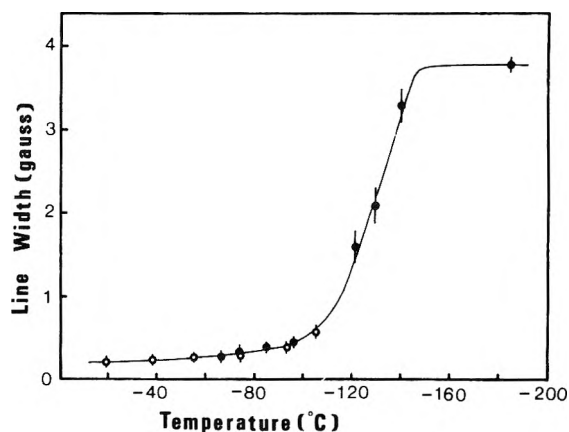


Figure 2. Temperature variation of the hydrogen atom line width in 0.5 M sulfuric acid solution (●) and in pure ice (○).

constant than a free hydrogen atom was reported by Marshall, Gabriel, and Serway.²⁶ The smaller deviation of the value at $-70\text{ }^{\circ}\text{C}$ can be taken as an indication of the weaker interaction of a hydrogen atom with its surroundings.

A quite similar narrowing phenomenon was observed in the same temperature range in 1 M hydrochloric acid solution, though the concurrent polarization effect was somewhat different from the case in sulfuric acid solution. (See the later section.)

No hydrogen atom signal was detectable in pure ice below $-130\text{ }^{\circ}\text{C}$ even during a high dose rate irradiation, $\sim 1\text{ Mrad/min}$. However, a narrow and polarized hydrogen atom signal emerged above $-110\text{ }^{\circ}\text{C}$. The degree of polarization was apparently smaller than the acidic cases, but there was no appreciable difference in the line width above $-110\text{ }^{\circ}\text{C}$ between pure ice and the acidic cases. These results are included in Figures 1 and 2. In the case of pure ice no reduction in the cavity Q value was noticeable up to its melting point.

B. Discussion on Narrowing. The line width of trapped hydrogen atoms is thought to arise mostly from hyperfine interactions with protons of nearby water molecules. The narrowing means fluctuation of this local magnetic field. Two possible interpretations can be considered: One is to explain this by tumbling motion of water molecules surrounding *trapped hydrogen atoms*, and the other is to attribute this to translational diffusion of hydrogen atoms. There is no phase

transition in usual hexagonal ice, and molecular reorientation in pure ice, as measured by dielectric relaxation²⁷ or nuclear spin relaxation,²⁸ is very slow. In fact the narrowing of the proton NMR line width, which is associated with much smaller coupling energy than this hydrogen atom line width, does not begin until -50°C .²⁸ Molecular reorientation coupled with a certain specific defect may be very fast, but such motion will probably lead to an escape of a hydrogen atom trapped within the cage of the defect. Further, if one assumes the former mechanism of narrowing, considerable line width, about 1 G, should remain after narrowing just as in the case of radicals in plastic crystals²⁹ where molecules are rotating rapidly but lack freedom of diffusional motion. The observed small line width at high temperatures suggests this is not the case. Therefore, the narrowing observed in pure ice should not be attributed to tumbling motion of water molecules surrounding trapped hydrogen atoms, but should be attributed to the translational diffusion of hydrogen atoms. This reasoning may not necessarily be applicable to concentrated acid solution. As described later, however, other radicals in the central part of ESR spectra are still very broad above -110°C , and the hydrogen atom signals alone show the narrowing phenomenon. This means that diffusional motion is most likely responsible also in acidic cases. At temperatures above -110°C hydrogen atoms must be diffusing as freely as in pure ice. Probably onset of some local motion in the vicinity of the solutes, as is inferred from the slight decrease in the cavity Q value, must have led to the loss of the hydrogen atom trapping ability of the solutes.

Not only the dipolar hyperfine coupling but also the isotropic hyperfine coupling with nearby protons is considered to be contributing to the line width. Helbert and Kevan³⁰ in fact showed the presence of a small isotropic interaction by an ENDOR experiment in acidic ices. Absence of any additional structure in a narrowed hydrogen atom line does not conflict at all with their observation, because such splittings are not expected in this diffusion-induced narrowing which involves a change of interacting protons with each diffusional step.

A simple classical method³¹ was used to obtain quantitative insight. The method deals with the problem on the basis that the narrowing is induced by adiabatic random fluctuation of the local field. It is assumed that the fluctuation is stationary and that the instantaneous distribution of the local field is Gaussian with the same second moment as is possessed by the absorption line of rigidly trapped hydrogen atoms. Then the relaxation function, namely, Fourier transform of a line shape function $I(\omega)$ expressed in terms of angular frequency ω , is given as follows:³¹

$$G(t) = \exp \left\{ i\omega_0 t - \int_0^t (t - \tau) G_\omega(\tau) d\tau \right\} \quad (1)$$

Here, ω_0 is the angular frequency at the center of the resonance, and $G_\omega(\tau)$ is the correlation function for the fluctuating local field. For the sake of simplicity an exponential correlation function was assumed, that is

$$G_\omega(\tau) = \omega_p^2 \exp(-|\tau|/\tau_c) \quad (2)$$

where ω_p^2 is the second moment of the distribution of the local field, and τ_c is a formally introduced correlation time and this is supposed to change with temperature. Actually the local field must be composed of various degrees of contributions from many protons, and the component associated with distant protons will vary more slowly, or with a larger correlation time, than the one associated with nearby protons. However,

because of the dipolar character of the coupling those protons that are more than several times as distant as the nearest ones give a negligibly small contribution to the line width. Therefore, although τ_c may not be taken simply to denote the mean length of time between two successive jumps in the diffusion process, it will serve at least as an order of magnitude estimate of that value.

For practical convenience the first derivative curves were directly calculated numerically with varying τ_c , and the line widths were compared with the measured values. The same ω_p^2 , taken from the measurement of the line width in 0.5 M sulfuric acid solution at -185°C , was used for both the sulfuric acid solution and pure ice. The measured value was 3.8 G at the earliest stage of irradiation. A much larger width of about 7 G is reported for the trapped hydrogen atoms in pure ice³² at 4.2 K, while similar but somewhat larger values have been obtained in acidic ices at 77 K.³³ A small contribution from electron spin-spin interaction was inferred in the latter case. In the present model a different assumption for the value of ω_p^2 leads only to a change in the scale of τ_c by the ratio of two ω_p^2 values.

The result is shown in Figure 3 as a plot of τ_c against the reciprocal of temperature. In this treatment a nonadiabatic component of the line width is neglected.³⁴ This is justified at least with regard to the contribution from diffusional motion, because τ_c^{-1} would be still fairly larger than the resonant frequency ω_0 , if half of the line width, which is the maximum contribution, is assumed to come from the nonadiabatic term. It is seen from Figure 3 that the narrowing in the sulfuric acid solution is dividable in two stages with different activation energies, namely, the one below -110°C with 3.8 ± 1.0 kcal/mol and the other above -110°C with 1.2 ± 0.4 kcal/mol. The higher activation energy of the former stage must be related to the traps formed by the sulfuric acid solute, while the activation energy above -110°C coincides within the errors with the one obtained in pure ice. The former value, 3.8 ± 1.0 kcal/mol, is somewhat smaller than the one, 5.79 ± 0.12 kcal/mol, obtained by Sprague and Schulte-Frohlinde⁵ from the measurement of the rate of disappearance of hydrogen atoms in sulfuric acid glass near the liquid nitrogen temperature, but they also suggested the presence of a shallower trap, about 4.1 kcal/mol deep, which is supposed to be occupied immediately after irradiation. The large difference in the temperature range and in the solute concentration may not be disregarded in this comparison, as in fact some change in the state of solvation of the solute is presumed.

Although one cannot tell whether the activation energy in pure ice, 1.2 kcal/mol, is involved in the primary jump process between nearest neighbor interstitial sites or is associated with an escape from a certain specific defect in the lattice, it must be the controlling factor of the diffusion of hydrogen atoms in pure ice. The line width below -110°C in pure ice is expected to vary much more slowly than in the sulfuric acid solution, and a large difference in τ_c values would be apparent in that temperature range. Fluornoy, Baum, and Siegel⁴ have measured the thermal decay of trapped hydrogen atoms in pure ice between 20 and 50 K. Although the activation energy could not easily be specified because of the complexity involved in the decay curves, they suggested activation energies of ~ 1 kcal/mol at 30 K and ~ 2.5 kcal/mol at 50 K. Thus the present result is at least not unreasonable. A simple linear extrapolation of the τ_c line of pure ice in Figure 3 toward lower temperatures predicts a significant change of τ_c at several tens of degree K, that is, τ_c changes from $\sim 3 \times 10^{-4}$ s at 40 K to $\sim 1 \times 10^3$ s at 20 K, if so extrapolated. This certainly corresponds

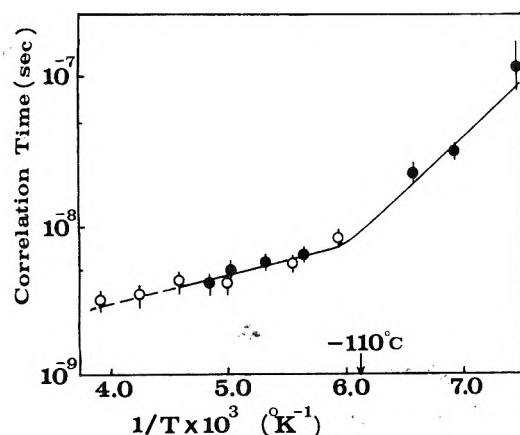


Figure 3. Correlation time vs. reciprocal temperature: ●, 0.5 M sulfuric acid solution; ○, pure ice.

to the observation by Fluornoy et al.⁴ that the diffusion is very slow below 20 K but that it is fairly rapid above 40 K.

The τ_c 's of an order of 10^{-9} s, as found in the both cases above -110°C , are considered to be several hundred times longer than the one expected in the liquid phase, and this could have some consequence on the development of polarization.

C. Polarization Effect. Before describing further about the polarization phenomenon, mention should be made of other radicals present in the spectrum in relation to the steady state character of the system during irradiation. In the case of the sulfuric acid solution, SO_4^- radicals, which supposedly caused the serious dose effect at low temperatures, decay so rapidly above -130°C that they are hardly seen in the spectrum at temperatures where the polarization is observed. An asymmetric singlet persists in the spectrum, which is probably another type of more stable sulfuroxy radical, but its yield is very small. Next, in hydrochloric acid solution a complex spectrum, mostly of Cl_2^- , is observed at low temperatures around 77 K, but only a very small part of this remains under irradiation above -130°C . Unlike hydrogen atoms these radicals in the acidic solutions did not show narrowing of the line width. In pure ice no clear signal was seen in the central part of the spectrum above -110°C . This is not surprising because the hydroxyl or the hydroperoxy radical may still have a broad line width and yet must be reacting quickly.¹⁷ Fortunately, in none of these three cases have the signal from hydrogen atoms experienced a large change during the course of irradiation above -110°C . There was certainly some dose effect that caused the scattering of the data to an extent of $\pm 20\%$, but it was much less prominent than in the low temperature range below -140°C . Thus these systems may be regarded to be in an approximate steady state during irradiation. Of course, this does not mean that radiolytic products in these systems are stable enough against primary radicals. In pure ice it was shown by Ghormley and Stewart³⁵ that the yield of radiolytic products at -78°C saturates to constants quickly around 0.1 Mrad. In this case rapid back reactions serve to establish the steady state condition with the progress of irradiation.

Dose rate is an important variable in the present method of continuous irradiation. In Figure 4a are shown the results of the dose rate dependence of line intensities in 0.5 M sulfuric acid solution at -77°C and in pure ice at -74°C . Unlike the result by Neta and Fessenden in the liquid phase,⁷ the two lines of hydrogen atoms have different dependence on the dose

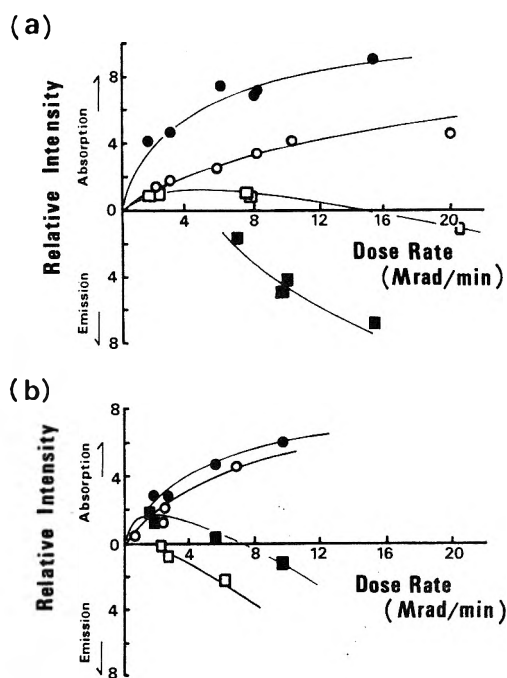


Figure 4. Dose rate dependence of the hydrogen atom signal intensity: (a) 0.5 M sulfuric acid solution at -77°C (●, high-field line; ■, low-field line), and pure ice at -74°C (○, high-field line; □, low-field line); (b) 0.1 M sulfuric acid solution at -76°C (●, high-field line, ■, low-field line), and 0.5 M sodium sulfate solution at -73°C (○, high-field line; □, low-field line). See footnote 24.

rate. The low-field line in pure ice changes from an absorption line to an emission line at about 14 Mrad/min. This behavior is quite natural when one considers the effect of spin-lattice relaxation and the fact that the interval between polarizing collisions becomes smaller with increase in the dose rate. A similar trend is seen in the case of sulfuric acid solution. The dependence of the high-field line in these systems is not simple either, and this is partly because of the complex reaction schemes involved. The degree of polarization cannot easily be specified because of unequal polarization of the two lines (see below), but in view of the small polarization at low dose rates it is at most several times the polarization in thermal equilibrium.

There is a considerable difference between 0.5 M sulfuric acid solution and pure ice, especially in the relative intensity of the two lines. The possibility of the reaction of electrons with acidic protons was at first presumed, for it could greatly increase the yield of hydrogen atoms in acidic ice. However, the difference was much less pronounced when 0.1 M sulfuric acid solution was used, and sodium sulfate solution (0.5 M) showed emissive low field lines comparable to the case of 0.5 M sulfuric acid solution (Figure 4b). These suggest that the reaction between acidic protons and electrons is not important even at these higher temperatures. The G value, the 100-eV yield, of hydrogen atom formation in pure ice is reported to be 0.9.³⁶ The additional increase in the G value in sulfuric acid solution, contributed by the reaction of electrons with the nondissociated or partially dissociated form of the acid, is estimated to be 0.2 in 0.5 M solution,¹⁵ and therefore is a minor contribution compared to the hydrogen atom formation in the solvent ice. The above-mentioned difference between the two cases should be ascribed partly to the presence of sulfate ion, which is presumably acting as a hydroxyl radical scavenger.

As noted in the preliminary report,¹⁴ 1 M hydrochloric acid

solution presents a remarkable example of polarization. In Figure 5 the emission line of the low-field is much stronger than the high-field line at the highest dose rate. Measurement at a different temperature in this system showed the same effect. A similar trend may be involved in the 0.5 M sulfuric acid solution at high dose rates, where the two lines have about the same intensity in spite of the presumed low degree of polarization. Besides, it was noted that the low-field line of pure ice becomes more emissive and becomes about 1.5 times more intense than the high-field line when a small amount of methanol, 0.2 M, is added as a radical scavenger. (The experiments with these additives are not detailed here in order to avoid complications.)

It has been reported that the two lines of hydrogen atoms appear always in about the same intensity in the liquid phase experiments.⁷⁻⁹ Obviously such unequal polarization is not expected from the radical pair theory that postulates only the mixing of a singlet configuration and a triplet with zero z component in the pair, the $S-T_0$ mixing. A simple explanation is possible if it is assumed that the high-field line has a shorter spin-lattice relaxation time, T_1 , than the other. Cross relaxation with other radicals is a possible cause for such field dependent relaxation times. However, there is no noticeable overlap of other signals with either hydrogen atom line, and moreover, the contrary trend observed at 77 K disqualifies the above hypothesis. The high-field line in the hydrochloric acid solution was found to be slightly more easily power saturated at 77 K than the low-field line. A similar effect has been reported in both sulfuric acid glass³⁷ at 77 K and in pure ice at 4.2 K.³⁸ These are presumably because of the presence of a small cross relaxation in the low-field line.³⁹

D. Discussion on the Polarization Effect. The appearance of polarized hydrogen atom signals above -110°C is not by itself a surprising result if one thinks of a possible difference in the temperature dependence of the spin-lattice relaxation and the polarization effect. It is, however, very difficult at this moment to give a clear explanation about the observed results. A serious difficulty is that the polarization of the high-field line is quite uncertain. It seems positive that in the liquid phase the high-field line is polarized in enhanced absorption to the same extent as the low-field line is polarized in emission.⁸ However, the observed unequal polarization of the two lines does not allow one to postulate such a simple relationship. The discussion here is concentrated upon the consideration about the possible consequence of the relatively slow diffusional motion of hydrogen atoms on the polarization in solid ice, especially on the difference of the polarization in the two lines.

The radical pair theory was originally proposed by Kaptein and Oosterhoff¹⁹ and by Closs and Closs.²⁰ Adrian¹² has made an important modification by introducing a reencounter process in the interaction of a pair. Recently a rigorous calculation of this problem with the stochastic-Liouville method was carried out by Pedersen and Freed⁴⁰ and also by Evans, Fleming, and Lawler.⁴¹ In these theories the mixing of a singlet S and a triplet T_0 configuration, induced by the difference in the magnetic interaction in the pair, was supposed to produce the polarization. On the other hand, Atkins and his co-workers observed a totally emissive ESR spectrum of a ketyl radical formed via an excited triplet precursor, and proposed the mixing of S with $T_{\pm 1}$ configurations.⁴² The off-diagonal element of the hyperfine interaction is a possible source of this mixing. The $S-T_{\pm 1}$ mixing has often been neglected under the simplification of the strong field approximation, but the hyperfine coupling energy of a hydrogen atom is as large as about

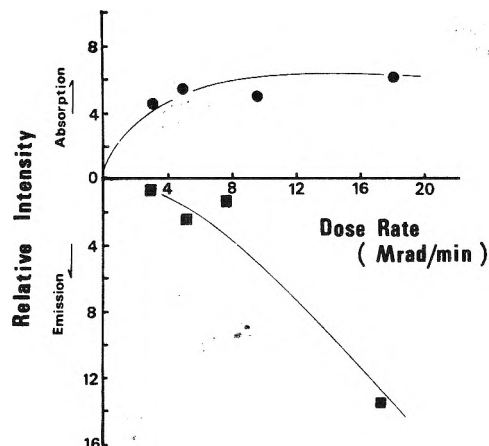


Figure 5. Dose rate dependence of the hydrogen atom signal intensity in 1 M hydrochloric acid solution at -78°C : \bullet , high-field line; \blacksquare , low-field line. See footnote 24.

one-sixth of the X-band microwave frequency. This $S-T_{\pm 1}$ mixing could cause a difference in the polarization of the two hyperfine lines. Fessenden^{8,13} treated his results phenomenologically on the base of the hypothesis of adiabatic recombination and separation of a radical pair.⁴³ It is worthwhile to note that if the $S-T_{\pm 1}$ mixing terms are included in the consideration of the adiabatic levels, the reaction paths along J , the exchange interaction, are thereby completely altered. However, in view of the rapidly changing nature of the exchange energy (see below) it seems highly improbable that the adiabaticity is retained during the passage through the small J part of the reaction paths where all the levels lie in close proximity.

Let us consider the time evolution of the wave function that describes the state of a pair of interacting hydrogen atoms, and let us assume that the diffusion of a hydrogen atom is as slow as to require time of $10^{-10} \sim 10^{-9}$ s to jump into a neighboring interstitial site. The exchange energy J between two hydrogen atoms at a large separation is expressed in terms of the distance R by $J = -0.821R^{5/2} \exp(-2R)$ in the atomic unit according to Herring and Flicker.⁴⁴ The lattice constants of hexagonal ice are 4.5 Å in a , b axis and 7.1 Å in c axis. It is readily seen that J is much larger than the magnetic interactions when the two hydrogen atoms are in the same interstitial site and that J decreases so rapidly within the nearest neighbor site⁴⁵ that J becomes much smaller than the latter at the distance of the second neighbor site. Clearly the development of polarization is possible only at the second stage of separation where one of the pair stays in the nearest neighbor site. The reencounter process, namely, a long excursion of one of the pair, is not important in this slow diffusion model because of the long time interval between the first and the second encounter. As we are considering a random encounter of hydrogen atoms, the diminution of the singlet component of the wave function by recombination reaction must take place at the first stage of separation for any polarization to be effected.

Both the $S-T_0$ and the $S-T_{\pm 1}$ mixing must be operating at the second stage. In order to compare these two types of mixing let us cite here the results on the development of polarization obtained by solving the time-dependent Schrödinger equation with sudden approximation, i.e., with an assumption that J changes suddenly to a constant comparable to the magnetic interactions, making minor modifications relevant to the present problem. For simplicity the pair is

assumed to be a triplet initially, and all 12 triplet sublevels with different electron and nuclear configuration are given the same amplitude of unity at time zero, i.e.

$$|C_{T_{-1}^{\alpha n \beta n}}(0)|^2 = |C_{T_1^{\alpha n \beta n}}(0)|^2 = |C_{T_0^{\alpha n \beta n}}(0)|^2 = \dots = 1$$

This initial condition leads to the final population of six spins into each energy level of an isolated hydrogen atom in the case of no polarization effect. When we first neglect the mixing of $T_{\pm 1}$ configurations, the contribution from the S- T_0 mixing is given in the form of eq 3 for the polarization of the low-field line¹⁹

$$P_{ST_0^{\beta n}}(t) = 2|C_s^{\beta n \alpha n}(t)C_{T_0^{\beta n \alpha n}}(t) + C_s^{\beta n \alpha n^*}(t)C_{T_0^{\beta n \alpha n}}(t)|^2 = 4aJ(a^2 + J^2)^{-1} \sin^2 \{(a^2 + J^2)^{1/2}t\} \quad (3)$$

where the polarization at time t , $P_{ST_0^{\beta n}}(t)$, is defined as the difference in the resultant population in the two β_n levels, and a is half of the hyperfine coupling constant and J is the exchange energy both in the unit of \hbar , the Planck constant. The first equation is added just to show how this polarization is expressed in terms of the coefficients of the S and T_0 components of the wave function (the asterisk denotes a complex conjugate). The negative J gives emissive polarization to the low-field line. The polarization of the high-field line is just opposite in the sign. On the other hand, Adrian has shown in a simplified calculation that the S- $T_{\pm 1}$ mixing induces the same amount of polarization in the both lines given in^{46,47}

$$P_{ST_{\pm 1}^{\alpha n}} = P_{ST_{\pm 1}^{\beta n}} = \sum_{\text{nuclear configuration}} \{|C_{T_{+1}^{\alpha n \beta n}}(t)|^2 - |C_{T_{-1}^{\alpha n \beta n}}(t)|^2\} = (4a^2/\omega_+^2) \sin^2 \omega_+ t - (4a^2/\omega_-^2) \sin^2 \omega_- t$$

where

$$\omega_{\pm} = \{a^2 + (J \pm \frac{1}{2}g\beta_0 H_0)^2\}^{1/2} \quad (4)$$

Here, a and J are as used in eq 3 and $\frac{1}{2}g\beta_0 H_0$ is the electron Zeeman energy in the same units. The initial condition and the definition of polarization⁴⁷ are the same as used for eq 3. The S- T_{-1} process prevails over the S- T_{+1} process in the case of the negative J , resulting in a net emissive contribution to the both lines.

It is clear that the contribution from eq 4 is negligible compared to the other when the time t is very small, that is, when $1/t$ is much larger than the magnetic interactions a or $\frac{1}{2}g\beta_0 H_0$. The second stage of $10^{-10} \sim 10^{-9}$ s is fairly long in this respect, and a certain contribution from eq 4 can be expected even if the pair may not spend all the time having J comparable to the magnetic interactions at that stage.

In view of the rapid change of J within the distance of the nearest neighbor site⁴⁵ it will be more pertinent to assume that J is fluctuating with time. An important difference between the two types of mixing becomes apparent when one considers that the pair may sometimes experience large J during this second stage of separation. The polarization induced by the S- T_0 mixing will be quenched if the strong J interaction continues for a certain period of time that let $Jt \gg 1$. This is actually the "spin exchange interaction", and has been often noted in the treatment of the radical pair theory. It is because such an interaction gives occasion to a large change in the difference of the phase factors of C_s and C_{T_0} on which this S- T_0 polarization depends (eq 3). The contribution from the S- $T_{\pm 1}$ mixing process, on the other hand, will not be quenched, since it rests solely on the amplitude of the coefficients $C_{T_{-1}}$, C_{T_1} , as seen in eq 4. Clearly the

final polarization depends on how one postulates about the motional state of the pair at the second stage, but it is thus well expected that the low-field line may be more strongly polarized than the high-field line. It is to be added that this difference in the two types of mixing may also be important in the possible secondary effect of encounters on the steady state polarization of the whole system.

The discussions on the temperature dependence of the polarization and on the effect of the solutes should be deferred until reliable information is available concerning the spin-lattice relaxation time and the reaction kinetics in solid ice. The resolution of the problem of the secondary reactions will be necessary and it may require elaborate work, but we think that this system deserves further investigation.

Acknowledgment. We wish to express thanks to Professor K. Hasegawa, Mr. M. Onoue, and Mr. T. Kawanishi for their help in the experimental setup and for operating the accelerator. Part of the analysis was made at the Royal Institute of Technology, Stockholm, Sweden. One of the authors, H.S., is grateful to Professor B. Rånby of the Department of Polymer Technology for his hospitality and to Dr. T. Reitberger of the Department of Nuclear Chemistry for his help in the supplementary experiment. He is also indebted to the Japan Sweden Foundation for its support to him.

References and Notes

- (1) See for review, L. Kevan in "Radiation Chemistry of Aqueous Systems", G. Stein, Ed., Weizman Science Press of Israel, Jerusalem, 1968, p 21.
- (2) R. Livingston, H. Zeldes, and E. H. Taylor, *Phys. Rev.*, **94**, 725 (1954).
- (3) L. H. Piette, R. C. Rempel, H. E. Weaver, and J. M. Fluornoy, *J. Chem. Phys.*, **30**, 1623 (1959).
- (4) J. M. Fluornoy, L. H. Baum, and S. Siegel, *J. Chem. Phys.*, **36**, 2229 (1962).
- (5) E. D. Sprague and D. Schulte-Frohlinde, *J. Phys. Chem.*, **77**, 1222 (1973).
- (6) C. J. Ultee and C. R. Kepford, *J. Chem. Phys.*, **52**, 3462 (1970).
- (7) P. Neta, R. W. Fessenden, and R. H. Schuler, *J. Phys. Chem.*, **75**, 1654 (1971).
- (8) N. C. Verma and R. W. Fessenden, *J. Chem. Phys.*, **58**, 2501 (1973).
- (9) B. Smaller, E. C. Avery, and J. R. Remko, *J. Chem. Phys.*, **55**, 2414 (1971).
- (10) R. W. Fessenden and R. H. Schuler, *J. Chem. Phys.*, **39**, 2147 (1963).
- (11) See for review, P. W. Atkins and K. A. Mclauchlan in "Chemically Induced Magnetic Polarization", A. R. Lepley and G. L. Closs, Ed., Wiley, New York, N.Y., 1973, p 42.
- (12) F. J. Adrian, *J. Chem. Phys.*, **54**, 3918 (1971).
- (13) R. W. Fessenden, *J. Chem. Phys.*, **58**, 2489 (1973).
- (14) H. Shiraishi, H. Kadoi, Y. Katsumura, Y. Tabata, and K. Oshima, *J. Phys. Chem.*, **78**, 1336 (1974).
- (15) L. Kevan, P. N. Moorthy, and J. J. Weiss, *Nature (London)*, **199**, 689 (1963).
- (16) For example, D. M. Brown and F. S. Dainton, *Trans. Faraday Soc.*, **62**, 1139 (1966).
- (17) I. A. Taub and K. Eiben, *J. Chem. Phys.*, **49**, 2449 (1968).
- (18) G. Nilsson, H. Christensen, P. Pagsberg, and S. O. Nielsen, *J. Phys. Chem.*, **76**, 1000 (1972).
- (19) R. Kaptein and J. L. Oosterhoff, *Chem. Phys. Lett.*, **4**, 195 (1969).
- (20) G. L. Closs and L. E. Closs, *J. Am. Chem. Soc.*, **91**, 4549, 4550 (1969).
- (21) D. A. Hutchinson, S. K. Wong, J. P. Colpa, and J. K. S. Wan, *J. Chem. Phys.*, **57**, 3308 (1972).
- (22) H. Shiraishi, H. Kadoi, K. Hasegawa, Y. Tabata, and K. Oshima, *Bull. Chem. Soc. Jpn.*, **47**, 1400 (1974).
- (23) N. Tamura, Y. Oshima, K. Yotsumoto, and H. Sunaga, *Jpn. J. Appl. Phys.*, **9**, 1148 (1970).
- (24) It was estimated that about 3×10^{-8} M hydrogen atoms would give unit integrated intensity at -100 °C in case of no polarization effect. This scaling of the ordinate is retained for Figures 4a, 4b, and 5, but note that errors of $\pm 20\%$ should be taken into account in the comparison between different samples.
- (25) This decrease was much less pronounced when a thinner 3-mm diameter sample was used instead of a 4-mm sample.
- (26) S. A. Marshall, J. R. Gabriel, and R. A. Serway, *J. Chem. Phys.*, **45**, 192 (1966).
- (27) For example, see, A. Hoppel, D. B. Knoll, and W. B. Westphal, *J. Chem. Phys.*, **54**, 134 (1971).
- (28) K. Kume, *J. Phys. Soc. Jpn.*, **15**, 1493 (1960).
- (29) See, for example, S. Ogawa and R. W. Fessenden, *J. Chem. Phys.*, **41**, 994 (1964).

- (30) J. Helbert and L. Kevan, *J. Chem. Phys.*, **58**, 1205 (1973).
 (31) A. Abragam, "The Principles of Nuclear Magnetism". Clarendon Press, Oxford, 1961, p 439.
 (32) H. N. Rexford and W. Gordy, *Phys. Rev.*, **125**, 242 (1962).
 (33) J. Zimbrick and L. Kevan, *J. Chem. Phys.*, **47**, 5000 (1967).
 (34) The dipolar electron spin-spin interaction was also neglected because of the low concentration of the radicals.
 (35) J. A. Gormley and A. C. Stewart, *J. Am. Chem. Soc.*, **78**, 2934 (1956).
 (36) S. Siegel, J. M. Fluornoy, and L. H. Baum, *J. Chem. Phys.*, **36**, 2229 (1962). There have been discussions about this value. See ref 1.
 (37) J. Kroh, B. G. Green, and J. W. T. Spinks, *Can. J. Chem.*, **40**, 413 (1962).
 (38) H. S. Judeikis, J. M. Fluornoy, and S. Siegel, *J. Chem. Phys.*, **37**, 2272 (1962). See also ref 31.
 (39) Cross relaxation problems of hydrogen atoms with paramagnetic ions were examined by S. K. Wong and J. K. S. Wan, *J. Chem. Phys.*, **55**, 4940 (1971).
 (40) J. B. Pedersen and J. H. Freed, *J. Chem. Phys.*, **58**, 2746 (1973).
 (41) G. T. Evans, P. D. Fleming, III, and R. G. Lawler, *J. Chem. Phys.*, **58**, 2071 (1973).
 (42) P. W. Atkins, R. C. Gurd, K. A. Mclauchlan, and A. F. Simpson, *Chem. Phys. Lett.*, **8**, 55 (1971).
 (43) Polarization by adiabatic separation of a radical pair has been proposed by H. Fischer, *Chem. Phys. Lett.*, **4**, 611 (1970), and also by S. H. Glarum and J. H. Marshall, *J. Chem. Phys.*, **52**, 555 (1970).
 (44) C. Herring and M. Flicker, *Phys. Rev. A*, **134**, 362 (1964).
 (45) If a distance range from 2.25 to 6.75 Å is tentatively assumed for the two hydrogen atoms in the nearest neighbor sites, J changes from 4×10^{13} to 3×10^7 Hz within that range.
 (46) F. J. Adrian, *Chem. Phys. Lett.*, **10**, 70 (1971). In his simplified calculation the $S-T_{+1}$ and the $S-T_{-1}$ mixing are treated separately. Participation of T_0 states in the wave equation and contribution of the hyperfine interaction to the energy of $T_{\pm 1}$ states are deliberately neglected.
 (47) Rigorously speaking, polarization should be defined on the basis of exact eigenfunctions of an isolated hydrogen atom. According to a preliminary calculation which does not involve the simplifications made by Adrian in ref 46, the contribution of the $S-T_{\pm 1}$ mixings is rather different from eq 4, when the polarization is defined rigorously as mentioned above. However, the essential point in the discussion, concerning the effect strong J interaction, remains valid.

Kinetics of the Reaction of Atomic Oxygen with Phosphorus Trifluoride. Electron Spin Resonance Determination

Ira B. Goldberg* and Harry R. Crowe

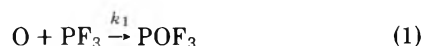
Science Center, Rockwell International, Thousand Oaks, California 91360 (Received April 1, 1976)

Publication costs assisted by Rockwell International

The reaction rate constant of the addition of atomic oxygen ($^3P_{0,1,2}$) to excess PF_3 was determined by fast flow ESR measurements to be $(2.28 \pm 0.06) \times 10^{11} \text{ cm}^3 \text{ mol}^{-1} \text{ s}^{-1}$ at 298 K at pressures between 0.6 and 2.9 Torr. The stoichiometry of the overall reaction of O and PF_3 was 1:1 indicating that the reaction proceeds by the mechanism $O + PF_3 = POF_3$.

Introduction

We report here studies of the kinetic behavior of the reaction of atomic oxygen with phosphorus trifluoride



using fast flow-electron spin resonance techniques. While considerable effort has been devoted to the synthesis and structure of phosphorus compounds,¹ little attention has been devoted to their fundamental kinetic behavior. A recent paper² reported the kinetics of the stepwise additions of atomic fluorine to PF_3



and



A qualitative study of the reaction of F_2 with various F-atom acceptors including PF_3 has also been reported.³

Other systems containing phosphorus have been qualitatively examined. Electric discharges have been used in the synthesis of POF_3 from O_2 and PF_3 ;¹ however, this has been shown to be a complex chemical system,⁴ partially due to the

fact that reactant pressures are quite high, allowing secondary processes including polymerization, to occur.

Reactions of PH_3 with H ,⁵ N ,⁶ and O ⁷ leads to elimination of H. In the latter case, the reaction rate constant, k_4



was calculated to be $3.1 \times 10^{10} \text{ cm}^3 \text{ mol}^{-1} \text{ s}^{-1}$.⁷ However, in presence of moisture, emission from PO is observed upon mixing the reactants. A brief report on the reactions of PCl_3 and PCl_5 with nitrogen also indicated the formation of PN .⁸

In this study, the possibility of abstraction of F as well as the fragmentation of POF_3 were also considered as possible reaction paths. It is not likely that O can abstract F from PF_3 since this reaction is endothermic by about 86 kcal/mol.⁹ There is a possibility of the elimination of F following the addition of O, because of the high exothermicity of the reaction; however, this does not appear to occur.

Experimental Section

The fast flow reactor was similar to the design of Westenberg and de Haas.¹⁰ The pressure along the reactor was monitored at five points using a capacitance manometer (MKS Corp., Baratron Model 170). Before entering the ESR

cavity, the reactor is uniformly tapered over a 3 cm length from 3.76 cm i.d. to 22.2 cm i.d. This result is a threefold increase in velocity in the narrow tube and thus decreases the concentration gradient for ESR detection. Flow rates of reactants and the diluent (He) were monitored using mass flow meters (Tylan Corp., Model FM300 and FM302) which were calibrated for each gas. These have the advantage of being independent of pressure and reproducible to within $\pm 0.5\%$, although they are limited to a narrow range of flow rates.

Oxygen was generated by passing N_2O through a microwave discharge (2.45 GHz, 130 W). No NO was detected downstream of the discharge. The maximum amount of nitrogen generated in any experiment was about 0.04 times that of the oxygen.

The ESR spectrometer was a modified Varian V-4502 instrument equipped with a Magnion 38-cm magnet with pole pieces tapered to a 20-cm face, a TE_{01n} wide access cavity, auxiliary homogeneity coils,¹¹ and a dedicated computer (Digital Equipment Corp., PDP 8m). Programs used to control the spectrometer and the interface are described in ref 12. Double integrations were carried out in floating point and replicate scans were typically reproducible to $\pm 2\%$. This technique will be discussed elsewhere. Since the peak-to-peak height of the derivative at a given pressure was found to be linear with concentration, the relative signal amplitudes were used as a measure of the relative concentrations in the kinetic determinations and titrations. However, the O-atom signal in the absence of PF₃ was recorded before and after each experiment to determine an accurate value of the initial oxygen concentration.

Results and Discussion

Titrations and Stoichiometry. The concentration of oxygen atoms was determined by ESR. Rather than using O₂ as a standard for concentration, where there is some uncertainty in the transition probability, the instrument sensitivity was calibrated by titrating F with H₂.¹³ F was generated by microwave discharge of CF₄. The standard deviation of eight measurements was 3% of the mean value. The fact that no F₂ was produced by wall recombination or in the discharge was verified by carrying out titrations in which H₂ was injected at different points in the reactor. Any F₂ produced would result in the consumption of H₂ without a decrease in the F-atom signal near the start of the titration.

The theory of calculating the absolute concentrations of atoms from ESR data is given by Westenberg and de Haas.^{14,15} The pressure, p , of an atom is related to the magnetic and instrumental parameters by

$$p = \frac{2kT}{\beta h \nu_0} \left\{ \frac{g_{\text{eff}} Z}{\sum [g_J^2 |J_J|^2 \exp(-E/kT)]} \right\} K_1 \cdot I \quad (5)$$

where K_1 is an instrumental constant, I is the double integral of the ESR signal, and the other variables utilize standard notation. The parameter in brackets in eq 5 is assigned the variable Q . Values of Q for atoms and diatomic molecules have been tabulated.¹⁵ The value of Q for the fluorine line utilized for the standardization was 1.582 (transition $M_J = -1/2$, $M_I = 1/2$ to $M_J = 1/2$, $M_I = 1/2$). All of the six lines due to O(³P₂) and O(³P₁) were utilized in these experiments. The value of Q in this case was 0.2048. Since the ESR detector was biased in the square-law region, the double integral was normalized to the square root of the incident power.

Titrations of O with PF₃ yielded a stoichiometry of (1.02 \pm 0.04):1. The nitrogen-atom concentration decreased to 0.7

times its initial value at the end point of the titration. At most, this would cause a 1% error in the stoichiometry.

Rate Constant Determinations. Rate constants determined at 298 K are summarized in Table I. Values for $C^0_{PF_3}/C^0_O$, where C^0 represents the initial concentrations, of 3.7 to 12 were used. The mean value of k_1 was 2.28×10^{11} cm³ mol⁻¹ s⁻¹ with a standard deviation of 0.06×10^{11} .

Figure 1 shows the time dependence of the relative concentrations for the third reaction listed in Table I, where the value of $C^0_{PF_3}/C^0_O$ is 3.70. The rate equation governing reaction 1 is

$$dC_O/dt = -k_1 C_O C_{PF_3} \quad (6)$$

Solving eq 6 gives the result

$$-k_1 t = \frac{1}{(C^0_{PF_3} - C^0_O)} \ln \left[\frac{C_O}{C^0_O} \frac{C^0_{PF_3}}{(C^0_{PF_3} - C^0_O + C_O)} \right] \quad (7)$$

where $C^0_{PF_3} - C^0_O + C_O$ is equal to C_{PF_3} . For the reaction to be pseudo-first order in the time zone during which the reaction is monitored, the value of C_{PF_3} must remain approximately constant. This is true if $C^0_{PF_3}$ were in large excess at the start of the reaction or if $C^0_{PF_3}$ were greater than C^0_O and the reaction was allowed to proceed to the point where $C_{PF_3} \gg C_O$. It is advantageous to monitor as much of the reaction as possible.

In Figure 1, $\ln(C_O/C^0_O)$ and $\ln\{(C_O/C^0_O)(C^0_{PF_3}/C_{PF_3})\}$ are plotted against the time of the reaction. The initial time, $t = 0$, of the reaction is arbitrary and was extrapolated from the upper line. As the reaction progresses, the ratio $C^0_{PF_3}/C_{PF_3}$ approaches a constant value, and slopes of both curves in Figure 1 become parallel as indicated by the broken line. The TE_{01n} cavity has a zone of detection of about 6 cm, however, only the central 3.4 cm is responsible for at least 82% of the signal. Since the velocity at the cavity is about three times greater than in the larger diameter tube where the reaction is monitored, the time zone of the reaction within the cavity is 0.5 ms. During this time, the change in the PF₃ concentration is small. Westenberg and de Haas¹⁶ have shown that for pseudo-first-order reaction, the ESR response corresponds to the atom concentration at some arbitrary fixed point within the zone of the cavity. In the reactions studied here, the PF₃ concentration can be considered constant over the length of the cavity. This treatment of the data is similar in principle to that used by Takacs and Glass.¹⁷

The diffusion coefficient of O in He has been measured at 1 atm and 280 K. Assuming ideal gas behavior, the diffusion coefficients corrected to 0.6 and 2 Torr are 1300 and 390 cm²/s, respectively. The time required to establish a uniform radial concentration is in the order of r^2/D , where D is the diffusion coefficient and r is the tube radius. At 2 Torr, this time is about 7 ms, while at 0.6 Torr it is 2.7 ms. At 0.6 Torr this time is small in comparison to the reaction time, while at 2 Torr, it is $1/4$ of the reaction time utilized in the measurements. Previous experiments have shown that this is still adequate to obtain reasonable values of the rate constant.¹⁸

Reaction Path. Reaction 1 is 130 ± 3 kcal exothermic⁹ so that it is possible that a reaction subsequent to the addition of oxygen could be



The energy of the PF bond in POF₃ is not known. In PF₅, the dissociation energy is about 95 kcal, while in PF₃ it is 139 ± 15 kcal.⁹ The P-F bonds in POF₃ and PF₃ are predominantly through sp³ hybridization. However, the PF bond distance in POF₃ is considerably shorter and less distorted than in PF₃.⁹

TABLE I: Summary of Measurements of the Rate Constant of $O + PF_3 = POF_3$ at 298 K

$C^0_O \times 10^{10}$, $m\text{ cm}^{-3}$	$C^0_{PF_3} \times 10^{10}$, $m\text{ cm}^{-3}$	P , Torr	$\bar{v} \times 10^{-3}$ cm/s	$k \times 10^{-11}$ $\text{cm}^3 \text{ mol}^{-1} \text{ s}^{-1}$
0.357	2.27	0.598	2.49	2.23
0.362	3.85	0.594	2.51	2.22
0.350	1.30	0.606	2.45	2.26
0.179	1.78	0.598	2.48	2.33
0.214	1.22	1.06	3.12	2.37
0.211	1.91	1.05	3.14	2.26
0.227	2.76	1.05	3.15	2.29
0.268	2.14	2.00	4.00	2.21
0.257	1.14	2.00	4.00	2.24
0.370	2.55	2.01	4.01	2.34

$$A\bar{v}k = 2.28 \times 10^{11} \text{ cm}^3 \text{ mol}^{-1} \text{ s}^{-1}$$

$$\sigma = 0.06 \times 10^{11} \text{ cm}^3 \text{ mol}^{-1} \text{ s}^{-1}$$

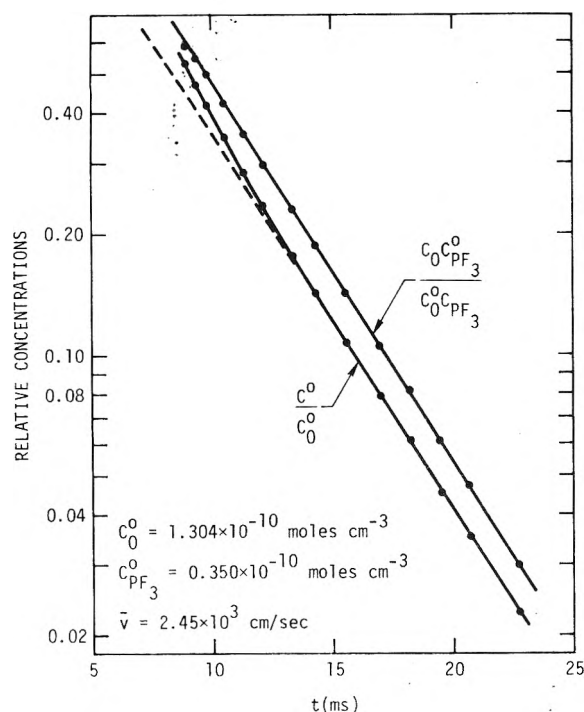


Figure 1. Plot of $\ln(C_O/C^0_O)$ and $\ln[(C_O/C^0_O)(C^0_{PF_3}/C_{PF_3})]$ vs. time for the reaction of $O + PF_3$.

As a result, the actual bond strength may be equal to or greater than that of PF_3 .

Since the value of k_2 is $8.6 \times 10^{12} \text{ cm}^3 \text{ mol}^{-1} \text{ s}^{-1}$, a search for F must be carried out at a large excess of O. Experimentally, sufficient PF_3 was added to the flow stream to decrease the O-atom signal to 96% of its initial value (partial pressure $\sim 2.0 \mu$). The magnetic field region in the vicinity of F-atom absorption was then investigated by extensive signal averaging at slow sweep rates. A line which was independent of the presence of PF_3 was observed which may have been due to O_2 or $N(^2D_{5/2})$.¹⁹ Reaction 8 is, therefore, not likely to contribute significantly to the overall mechanism.

In the presence of excess PF_3 no visible luminescence was observed from the reaction in a darkened room. The reaction was not monitored using a photomultiplier. The exothermicity of 130 kcal/mol is sufficient to produce radiation well into the uv region.

An analogy between the additions of O to PF_3 and to olefins^{20,21} can be made. In the series of olefins, ethylene to butene, the rate constant increases from 4.9×10^{11} to 1.4×10^{13}

$\text{cm}^3 \text{ mol}^{-1} \text{ s}^{-1}$ as the size of the molecule increases.²¹ The rate constant for reaction of O with C_2F_4 is $5.3 \times 10^{11} \text{ cm}^3 \text{ mol}^{-1} \text{ s}^{-1}$.²² These reactions are thought to proceed by the formation of an excited triplet state which cyclizes at low total pressures or fragments at high pressures.²⁰ POF_3 does not fragment; but it is also possible that the initial state may be described by a short-lived triplet in which an sp^3 hybrid bond is formed with O, and unpaired electrons occupy the d orbital of phosphorus and the p orbital of oxygen prior to formation of the P-O double bond. A determination of the activation energy would contribute to a better understanding of this mechanism.

Conclusions

The rate constant of the reaction $O + PF_3 \rightarrow POF_3$ was found to be $2.28 \times 10^{11} \text{ cm}^3 \text{ mol}^{-1} \text{ s}^{-1}$. This rate was independent of pressure between 0.6 and 2.0 Torr. No fragmentation into F atoms was detected nor was any visible luminescence observed.

Acknowledgment. The authors thank Drs. Donald Pilipovich, Robert Coombe, and A. T. Pritt for helpful discussions. Computer programs utilized in this work for data analysis an acquisition were developed under support of the Office of Naval Research.

References and Notes

- (1) R. Schmutzler, *Adv. Fluorine Chem.*, **5**, 31 (1965).
- (2) I. B. Goldberg, H. R. Crowe, and D. Pilipovich, *Chem. Phys. Lett.*, **33**, 347 (1975).
- (3) G. L. Schott, S. W. Rabideau, A. V. Nowak, and R. W. Getzinger, 4th Conference on Chemical and Molecular Lasers, Oct. 1974, St. Louis, Mo., p 17.
- (4) U. Wannagat and J. Rademachers, *Z. Anorg. Allg. Chem.*, **289**, 66 (1957).
- (5) H. Guenebaut and B. Pascat, *C. R. Acad. Sci.*, **256**, 677 (1963).
- (6) H. Guenebaut and B. Pascat, *C. R. Acad. Sci.*, **256**, 2850 (1963).
- (7) P. B. Davies and B. A. Thrush, *Proc. R. Soc. London, Ser. A*, **302**, 243 (1968), and references therein.
- (8) H. Guenebaut, B. Pascat, C. Couet, and L. Marsigny, *C. R. Acad. Sci.*, **257**, 135 (1963).
- (9) JANAF Thermochemical Tables, National Bureau of Standards Reference Data Series, Washington, D.C.
- (10) A. A. Westenberg and N. de Haas, *J. Chem. Phys.*, **50**, 707 (1969); **46**, 490 (1967).
- (11) I. B. Goldberg and H. R. Crowe, *J. Magn. Reson.*, **18**, 497 (1975).
- (12) I. B. Goldberg, H. R. Crowe, and R. S. Carpenter, *J. Magn. Reson.*, **18**, 84 (1975).
- (13) R. Foon and M. Kaufman, *Prog. React. Kinet.*, **8**, 81 (1975).
- (14) A. A. Westenberg and N. de Haas, *J. Chem. Phys.*, **40**, 3087 (1964).
- (15) A. A. Westenberg, *Prog. React. Kinet.*, **7**, pt. 1, 23 (1973).
- (16) A. A. Westenberg and N. de Haas, *J. Chem. Phys.*, **46**, 490 (1967).
- (17) G. A. Takacs and G. P. Glass, *J. Phys. Chem.*, **77**, 1060 (1973).
- (18) I. B. Goldberg and G. R. Schneider, *J. Chem. Phys.*, **65**, 147 (1976).
- (19) H. E. Radford and K. M. Evenson, *Phys. Rev.*, **168**, 70 (1968).
- (20) R. J. Cvetanovic, *Adv. Photochem.*, **1**, 115 (1963).
- (21) J. T. Herron and R. E. Muie, *J. Phys. Chem. Ref. Data*, **2**, 467 (1973).
- (22) D. Saunders and J. Hecklin, *J. Am. Chem. Soc.*, **87**, 2088, 4062 (1965); *J. Phys. Chem.*, **70**, 1950 (1966).

Effect of Molecular Parameters on the Carbon-13 Spin-Lattice Relaxation Behavior in Alicyclic Compounds

Richard A. Komoroski^{1a} and George C. Levy^{*1b}

Department of Chemistry, Florida State University, Tallahassee, Florida 32306 (Received February 23, 1976)

Publication costs assisted by the National Science Foundation

The effect of molecular weight, viscosity, and functional group on the rate and anisotropy of molecular rotation in neat liquids has been studied for three homologous series of compounds: the cycloalkanols, their methoxy derivatives, and the cycloalkanones. Carbon-13 spin-lattice relaxation times were used for this purpose. The average T_1 values generally decrease with increasing molecular weight in all three series. The overall rotation of the alcohols is considerably more anisotropic than in the methyl ethers for small ring sizes. Anisotropic motion generally becomes less pronounced in both series as ring size increases. The overall reorientation of all the cyclic ketones is essentially isotropic. The effect of functional group on the molecular rotation of the four- and six-membered rings was investigated. The microviscosity factor generally increases with increasing van der Waals volume of the functional group for the cyclohexyl derivatives. The ^{13}C spin relaxation behavior in the three homologous series is examined in terms of simple rotational diffusion and microviscosity theory. For the methyl ethers, a single microviscosity factor describes the rotational diffusion. For the cycloalkanols, the microviscosity factor decreases with increasing ring size.

Carbon-13 spin-lattice relaxation time (T_1) measurements have proven useful in the study of molecular rotational motions in organic molecular systems.² Considerable information on the rate and anisotropy of overall molecular tumbling can be obtained from T_1 's of individual carbons in relatively rigid frameworks.³ Relaxation measurements have also been used to probe detailed internal motions along aliphatic chains in a number of systems,⁴ providing insight into molecular aggregation and solvation. These results derive from the inverse relationship between the ^{13}C - ^1H dipolar relaxation time (under proton decoupled conditions) and the rotational correlation time observed for most organic molecules within the so-called extreme-narrowing region.

Recently, Grant and Werbelow^{5a,b} and Canet, Vold, and Vold^{5c} have discussed the importance and utility of cross-correlation terms for full interpretation of ^{13}C T_1 ^{5a,b} and T_2 ^{5c} data. One of these references showed that the effect of cross-correlation terms on ^{13}C spin-lattice relaxation is not completely negated by wide-band proton decoupling, a finding not anticipated by earlier work.² Deviations from behavior predicted from the simple theories² are expected to become significant in cases of CH_2 carbon relaxation, when two or more relaxation mechanisms are operative, or with molecules undergoing slow molecular reorientation (outside of extreme spectral narrowing).

While the advent of these new theoretical results⁵ places restrictions on the exact quantitative interpretation of the present data, no major changes in the interpretation of these results are expected. Indeed it is likely that systematic quantitative deviations in determined T_1 's are small and similar for all of these similar molecular systems.

Roberts and co-workers^{6a} have examined the effect of molecular weight on the ^{13}C T_1 's of some cycloalkanes. A detailed study of anisotropic molecular motion in a number of methylcycloalkanes has also appeared.^{6b} In the latter study,^{6b} ^{13}C T_1 data were used to calculate the three components of the rotational diffusion tensor.

In order to investigate the effect of molecular weight, viscosity, and functional group on the rate and anisotropy of

molecular rotation in neat liquids, we have examined the ^{13}C spin-lattice relaxation behavior in several homologous series of alicyclic compounds, viz., the cycloalkanols, their methoxy derivatives, and the cycloalkanones. A preliminary report on a number of these compounds has appeared.⁷ The effect of a number of substituents on the rotational motion of four- and six-membered rings is also investigated. Comparisons within and among the various series are made using the theory of rotational Brownian motion and microviscosity.

Experimental Section

Samples were obtained from commercial sources, except for the methyl ethers which were prepared by methylation of the alcohols, and the deuterated derivatives, which were prepared by exchange of the α protons in the ketones and subsequent reduction. Proton decoupled natural abundance ^{13}C Fourier transform NMR spectra were recorded at 67.9, 25.1, and 22.6 MHz on Bruker HX-270, Varian XL-100, and Bruker HFX-90 NMR spectrometers, respectively. Chemical shifts were measured with respect to 10% internal tetramethylsilane, except as noted. Carbon-13 spin-lattice relaxation times were measured at 25.1 MHz using the Freeman-Hill modification⁸ of the inversion recovery⁹ pulse sequence. At 67.9 MHz the majority of T_1 's were measured using the standard $[180^\circ - \tau - 90^\circ - T]_n$ inversion recovery pulse sequence.⁹ Some T_1 measurements at 67.9 MHz were carried out using the so-called fast inversion recovery (FIRFT) pulse sequence.¹⁰ Nuclear Overhauser enhancements were measured using a gated decoupling technique.¹¹ Measurements on the neat liquid samples at 67.9 MHz were carried out in 8-mm tubes, with acetone- d_6 for field/frequency locking contained in a 10-mm o.d. external annulus. Tubes of 12 mm o.d. were used at 25.1 MHz. Viscosities were measured using an Ostwald viscometer.

Results and Discussion

Chemical Shifts. Table I gives the ^{13}C chemical shifts (with respect to tetramethylsilane) for all resolved resonances in the ^{13}C spectra of most of the alicyclic compounds investigated

TABLE I: Carbon-13 Chemical Shifts in Some Cyclic Compounds^a

Compound	C-1	C-2	C-3	C-4	C-5	C-6	C-7	Me
Bromocyclobutane	41.81 (18.5)	35.84 (12.5)	19.20 (-4.1)					
Chlorocyclobutane	52.28 (29.0)	35.34 (12.0)	16.79 (-6.5)					
Cyclobutanecarboxylic acid	38.86 (15.6)	25.81 (2.5)	19.02 (-8.5)					
Cyclobutylamine·HCl ^b	45.44 (22.1)	27.04 (3.7)	14.78 (-8.5)					
Cyclobutanol	66.98 (43.7)	33.71 (10.4)	12.56 (-10.7)					
Cyclopentanol	73.48	35.48	23.70					
Cyclohexanol	69.80	35.78	24.68	26.20				
Cycloheptanol	72.34	37.78	23.32	28.65				
Cyclooctanol	71.59	34.73	23.24	27.96	25.70			
Cyclononanol ^c	72.01	33.80	21.86	27.36	25.06			
Cycloundecanol	70.83	35.13	23.26	26.82	26.50	26.32		
Cyclododecanol ^c	68.11	32.29	20.94	24.27 ^d	23.38 ^d	23.30	23.85	
Cyclotridecanol ^c	70.58	34.95	23.01	26.53 ^d	26.17 ^d	26.03 ^d	26.17	
Methoxycyclopentane	83.19	32.44	24.08					56.03
Methoxycyclohexane ^c	77.96	31.52	23.59	25.97				54.90
Methoxycycloheptane	81.41	33.91	23.40	29.06				55.64
Methoxycyclooctane	81.14	31.33	23.32	28.04	25.91			55.60
Methoxycyclododecane	78.76	28.64	20.90	25.43 ^d	23.54 ^d	23.54	25.00	55.76
Cyclobutanone	207.72	47.95	10.08					
Cyclopentanone	217.95	38.15	23.59					
Cyclohexanone	208.84	42.03	27.43	25.45				
Cycloheptanone	212.05	43.90	30.92 ^d	24.77 ^d				
Cyclooctanone	214.73	42.00	27.80 ^d	26.07 ^d	25.35			
Cyclononanone	217.26	43.61	27.11 ^d	25.24 ^d	24.48 ^d			
Cyclodecanone	211.22	41.96	25.42 ^d	25.24 ^d	23.69 ^d	25.60		
Cycloundecanone	210.94	41.78	26.46 ^d	25.49 ^d	24.66 ^d	22.76 ^d		
Cyclododecanone ^c	212.09	40.41	24.88 ^d	24.88 ^d	24.38 ^d	22.65 ^d	24.38 ^d	
Cyclotridecanone	209.14	41.78	26.89 ^d	26.32 ^d	26.14 ^d	24.99 ^d	23.48 ^d	

^a Run as the liquids at 35 °C with internal TMS, except as noted. Accuracy ± 0.05 ppm. Values in parentheses are the shift changes from cyclobutane, taken as 23.3 ppm. ^b 1 M in D₂O. Shifts reported vs. external TMS. ^c Approximately 10% solution in CCl₄, 10% TMS internal standard. ^d Assignments ambiguous.

in this paper. Peak assignments for the cyclic alcohols possessing five- to eight-membered rings have been given by Roberts et al.,¹² and have been extended by us to larger ring sizes and to the corresponding methyl ethers.⁷ However, the previous assignments¹² for carbons 4 and 5 of cyclooctanol have been reversed on the basis of observed integrated peak intensities. Assignments for a number of resonances in the ¹³C spectra of the cycloalkanones have also been given.^{13,14} The values reported here are in satisfactory agreement with those previously reported, except for the carbonyl carbons of cyclononanone and cyclododecanone.¹⁵

Replacement of the hydroxyl proton in the cycloalkanols with a methyl group results in a 8–11-ppm downfield shift change of C-1, with roughly a 3–4-ppm upfield shift change for C-2. Upon going from cyclododecanol to methoxycyclododecane, an approximately 1-ppm shift downfield is seen for C-7 and the resonance tentatively assigned to C-4. The methoxy carbon resonance in the cyclic ethers occurs at about 56 ppm, with the largest variations occurring for the 5- and 6-membered rings. Listed with the ¹³C shifts in some cyclobutyl derivatives are the shift changes (in parentheses) for the corresponding carbons relative to cyclobutane (taken as 23.3 ppm¹⁵). Rather large changes are seen for C-3 in these compounds, probably due to steric and electric field interactions in the puckered cyclobutyl ring.

Effect of Size on the Rate and Anisotropy of Molecular Rotation. In Tables II–IV are the ¹³C *T*₁ values for some cycloalkanols, cyclic methyl ethers, and cycloalkanones, respectively. As expected, the slower overall molecular reorientation which accompanies increasing ring size generally results in decreasing *T*₁ values for all three series of compounds. Similar dependences of average *T*₁ values on molec-

ular size have been observed for the cycloalkanes^{6a} and methyl-substituted cycloalkanes^{6b} when the contribution to *T*₁ from the spin–rotation (SR) relaxation mechanism is taken into account in the smallest ring sizes.^{2a} Spin–rotation contributes negligibly to the spin–lattice relaxation behavior of the carbons in the molecules listed in Tables II and III, as evidenced by the full NOE values of 3 for neat cyclobutanol and methoxycyclopentane, in which SR relaxation would most likely be operative.

The ¹³C *T*₁ values for neat cycloheptanol at 35 °C are somewhat longer than those of cyclohexanol, instead of between those for cyclohexanol and cyclooctanol, as might be expected on the basis of ring size and molecular weight. This behavior corresponds to the behavior of the viscosities among the neat cycloalkanols (see Table II). Cyclononanol and cyclododecanol (the latter of which is a solid at 35 °C) were both run at elevated temperatures. The *T*₁ values for cycloundecanol are such that the extreme narrowing condition is not fulfilled at 67.9 MHz. At the typical ¹³C resonances frequencies encountered with electromagnets, approximately 20% shorter *T*₁'s would be observed for cycloundecanol.

Theory predicts¹⁶ and it has been shown experimentally^{2d,16} that ¹³C *T*₁'s will be inversely proportional to the number, *N*, of attached hydrogens for rigid frameworks rotating isotropically in solution. Hence the ratio of a methine carbon *T*₁ to that of a methylene carbon will be 2:1 if the carbons are undergoing the same motional behavior. This is not the case for most of the cyclic alcohols and methyl ethers listed in Tables II and III. In several cases methine and methylene carbon *T*₁'s are roughly in the ratio 2 to 1, taking into account experimental errors. Deviation from this behavior can be attributed to anisotropic (overall or internal) motion of the

TABLE II: ^{13}C T_1 's in Some Cycloalkanols^a

Compound	C-1	C-2	C-3	C-4	C-5	C-6	C-7	η , cP	f_r
Cyclobutanol ^b	3.2	3.1	4.3					3.97	0.164
1 M in 85% CCl_4 -15% acetone- d_6	12.4	10.7	11.6						
0.2 M in 85% CCl_4 -15% acetone- d_6	21.8	13.9	12.7						
Cyclopentanol	2.5	4.1	3.3					5.97	0.118
Cyclohexanol	0.72	0.59	0.60	0.32				26.6	0.079
0.4 M in 85% CCl_4 -15% acetone- d_6	11.5	7.4	7.6	5.6				0.74	
Cycloheptanol	0.87	1.00	0.83	1.14				23.4	0.065
Cyclooctanol	0.32	0.28	0.24	0.35	0.24			62.2	0.059
Cyclononanol, 41 °C	0.40	0.26	0.25	0.26	0.24			110	
Cycloundecanol	0.20	0.12	0.13	0.14	0.14	0.14		~170	0.035 ^d
Cyclododecanol, 83 °C	0.81	0.48	0.55	0.62 ^c	0.53 ^c	0.53	0.50		
20% in CCl_4	0.80	0.50	0.50	0.56 ^c	0.57 ^c	0.50	0.51	1.42	
30% in CDCl_3	1.59	0.84	0.84	0.99 ^c	1.01 ^c	0.84	0.76	1.18	
40% in $\text{Me}_2\text{SO}-d_6$	0.70	0.41	0.52	0.51 ^c	0.53 ^c	0.53	0.50	4.79	
Cyclotridecanol, 1.5 M CDCl_3	2.45	1.59	1.55	1.61 ^c	1.74 ^c	1.73 ^c	1.60	0.96	
2,2,6,6-cyclohexanol- d_4 , 43 °C	3.30		2.31	1.18					
2,2,12,12-cyclododecanol- d_4 , 40 °C, 1.5 M in CDCl_3	3.48		1.81	2.09 ^c	1.82 ^c	1.94	1.82		

^aIn seconds. Estimated accuracy $\pm 10\%$. Relative accuracy is considerably better. Compounds were run as the neat liquids at 35 ± 2 °C except as noted. ^bAll carbons of cyclobutanol exhibited the full NOE of 3. ^cAssignments ambiguous, see Table I. ^dCalculated from the T_1 value of 0.17 s expected for C-1 at 22.63 MHz.

TABLE III: ^{13}C T_1 's in Some Cyclic Methyl Ethers^a

Compound	C-1	C-2	C-3	C-4	C-5	C-6	C-7	Me	η , cP	f_r
Methoxycyclopentane ^b	23.4	17.3	19.4					15.2	0.53	0.116
Methoxycyclohexane	13.4	8.2	8.4	7.4				11.6	0.91	0.105
Methoxycycloheptane	11.3	7.5	7.8	8.6				10.4	1.06	0.094
Methoxycyclooctane	7.7	4.6	5.1	5.0	4.4			9.4	1.62	0.081
Methoxycyclododecane	1.5	0.77	0.85	0.86 ^c	0.82 ^c	0.81	0.85	3.6	4.44	0.109

^aNeat, 35 ± 2 °C. Average of two separate runs. Estimated accuracy $\pm 10\%$. Relative accuracy is considerably better. ^bAll carbons exhibited the full NOE of 3 within experimental error. ^cAssignment ambiguous. See Table I.

TABLE IV: ^{13}C T_1 's in Some Cycloalkanones^a

Compound	C-2	C-3	C-4	C-5	C-6	C-7	η , cP	f_r
Cyclobutanone ^b	21.7	21.6					0.55	0.037 ^g
Cyclopentanone ^c	12.2	12.0					0.92	0.079
Cyclohexanone	8.1	8.0	7.6				1.82	0.052
Cycloheptanone ^d	8.7	7.7 ^f	7.7 ^f				2.45	0.031
Cyclooctanone ^e	4.2	4.2 ^f	4.2 ^f	4.2			3.84	0.037
Cyclononanone	3.3	3.3 ^f	3.4 ^f	3.2 ^f			7.23	0.023
Cyclodecanone	1.29	1.31 ^f	1.38 ^f	1.21 ^f	1.53			
Cycloundecanone	1.15	1.27 ^f	1.23 ^f	1.28 ^f	1.13 ^f		9.45	0.041
Cyclotridecanone	0.69	0.85 ^f	0.73 ^f	0.80 ^f	0.79 ^f	0.68 ^f	12.6	0.044

^aRun at 35 ± 2 °C as neat liquids, except as noted. Estimated accuracy $\pm 10\%$. Relative accuracy is considerably better. ^bNOE values 1.8 (C-2) and 2.0 (C-3) were found for this compound. ^cFull NOE values of 3 were found for the carbons of this compound. ^d40 °C. ^e46 °C. ^fAssignments ambiguous. See Table I. ^gCalculated from T_1^{DD} of 54 s for C-2.

molecules in solution (or may result in part from arguments as presented in ref 5).

For the cyclic alcohols larger than cyclobutanol the degree of motional anisotropy generally decreases with increasing size. The large T_1 differential observed between the C-2 or C-3 carbons and the C-4 carbon in cyclohexanol is probably due largely to favorable alignment of the 4-carbon C-H vectors with the principal axis of molecular reorientation. For cyclononanol and larger rings, little change is seen in the degree of motional anisotropy, as measured by the methylene-to-methine NT_1 ratio. Completely isotropic motion is apparently not obtained, even for cyclotridecanol.

Calculations¹⁷ utilizing a computer program designed to

calculate the principal components of the rotational diffusion tensor for anisotropic motion^{6b} have been carried out for neat cyclohexanol using the ^{13}C T_1 data in Table II. The calculations show a faster rotation ($\sim 1.8 \times 10^{10}$ radians/s) about the principal inertial axis (in the plane containing the OH group), with rotation about the remaining two axes ($\sim 0.6 \times 10^{10}$ radians/s) being roughly equivalent. Unfortunately, quantitative conclusions are clouded by the likelihood that, in strongly associated systems like neat alcohols, the rotational diffusion axes will not be aligned along the inertia axes.¹⁸ Moreover, such detailed calculations are less meaningful for small molecules, such as cyclohexanol, which contain a paucity of non-equivalent CH vectors. For the larger molecules studied in this

paper, the ^{13}C T_1 's indicate near isotropic rotation, obviating the need for detailed calculations of rotational anisotropy.

For neat cyclobutanol at 35 °C, the NT_1 values of C-2 and C-3 are roughly two and three times, respectively, that of C-1. Dilution to 1 M in 85% CCl_4 -15% acetone- d_6 not only results in a considerable lengthening of all T_1 's of cyclobutanol, but also causes a slight attenuation of the motional anisotropy. Dilution to 0.2 M results in an even greater leveling of NT_1 values across the ring. It is not known whether further dilution of cyclobutanol would result in even more isotropic rotational behavior. Dilution of neat cyclohexanol to 0.4 M in the same solvent system used for cyclobutanol also results in a substantial lessening of the observed motional anisotropy, as well as a lengthening of T_1 's.

Also given in Table II are the ^{13}C T_1 's for cyclododecanol in three different solvents. For a 20% solution in CCl_4 and a 40% solution in $\text{Me}_2\text{SO}-d_6$, the T_1 behavior is very close to that of neat cyclododecanol at 83 °C. For a 30% solution in CDCl_3 , the T_1 's are roughly twice that observed in the other two solutions. No measurable differences in motional anisotropy were observed among the three solutions. Solution viscosities do not correlate with the relative T_1 values in the different solvents.

A comparison of the data in Tables II and III shows that the T_1 value for each carbon in the neat methyl ether is considerably longer than the corresponding value in the neat alcohol at the same temperature. Formation of the methyl ether removes the considerable restriction to overall motion that occurs in the alcohols due to intermolecular association. The removal of hydrogen-bonding capability results in roughly an order of magnitude increase in T_1 . Moreover, the absence of strong intermolecular association (that occurs in the alcohols) also results in a lessening of the observed motional anisotropy for a given ring size. For the methyl ethers the lessening of motional anisotropy with increasing ring size is more gradual than for the cycloalkanes. The presence of a substituent group makes a smaller perturbation for the larger rings. However, even for methoxycyclododecane, NT_1 of some methylene carbons is consistently longer than for C-1.

Upon going from the alcohols to the methyl ethers, no significant changes occur in the pattern of NT_1 values for the methylene carbons in a given ring for $n = 6$ and above. For the five-membered ring, the NT_1 of C-2 is substantially longer than for C-3 in cyclopentanol, while for methoxycyclopentane T_1 of C-3 is slightly longer than for C-2. This behavior may be due to a substantial difference in the principal diffusion axes in the two cases, or may result from librational motions in the ring.

In the above discussion the assumption has been made that the predominant conformation(s) of the ring has not been altered significantly by introduction of the methyl group. It is possible that, in a given ring, the addition of the methyl group results in significant ring conformational changes.

The ratio of the methyl T_1 to that of a ring methylene or methine carbon T_1 increases as the size of the ring increases in the cyclic ethers. This behavior can be attributed to the higher relative contribution to $1/\tau_{\text{eff}}$ from internal spinning of the methyl group in the larger rings, compared to the contribution from overall anisotropic molecular reorientation. This is not the case for the methyl-substituted cycloalkanes with five- to eight-membered rings,^{6b} where calculations show that the methyl groups in these compounds are relaxed via the overall motion and do not undergo appreciable internal spinning on the time scale of anisotropic overall reorientation. The additional degree of freedom present for the methoxy

group in the cyclic ethers allows for effective rotational freedom of this moiety.

Unlike the first two series of compounds, molecular reorientation for all of the cycloalkanones is essentially isotropic. The presence of the carbonyl oxygen does not result in any measurable rotational anisotropy. Small variations across the ring are seen in some cases. For a given ring size, the average T_1 in the cycloalkanones is longer than that in the cycloalkanes, and approximately the same as that observed for the methyl ethers. It is interesting that the cycloalkanones, while being more viscous than the methyl ethers, exhibit less motional anisotropy. The T_1 values exhibited by the cycloalkanones are roughly one-half those observed for the cycloalkanes,^{6a} for a given ring size. Since the carbons in cyclopentanone exhibit the full NOE of 3, nondipolar mechanisms contribute negligibly to the relaxation behavior of this compound and the larger ones. NOE's of 1.8 (C-2) and 2.0 (C-3) were found for cyclobutanone, indicating the presence of a substantial contribution from a nondipolar (probably the spin-rotation) mechanism.

At this juncture we consider the possibility that internal motions or librations are contributing to the spin-relaxation behavior of the ring carbons in the alicyclic compounds listed in Tables II-IV. ^{13}C T_1 's have been used to monitor internal motions in the proline ring in some peptides¹⁹ and diketopiperazines.²⁰ Internal motion will contribute to the observed T_1 if the correlation time for the internal motion is comparable to or faster than that for overall rotation and if the internal motion or libration is of sufficient amplitude, i.e., experiences a sufficiently large angular displacement. Since the energy barriers between stable conformations of most intermediate sized rings are greater than 5 kcal mol⁻¹, it is not expected that pseudorotation or other conformational exchange processes will contribute significantly to observed T_1 behavior for those rings. The exceptions to this are the four-, five-, and seven-membered rings. It is possible that sufficiently fast internal motions are present in these latter rings to make a contribution to the observed T_1 of some or all carbons. It is also possible that small differences seen in T_1 across the larger rings, for example, carbon 4 of cyclooctanol and carbons 3-6 of cyclododecanol, may be primarily due to internal librational motions within energetically allowed conformations.

As previously pointed out, completely isotropic motion is apparently not obtained even in cyclotridecanol or methoxycyclododecane, particularly when the NT_1 value of the C-1 carbon is compared to those for the ring methylenes. This phenomenon may arise from a residual anisotropy of overall molecular reorientation, or may be due to conformational or librational motions in the ring that affect some C-H vectors more than others, or to both. However, there are possibilities that arise not from motional considerations, but rather from an uncertainty in the number and distance of hydrogens which can contribute to the relaxation behavior of a given carbon. In such a case, NT_1 values lose significance.

It is conceivable that a high concentration of spatially close nonbonded protons could result in small but significant contributions to the relaxation of protonated carbons in small organic molecules.^{6b} Another possibility is that the distance between C-1 and its directly bonded proton is shorter than the methylene C-H distance. The variation in C-H bond lengths as it affects ^{13}C relaxation rates has been touched upon by several authors.^{3a,21-23} Due to the inverse sixth power dependence of dipolar relaxation rates on distance, a 3-4% change in average bond length will result in a 19-25% change in T_1 . Differences in bond length are often associated with

differences in hybridization at the carbons in question. Unfortunately, there are very little data available²⁴ that are accurate enough to properly assess the importance of bond distance variations in motional studies based on ¹³C T_1 's. It is unlikely that variations in C–H bond lengths can be invoked in order to explain the small T_1 differences for the large alicyclic compounds considered in this study, since only aliphatic carbons are involved. In the strained rings, particularly the cyclobutyl derivatives (Table V), C–H bond distance variations may be appreciable.²⁵

Contributions to the spin–lattice relaxation behavior of a given carbon from nonbonded protons will depend on the number and distance of such protons, as well as the number of directly bonded protons. In some of the cyclic systems studied here, it is possible that, due to steric crowding, protons from carbons several bonds away may contribute to the relaxation of a given carbon. A simple calculation utilizing standard bond distances and angles show that an approximately 5% difference in the NT_1 values for a methine and methylene carbon in the cycloalkanols or methyl ethers would be expected, assuming isotropic reorientation and that only protons on nearest neighbor carbons are involved. This requires a relative accuracy of better than 3% in the measurement of the two T_1 values concerned. Given the inaccuracies involved in T_1 measurements,²⁶ this standard is difficult to achieve.

In an attempt to assess the contribution of neighboring protons to the relaxation of the methine carbon in cyclohexanol and cyclododecanol, derivatives were prepared in which the neighboring carbons (C-2 and C- ω) were fully deuterated. The T_1 's for neat cyclohexanol- d_4 and for 1.5 M cyclododecanol- d_4 in CDCl₃ are given in Table II. An inspection of the relative T_1 values in the two rings shows no consistent pattern which could be attributed to removal of the contribution of neighboring protons to the relaxation of C-1.

Anisotropic Motion in Some Cyclobutyl and Cyclohexyl Derivatives. In Table V are the ¹³C T_1 's for a number of cyclobutyl derivatives. For C-1 of bromocyclobutane, scalar relaxation with the attached bromine nucleus^{2a} may contribute substantially to the observed spin–lattice relaxation behavior. The value listed in Table V for C-1 of bromocyclobutane represents T_1^{DD} , the T_1 arising from ¹³C–¹H dipolar relaxation only. The T_1^{DD} was calculated from the observed T_1 of 13.2 s and the NOE value of 1.8 for C-1 (obtained from the relative integrated intensity of C-1 compared to C-2 and C-3, which were assumed to relax completely by the dipolar mechanism). The data in Table V reveal no consistent trend for motional anisotropy in these derivatives. For example, in neat cyclobutanol the T_1 for C-3 is substantially larger than for C-2, while in neat cyclobutane carboxylic acid the reverse is true. The motional anisotropy of the neat halogen derivatives is much less than for the neat alcohol or carboxylic acid. In fact, the behavior in the chloro and bromo compounds is comparable to that of dilute cyclobutanol in CCl₄ or of cyclobutylamine·HCl in D₂O. It may be that changing contributions from anisotropic overall reorientation and from libration of the cyclobutyl ring are responsible for the relative T_1 variations seen in the cyclobutyl derivatives.

For the cyclohexyl derivatives (Table VI) the NT_1 pattern is the same for all the compounds studied. That is, the NT_1 values of C-2 and C-3 are essentially equal to each other in every case, and are always longer than or approximately equal to NT_1 for either C-4 or C-1. Also, the NT_1 value of C-4 is for the most part equal to or slightly longer than for C-1. Of course, the absolute values of NT_1 vary among the cyclohexyl

TABLE V: ¹³C T_1 's in Some Cyclobutyl Derivatives^a

Compound	C-1	C-2	C-3
Cyclobutanol	3.2	3.2	4.3
Cyclobutanol 0.2 M in CCl ₄	21.8	13.9	12.7
Cyclobutylamine·HCl 1.0 M in D ₂ O, 50°C	18.3	11.4	13.9
Cyclobutanecarboxylic acid	3.6	4.8	2.8
Chlorocyclobutane	28.6	19.3	19.4
Bromocyclobutane	33 ^b	15.0	14.6

^aIn seconds for the neat liquids at 35 °C, except as noted. Estimated accuracies $\pm 10\%$; relative accuracy is considerably better.

^b T_1^{DD} only (see text).

derivatives, depending on functional group (see below). The consistency in the pattern of NT_1 values in the cyclohexyl derivatives suggests that anisotropic overall rotation is the major factor in determining the pattern across the ring.

Behavior of the Microviscosity Factor. It is interesting to explore how the ¹³C T_1 's for the three homologous series of compounds depend on macroscopic solution viscosity (η) within a given series. An analysis of the T_1 and viscosity data in Tables II–IV, using C-1 for the alcohols and ethers and C-2 for the ketones, reveals that the variation of $1/NT_1$ with η is approximately linear in each series. For the cycloalkanones and methyl ethers, the dependence of T_1 on η is roughly the same. For the cycloalkanols, a much larger change in η is necessary to produce a given change in T_1 .

In Figure 1 is a log–log plot of $1/T_1$ of the C-1 and methyl carbons of the methyl ethers vs. viscosity. The dependence of the methyl carbon $1/T_1$ is markedly less than for C-1 due to the additional degrees of internal motion present for this group. The good correlation between $1/T_1$ and macroscopic viscosity within this and the other two series most probably arises from the high degree of similarity of the molecules within a series.

The ¹³C T_1 for a protonated carbon under conditions of complete proton decoupling is related to the correlation time, τ_c , for overall molecular reorientation by the relation

$$1/NT_1 = \hbar^2 \gamma_C^2 \gamma_H^2 r_{CH}^{-6} \tau_c \quad (1)$$

where γ_H and γ_C are the magnetogyric ratios of ¹H and ¹³C, respectively, r_{CH} is the carbon–hydrogen bond distance, and N is the number of directly bonded hydrogens. Equation 1 applies for isotropic small-step rotational diffusion when the extreme narrowing condition [$(\gamma_C + \gamma_H)\tau_c \ll 1$] is satisfied.^{2a} The most commonly used model for a priori calculation of the rotational correlation time is a modified version of the hydrodynamic (Stokes–Einstein) model with “sticking” boundary conditions, given by

$$\tau_c = \eta V_m f_r / kT \quad (2)$$

Here η is the macroscopic viscosity of the liquid in poise, V_m is the molecular volume, k is the Boltzmann constant, and T is the absolute temperature. The quantity f_r is the microviscosity factor of Gierer and Wirtz,²⁷ and is predicted to have a value of 1/6 for pure liquids. The microviscosity factor has often been treated as essentially an “adjustable” parameter used to evaluate the applicability of the Stokes–Einstein model to the rotational motion of liquid molecules.²⁸

The molecular volume can be estimated from the density by assuming hexagonal close packing of “spherical” molecules. Hence

$$V_m = 0.74M_w/N_{0\rho} \quad (3)$$

TABLE VI: ^{13}C T_1 's in Some Cyclohexyl Derivatives^a

Compound	C-1	C-2	C-3	C-4	η , cP	f_r	V_w , ^b cm ³ /mol of substituent group
Cyclohexane	19.5				0.83	0.043	3.4 ^c
Cyclohexanone		8.1	8.0	7.6	1.82	0.052	6.7
Cyclohexanol	0.70	0.59	0.60	0.32	26.6	0.079	7.0
Cyclohexylamine	10.0	7.4	7.9	6.4	1.71	0.081	10.5
Methylcyclohexane	14.1	10.9	11.0	10.0	0.64	0.138	13.7
Methoxycyclohexane	13.4	8.2	8.4	7.4	0.91	0.105	17.4

^aIn seconds at 35 °C for the neat liquids. Estimated accuracy $\pm 10\%$. Relative accuracy is considerably better. ^b From ref 30. ^c From ref 29, converted to cm³/mol.

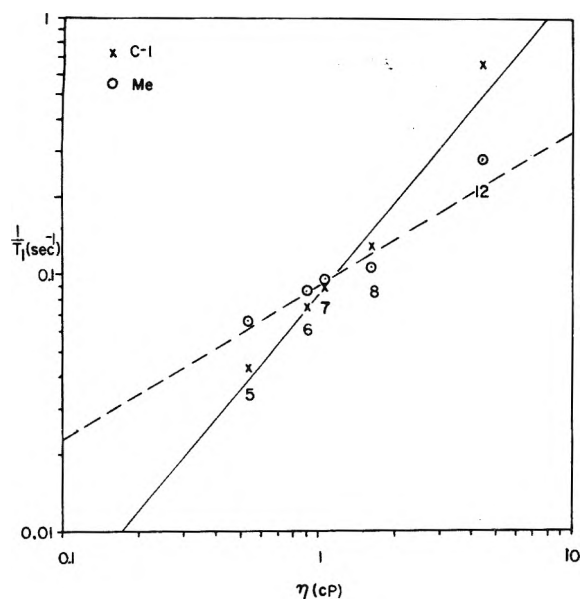


Figure 1. Log-log plot of $1/T_1$ (s^{-1}) vs. η (cP) for C-1 and the methyl carbon in a series of cyclic methyl ethers. The numbers indicate the ring size corresponding to the experimental points.

where N_0 is Avogadro's number, ρ is the density, and M_w is the molecular weight. The molecular volume can also be estimated as the van der Waals volume²⁹ calculated from atomic increments.³⁰ However, the use of atomic increments for largely folded molecules or for the cyclic molecules studied in this paper is hampered by the presence of a substantial percentage of "interior" volume, inaccessible to other molecules, and unaccounted for using atomic increments.²⁹ Hence we have used eq 3 for estimates of molecular volumes.

Combination of eq 1 to 3 yields an expression directly relating T_1 to basic physical parameters of the liquid: η , M_w , and ρ .³¹

$$\frac{1}{NT_1} = \frac{0.74\hbar^2\gamma_C^2\gamma_H^2}{r_{CH}^6kTN_0} f_r \left[\frac{\eta M_w}{\rho} \right] \quad (4)$$

It is interesting to quantitatively compare the behavior of the three homologous series of alicyclic compounds studied in this work with that predicted from eq 4. Such series are well suited to investigate the effect of size and molecular weight on the molecular motion in neat liquids, since the molecular interactions arising from the properties of the substituent group can be expected to be roughly constant throughout the series. The values of f_r corresponding to fulfillment of eq 4 for each compound studied are listed in Tables II-IV. The T_1 values of C-1 of the cycloalkanols and methyl ethers, and C-2 of the cycloalkanones were used in the calculation.

The microviscosity factors for the cyclic methyl ethers (Table III) fall in the range 0.081–0.116, i.e., intermediate between the predicted value of 1/6, and the value 1/12, which has been suggested on the basis of deuterium spin-lattice relaxation time measurements on a wide range of pure liquids.²⁸ The relatively narrow range of f_r values in Table III indicates that the rotational diffusion of the molecules studied in this series of similar compounds can be approximately described by eq 4 using a single value of f_r . Except in the case of methoxycyclododecane, the f_r values seem to decrease slightly with increasing size.

Considering the variation in size and shape among the molecules of this series, it is surprising that essentially the same microviscosity factor is obtained in each case. It is possible that the assumption of isotropic rotational diffusion, implicit in eq 4, masks a more complex behavior of f_r .

No consistent trend is seen for the f_r values of the cycloalkanones (Table IV). Most fall in the range 0.023–0.052, and hence are substantially lower than encountered for the cyclic methyl ethers. In view of the more compact structures of the cycloalkanones compared with the methyl ethers, the smaller f_r values might be expected. Of course, this compactness is also reflected in the essentially isotropic reorientation of the cycloalkanones.

A definitive argument is not available to explain the substantial variation that occurs in the microviscosity factors for the cyclic ketones. Intermolecular interactions are expected to be quite similar for all of these compounds, and thus the variations in f_r may reflect detailed differences in molecular shape. Inspection of space-filling models revealed no obvious correlations. Internal motions may also be a contributing factor.

The cycloalkanols (Table II) exhibit a behavior different from the other two classes of compounds studied in this paper. As the ring size increases, the microviscosity factor obtained from eq 4 falls from approximately 1/6 (cyclobutanol) to a value (0.035 for cycloundecanol) typical of the cycloalkanones. The rotational diffusion of the cycloalkanols cannot be described by a single value of f_r .

The behavior of the cycloalkanols can be explained qualitatively as follows. From eq 2 we can see that the molecular motion depends directly on both the microviscosity (ηf_r) and the molecular size (V_m). A dependence on molecular size also is present indirectly in the viscosity.³² In addition, reflected in the microviscosity is the "structure" of the liquid, or some measure of the strength of the intermolecular interactions.³² Structured liquids can be thought of as consisting of aggregates of various sizes that are long-lived compared to the rotational correlation time.³³ In this case the overall rotation of the molecule (with no internal rotations) is that of the aggregate.

For the cycloalkanols of small ring size, hydrogen-bonded

aggregates consisting of relatively large numbers of molecules can be formed, since there are more OH groups per unit volume and since steric restrictions due to ring size are minimal. Hence the liquid is relatively structured. As ring size increases, intermolecular association is not as favored. Fewer molecules are accommodated in a typical aggregate. This results in a "less structured" liquid, and hence a smaller microviscosity factor. A lessening of the motional anisotropy is also obtained. Of course, molecular shape may also be a contributing factor in the trend exhibited by f_r in Table II. However, such a trend was not seen for the other two series of compounds.

It is interesting to compare the values of f_r for the three series of compounds in Tables II–IV to values found previously for some neat liquids. In a recent report,²³ ^{13}C T_1 's were used to obtain values of the Kivelson parameter (κ) (essentially identical with the microviscosity factor f_r of Gierer and Wirtz) for the pure liquids norbornadiene, 2-methylenenorbornene, and α - and β -pinene at several temperatures.²³ The Kivelson parameter ranges from approximately 0.07 to 0.1 for these compounds. The parameter κ has been interpreted theoretically in terms of anisotropic intermolecular potential energy,³⁴ and gives the ratio of the intermolecular torques on the solute molecules to the intermolecular forces on the solvent molecules. For relatively symmetric molecules, weak intermolecular torques will result in small κ 's. Due to the intermolecular hydrogen bonding present in the neat cycloalkanols, their f_r values cannot be readily compared to those of non-hydrogen bonded liquids. The κ values reported²³ for the quasispherical hydrocarbon molecules listed above are quite similar to those observed here for the cyclic methyl ethers. However, the cycloalkanones (except cyclopentanone) exhibit f_r values which are one-half to one-third those of the hydrocarbons.

The above discussion has centered around the effect of molecular size on the rotational diffusion of molecules in neat liquids, keeping the substituent group, and hence the nature of the intermolecular interactions, the same. It is also informative to examine the variations with different substituents on a given ring.

Assink, DeZwaan, and Jonas³⁵ have correlated the microviscosity factor, calculated from deuterium T_1 's, with molecular shape in a series of monosubstituted benzenes. The molecular shape was represented by the van der Waals volume³⁰ of the substituent group. We have performed a similar analysis for the ^{13}C data of a series of cyclohexyl derivatives. In the last two columns of Table IV are listed the f_r values (calculated from C-1, except for cyclohexanone, where C-2 was used) and the van der Waals volumes (V_w)³⁰ of the substituent groups in a series of cyclohexyl derivatives. Comparison of the last two columns in Table VI indicates that the microviscosity factor, as determined from ^{13}C T_1 's, correlates reasonably well with substituent van der Waals volume and hence molecular shape. It is particularly surprising that the results for cyclohexanol fit the general trend of the cyclohexyl derivatives. It might be expected that this relatively structured liquid (as evidenced by the short T_1 's and highly anisotropic motion) would exhibit a microviscosity factor more like that of a much larger molecule.

The above discussion is based on a modified Stokes–Einstein model for rotational diffusion with "sticking" boundary conditions. Hu and Zwanzig³⁶ have treated the case of ellipsoids rotating in a viscous fluid with "slipping" boundary conditions. It was found that the ratio of the "slip" frictional coefficient to the "stick" frictional coefficient varies from unity to zero as the axial ratio of the ellipsoids varies from zero

(highly asymmetric) to unity (spherical). The "slip" model has been shown to be valid for a number of organic molecules using depolarized Rayleigh scattering and ^{13}C spin–lattice relaxation techniques.^{3h,37} As for the previous work^{3h,37} the alicyclic compounds studied here may be alternatively treated using a hydrodynamic model with slipping boundary conditions. We feel that the qualitative conclusions of the present paper would not be substantially altered by performing such a treatment.

Acknowledgments. We are grateful to the National Science Foundation and the Research Corporation for financial support of this research. The Bruker HX-270 spectrometer was purchased through a departmental grant from the National Science Foundation. We thank Dr. R. E. Echols for preparation of the methyl ethers and the deuterated derivatives. We also thank Linda Stork, James Michael Hewitt, Bob Schwartz, and Joann Sullivan for experimental assistance and Professors D. M. Grant and J. D. Roberts, and Dr. S. Berger for providing preliminary calculations for cyclohexanol.

References and Notes

- (1) (a) Present address: T. R. Evans Research Center, Diamond Shamrock Corp., Painesville, Ohio 44077. (b) Alfred P. Sloan Research Fellow, 1975–1977.
- (2) (a) J. R. Lyster and G. C. Levy, *Top. Carbon-13 NMR Spectrosc.*, **1** (1974); (b) G. C. Levy, *Acc. Chem. Res.*, **6**, 161 (1973); (c) E. Breitmaier, K. Spohn, and S. Berger, *Angew. Chem., Int. Ed., Engl.*, **14**, 144 (1975); (d) A. Allerhand, D. Doddrell, and R. Komoroski, *J. Chem. Phys.*, **55**, 189 (1971).
- (3) (a) G. C. Levy, J. D. Cargioli, and F. A. L. Anet, *J. Am. Chem. Soc.*, **95**, 1527 (1973); (b) G. C. Levy, *J. Chem. Soc., Chem. Commun.*, **47** (1972); (c) G. C. Levy, *J. Magn. Reson.*, **8**, 122 (1972); (d) D. M. Grant, R. J. Pugmire, E. P. Black, and K. A. Christensen, *J. Am. Chem. Soc.*, **98**, 8465 (1973); (e) G. C. Levy, D. M. White, and F. A. L. Anet, *J. Magn. Reson.*, **6**, 453 (1972); (f) K. T. Gillen, M. Schwartz, and J. H. Noggle, *Mol. Phys.*, **20**, 899 (1971); (g) T. K. Leipert, J. H. Noggle, and K. T. Gillen, *J. Magn. Reson.*, **13**, 158 (1974); (h) D. R. Bauer, G. R. Alms, J. I. Brauman, and R. Pecora, *J. Chem. Phys.*, **61**, 2255 (1974); (i) E. von Goldammer, H.-D. Ludemann, and A. Muller, *ibid.*, **60**, 4590 (1974); (j) L. J. Burnett and S. B. W. Roeder, *ibid.*, **60**, 2420 (1974); (k) E. von Goldammer, H.-D. Ludemann, and O. Roder, *Chem. Phys. Lett.*, **26**, 387 (1974); (l) R. Rowan and B. D. Sykes, *J. Am. Chem. Soc.*, **96**, 7000 (1974); (m) R. S. Becker, S. Berger, D. K. Dalling, D. M. Grant, and R. J. Pugmire, *ibid.*, **96**, 7008 (1974).
- (4) (a) G. C. Levy and G. L. Nelson, *J. Am. Chem. Soc.*, **94**, 4897 (1972); (b) G. C. Levy, *J. Chem. Soc., Chem. Commun.*, 768 (1972); (c) N. J. M. Birdsall, A. G. Lee, Y. K. Levine, J. C. Metcalfe, P. Partington, and G. C. K. Roberts, *ibid.*, 757 (1973); (d) D. Doddrell and A. Allerhand, *J. Am. Chem. Soc.*, **93**, 1558 (1971); (e) G. C. Levy, R. A. Komoroski, and J. A. Halstead, *ibid.*, **96**, 5456 (1974); (f) J. R. Lyster, Jr., H. M. McIntyre, and D. A. Torchia, *Macromolecules*, **7**, 11 (1974); (g) E. Williams, B. Sears, A. Allerhand, and E. H. Cordes, *J. Am. Chem. Soc.*, **95**, 4871 (1973); (h) R. T. Roberts and C. Chachaty, *Chem. Phys. Lett.*, **22**, 348 (1973); (i) C. Chachaty, Z. Wolkowski, F. Pirion, and G. Lukacs, *J. Chem. Soc., Chem. Commun.*, 951 (1973); (j) Y. K. Levine, N. J. M. Birdsall, A. G. Lee, and J. C. Metcalfe, *Biochemistry*, **11**, 1416 (1972); (k) G. C. Levy, *J. Am. Chem. Soc.*, **95**, 6117 (1973).
- (5) (a) L. G. Werbelow and D. M. Grant, *J. Chem. Phys.*, **63**, 4742 (1975); (b) *ibid.*, 544 (1975); (c) D. Canet, R. L. Vold, and R. R. Vold, *ibid.*, **64**, 900 (1976).
- (6) (a) S. Berger, F. R. Kreissl, and J. D. Roberts, Jr., *J. Am. Chem. Soc.*, **96**, 4348 (1974); (b) S. Berger, F. R. Kreissl, D. M. Grant, and J. D. Roberts, *ibid.*, **97**, 1805 (1975).
- (7) G. C. Levy, R. A. Komoroski, and R. E. Echols, *Org. Magn. Reson.*, **7**, 172 (1975).
- (8) R. Freeman and H. D. W. Hill, *J. Chem. Phys.*, **54**, 3367 (1971).
- (9) R. L. Vold, J. S. Waugh, M. P. Klein, and D. E. Phelps, *J. Chem. Phys.*, **48**, 3831 (1968).
- (10) D. Canet, G. C. Levy, and I. R. Peat, *J. Magn. Reson.*, **18**, 199 (1975).
- (11) R. Freeman, H. D. W. Hill, and R. Kaptein, *J. Magn. Reson.*, **7**, 327 (1972).
- (12) J. D. Roberts, F. J. Weigert, J. I. Kroschwitz, and H. J. Reich, *J. Am. Chem. Soc.*, **92**, 1338 (1970).
- (13) F. J. Weigert and J. D. Roberts, *J. Am. Chem. Soc.*, **92**, 1347 (1970).
- (14) J. B. Stothers and P. C. Lauterbur, *Can. J. Chem.*, **42**, 1563 (1964).
- (15) J. B. Stothers, "Carbon-13 NMR Spectroscopy," Academic Press, New York, N.Y., 1972.
- (16) K. F. Kuhlmann, D. M. Grant, and R. K. Harris, *J. Chem. Phys.*, **52**, 3439 (1970).
- (17) G. C. Levy, R. A. Komoroski, H. Pearson, J. D. Roberts, D. M. Grant, and S. Berger, unpublished results.
- (18) W. T. Huntress, *Adv. Magn. Reson.*, **4**, 1 (1970).
- (19) (a) R. Deslauriers and I. C. P. Smith, *Top. Carbon-13 NMR Spectrosc.*, **2**,

- chapter 1 (1975); (b) D. A. Torchia and J. R. Lyerla, Jr., *Biopolymers*, **13**, 97 (1974); (c) R. A. Komoroski, I. R. Peat, and G. C. Levy, *Biochem. Biophys. Res. Commun.*, **65**, 272 (1975).
- (20) R. Deslauriers, Z. Grzonka, K. Schaumburg, T. Shiba, and R. Walter, *J. Am. Chem. Soc.*, **97**, 5093 (1975).
- (21) A. Allerhand and R. A. Komoroski, *J. Am. Chem. Soc.*, **95**, 8228 (1973).
- (22) R. A. Komoroski, Ph.D. Thesis, Indiana University, Bloomington, Ind., 1973.
- (23) J. Grandjean and P. Laslo, *Mol. Phys.*, **30**, 413 (1975).
- (24) (a) "Tables of Interatomic Distances and Configuration in Molecules and Ions", Supplement, Special Publication No. 18, The Chemical Society, London, 1965; (b) "Molecular Structures and Dimensions", Vol. A1, O. Kennard et al., ed., International Union of Crystallography, 1972.
- (25) K. C. Cole and D. F. R. Gilson, *J. Chem. Phys.*, **60**, 1191 (1974).
- (26) G. C. Levy and I. R. Peat, *J. Magn. Reson.*, **18**, 500 (1975).
- (27) A. Gierer and K. Wirtz, *Z. Naturforsch. A*, **8**, 532 (1953).
- (28) J. A. Glasel, *J. Am. Chem. Soc.*, **91**, 4571 (1969).
- (29) J. T. Edwards, *J. Chem. Educ.*, **47**, 261 (1970).
- (30) A. Bondi, *J. Phys. Chem.*, **68**, 441 (1964).
- (31) J. H. Noggle and R. E. Schirmer, "The Nuclear Overhauser Effect", Academic Press, New York, N.Y., 1971, pp 26-31.
- (32) H. G. Hertz, *Ber. Bunsenges. Phys. Chem.*, **75**, 183 (1971).
- (33) H. G. Hertz and M. D. Zeidler, personal communication.
- (34) R. E. D. McClung and D. Kivelson, *J. Chem. Phys.*, **49**, 3380 (1968).
- (35) R. A. Assink, J. CeZwaan, and J. Jonas, *J. Chem. Phys.*, **56**, 4975 (1972).
- (36) C. M. Hu and R. Zwanzig, *J. Chem. Phys.*, **60**, 4354 (1974).
- (37) D. R. Bauer, J. I. Brauman, and R. Pecora, *J. Am. Chem. Soc.*, **96**, 6840 (1974).

Axial and Equatorial Bond Orientation around Phosphorus in 1,3,2-Dithiaphosphorinanes. Use of $J(^{31}\text{P}^1\text{H})$ and $J(^{31}\text{P}^{13}\text{C})$ for Stereochemical Assignments

J. Martln, J. B. Robert,* and C. Taleb

Laboratoire de Chimie Organique Physique, Département de Recherche Fondamentale, Centre d'Etudes Nucléaires de Grenoble, 85 X 38041, Grenoble Cedex, France (Received April 19, 1976)

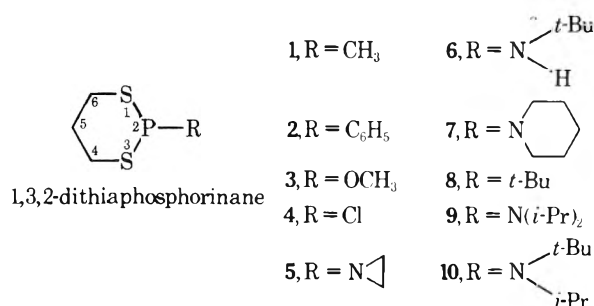
Publication costs assisted by C.E.A. France

The total NMR spectral analysis (^1H , ^{13}C , and ^{31}P) of ten 2-R-1,3,2-dithiaphosphorinanes bearing different R groups (CH₃, **1**; C₆H₅, **2**; OCH₃, **3**; Cl, **4**; c-C₂N, **5**; N(H)*t*Bu, **6**; c-C₅N, **7**; *t*-Bu, **8**; N(*i*Pr)₂, **9**; and N(*i*Pr)*t*Bu, **10**) have been analyzed. For compounds 1-5, the P-R bond is axial, and for compounds 9 and 10 it is equatorial. In the case of compound 6-8, there exists at room temperature a conformational equilibrium. The NMR coupling constants $^3J(\text{PH})$, $^4J(\text{PH})$, and $^4J(\text{PC})$ are highly sensitive to bond orientation around the phosphorus and can be used as a tool for stereochemical assignment.

Introduction

In 2-R-1,3,2-dioxaphosphorinanes, the preferred orientation of the P-R bond has been established for various R groups from dipole moment measurements,^{1a} NMR chemical shifts,^{1b} deductive reasoning concerning the stereochemical course of exchanging one R group for another, and x-ray work^{1c} on the corresponding four coordinated phosphorous compounds. Electronegative R groups (Cl, F, OCH₃, OC₆H₅) have a strongly preferred axial orientation. For R = alkyl, there exists an equilibrium which shows an increasing amount of the equatorial form as the bulk of the substituent R increases.¹⁻³ In the case of a trivalent nitrogen atom directly bonded to the phosphorus atom, the extracyclic P-N bond can adopt either an axial or an equatorial orientation, depending upon the nature of the groups attached to the nitrogen atom.⁴⁻⁷

In 2-R-1,3,2-dithiaphosphorinanes, the very few conformational studies support a chair conformation for the ring with axial orientation of the extracyclic P-R bond.⁸⁻¹⁰ We report here the full NMR spectral analysis (^1H , ^{13}C , ^{31}P) of several 2-R-1,3,2-dithiaphosphorinanes (1-10) in which the ring carbon atoms bear only hydrogen atoms, thus obtaining as much stereochemical information as possible from the NMR data. Depending upon the nature of the R group, the P-R bond is shown to adopt an axial or an equatorial orientation.



NMR Spectral Analysis

Proton NMR spectra of compounds 1-10 were recorded at 100 and 250 MHz. They display similar multiplets for the ring protons representing AA'BB'CDX patterns (X phosphorus). The spectral analyses are considerably more difficult than those of the corresponding 1,3,2-dioxaphosphorinanes due to the smaller low field shift induced by a sulfur atom as compared to that induced by an oxygen atom. ^{31}P decoupled spectra were recorded in order to obtain simpler spectra from which good approximate values for the chemical shifts and coupling constants could be extracted. The final parameters have been obtained using the iterative NMR program LAOCOON 3 (Figure 1). The NMR data (^1H , ^{13}C , and ^{31}P) are presented in Tables I (^1H) and II (^{13}C , ^{31}P).

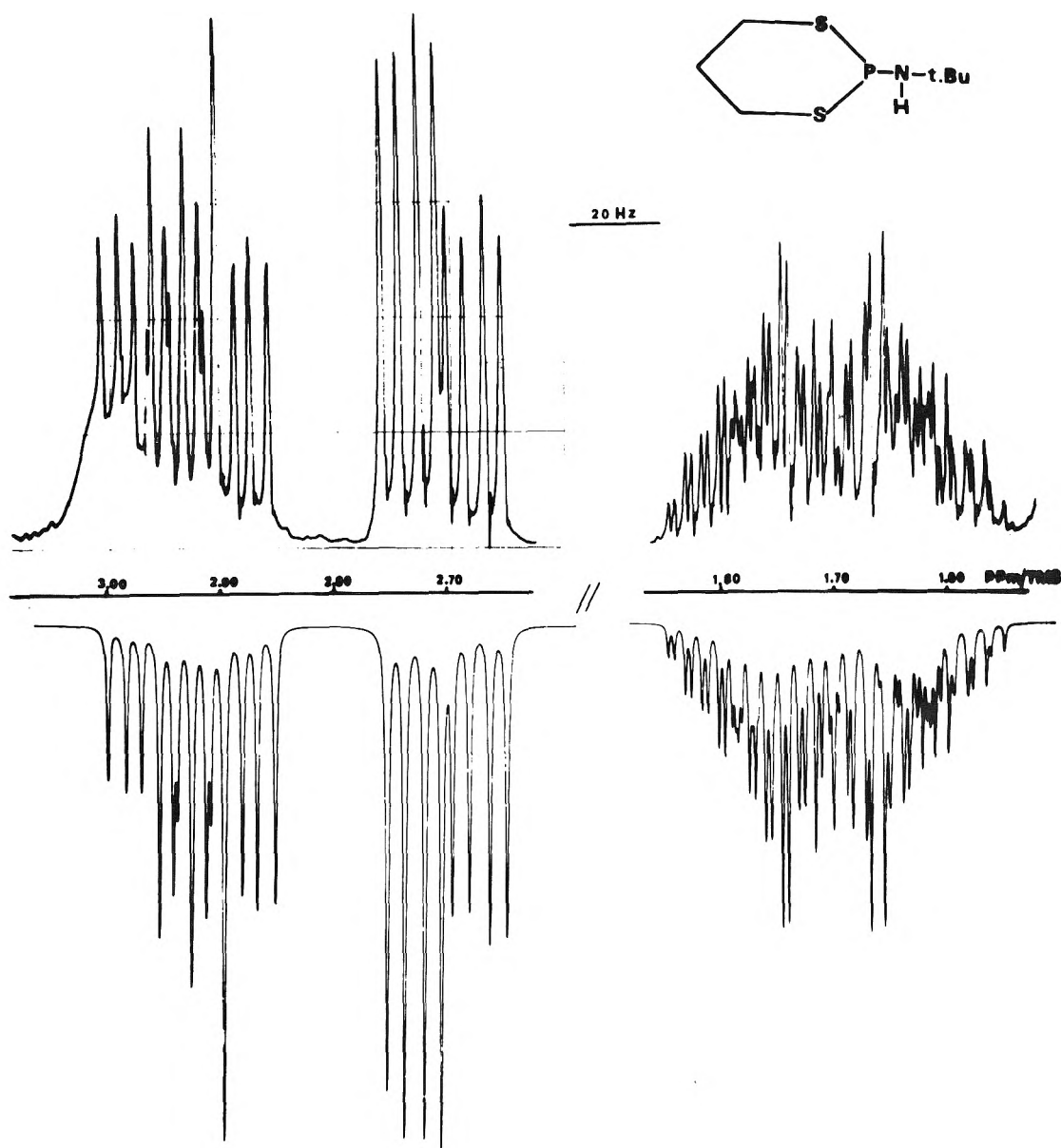


Figure 1. Observed and calculated proton NMR spectrum (250 MHz) of 2-*tert*-butylamino-1,3,2-dithiaphosphorinane (6).

Discussion of the Results

The NMR results concerning compounds 1–5 are quite comparable and are characterized by the following main features:

(i) A large ${}^3J(\text{H}_{4a}\text{H}_{5a})$ value of about 12 Hz, indicative of axial–axial coupling, which allows the assignment of axial and equatorial protons on C_4 , C_6 , and C_5 . All of the ${}^3J(\text{HH})$ values are close to the ones measured on 2-phenyl-1,3-dithiane¹⁰ which shows in the solid state a somewhat flattened chair conformation with the phenyl group in the equatorial position.¹¹

(ii) Two small ${}^3J(\text{PSCH})$ coupling constants with ${}^3J(\text{PSCH}_{4a}) > {}^3J(\text{PSCH}_{4e})$. In contrast to the dioxaphosphorinanes, the ${}^3J(\text{PH})$ coupling constant corresponding to the axial proton is higher than the one corresponding to the equatorial proton.

(iii) A large ${}^4J(\text{PSCCH}_{5e})$ coupling ranging from 7.7 to 10 Hz. It is noteworthy that in the 1,3,2-dioxaphosphorinanes and in the 1,3,2-diazaphosphorinanes¹² the two ${}^4J(\text{PH})$ values

are smaller than the ${}^3J(\text{PH})$ values. The difference observed between the two ${}^4J(\text{PSCCH})$ values indicates that such a coupling is highly dependent upon geometrical parameters.

(iv) A near zero value for ${}^3J(\text{PSCC}_5)$. From previous studies on 2-R-1,3,2-dioxaphosphorinanes which exist in a rigid chair conformation, the ${}^3J(\text{POCC}_5)$ NMR coupling is larger for an equatorial P–R bond than for an axial one.^{13,14} A typical value is 10 Hz for a P–R equatorial bond and 5 Hz for an axial P–R one.

(v) A chemical shift difference $\delta(\text{H}_{4a}) - \delta(\text{H}_{4e})$ larger than 0.5 ppm, for all the spectra recorded in the same solvent. This chemical shift difference which ranges from 1.19 ppm for 5 to 0.52 ppm for 2 is highly dependent upon the nature of the R group, and it correlates well with the chemical shift difference observed on the corresponding dioxaphosphorinanes^{6,15} which are known to exist in a rigid chair conformation with an axial P–R bond.

The full set of the ${}^3J(\text{HH})$ values for compounds 1–5 and mainly the large ${}^3J(\text{H}_{4a}\text{H}_{5a})$ coupling as compared with the values measured in 1,3-dithianes¹⁰ indicate that in these

TABLE I: ^1H NMR Spectral Data for 2-R-1,3,2-Dithiaphosphorinanes

Compd	Solvent	Chemical shifts δ^a				$J(\text{HH})$ coupling constants b					
		H(4a) c	H(4e) c	H(5a)	H(5e)	4a-4e	4a-5e	4a-5a	4e-5e	4e-5a	5a-5e
1	C_6D_6	2.78	2.14	1.85	1.46	-14.0	2.1	12.0	6.0	2.5	-14.5
2	C_6D_6	2.51	1.99	1.91	1.28	-13.9	2.1	12.3	5.4	2.5	-14.7
3	C_6D_6	2.97	2.02	1.88	1.36	-13.7	2.5	12.0	5.5	2.7	-14.2
4	C_6D_6	3.23	2.36	1.82	1.68	-14.0	2.2	12.5	5.2	2.6	-15.0
5	C_6D_6	3.45	2.26	2.05	1.70	-13.7	2.2	12.0	5.5	2.7	-14.5
6	C_6D_6	2.71	2.93	1.64	1.76	-14.4	3.7	7.6	8.6	3.6	-14.1
7	C_6D_6	2.60	2.72	1.40	1.43	-14.3	3.1	10.3	6.6	2.6	ind.
8	CDCl_3^d	2.96	3.12	1.77	2.08	-14.5	2.0	11.5	5.5	2.6	-14.8
9	CDCl_3^d	2.89	2.93	1.51	1.89	-14.1	2.7	12.2	4.7	2.6	-14.4
10	C_6D_6	2.74	2.70	1.30	1.60	-14.1	2.2	12.4	4.5	2.6	-15.0

a Chemical shifts in ppm downfield from TMS as internal reference. b Values in Hz. RMS error calculated line position 0.20; J_{gem} values are assumed to be negative. c For compounds existing in a rigid conformation (1-5, 9, 10) a refers to axially oriented protons, and e to equatorially oriented protons. d The ^1H NMR spectrum of compounds 8 and 9 have been recorded in CDCl_3 because of a very small difference $\delta(\text{H}_{4e}) - \delta(\text{H}_{4a})$ in C_6D_6 which makes an accurate spectral analysis extremely difficult. The NMR couplings are similar in both solvent.

TABLE II: ^{13}C and ^{31}P NMR Parameters for 2-R-1,3,2-Dithiaphosphorinanes

Compd	Chemical shifts a			Phosphorus-proton and phosphorus- $^{13}\text{C}^b$ coupling constants					
	^{31}P	$^{13}\text{C}(4)$	$^{13}\text{C}(5)$	P-4a c	P-4e	P-5a	P-5e	P-C $_4$	P-C $_5$
1	23.4	22.6	26.8	3.5	0.0	2.5	8.0	12.0	0.0
2	40.0	24.1	25.8	3.1	0.1	2.6	7.9	12.5	0.0
3	153.0	24.8	27.1	2.5	0.5	2.7	8.0	14.0	0.0
4	139.7	24.2	24.7	4.2	1.4	4.2	10.0	14.4	1.5
5	117.5	23.5	26.3	2.2	0.0	2.7	7.7	13.7	0.0
6	87.5	25.8	26.1	11.6	0.1	1.3	3.1	10.0	3.8
7	122.9	26.4	24.1	0.0	14.7	ind.	1.1	10.0	6.1
8	97.3	29.8	28.8	1.6	16.5	2.1	1.0	9.1	8.4
9	121.0	28.7	24.2	1.2	21.1	0.9	0.7	10.5	10.8
10	125.0	32.7	28.1	4.0	26.0	1.0	1.0	15.6	12.1

a ^{31}P chemical shifts in ppm downfield from external 85% H_3PO_4 ; ^{13}C chemical shifts in ppm downfield from TMS as internal reference. b Values in Hz. c For a and e designation of protons, see Table I.

molecules, the $\text{SCH}_2\text{CH}_2\text{CH}_2\text{S}$ fragment adopts a rigid C_s conformation. The R ratio defined as $R = J_{\text{trans}}/J_{\text{cis}} = (J_{\text{aa}} + J_{\text{ee}})/(J_{\text{ae}} + J_{\text{ea}})^{16}$ allows a good estimate of the torsional angle Ψ and of the various H-C-C-H dihedral angles ($\Phi_{\text{aa}} = 120 + \Psi$; $\Phi_{\text{ee}} = 120 - \Psi$; $\Phi_{\text{ae}} = \Phi_{\text{ea}} = \Psi$). The Ψ angles for compounds 1-5 are within a 1.5° range with a mean value of 65° . A conformational study of 2-R-2-thiono-1,3,2-dithiaphosphorinanes ($R = \text{Cl}$, $R = \text{CH}_3$) 17 by use of x-ray structure analysis and NMR data showed us that the R ratio gives very reliable values for the 1,3,2-dithiaphosphorinane rings (63° as compared to 62 and 61.5° from x-ray data).

On the basis of the previous stereochemical studies on 1,3,2-dithiaphosphorinanes 8 and from the similar trends observed on compounds 1-5, the NMR results obtained on these compounds are best explained in terms of a fixed chair conformation and of an axial preference for the various substituents on phosphorus.

The NMR parameters of molecules 9 and 10 are characterized by a large $^3J(\text{H}_{4a}\text{H}_{5a})$ value as observed for compounds 1-5 but conversely one notes: (i) A large $^3J(\text{PSCH}_{4e})$ coupling constant (21.1 and 26.0 Hz for 9 and 10, respectively) as compared with the values measured in compounds 1-5. Such an increase of the $^3J(\text{PH}_{4e})$ value has already been observed in the 1,3,2-dioxaphosphorinanes when the P-N bond is changed from axial to equatorial orientation. 5,6 (ii) A small $^4J(\text{PSCCH}_{5e})$ coupling constant. (iii) A large $^3J(\text{PSCC}_5)$ value as compared to the near zero value measured in compounds 1-5. As already mentioned in previous studies on 2-R-1,3,2-dioxaphosphorinanes, it was established that the $^3J(\text{POCC}_5)$

NMR coupling is larger for an equatorial P-R bond than for an axial one. 13,14 (iv) A fairly small chemical shift difference $\delta(\text{H}_{4a}) - \delta(\text{H}_{4e})$ which is smaller than 10 Hz for a spectrum recorded in benzene at 250 MHz. Such a small $\delta(\text{H}_{4a}) - \delta(\text{H}_{4e})$ difference is also observed in 2-amino-1,3,2-dioxaphosphorinanes with an equatorially oriented P-N bond. 5,6

The $^3J(\text{HH})$ NMR coupling values obtained on compounds 9 and 10 show that these molecules also exist in a rigid C_s conformation. The R values, 3.19 and 3.31, respectively, indicate a smaller puckering of the ring in the $\text{SCH}_2\text{CH}_2\text{CH}_2\text{S}$ fragment than for compounds 1-5. Comparison of the $^3J(\text{PH}_{4e})$, $^4J(\text{PH}_{5e})$, $^3J(\text{PC}_5)$, and $\delta(\text{H}_{4e}) - \delta(\text{H}_{4a})$ values obtained in compounds 9 and 10 and in the set of compounds 1-5 in which the P-R bond is axially oriented lead us to the conclusion that in compounds 9 and 10, the P-R bond lies in the equatorial orientation. Such an assignment is supported by the upfield shift of several parts per million observed on the $^{13}\text{C}_4$ (γ effect) 18 in going from compound 9 and 10 to the set of compounds 1-5.

In the molecules 6-8, the $^3J(\text{PSCH})$, $^3J(\text{PSCC}_5)$, and $^4J(\text{PSCCH})$ coupling constants have intermediate values between the corresponding ones observed in molecules 9 and 10 and the set of molecules 1-5. The $^3J(\text{HH})$ coupling constants clearly indicate that molecules 6-8 do not exist in a rigid unique C_s conformation (chair or boat) which would give a $^3J(\text{HH})$ value of 12 Hz instead of the 7.6-, 10.3-, and 11.5-Hz values obtained. These results can be interpreted in terms of a chair-chair equilibrium with the P-R bond occupying alternately the axial and equatorial orientation. We exclude a

flexible pseudorotating twist form for two reasons. First, it should give more identical $^3J(\text{HH})$ and $^3J(\text{PSCH})$ NMR couplings, and second the $^3J(\text{H}_{4a}, \text{H}_{5a})$ and $^3J(\text{H}_{4e}, \text{H}_{5e})$ couplings show an opposite trend of variation in going from 6 to 8, a result which is in agreement with the existence of an equilibrium between conformers of different energy. An additional answer to this question, chair-chair equilibrium or twist conformation, could be given by low-temperature NMR experiments. However, the complexity of the proton spectra (AA'BB'CDX) and some solubility problems have thus far precluded such studies. As the $^3J(\text{HH})$ values are not known for 6–8 locked in a rigid conformation, it is not possible to calculate an exact value for the two conformer populations, only approximate values can be obtained. Moreover, the examination of $^3J(\text{HH})$ does not allow the determination of the predominant conformation, P–R axial or P–R equatorial. However, such a question can be answered by use of the bond orientation at phosphorus. Typical values for the two orientations, taken as the mean values obtained on the compounds showing a strongly biased equilibrium (1–5, 9, 10), are presented in Table III. Thus, the examination of the coupling constants appear to be a good tool for stereochemical assignment. Since such coupling values are not only dependent upon the bond orientation around phosphorus but also, to a lesser extent, upon the nature of the R group attached to the phosphorus, they do not allow precise population analysis determination. However, combining the values of Table III and the $^3J(\text{HH})$ couplings, the following stereochemical conclusions may be drawn: the equatorial orientation is predominant in compound 7 (~60%) and 8 (~80%), and the equilibrium close to 50% for 6.

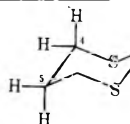
The results presented here show that as previously observed for 2-R-1,3,2-dioxaphosphorinanes, the extracyclic P–R bond of the 2-R-1,3,2-dioxaphosphorinanes can adopt axial or equatorial orientation. For an alkyl group, the tendency to adopt the axial orientation is more pronounced for the 1,3,2-dithiaphosphorinanes than for the 1,3,2-dioxaphosphorinanes. When R is methyl or phenyl the 2-R-1,3,2-dithiaphosphorinanes are biased with the P–R bond in the axial orientation, while the corresponding 1,3,2-dioxaphosphorinanes show an equilibrium between the two conformations P–R axial or P–R equatorial.^{1–3} The same trend is observed in the solid state conformation of the corresponding 2-thiono derivatives. For example, 2-methyl-2-thiono-1,3,2-dioxaphosphorinane exists in the solid state in chair conformation with an equatorial PCH₃ bond¹⁹ but 2-methyl-2-thiono-1,3,2-dithiaphosphorinane shows a chair form with an axial P–CH₃ bond.¹⁷ The extracyclic P–N bond is axial for a nonplanar nitrogen atom (aziridine) in which the P–N bond is longer than in the case of a planar nitrogen.²⁰ Bulky groups attached to the nitrogen give rise to severe 1,3 nonbonded interactions as a consequence of the rotational preference of the rotameric conformation around the P–N bond²¹ which displaces the equilibrium toward the P–N equatorial orientation.

Experimental Section

The synthesis of the 1,3,2-dithiaphosphorinanes used in this study were conducted in an inert gas atmosphere using rigorously anhydrous solvents. It is noteworthy that pure samples of compounds 1, 3, and 5–10 kept under vacuum in sealed tubes show additional ³¹P NMR peaks which appear with time. These extra peaks are due to three coordinated phosphorus species as shown by the ³¹P chemical shifts, and are now under investigation.

TABLE III: Stereochemical Dependence of the NMR Coupling Constants (Hz) in 1,3,2-Dithiaphosphorinanes^a

P–R bond orientation	3J (PH _{4e})	4J (PH _{5e})	3J (PC ₅)
Axial	0.5	8.0	0.5
Equatorial	23.5	1.0	11.5



^a The values reported in this table correspond to mean values.

2-Methyl-1,3,2-dithiaphosphorinane (1). The synthesis was accomplished by use of the procedure described for the corresponding 1,3,2-dithiaphospholane.²² At room temperature, methylphosphonous dichloride (5.25 g, 0.045 mol) was added dropwise to a solution of 1,3-propanedithiol (4.75 g, 0.045 mol) in benzene. After addition, the solution was heated for 2 h at 60 °C. After evaporation of benzene, the compound was purified by sublimation to obtain 2.6 g of 2-methyl-1,3,2-dithiaphosphorinane (38% yield): mp 50 °C. Anal. Calcd. for C₄H₉PS₂: C, 31.56; H, 5.96; P, 20.35; S, 42.13. Found: C, 31.75; H, 5.97; P, 20.25; S, 42.25.

2-Phenyl-1,3,2-dithiaphosphorinane (2). This compound was prepared by the same procedure as described for 1 using phenylphosphonous dichloride instead of methylphosphonous dichloride. 2 was purified by crystallization in methanol or acetonitrile (75% yield); mp 48 °C. Anal. Calcd. for C₉H₁₁PS₂: C, 50.51; H, 5.18; P, 14.47; S, 29.97. Found: C, 50.94; H, 4.87; P, 14.13; S, 28.70.

2-Methoxy-1,3,2-dithiaphosphorinane (3). To a benzene solution of methanol (2.30 g, 0.071 mol) and triethylamine (8 g, 0.079 mol) at 0 °C was added dropwise 2-chloro-1,3,2-dithiaphosphorinane (12.4 g, 0.071 mol). After 24 h, the mixture was filtered and concentrated. Molecular distillation (70 °C, 1 mm) gave a colorless liquid which becomes viscous with time. This compound can also be purified by chromatography on a silica column, using benzene as eluent. Anal. Calcd. for C₄H₉PS₂O: C, 28.56; H, 5.39; P, 18.41; S, 38.12. Found: C, 28.70; H, 5.33; P, 18.56; S, 38.02.

2-Chloro-1,3,2-dithiaphosphorinane (4). This compound was prepared in a 90% yield by reaction of phosphorus trichloride on 1,3-propanedithiol according to the procedure of Arbuzov and Zoroastrova for the 2-chloro-1,3,2-dithiaphospholane.²³ It was purified by sublimation: mp 45 °C. Anal. Calcd. for C₃H₆PS₂Cl: C, 20.87; H, 3.50; P, 17.94. Found: C, 20.53; H, 4.19; P, 17.98.

2-Amino-1,3,2-dithiaphosphorinanes (5–7, 9, 10). All of these compounds were prepared by the same experimental procedure. 2-Chloro-1,3,2-dithiaphosphorinane (1 mol) was added dropwise to a benzene solution of the amine (2 mol) at ca. 0 °C. The solution was stirred for 24 h and the amine hydrochloride filtered off. After evaporation of the solvent, purification was done by molecular distillation. The identification of each compound was performed by NMR spectral analysis (¹H, ¹³C, ³¹P) and mass spectrometry. The symmetry of the spectrum, the integration of the peak area, and the ³¹P chemical shift demonstrate without any ambiguity the formula of each compound. The mass spectra show peaks corresponding to the molecular weights.

2-tert-Butyl-1,3,2-dithiaphosphorinane (8). 1,3-Propanedithiol (5.31 g, 0.049 mol) was added dropwise to a benzene solution (100 cm³) of tert-butylphosphonous dichloride (7.84 g, 0.049 mol) and pyridine (7.76 g, 0.098 mol). The mixture is stirred for 2 weeks at 50 °C and the pyridinium salt is

filtered off. A ^{31}P NMR spectrum of the benzene solution shows four peaks at 97.3, 104.0, 115.5, and 121.0 ppm respectively, with respect to a 85% H_3PO_4 solution as external reference. Column chromatography over silica and performed under nitrogen using as eluent a 3:1 mixture of hexane-benzene, allows isolation of compound 8 (δ ^{31}P 97.3 ppm). The compound is identified by NMR spectroscopy ^1H , ^{13}C , ^{31}P , and the mass spectrum which shows a peak at m/e 194. The fact that the isolated compound is a six-membered ring is shown by the identification of its 2-thiono derivative. The extra peaks observed in the benzene solution correspond to cyclic polymeric species which will be described in a forthcoming paper. Anal. Calcd. for $\text{C}_7\text{H}_{15}\text{PS}_2$: C, 43.27; H, 7.78; P, 15.94; S, 33.00. Found: C, 43.74; H, 7.51; P, 15.80; S, 32.17.

Acknowledgments. The NMR spectra were recorded at the "Laboratoire Grenoblois de Résonance Magnétique Nucléaire", on a Cameca 250-MHz spectrometer (^1H) and a Varian-Informatek Spectrometer (^{13}C , ^{31}P). We thank Mr. R. Nardin and Mr. H. Reutenauer for skillful assistance in recording the NMR spectra.

References and Notes

- (1) (a) D. W. White, G. K. McEwen, and J. G. Verkade, *Tetrahedron Lett.*, 5369 (1968); C. Bodkin and J. P. Simpson, *J. Chem. Soc. D*, 829 (1969); B. A. Arbousov and R. P. Archinova, *Dokl. Akad. Nauk SSSR*, **195**, 835 (1970); B. A. Arbousov, R. P. Archinova, A. N. Verechaguin, S. G. Voulfson, O. N. Nouredinova, and L. Z. Nikonova, *Khim. Keterocycl. Soedin.*, **10**, 1324 (1971); (b) W. G. Bentrude, K. C. Yee, R. D. Bertrand, and D. H. Grant, *J. Am. Chem. Soc.*, **93**, 797 (1971); W. G. Bentrude and J. H. Hargis, *ibid.*, **92**, 7136 (1970); W. G. Bentrude and K. G. Yee, *Tetrahedron Lett.*, 3999 (1970); K. Bergensen and P. Albrigtsen, *Acta Chem. Scand.*, **26**, 1680 (1972); (c) M. G. B. Drew, J. Rodgers, D. W. White, and J. G. Verkade, *J. Chem. Soc. D*, 227 (1971); J. Rodgers, D. W. White, and J. G. Verkade, *J. Chem. Soc. A*, 77 (1971); M. G. B. Drew and J. Rodgers, *Acta Crystallogr., Sect. B*, **28**, 924 (1972); M. Haque, C. N. Caughlan, J. M. Hargis, and W. G. Bentrude, *J. Chem. Soc. A*, 1786 (1970); A. Okruszek and W. J. Stec, *Z. Naturforsch. B*, **30**, 430 (1974); **31**, in press.
- (2) D. W. White, *Phosphorus*, **1**, 33 (1971).
- (3) J. P. Albrand, J. P. Dutasta, and J. B. Robert, *J. Am. Chem. Soc.*, **96**, 4584 (1974), and unpublished results for R ethyl and R isopropyl.
- (4) J. A. Mosbo and J. G. Verkade, *J. Am. Chem. Soc.*, **94**, 8224 (1972); **95**, 4659 (1973).
- (5) W. G. Bentrude and H. W. Tan, *J. Am. Chem. Soc.*, **94**, 8222 (1972); **95**, 4666 (1973).
- (6) A. Cogne, A. C. Guimaraes, J. Martir, R. Nardin, J. B. Robert, and W. Stec, *Org. Magn. Reson.*, **6**, 629 (1974).
- (7) W. J. Stec and A. Okruszek, *J. Chem. Soc., Perkin Trans. 1*, 1828 (1975).
- (8) R. O. Hutchins and B. E. Maryanoff, *J. Am. Chem. Soc.*, **94**, 3266 (1972).
- (9) E. E. Nifant'ev, A. A. Eorissenko, A. I. Zavalichina, and S. F. Sorokina, *Dokl. Akad. Nauk SSSR*, **219**, 881 (1974).
- (10) J. Martin and J. B. Robert, *Org. Magn. Reson.*, **7**, 76 (1975).
- (11) H. T. Kalf and G. Romers, *Acta Crystallogr.*, **20**, 490 (1966).
- (12) R. O. Hutchins, B. E. Maryanoff, J. P. Albrand, A. Cogne, D. Gagnaire, and J. B. Robert, *J. Am. Chem. Soc.*, **94**, 9151 (1972).
- (13) E. E. Nifant'ev, A. A. Borissenko, and N. M. Sergue'v, *Dokl. Akad. Nauk SSSR*, **208**, 651 (1973).
- (14) M. Haemers, R. Ottinger, D. Zimmerman, and J. Reisse, *Tetrahedron Lett.*, 2241 (1973).
- (15) D. Gagnaire, J. B. Robert, and J. Verrier, *Bull. Soc. Chim. Fr.*, 2392 (1968).
- (16) J. B. Lambert, *Acc. Chem. Res.*, **4**, 87 (1971).
- (17) A. Grand, J. Martin, and J. B. Robert, *Acta Crystallogr., Sect. B*, **32**, 1244 (1976).
- (18) D. M. Grant and B. V. Cheney, *J. Am. Chem. Soc.*, **89**, 5315 (1967); D. K. Dalling and D. M. Grant, *ibid.*, **89**, 5318 (1967); A. J. Jones, E. L. Eliel, D. M. Grant, M. C. Knoeber, and W. F. Bailey, *ibid.*, **93**, 4772 (1971); F. G. Riddell, *ibid.*, **93**, 1030 (1971); M. Haemers, R. Ottinger, D. Zimmermann, and J. Reisse, *Tetrahedron*, **29**, 3539 (1973); H. W. Tan and W. G. Bentrude, *Tetrahedron Lett.*, 619 (1975); S. I. Featherman and L. D. Quin, *J. Am. Chem. Soc.*, **97**, 4349 (1975).
- (19) J. P. Dutasta, A. Grand, and J. B. Robert, *Tetrahedron Lett.*, 2655 (1974).
- (20) L. V. Vilkov, L. S. Khaikin, and V. V. Evdokimov, *Zh. Strukt. Khim.*, **13**, 7 (1972).
- (21) E. D. Morris and C. E. Nordman, *Inorg. Chem.*, **8**, 1673 (1969).
- (22) M. Wieber, J. Otto, and M. Schmidt, *Angew. Chem., Int. Edit. Engl.*, **3**, 586 (1964).
- (23) A. E. Arbousov and V. H. Zoroastrova, *Izv. Akad. Nauk SSSR, Otd. Khim. Nauk*, 770 (1952).

Intramolecular Torsional Potential and Dielectric Properties of 2,3-Butanedione

Giles L. Henderson* and Gevert H. Meyer

Department of Chemistry, Eastern Illinois University, Charleston, Illinois 61920 (Received October 14, 1975; Revised Manuscript Received July 1, 1976)

Dipole moment measurements have been carried out on 2,3-butanedione in solution, pure liquid, and the vapor phase. A dipole moment of 1.03 ± 0.01 D was observed for dilute solutions of 2,3-butanedione in carbon tetrachloride at 298.15 K. Pure liquid samples at 298.15 K exhibit an anomalous dipole of 1.36 ± 0.01 D. The following results were obtained for vapor phase measurements: 1.03, 1.05, 1.07, 1.11, 1.20, and 1.25 ± 0.015 D at 310.15, 330.15, 350.15, 370.15, 431.69, and 472.10 ± 0.02 K, respectively. The acetyl torsional potential was characterized from the observed temperature dependence of the dipole moment. This torsional mode was described by a potential function of the form: $V(\phi) = \frac{1}{2} \sum_n^3 V_n (1 - \cos n\phi)$ where ϕ is the acetyl torsional angle. The temperature dependence of the dipole moment was analyzed using statistical thermodynamic methods to determine the internal rotation potential parameters. A numerical least-squares fit of the data yields $V_1 = 2660 \pm 30 \text{ cm}^{-1}$ ($7.60 \pm 0.09 \text{ kcal/mol}$) and $V_2 = V_3 = 0.0 \text{ cm}^{-1}$. A multiparameter potential function has been employed for the first time to characterize the temperature dependence of the dipole moment of 2,3-butanedione. The results of this study indicate that in contrast to diethanal (glyoxal), the *cis* conformer of 2,3-butanedione is unstable, which accounts for the failure of other experimental methods to observe this species.

Introduction

Both the *cis* and *trans* conformer of conjugated 1,2-dicarbonyl compounds are stabilized by partial π bonding due to p orbital overlap between the adjacent carbonyl carbon atoms. Thus it might be expected that, in general, both conformers may exist as stable species. Indeed the *cis* conformer of glyoxal $\text{H}-\text{C}(=\text{O})-\text{C}(=\text{O})\text{H}$ has been observed. It was first detected in 1970 by Currie and Ramsey¹ with the appearance of an electronic band at 4875 Å in the uv-emission spectrum. In 1972 Durig, Tong, and Li² reported the microwave spectrum of *cis*-glyoxal. However, several investigators have failed to document the stability of *cis*-2,3-butanedione (biacetyl). Durig, Hannum, and Brown³ systematically examined the infrared spectrum of solid, liquid, and vapor phase biacetyl. They observed the acetyl torsional mode of the *trans* isomer at 52 cm^{-1} (Fateley⁴ and co-workers reported a value of 48 cm^{-1}), but no evidence was found for the existence of a stable *cis* conformer. Recent electron diffraction studies by Hagen and Hedberg⁵ concluded that vapor phase biacetyl exists only in the *trans* configuration.

Information about intramolecular rotation about the C-C bond in 1,2-dicarbonyl compounds can also be obtained from the temperature dependence of the molecular dipole moment.⁶ In the *trans* configuration, the two rotatable dipoles exactly cancel each other while in the *cis* position the two dipoles would yield a maximum resultant dipole moment. For cases where the two dipoles undergo free rotation, all positions around the C-C bond are equally probable and the molecular dipole is temperature independent. In cases where rotation is hindered by a potential barrier, thermal effects will be observed in the molecular dipole. If the *trans* conformer is of lower energy than the *cis* conformer, the dipole moment will be minimum at absolute zero. As the temperature is raised the Boltzmann population of excited librator states possessing large torsional amplitudes will increase and the root mean square dipole moment averaged over all the molecules increases.⁷ This effect will be greatly enhanced if the polar *cis* configuration is stabilized by the intramolecular torsional potential.

Temperature dependence of the dipole moment of biacetyl has been studied on two previous occasions: Zahn⁸ in 1932 and Bloom and Sutton⁹ in 1941. A serious discrepancy between their results can be seen in Figure 1. Zahn⁸ makes no mention of his experimental methods or source of materials. Moreover he made no attempt to fit his data to any type of torsional potential function. In the absence of modern day computation facilities, Bloom and Sutton⁹ attempted to fit their data only to single parameter potential functions. However, their functions fail to allow the existence of both stable *trans* and *cis* conformers.

The present study of biacetyl was undertaken to resolve the existing discrepancy in the dipole moment and to obtain an optimum multiparameter torsional potential to assess the relative stability of *cis*-biacetyl.

Experimental Section

Materials. The materials used for dielectric calibration standards for pure liquid and solution measurement are given in Table I. These standards were purified by the methods described by Weissberger.¹¹ The 2,3-butanedione was purchased from Eastman Kodak and fractionally distilled twice with the middle fraction of the second distillate used for measurements. All liquid standards were stored in the dark over type 4A molecular sieves that had been freshly prepared by heating at 320 °C for 3 h in a thermostated furnace. The gas cell used in vapor phase dielectric measurements was calibrated with prepurified grade nitrogen gas purchased from Matheson Gas Co.

Equipment and Apparatus. Indices of refraction of liquid samples were measured with a Bausch and Lomb Abbe refractometer. Densities were determined with a Weld pycnometer. Dielectric measurements were made at 2.6 MHz with a heterodyne beat dielectrometer constructed in this laboratory. Solution and pure liquid measurements were made in a 15 ml, 20 pF liquid cell, Model 2TN20LV obtained from Balsbaugh Laboratories, Duxbury, Mass. This cell was modified so that samples could be introduced by means of a vacuum and removed by pressurizing the cell with nitrogen gas.

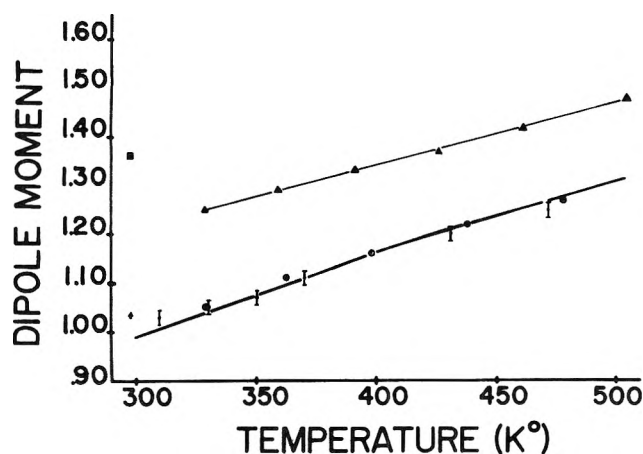


Figure 1. Comparison of results with other dipole studies: (□) pure liquid measurement; (•) solution measurement; (▲) LeFevre's solution measurement; (△) Zahn's vapor phase measurements; (○) Bloom and Sutton's vapor phase measurements; (⊖) our vapor phase measurements. The corresponding solid line through our experimental points gives the optimum calculated root mean square dipole moments for $V_1 = 2660 \text{ cm}^{-1}$ and $V_2 = V_3 = 0.0 \text{ cm}^{-1}$.

TABLE I: Dielectric Standards

Material	ϵ^{25}
Cyclohexane	2.015 ¹⁰
Carbon tetrachloride	2.228 ¹⁰
Benzene	2.275 ¹¹
Chloroform	4.781 ¹⁰
Chlorobenzene	5.621 ¹⁰
Ethyl acetate	6.02 ₁ ¹⁰
Methyl benzoate	6.57 ₀ ¹⁰
Nitrogen	1.000 547 2 ^a

^a At 20.00 °C and 760 Torr pressure.¹²

The cell was thermostated by a water bath within ± 0.03 °C.

A custom built 1000-pF dielectric cell¹³ and vacuum line were used for vapor phase measurements. The temperature of the cell was maintained within ± 0.02 °C with a YSI Model 71A Thermistemp temperature controller and an insulated oil bath.

The gas cell was connected by means of a vacuum line to a mercury manometer, a regulated nitrogen gas supply, and to a biacetyl sample reservoir thermostated at approximately 15 °C to maintain an equilibrium vapor pressure in the cell on the order of 31 Torr at all cell temperatures. The dielectric cells were connected to the tank circuit of the dielectrometer with RG-58 coaxial cable enclosed in rigid $\frac{5}{16}$ -in. copper tubing to enhance the stability of the radiofrequency oscillator.

Calibration and Measurements. The turning mechanism of a war surplus frequency meter (Model BC22IN) was used to measure changes in capacitance. Although the BC22IN provides a high precision variable capacitor and vernier dial mechanism, an accurate calibration technique is required since measured changes in capacitance and dielectric constants are nonlinear with respect to dial readings. This was done for both the liquid and gas cells by measuring a series of standard materials (Table I) of known dielectric constant as a function of null point dial settings. The parameters for polynomial calibration functions were then obtained using a non-linear least-squares fit.¹⁴ The calibration function could then be used to calculate the dielectric constant of an un-

known sample directly from the observed null point dial setting of the BC22IN.

Since the vapor phase experiments required measuring very small changes in dielectric constants, on the order of 1×10^{-4} , it was necessary to correct for any background drift in the frequency of the rf oscillators. This was accomplished by observing the null point of the evacuated cell before and after each sample measurement. Thus all measurements could be plotted with respect to time and appropriate drift corrections made, i.e., a positive deviation in the background was subtracted from the observed dial setting. Separate calibration functions were obtained at each cell temperature by observing null points for nitrogen gas pressures of 200, 250, 300, 350, and 400 Torr. Approximately 75 nitrogen calibration and 45 biacetyl null point observations were made over a period of 6 h for each temperature. A total of over 2000 vapor phase measurements were made over the accessible temperature range.

Results

The dielectric constant, index of refraction, and density of pure liquid biacetyl were measured at 25.00 °C as $\epsilon = 4.713 \pm 0.002$; $n_D = 1.3922 \pm 0.0001$, and $\rho = 0.981 \pm 0.001 \text{ g/ml}$, respectively. The dipole moment was then calculated from the Onsager¹⁵ equation:

$$\mu = 1.36 \pm 0.01 \text{ D}$$

The dielectric constant and densities of several dilute solutions of biacetyl in CCl_4 were measured at 25.00 °C as a function of mole fraction of biacetyl and are given in Table II. Both the dielectric constants and the densities were found to be linear with respect to mole fraction:

$$\epsilon = a\bar{X}_2 + \epsilon_1$$

$$\rho = b\bar{X}_2 + \rho_1$$

where ϵ_1 and ρ_1 represent the dielectric constant and the density of the solvent. The slopes a and b were found by a linear least-squares fit of the data in Table II: $a = 1.099$, and $b = -0.6269$. These parameters were then used to calculate the dipole moment of the solute by the Hederstrand method:^{16,17} $P_{2m} = 44.86 \text{ cm}^3$, $P_{2d} = 22.99 \text{ cm}^3$, $P_{2\mu} = 21.87 \text{ cm}^3$, $\mu = 1.03 \pm 0.01 \text{ D}$.

Vapor phase dielectric data were used to calculate the dipole moment over the temperature range of 310.15–472.10 K by means of the Debye equation.^{17,18}

The average values of the molar polarization and dipole moments are given in Table III for each temperature.

Discussion

Comparison with Other Dipole Studies. Our dipole moment measurements are compared with Zahn's⁸ vapor phase, Bloom and Sutton's⁹ vapor phase, and LeFevre's¹⁹ solution measurements in Figure 1. Our dipole moment for pure liquid biacetyl (1.36 D) was found to be much higher than expected. Such anomalous deviations have been observed in polar liquids and have been attributed²⁰ to strong dipole-dipole intermolecular interactions. These interactions can be minimized by measuring dipole moments in dilute solutions rather than in the pure liquid state.

Both LeFevre's and our solution dipole measurements are in good agreement with Bloom and Sutton's vapor phase data extrapolated to 298 K: Bloom and Sutton's extrapolated dipole = 1.01 D; LeFevre's solution dipole = 1.04 D; our solution dipole = 1.03 D. Although the slope of Zahn's vapor phase

TABLE II: Dilute Solution Measurements in CCl₄ at 25.00 °C

\bar{X}_2	ϵ	ρ
0.000 00	2.232	1.584
0.015 64	2.247	1.580
0.026 03	2.257	1.573
0.030 47	2.271	1.566
0.045 69	2.281	1.558
0.060 75	2.298	1.548

TABLE III: Dipole Moment and Molar Polarization of Biacetyl

T, K	P_m, cm^3	μ, D
310.15	43.9	1.03
330.15	43.1	1.05
350.15	42.9	1.07
370.15	43.2	1.11
431.69	43.5	1.20
472.10	43.3	1.25

measurements is nearly equal to ours, there appears to be some systematic error, resulting in a constant positive deviation. Since Zahn gives no experimental details, we can only speculate that an impure dielectric reference gas resulted in a systematic calibration error.

There is good correlation between Bloom and Sutton's and our vapor phase data at all temperatures. Although it appears that Bloom and Sutton's data may be more precise, our dipoles are slightly lower throughout the experimental temperature range. However, this difference is primarily due to the value assumed for the distortion polarization: Bloom and Sutton use $P_d = 22.7$, we use $P_d = 22.99$ calculated from the density and index of refraction cited in the Results section.

Dipole Moment and Intramolecular Rotation. Beach and Stevenson^{21,22} have shown that the observed or average dipole moment of a molecule containing two movable dipoles restricted to internal rotation can be expressed as a function of temperature:

$$\mu^2 = A - B \langle \cos \phi \rangle \quad (1)$$

where $A = m_1^2 + m_2^2 - 2m_1m_2 \cos \alpha_1 \cos \alpha_2$ and $B = 2m_1m_2 \sin \alpha_1 \sin \alpha_2$. m_1 and m_2 are the magnitudes of the two movable dipoles. α_1 and α_2 are the angles made by the dipoles with the axis of rotation. ϕ is the angle describing internal rotation as depicted in Figure 2. $\langle \cos \phi \rangle$ represents the expectation value of the $\cos \phi$ averaged over the intramolecular rotational potential, $V(\phi)$:

$$\langle \cos \phi \rangle = \frac{\int_0^\pi \cos \phi \exp(-V(\phi)/kT) d\phi}{\int_0^\pi \exp(-V(\phi)/kT) d\phi} \quad (2)$$

For biacetyl, $\alpha_1 = \alpha_2 = 120.3^\circ$ as determined by electron diffraction.⁵ The value for $m_1 = m_2$ was taken as 2.83 D which is the average carbonyl dipole moment calculated for: acetone²³ ($\mu_{\text{CO}} = 2.86$ D); camphorquinone¹⁹ ($\mu_{\text{CO}} = 2.72$ D); and *cis*-glyoxal² ($\mu_{\text{CO}} = 2.90$ D). From the above m and α values we calculate $A = B = 11.91$ D².

The torsional potential associated with internal rotation about the C-C bond axis of biacetyl can be expressed in the form of a Fourier expansion:

$$V(\phi) = \frac{1}{2} \sum_n V_n (1 - \cos n\phi) \quad (3)$$

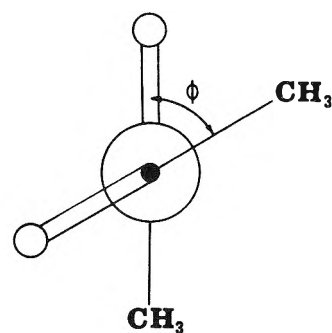


Figure 2. Note that the torsional angle ϕ is zero for the trans configuration.

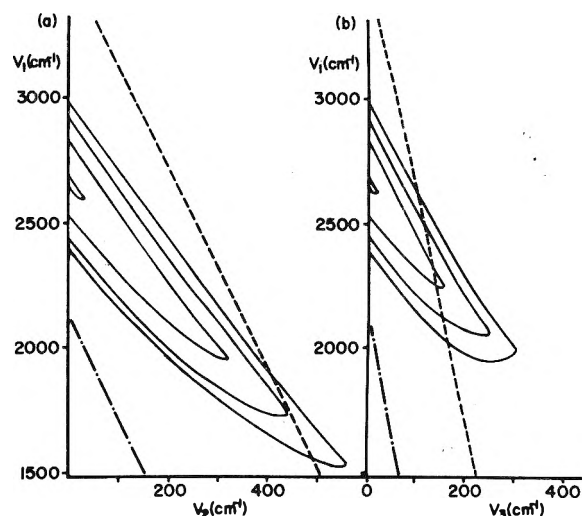


Figure 3. Dipole regression contours; from outer to inner: $R = 0.04, 0.03, 0.02$ and 0.0015 for (a) $V(\phi) = \frac{1}{2} V_1 (1 - \cos \phi) + \frac{1}{2} V_2 (1 - \cos 2\phi)$ and (b) $V(\phi) = \frac{1}{2} V_1 (1 - \cos \phi) + \frac{1}{2} V_3 (1 - \cos 3\phi)$. (---) Constraints on the potential parameters from ir data.⁴ (- - -) Constraints on the potential parameter from electron diffraction data⁵ (see Potential Parameter and Torsional Librational Frequency in the Discussion).

As a first approximation, the series is terminated after the V_2 term. This two parameter function describes interactions which are either periodic in $\phi = \pi$ or $\phi = 2\pi$ and exhibits minima for the trans and cis forms. A V_3 term must be included to describe interactions periodic in $\phi = \frac{2}{3}\pi$ stabilizing a gauche form. Such a trigonal potential barrier would be given by the bent "banana" bond model of the C=O double bond.⁴ It has been suggested²⁴ that other nonbonded interactions could also contribute to the stability of a gauche conformation in conjugated molecules. However, in the case of glyoxal, the metastable form has been shown to be cis rather than gauche.^{1,2}

Determination of the Potential Parameters. The dipole moment can be calculated as a function of temperature for any given torsional potential from eq 1-3. The potential parameters that best fit the experimental temperature dependence of the dipole moment were found by a numerical least-squares fit. This was accomplished by calculating a regression value R to determine the quality of the fit while systematically varying the potential parameters

$$R = \sum_{i=1}^n \delta_i^2$$

where δ = the difference between the calculated and observed dipole moments and the best fit corresponds to a minimum

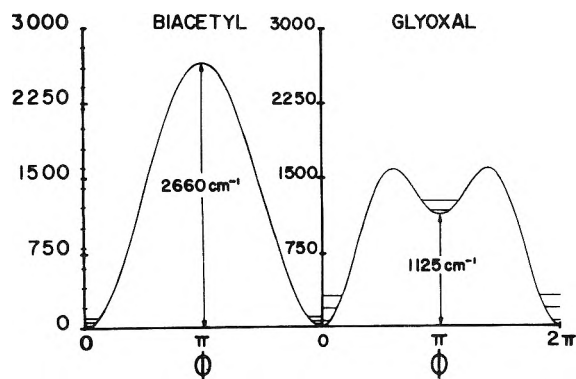


Figure 4. The torsional potentials for biacetyl and glyoxal.² The biacetyl potential corresponds to $V_1 = 2660 \text{ cm}^{-1}$ and $V_2 = V_3 = 0.0 \text{ cm}^{-1}$.

regression. The integrals in eq 2 were evaluated by numerical methods on an IBM-360 computer using Simpson's rule. A three parameter search was carried out using the potential function given by eq 3 where $n = 1$ to $n = 3$; $0.0 \leq V_1 \leq 4000 \text{ cm}^{-1}$; $0.0 \leq V_2 \leq 2000 \text{ cm}^{-1}$; and $0.0 \leq V_3 \leq 2000 \text{ cm}^{-1}$.

The dipole moments dependence on the torsional potential function can be illustrated with regression contour maps. Figure 3 depicts two special cases: (a) $V_3 = 0.0$ on the left-hand side and (b) $V_2 = 0.0$ on the right-hand side. The precision limits of our dipole measurements allow acceptable values of the potential parameters to lie anywhere within a regression contour of $R = 0.0015$. The best fit corresponds to $V_1 = 2660 \text{ cm}^{-1}$ and $V_2 = V_3 = 0.0 \text{ cm}^{-1}$. The calculated temperature dependence of the dipole moment is compared to the experimental observation in Figure 1. The same calculations were carried out with Bloom and Sutton's dipole data and yield $V_1 = 2630$, $V_2 = V_3 = 0.0 \text{ cm}^{-1}$.

Potential Parameter and Torsional Librational Frequency. The torsional quantum levels corresponding to a potential of the form given in eq 3 cannot be represented by a closed analytical expression. However, the lowest levels can be approximated by a harmonic oscillator model since the potential function is parabolic for small torsional displacement angles:⁴

$$V(\phi) = \frac{1}{4}(V_1 + 4V_2 + 9V_3)\phi^2 = \frac{1}{4}V^*\phi^2 \quad (4)$$

and the torsional oscillation frequency is

$$\bar{\nu} = \frac{1}{2\pi c} \sqrt{\frac{V^*}{2\mu_i}} \quad (5)$$

where μ_i is the reduced moment of inertia.²⁵ Using this harmonic oscillator approximation, $V^* = V_1 = 2660 \text{ cm}^{-1}$, and a reduced moment of inertia from recent electron diffraction structure parameters of the trans conformation,⁵ we calculate the $1 \leftarrow 0$ torsional transition frequency as 43 cm^{-1} . This result seems in good agreement with the observed far-ir spec-

trum. Both Durig³ et al. and Fateley et al.⁴ have observed prominent absorption between 35 and 65 cm^{-1} . Hagen and Hedberg⁵ obtain a value for the root mean square torsional amplitude of $\delta = 24^\circ$ from an analysis of their electron diffraction data. We calculate a value for the torsional barrier height from eq 2 and 3 using $\langle \phi \rangle = 24^\circ$ and Hagen and Hedberg's nozzle temperature 228° C as $V^* = 2124 \text{ cm}^{-1}$. Both the harmonic oscillator estimate of V^* from ir data⁴ and the V^* calculated above from electron diffraction data⁵ result in the constraints of V_1 , V_2 , and V_3 given by $V^* = V_1 + 4V_2 + 9V_3$ and depicted in Figure 3.

The shape of the dipole regression contours in Figure 3 strongly suggests that only the trans conformer of biacetyl is stable. The optimum potential derived from this study for biacetyl is compared with the torsional potential of glyoxal² in Figure 4. This study indicates that in contrast to glyoxal there is no detectable minimum in the biacetyl torsional potential at $\phi = \pi$ and hence spectroscopic detection of the cis configuration would seem highly improbable.

References and Notes

- (1) G. N. Currie and D. A. Ramsay, *Can. J. Phys.*, **49**, 317 (1971).
- (2) J. R. Durig, C. C. Tong, and Y. S. Li, *J. Chem. Phys.*, **57**, 4425 (1972).
- (3) J. R. Durig, S. E. Hannum, and S. C. Brown, *J. Phys. Chem.*, **75**, 1946 (1971).
- (4) W. G. Fateley, R. K. Harris, F. A. Miller, and R. E. Witkowski, *Spectrochim. Acta*, **21**, 231 (1965).
- (5) K. Hagen and K. Hedberg, *J. Am. Chem. Soc.*, **95**, 8266 (1973).
- (6) C. P. Smyth, "Dielectric Behavior and Structure", McGraw-Hill, New York, N.Y., 1955, Chapter XI.
- (7) Dielectric measurements are sensitive to the square of the dipole moment as can be seen from the Debye equation:

$$P_m = \frac{\epsilon - 1}{\epsilon + 2} \frac{M}{\rho} = \frac{4\pi N}{3} \left(\alpha_0 + \frac{\mu^2}{3KT} \right)$$
- (8) C. T. Zahn, *Phys. Rev.*, **40**, 291 (1932).
- (9) G. I. M. Bloom and L. E. Sutton, *J. Chem. Soc.* 727 (1941).
- (10) "Dielectric Constants of Pure Liquids", National Bureau of Standards, Circular No. 514.
- (11) A. Weissberger, "Technique of Organic Chemistry", 2d ed, Vol VII, Interscience, New York, N.Y., 1955.
- (12) "Dielectric Constants of Reference Gases at 20° C and 1 atmosphere", National Bureau of Standards, Circular No. 537.
- (13) Constructed by Dorsett Instrument and Machine Co., R. R. 10, Box 5, Bloomington, Ind. 47401.
- (14) G. Henderson and A. Gajjar, *J. Chem. Educ.*, **48**, 693 (1971).
- (15) L. Onsager, *J. Am. Chem. Soc.*, **58**, 1486 (1936).
- (16) G. Medstrand, *Z. Phys. Chem.*, **2B**, 428 (1929).
- (17) The atomic polarization is taken as 10% of the electronic polarization. Hence $P_d = P_E + P_A = 1.1R_m$ where R_m = molar refractivity calculated for the sodium D line.
- (18) P. Debye, *Phys. Z.*, **13**, 97 (1912).
- (19) P. Cureton, C. G. LeFevre, and R. J. W. LeFevre, *J. Chem. Soc.*, 4447 (1961).
- (20) Reference 6, p 31.
- (21) J. Y. Beach and D. P. Stevenson, *J. Chem. Phys.*, **6**, 635 (1938).
- (22) Beach and Stevenson give $\mu^2 = A + B(\cos \phi)$ and express the torsional potential as $V(\phi) = \frac{1}{2} \sum_n V_n (1 + \cos n\phi)$. However, we have chosen to write the potential in the more conventional form $V(\phi) = \frac{1}{2} \sum_n V_n (1 - \cos n\phi)$ which requires that $\mu^2 = A - B(\cos \phi)$.
- (23) A. L. McClellan, "Table of Experimental Dipole Moments", W. H. Freeman, San Francisco, Calif., 1963.
- (24) M. J. S. Dewar and A. J. Harget, *Proc. R. Soc. London, Ser. A*, **315**, 443 (1970).
- (25) K. S. Pitzer, *J. Chem. Phys.*, **14**, 239 (1946).

Free Radical Oxidation of Organic Disulfides

M. Bonifačić and K.-D. Asmus*

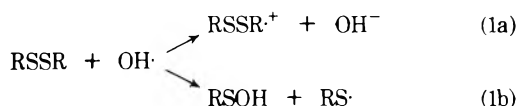
Hahn-Meitner-Institut für Kernforschung Berlin GmbH, Bereich Strahlenchemie,
D 1000 Berlin 39, West Germany (Received May 17, 1976)

Publication costs assisted by Hahn-Meitner-Institut für Kernforschung Berlin GmbH

The oxidation of aliphatic organic disulfides by 1,3,5-trimethoxybenzene and thioether radical cations, $\text{SO}_4^{\cdot-}$ and $\text{Br}_2^{\cdot-}$ radical anions, and by the unstable metal ions Ag^{2+} , $\text{Ag}(\text{OH})^+$, and Tl^{2+} leads to the formation of $\text{RSSR}^{\cdot+}$ radical cations as primary reaction product with 100% efficiency. Oxidation by $\text{Tl}(\text{OH})^+$, the hydroxyl radical $\text{OH}\cdot$, and the bicarbonate radical $\text{HCO}_3^{\cdot-}$ leads to the formation of $\text{RSSR}^{\cdot+}$ in 80, 55, and ca. 10% yield, respectively. The rate constants for the oxidation processes are in the 10^7 – $3 \times 10^9 \text{ M}^{-1} \text{ s}^{-1}$ range. The various oxidation mechanisms and the role of $\text{RSSR}^{\cdot+}$ radical cations as a mediator for electrons are discussed.

Introduction

The oxidation of organic disulfides by hydroxyl radicals in aqueous solutions has been the subject of several recent publications.^{1–6} It has been shown that ion pair formation and dissociative OH addition occur with about equal probability in neutral solutions.^{5,6} At low and high pH RSH and RSO· radicals are also observed.



The radical cations $\text{RSSR}^{\cdot+}$ have been identified by pulse radiolysis conductivity studies and by their optical absorption spectra.^{5,6} The nonionic species have been characterized through steady state analysis of stable reaction products^{1,2,6} and EPR trapping experiments.^{3,4}

Oxidation reactions in general can be initiated not only by hydroxyl radicals but also by a variety of other species such as $\text{Br}_2^{\cdot-}$, $\text{SO}_4^{\cdot-}$, Tl^{2+} , Ag^{2+} , $\text{HCO}_3^{\cdot-}$, etc. These oxidizing species can be generated most conveniently by radiation chemical methods, particularly pulse radiolysis, but also by photochemical or conventional chemical methods.

Oxidation of organic compounds by the above radicals often leads to the formation of the same products. In some instances, however, results suggest that the oxidation mechanism may also proceed via different pathways depending on the nature of the oxidant. For example, O'Neill et al.,⁸ who studied the oxidation of methoxybenzenes, could demonstrate that Tl^{2+} and $\text{OH}\cdot$ lead to quite different yields of methoxy radical cations. Even the various forms of the same oxidation state of a metal ion can exhibit different oxidizing properties. For example, $\text{Tl}(\text{II})$ has been found to exist in the equilibria^{9,10}



($\text{p}K = 7.7$ and 4.6 , respectively); Tl^{2+} and $\text{Tl}(\text{OH})^+$ are good oxidants.^{8–10} $\text{Tl}(\text{OH})_2$ can even act as a reductant.¹⁰

The present pulse radiolysis study has been undertaken to obtain information on the primary reaction products of the reaction of organic disulfides and various oxidative radicals and ions. Particular emphasis has been put on the determination of the yield of radical cations $\text{RSSR}^{\cdot+}$. The results are compared with the $\text{OH}\cdot$ radical induced oxidation mechanism.

Experimental Section

Commercially available sulfur organic compounds were fractionally distilled and the purity (>99%) was checked gas chromatographically.⁶ All other chemicals were of analytical grade.

Solutions were generally prepared from Millipore filtered deionized water. Deoxygenation was achieved by bubbling the solutions with argon or N_2O . The latter was used if hydrated electrons were to be converted to $\text{OH}\cdot$ radicals ($\text{N}_2\text{O} + e_{\text{aq}}^- \rightarrow \text{N}_2 + \text{OH}^- + \text{OH}\cdot$).

The experimental technique has already been described.¹¹ The pulse experiments were done with high energy electrons from a 1.6-MeV Van de Graaff generator (10 mA) at pulse lengths of 0.5–2 μs and an absorbed dose of ca. 700 rads/1- μs pulse duration.

Dosimetry was based on optical measurements of $\text{C}(\text{NO}_2)_3^-$ ions ($\epsilon_{350 \text{ nm}} = 1.5 \times 10^4 \text{ M}^{-1} \text{ cm}^{-1}$) formed during the reduction of tetranitromethane (TNM) by e_{aq}^- and $(\text{CH}_3)_2\dot{\text{C}}\text{OH}$ in pulsed, deoxygenated solutions of 10^{-3} M TNM and $2 \times 10^{-1} \text{ M}$ 2-propanol (pH 4–5). This process occurs with a yield of $G(\text{C}(\text{NO}_2)_3^-) = 5.6$.¹² (The G value represents the number of species formed or destroyed per 100 eV absorbed energy in a radiation induced process.)

All experiments were carried out at room temperature.

Results and Discussion

Oxidation by Ag(II). The oxidation of $\text{C}_2\text{H}_5\text{SSC}_2\text{H}_5$ by Ag^{2+} ions has been observed in pulse irradiated, N_2O saturated solutions of the disulfide (10^{-4} M) and $2 \times 10^{-3} \text{ M}$ Ag^+ at pH 4. Under these conditions $\text{OH}\cdot$ radicals which are produced with $G = 5.5$ (species per 100-eV absorbed energy) will almost quantitatively react with the silver ions to form Ag^{2+} ¹³ ($k = 6.9 \times 10^9 \text{ M}^{-1} \text{ s}^{-1}$). (A higher Ag^+ concentration could not be used because of the possibility of direct reaction of Ag^+ with e_{aq}^- .) The formation of Ag^{2+} was indicated by an immediate increase in optical absorption at 300 nm (Figure 1a). (A maximum absorption at 270 nm has been found.¹⁵) In the absence of other reactants Ag^{2+} has a considerable lifetime ($t_{1/2} > 1 \text{ ms}$) and decays by a second-order process. In the presence of 10^{-4} M $\text{C}_2\text{H}_5\text{SSC}_2\text{H}_5$ it disappears exponentially with $t_{1/2} = 20 \mu\text{s}$. At 420 nm a corresponding increase in optical absorption occurs (Figure 1b). The absorption spectrum taken at the time of complete decay of the 300-nm absorption and full development of the 420-nm absorption is shown in Figure

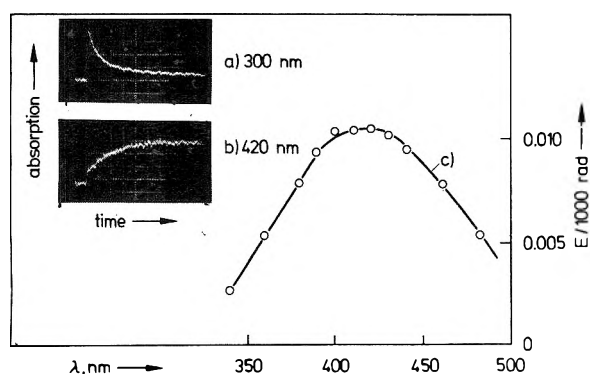


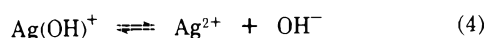
Figure 1. Optical absorption-time curves at 300 (a) and 430 nm (b) of pulse irradiated, N_2O saturated solutions of 2×10^{-3} M Ag^+ and 10^{-4} M $C_2H_5SSC_2H_5$ (pH 4). Time scale: $20 \mu s$ per large division; dose: ca. 700 rads. (c) Spectrum taken $180 \mu s$ after the pulse.

1c. It is identical with that of the disulfide radical cation formed in the electron transfer process

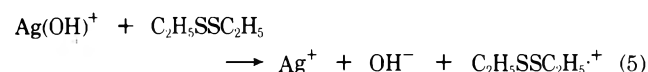


The rate constant for reaction 3 derived from Figures 1a and 1b and similar curves at several disulfide concentrations is $k_3 = (3.5 \pm 0.5) \times 10^8 \text{ M}^{-1} \text{ s}^{-1}$. The yield of $C_2H_5SSC_2H_5^+$ radical cations calculated from the maximum absorption at 420 nm and the known extinction coefficient of $\epsilon = 1.8 \times 10^3 \text{ M}^{-1} \text{ cm}^{-1}$ amounts to $G = 5.5$. This yield is identical with $G(OH\cdot) = G(Ag^{2+})$, i.e., oxidation of the disulfide by Ag^{2+} in contrast to direct oxidation by $OH\cdot$ radicals quantitatively leads to the radical cation as a primary product.

No change in $C_2H_5SSC_2H_5^+$ yield is observed over the pH range 3.5–8.0. Since $Ag(II)$ exists in the equilibrium



with a $pK = 5.3^{15}$ this means that the reaction

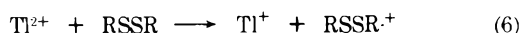


also leads quantitatively to disulfide radical cations. The rate constant $k_5 = (7.0 \pm 0.5) \times 10^8 \text{ M}^{-1} \text{ s}^{-1}$ has been determined.

Basically the same results are obtained for the oxidation of CH_3SSCH_3 by Ag^{2+} and $Ag(OH)^+$. The corresponding radical cation yields and rate constants are summarized in Table I together with the data of the other oxidation systems studied.

Oxidation by $Tl(II)$. The reaction of $Tl(II)$ with disulfides has been observed through the decay of the $Tl(II)$ absorptions ($\approx 260 \text{ nm}$)^{9,10,16} and the formation of the $RSSR^+$ absorptions. Solutions were generally N_2O saturated and contained 2×10^{-3} M Tl^+ and various lower concentrations of disulfide. The pH was adjusted by $HClO_4$ or $NaOH$. Under these conditions all $OH\cdot$ radicals reacted with Tl^+ within the duration of the pulse to form Tl^{2+} , $Tl(OH)^+$, or $Tl(OH)_2$ depending on the pH of the solution (see eq 2). Subsequently, reaction of these species with the disulfide could occur. The absorption-time curves obtained were principally similar to those given in Figure 1.

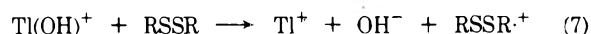
In acid solution (pH 3.5) the reaction



quantitatively leads to disulfide radical cations, i.e., occurs with $G = 5.5$. The rate constants for reaction 6 (see Table I)

are on the order of $2 \times 10^9 \text{ M}^{-1} \text{ s}^{-1}$. They are therefore markedly higher than for the oxidation of $RSSR$ by Ag^{2+} .

At pH 5.5–6.0 the reaction



was observed. The rate constants for these reactions are of the same order as k_6 . An interesting result is, however, obtained with respect to the yield of disulfide radical cations. It dropped to $G(RSSR^+) = 4.7$ and 4.6 for the dimethyl and diethyl disulfide, respectively. Since the $Tl(OH)^+$ absorption disappears completely in the presence of disulfide, i.e., $Tl(OH)^+$ quantitatively seems to react with $RSSR$, this would indicate that ca. 20% of the $Tl(OH)^+$ lead to oxidation products other than radical cations.

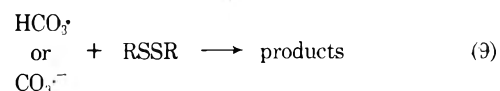
The reaction



investigated at pH >7.5 is difficult to observe. It is comparatively slow, i.e., rather high $RSSR$ concentrations have to be applied to obtain a pseudo-first-order disappearance of the $Tl(OH)_2$ absorption. To avoid direct reaction of $OH\cdot$ with $RSSR$ the Tl^+ concentration also would have to be increased which, however, also leads to an unwanted $Tl^+ + e_{aq}^-$ reaction. Therefore only an upper limit of $1 \times 10^8 \text{ M}^{-1} \text{ s}^{-1}$ can be estimated for k_8 . The yield of $RSSR^+$ radical cations from this reaction could not be determined within reasonable limits of error. The observable $RSSR^+$ absorption from reaction 8 is very small. This, however, is not only due to a possible reaction other than electron transfer, but also results from incomplete reaction of $Tl(OH)_2$ with $RSSR$ as well as from partial neutralization of $RSSR^+$ with OH^- within this pH range.

Oxidation by HCO_3^- and CO_3^{2-} . The reactions of the oxidized form of carbonate with disulfides have been studied in pulse irradiated, N_2O saturated solutions of 0.1–1.0 M HCO_3^- or CO_3^{2-} and low concentrations of disulfides. Since the pK of $HCO_3^- (= CO_3^{2-} + H_{aq}^+)$ is 9.6¹⁷ experiments were carried out at pH ≈ 8 and ≈ 11 . (The radicals $HCO_3\cdot$ and $CO_3^{2-\cdot}$ are formed in the reaction of $OH\cdot$ and HCO_3^- or CO_3^{2-} .^{17,18})

The rate constants for the reactions



were derived from the decay of the radical absorptions at 600 nm. In the absence of $RSSR$ both $HCO_3\cdot$ and $CO_3^{2-\cdot}$ are very long lived ($t_{1/2} > 10 \text{ ms}$). With added $RSSR$ they disappear completely according to an exponential rate law and with $t_{1/2}$ being inversely proportional to the disulfide concentration. The rate constants are found to be in the range of 10^7 – $10^8 \text{ M}^{-1} \text{ s}^{-1}$ (see Table I) and are similar to those determined in photolytic experiments for the corresponding reactions of $HCO_3\cdot$ and $CO_3^{2-\cdot}$ with some biochemically interesting disulfides.¹⁹

The yield of radical cations, $RSSR^+$, at low pH, where neutralization by OH^- ions does not yet occur, amounts to $G \approx 0.6$. Almost 90% of $HCO_3\cdot$ therefore do not lead to $RSSR^+$ in their reaction with disulfides. No radical cations could be observed for the reaction of $CO_3^{2-\cdot}$ with $RSSR$. However, even if $RSSR^+$ were formed their lifetime at the pH necessary for observation of $CO_3^{2-\cdot}$ reactions would be too short for detection due to neutralization by OH^- ions.

Oxidation by $SO_4^{\cdot-}$. The reaction of $SO_4^{\cdot-}$ radical anions with disulfides was studied in pulsed, argon saturated solutions of 10^{-1} M $S_2O_8^{2-}$ and low $RSSR$ concentrations under slightly acid conditions (pH ≈ 4.5). In such solutions $OH\cdot$ radicals which are present with $G = 2.7$ will directly react with $RSSR$ according to reaction 1. Since $OH\cdot$ forms $RSSR^+$ with

TABLE I: Oxidation of CH₃SSCH₃ and C₂H₅SSC₂H₅ by Various Oxidizing Species^f

Oxidant	CH ₃ SSCH ₃			C ₂ H ₅ SSC ₂ H ₅		
	<i>k</i> , M ⁻¹ s ⁻¹	<i>G</i> (RSSR ^{•+})	%(RSSR ^{•+})	<i>k</i> , M ⁻¹ s ⁻¹	<i>G</i> (RSSR ^{•+})	%(RSSR ^{•+})
Ag ²⁺	5.2 × 10 ⁸	5.5	100	3.5 × 10 ⁸	5.5	100
Ag(OH) ⁺	5.6 × 10 ⁸	5.4	100	7.0 × 10 ⁸	5.5	100
Tl ²⁺	2.3 × 10 ⁹	5.5	100	1.4 × 10 ⁹	5.5	100
Tl(OH) ⁺	1.5 × 10 ⁹	4.7	85	1.4 × 10 ⁹	4.6	84
Tl(OH) ₂	≤10 ⁸	≤1	≤20	≤10 ⁸	≤1.5	≤30
HCO ₃ ⁻	1.0 × 10 ⁸	≈0.6	≈10	4.5 × 10 ⁷	≈0.6	≈10
CO ₃ ⁻	8.0 × 10 ⁷			6.6 × 10 ⁷		
SO ₄ ⁻	3.8 × 10 ⁸	4.2 ^c	100	2.6 × 10 ⁸	4.3 ^c	100
Br ₂ ⁻	2.2 × 10 ⁹	5.5	100	1.8 × 10 ⁹	5.4	100
TMB ^{•+}	2.2 × 10 ⁹	5.6	100	2.1 × 10 ⁹	5.5	100
(CH ₃) ₂ S ^{•+}	<i>a</i>	<i>b</i>	100	<i>a</i>	<i>b</i>	100
(C ₂ H ₅) ₂ S ^{•+}	<i>a</i>	<i>b</i>	100	<i>a</i>	<i>b</i>	100
((CH ₃) ₃ C) ₂ S ^{•+}				5.0 × 10 ⁹	2.5 ^d	100 ^d
OH ^{•e}	1.7 × 10 ¹⁰	3.1	56	1.4 × 10 ¹⁰	3.0	55

^a Rate constant depends on thioether concentration (see text and ref 24). ^b Yield depends on thioether concentration (see text and ref 24). ^c Argon saturated solutions; total yield of RSSR^{•+} results from the reactions SO₄⁻ + RSSR and OH[•] + RSSR (see text). ^d The thioether radical is formed with only *G* = 2.5 (see text). ^e Taken from ref 24. ^f *k*, rate constant for the oxidation process; *G*(RSSR^{•+}), yield of RSSR^{•+} from N₂O saturated solutions unless otherwise noted; %(RSSR^{•+}), percentage yield of oxidant leading to RSSR^{•+} radical cations. The accuracy of the results is estimated to ±10%.

55% efficiency⁶ *G*(RSSR^{•+}) = 2.7 × 0.55 = 1.5. The hydrated electrons which are also present with *G* = 2.7 react with the peroxydisulfate in a fast reaction (*k* = 1.1 × 10¹⁰ M⁻¹ s⁻¹)²⁰



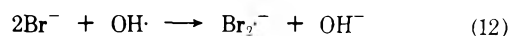
The subsequent reaction



is very difficult to study since the SO₄⁻ unfortunately has a very similar optical absorption (λ_{max} = 450 nm, ε = 1 × 10³ M⁻¹ cm⁻¹)^{20,21} and lifetime as RSSR^{•+}. Only at about 300 nm SO₄⁻ has a comparatively higher absorption than RSSR^{•+} and a faster decay is indicated in the presence of disulfide. From this estimates of *k*₁₁ = 5 × 10⁸ and 3 × 10⁸ M⁻¹ s⁻¹ are derived for CH₃SSCH₃ and C₂H₅SSC₂H₅, respectively. It should be mentioned, however, that the overall absorptions at this wavelength are very small and the observed signals could be artifacts. In order to positively prove reaction 11, the following experiments have been done: SO₄⁻ is known to react with alcohol,^{21,32} e.g., the SO₄⁻ absorption is seen to decay increasingly faster upon addition of CH₃OH (*k*(SO₄⁻ + CH₃OH) = 2 × 10⁷ M⁻¹ s⁻¹). On the other hand, RSSR^{•+} does not react with CH₃OH. If therefore reaction 11 occurred, i.e., the observable absorption was due to RSSR^{•+}, its decay should not be affected upon addition of methanol. This was indeed found by pulsing a solution of 10⁻¹ M S₂O₈²⁻, 2 × 10⁻³ M CH₃SSCH₃, and 3.2 × 10⁻³ M CH₃OH (pH 3.8). The half-life for the decay of the absorption at 440 nm remained the same with and without the methanol present (*t*_{1/2} = 75 μs), whereas in the absence of the disulfide *t*_{1/2} of the absorption (now due to SO₄⁻) is reduced to 10 μs by the alcohol.

The total yield of RSSR^{•+} radical cations formed in the solutions mentioned at the beginning of this section amounts to *G* = 4.2. With *G* = 1.5 resulting from direct OH[•] reaction (see above) this leaves another *G* = 2.7 formed through reaction 11. It therefore seems that SO₄⁻ which is formed with *G* = 2.7 quantitatively oxidizes the disulfides to radical cations through an electron transfer process.

Oxidation by Br₂⁻. Another powerful oxidant is Br₂⁻ formed in the overall reaction²²



Its reaction with disulfides was studied in pulsed, N₂O saturated solutions of 2 × 10⁻² M Br⁻ and (2–5) × 10⁻⁴ M RSSR at pH 4–5. The rate constants for the reactions



were derived from either the decay of the Br₂⁻ absorption at 360 nm or the formation of the RSSR^{•+} absorption at 430 nm and are also listed in Table I. Br₂⁻ is seen to oxidize disulfides as rapidly as Tl²⁺ and Tl(OH)⁺ ions.

The RSSR^{•+} yields (see also Table I) equal *G*(OH[•]) = *G*(Br₂⁻), i.e., the oxidation of disulfides is quantitatively described by reaction 13.

Oxidation by 1,3,5-Trimethoxybenzene Radical Cations. The oxidation of 1,3,5-trimethoxybenzene (TMB) in acid solution leads to radical cations TMB^{•+} in the reaction sequence



with a neutral OH radical addition product as an intermediate.⁸ The yield of TMB^{•+} is essentially controlled by the competition between the bimolecular decay of two TMB(OH)[•] radicals and the reaction of TMB(OH)[•] with H_{aq}⁺.

The reactions of disulfides with TMB(OH)[•] and TMB^{•+} can easily be studied since these species show strong optical absorptions peaking at 340 and 580 nm, respectively,⁸ and are practically transparent where RSSR^{•+} absorbs.

The pulse experiments were carried out with N₂O saturated solutions of 10⁻³ M TMB and (0.5–1.0) × 10⁻⁴ RSSR at different pH's. In acid solution the radical cation TMB^{•+} is seen to react with disulfides according to



with rate constants (see Table I) on the order of 2 × 10⁹ M⁻¹ s⁻¹.

At neutral pH where only TMB(OH)[•] exists, no reaction

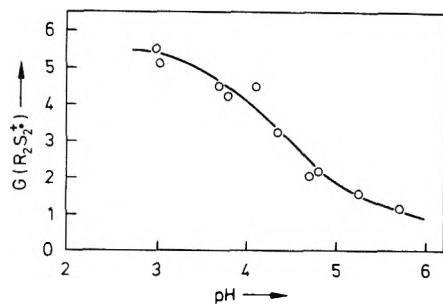


Figure 2. Yield of disulfide radical cations as a function of pH formed in pulse irradiated, N₂O saturated solutions of 10⁻³ M 1,3,5-trimethoxybenzene and 10⁻⁴ M CH₃SSCH₃.

could be observed, i.e., the decay of the optical absorption of TMB(OH)· was not affected by the addition of disulfide to the solution.

The yield of RSSR·⁺ is shown in Figure 2. At low pH $G(\text{RSSR}\cdot^+) = G(\text{TMB}\cdot^+) = G(\text{OH}\cdot)$ indicating that reaction 15 is quantitative. The RSSR·⁺ yield then decreases with increasing pH and essentially follows and thereby substantiates the curve published for the yield of TMB·⁺ radical cations as a function of pH.⁸

Oxidation by Thioether Radical Cations. Positively charged radical ions are also formed in the reaction of hydroxyl radicals with another class of sulfur organic compounds, namely, thioethers.²³⁻²⁵ For simple aliphatic thioethers they predominantly exist as complexed ions in the equilibrium²⁴



Pulse radiolysis experiments have been carried out to determine whether RSSR·⁺ could oxidize R₂S or (R₂S)₂⁺/R₂S⁺ could oxidize RSSR. No reaction could be observed between the disulfide radical cation and thioethers. In solutions of high RSSR concentration (2 × 10⁻³ M) the transient RSSR·⁺ absorption is not affected upon addition of thioether, and also the characteristic (R₂S)₂⁺ absorption at 480–500²⁴ nm does not appear, i.e.



On the other hand, in solutions containing high concentrations of thioethers the (R₂S)₂⁺ absorption is seen to decay upon addition of disulfide and the (R₂S)₂⁺ absorption is replaced by a spectrum identical with that of RSSR·⁺. The oxidation of dimethyl disulfide by thioether radical cations occurs with $k = 2.3 \times 10^7$, 2.7×10^7 , and $\leq 5 \times 10^6 \text{ M}^{-1} \text{ s}^{-1}$ in solutions containing 10⁻² M (CH₃)₂S, (C₂H₅)₂S, and (CH₂)₄S, respectively, together with low ($\approx 10^{-4}$ M) concentrations of the disulfide. These rate constants indicate relatively slow processes. However, the respective k 's increase with decreasing thioether concentration. For example, $k = 2.7 \times 10^7$, 5.6×10^7 , 6.3×10^7 , 7.8×10^7 , 1.4×10^8 , and $2.0 \times 10^8 \text{ M}^{-1} \text{ s}^{-1}$ for solutions containing 1.0 × 10⁻², 5.3 × 10⁻³, 3.6 × 10⁻³, 1.8 × 10⁻³, 1.0 × 10⁻³, and 5 × 10⁻⁴ M (C₂H₅)₂S, respectively. This would suggest that the underlying process is the reaction of the uncomplexed R₂S⁺ radical cation



with R₂S⁺ having to be formed through the equilibrium given in eq 16. This conclusion is also in agreement with our previous finding that the complexed radical cation (R₂S)₂⁺ is rather stable and reactions essentially occurred through the uncomplexed R₂S⁺.²⁴

Further support for this mechanism arises from the corre-

sponding results from N₂O saturated solutions containing di-*tert*-butyl thioether (10⁻³ M) and diethyl disulfide (10⁻⁴ M). In contrast to the other thioethers no complexed radical cations are formed (probably due to steric reasons)²⁴ and the monomer radical cation is immediately available for the reaction



The rate constant measured for this process is $k_{19} = 5 \times 10^9 \text{ M}^{-1} \text{ s}^{-1}$. It therefore appears that this high rate constant, indicating an almost diffusion controlled process, is representative of an electron transfer reaction between a disulfide and an uncomplexed thioether radical cation.

The yield of RSSR·⁺ formation through reaction 18 is identical with $G((\text{R}_2\text{S})_2^+)$, i.e., $G(\text{R}_2\text{S}^+)$ except for the di-*tert*-butyl thioether. In the latter case the absolute yield of R₂S⁺ could not yet be determined, since this species is not the only positively charged oxidation product. In addition several overlapping absorptions in the 300-nm range precluded any quantitative conclusions.²⁶ It appears, however, that only the R₂S⁺ radical cation is able to oxidize disulfides. Upon addition of RSSR to the pulsed di-*tert*-butyl thioether solution part of the 300-nm absorption is seen to decay faster with increasing RSSR concentration and the RSSR·⁺ absorption at about 430 nm is formed. The yield of RSSR·⁺ amounts to $G = 2.5$. This value is therefore considered to represent the yield of ((CH₃)₃C)₂S⁺ formed initially during the oxidation of di-*tert*-butyl thioether by hydroxyl radicals.

Conclusion

The oxidation of disulfides depends on the nature of the oxidizing species. Ag²⁺, Ag(OH)⁺, Tl²⁺, Br₂⁻, R₂S⁺, TMB·⁺, and SO₄⁻ are only involved in an electron transfer process and quantitatively form an RSSR·⁺ radical cation in their reaction with a disulfide. Other oxidants as Tl(OH)⁺, OH·, and HCO₃⁻ (most likely also CO₃⁻) only partially yield RSSR·⁺. This could be explained if the transition state complexes between these latter oxidants and disulfides stabilize not only by an electron transfer process leading to RSSR·⁺, but also by nonionic fragmentation into radicals and smaller molecules as has already been established in detail for the OH· radical reaction with disulfides.¹⁻⁶ Tl(OH)⁺ and HCO₃⁻ may in fact act as quasi-OH· donors. They cannot be considered to provide free hydroxyl radicals, however, since $G(\text{RSSR}\cdot^+)$ from HCO₃⁻, for example, is much lower than from free OH· radicals.

It is interesting to compare the Tl(OH)⁺ and Ag(OH)⁺ results. The reduced efficiency of Tl(OH)⁺ to form RSSR·⁺ does not seem to be related to its reactivity toward disulfides. The rate constant for the reaction of Tl(OH)⁺ is about five times higher than that of Ag(OH)⁺. Looking at the absorption spectra of Tl²⁺/Tl(OH)⁺ and Ag²⁺/Ag(OH)⁺^{10,15} it appears that different electronic structures may apply to these two systems. This could possibly be one of the reasons why Ag(OH)⁺ only undergoes electron transfer and Tl(OH)⁺ may also act through another reaction route.

It also seems noteworthy that of the structurally similar HCO₃⁻ and SO₄⁻ only the latter forms RSSR·⁺ ions. Owing to the spectral problems discussed earlier the results concerning SO₄⁻ are, however, somewhat ambiguous. We are not able to either prove or exclude the possibility of an intermediate SO₄⁻ adduct to RSSR which then could rearrange by an overall electron transfer mechanism (SO₄⁻ adducts have been discussed occasionally in the literature).²⁷⁻²⁹

The rate constants measured for the reactions of the various oxidizing species in general are in good agreement with other

TABLE II: Rate Constants for the Bimolecular Decay of $\text{RSSR}^{\cdot+}$ Formed in the Reaction of Various Oxidizing Species with $\text{CH}_3\text{SSCH}_3^c$

Oxidant	Ionic strength	%($\text{RSSR}^{\cdot+}$)	$2k_2, \text{M}^{-1} \text{s}^{-1}$
Ag^{2+}	3×10^{-3}	100	6.8×10^8
Tl^{2+}	3×10^{-3}	100	7.4×10^8
Br_2^-	3×10^{-3}	100	6.5×10^8
	2×10^{-2}		1.1×10^9
	1×10^{-1}		1.5×10^9
$\text{Tl}(\text{OH})^+$	3×10^{-3}	85	2.8×10^9
$\text{SO}_4^{\cdot-}$ ^a	3×10^{-2}	87 ^a	3.1×10^9
OH^{\cdot} ^b		55	6.0×10^9

^a In the argon saturated solution of $\text{S}_2\text{O}_8^{2-}$ the reaction $\text{OH} + \text{RSSR}$ leads to $\text{RSSR}^{\cdot+}$ with 55% efficiency while e_{aq}^- are quantitatively converted to $\text{SO}_4^{\cdot-}$ and $\text{RSSR}^{\cdot+}$. ^b Taken from ref 24. ^c The accuracy of $2k_2$ is estimated to $\pm 15\%$.

published data.^{7,8,17,19,24} High rate constants have been found, for example, for the oxidation reactions of Br_2^- , Tl^{2+} , and TMB^+ , while HCO_3^- and CO_3^- were found to react considerably slower.

The present experiments also serve as additional proof for part of the mechanism published for the disulfide oxidation by hydroxyl radicals.^{4,6} To explain the decay of the $\text{RSSR}^{\cdot+}$ radical cation two simultaneous reactions



and

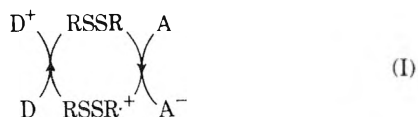


had to be proposed.⁶ (RSOH is formed by reaction 1b with about equal yield as $\text{RSSR}^{\cdot+}$.) The second-order rate constants for the decay of the $\text{RSSR}^{\cdot+}$ absorption in the various systems are summarized in Table II. The lowest rate constants are found for those solutions ($\text{Ag}(\text{II})$, Br_2^- etc.) where $\text{RSSR}^{\cdot+}$ is the only primary oxidation product and its decay solely occurs through reaction 20. The smaller the yield of $\text{RSSR}^{\cdot+}$, i.e., the higher the probability for $\text{RSSR}^{\cdot+}$ to react also with an uncharged species (RSOH or possibly still other species), the higher the rate constant which is observed for its overall decay. In addition kinetic salt effect experiments show a corresponding effect on the second-order rate constant. Only if $\text{RSSR}^{\cdot+}$ is the sole primary species, a bimolecular reaction of two singly charged species of the same sign is clearly indicated.

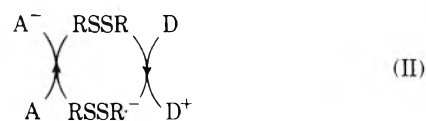
In our previous papers it has been shown that $\text{RSSR}^{\cdot+}$ radical cations can act themselves as oxidants by accepting an electron from suitable partners, e.g.



thereby undergoing a repair process.^{5,6} Disulfides may therefore be involved in an electron transfer chain



where the electron acceptor A could be a species such as Ag^{2+} , Br_2^- , R_2S^+ , TMB^+ , etc. and the electron donor D a species such as Fe^{2+} , RSOH , etc. Similarly it has been established that disulfides could also mediate electrons through their anionic form^{30,31}



where the donor D could even be a free or solvated electron. These mechanisms can be considered to be of particular significance for biochemical processes. Mechanism I as can be seen from our present experiments strongly depends on the nature of the oxidant, i.e., the electron acceptor A, since several of them such as OH^- , $\text{Tl}(\text{OH})^+$, HCO_3^- , do not only yield $\text{RSSR}^{\cdot+}$ and thus lead to partial destruction of the disulfide. On the other hand, mechanism II leads to regeneration of RSSR only in solutions with $\text{pH} > \text{pK}(\text{RSSRH}^-)$, i.e., mostly in basic environment. The protonated form of the disulfide anion, RSSRH , is very unstable and decays into fragments prior to a possible electron transfer to another species. Mechanism I can operate at any $\text{pH} < 8-9$. At higher pH neutralization of $\text{RSSR}^{\cdot+}$ by OH^- ions also leads to irreversible fragmentation.

References and Notes

- (1) (a) J. W. Purdie, *J. Am. Chem. Soc.*, **89**, 226 (1967); (b) *Can. J. Chem.*, **47**, 1029 (1969); (c) *ibid.*, **47**, 1037 (1969); (d) *ibid.*, **49**, 725 (1971).
- (2) (a) T. C. Owen, A. C. Wilbraham, J. A. Roach, and D. R. Ellis, *Radiat. Res.*, **50**, 234 (1972); (b) T. C. Owen and A. C. Wilbraham, *ibid.*, **50**, 253 (1972); (c) T. C. Owen and D. R. Ellis, *ibid.*, **53**, 24 (1973).
- (3) W. A. Armstrong and W. G. Humpheys, *Can. J. Chem.*, **45**, 2589 (1967).
- (4) B. C. Gilbert, H. A. H. Laue, R. O. C. Norman, and R. C. Sealy, *J. Chem. Soc., Perkin Trans. 2*, 892 (1975).
- (5) H. Möckel, M. Bonifačić, and K.-D. Asmus, *J. Phys. Chem.*, **78**, 282 (1974).
- (6) M. Bonifačić, K. Schäfer, H. Möckel, and K.-D. Asmus, *J. Phys. Chem.*, **79**, 1496 (1975).
- (7) G. E. Adams, J. E. Aldrich, R. H. Bisby, R. B. Cundall, J. L. Redpath, and R. L. Willson, *Radiat. Res.*, **49**, 278 (1972).
- (8) (a) P. O'Neill, S. Steenken, and D. Schulte-Frohlinde, *Angew. Chem.*, **87**, 417 (1975); (b) *Angew. Chem., Int. Ed.*, 430 (1975); (c) *J. Phys. Chem.*, **79**, 2773 (1975).
- (9) P. O'Neill and D. Schulte-Frohlinde, *J. Chem. Soc., Chem. Commun.*, 387 (1975).
- (10) M. Bonifačić and K.-D. Asmus, *J. Chem. Soc., Dalton Trans.*, in press.
- (11) A. Henglein, *Allg. Prakt. Chem.*, **17**, 296 (1966).
- (12) (a) K.-D. Asmus, *Int. J. Radiat. Phys. Chem.*, **4**, 417 (1972); (b) K.-D. Asmus, H. Möckel, and A. Henglein, *J. Phys. Chem.*, **77**, 1218 (1973).
- (13) J. Pukies, W. Roebke, and A. Henglein, *Ber. Bunsenges. Phys. Chem.*, **72**, 842 (1968).
- (14) G. C. Barker and P. Fowles, *Trans. Faraday Soc.*, **66**, 1661 (1970).
- (15) M. Bonifačić, K.-D. Asmus, P. O'Neill, and S. Steenken, to be submitted for publication.
- (16) B. Cercek, M. Ebert, and A. J. Swallow, *J. Chem. Soc. A*, 612 (1966).
- (17) (a) S. Chen, V. W. Cope, and M. Z. Hoffman, *J. Phys. Chem.*, **77**, 1111 (1973); (b) S. Chen and M. Z. Hoffman, *J. Chem. Soc., Chem. Commun.*, 991 (1972).
- (18) (a) J. L. Weeks and J. Rabani, *J. Phys. Chem.*, **70**, 2100 (1966); (b) G. E. Adams and J. W. Boag, *Proc. Chem. Soc.*, 112 (1964).
- (19) S. Chen and M. Z. Hoffman, *Radiat. Res.*, **56**, 40 (1973); **62**, 18 (1975).
- (20) W. Roebke, M. Renz, and A. Henglein, *Int. J. Radiat. Phys. Chem.*, **1**, 39 (1969).
- (21) E. Heckel, A. Henglein, and G. Beck, *Ber. Bunsenges. Phys. Chem.*, **70**, 149 (1966).
- (22) (a) H. C. Sutton, G. E. Adams, J. W. Boag, and B. D. Michael in "Pulse Radiolysis", M. Ebert, J. P. Keene, A. J. Swallow, and J. H. Baxendale, Ed., Academic Press, London, 1965, pp 61-81; (b) B. Cercek, M. Ebert, C. W. Gilbert, and A. J. Swallow, *ibid.*, 1965, pp 83-98.
- (23) G. Meißner, A. Henglein, and G. Beck, *Z. Naturforsch. B*, **22**, 13 (1967).
- (24) M. Bonifačić, H. Möckel, D. Bahnemann, and K.-D. Asmus, *J. Chem. Soc., Perkin Trans. 2*, 675 (1975).
- (25) (a) B. C. Gilbert, D. K. C. Hodgeman, and R. O. C. Norman, *J. Chem. Soc., Perkin Trans. 2*, 1748 (1973); (b) B. C. Gilbert, J. P. Larkin, and R. O. C. Norman, *ibid.*, 272 (1973).
- (26) Unpublished results.
- (27) R. O. C. Norman, P. M. Storey, and P. R. West, *J. Chem. Soc. B*, 1087 (1970).
- (28) R. O. C. Norman and P. M. Storey, *J. Chem. Soc. B*, 1099 (1970).
- (29) C. Walling and D. M. Camaioni, *J. Am. Chem. Soc.*, **97**, 1603 (1975).
- (30) G. E. Adams, G. S. Naughton, and B. D. Michael in "Excitation and Ionization", G. Scholes and G. R. A. Johnson, Ed., Taylor and Francis, London, 1967.
- (31) R. L. Willson, *J. Chem. Soc., Chem. Commun.*, 1424 (1970).
- (32) J. L. Redpath and R. L. Willson, *Int. J. Radiat. Biol.*, **27**, 389 (1975).

COMMUNICATIONS TO THE EDITOR

Dependence of Molybdenum(V) Electron Paramagnetic Resonance Signals on Temperature

Publication costs assisted by the National Science Foundation

Sir: It has been known for over 10 years that when Mo/ γ -Al₂O₃ catalysts are reduced, an EPR signal due to Mo⁵⁺ is developed.¹ This signal has been ascribed to Mo⁵⁺ formed from Mo⁶⁺ in O_h symmetry which, upon reduction, loses oxygen ligands to form Mo⁵⁺ in square pyramidal coordination and belonging to the C_{4v} symmetry point group.² Recently, based on comparison³ with Mo⁵⁺ spectra in Bi₂(MoO₄)₃ and on Q-band EPR evidence, we noted that this EPR signal could equally well originate from Mo⁵⁺ in a tetragonally distorted T_d symmetry.⁴ A comparison of the values of g_{\parallel} and g_{\perp} is a customary approach to assignment of crystal field symmetry. However, the lack of suitable literature data on well-defined Mo⁵⁺ systems makes distinction between the two symmetries on this basis unsatisfactory.

Some unexpected results were obtained from experiments made to better define this important system and a preliminary report of these is given here. Recently, Hall and Lo Jacono introduced evidence suggesting that the Mo⁵⁺ EPR signal corresponds to only about 10% of the Mo⁵⁺ ions produced upon reduction.⁵ If so, then a central problem concerns the reason why only a small fraction of the Mo⁵⁺ ions are observable at room temperature. Several explanations can be offered. One is the presence of the greater portion of the Mo⁵⁺ ions in a symmetry, such as O_h, which facilitates fast spin-lattice relaxation at room temperature and results in lines too broad to detect even at liquid nitrogen temperature. This could be verified by obtaining spectra at even lower temperatures, e.g., at 4.2 K where the spin-lattice relaxation times should be slow enough to narrow the line to an acceptable signal-to-noise ratio. Another possibility is line broadening by strong interactions between spins of adjacent ions. If the first process is a significant mechanism resulting in Mo⁵⁺ loss, the signal intensity will increase as the line becomes narrower upon going to low temperatures, but if the second process is taking place, the line shape and intensity could only be affected by going to temperatures sufficiently high to overcome the interaction energy between the spins.

We have performed experiments by EPR between 4.2 and 560 K on several samples treated with hydrogen in an all-glass circulating system with a liquid nitrogen trap to remove water produced upon reduction. The catalyst which consisted of 8% Mo/ γ -Al₂O₃ was reduced to varying extents by changing the hydrogen pressure, temperature, and time of reduction. Afterwards, aliquots were transferred to 4-mm quartz tubes sealed onto the side of the reactor. They were then sealed off under vacuum or in the ambient H₂. During the low-temperature EPR experiments, the temperature was measured using a calibrated chromel-constantan thermocouple. The EPR line intensities were normalized against a Cr³⁺ ruby standard

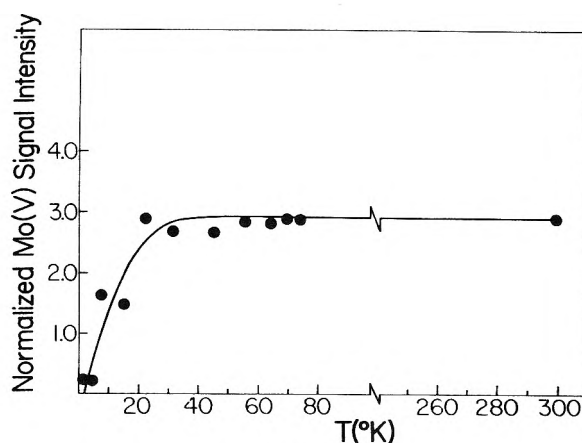


Figure 1. Dependence of Mo⁵⁺ EPR signals on temperature.

which in turn was calibrated at various temperatures against a DPPH standard.

Figure 1 shows a plot of the normalized Mo⁵⁺ signal intensity vs. temperature. This signal exhibits a line width of 80 G which is invariant in the temperature range studied. The normalized intensity of the Mo⁵⁺ line remains constant down to a temperature of 15 ± 5 K, at which temperature it undergoes a sudden decrease to a value of about 0.09 of its intensity at liquid nitrogen temperature. In light of these results, saturation studies were performed on some representative samples at 4.2 K. The peak-to-peak intensity of the signal increased linearly with the square root of power indicating the absence of saturation.

These results can only lead us to conclude that the Mo⁵⁺ ions seen by EPR are present in a symmetry resulting in a low lying singlet ground state which explains the invariance of the line shape and intensity down to such low temperatures. Furthermore, these ions must exhibit weak spin-spin interactions, since the temperature required to overcome them, i.e., the transition point in Figure 1, is very close to liquid helium temperature. As to the question of the absence of 90% of the EPR line intensity resulting from Mo⁵⁺ calculated to be on the surface, our present hypothesis is that these ions must exist in an environment different from the ones observed by EPR, and that these ions are strongly interacting since this interaction energy cannot be overcome at the upper limits of the temperature studied.

Acknowledgments. Support of this work by the National Science Foundation (Grant No. CHE74-11539) and by the Graduate School of the University of Wisconsin-Milwaukee is gratefully acknowledged.

References and Notes

- G. K. Borekov, V. A. Dzis'ko, V. M. Emel'yanova, Y. I. Pechnerskaya, and V. B. Kazanskii, *Dokl. Akad. Nauk SSR*, **150**, 829 (1963).

- (2) K. S. Seshardi and L. Petrakis, *J. Catal.*, **30**, 195 (1973).
 (3) A. F. Van den Elzen and G. D. Rieck, *Acta Crystallogr., Sect. B*, **29**, 2433 (1973).
 (4) S. Abdo, M. Lo Jacono, R. B. Clarkson, and W. Keith Hall, *J. Catal.*, **36**, 330 (1975).
 (5) W. Keith Hall and M. Lo Jacono, "The Surface Chemistry of Molybdena-Alumina Catalysts," presented to the Vth International Congress on Catalysis, London, July, 1976, paper A-16.

Laboratory for Surface Studies
 Department of Chemistry
 University of Wisconsin
 Milwaukee, Wisconsin 53201

Received February 9, 1976

Suheil Abdo
 R. B. Clarkson
 W. Keith Hall*

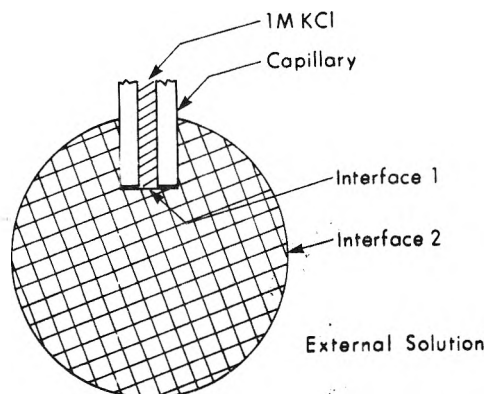


Figure 1. Diagrammatic representation of the measurement system.

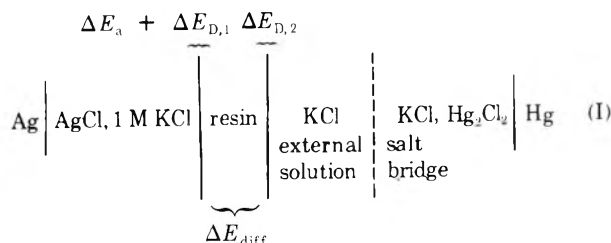
Comment on "Biological Ion Exchanger Resins. VI. Determination of the Donnan Potentials of Single Ion Exchange Beads with Microelectrodes", by M. Goldsmith, D. Hor, and R. Damadian¹

Publication costs assisted by the University of Alberta

Sir: The concept of the Donnan potential, as it is commonly used to explain certain aspects of the behavior of ion-exchange resins, refers to the potential difference between the resin and the external solution, and as such is a single phase boundary potential.² While the experiments of Goldsmith et al. have revealed some interesting electrochemical behavior, we question their two fundamental claims of: (1) having measured an interfacial Donnan potential, and (2) having measured single-ion activities of potassium ion in the resin phase. Furthermore, we propose that their data can be explained in terms of well-known properties of ion-exchange membranes.²

Any resin surface constitutes an interface, whether it be the spherical surface of the resin bead or the interface between the punctured bead and capillary electrode tip. See Figure 1. For example, cutting a resin bead in half, grinding it into small particles, or puncturing it with a microelectrode merely exposes fresh resin "surface" and does not provide access to the internal resin phase in an electrochemical sense. The punctured resin bead becomes an ion-exchange membrane separating the potassium chloride solution in the capillary from that in the petri dish.

The cell representation for the potentiometric measurement system employed is



The terms in (I) are defined as follows: $\Delta E_{D,1}$ is the Donnan potential at the interface between the resin and 1 M potassium chloride capillary solution; $\Delta E_{D,2}$ is the Donnan potential at the resin-petri dish solution interface; ΔE_{diff} is the diffusion potential between the two interfaces; ΔE_a includes any residual junction potential between solution in the capillary and solution just outside the capillary tip in the puncture well, along with any asymmetry potential arising from differences

in the nature of the aged resin external surface and the freshly exposed surface. This term is probably small. All other potential differences in the cell are compensated for by the calibration procedure. It is necessary to recognize that the potential difference in the vicinity of the electrode tip is primarily an interfacial potential, similar in character and origin to that between the resin and external solution.

The reported voltages (ΔE_{measd}) are given by

$$\Delta E_{\text{measd}} = \Delta E_{D,1} - \Delta E_{D,2} + \Delta E_{\text{diff}} + \Delta E_a \quad (1)$$

where the first three terms on the right constitute the conventional "membrane potential". Assuming that both the concentration of potassium chloride in the capillary (1 M) and ΔE_a remain constant from measurement to measurement, then the cell voltage at 25 °C can be related to the activity in the external solution (a_{K^+}) by the limiting equation^{2,3}

$$\Delta E_{\text{measd}} = \Delta E^0 - 0.0591 \log a_{K^+} \quad (2)$$

A plot of $\log a_{K^+}$ vs. ΔE_{measd} would show a "Nernstian" slope, as is true for many membrane electrodes (see Figure 1 of Goldsmith et al.).

When the concentration of potassium chloride in the external solution is equal to that in the capillary (i.e., 1 M) then $\Delta E_{\text{measd}} = \Delta E_a$, since $\Delta E_{D,1} = \Delta E_{D,2}$ and $\Delta E_{\text{diff}} = 0$. Using 0.605, the mean ionic activity coefficient of potassium chloride,⁴ as the activity coefficient of 1 M K^+ , a concentration of 1 M corresponds to an activity of 0.605. The voltage at this activity of K^+ in the external solution can be read from Figure 1 of Goldsmith et al. as 4 MV. This is the value of ΔE_a and can be seen to be quite small.

The limiting equation (eq 2) is valid up to external solution ionic strength of about 0.1, above which the resin becomes less cation permselective.² This may account for the deviation from Nernstian slope at K^+ activities greater than 0.1.

In conclusion, it is impossible to potentiometrically measure the (Donnan) interfacial potential between an ion-exchange resin phase and external solution without introducing a second interfacial potential, and thereby measuring a trans-membrane voltage. Consequently, intraresin ion activities are inaccessible in this experiment.⁵

Acknowledgments. This work was supported by the National Research Council of Canada and the University of Alberta.

References and Notes

- (1) M. Goldsmith, D. Hor, and R. Damadian, *J. Phys. Chem.*, **79**, 342 (1975).
 (2) F. Helfferich, "Ion Exchange", McGraw-Hill, New York, N.Y., 1962, Chapter 8.

- (3) The sign in this equation and the sign of the slope in the plot of $\log a_{K^+}$ vs. ΔE_{meas} can be reversed in theory by writing the cell representation backwards or in practice by reversing the polarity of the potentiometer.
- (4) H. S. Harned and B. B. Owen, "The Physical Chemistry of Electrolytic Solutions", 3d ed, Reinhold, New York, N.Y., 1958, p 731.
- (5) Shortly after preparing the above comments, the work of G. A. Kurella came to our attention. Kurella performed an experiment similar to that of Goldsmith et al., using a sulfonated polystyrene-2% divinylbenzene resin (KU-2). His interpretation of his findings are essentially the same as that which we have proposed for the Goldsmith et al. results. G. A. Kurella in A. Kleinzeller and A. Kotyk, Ed., "Symposium on Membrane Transport and Metabolism", Academic Press, New York, N.Y., 1961.

Department of Chemistry
University of Alberta
Edmonton, Alberta, Canada T6G 2G2

F. F. Cantwell*
Rolf Saetre

Received April 6, 1976

Reply to "Comment on Biological Ion Exchanger Resins. VI. Determination of the Donnan Potentials of Single Ion Exchange Beads with Microelectrodes", by F. Cantwell and R. Saetre

Publication costs assisted by the Downstate Medical Center

Sir: Cantwell and Saetre have raised certain objections to the work published in this journal in January, 1975.¹ Their objections raise several important points to which I would like to respond.

I quite disagree with their statement that the measurements in question do "not provide access to the internal resin phase in an electrochemical sense", but rather that the microelectrode is merely being exposed to fresh surface. When the bead surface "reseals itself" around the shank of the penetrating microelectrode, the only complete electrical circuit involves the movement of current through the body of the resin bead. Since the potential "seen" by the microelectrode does not change by exposing it to the fresh internal "surfaces" of the bead, one might conclude, as these correspondents did, that we have merely exposed fresh surface. However, the more appropriate conclusion is that the resin is a homogeneous system of charge. Were the charge density of the resin to vary with distance from the surface, the microelectrode would register a change in potential with depth of puncture. Thus, I believe that we have indeed provided access to the internal phase in an electrochemical sense.

The main objection of the correspondents appears to be the impossibility of measuring a Donnan potential. In publishing our results, I was quite aware of the theoretical impossibility of directly measuring either Donnan potentials or single-ion activities. At the beginning of the Results section of our publication,¹ we stated "The Donnan potential of a resin bead cannot be directly measured since it is a single electrode potential and as such is undefined". To accept the impossibility of an absolute measurement, however, is not to give up all attempts at meaningful experimental approximations. If it were, we would deprive ourselves of such useful tools as pH determinations which, because of their single-ion definition, are not absolutely measurable. Indeed, any experimental attempt to determine a Donnan potential actually measures a "Donnan potential difference" plus some small electrokinetic voltages. Although many ion-exchange membranes are heterogeneous in nature, Cantwell and Saetre are quite correct

in stating that the electrochemical cell used in our measurements is analogous to a membrane electrode system. I believe, however, that naming the determined voltage a "membrane potential" will lead to a great deal of confusion. A term more descriptive of the origins of the voltage would be the "Donnan potential difference".

The confusion I am referring to arises because the use of the term "membrane potential" by electrochemists studying ion-exchange membranes infers something quite different from the "membrane potential" observed by electrophysiologists studying biological systems. The former are dealing with a Donnan potential difference which has an electrokinetic component of increasing magnitude as the permselectivity of the exchanger decreases. The voltage in this system arises primarily from the existence of a separate fixed charge phase which may be allowed to come to equilibrium with its environment. The biological "membrane potential" is widely construed to be different, and is based on the following rationale.

1. Voltages determined across the cellular surface do not agree with the theoretical Donnan potential predicted from the actual ion distribution.

2. Since the measured voltage must equal the Donnan potential if the voltage is an equilibrium voltage, deviations from the predicted Donnan equilibrium value must mean that electrokinetic potentials (usually assumed to be diffusion potentials) are present.

3. Since the ion composition of the cell and its surroundings does not change with time, a diffusion potential can only exist if an ion, diffusing in one direction, is returned in the form of a noncharged complex.

4. In order to form such noncharged complexes, there must exist ion carriers which ferry charges unidirectionally (at the expense of metabolic energy) and thus allow a diffusion potential to arise without a net movement of ions. These carriers are therefore referred to as "electrogenic ion pumps".

For reasons of cellular anatomy, the measured cellular voltage is called a "membrane potential". Thus, the "membrane potential" of artificial ion exchangers owes its existence to the fixed charges of the exchanger phase, while the biological "membrane potential" is widely assumed to be largely an electrokinetic voltage which owes its existence to "electrogenic ion pumps". In general, the title "membrane potential" implies that the origin of the voltage lies not with the existence of a fixed charge phase, but rather with the "permeability" of charges through a membrane, and the existence of electrokinetic phenomena.

This implication is quite clear in the interpretation which Cantwell and Saetre give to the deviation from Nernstian slope which the resin displayed at high external salt activity. They attribute the nonideal behavior to a loss in permselectivity, analogous to what occurs in a dialyzing membrane. We would point out, however, that the deviations from Nernstian behavior were always accompanied by a quite noticeable contraction of the resin bead. Such a contraction must necessarily cause an increase in intraresin cation molality. Thus, the deviation from ideality is quite easily interpretable from the Donnan viewpoint and further complications should be avoided until they offer additional insights.

With regard to the biological concept of the "membrane potential", it has several significant difficulties. First among these is that "electrogenic ion pumps" have yet to be chemically isolated despite intense efforts. Second, the necessity of postulating such pumps rests on the belief that the ion distributions in biological systems are not consistent with equi-

librium or near-equilibrium voltages. This fundamental belief has never, in fact, been adequately tested, in that the standard state potential difference is not included in calculations. This factor cannot be omitted since most cells are 30–40% non-aqueous by weight. In tissues where this factor is included, the necessity for electrogenic pumps has disappeared.^{2–5} With the continuing demise of such pumps, the term “membrane potential” may attain a clearer meaning in the future. However, until the situation in electrophysiology is corrected, the designation of the voltages we measured as “membrane potentials” can only lead to greater confusion.

References and Notes

- (1) M. Goldsmith, D. Hor, and R. Damadian, *J. Phys. Chem.*, **79**, 342 (1975).
- (2) G. Ling, *J. Gen. Physiol.*, **43**, 149 (1960).
- (3) N. Joseph, M. Engel, and H. Catchpole, *Nature (London)*, **191**, 1175 (1961).
- (4) N. Joseph, M. Engel, and H. Catchpole, *Nature (London)*, **203**, 931 (1964).
- (5) H. Catchpole, N. Joseph, and M. Engel, *Fed. Proc.*, **25**, 1124 (1966).

Department of Medicine and
Program in Biophysics
State University of New York at Brooklyn
Brooklyn, New York 11203

Michael Goldsmith

Received May 3, 1976

Ferrioxalate Actinometry. A Warning on Its Correct Use

Sir: While recalibrating the ferrioxalate actinometer,^{1,2} we found it to be erratic and irreproducible, a complaint we have subsequently heard from numerous photochemists. We have traced the problem to an apparently previously unrecognized slow photodegradation of the 1,10-phenanthroline (phen) solutions which makes the development time dependent on the age of the phen solution and the order of addition of reagents; using published procedures errors can be >40%.

We followed the procedures of Hatchard and Parker¹ using reagent grade chemicals. Two bottles of phen (G. Frederick Smith Chemical Co.) and several preparations of potassium ferrioxalate and buffer¹ were used. Our original data were taken with the phen solutions stored in thin-walled clear Pyrex bottles under fluorescent room lights.

Typical development data for a uv photolysis of 0.006 M potassium ferrioxalate are given in Figure 1. The slow development of the phen first solutions and the dual terminal absorbances arose only with the aged phen solutions and were insensitive to the preparation or age of the other components. When aged phen was added first, longer delays before addition of the buffer produced lower initial absorbances and longer development times. Addition of Fe²⁺ to premixed phen-buffer solutions yielded behavior like the buffer first results. The problems were common to all Fe²⁺ sources.³ Addition of NH₄F, recommended to accelerate color development,⁴ was without effect on the development times or the presence of two final absorbances. Where two “terminal” absorbances resulted, the buffer first value was the correct one, although it took up to ~5–6 h to develop.⁵ Phen solutions prepared within a few weeks of use, however, always yielded immediate

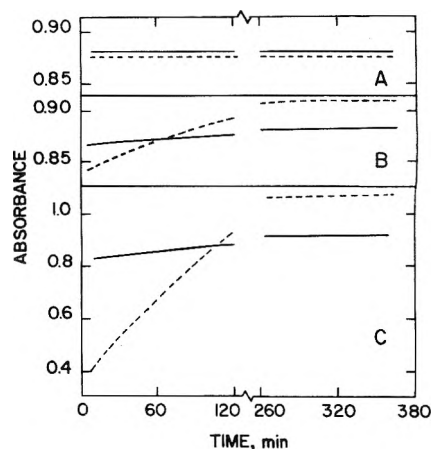


Figure 1. Development of longwave uv photolyzed 0.006 M ferrioxalate developed with: (A) fresh phen solution; (B) 7-week old phen solution; (C) 8-month old phen solution. (—) Buffer added to ferrioxalate followed by phen. (---) Phen added to ferrioxalate followed by buffer. In A the phen first curve is shifted upward by 0.01 for visualization. Absorbances cannot be compared for different samples of phen because of differing quantum doses. Each solution was diluted to 25 ml and contained 1 ml of irradiated ferrioxalate, 2 ml of 0.1% phen solution, and 1 ml of acetate buffer. All measurements were in a 1-cm cell. Phen solutions were stored in thin-walled Pyrex bottles under fluorescent room lights.

(<3 min) color formation with terminal absorbances independent of the order of addition of reagents.⁶

The recommended development times are 30 min or at least 1 h,² and absorbances were claimed stable for at least several hours.¹ Thus, errors could be ~-40 to +20%.

The origin of the problem was traced to photolysis of the phen solution by the fluorescent room lights. Solutions in either thick-walled glass or polyethylene bottles were set out under the room light and control solutions were placed in the dark. After 3.5 months, using standard Fe²⁺ the dark controls still developed immediately (<2 min) regardless of the order of addition of reagents. Light exposed solutions developed to within 1% of the terminal value within 2 min if the buffer was added first. The characteristic slow development arose, however, if the phen was added first; no overshoot was observed during 2 h. The polyethylene stored sample gave 7, 5, and 3% low results and the sample stored in glass gave 30, 23, and 12% low results at 2, 30, and 60 min, respectively, after addition of reagents.

Similar effects could be induced by irradiating fresh phen solutions with a 1000-W Hg-Xe arc lamp.⁷ Air saturated phen solutions irradiated for 15–60 min yielded low initial Fe²⁺ results with slow rises to the correct absorbances for the phen added first. The error increased with irradiation time. After developing for 3 min the absorbance was 60% low for a 1-h photolysis. Deoxygenating the phen solution with N₂ during a 1-h irradiation almost eliminated the initial low absorbance reading (2% low at 3 min).

These results suggest the initial low absorbances arise at least in part from formation of a new ligand which complexes the Fe²⁺ in acid and is only slowly displaced by phen when buffer is added. Longer delays between addition of phen and buffer permit more of the interfering complex to form. The new ligand is probably a photooxidation product of phen, possibly formed by self-sensitized singlet oxygen attack on the reactive 5,6 double bond.⁸ The differences between samples in different containers probably arises from different photochemical modes at different wavelengths coupled with thermal reactions.

For most accurate use of the ferrioxalate actinometer we

make the following recommendations: (1) Solutions of phen should be stored in the dark and kept for no more than 3 months. (2) As a precaution, buffer should be added before phen—the opposite of the current recommendations.^{1,2,9} (3) With good phen development is immediate (<2 min), but 30 min¹ allows a good safety margin. (4) NH₄F should not be used.

Acknowledgment. We gratefully acknowledge the support of the National Science Foundation (Grant No. MPS-74-17916) and thank F. Wilkinson and S. H. Peterson for comments on the ferrioxalate system. We thank R. B. Martin for use of his Cary 11 and 14, F. S. Richardson for use of his laser, and E. Sinn for a sample of 1,10-phenanthroline *N*-oxide.

References and Notes

- (1) C. G. Hatchard and C. A. Parker, *Proc. R. Soc. London, Ser. A*, **235**, 518 (1956).
- (2) J. G. Calvertt and J. N. Pitts, Jr., "Photochemistry", Wiley, New York, N.Y., 1968.
- (3) Similar results were obtained with standard ferrous ammonium sulfate solutions, 0.15 M potassium ferrioxalate photolyzed at 458 nm, and standard Fe²⁺ solutions to which aliquots of unexposed 0.15 M ferrioxalate were added.
- (4) J. H. Baxendale and N. K. Bridge, *J. Phys. Chem.*, **59**, 783 (1955).
- (5) For standard Fe²⁺ solutions or synthetic photolyzed solutions made from ferrioxalate and standard Fe²⁺, we find $\epsilon_{510} \sim 11\,000$, the accepted value, only when the buffer is added first. Using freshly prepared phen, we obtain an ϵ of $11\,100 \pm 100$, regardless of the addition order.
- (6) The method of preparation of the phen solution was unimportant: The phen was dissolved in distilled water while stirring: (a) at $\sim 50^\circ\text{C}$, (b) at $\sim 50^\circ\text{C}$ followed by heating at 97°C for 30 min, (c) at $\sim 50^\circ\text{C}$ and then refluxing for 1 week, (d) at room temperature. All solutions gave indistinguishable results in standard Fe²⁺ determinations.
- (7) Filtered through Pyrex optics and 5 cm of aqueous CuSO₄·5H₂O (100 g/l).
- (8) 1,10-Phenanthroline *N*-oxide mixed with phen can produce low initial absorbances and slow development times if the mixture is added before the buffer, but even with 20% of the oxide in the phen the effect is rather small. The photolyzed solutions, however, contained no detectible amounts of the oxide as shown by thin layer chromatography.
- (9) N. F. Davis, C. E. Osborne, and H. A. Nash, *Anal. Chem.*, **30**, 2035 (1958).

Department of Chemistry
University of Virginia
Charlottesville, Virginia 22901

W. D. Bowman
J. N. Demas*

Received March 17, 1976

Enthalpy–Entropy Compensation and Order in Alkane and Aqueous Systems

Publication costs assisted by Imperial Oil Enterprises Limited

Sir: Thermodynamic¹ and depolarized Rayleigh scattering² studies indicate the presence of short-range orientational order in liquids such as *n*-hexadecane where the molecules are long chains. The presence of order is revealed by thermodynamic effects associated with loss of order when a "probe" liquid such as *n*-C₆, 2,2-dimethylbutane, or cyclohexane is mixed with the *n*-C₁₆. Table I shows values of the molar heat of mixing or excess heat (h^E) at equimolar concentration using *n*-C₆ as the probe, mixed first with a highly branched C₁₆ isomer which has little orientational order, 2,2,4,4,6,8,8-heptamethylnonane (br-C₁₆). The negative h^E value is explained, using the Prigogine–Flory theory,^{1a} as a "free volume effect" associated with volume changes occurring during the mixing

TABLE I: Equimolar Excess Thermodynamic Quantities at 25 °C

	h^E , J mol ⁻¹	Ts^E , J mol ⁻¹	g^E , J mol ⁻¹
<i>n</i> -C ₆ + br-C ₁₆	-68 ^a	20	-88
<i>n</i> -C ₆ + <i>n</i> -C ₁₆	110 ^a	180	-70
Order-decrease contribution	178	160	18

^a Reference 1a.

process (V^E is negative). No other interaction need be assumed between the molecules which are of the same chemical nature. For *n*-C₆ + *n*-C₁₆ h^E is endothermic, indicating that the negative free volume term has now been outweighed by a new endothermic contribution from the decrease of *n*-C₁₆ order caused by the *n*-C₆ probe. The free volume terms are similar for both systems so that the difference in h^E values represents h^E (order-decrease) given in the table.

We have now measured the excess (nonideal) Gibbs free energy for the *n*-C₆ + br-C₁₆ system using a Cahn electrobalance to determine the composition of the solution in equilibrium with a known pressure of *n*-C₆ vapor. The value of Ts^E in Table I may be explained through a negative free volume contribution arising from volume changes during mixing, plus the positive Flory–Huggins excess entropy for mixing components of unequal molecular size. On the other hand, Ts^E for *n*-C₆ + *n*-C₁₆ is considerably larger, indicating the presence of a positive contribution arising from the destruction of orientational order in the *n*-C₁₆. As with h^E , the differences between the *n*-C₁₆ and br-C₁₆ values of Ts^E and g^E correspond to the "order-decrease" contributions for the *n*-C₁₆ system.

It is intuitively evident that the order-decrease contributions in h^E and Ts^E should both be positive. The g^E (order-decrease) is also positive showing that order stabilizes the system. However, its relatively small size is striking. It indicates a considerable degree of enthalpy–entropy compensation. Data similar to that in Table I have been obtained for 2,2-dimethylbutane and cyclohexane probes. Compensation of the enthalpy and entropy order-decrease contributions is again found. A simple explanation of this phenomenon can be given. Reference 1b showed that, for various mixtures containing long-chain alkanes, h^E (order-decrease) falls off rapidly with increasing temperature, and approaches zero, indicating a similar behavior for the orientational order in long-chain *n*-alkanes. It is clear that since c_p^E is large and negative, s^E (order-decrease) must also fall off rapidly with T , as seen in Figure 1, and at some temperature T_1 will be virtually zero. At this temperature g^E (order-decrease) must also be zero. If T_0 is a lower experimental temperature at which g^E is determined, then from elementary thermodynamics

$$g^E(\text{order-decrease}, T_0) = g^E(\text{order-decrease}, T_1) + \int_{T_1}^{T_0} -s^E(\text{order-decrease}) dT = \int_{T_0}^{T_1} s^E(\text{order-decrease}) dT \quad (1)$$

and corresponds to the small hatched area in Figure 1. In contrast, the quantity T_0s^E (order-decrease) corresponds to the large rectangle. By inspection

$$g^E(\text{order-decrease}) \ll Ts^E(\text{order-decrease}) \sim h^E(\text{order-decrease}) \quad (2)$$

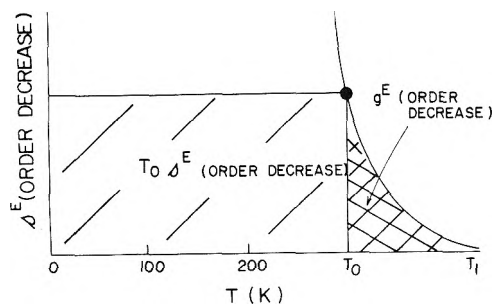


Figure 1. Plot of s^E (order-decrease) against T to show that g^E (order-decrease) $\ll T s^E$ (order-decrease). The curved line represents s^E (order-decrease) falling to zero at T_1 . The point represents the value at the experimental temperature T_0 , the rectangle corresponding to the product $T_0 s^E$ (order-decrease). The value of g^E (order-decrease) at T_0 is given by the hatched area.

Thus, compensation between the order-decrease enthalpy and entropy effects will occur in any system where the order falls off and disappears with T . This should also be true for systems where the order, or structure is *increased* by the introduction of the probe. Here the order-increase contributions to the excess quantities would all be negative. The predicted temperature dependences of both order-decrease and -increase contributions are sketched in Figure 2.

An increase of order caused by the introduction of a solute has not been found in hydrocarbon systems, but it is usual when the ordered solvent is water and the probe is hydrophobic, i.e., a rare gas or a hydrocarbon. Furthermore, it is known that the enhancement of structure becomes less with increasing temperature and may be considered to cease at some temperature above 100 °C, hence order-increase contributions should be as in Figure 2. Experiments lead to thermodynamic functions for the transfer of hydrocarbons and rare gases from an inert solvent, such as a hydrocarbon, into water. If ΔH , ΔS , and ΔG of transfer reflected only the order-increase contributions, all would be negative with ΔG small due to enthalpy-entropy compensation. Experimentally,^{3,4} ΔS (transfer) is negative, ΔH (transfer) is negative becoming positive at higher T , but these quantities do not compensate so that ΔG (transfer) is large and positive, corresponding to the hydrophobic character of the solute-water interaction. However, as in alkane systems, order or structure does not make the only contribution to the thermodynamic quantities. It is clear that the entry of a hydrocarbon or inert gas into water should be accompanied by a second, positive effect in H and G , a "normal" contribution when molecules

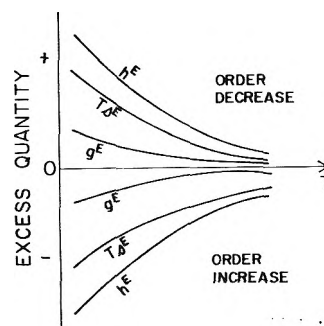


Figure 2. Schematic of the temperature dependence of contributions to excess quantities due to decrease and increase of solvent order.

of widely different chemical nature come into contact. Thus the net effect of the "normal" and order-increase contributions to ΔG (transfer) would be positive. The origin of hydrocarbon-water antipathy and of the hydrophobic bond lies in the positive "normal" contribution rather than in the negative order-increase contribution which actually *stabilizes* the hydrocarbon-water system. This interpretation is essentially that given by Shinoda and Fujihara.⁵ Most current thought based primarily on ref 3 and 4 stresses only order-increase and holds that, due to a lack of enthalpy-entropy compensation, water structuring leads to a positive ΔG (transfer). This, however, is not consistent with the observed rapid decrease with T of water structuring, which should lead to enthalpy-entropy compensation and small negative ΔG . For this reason we prefer the Shinoda-Fujihara picture.

Acknowledgment. We thank Imperial Oil Enterprises Limited and the National Research Council of Canada for financial support.

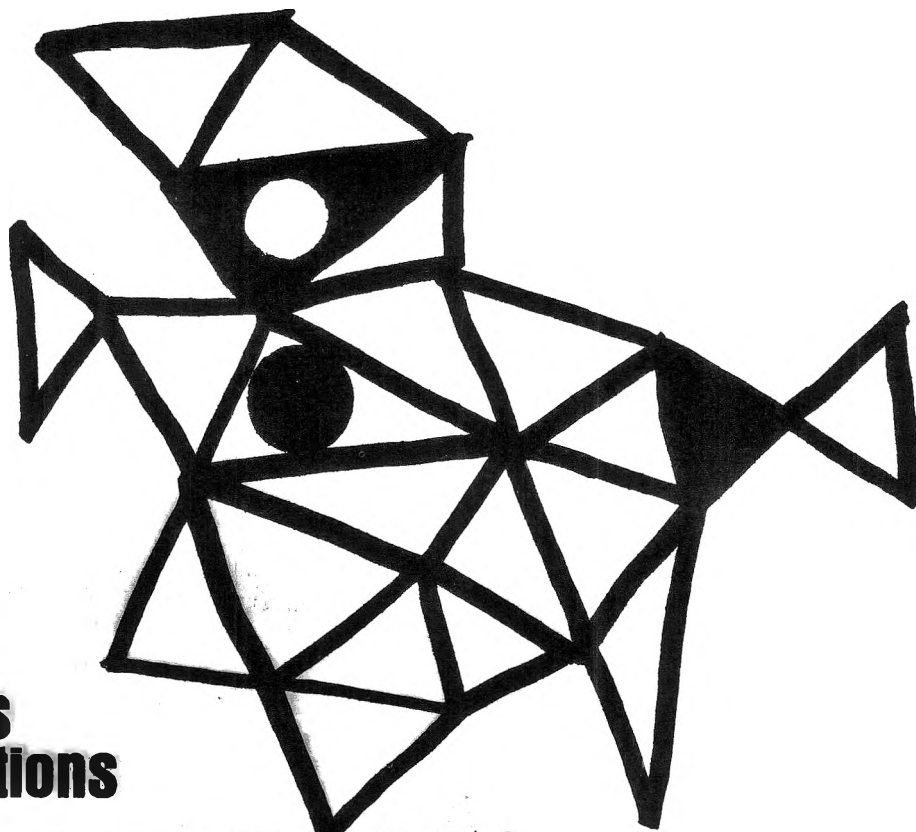
References and Notes

- (1) (a) V. T. Lam, P. Picker, D. Patterson, and P. Tancrede, *J. Chem. Soc., Faraday Trans. 2*, **70**, 1465 (1974); (b) M. D. Croucher and D. Patterson, *ibid.*, **70**, 1479 (1974).
- (2) P. Bothorel, *J. Colloid Sci.*, **27**, 529 (1968), and references in ref 1a.
- (3) G. Nemethy and H. A. Scheraga, *J. Chem. Phys.*, **36**, 3401 (1962).
- (4) W. Kauzmann, *Adv. Protein Chem.*, **14**, 1 (1959).
- (5) K. Shinoda and M. Fujihara, *Bull. Chem. Soc. Jpn.*, **41**, 2612 (1968).

Chemistry Department
McGill University
Montreal, Quebec, Canada H3C 3G1

D. Patterson*
M. Barbe

Received June 3, 1976

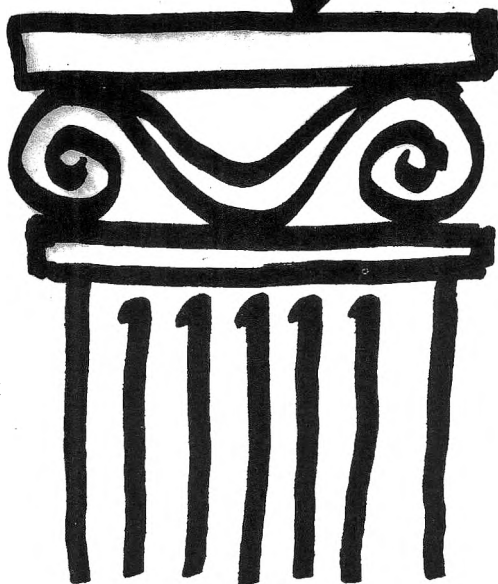


**New concepts
new techniques
new interpretations**

**... together
with valuable reports
on classical areas**

They are all waiting for you between the covers of our well-balanced JOURNAL OF PHYSICAL CHEMISTRY. Whatever your particular interest in physical chemistry, you'll find the JOURNAL's broad range of experimental and theoretical research reports are relevant and beneficial to your work. Each biweekly issue brings you an average of 30 authoritative, comprehensive reports on fundamental aspects of atomic and molecular phenomena, as well as timely notes, communications and reports plus the proceedings of selected symposia.

Join your fellow physical chemists who rely on JPC as an excellent biweekly source of data in both new and classical areas. Just complete and return the form to start your own subscription.



**Journal of
Physical
Chemistry**

**The Journal of Physical Chemistry
American Chemical Society**
1155 Sixteenth Street, N.W.
Washington, D.C. 20036

1976

Yes, I would like to receive the JOURNAL OF PHYSICAL CHEMISTRY at the one-year rate checked below:

	U.S.	Canada**	Latin America**	Other Nations**
ACS Member One-Year Rate*	<input type="checkbox"/> \$24.00	<input type="checkbox"/> \$30.25	<input type="checkbox"/> \$29.75	<input type="checkbox"/> \$30.25
Nonmember	<input type="checkbox"/> \$96.00	<input type="checkbox"/> \$102.25	<input type="checkbox"/> \$101.75	<input type="checkbox"/> \$102.25

Bill me Bill company Payment enclosed

Air freight rates available on request

Name _____

Street _____ Home
Business

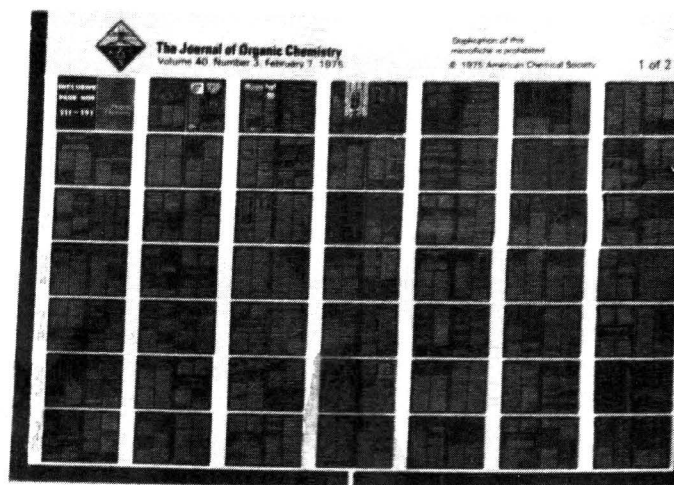
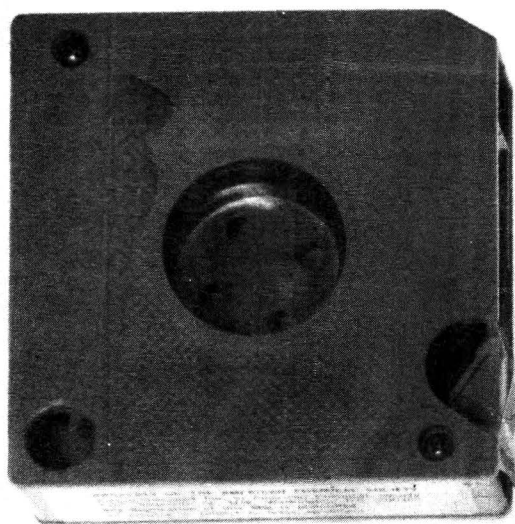
City _____ State _____ Zip _____

Journal subscriptions start January '76

*NOTE: Subscriptions at ACS member rates are for personal use only. **Payment must be made in U.S. currency, by international money order, UNESCO coupons, U.S. bank draft, or order through your book dealer.



... another ACS service



MICROFORMS

American Chemical Society publications in microform

MICROFILM OR MICROFICHE?

With the ACS microform program you can receive either, or both

Microfilm

All periodical publications back to volume one

Copying privileges included with current subscriptions

All non-print supplementary materials provided free on microfiche

Archival quality silver halide film supplied as you request; positive or negative; 16 or 35mm; cartridge, reel, or cassette.

Microfiche

Current issues of primary journals, beginning with January 1975

Individual issues or full volumes available

Supplementary materials also available on microfiche

Fiche supplied are archival quality silver halide, negative, 105 x 148mm (4" x 6"); 24x, with eye legible headers, start and end targets, and page numbers

For information about our microfilm/microfiche write:

Microform Program

Special Issues Sales
American Chemical Society
1155 16th Street, N.W.
Washington, D.C. 20036
(202) 872-4363